Novel Iridium (III) complexes for photocatalytic H_2 generation from H_2O using sunlight

Suraj Soman

A Thesis presented to Dublin City University for the degree of Doctor of Philosophy

2011

Novel Iridium (III) complexes for photocatalytic H_2 generation from H_2O using sunlight

A Thesis presented to Dublin City University for the degree of

Doctor of Philosophy

by

Suraj Soman M.Sc.

Supervisors : Professor Johannes G. Vos and Dr Mary T. Pryce

School of Chemical Sciences
Dublin City University
Dublin 9, Ireland

2011

Dedication

Dedicated to my parents Soman V. A and Santhadevi

And to my wife Anila

I hereby certify that this material, which I now submit for assessment on the programme of study leading to the award of Doctor of Philosophy is entirely my own work, that I have exercised reasonable care to ensure that the work is original, and does not to the best of my knowledge breach any law of copyright, and has not been taken from the work of others save and to the extent that such work has been cited and acknowledged within the text of my work.

Signed:______________________

Suraj Soman

I.D. No. 58118799

Date:________________________

Abstract

The design and synthesis of economically viable homogeneous and heterogeneous transition metal complexes for photocatalytic hydrogen generation using visible light irradiation and as OLED's are under intense investigation. Transition metal complexes are drawing great interest as they offer highly efficient room temperature phosphorescence. In particular iridium (III) complexes are considered to be the most promising since they exhibit: (1) good photo and thermal stabilities, (2) high phosphorescence quantum efficiency, (3) very large values for excited state lifetimes, (4) facile colour tuning through ligand structure control and (5) large cross section for exciton formation. Such characterstic features are attributed to the efficient spin-orbit coupling provided by the Ir metal as well as the strong structural or electronic interactions between the Ir metal and ligands.

Chapter 1 starts up with the general introduction to various technologies used at present for H_2 production followed by its storage, distribution and utilisation. Basic mechanism for natural photosynthesis is described along with different artificial photosynthetic systems giving special attention to intermolecular and intramolecular photocatalyts. Effort has been taken to include most of the recent publications in these catagories. This is followed by a complete insight into the iridium chemistry starting with the iridium complexes using (N^N) co-ordinating ligands and multimetal complexes derived from it followed by Ir complexes with the cyclometallating ligands which then moves along the synthetic aspects and photophysics of the tris complexes and then to the importance of iridium terpyridine complexes. A brief history on the basic excited state properties of iridium metal complexes is described after that. The chapter ends up with the application of the iridium complexes mainly concentrating on the OLED's.

Chapter 2 details the basic synthetic procedures and instruments employed in the studies presented in later chapters. Various techniques used for the characterisation of the complexes including 1D and 2D Nuclear Magnetic Resonance Spectroscopy (NMR), Mass Spectroscopy, Elemental Analysis (CHN), High Performance Liquid Chromatography (HPLC), Absorption and Emission spectroscopy, Time Corelated Single Photon Counting (TCSPC), Laser Flash Photolysis and Gas Chromatography (GC) are briefly described in this chapter.

Chapter 3 deals with the synthesis of iridium polypyridyl complexes with various cyclometallating ligands used for intermolecular and intramolecular photocatalytic H_2 generation from H_2O. A series of heteroleptic iridium monomers and hetrodinuclear Ir-Pt/Pd dimers, which are potential candidates for photocatalytic H_2 generation, are described along with preliminary photophysics measurements and photocatalytic H_2 production results as Turn Over Numbers (TON's) measured using gas chromatography.

Chapter 4 describes the detailed excited state photophysics of novel iridium complexes. Absorption and emission spectra of these novel complexes are taken in different solvents in order to examine any solvatochromic effects. Deaeration was done using freeze pump thaw method in order to remove any oxygen present in the samples that can cause quenching. Temperature dependent emission measurements were carried out in temperature range 77 K to 298 K in every 10 K temperature interval. Temperature dependent lifetime measurements were also carried out in temperature range 77 K to 298 K in every 10 K temperature interval using TCSPC and a cryostat.

Chapter 5 gives an account on the novel high yield synthesis, characterisation, reaction mechanism and excited state photophysics of Ir(polypyridyl)$_2$Cl$_2$ complexes and their deuteriated analogous. Taking [Ir(bpy)$_2$Cl$_2$]PF$_6$ as the standard complex significant effort has been made to figure out the synthetic mechanism of the reaction with the aid of NMR and HPLC done in a concomitant way. This section also explains the novel synthetic method for removing the inner sphere chlorides as triflate complexes and binding the triflate intermediates to other polypyridyl ligands. Detailed study has been carried out on probing the excited state photophysics of these complexes. Excited state lifetimes measured using both TCSPC and laser flash photolysis which provided promising evidence on the effect of deuteriation on lifetimes and the role these complexes can play in OLED applications. Effort has taken in order to study intermolecular photocatalysis with these complexes.

Chapter 6 gives an overview of all the work that has been carried out up to date and a future research plan is also included.

Acknowledgements

Firstly I would like to thank my supervisors Prof. Han Vos and Dr. Mary T. Pryce for giving me an opportunity to carry out my research at Dublin City University (DCU), Ireland. Your guidance, support and encouragement given to me throughout the course of my work has allowed this thesis come to fruition. Whenever I am struck up in between my reactions, go to Han, knock the door, you will surely get a solution. Thanks a lot for giving me the freedom to work in the area where I am interested. I am also grateful for the amount of time and effort that went into reading and correcting this work. I am not getting any words to tell about Mary as she is exceptional, the mental support given by her in all the difficult situations helped me to complete this 3 years smoothly. A heartfelt Thank You for you. I will surely disturb you again in future as I need your help, support and advices throughout my life.

To my parents, no words are there to explain the amount of love and support given by you which helped me to reach upto now. Amma you are the one behind all my success, I love you so much. The care and affection given to me during my school and college days made me to aim at the stars. I wont forget the study leave times when you took leave for the whole month and helped me out in acheving my ambitions. To Achan, you are my best friend, all else is included. Your support, encouragement and motivation has finally given its way leading me upto here. Both of you took all my tensions for yourself and let me go just through my studies. I am so lucky to get you both. Love you both. At this point I am happy to say that I will be back soon to you to spent the rest of my life with you both. Heartfelt love to chechiamma for her wishes for my goodness. Thanks a lot to Asokan achan, sulu amma and kannan for all your support and blessings given to me. Asokan acha, I really wanted to be patient and calm like you but its not working up for me but I will still try. To my sister sini chechi for all her support, care, love and encouragement given to me. To shaji chettan for all his support even during my school days with which I can master up with my papers, especially with english and physics and mathematics. To lachu and appu for the love they are giving to me. Love you all a lot. To members of the extended family you can now stop asking me if I am still a student…I have a job!

Now to my wife Anila, you are being the energy and motivation for me from the past years. You are my soul, I am really lucky to have you as my wife. Love you a lot. Sorry for those hard days working late in labs, stress, tensions and all. I know I made you feel bad many times but still you understand all these things and helped me out to get through. But here on I am confident that life will be entirely different for both of us. I am confident as I told you 5 years back if you are with me I can achieve anything in this world. Thanks a lot for proof reading my thesis and figuring out the mistakes.

I would like to say a huge thank you to all the technicians in School of Chemical Sciences, DCU, for all your help. Veronica, Ambrose, John, Damien, Mary, Catherine, Vinny, and Brendan, I'm sure I've left out a few but to all I'm very appreciative of your help. Brendan, thanks a lot for all the surgeries done on TCSPC, hope that our patient will now stay alive for a long time. Thanks a lot John for making NMR so much handy for us and all your help and new ideas.

And now to my postgraduate friends and colleagues!! I've had great pleasure working alongside with all of you over the past 3 years. It's difficult to know where to begin but I guess the HVRG is the best place to start. Nadia, Evan and Laura for giving me a hearty welcome to the lab and giving me the push to start up my research in my first month. Dr. Danilo Dini for his kind advice, directions and for the company given to for the late night walks to Drumcondra. Dr. Hamid Ahmed for his help given to me with the HPLC and for making the lab alive all the time. To my brother Gurmeet, the master of organic synthesis, thanks a lot for treating me as your younger brother and being with me in all hard times as a big piller of support to get through the hardships, and correcting me when I do something wrong. Now to my sweet girls, Emma, Nikki and Jen, you three changed my life in Ireland itself. Its a really great time being with you three. I will miss you all a lot. Emma, thanks a lot once more for saving me from that devil house owner in drumcondra, and more than above the mental support and courage given to me in past 3 years made it easier for me to finish everything smoothly. I am sure we all will be in touch throughout the life. Declan for the wonderful evenings we had together late night in lab. Dr. Robert Groarke for all his help and support with the photophysics part and teaching me SPC and its various aspects. Thanks for the physical help also (shifting the vacuum pump). Avi and Nivi, thanks for all your support. Dr. Martin Schulz for all your directions to make things in a proper german way, thanks a lot for your help with the publications. Thanks a lot to Dr. Wesley Browne for your suggestions on the bis polypyridyls which give me a good start, hope that our triazole paper will be out in few months time. Now to all my friends very close to heart in Chemical Sciences, with the help of them I understand more about Ireland, the culture over here, festivals, night outs and a lot lot more. Thanks to you all - Zoe, Kieran, Elaine, Ciaran, Shane, Jamie, Kelly – for all those wonderful days. The list is endless and I can't mention everyone but a thank you to you all, you made everyday life enjoyable. It has been a really great time.

Outside the lab, I owe my gratitude to many people as well. To all my friends and their family over here in Dublin for those very nice get togethers and parties and picnics in the past years which took us out from the world of chemistry for some while. I should thank Gurmeet and Pavneet for being with us in all difficult situations and you both are so close to our heart, will miss you a lot. To my elder brother in Ireland, one of the gift that ireland gave me Mr. Madhukumar Bhasker and family. No words to express our love and gratitude to you. Thanks a lot for all your directions and help for cheering me up and getting me go through the right track. Thanks a lot for being my elder brother over here. To Dr. Rajani, Dr. Bincy and Sithara, thanks a lot for all those loving memories with all of you.

Thanks a lot for my teachers over in school and college. Antony sir for giving me the start of chemistry, Manoj sir for all those support given to me in helping up in developing my new ideas, to present up in science fairs and we won continuously for 4 years in district level. Those nice days created the flame inside my mind to dedicate my life to research. Thanks a lot to all of you. Achutan sir, for being a constant support for me. Thanks to my teachers over in the higher seconday school, Francis sir, Sabu sir, Mini miss, Thomas sir, Sen sir for their constant support and encouragement. From my college days thanks to all teachers in St.George College, Aruvithura and St. Thomas College, Palai for being a constant support for me in achieving my goals. To Dr. Sunny Kuriakose and Dr. Tessymol, no words to tell about you both, you considered me as a part of your family and only with your blessings and support I am here now. Sunny sir you are the person who showed me the wonderful and vast world of chemistry. Thanks a lot from my heart. To Sally miss and family for the encouragement and support given to me for achieving my goal of a rank during my bachelors. The flawless effort made by many teachers who shed light on α, β's of life with τ, μ, ε's of chemistry

To all my friends back in home Syam, Arathi, Afsal, Rajkumar, Tom, Renjith, Sujith, John, Sarath, Nikhil, and to by sister sajini, thanks a lot for all of your support and encouragement.

To Dr. Suresh Das, director of NIIST, Trivandrum for giving me a real opening into the international chemistry. Thanks a lot to you and family for giving me support to start up my reseach here in DCU. Thanks to Prof. George Thomas and Prof. George for their help and support given to me during my days in RRL. My heartfelt thanks to Dr. N. S. Saleeshkumar, you are one of the exceptional person that I can find in the area of research who is so willing to help others. Your are the best chetta. All your support and advices at the beginning stage of my research and throughout the past 3 years helped me a lot. We will surely start up some collabrations in the near future itself. Thanks to Dr. Shinto, Dr. Pramod, Dr. Prateesh, Dr. Vijayakumar, Dr. Yoosuf, Dr. Basheer and Dr. Narayan for their help, support and encouragement.

And finally, thanks to Almighty for giving me blessings without which I wont be able to achive my goals in life.

Table of contents

Appendices

Appendix A Posters, presentations and publications

Appendix B Supplementary data from chapter 2 and chapter 3

Appendix C Supplementary data from chapter 4

Appendix D Supplementary data from chapter 5

Appendix E Synthesis of $[Ru(bpy)_2(pztr)]^+$, separation of its isomers and photophysics

Appendix F Photophysics of Ru (II) complexes

Glossary

Abbreviations used throughout this thesis

ACN	acetonitrile
COSY	correlated spectroscopy
CFSE	crystal field stabilisation energy
CT	charge transfer
GS	ground state
HOMO	highest occupied molecular orbital
IC	internal conversion
ISC	inter system crossing
^{1}LLCT	singlet ligand to ligand charge transfer state
^{3}LLCT	triplet ligand to ligand charge transfer state
LUMO	lowest unoccupied molecular orbital
^{1}MLCT	singlet metal to ligand charge transfer state
^{3}MLCT	triplet metal to ligand charge transfer state
^{1}MC/^{1}dd	singlet metal centered
^{3}MC/^{3}dd	triplet metal centered
π-π^*/IL/LC	intraligand or ligand centered transition
OLED	organic light emitting device
PS	photosensitizer
SR	sacrificial reductant
WRC	water reduction catalyst
TEOA	triethanolamine

Abbreviations of compounds discussed in this thesis

bpy	2,2'-bipyridine
dmbpy	4,4'-dimethyl-2,2'-bipyridine
dtbpy	4,4'-ditertiarybutyl-2,2'-bipyridine
dpbpy	4,4'-diphenyl-2,2'-bipyridine
phen	1,10-phenanthroline
dpphen	4,7-diphenyl-1,10-phenanthroline
bpp	2-(6-(pyridin-2-yl)pyridin-3-yl)pyridine
tpy	2,2':6',2"-terpyridine
bpm	2,2'-bipyrimidine
dpp	2,3-di(pyridin-2'-yl)-pyrazine
ppy	2-(phenyl)-pyridine
thpy	2-(thiene-2'-yl)-pyridine
Hpytr	3-(pyridin-2'-yl)-1H-1,2,4-triazole
Hpztr	3-(pyrazin-2'-yl)-1H-1,2,4-triazole

Chapter I

Introduction

In this chapter areas relevent to the studies done in the remaining chapters will be introduced. Firstly various approaches for H_2 production are discussed along with natural and artifical photosynthesis and various photocatalytic complexes reported in the literature for intramolecular and intermolecular photocatalysis. Secondly discussion focuses on the developments with respect to the synthesis and characterisation of Ir (III) polypyridyl complexes with particular emphasis on photophysics. Other areas, which have specific relevance to individual chapters, will be introduced in those chapters.

1.1 Introduction

Energy affects all aspects of modern life. Energy is an essential commodity for increasing productivity in both agriculture and industry. The world's energy requirements have been increasing due to a growing world population, technological development, and higher living standards. Due to world population growth and the advance of technologies that depend on fossil fuels, reserves of fossil fuel eventually will not be able to meet the energy demand. The most important property of any energy source is its environmental compatibility. Our current energy infrastructure is dominated by fossil fuel use, which leads to greenhouse gas emissions. One of the major challenges facing humanity is to develop a renewable source of energy to replace our dependence on fossil fuels. Ideally, this new source should be abundant, inexpensive, environmentally clean, and widely distributed geographically. Different renewable alternatives have been considered which may provide potential solutions to the current environmental issues. Renewable energy should be a clean or inexhaustible energy like hydrogen energy, solar energy, wind energy, biomass energy, hydropower energy, geothermal energy and tidal energy. The most important benefit of renewable energy systems is the decrease of environmental pollution.[1,2]

Of the few potential energy sources that might meet these criteria, sunlight is the most attractive. The sun delivers energy to the earth's surface at an average rate which is about four orders of magnitude larger than the current rate of worldwide technological energy use. Although practical methods for conversion of sunlight to electricity exist, solar generated electricity currently does not compete successfully with that from fossil fuels. The diurnal nature of solar radiation, the fluctuation of sunlight intensity at the earth's surface as a function of the season and weather conditions, and the diffuse nature of solar energy, makes it impractical for powering land vehicles. This in turn will necessitate either great advances in batteries or other devices for storing electricity, or generation of fuels from sunlight. For example, generation of hydrogen from water using sunlight and using it as a fuel.[3]

Hydrogen is potentially an ideal energy carrier, as it is nonpolluting and gives up both its electrons upon oxidation to form only water. Although it is the most abundant element in the universe, elemental hydrogen is not present in great quantities on earth; most of the hydrogen present in earth is bonded to oxygen in the form of water. A number of challenges must be overcome for hydrogen to be used widely as a sustainable energy source. In order to achieve the full environmental benefit of hydrogen as an energy carrier, low carbon intensive, low polluting, and lower cost processes for producing hydrogen from renewable energy sources need to be developed. Scientific advances are needed to develop more energy-efficient and cost-effective methods for purification and delivery, and storage of hydrogen systems, especially for vehicular on board storage, and to enable more durable fuel cells for converting hydrogen into electrical energy. The development of heterogeneous catalytic systems for hydrogen production from water under irradiation has been investigated during last three decades. Intramolecular photocatalysts, however, are very attractive in the sense that their chemical and photochemical properties can be understood and tuned at the molecular level. Moreover, intramolecular catalytic system may be covalently bound to photosensitiser, which leads to more efficient electron transfer. Molecular devices for water splitting based on such systems are of great interest.[4]

1.2 Solar hydrogen - fuel for the future

Hydrogen can be obtained from diverse resources, both renewable (hydro, wind, wave, solar, biomass and geothermal) and non-renewable (coal, natural gas and nuclear). It can be stored as a fuel and used in transportation and distributed heat and power generation systems using fuel cells, internal combustion engines or turbines, with the only by-product at the point of use being water. Hydrogen can also be used as a storage medium for electricity generated from intermittent, renewable resources, such as solar, wind, wave and tidal power; it thereby provides the solution to one of the major issues of sustainable energy, namely the problem of intermittency of supply. The ability of hydrogen to replace fossil fuels in the transportation sector could address one of the world's major environmental problems.[5] The importance of hydrogen as a potential energy carrier has increased significantly over the last decade, owing to rapid advances in fuel cell technology. Fuel cells, operating using hydrogen or hydrogen-rich fuels, have the potential to become major factors in catalysing the transition to a future sustainable energy system with low carbon dioxide emissions. Figure 1.1 illustrates the central role of hydrogen as an energy carrier linking multiple hydrogen production methods and various end-user applications. One of the principal attractions of hydrogen as an energy carrier is obviously the diversity of production methods from a variety of resources. Hydrogen can be produced from coal, natural gas and other hydrocarbons by a variety of techniques, from water by electrolysis, photolytic splitting or high-temperature thermochemical cycles, from biomass and even municipal waste. Such a diversity of production sources contributes significantly to the security of energy supply.

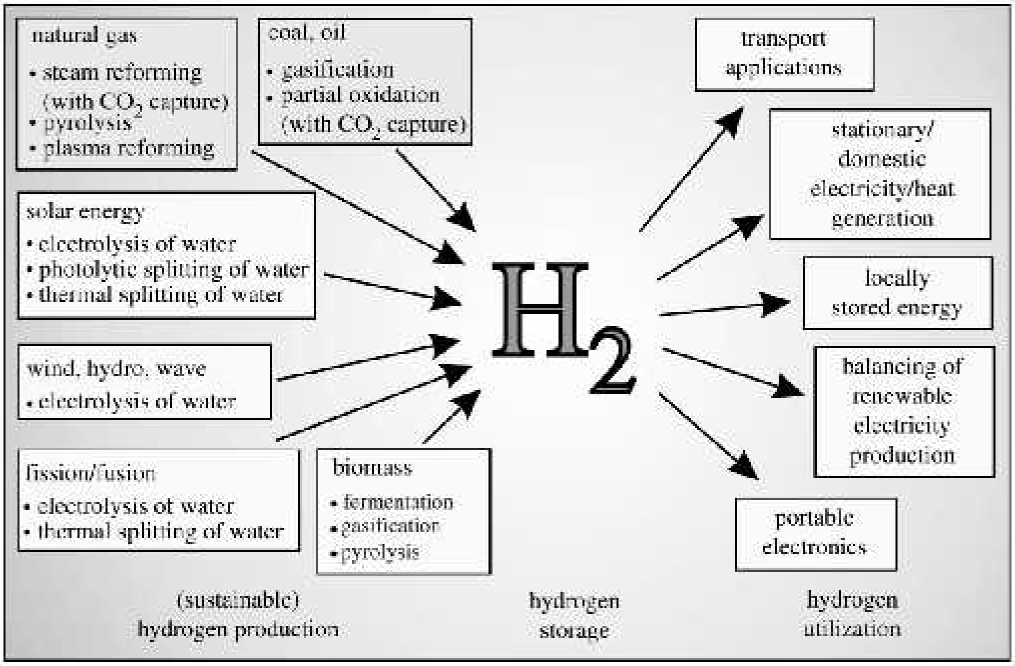

Figure 1.1 *Hydrogen as an energy carrier linking multiple hydrogen production methods, through storage to various end-users.*[14]

The conversion of solar energy into electricity or other forms of energy is a very promising way to solve the energy crisis problem. Since the total solar energy that reaches the earth surface exceeds our total energy consumption by a factor of thousands, an attractive solution would be large scale conversion of solar energy to electricity and fuel. Many attempts were made to convert solar energy into electricity, especially after the discovery of new devices capable of utilising sunlight, i.e. dye-sensitised solar cells. Another way to utilise solar energy is water splitting with production of molecular hydrogen and oxygen. Molecular hydrogen is an ideal fuel because the only product of combustion is water, when combustion is made in pure oxygen. [6,7] Many studies on visible light-driven water splitting, into hydrogen with either heterogeneous or homogeneous systems have been reported since late 1970s.[8,9,10] The key components of these photochemical H_2 evolving systems are usually a light-harvesting photosensitiser, a sacrificial electron donor, and a proton-reduction catalyst. With the aim of developing light driven H_2

evolving devices, several photoinduced molecular devices for homogeneous hydrogen generation were constructed in recent years.[11,12] Solar energy stored in hydrogen is available at any time and at any place on Earth, regardless of when or where the solar irradiance (or the hydropower, biomass, ocean energy or wind energy) was converted. The fundamental discrepancies in the times and places of solar energy supply and human energy demands can be overcome using hydrogen. Solar hydrogen combines the advantages of hydrocarbons with the advantages of solar energy (ecological acceptability, renewability and low risk).

A typical energy chain for hydrogen will comprise hydrogen production, distribution and delivery through hydrogen storage and ultimately its utilisation. The energy chain for sustainable hydrogen energy will involve the harvesting of sunlight or other energy sources to yield hydrogen as the energy carrier, and the storage and distribution of this energy carrier to its utilisation at an end device centered on either fuel cells or combustion where it is converted to power. The ultimate realization of a hydrogen-based economy could potentially confer enormous environmental and economic benefits, together with enhanced security of energy supply. Perhaps, the most telling argument for a sustainable hydrogen economy is the potential (globally) to drastically reduce carbon emissions. However, the transition from a carbon-based (fossil fuel) energy system to a hydrogen-based economy involves significant scientific, technological and socioeconomic barriers to the implementation of hydrogen as the clean energy source of the future.[13]

1.3 Main Approaches for Hydrogen production

Hydrogen is the third most abundant chemical element in the Earth's crust, but it is invariably bound in chemical compounds with other elements. It must, therefore, be produced from other hydrogen-containing sources using energy, such as electricity or heat. At present, hydrogen is produced in large quantities from fossil fuels by steam reforming of natural gas and partial oxidation of coal or heavy hydrocarbons.[14] These methods can take advantage of economies of scale and are currently the cheapest and most established techniques for the large-scale production of hydrogen. They can be used in the short to middle term to meet hydrogen fuel demand and enable the production and testing of technologies related to hydrogen production, storage, distribution, safety and use. However, in the long term, it is clearly unsustainable that the hydrogen economy is driven by hydrogen derived from hydrocarbons. However, to achieve the benefits of a truly sustainable hydrogen energy economy, hydrogen has to be produced from non-fossil resources, such as water.[15,16,17] Hydrogen can be produced by splitting water through various processes, including electrolysis, photo-electrolysis, high temperature decomposition and photo-biological water splitting. The commercial production of hydrogen by electrolysis of water achieves an efficiency of 75 % but the cost is currently several times higher than that produced from fossil fuels. Electricity derived from renewable energy resources (e.g. wind, wave, tidal) might provide local hydrogen needs, but it will not meet the volumes of hydrogen required globally for its widespread use as the new energy source.[18]

Among the different approaches, photocatalysis has received much attention as a possible method for photochemical conversion and storage of solar energy. Photosynthetic bacteria represent a method with appreciable efficiency for hydrogen evolution using solar energy. The various renewable pathways for H_2 production from solar energy are shown in figure 1.2 below.

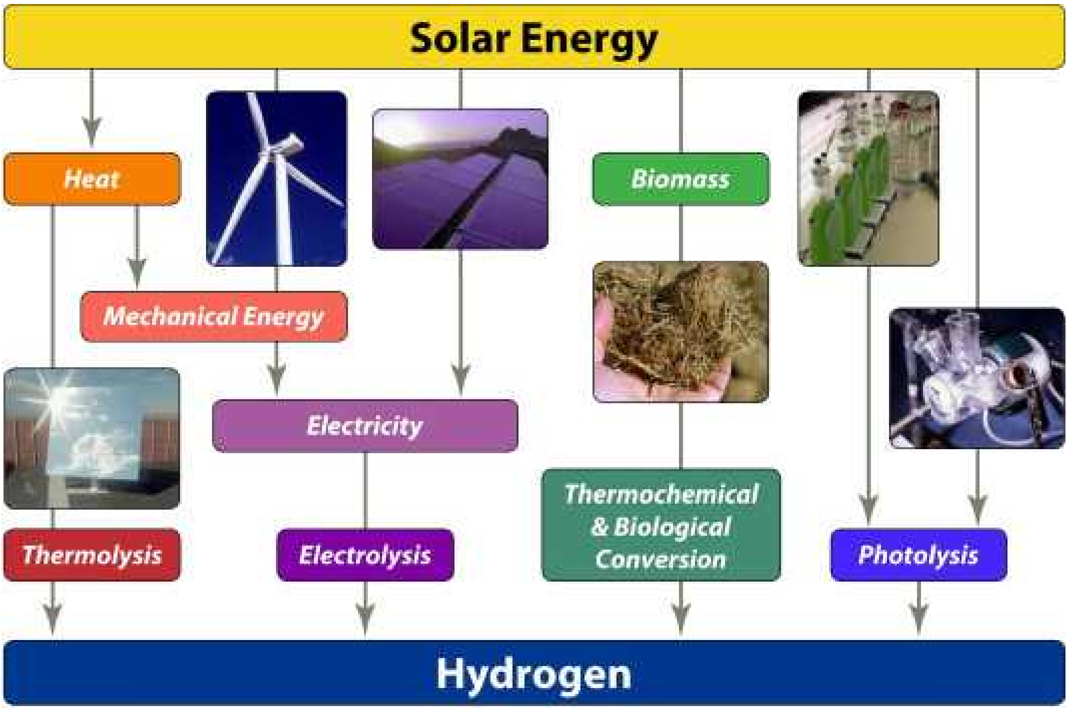

Figure 1.2 *Renewable pathways for hydrogen production.*[47]

Achieving low-cost and efficient solar energy production of hydrogen requires the development of innovative materials, emerging physical phenomena, novel synthetic techniques and new design concepts. Some of the main technologies used for hydrogen production and their status of development are summarised below.

1.3.1 Electrochemical processes

Water electrolysis is one of the most important industrial processes for hydrogen production today, and is expected to become even more important in the future. The three major technologies currently under consideration for electrolytic hydrogen production are classified as alkaline, polymer membrane and ceramic oxide electrolyte. Developments of solid electrolytes for water electrolysis at intermediate temperatures are also important.[19] A principal focus of modern research in hydrogen production by electrolysis is to discover electrode materials that exhibit good electrochemical stability and show interesting activity for the typical electrochemical reactions. It is also desirable that these materials be inexpensive, abundantly available, easy to manipulate and nonpolluting.

1.3.2 Concentrating solar power Technologies (CSP)

Concentrating solar power (CSP) systems use large mirrors to focus direct solar radiation onto a small absorber area, in order to generate heat at temperatures ranging from 200 ^{0}C to 1000 ^{0}C. CSP plants offer possibilities to convert solar radiation on a large scale into a solar chemical fuel such as hydrogen (figure 1.3). Chemical fuels have the advantages of being storable and transportable. Various new concepts were recently developed for solar thermal hydrogen production.[20] The majority of those are solar thermochemical cycles, solar steam reforming of natural gas and methane cracking. Moreover, the high temperature electrolysis can also produce hydrogen by using electricity and heat from solar thermal power plants.

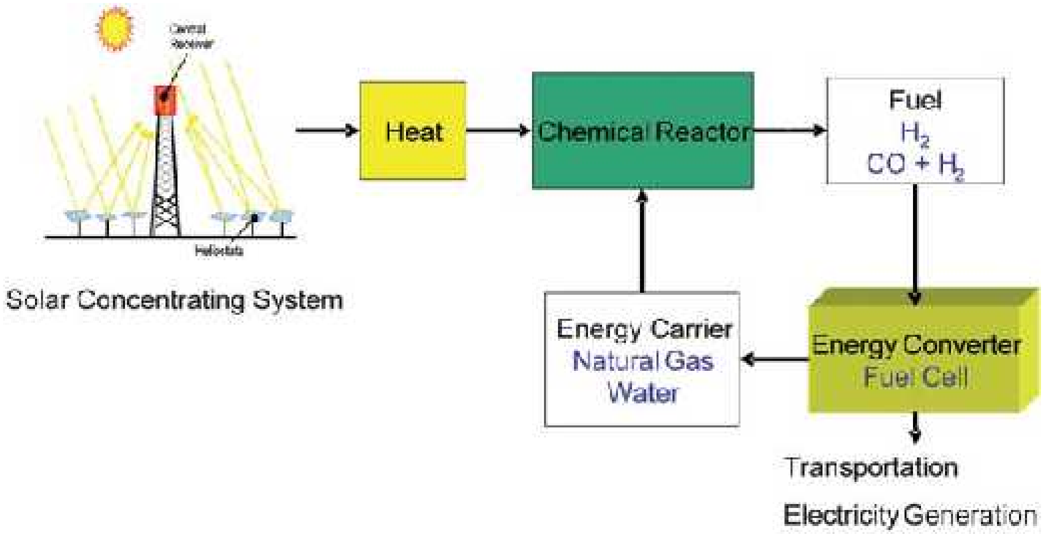

Figure 1.3 *Principle of solar fuel production.*[149]

1.3.3 Photochemical processes

Hydrogen production by solar energy is direct photochemical reduction of water. Of the various possible methods, nature provides a blueprint for converting solar energy in the form of chemical fuels.[21] A leaf is a synergy of elaborated structures and functional components in order to produce the highly complex machinery for photosynthesis in which light harvesting, photoinduced charge separation, and catalysis modules combine to capture solar energy and split water into oxygen and ‘‘hydrogen’’ efficiently. In artificial photocatalytic systems the photosensitiser is excited by visible light and can thereafter effect redox reactions, yielding electrons for the water reduction. One of the benefits of this system is that several sensitisers with different absorption characteristics can be used simultaneously, leading to higher quantum yields per unit area. Thus, the design of efficient, cost-effective artificial systems by the coupling of leaf like hierarchical structures and analogous functional modules under the guidance of the key steps of natural photosynthesis would be a major advance in the development of materials for energy conversion. Further details are given in section 1.7 and section 1.8.

1.3.4 Photocatalytic H_2 Production

Photocatalytic water splitting employs light and semiconductors to split water. The photocatalytic water splitting will be advantageous for the large-scale application of solar hydrogen production because of its simplicity. Water splitting using light energy has been studied for a long time using powder and electrode systems since the Honda–Fujishima effect was reported.[22,23] There is no doubt that photocatalytic water splitting will contribute to green sustainable chemistry. The final target of this research field is to achieve artificial photosynthesis and solar hydrogen production from water. Figure 1.4 shows the main processes in a photocatalytic reaction. The first step (i) is absorption of photons to form electron–hole pairs. The second step (ii) in Figure 1.4 consists of charge separation and migration of photogenerated carriers and the final step (iii) in Figure 1.4 involves the surface chemical reactions.

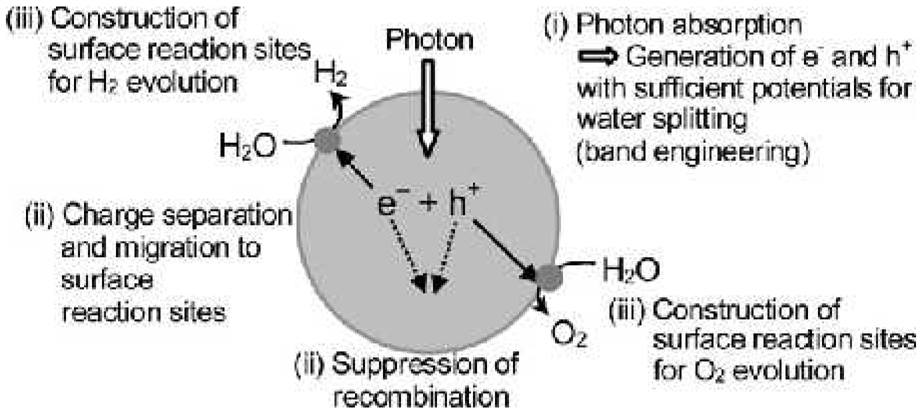

Figure 1.4 *Main processes in photocatalytic water splitting.*[150]

Water splitting proceeds on heterogeneous photocatalysts with semiconductor properties as schematically shown in Figure 1.5. Semiconductors have the band structure in which the conduction band (CB) is separated from the valence band (VB) by a suitable band gap. Irradiation results in generation of electrons and holes in the CBs and VBs, respectively. The photogenerated electrons and holes cause redox reactions similarly to electrolysis. Water molecules are reduced by the electrons to form hydrogen and are oxidised by the holes to form oxygen (for overall water splitting). Important points in the semiconductor photocatalyst materials are the width of the band gap and energy levels of the CBs and VBs. The bottom level of the CB has to be more negative than the redox potential of H^+/H_2 (0 V vs. NHE), while the top level of the VB has to be more positive than the redox potential of O_2/H_2O (1.23 V). Therefore, the band gap should be wider than 1.23 eV.

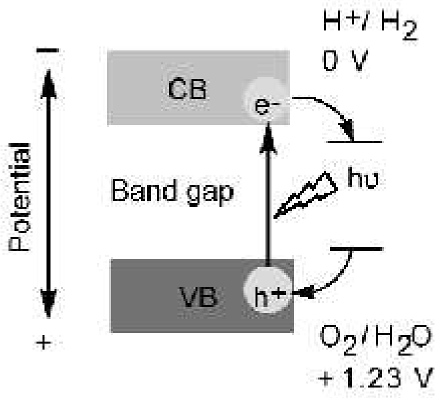

Figure 1.5 *Principle of water splitting on semiconductor photocatalysts.*[150]

1.3.5 Photobiological H_2 Production

Photosynthetic green algae and cyanobacteria provide a promising pathway for generating hydrogen on a large scale. Green algae and cyanobacteria can use solar energy to convert water into hydrogen gas, an energy carrier whose use does not emit greenhouse gases.[24] Hydrogen production by these microorganisms depends on the availability of plentiful resources, namely water as a substrate and solar energy as the energy source. Moreover, the oxygen and hydrogen that such cells produce could be used in a fuel cell to generate electricity (Figure 1.6).

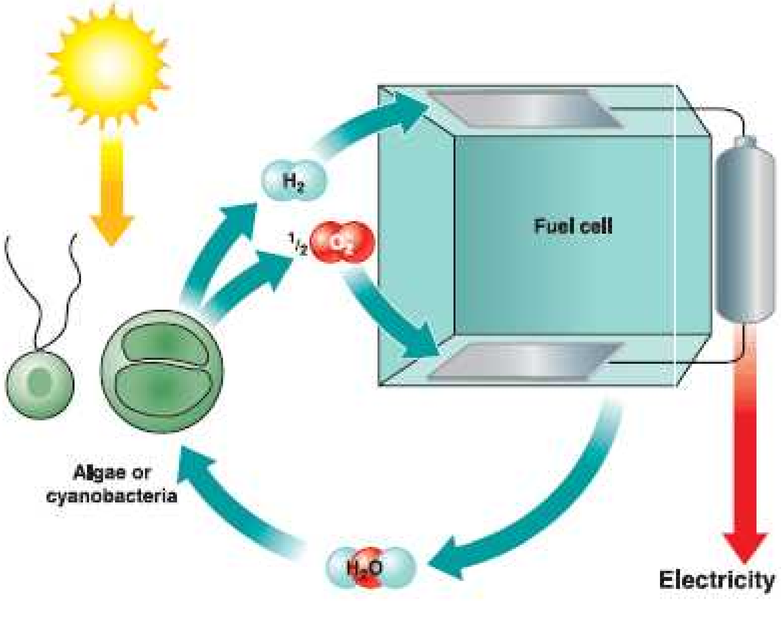

Figure 1.6 *Photobiological H_2 production and its utilisation in a H_2 fuel cell taken from Ref : http://www.microbemagazine.org/309-photobiological hydrogen production*

Green algae and cyanobacteria absorb light through pigments that are associated with two photosystems, photosystem I (PSI) and photosystem II (PSII). The absorbed light energy is transferred from the antenna pigments to chlorophyll reaction center molecules where charge separation occurs, yielding oxidants and reductants. PSI generates a reductant that eventually reduces the iron-sulfur protein ferredoxin, which plays several roles. Its main function is to provide electrons to generate NADPH via ferredoxin-NADP oxidoreductase. NADPH, along with ATP, is needed for fixing carbon dioxide and for producing carbohydrates. However, in the absence of carbon dioxide and under anaerobic conditions, reduced ferredoxin or NADPH reduces protons to yield hydrogen gas, a reaction catalysed by hydrogenase. Ferredoxin links photosynthetic electron transport directly to hydrogen production in green algae, whereas NADPH is the likely electron donor to hydrogenease in cyanobacteria.

1.4 Technologies for hydrogen storage, distribution and utilisation

1.4.1 Hydrogen Storage

Viable hydrogen storage is considered by many as one of the crucial and the most technically challenging barriers to the widespread use of hydrogen as an effective energy carrier.[25] Hydrogen contains more energy on a weight-for-weight basis than any other substance. Unfortunately, since it is the lightest chemical element of the periodic table, it also has a very low energy density per unit volume. The hydrogen economy will require two types of hydrogen storage systems; one for transportation and another for stationary applications. Both have different requirements and constraints. The transportation sector is believed to be the first high-volume user of hydrogen in the future hydrogen economy. The hydrogen storage requirements for transportation applications are far more stringent than those for stationary applications. There are four technologies available today to store hydrogen aboard vehicles

- Liquefied hydrogen used by NASA and considered for airliners.
- Metal hydrides used for example by Mazda and by Daimler-Benz in passenger cars.
- Compressed hydrogen gas used on urban transport buses built by Ballard.
- Carbon sorption yet to be used on vehicles.

A serious downside of these methods is the significant energy penalty, up to 20 % of the energy content of hydrogen is required to compress the gas and up to 30 % to liquefy it. Another crucial issue that confronts the use of high-pressure and cryogenic storage centers, is public perception and acceptability associated with the use of pressurised gas and liquid hydrogen containment. This clearly represents a particularly challenging set of credentials for designing the ideal storage material.

The most promising stationary hydrogen storage materials are a class of ionic–covalent hydrides formed by light elements, such as lithium, boron, sodium, magnesium and aluminium. Hydrogen absorption/desorption in these materials usually involves high-temperature solid-phase transitions. However, much more fundamental research is required to understand the physical and chemical processes governing the hydrogen storage and release and to improve the hydrogen absorption/desorption characteristics in this class of materials to meet hydrogen storage requirements.

1.4.2 Hydrogen Distribution

The current transportation system for delivering conventional fuels to consumers cannot be easily transformed for use with hydrogen. The present options for transporting hydrogen include compressed gas (200 bar) in steel tube cylinders, liquid hydrogen tanks and a few examples of local networks of hydrogen pipelines.[26] All these options are expensive and contribute significantly to the cost of hydrogen for end-users. New concepts will be needed to reduce delivery costs while retaining high safety standards from the point of production through to refueling end-users. The basic components of a hydrogen delivery infrastructure therefore need to be developed. The construction of a new hydrogen network would require significant investment accompanied by research and development of new materials, low-cost compressor technology, seals, sensors and controls, as well as new refilling stations. In those areas where natural gas is not available, hydrogen could be best produced on-site from water, methanol or ammonia, via electricity ideally from renewable energy sources, e.g. wind or solar, or from biofuels. Localised hydrogen production might fit better with accessible fuel distribution. When high penetration rates of hydrogen in energy sector are reached, the ideal long-term option for hydrogen distribution will be a grid of hydrogen pipelines connecting centralised hydrogen production facilities with stationary users and mobile filling stations.

1.4.3 Hydrogen Utilisation

The widespread use of hydrogen as an energy carrier will depend significantly on the availability of efficient, clean and economic techniques for its utilisation and conversion to electricity/heat. The synergistic complementarity of hydrogen and electricity represents one of the most appealing routes to a sustainable energy future, and fuel cells provide, arguably, the most efficient conversion device for converting hydrogen and other hydrogen-bearing fuels into electricity.[27] A fuel cell is a device similar to a continuously recharging battery; a fuel cell generates electricity by the electrochemical reaction of hydrogen and oxygen from the air. An important difference is that batteries store energy, while fuel cells can produce electricity continuously as long as fuel and air are supplied. Several types of fuel cells operating on a variety of fuels and suitable for different energy applications have been developed, but all share the basic design of two electrodes (anode and cathode) separated by a solid or liquid electrolyte or membrane (Figure 1.7). Hydrogen (or a hydrogen-containing fuel) and oxygen are fed into the anode and cathode of the fuel cell and the electrochemical reactions assisted by catalysts take place at the electrodes. The electrolyte or membrane enables the transport of ions between the electrodes while the excess electrons flow through an external circuit to provide electrical current.

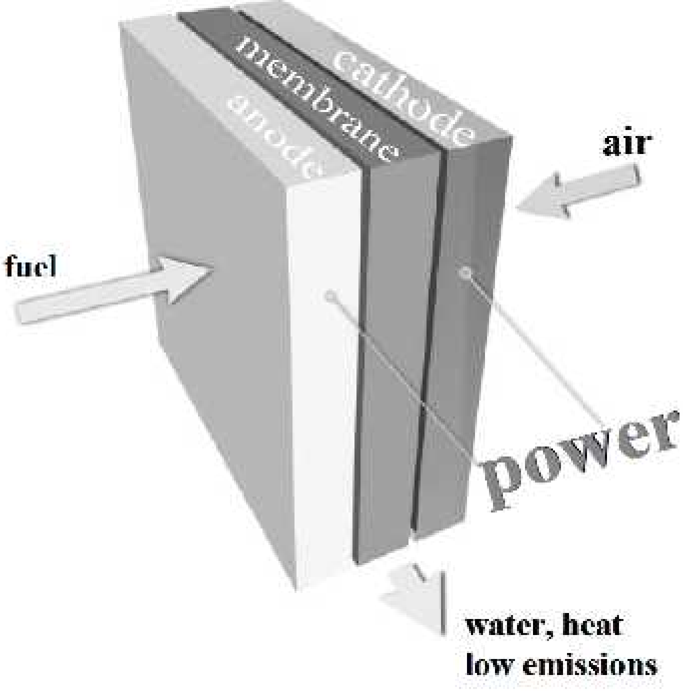

Figure 1.7 *Schematic of a fuel cell.*[147]

Because fuel cells are not subject to the intrinsic limitations of the Carnot cycle, they convert fuel into electricity at more than double the efficiency of internal combustion engines. In transportation, hydrogen fuel cell engines operate at an efficiency of up to 65%, compared to 25% for present-day petrol driven car engines. When heat generated in fuel cells is also used in combined heat and power (CHP) systems, an overall efficiency in excess of 85% can be achieved. Unlike internal combustion engines or turbines, fuel cells demonstrate high efficiency across most of their output power range. This scalability makes fuel cells ideal for a variety of applications from mobile phone batteries through vehicle applications to large-scale centralised or decentralised stationary power generation. Hydrogen fuel cells emit only water and have virtually no pollutant emissions, even nitrogen oxides, because they operate in the temperature range of 60 ^{0}C – 120 ^{0}C, which is much lower than the normal operating temperature of internal combustion engines. Hydrogen-powered fuel cell vehicles provide a route, in theory, to real (i.e. complete life cycle) zero emissions if the hydrogen fuel could be sourced from renewable routes.[28]

1.5 Natural Photosynthesis

Nature has created a process which is capable of harvesting the solar energy that reaches our planet and to use it to sustain life. This process is called photosynthesis and the chemical reactions within it are probably the most important reactions taking place on earth.[29] It is the photosynthesis in cyanobacteria, certain algae and higher plants that produce the oxygen we breathe, most of our food and much of our raw materials. If mankind could understand and mimic the basic principles of photosynthesis, an endless and non-polluting energy source would become accessible.

Photosynthetic organisms capture sunlight very efficiently and convert it into organic molecules. These molecules are the building blocks of all living organisms and without photosynthesis life on our planet would not have evolved in the way that we know. At the heart of the photosynthetic process, is the splitting of water by sunlight into oxygen and ‘hydrogen’. The oxygen is released into the atmosphere where it is available for us to breathe and to use for burning fuels to drive our technologies. The ‘hydrogen’ is not normally released into the atmosphere but instead is combined with carbon dioxide to make sugars and other organic molecules of various types. When fuels are burnt (fossil, biomass and other biofuels) to release energy, the 'hydrogen' stored in these organic molecules are combined with atmospheric oxygen, so completing a cycle that started millions of years ago. Similarly, energy is also released from the organic molecules which constitute our food, when they are metabolised within our bodies by the process of respiration. Thus in the biological world, photosynthesis brings about the splitting of water into oxygen and 'hydrogen' while respiration is the reverse, combining oxygen and hydrogen in a carefully controlled and highly efficient way so as to create metabolic energy. Therefore, from an energetic view, the synthesis of organic molecules represents a way of storing hydrogen and therefore storing solar energy in the form of chemical bonds (Figure 1.8).

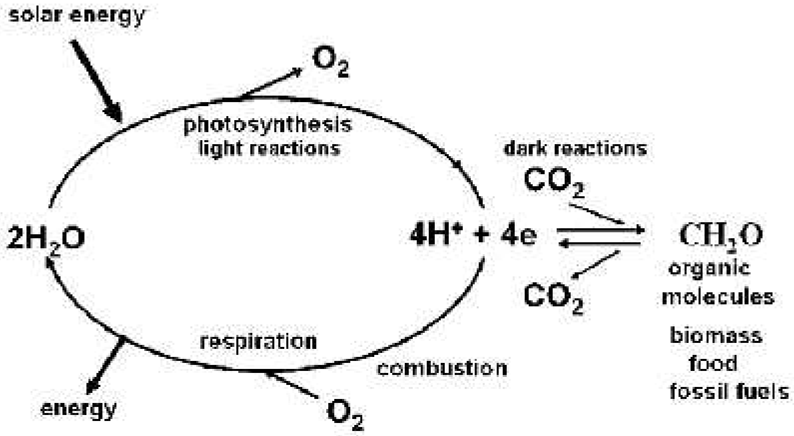

Figure 1.8 *A diagrammatic representation of energy flow in biology. The light reactions of photosynthesis (light absorption, charge separation, water splitting, electron/proton transfer) provides the reducing equivalents in the form of energised electrons (e) and protons (H^+) to convert carbon dioxide (CO_2) to sugars and other organic molecules which make up living organisms.(taken from the review of James Barber)*[151]

1.5.1 Basic Mechanism of Natural Photosynthesis

The protein complexes of the photosynthetic machinery are located in the thylakoid membrane of the chloroplasts. This machinery includes light harvesting proteins, reaction centers, electron transport chains and ATP synthase (ATP = adenosine triphosphate). The initial step in photosynthesis is the absorption of light by the light harvesting complex II (LHC II). LHC II consists of an antenna system that absorbs light and transfers the energy to the reaction centre (P680) of photosystem II (PS II). The excited P680 reduces a nearby pheophytin (pheo) to form a primary charge separation (eq 1.1).

$$\text{P680 pheo} \xrightarrow{h\upsilon} \text{P680}^{+}\,\text{pheo}^{-} \qquad (1.1)$$

The negative charge is transferred through an ingenious chain of electron acceptors via the cytochrome bf complex to photosystem I (PS I). In PS I another reaction centre (P700) is responsible for providing the reducing power for the conversion of $NADP^+$ to NADPH. In plants, light-dependent reactions occur in the thylakoid membranes of the chloroplasts and use light energy to synthesise ATP and NADPH. The light-dependent reaction has two forms: cyclic and non-cyclic. In the non-cyclic reaction, the photons are captured in the light harvesting antenna complexes of photosystem II by chlorophyll and other accessory pigments. When a chlorophyll molecule at the core of the photosystem II reaction center obtains sufficient excitation energy from the adjacent antenna pigments, an electron is transferred to the primary electron-acceptor molecule, pheophytin, through a process called photoinduced charge separation. These electrons are shuttled through an electron transport chain, the so called Z scheme shown in figure 1.9 that initially functions to generate a chemiosmotic potential across the membrane.[30]

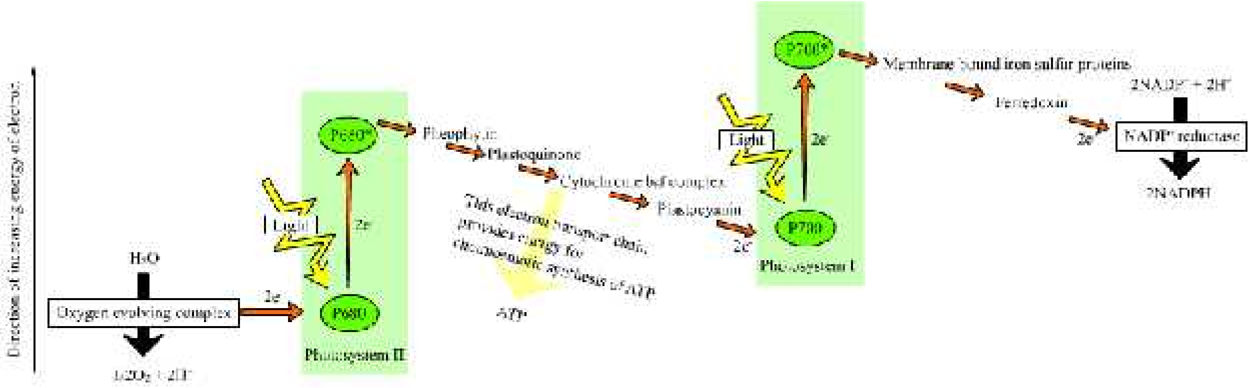

Figure 1.9 *A simplified Z-scheme of the light reactions of photosynthesis (taken from http://en.wikipedia.org/wiki/Photosynthesis)*

An ATP synthase enzyme uses the chemiosmotic potential to make ATP during photophosphorylation, whereas NADPH is a product of the terminal redox reaction in the *Z* scheme. The electron enters a chlorophyll molecule in Photosystem I. The electron is excited due to the light absorbed by the photosystem. A second electron carrier accepts the electron, which again is passed down lowering energies of electron acceptors. The energy created by the electron acceptors is used to move hydrogen ions across the thylakoid membrane into the lumen. The electron is used to reduce the co-enzyme NADP, which has functions in the light-independent reaction. The cyclic reaction is similar to that of the non-cyclic, but differs in the form that it generates only ATP, and no reduced NADP (NADPH) is created. The cyclic reaction takes place only at photosystem I. Once the electron is displaced from the photosystem, the electron is passed down the electron acceptor molecules and returns to photosystem I, from where it was emitted, hence the name cyclic reaction.

1.6 Artificial Photosynthesis

1.6.1 Introduction

The conversion of solar energy into fuel by artificial photosynthetic systems is certainly one of the most challenging goals in chemistry.[31,32,33,34] For solar fuel production to be economically and environmentally attractive, the fuels must be formed from abundant, inexpensive raw materials such as water and carbon dioxide. Water should be split into molecular hydrogen and molecular oxygen, and carbon dioxide in aqueous solution should be reduced to ethanol with the concomitant generation of dioxygen.[6] From many points of view, the most attractive fuel-generating reaction is the cleavage of water into hydrogen and oxygen as given in eqn 1.2.

$$2H_2O + 4h\upsilon \longrightarrow 2H_2 + O_2 \qquad (1.2)$$

Such a process, of course, has to be sensitised as water cannot be electronically excited by sunlight.[35] Combustion of molecular hydrogen, H_2, with oxygen produces heat and water, and combination of molecular hydrogen and oxygen in a fuel cell generates electricity, heat, and water. Once obtained, hydrogen can also be used to obtain methanol, a liquid fuel. Clearly, if hydrogen could promptly replace oil, both the energy and the environmental problems of our planet would be solved. Clearly, clean hydrogen can only be obtained by exploiting renewable energies, and this can be done, in principle, by photochemical water splitting or through the intermediate production of electricity (e.g. by wind or photovoltaic cells) followed by water electrolysis.

1.6.2 Components of an Artificial Photosynthetic System

A possible way to construct artificial photosynthetic systems for practical solar fuels production is that of mimicking the molecular and supramolecular organization of the natural photosynthetic process: light harvesting should lead to charge separation, that must be followed by charge transport to deliver the oxidizing and reducing equivalents to catalytic sites, where evolution of oxygen and hydrogen should separately occur. Therefore, a plausible artificial photosynthetic system should include the following basic features (Figure 1.10)[7] 1) an antenna for light harvesting, 2) a reaction center for charge separation, 3) catalysts and 4) a membrane to provide physical separation of the products.

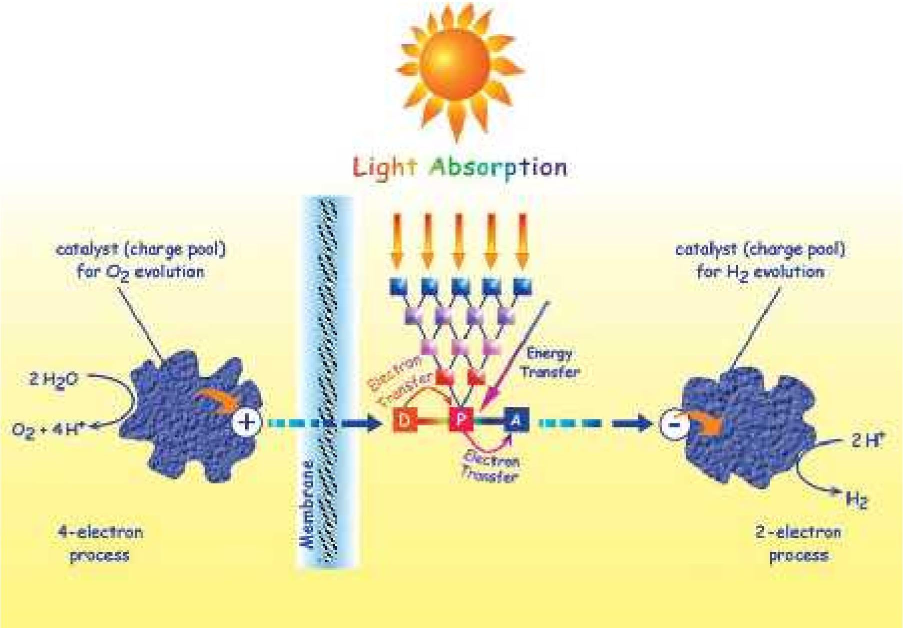

Figure 1.10 *Schematic representation of photochemical water splitting (artificial photosynthesis). Five fundamental components can be recognised - an antenna for light harvesting, a charge-separation triad D-P-A, a catalyst for hydrogen evolution, a catalyst for oxygen evolution, and a membrane separating the reductive and the oxidative processes.*[7]

The achievement of efficient conversion of light into chemical energy requires the involvement of supramolecular structures with very precise organization in the dimensions of space (relative location of the components), energy (excited states energies and redox potentials), and time (rates of competing processes). Such an organization, which in natural systems comes as a result of evolution and is dictated by intricate intermolecular interactions, can be imposed in artificial systems by molecular engineering exploiting covalent or non-covalent bonding.[36]

Molecular photocatalytic systems can be either intermolecular or intramolecular. The former one relies on the collision induced electron transfer between the different species involved which has low catalytic efficiencies due to the presence of various reaction intermediates. The intramolecular system consisting of a light harvesting unit and a catalytic centre which are bound together using a proper bridging ligand is based on the fundamental biological construction principles and allows more efficient light driven reactions such as oxidation and reduction of water.

1.7 Intermolecular Photocatalytic Systems

1.7.1 Systems based on light-induced hydride transfer

In organic photochemistry, benzophenone is a widely used photosensitiser which, in its excited state and in the presence of a platinum catalyst, is capable of oxidizing secondary alcohols to give ketones and hydrogen.[37,38,39] The addition of methyl viologen (MVZ^+; 1,1'-dimethyl-4,4'-bipyridinium dication), acting as an electron relay compound, increases the quantum yield of light-induced hydrogen formation.

However, one great disadvantage of these systems is that benzophenone does not absorb in the visible light region and therefore its practical application for conversion of solar energy is limited. Several other dyes of the benzophenone type (fluorenone and its derivatives, pyrrolizinone, etc.) have been investigated with respect to a bathochromic shift of the absorption (maximum) and to light-induced H_2 formation.[40] It was shown that suitable modifications of the structure of polycyclic aromatic ketones give stronger absorbances and a bathochromic shift of the lowest energy absorption band. However, although compounds possess higher absorption coefficients in the visible light region, (efficient) visible light-induced hydrogen formation could not be achieved.

1.7.2 Systems based on light-induced electron transfer

Classical intermolecular systems commonly employ $[Ru(bpy)_3]^{2+}$ as a light-harvesting complex. $[Ru(bpy)_3]^{2+}$ and its derivatives therefore have a long and rich history in inorganic chemistry and photochemistry. The parent compound, first prepared in 1936,[40] was later obtained by a more practical synthesis,[41] thus opening the way for Adamson's first use of the $[Ru(bpy)_3]^{2+}$ excited state as a photochemical reductant in 1972.[42] The potential of this excited state for water splitting was quickly noted by other authors,[43,44] and the numerous attempts to realise this reactivity directly grew into the field of three component catalysis. The first reports using $[Ru(bpy)_3]^{2+}$ for "water splitting" focused on the hydrogen half-reaction, using a modified photosensitiser that can be cast into films.[45,46] Though the H_2 generating properties of the systems were ill defined, this work was the predecessor of three component systems composed of a $[Ru(bpy)_3]^{2+}$ as sensitiser, colloidal Pt as a H_2 production catalyst, and methylviologen (MV^{2+}) as a mediator.[47] Brown *et. al.* [48] described the mechanism of the formation of dihydrogen from the photoinduced reactions of $[Ru(bpy)_3]^{2+}$ and $[Rh(bpy)_3]^{3+}$. They found that visible irradiation of aqueous solutions of $[Ru(bpy)_3]^{2+}$ and $[Rh(bpy)_3]^{3+}$ containing TEOA/$TEOAH^+$ (pH 8.1) and K_2PtCl_4 yielded dihydrogen as the end product of a series of electron transfer reactions. Irradiation with visible light gives rise to $^*[Ru(bpy)_3]^{2+}$ which in turn is oxidised by $[Rh(bpy)_3]^{3+}$ to produce $[Ru(bpy)_3]^{3+}$ and $[Rh(bpy)_3]^{2+}$. TEOA reduces $[Ru(bpy)_3]^{3+}$, and Rh(II) in the presence of platinum can either disproportionate or yield dihydrogen or in the absence of platinum disproportionates to give Rh (III) and Rh (I).[49]

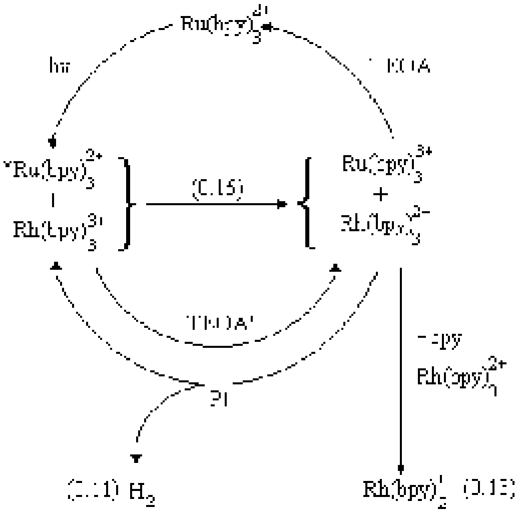

Figure 1.11 *Outline of reaction pathways leading to the production of H_2.*[49]

After excitation of a photosensitiser S, charge separation takes place: D is the electron donor and R is the electron relay

$$S + h\upsilon \rightarrow S^{*} \tag{1.3}$$

$$S^{*} + D \rightarrow S^{-} + D^{+} \tag{1.4}$$

$$S^{*} + R \rightarrow S^{+} + R^{-} \tag{1.5}$$

The photosensitiser in its excited state, is both a stronger oxidant and reductant than in its ground state because of its higher energy content. The light-induced charge separation can result either in a reduced S^- or in an oxidised photosensitiser S^+.[50] Whether oxidative quenching Eq. 1.4 or reductive quenching Eq. 1.5 takes place, depends on the redox potentials of the species involved. In both cases the light-induced electron transfer reaction results in a pair of products ($S^+ + R^-$ or S $^- + D^+$) which possess higher energy content and can undergo further reactions (Figure 1.12).

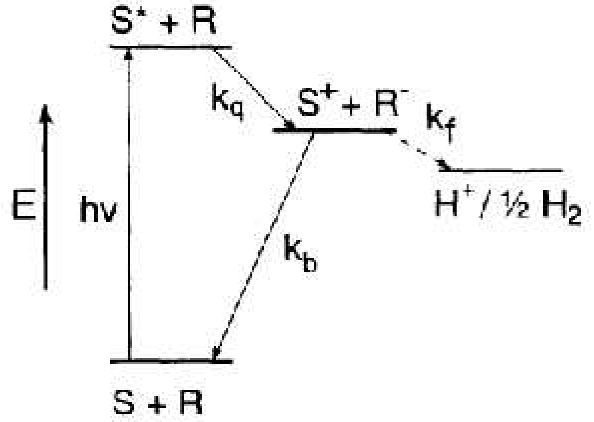

Figure 1.12 *Energy diagram for light-induced charge separation: S, photosensitiser; R, electron relay (electron acceptor) ; k_q, rate constant for quenching reaction; k_b, rate constant for back electron transfer reaction; k_f, rate constant for forward reaction (proton reduction).*[152]

When the "molecular electronegativity" Δ_{ME} of a compound is maximum then that compound acts as an electron acceptor. Δ_{ME} is defined as the sum of the oxidation and reduction potentials, i.e. $\Delta_{ME} = E°(M/M^+) + E°(M^-/M)$.[51] Light induced intermolecular electron transfer reactions are usually fast (eg: for $[Ru(bpy)_3]^{2+}*$ (S) quenched by viologens (R), kq = $10^9 Lmol^{-1}s^{-1}$) and thus in solutions they are limited by diffusion processes.[57] Fast electron transfer (quenching) reactions are necessary, since the photosensitiser's excited state lifetime is usually short (eg: for [^{3}Ru(bpy)$_3$]$^{2+}$*, τ = 0.64 μs). By thermal back reaction (k_b in Fig. 2) the initial state (S + R) is reached, producing heat. During the lifetime of the charge separated state (S$^+$ + R$^-$) (usually less than 1μs), other reactions (e.g. proton reduction and hydrogen formation; k_f in Figure 1.13) can occur.[52]

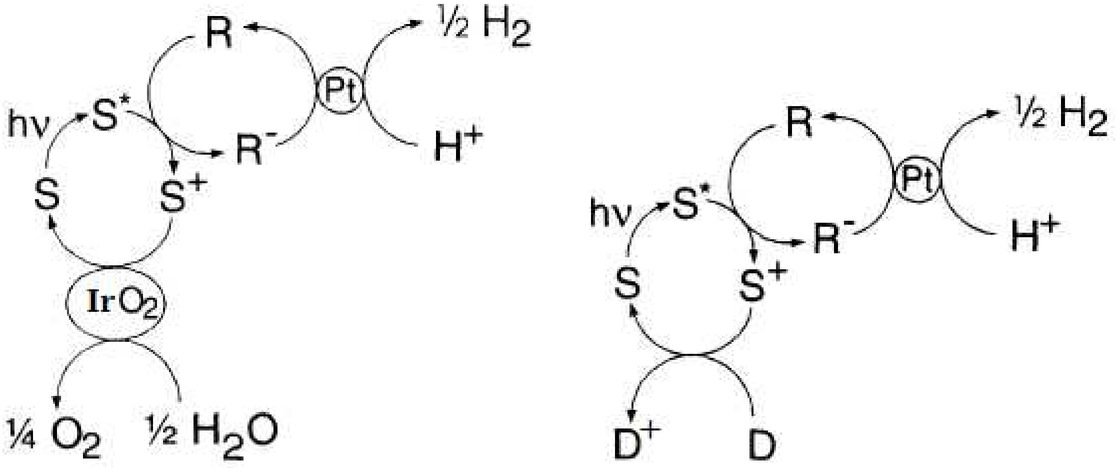

(a) **(b)**

Figure 1.13 *Reaction schemes for* ***(a)*** *light-driven cyclic water splitting and* ***(b)*** *light-induced "sacrificial" hydrogen formation: S, photosensitiser; R, electron relay (electron acceptor; e.g. MV^{2+}); D, "sacrificial" electron donor (e.g. EDTA, TEA); Pt, colloidal platinum catalyst; RuO$_2$, colloidal ruthenium oxide catalyst.*[152]

In the case of cyclic water splitting (Fig. 1.13(a)) the reduced electron acceptor R$^-$ (or photosensitiser S$^+$ in the case of oxidative quenching according to Eq. (1.6)) should reduce protons to hydrogen (in the presence of a suitable catalyst, e.g. Pt, RuO$_2$, Pd or Ni)[53] and the oxidised sensitiser S$^+$ (or electron donor D$^+$) should oxidise water to oxygen, Eq. 1.7.

$$R^-/S^- + H^+ \rightarrow R/S + 1/2H_2 \tag{1.6}$$

$$2D^+/S^+ + H_2O \rightarrow 2D/S + 2H^+ + 1/2O_2 \tag{1.7}$$

This also requires a suitable catalyst (e.g. RuO$_2$ or IrO$_2$) and still has to overcome additional drawbacks, e.g. RuO$_2$ is subject to corrosion (oxidation to the inactive RuO$_4$).[54] Moreover, cyclic water splitting requires catalysts which are selective for the forward reaction (i.e. H$_2$ and O$_2$ formation) and which do not increase the rate constants of back reactions. The overall reaction would be cyclic light-induced water splitting with oxygen and hydrogen as desired products. In order to study the hydrogen evolution, a "sacrificial" electron donor was introduced several years ago,[55] mimicking the oxygen evolution process and reducing the oxidised sensitiser (see Fig. 1.13(b)) and thus diminishing the back electron transfer. EDTA (ethylenediaminetetraacetic acid) and TEA (triethanolamine) were the mostly used "sacrificial" electron donor substances. With such "sacrificial systems", quantum yields (ϕ_{H2}) up to 18% can be achieved. The components S and R are not consumed during this cyclic reaction but may be destroyed as a result of different competing and consecutive processes. For example, oxidation and degradation of TEA may be represented as follows (Scheme 1.1). In these processes, different radical and cationic species are involved, and they, together with products from their decomposition, can potentially influence the structures and reactivities of photosensitisers and catalysts.

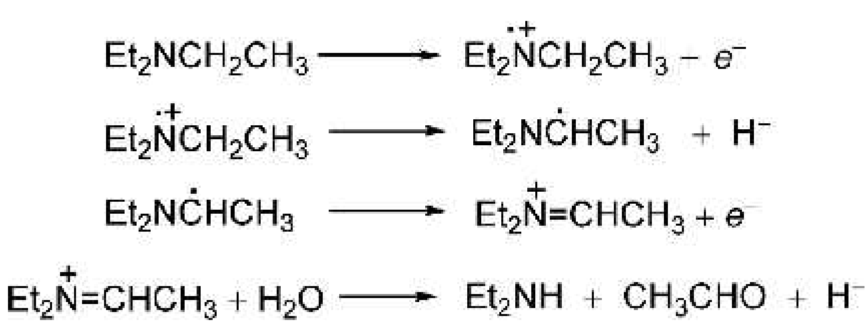

$$Et_2NCH_2CH_3 \longrightarrow Et_2\overset{\cdot+}{N}CH_2CH_3 - e^-$$
$$Et_2\overset{\cdot+}{N}CH_2CH_3 \longrightarrow Et_2N\dot{C}HCH_3 + H^-$$
$$Et_2N\dot{C}HCH_3 \longrightarrow Et_2\overset{+}{N}{=}CHCH_3 + e^-$$
$$Et_2\overset{+}{N}{=}CHCH_3 + H_2O \longrightarrow Et_2NH + CH_3CHO + H^-$$

Scheme 1.1 *Proposed reactions of TEA as a sacrificial electron donor in hydrogen photo-production systems.*

1.7.3 Iridium and Rhodium based intermolecular water reduction catalysts (WRCs)

It was found that the emission energy of ruthenium(II) tris-diimine complexes cannot be adjusted through ligand modification due to the presence of a low lying triplet metal centered (^{3}MC) excited state.[56] The detrimental effect of this very short-lived and accessible ^{3}MC state is further compounded by the fact that its populated anti-bonding, e_g* like molecular orbital (MO) weakens the metal ligand bond, promoting photosensitiser degradation through ligand dissociation. In an effort to alleviate the constraint of the ^{3}MC state, third row transition metals such as iridium and platinum have been targeted as more tunable photosensitisers, since their greater ligand field splitting allows for a broader range of populated/unpopulated MO gap energies. Additionally, the absolute energies corresponding to the highest populated and lowest unpopulated MOs of heteroleptic iridium complexes incorporating 2-phenylpyridine (ppy) and bpy can be adjusted independently of each other through chemical substitution on the peripheries of the ppy and bpy ligands, respectively.[57] This ability to selectively tune the critical MOs may prove indispensable in reuniting the PS with a pair of optimised catalysts. A reductive quenching mechanism is exclusively available to the iridium complexes which was substantiated through DFT calculations (Figure 1.14) resulting in higher photocatalytic efficiency compared to the ruthenium analogues. The lowest singly occupied molecular orbital (LSOMO) is exclusively metal centered in $[Ru(bpy)_3]^{2+}$ (95 percentile), while the analogous orbital of the Ir(III) complex exhibits mixed metal-based 5d and ppy-based π character. The highest singly occupied molecular orbitals (HSOMO) of both complexes are exclusively localised on the bpy ligands.

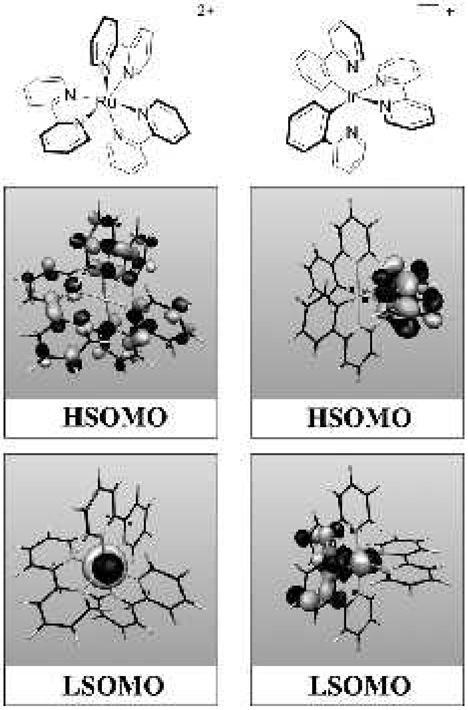

Figure 1.14 *Frontier orbitals of $[Ru(bpy)_3]^{2+}$ (left) and $[Ir(ppy)_2(bpy)]^+$ (right) in the triplet excited state obtained through DFT calculations.*[153]

To advance the discipline of water splitting, the Bernhard group has synthesised a variety of heteroleptic iridium (III) complexes of the general structure $[Ir(C^\wedge N)_2(N^\wedge N)]^+$ that exhibit a broad range of photocatalytic properties with $[Co(bpy)_3]^{2+}$ as shown in Figure 1.15 below (C^N = cyclometalating ligand and N^N = neutral diimine ligand).[58,59]

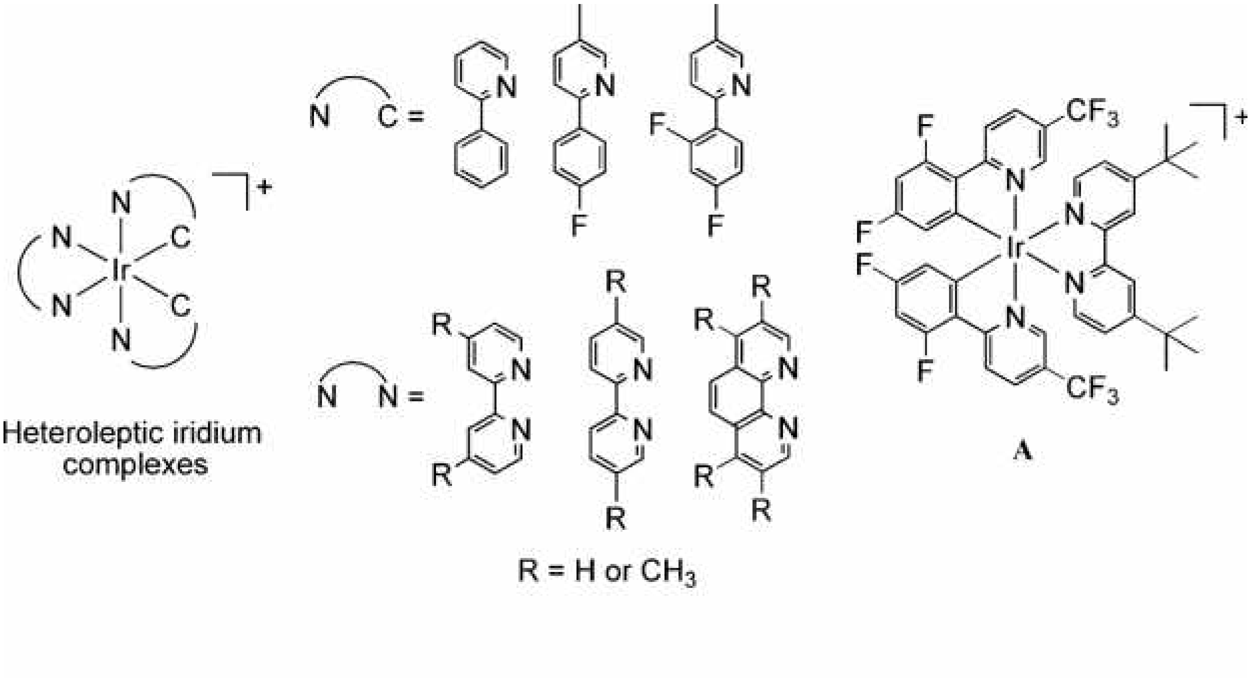

Figure 1.15 *Heteroleptic iridium photosensitisers used by Bernhard's group.*[58,59]

These heteroleptic iridium complexes were found to be superior to ruthenium polypyridine derivatives. On comparing the TON results, the turnovers are up to 920 based on the iridium photosensitiser $[Ir(F\text{-}mppy)_2(bpy)]^+$ (F-mppy = 5-methyl-2-(4-fluoro)phenylpyridine) and 18 based on $[Co(bpy)_3]^{2+}$, while it is 580 turnovers based on $[Ru(dmphen)_3]^{2+}$ and 12 turnovers based on $[Co(bpy)_3]^{2+}$.[11] The relative quantum yields of hydrogen determined in this work are 3 to 7 times as high as the results obtained with $[Ru(dmphen)_3]^{2+}$ as photosensitiser.[65] With introduction of the CF_3 group to the difluorophenylpyridine ligand and the *t*-butyl groups to the bipyridine ligand, both the lifetime and the reducing power of the excited iridium photosensitiser (**A**, Figure 1.15) are apparently enhanced, resulting in an increase in hydrogen production efficiency. The quantum yield of hydrogen at 465 nm with the modified iridium complex as photosensitiser is 14 times as high as that obtained with $[Ru(dmphen)_3]^{2+}$ as a light-harvesting unit.[12]

Tris-(2,2′-bipyridine)Rh(III), $[Rh(bpy)_3]^{3+}$, is an ideal candidate for the WRC (water reduction catalyst) component in homogeneous systems because it accumulates two electrons at a suitable potential for water reduction and is known to form hydrides.[60] Additionally, the one-electron reduction product, $[Rh(bpy)_3]^{2+}$, is kinetically unstable and rapidly disproportionates to form the doubly reduced species, eliminating the need for a concerted two-electron reduction by the photosensitiser.[61] Sutin and co-workers reported the use of the rhodium complex $[Rh(bpy)_3]^{3+}$ for photoinduced hydrogen formation in 1981.[60] This complex, in combination with $[Ru(bpy)_3]^{2+}$ and TEOA, can be reduced under irradiation with 450 ± 20 nm light to give rhodium(I) and hydrogen. The quantum yields of hydrogen evolution (up to 0.11) were found to be dependent on pH and concentrations of Rh and Ru complexes. It was recently found by Bernhard and co workers that the systems composed of cyclometallated iridium (III) complexes as photosensitisers and tris-2,2'-bipyridyl rhodium (III) complexes as catalysts are efficient in production of hydrogen from water.[62] The effectiveness of these systems is impressive: turnovers greater than 5000 with quantum yields up to 34 % can be achieved. Authors noted that the photoreaction conditions, such as solvents and sacrificial reductants, dramatically influence the performance of the catalytic systems. Triethylamine was found to be the most efficient sacrificial reductant, and a water/THF (80 %) mixture is optimal as a reaction medium.

The photocatalytic water reduction process reported above involves three critical components: the PS, the SR, and WRC. In the catalytic light cycle, the PS is responsible for the absorption of visible light to provide the energy necessary for the endothermic water reduction process to occur. In the catalytic dark cycle, the WRC collects the high-energy electrons from the light cycle and protons from water to produce hydrogen. The SR provides the electrons necessary for water reduction by replenishing the lowest singly occupied molecular orbital of the PS^* or PS^+, depending on the mechanism of quenching. In the case of cyclometallated iridium complexes the reaction is operating predominately through a reductive quenching mechanism, where the highly reactive $[Ir(N^\wedge C)_2(N^\wedge N)]^0$ species reduces the WRC components as outlined in scheme below.

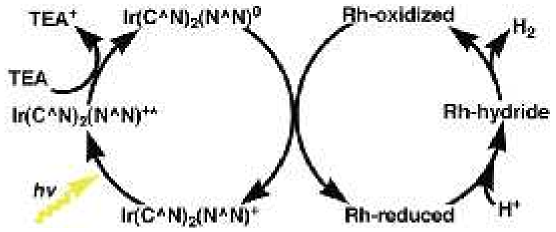

Figure 1.16 *General reaction scheme for photocatalytic hydrogen production by TEA-Ir-Rh system.*[62]

1.7.4 Bio-inspired iron based intermolecular photocatalytic systems

Recently, Moore and co-workers reported photoinduced hydrogen production catalysed by [FeFe]-hydrogenase ([FeFe]H_2ase) in a photoelectrochemical bio-fuel cell.[63] Although hydrogenases are more active and selective compared to reported hetero and homogeneous catalysts, they are not ideally suited for large-scale and long-term use because the reaction conditions are limited.[64] Among the several kinds of hydrogenases ([FeFe], [NiFe], and [Fe]-hydrogenases), [FeFe]H_2ases, depicted in figure 1.17,[65] seem to be more involved in the proton reduction to molecular hydrogen than other two kinds of hydrogenases. The catalytic activity of [FeFe]H_2ases can reach 6000–9000 molecules H_2 s^{-1} per site under optimal conditions.[66]

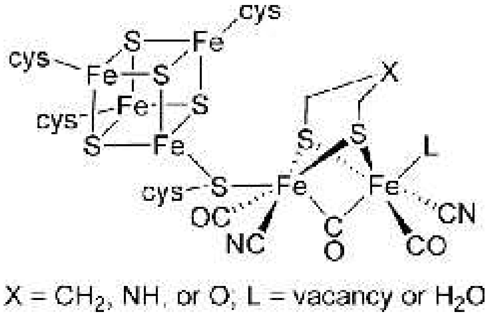

X = CH_2, NH, or O; L = vacancy or H_2O

Figure 1.17 *The structure of the active site (H-cluster) in [FeFe]H_2 ases.*[65]

Hydrogen was generated from the three-component system of $[Ru(bpy)_3]^{2+}$, ascorbic acid, and an all CO diiron complex **1** (figure 1.18) in action of light with λ > 400 nm, in which ascorbic acid acts as a proton source and its ascorbate anion functions as a reductive quencher for $*[Ru(bpy)_3]^{2+}$ to generate $[Ru(bpy)_3]^{3+}$.[67]

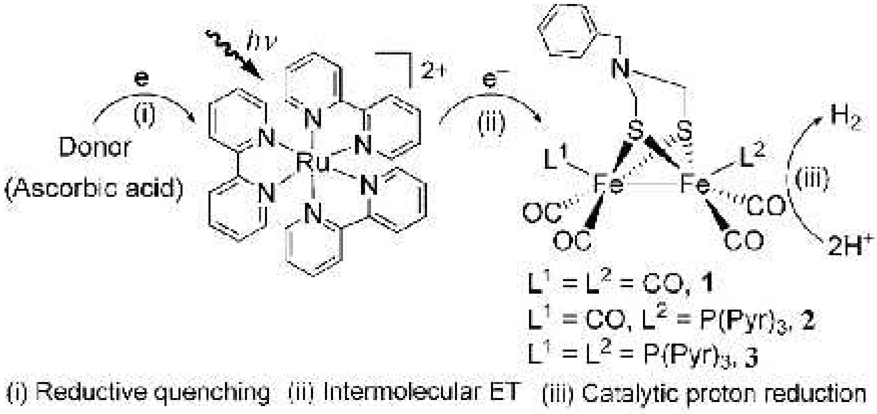

Figure 1.18 *The Fe-based homogeneous catalytic systems with ruthenium-polypyridine as photosensitiser for hydrogen generation.*[67]

The total amount of hydrogen evolved was 0.8 turnovers based on complex **1**.[67] One of the reason for relatively low activity is that the all CO diiron complex **1** (Figure 1.18) was gradually decomposed under irradiation. A special phosphine ligand, tris(*N*-pyrrolyl)phosphine (P(Pyr)$_3$), was introduced to the diiron complexes to improve the photo-stability of diiron complexes. The reduction potentials of complexes **2** and **3** for the Fe^IFe^I/Fe^0Fe^I process match the thermodynamic requirement for intermolecular electron transfer from $[Ru(bpy)_3]^{2+}$ to the diiron complex.[68] With **2** and **3** as catalysts in a 1 : 1 $CH_3CN–H_2O$ solution, the total turnovers for hydrogen evolution are 4.3 based on **2** and 86 based on $[Ru(bpy)_3]^{2+}$ in a 3 h photolysis, and for the system with P(Pyr)$_3$ disubstituted complex **3**, the turnovers are 1.7 based on **3** and 34 based on $[Ru(bpy)_3]^{2+}$. The photostabilities and catalytic activities of **2** and **3** are higher than that of the all-CO analogue **1**. These results indicate that CO-displacement of the all-CO diiron complex by P(Pyr)$_3$ ligand(s) improves the photostability and the catalytic activity of [2Fe$_2$S] model complexes to a certain extent in the photocatalysis reaction.

1.7.5 Cobalt based intermolecular photocatalyst systems

Some cobaloxime complexes have been found to be very efficient for hydrogen evolution.[69] Cobaloximes are considered as good catalytic candidates for photochemical hydrogen production. Lehn and co-workers pioneered the studies on homogeneous photogeneration of hydrogen using $[Co(dmgH)_2(OH_2)_2]$ (**1**, dmgH = dimethylglyoximate, figure 1.19) as catalyst with $[Ru(bpy)_3]^{2+}$ as photosensitiser and TEOA as sacrificial electron donor in the DMF solution.[154] The turnover based on the cobaloxime is 16 after 1 h irradiation. Addition of 6 to 15 equivalents of the dmgH$_2$ (dimethylglyoxime) ligand was found to be necessary to prevent complex **1** (figure 1.19) from dissociation and to replace the hydrogenated ligand formed by side reactions. Dissolution of CO_2 in the reaction solution resulted in an increase of the hydrogen production efficiency to about twice that observed in the absence of CO_2. It was proposed that this increase may be mainly a pH effect since CO_2 dissolution was expected to decrease the apparent “pH” of the medium.[154]

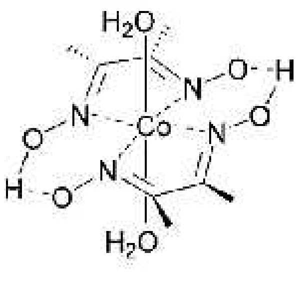

1

Figure 1.19 *Structure of the cobaloxime complex [Co(dmgH)$_2$(OH$_2$)$_2$]* ***(1)***

Recently, Eisenberg and co-workers developed an efficient three-component system with the cobaloxime [Co(dmgH)$_2$(py)Cl] **2** (Figure 1.20) as catalyst, platinum terpyridylphenylacetylide complex **3** (Figure 1.20) as photosensitiser, and TEOA as electron donor.[70] On increasing the concentration of electron donor (TEOA) to 2.4 (104-fold to that of the platinum-based photosensitiser) turnovers of 1000 based on platinum and 28 based on the cobalt catalyst were achieved after a 10 h irradiation (λ > 410 nm) in $CH_3CN–H_2O$ solution.

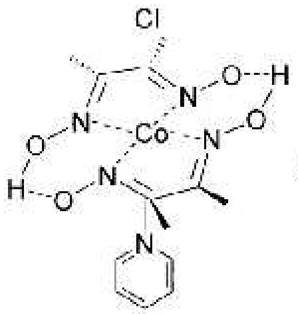

2

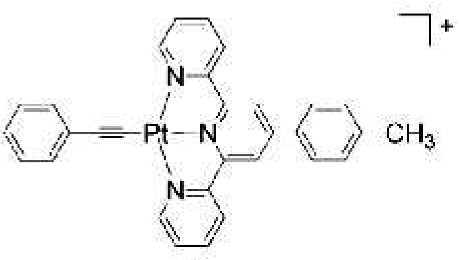

3

Figure 1.20 *The cobaloxime catalyst and the platinum photosensitiser used by Eisenberg's group.*[70]

The cobaloxime complex [Co(dmgBF$_2$)$_2$(OH$_2$)$_2$] **4** (figure 1.21) containing two BF$_2$-bridges was found to be highly efficient for photo-generation of hydrogen with a rhenium complex [Re(CO)$_3$Br(phen)] **5** (figure 1.21) (phen = phenanthroline) as photosensitiser in the presence of excess amounts of Et_3N and $Et_3NH^+BF_4^-$ in acetone under irradiation (λ = 380 nm).[71] The maximum turnover is 273 based on both photosensitiser and catalyst using 600 equiv. of both Et_3N and $Et_3NH^+BF^{4-}$ after 15 h irradiation. The quantum yield of hydrogen was 0.16 at 412 nm. The catalytic activity and stability of this multicomponent catalyst system can compete with some previously reported platinum based systems.[72] Similar systems, based on the cobalt catalyst $[Co(dmgH)_2]$ and rhenium photosensitiser $[Re(CO)_3Br(bipy)]$, are recently described.[73] The quantum yield of hydrogen is 26 ± 2 %. The rate of hydrogen evolution was found to be dependent on the photon flux (a linear dependence) and the concentration of cobalt catalyst (a quadratic dependence).

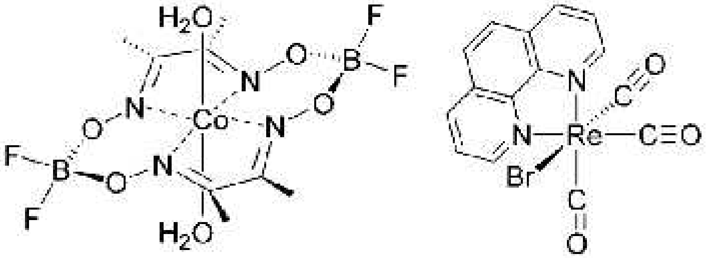

4

5

Figure 1.21 *The cobaloxime catalyst and the rhenium photosensitiser used by Fontecave's group.*[71]

1.8 Intramolecular Photocatalysis

Since the photolysis of water requires the transfer of redox equivalents, and typically light absorption is separated from the actual catalysis centre, there has been a considerable amount of recent work invested in linking a photosensitizing unit to a water reduction catalyst. Such bridged systems allow for increased electron transfer rates, while the adjustment of orbital energies and overlap allows for a long-lived charge-separated state. Connecting the photosensitiser to a water reducing catalyst may prove to be advantageous, but knowing for certain the nature of the active catalyst can be difficult. Since several recent examples of bridged systems use Pt^{2+} or Pd^{2+} based catalysts for proton reduction, the formation of a metallic colloid by reduction of the catalytic site is plausible.[74] While the catalytic activity of the molecular species cannot be ruled out, the formation of a potentially more efficient colloidal catalyst must be considered. In addition, the active state of such bridged catalysts could actually be a dissociated form of the precatalyst, thus functioning as a bimolecular system. Therefore, such systems must be studied in detail with carefully selected comparisons to determine the nature of the catalytic species.

1.8.1 Platinum and palladium based intramolecular photocatalytic systems

Sakai and co-workers reported the synthesis of heterobinuclear Ru–Pt complex **1** (Figure 1.22).[75] Under irradiation ($\lambda \geq 390$ nm) a water solution of this complex, in combination with EDTA as sacrificial electron donor, led to the evolution of hydrogen with a TON of 4.8.

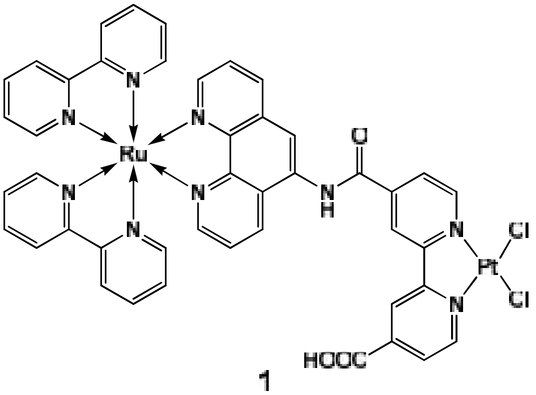

1

Figure 1.22 *A platinum (II) complex covalently bound to a ruthenium photosensitizer.*[75]

At the same time, Rau and co-workers reported the synthesis and catalytic properties of Ru–Pd complexes **2** and **3** (Figure 1.23).[76] A bridging ligand between the metals was tetrapyridophenazine. A turnover number of 56 was achieved when a water solution of the complex containing triethylamine was irradiated with 470 nm light. The formation of zero-valent metals in the reduction is probably one of the reasons for low stability of platinum and palladium-based catalysts. It was also found that binuclear Ru–Pd complexes of this type can catalyse the selective reduction of tolane to *cis*-stilbene under the same conditions.

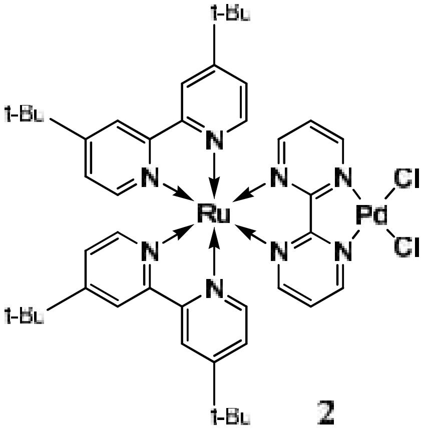

2

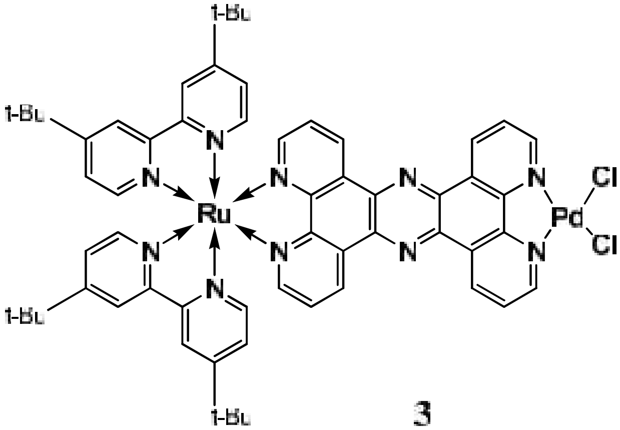

3

Figure 1.23 *Palladium(II) complex covalently bound to the ruthenium photosensitiser.*[76]

Another binuclear Ru–Pd complex **4** (Figure 1.24), active as a photocatalyst for hydrogen production, was reported by Hammarstrom's group.[77] Hydrogen evolution was monitored upon irradiation (λ ≥ 475 nm) of the complex in ACN–TEA. No hydrogen was detected in the dark; maximal turnover number was 30. Authors investigated the potential formation of colloidal palladium in this system by using transmission electron microscopy and X-ray photoelectron spectroscopy. On the basis of these measurements, the formation of colloidal palladium was confirmed. The appearance of the colloid correlates in time with hydrogen evolution. In conclusion, authors do not rule out that binuclear complex can function as homogeneous catalyst, but metallic palladium plays a major role. These important results indicate that great care should be taken when interpreting the mechanism of hydrogen production catalysed by supramolecular systems.

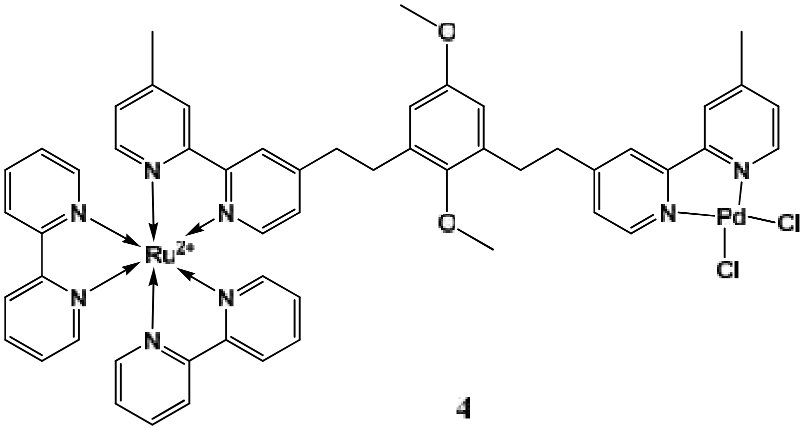

4

Figure 1.24 *A binuclear Ru–Pd complex reported by Hammarstroms group.*[77]

1.8.2 Iron based based intramolecular photocatalytic systems

Several ruthenium diiron dyads (**5**–**8**) were reported (figure 1.25), where the [2Fe$_2$S] model complexes of the [FeFe]H$_2$ase active site are attached to [Ru(bpy)$_3$]$^{2+}$ by different linkers.[78] The initial motif is to build photoactive catalysts for hydrogen production, however, the diiron catalytic centers in these ruthenium diiron dyads cannot be directly reduced by the excited photosensitiser, which was quenched either by energy transfer or by unwanted reductive quenching from the diiron moiety. It is mainly because the reduction potentials of the diiron complexes are more negative than the oxidation potential of the excited state of the ruthenium complex, making the direct electron transfer from the excited photosensitiser to the catalyst thermodynamically unfavourable.

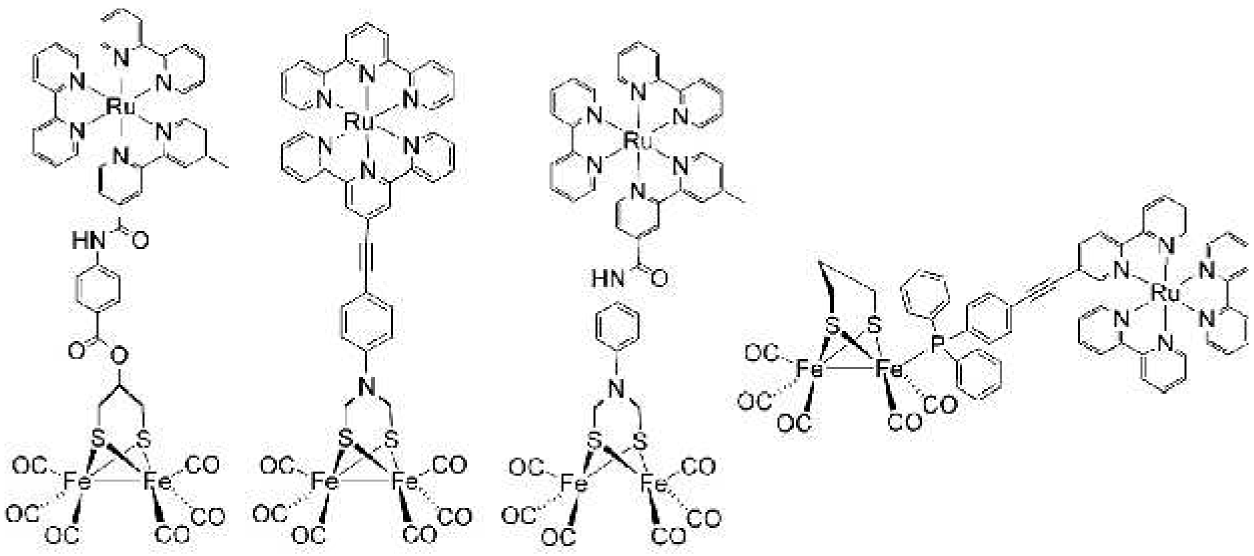

5 **6** **7** **8**

Figure 1.25 *Diiron complexes covalently linked to the ruthenium-polypyridine photosensitiser.*[78]

In addition to ruthenium-polypyridine complexes, a phenylsubstituted porphyrin and zinc-porphyrin complexes were also used as photosensitisers in the photoinduced electron transfer and hydrogen generation studies. Song and co-workers successfully prepared and well-characterised two light-driven dyad models (**9** and **10**, Figure 1.26), in which the photosensitiser, either a tetraphenyl porphyrin (TPP) or a zinc-porphyrin complex (ZnTPP), is coordinately bonded to a diiron complex.[79] Although it is possible that the marked quenching of the fluorescence bands of **9** and **10** in the steady-state emission spectra relative to those of their reference compounds TPP and ZnTPP is mainly due to the intramolecular electron transfer from the photoexcited porphyrin or metalloporphyrin-type moiety to the coordinately bonded diiron complex, the proposed electron transfer processes are not experimentally verified by time-resolved spectroscopy. Recently, a non-covalent assembly **11** (Figure 1.26) of a pyridyl functionalised hydrogenase active site model and a zinc tetraphenylporphyrin was obtained and characterised.[80] The photoinduced intramolecular electron transfer from the excited singlet state of the porphyrin to the diiron center was well verified by the fluorescence spectra and the laser flash photolysis technique. Because the two units, the zinc-porphyrin and the diiron complex, in the coordinately self-assembled dyad are able to separate from each other after the intramolecular electron transfer reaction, this dyad can effectively reduce the charge recombination and energy transfer as compared to covalently linked ruthenium diiron molecular dyads. Visible light-driven dihydrogen generation was observed from the zinc-porphyrin diiron dyad **11**.

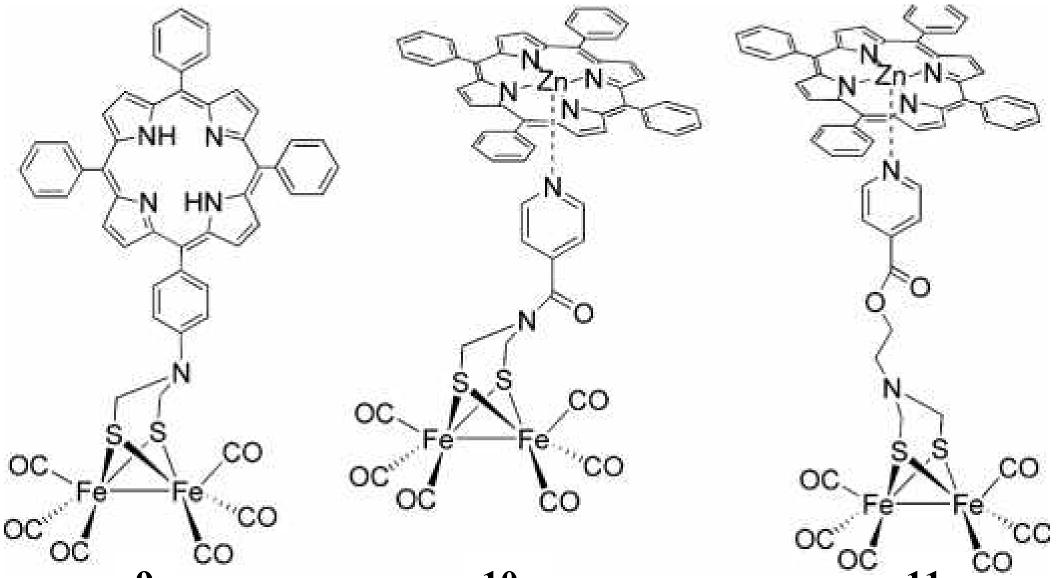

9 **10** **11**

Figure 1.26 *Diiron complexes covalently or coordinately linked to the porphyrin photosensitiser.*[79, 80]

Although the turnover number (TON) is relatively low (0.2), the zinc porphyrin diiron catalytic system is attractive because (i) no noble metal is involved in the catalytic system; (ii) both catalyst and photosensitiser are based on bio-inspired mimics; and (iii) it is the first photoactive hydrogenase model for successful light driven dihydrogen generation using a self assembling principle.

1.8.3 Cobalt based catalyst systems

By replacing one of the axial H_2O ligands of the cobaloxime with pyridine-functionalised ruthenium-polypyridine complexes, Fontecave and Artero *et al.* built a series of Ru–Co and Ir–Co heterobinuclear photocatalysts (**12–16**, Figure 1.27) for photochemical hydrogen generation from $Et_3NH^+BF_4^-$.[69,81] The Ru–Co dyads are more efficient in hydrogen production than their corresponding multicomponent systems under the same condition. Complex **13** containing the BF_2-bridged Co(II) center is superior to **12** with the H-bridged Co(III) center because the Co(II) state in **13** is more easily reducible and more resistant towards the side reactions, such as acidic hydrolysis and hydrogenation. The supramolecular photocatalyst **13** with the $[Ru(bpy)_2(L\text{-}pyr)]^{2+}$ (L-pyr =(4-pyridine)oxazolo[4,5-f]phenanthroline) unit as photosensitiser performs up to 103 turnovers in the presence of 100 equiv. of both Et_3N and $Et_3NH^+BF_4^-$ in acetone during a 15 h irradiation (λ >350 nm).[81] The systems based on **12–14** are almost inactive under visible light irradiation. Substitution of dmphen ligands for bpy in the ruthenium unit makes the Ru–Co supramolecular catalyst (**15**) active using visible light (λ > 380 nm), but the turnover remains low. A significant enhancement in catalytic activity was observed when the ruthenium-based photoactive moiety was replaced by the heteroleptic iridium unit. Turnover number reaches 210 based on **16** in the presence of 600 equiv. of both Et_3N and $Et_3NH^+BF_4^-$ following 15 h irradiation, which is higher than those reported for the other noble metal-based supramolecular systems such as the Ru–Pt, Ru–Pd, and Ru–Rh photocatalysts. In comparison, the maximum turnover for the corresponding Ir–Co multicomponent system is 165 under the same conditions and the quantum yield of hydrogen is 0.12. In common with the Ru–Co system reported by Lehn and co-workers,[82] the photocatalytic activity of the dyads decreased by a third upon addition of water to the reaction medium.

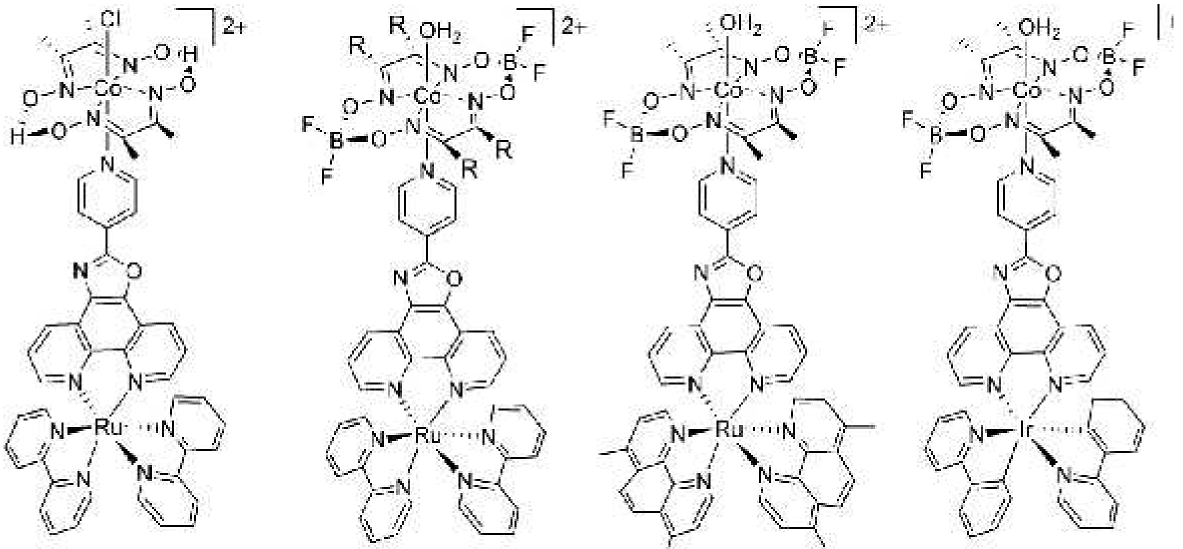

12

13.R=Me
14.R=Ph

15

16

Figure 1.27 *Photosensitiser-cobaloxime supramolecular catalysts reported by Fontecave's group.*[81]

A promising approach to the hydrogen photo-evolution was developed by Nocera's group.[83] This approach is based on the use of two-electron mixed-valence coordination complexes of the general formula M_n–M_{n+2}. Dirhodium **17** (Figure 1.28) and diiridium complexes with different bridging ligands are capable of generating hydrogen from HCl or HBr under irradiation. It was found that dirhodium compounds can also function as a photocatalysts.[84] Thus, the photocatalytic production of hydrogen from THF–HCl solution was observed upon irradiation with UV-vis light ($\lambda \geq 338$ nm). Activation of the Rh–Cl bond and photochemical instability of Rh^0–Rh^{II} intermediates involved in the catalytic cycle play crucial roles in this system.

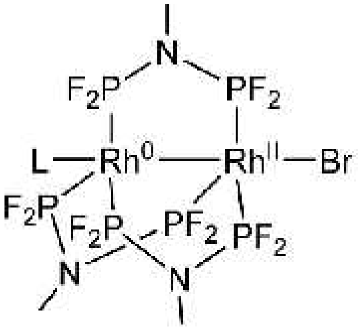

17

Figure 1.28 *A dirhodium mixed-valence cluster reported by Nocera's group.*[83]

1.9 History and Occurrence of Iridium Complexes

Iridium was discovered and named by a British scientist, Smithson Tennant. This metal had for some time been known to dissolve almost completely in aqua regia, but a small black residue always remained and was for a time thought to be graphite. In 1803 Tennant began a study of this material which ultimately resulted in the identification of both osmium and iridium. Iridium is a precious metal. Iridium is hard, fragile and can be easily worked between 1200 ^{0}C and 1500 ^{0}C. Tennant chose the name iridium, from the Greek iris, rainbow, "from the striking variety of colors which it gives while dissolving in marine acid". Iridium always occurs associated with other metals from the platinum group. The major source are the nickel-copper ores of Canada. Generally, iridium is regarded as a "catalytic" metal or as a useful metal centre for reactivity and model studies related to homogeneous catalysis. Effort has been made to portrait through the literature review section that iridium is more than that. In particular, some of its complexes display promising photophysical and photochemical properties. This section aims to provide an overview of iridium (III) polyamine complexes.

1.10 Families of Ir (III) polyamine complexes

As a third-row transition metal, iridium (III) is characterised by the great inertness of its coordination sphere, requiring harsh reaction conditions to substitute the classical chlorine ligands of the starting iridium salts. It is noteworthy that iridium (III) is capable of forming a large range of complexes, including mono-, bis- and tris-cyclometallated complexes (the last is a unique feature among all polyamine complexes of transition metals),[85] and that many more complexes are known with bidentate ligands than with terdentate ligands.

Two classes of complexes can be distinguished, depending on the extent to which the ligands contribute to the electron density at the metal centre. When some ligands are anionic (chloride, cyclometallating ligand), the emitting excited states have metal-to-ligand charge transfer (MLCT) character and there is sufficient charge compensation for the metal-centered oxidation to proceed. In contrast, when the ligands are neutral and donate less charge density to the metal, emission is ligand centered (LC) and no metal-based oxidation is observed. For both classes of complexes for which reduction processes have been investigated, these are exclusively ligand centered.

1.10.1 $[IrL_2Cl_2]^{n+}$ complexes [L = bidentate ligand, (N^N) species]

In 1969 DeSimone *et al.* reported the preparation of $[Ir(bpy)_2Cl_2]Cl$ by fusing $K_3IrCl_6 \cdot 3H_2O$ and bpy in the absence of any solvents at 270 ^{0}C for 15 min,[86]and unambiguously demonstrated the *cis*-configuration of the complex using NMR spectroscopy. From the literature it is clear that phenanthroline has been used much more often than bipyridine. This is due to the greater difficulty of obtaining pure samples of complexes with bpy ligands. *cis*-$[Ir(phen)_2Cl_2]Cl$ was first described in 1964 by Chiswell *et al.*,[87] prepared in 27 % yield by heating K_3IrCl_6 with 1,10-phenanthroline at 220 ^{0}C for 14 h. In 1971 Broomhead *et al.* reported a different synthesis.[88] In a first step $[Ir(phen)Cl_4]^-[phenH]^+$ was prepared in 90 % yield from $(NH_4)_3IrCl_6 \cdot 2H_2O$ and phen by reflux in acidic water for 2 h. The second step consisted of heating the phenanthrolinium salt in refluxing glycerol for 1 min, and gave *cis*-$[Ir(phen)_2Cl_2]Cl$ as a yellow solid. These early examples reflect the synthetic difficulties usually encountered when preparing simple iridium (III) complexes.

In 1990 Brewer *et al.* reported the preparation of various complexes of the type *cis*-$[IrL_2Cl_2]^+$ (L = bidentate chelate, figure 1.29) following a slightly modified procedure.[89]

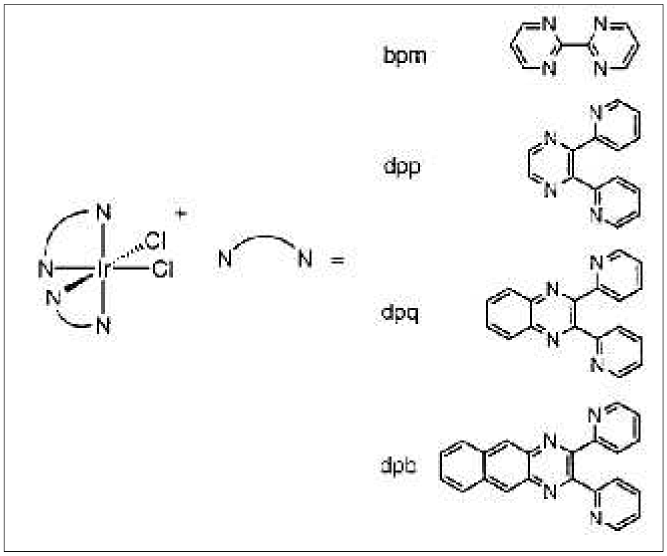

Figure 1.29 *Representation of* $[IrL_2Cl_2]^+$ *complexes [L = bidentate (N^N) chelate].*[89]

In contrast to related Rh^{III} complexes, in which the first reduction is metal centered, in these $[IrL_2Cl_2]^+$ complexes the first two reduction steps are ligand based. The ligands bpm, dpp, dpq, and dpb (figure 1.28) are all easier to reduce than bpy, and the first reduction potential for these $[IrL_2Cl_2]^+$ complexes is clearly related to the extent of electronic delocalisation over the ligand. After uptake of two electrons by the ligand system, a subsequent two-electron metal centered reduction takes place which leads to expulsion of the chloride ligands, generating a four-coordinate Ir^I complex [eqns. (1.8)–(1.11)].[89,90]

$$[Ir^{III}L_2Cl_2]^+ + e^- \rightleftharpoons [Ir^{III}LL^-Cl_2] \qquad (1.8)$$

$$[Ir^{III}LL^-Cl_2] + e^- \rightleftharpoons [Ir^{III}L^-L^-Cl_2]^- \qquad (1.9)$$

$$[Ir^{III}L^-L^-Cl_2] + 2e^- \rightleftharpoons [Ir^{I}L^-L^-Cl_2]^{3-} \qquad (1.10)$$

$$[Ir^{I}L^-L^-Cl_2]^{3-} \longrightarrow [Ir^{I}L^-L^-]^- + 2Cl^- \qquad (1.11)$$

A noteworthy feature of the above reduction pattern is that the reduced two-electron $[IrL^- L^-Cl_2]^-$ species are stable. This is one reason why multielectron reduction schemes are feasible based either on the monometallic complexes of the series in figure 1.29 or on multimetallic complexes. The mononuclear complexes described above have been extended to polynuclear mixed-metal systems with the ability to undergo intercomponent electron-transfer processes on irradiation. $[IrL_2Cl_2]^+$ (where L is the dpb ligand) was reacted with two equivalents of $[Ru(bpy)_2Cl_2]$ to give a diastereomeric mixture of the corresponding trinuclear complexes in 85–90 % yield after heating at reflux in EtOH–H_2O for 3 days.[90] The trinuclear complexes prepared by Brewer and coworkers (figure 1.30(a)) demonstrate rich electrochemistry. The two ruthenium (II) centres are oxidised simultaneously and there is also a series of one-electron reductions leading to the storage of four electrons in the bridging ligands before the peripheral bpy ligands are reduced.[91,92]

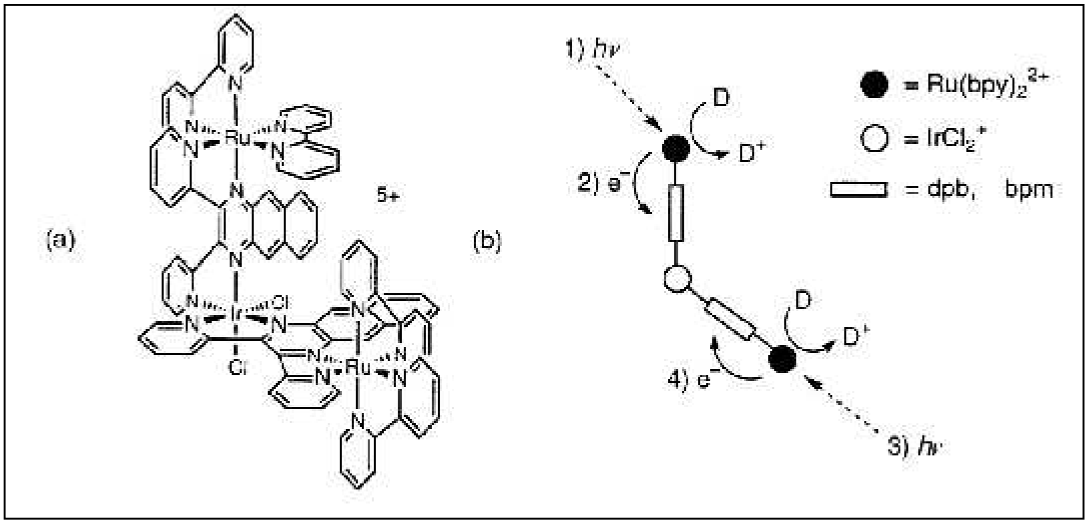

Figure 1.30 *(a) $[Ru(bpy)_2(dpb)IrCl_2(dpb)Ru(bpy)_2]^{5+}$ and (b) Photoinduced two-electron uptake by the bridging ligands.*[104]

For $[(bpy)_2Ru^{II}(dpb)Ir^{III}Cl_2(dpb)Ru^{II}(bpy)_2]^{5+}$, sequential reductions of the bridging ligands (BLs) occur at -0.12, -0.26, -0.90 and -1.22 V (*vs* Ag/AgCl).[91,92] The first two reduction processes in this trinuclear complex are easier than the analogous processes in the mononuclear precursor $[Ir(dpq)_2Cl_2]^+$. This can be ascribed to the stabilising effect of the Ru (II) centres towards reduced states involving iridium containing fragments. As a consequence of this remarkable electrochemical behaviour, an extension to systems driven by light was proposed.[91]

Figure 1.30(b) provides an illustration of a trinuclear complex containing the dpb ligand which can store multiple electrons. Irradiation of the peripheral Ru (II) centres leads to the transfer of two electrons to the BLs, following which the Ru (III) donors are re-reduced by the sacrificial electron donor (dimethylaniline). This basic photochemical device has potential future applications in one-step two-electron delivery to a substrate. Two years later, a similar trinuclear system was prepared using a different bridging ligand, bpm, which now can take up two electrons (four electrons are collected before the first bpy-localised reduction),[92] according to a reduction pattern of the type seen above (figure 1.30b). This reaction proceeded with a 60% isolated yield by heating the starting materials [Ru(bpy)$_2$Cl$_2$] and [Ir(bpm)$_2$Cl$_2$]$^+$ to reflux in EtOH–H$_2$O for 5 days. Further detailed photophysics on complexes of the type [IrL$_2$Cl$_2$]$^{n+}$ is considered in detail in chapter 5.

1.10.2 [IrL$_3$]$^{n+}$ complexes (L = bidentate (N,N) ligand)

In 1958 [Ir(bpy)$_3$]$^{3+}$ was first described by Martin *et al.*, as an orange solid, obtained by fusing K$_3$IrCl$_6$ and bpy for 20 min.[93] The lack of precise characterization available at that time led Chiswell *et al.* to attempt the preparation of [Ir(phen)$_3$]$^{3+}$ in 1964 under similar conditions.[87] Pale yellow complexes were obtained, although some uncertainty remains regarding their purity. In 1974, the procedure described by Demas *et al.* was much more precise.[94] K$_3$IrCl$_6$.3H$_2$O was first converted into a halide free sulfate upon treatment with K$_2$S$_2$O$_8$ and KHSO$_4$ in boiling water, evaporation to dryness, and fusion in air above 250 ^{0}C for 30 min. After cooling, it was mixed with bpy and fused under CO$_2$ at 230 ^{0}C for 6 h. A laborious work-up led to [Ir(bpy)$_3$]$^{3+}$ in a good 50 % yield (figure 1.31).

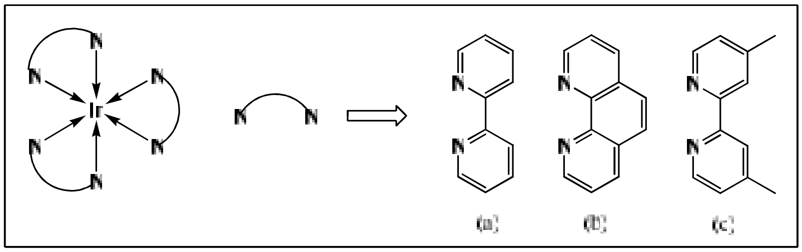

Figure 1.31 *Representation of (a) [Ir(bpy)$_3$]$^{3+}$ (b) [Ir(phen)$_3$]$^{3+}$ and (c) [Ir(dmbpy)$_3$]$^{3+}$.*

The metal-centered oxidation of $[Ir(bpy)_3]^{3+}$ occurs at a rather high potential, +2.17 V, while reduction (ligand centered) occurs at -0.76 V (*vs* NHE).[85,95] Its low temperature luminescence (77 K), which has a lifetime of 80 μs, has LC characteristics. At room temperature it exhibits a lifetime, τ = 2.4 μs, suggesting emission has some MLCT character (less than 20–30%).[85,96] From the onset of the emission spectrum, the energy level of the lowest-lying excited state, $[Ir(bpy)_3]^{3+}$, is estimated to be 2.81 eV. According to these electrochemical and spectroscopic data, $[Ir(bpy)_3]^{3+}$ is a good oxidizing agent.

From the reaction between $IrCl_3$ and bpy in glycerol at 180 ^{0}C for 2 h, performed in 1977 by Watts *et al.*, a complex was isolated, which was identified at that time as $[Ir(bpy\text{-}N^\wedge N)_2(bpy\text{-}N)(H_2O)]^{3+}$, a complex with one monodentate bpy in which the sixth coordination site is occupied by a water molecule.[97] Four years later using X-ray crystallography, Serpone *et al.* demonstrated that it was in fact $[Ir(N^\wedge N\text{-}bpy)_2(NH,C3\text{-}bpy)]^{3+}$, the monocyclometallated and N-protonated analogue of $[Ir(bpy)_3]^{3+}$.[98] Further published work confirmed this conclusion in subsequent years. Treatment of *cis*-$[Ir(bpy)_2Cl_2]^+$ with trifluoromethanesulfonic acid in *o*-dichlorobenzene led to *cis*-$[Ir(bpy)_2(OSO_2CF_3)_2]^+$ in 95 % yield, as reported by Meyer *et al.* in 1984.[99] This trifluoromethanesulfonato complex proved to be an excellent precursor to $[Ir(bpy)_3]^{3+}$, the substitution proceeding in 80 % yield by heating with bpy in ethylene glycol for 5 h.

1.10.3 [IrL$_2$Cl]$_2$ complexes [L = cyclometalating ligand, (N^C) species]

In 1984, Watts *et al.* prepared dichloro-bridged Ir^{III} dimers in 72 % yield using Hppy or benzo[*h*]quinoline as *N^C* cyclometallating ligands, by refluxing iridium trichloride hydrate with the ligand in 2-ethoxyethanol:water for one day (figure 1.32a).[100] Nonoyama and coworkers had developed another synthetic strategy in which the cyclometallating ligand (e.g. phenylpyridine, benzoquinoline, 2-phenylbenzothiazole, etc.) is reacted with $IrCl_3.nH_2O$ in 2-ethoxyethanol under an inert atmosphere giving the corresponding air-stable μ-chloro bridged precursor material.[101] Although this procedure is used widely, alternative protocols performing the cyclometallation reaction in trimethyl phosphate at significantly lower temperatures have been reported.[102] Six years later, by reacting potassium hexachloroiridium (IV) and potassium hexachloroiridium (III) with bpy in EtOH–H_2O, the Watts group obtained a dichloro-bridged dimer in which each iridium centre is surrounded by one *N,N*-coordinated bpy and one *N,C*-coordinated bpy (figure 1.32b).[103]

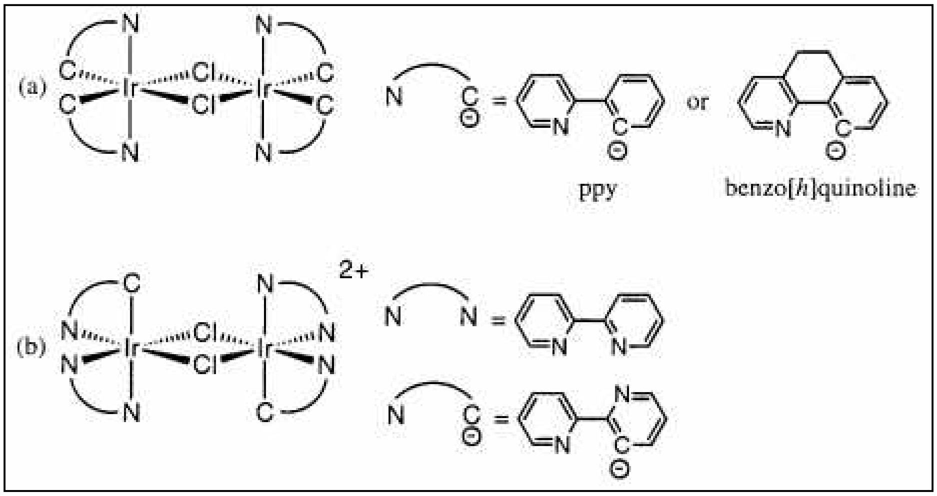

Figure 1.32 *Representation of cyclometallated dichloro-bridged dimers.*

1.10.4 $[IrL_3]^{n+}$ complexes (L = (N,C), (N,Si) and (N, S) ligands), homoleptic and heteroleptic

The interest in iridium compounds (iridium (I) and iridium (III) species) has especially been boosted by the different fields of application ranging from very efficient catalysts to important emitter materials in OLEDs. Although the catalytic activity of iridium complexes has been well-known for a significant period of time,[104] a new era of utilisation has commenced its rapid development with the first reports on electrophosphorescent devices.[105] In particular, the very desirable material properties such as reversible electrochemistry, appropriate triplet lifetimes, synthetic versatility, colour tuning of the emission wavelengths by ligand modifications and the robust nature of many iridium (III) complexes render these compounds ideal candidates for the fabrication of highly efficient phosphorescent OLEDs.[106,107,108] Neutral electrophosphorescent iridium (III) compounds are definitely the most common phosphorescent dopants in OLEDs distinguishing two classes, namely homoleptic compounds containing three cyclometalating ligands and heteroleptic iridium complexes with two cyclometalating ligands and an ancillary ligand. Despite intense studies on neutral iridium complexes being a topic of worldwide scientific efforts, charged derivatives also receive more and more attention due to possible applications in light-emitting electrochemical cells (LECs).[109] The general synthetic methods followed at present for the synthesis of homoleptic iridium complexes is summarised in Scheme 1.2.

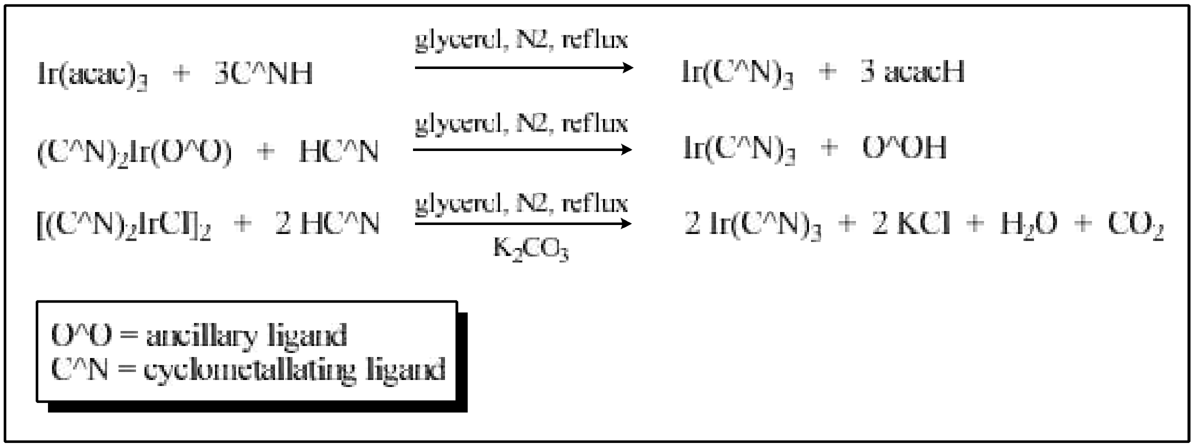

Scheme 1.2 *General synthetic pathways followed for homoleptic tris iridium complexes.*

1.10.4.1 Homoleptic Complexes

The first report on homoleptic *tris*-cyclometallated iridium (III) compounds was published in the early 1980's being observed as a byproduct of the synthesis of di-μ-chloro*tetrakis*(κ^2(C^2,N)-2-phenylpyridine) diiridium (III). Since that time and enforced by the excellent electroluminescent properties of e.g. Ir(ppy)$_3$ (ppy = phenylpyridine) as well as the possibility of efficient colour-tuning by simple changes or modifications of the cyclometallating ligand, numerous optimised protocols have been presented giving *tris*-cyclometallated complexes in acceptable yields. Among them, ligand exchange reactions starting from Ir(acac)$_3$, solvent-free procedures or approaches conducted at high temperatures of 170 - 195 ^{0}C in the presence of silver triflates have been proposed.[108] However, the harsh reaction conditions, comparably low yields and the number of byproducts[110] are considered to be significant drawbacks of homoleptic iridium complexes.

Additionally, the rate of formation of the *facial* and *meridional* isomer was found to be influenced by the reaction conditions. *fac*-[Ir(ppy)$_3$] was reported as a side-product in the preparation of [Ir(ppy)$_2$Cl]$_2$ by Watts *et al.* in 1985, which was isolated soon afterwards in low yield from washing filtrates.[111] Subsequently, other complexes containing substituted ppy were prepared in good yields (40-75%) by reaction of [Ir(acac)$_3$] with Hppy in refluxing glycerol for 10 h.[112] The facial arrangement of the ligands can be explained by the strong *trans*-effect of Ir–C bonds: after coordination of a first ppy, the oxygen atom (from acac) located *trans* to the Ir–C bond is labilised and this vacant coordination site is filled by the nitrogen atom of another ppy. In this way a series of tris-cyclometallated complexes was obtained by Watts *et al.*, which proved to be strong photoreductants.[111,112]

The first tris (N^Si) ligated metal complex was reported the following year, by Watts *et al.*[113] It was obtained in 60 % yield by reaction of [Ir(PPh$_3$)$_3$(CO)(H)] with (8-quinolyl)dimethylsilane in refluxing toluene for 24 h (figure 1.33). A different procedure was later used by Güdel *et al.* for the preparation of *fac*-[Ir(thpy)$_3$].[114] In this case, [Ir(thpy)$_2$Cl]$_2$, excess Hthpy and silver triflate were heated at 110 ^{0}C for one day to give the desired orange complex in 58 % isolated yield (figure 1.33).

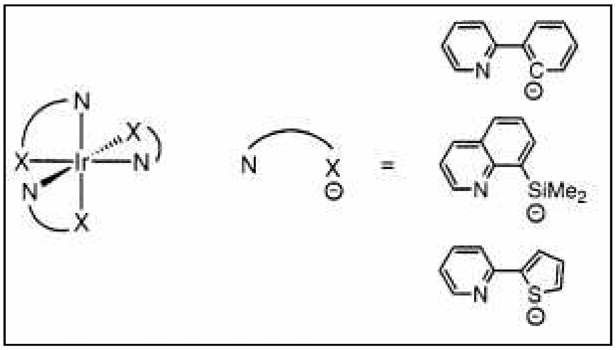

Figure 1.33 *Representation of tris-cyclometallated complexes with (N,C), (N,Si) and (N,S) ligands.*

1.10.4.2 Heteroleptic Iridium Complexes

The difficulties in preparing *tris*-cyclometallated iridium complexes is overcome by incorporating ancillary ligands such as acetylacetonates, picolinates, triazolates, tetrazolates or quinolinolates.[115,116,117] Although the preparation of heteroleptic iridium (III) compounds starts, again, from the corresponding μ-chloro bridged precursor materials, the subsequent bridge-splitting step is clearly facilitated giving the products in better or even quantitative yields. Colour tuning is usually achieved by changing the nature of the cyclometallating ligand but, on the other hand, requires the synthesis of different precursors.[108,118] Despite this being considered to be a significant drawback of this approach, many heteroleptic iridium complexes bearing ancillary ligands exhibit very desirable material properties such as high quantum yields even at room temperature or good thermal stabilities providing the possibility of vacuum deposition processes.

As a consequence, they are frequently used as phosphorescent dopants in OLEDs.[119,120] Some frequently used cyclometalating and ancillary ligands are shown in figure 1.34.

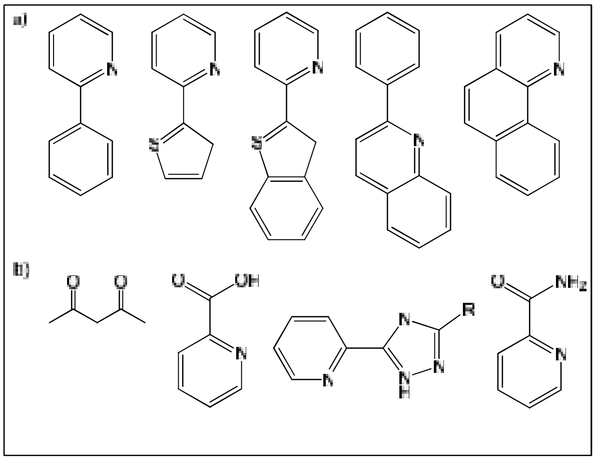

Figure 1.34 *Commonly used a) cyclometallating and b) ancillary ligands for homo and heteroleptic iridium(III) complexes.*

1.10.5 [IrL$_2$]$^{n+}$ complexes (L = terdentate ligand)

1.10.5.1 IrLCl$_3$ species

In 1937, working on the coordination chemistry of terpy and various metals, Morgan and Burstall reported in a historic paper the preparation of [Ir(terpy)Cl$_3$] by reaction of Na$_3$IrCl$_6$ and terpy in water.[121] Fifty five years later, Brewer *et al.* prepared [Ir(tpp)Cl$_3$] in 45 % yield by reacting IrCl$_3$: 13H$_2$O and tpp in refluxing ethylene glycol for 25 min.[122] A dinuclear complex was also synthesised, using tpp as bridging ligand: [(terpy)Ru-(tpp)IrCl$_3$]$^{2+}$ was obtained in 62 % yield from [Ir(tpp)Cl$_3$] and [Ru(terpy)Cl$_3$] after heating at reflux in DMF–EtOH for 4 h (figure 1.35). For this complex, the emission is of Ru→ tpp CT nature, irrespective of the excitation wavelength.[113]

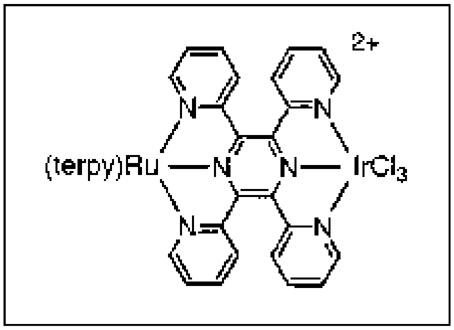

Figure 1.35 *Representation of the Ir-Ru dimer with ligand tpp, [(terpy)Ru(tpp)IrCl$_3$].*

1.10.5.2 $[IrL_2]^{3+}$ complexes ((N^N^N) species)

In 1990, Demas and co-workers reported the first synthesis of $Ir(terpy)_2^{3+}$ following the initial stage of the procedure they had used in 1974 for the synthesis of $Ir(bpy)_3^{3+}$.[123] The iridium sulfate (prepared *in situ* from K_3IrCl_6) was reacted with terpy in refluxing ethylene glycol for a few minutes, and at 150 ^{0}C for 6 h. Tedious workup and purification were necessary to isolate the desired complex (figure 1.36).

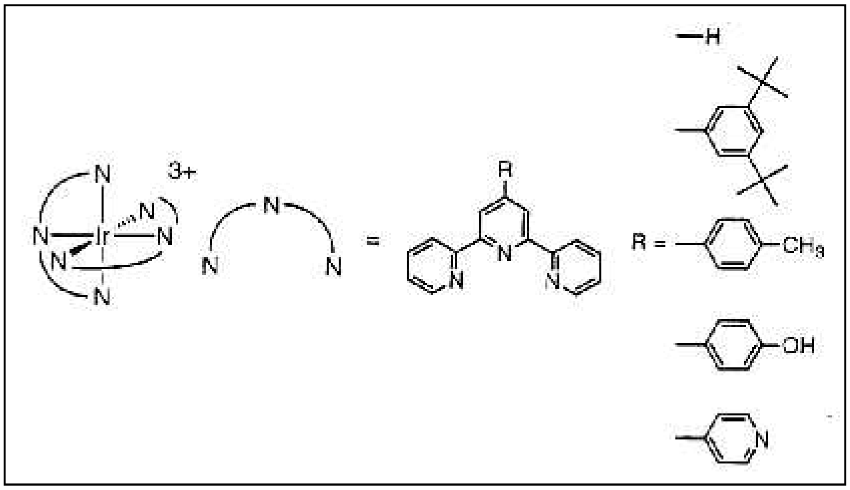

Figure 1.36 *Representation of bis-terpyridine complexes.*

In 1999 a different method was reported,[124] based on the stepwise coordination of two terpy ligands under milder conditions. Depending on the solubility of the ligand, the first coordination required refluxing EtOH or heating at 160 ^{0}C in ethylene glycol. After isolation of the $[Ir(terpy)Cl_3]$ intermediate, the second chelation was achieved in ethylene glycol, at temperatures between 140 ^{0}C and reflux (196 ^{0}C). Purification proceeded either by crystallisation or by column chromatography on silica gel. Isolated yields were 10 - 25 % with respect to $IrCl_3$.

Iridium bis-terpyridine complexes are luminescent at room temperature, with λ_{em}= 458 nm for unsubstituted terpy and 506 nm for 4'-arylterpys. The emission is a ligand phosphorescence,[122] possibly with some MLCT character for 4-arylterpys.[123] This gives highly energetic excited states with a lifetime on the microsecond timescale, in striking contrast to the ruthenium (II) analogues. With a reduction potential of +1.6 V/SCE, the excited state is also a powerful oxidant. More recently, Williams *et al.* used the same synthetic pathway to prepare bis-terpy complexes bearing pH-sensitive groups (phenol and pyridine, figure 1.36).[125] [(tterpy)Ir(terpy-py)]$^{3+}$ is luminescent at pH > 6, but its luminescence intensity drops by about one order of magnitude for pH < 4. This complex constitutes a potentially useful pH sensor. The authors ascribe the pH-dependence of the luminescence to a change from predominantly LC emission at higher pH to predominantly MLCT emission at lower pH values, as a consequence of protonation of the appended pyridine site.[125]

1.11 Multinuclear iridium complexes

Reaction of [Ir(ppy)$_2$Cl]$_2$ with HAT in refluxing CH$_2$Cl$_2$–MeOH gave the orange complex [Ir(ppy)$_2$(HAT)]$^+$ in 80 % yield (figure 1.37a).[126] Irradiation of this complex with visible light leads to luminescent states. At room temperature, [Ir(ppy)$_2$(HAT)]$^+$ emits at $\lambda > 770$ nm ($\tau < 10$ ns) while at 77 K it has dual-emission properties. The two states responsible for the low-temperature behavior, which are not thermally equilibrated at 77 K, are identified as MLCT and sigma-bond-to-ligand CT (SBLCT) states (figure 1.37c), with lifetimes of 1.5μs and 3μs.[126]

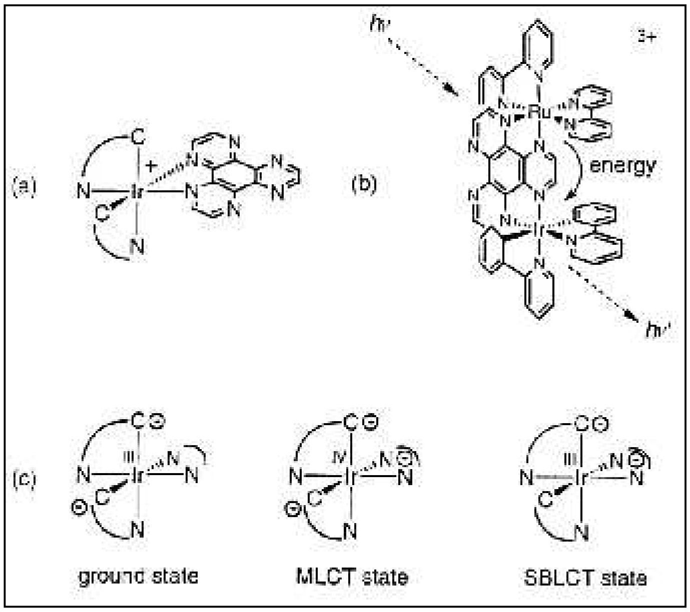

***Figure 1.37** (a) Representation of Ir(ppy)$_2$(HAT)$^+$, (b) Energy transfer in [Ru(bpy)$_2$(HAT) Ir(ppy)$_2$]$^{3+}$ and (c) Ground and excited states.*

The synthesis of a dinuclear complex incorporating Ru (II) and Ir (III) centers linked *via* the bridging ligand HAT was reported by Kirsch-De Mesmaecker *et al.* [(bpy)$_2$Ru(HAT)Ir(ppy)$_2$]$^{3+}$

(figure 1.37b) was obtained by reacting $[Ru(bpy)_2(HAT)]^+$ with $[Ir(ppy)_2Cl]_2$ in refluxing CH_2Cl_2–MeOH for 6 h.[127] In this dinuclear complex, the emission is identified as Ir-centred, SBLCT in nature (λ_{max} = 760 nm, τ < 10 ns), consistent with Ru → Ir energy transfer.[128]

A different dinuclear complex, $[(bpy)_2Ru(bpt)Ir(ppy)_2]^{2+}$, was synthesised by Reedijk *et al.* by reacting $[Ru(bpy)_2(bpt)]^+$ and $[Ir(ppy)_2Cl]_2$ in refluxing 2-methoxyethanol for 2 days.[129] In this complex (figure 1.38), the two metal centres are linked *via* a bridging ligand containing a monoanionic triazole unit. Because of this electronic feature, the MLCT states localised on the two moieties involve the peripheral ligands and not the bridging ligand (as is usual for most dinuclear complexes). In $[(bpy)_2Ru(bpt)Ir(ppy)_2]^{2+}$, emission is only observed from the Ru based unit and the direction of intercomponent energy transfer is Ir → Ru, *i.e.* in the opposite direction from that observed for $[(bpy)_2Ru(HAT)Ir(ppy)_2]^{3+}$.

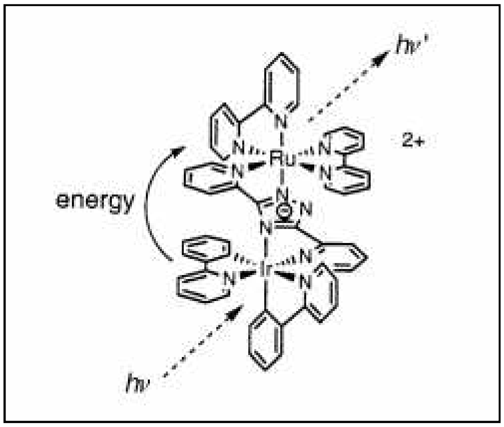

Figure 1.38 *Energy transfer in* $[Ru(bpy)_2(bpt)Ir(ppy)_2]^{2+}$.

Continuing the series from mono and dinuclear complexes to multinuclear compounds led Serroni, Campagna *et al.* to investigate tetranuclear heterometallic complexes.[130] These were obtained as a mixture of diastereoisomers by the reaction of $[Ir(ppy)_2Cl]_2$ with $M(dpp)_3^{2+}$ (M = Ru (II), Os (II)) in refluxing CH_2Cl_2 for 2.5 h, in 73 % and 70 % yields respectively (figure 1.39). Using similar reaction conditions (CH_2Cl_2–MeOH, 2 h reflux) Neve, in collaboration with the same group, prepared $[Ir(ppy)_2L]^+$ complexes where L is a substituted 6'-phenylbipyridine.[131] The emission is ascribed to MLCT states with partial SBLCT character.

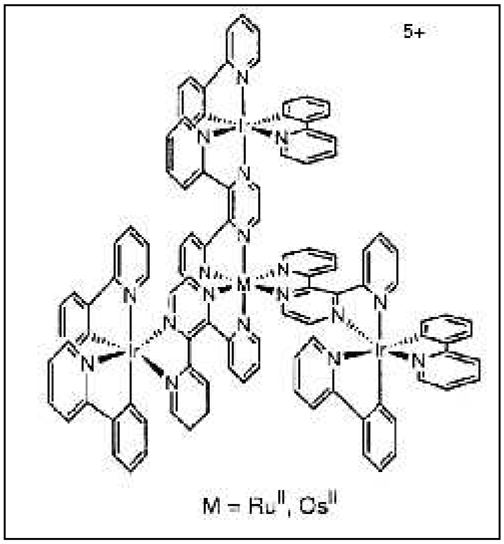

Figure 1.39 *Representation of* $\{M[(dpp)Ir(ppy)_2]_3\}^{5+}$ *(M = Ru (II), Os (II)).*

The coordination chemistry of iridium (III) was originally carried out under harsh reaction conditions. The more recent use of milder conditions has opened the way to the use of ligands bearing chemically sensitive groups.[124] This synthetic approach has led to the preparation of porphyrinic arrays built around an $Ir(terpy)_2^{3+}$ core, with appended electron donors and acceptor units (figure 1.40).[124,155,156] In this triad, excitation of the free-base porphyrins with visible light yields, with 50% efficiency, a charge separated state which has a lifetime of 3.5 ns at room temperature.[156]

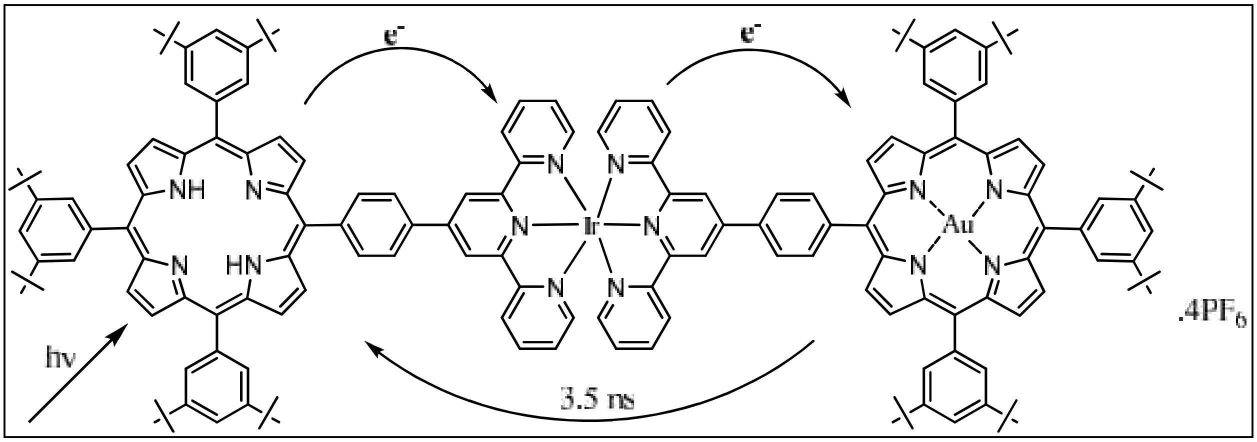

Figure 1.40 *A porphyrinic molecular triad which undergoes photoinduced charge separation.*[156]

1.12 Photophysical properties of iridium (III) complexes

Most of the experiments were carried out on iridium polypyridyl complexes. These are octahedral complexes of Ir (III) possessing a center of symmetry. The symmetry selection rule states that it is a necessary condition for a transition to be "allowed" and that the electron moves from an orbital that is even with respect to inversion through the center of symmetry, to an orbital that is uneven with respect to inversion. Since all d orbitals in an octahedral complex are even with respect to inversion, d-d transitions are "forbidden". Under visible irradiation these complexes undergo strong *intra ligand charge transfer transitions* (ILCT). What is called a *charge transfer* is nothing but a transition with a very large transition dipole moment. In the case of transition metal complexes in addition to ligand-based transitions, electron density can be transferred from d or n orbitals localised on the metal ion to a π^* orbital on the ligand. If the lowest unoccupied molecular orbital (LUMO) is located on the metal ion, the opposite charge transfer (LMCT) is observed.[145,157,158]

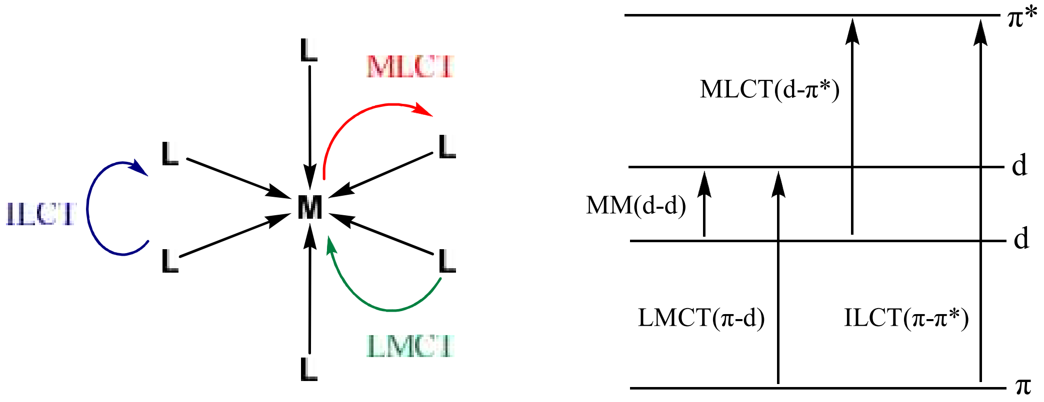

***Figure 1.41** Charge transfers in a transition metal complex*

Tuning of the photophysical properties of iridium (III) complexes has received considerable attention because of a series of practical applications such as flat-panel displays. Even though numerous organo iridium compounds have been reported to give efficient electroluminescence in the red, green and blue spectral region,[132,133] further scientific efforts are necessary to provide a general toolbox for synthesizing iridium compounds with absorption and emission characteristics tailored towards particular needs.[134] In this context, not only numerous reports on the synthesis and photophysical characterization of novel iridium (III) complexes have been published, but also quantum mechanical calculations are becoming more and more important in the design of phosphorescent emitter materials.[135, 136, 137] The absorption and emission spectra of these phosphorescent metal complexes are in general influenced by various parameters such as the valence electron configuration at the metal, the type of the electronic transitions or the correlation among lower lying electronic excited states. Similar to fluorescent small molecules also the photophysical behavior of transition metal complexes can be properly described with molecular orbitals, however, the performance of accurate quantum mechanical calculations is far more complicated. Nevertheless, it has been shown that frontier molecular orbitals are not equally delocalised in heavy metal complexes resulting in different electronically excited states.[159]

Among them, metal centered (MC) excited states are typically present in metal complexes with partially filled d shells at the metal center. The corresponding d-d transitions are Laporte-forbidden and, consequently, exhibit very low transition probabilities. Metal-to-ligand charge-transfer (MLCT) states involve electronic transitions from metal based d orbitals to a ligand centered π* antibonding orbital. Emissive MLCT states are particularly observed in d^6 and d^8 transition metal complexes and play, therefore, a major role in the photophysics of iridium (III) compounds. Intraligand (IL) π-π* excited states originate from electronic transitions of the ligand. If the metal perturbation upon coordination is minimised, their spectral properties often closely resemble the free ligand states. Finally, ligand-to-metal charge transfer (LMCT) excited states are occasionally observed in complexes with metal atoms in high oxidation states or in d^{10} complexes. All these transitions determine the photophysical properties of transition metal complexes and can be used for the interpretation of experimentally observed spectra or prediction of absorption and emission characteristics of novel compounds.[157,158,159] Hence, this elementary knowledge of the described processes is necessary to rationalise the impact of ligand modifications on the photophysical properties of phosphorescent dyes or to design highly efficient materials for photocatalysis and OLED applications. Along these lines, the absorption spectra of classical phosphorescent iridium (III) complexes typically display absorption bands with extinction coefficients between approximately 50000 and 6000 L mol^{-1} cm^{-1}. The weak absorption features between 400 and 500 nm can be attributed to spin-allowed and spin-forbidden metal-to-ligand charge-transfer (MLCT) transitions, while the strong absorption bands peaking in the UV-region usually originate from intraligand (IL) π-π* transitions.

After excitation of the iridium complex, the strong spin-orbit coupling induced by the metal center gives the formally forbidden triplet to singlet ground state transition a significant allowedness.[138] In this context, the energies of the lowest excited states play a major role as they can be tuned by adjusting the metal and ligand orbitals through substituent effects or *via* changing the ligand structures. In other words, chemical modifications or complete alterations of the cyclometallating or ancillary ligands pave the way to very efficient emission color tuning but also provide the possibility of tuning the corresponding absorption characteristics towards particular needs.[158,159]

Tremendous emission colour-versatility has been achieved with iridium (III) luminophores applying the above described tuning procedures giving materials with a broad range of excited state lifetimes (from nanoseconds to microseconds; here it should be noted that a long lifetime will increase the probability of excited state quenching processes and increases diffusion of the excited state, which will in turn call for efficient concepts to confine the excitation in the emissive layer) and quantum yields approaching 100%.[105,118,135] As a consequence, phosphorescent iridium complexes have emerged as the most promising class for practical OLED applications and the number of new phosphorescent dyes with emission wavelengths covering the entire visible spectrum is still growing.[139,141] Some selected examples of organoiridium complexes emitting in the blue, green and red spectral region are depicted in figure 1.42. Detailed photophysics of cyclometallated iridium complexes are also discussed in chapter 4.

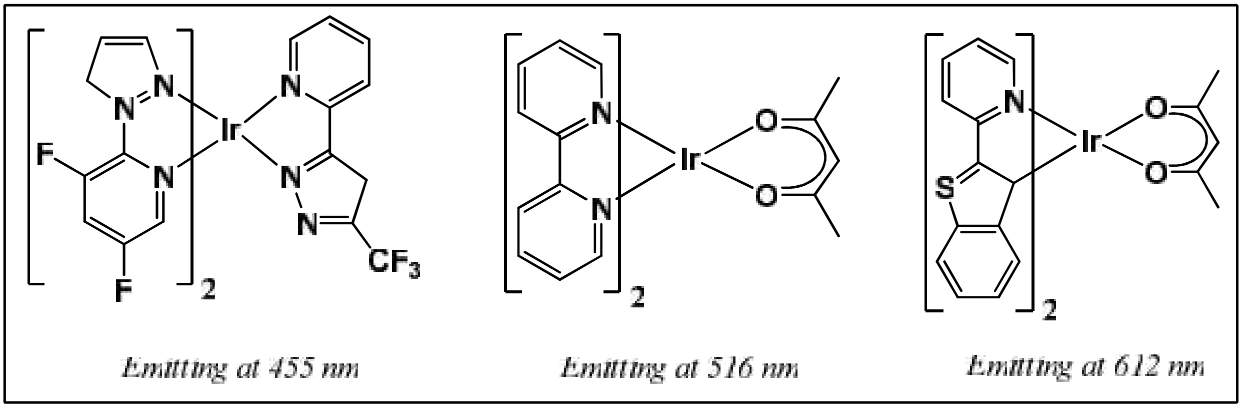

Emitting at 455 nm *Emitting at 516 nm* *Emitting at 612 nm*

Figure 1.42 *Selected examples of phosphorescent iridium complexes with emission maxima in the blue, green and red spectral region.*[118,119]

1.13 Iridium complexes as OLED’s

Research on organic light-emitting diodes (OLEDs), has been focused on devices composed of thin films containing organic/organometallic molecules that directly convert electricity into light (figure 1.43).[139] Heavy metal organometallic complexes have recently gained tremendous research interest for fabricating highly efficient phosphorescent OLEDs by taking advantage of the 1:3 exciton singlet/triplet ratio predicted by simple spin statistics.[135] These phosphorescent emitters are mainly derived from the family of the third-row transition metal (Re^{I}, Os^{II}, Ir^{III} and Pt^{II}) complexes,[140] although examples with some second-row transition metals such as Ru^{II} are also known. The three key electronic processes are, (i) charge injection, (ii) charge transport, and (iii) electron-hole recombination (i.e. exciton formation). Efficiency must be separately optimised in order to improve the overall OLED performance. The basic Organic Light-Emitting Diode (OLED) structure typically consists of an organic, light emitting layer between a transparent anode and a metallic cathode. In the more advanced structure the organic layers comprise a hole-injection layer, a hole-transport layer, an emissive layer, and an electron-transport layer to optimise the light output. When an appropriate voltage is applied to the cell, the injected positive and negative charges recombine in the emissive layer to produce electroluminescent light. When used to produce displays, the OLED technology produces self-luminous displays that do not require backlighting. These thin compact displays have a wide viewing angle of up to 160 degrees and require very low voltage, only 2-10 volts.

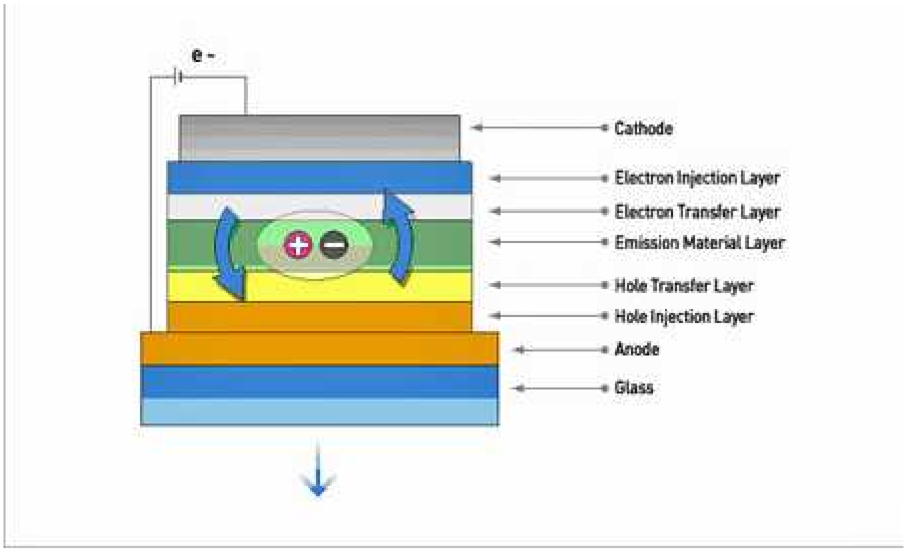

Figure 1.43 *A simple OLED structure (ref: http://www. hwsands.com).*

The pioneering work by Forrest and Thompson based on the utilisation of triplet emitters rather than of singlet emitters was a breakthrough in tackling the recombination efficiency issue,[141] and has since triggered a substantial amount of research activities on phosphorescent molecules with much success. This strategy enhances light emission efficiency by efficient electrophosphorescence. The advantage of triplet emitters over the singlet emitting counterparts is that they can capture energy from both singlet and triplet excited states, lifting the upper limit of the internal quantum efficiency of the usual fluorescent dopant based devices from 25 % to nearly 100 %. Phosphorescent emitters with heavy metal ions allow for circumvention of this limitation if the excitons generated by hole-electron recombination reside at a site where efficient spin orbit coupling leads to efficient singlet triplet state mixing which eliminates the spin forbidden nature of the radiative relaxation of the triplet state. Of all the systems investigated to date, [Ir(ppy)$_3$] and [Ir(ppy)$_2$(acac)] (Hppy = 2-phenylpyridine, Hacac = acetylacetone) are the most well-studied compounds in this area.[119] Neutral iridium (III) cyclometallated complexes have been widely employed as phosphorescent dyes in high-efficiency OLEDs with external quantum efficiency of up to 19 % using the multilayered device structure.[142] The phosphorescence colour tuning capability of these metallophosphors proceeded via relevant modifications of the ligand structures and has been well documented for important applications in full-colour displays.[115,143]

Cyclometallated iridium (III) complexes with various peripheral chelating ligands are of major interest due to their high quantum yields, short lifetimes, or color-tunability. Chelating ligands play an important role in organic light-emitting diodes (OLEDs)[144] and other electroluminescent technologies.[105,106] For the purpose of design and synthesis of luminescent complexes, cyclometallated aromatics have been commonly used,[145] the success of which is attributed to the following factors. Firstly compared with other organic ligands, aromatic cyclometallates tend to form the strongest bonding interaction with transition metal elements. Secondly the stronger metal ligand bonding should increase the d–d energy gap and afford less radiationless quenching due to the suppressed population to the higher lying, repulsive d–d excited state. This is particularly true for the third row transition metal elements. Finally the occurrence of close lying, ligand centered π–π* electronic transitions allows facile tuning of emission wavelength.

OLEDs may revolutionise display technologies in the scientific community. The key advantages of OLEDs for flat-panel display applications are their self-emitting property, high luminous efficiency, full color capability, wide viewing angle, high contrast, low power consumption, low weight, potentially large area color displays and flexibility.[105,135,160] Unlike liquid crystal displays (LCDs), OLEDs display can be printed on to a surface using an inkjet or even screen printing technology. They are also more energy efficient and are generally lower in cost than LCDs. In view of this, the rapidly growing market for OLED technology is driving both the academic and industrial communities towards the development of new functional materials for advanced manufacturing technologies.

1.14 Bibliography

---

1. N. S. Lewis, D. G. Nocera, *Proc. Natl. Acad. Sci. U. S. A.,* **2006**, 103, 15729.
2. J. P. McEvoy, G. W. Brudvig, *Chem. Rev.,* **2006**, 106, 4455.
3. K. N. Ferreira, T. M. Iverson, K. Maghlaoui, J. Barber, S. Iwata, *Science*, **2004**, 303, 1831.
4. M. Roeb, M. Neises, J. Sack, P. Rietbrock, N. Monnerie, J. Dersch, M. Schmitz, C. Sattler, *Int. J. Hydrogen Energy,* **2009**, 34, 4537.
5. M. Z. Jacobson, W. G. Colella, D. M. Golden, *Science*, **2005**, 308, 1901.
6. R. Eisenberg, D. G. Nocera, *Inorg. Chem.,* **2005**, 44, 6799.
7. N. Armaroli, V. Balzani, *Angew. Chem. Int. Ed.,* **2007**, 46, 52.
8. J. M. Lehn, J. P. Sauvage, *Nouv. J. Chim.,* **1977**, 1, 449.
9. K. Kalyanasundaram, J. Kiwi, M. Gratzel, *Helv. Chim. Acta.,* **1978**, 61, 2720.
10. M. Gratzel, *Acc. Chem. Res.,* **1981**, 14, 376.
11. A. J. Esswein, D. G. Nocera, *Chem. Rev.,* **2007**, 107, 4022.
12. S. Rau, D. Walther, J. G. Vos, *Dalton Trans.,* **2007**, 9, 915.
13. S. Rodat, S. Abanades, J. L. Sans, G. Flamant, *Int. J. Hydrogen Energy.,* **2010**, 35, 7748.
14. T. I. Sigfusson, *Phil. Trans. R. Soc. A.,* **2007**, 365, 1025.
15. J. A. Turner, *Science.,* **2004**, 305, 972.
16. S. A. Sherif, F. Barbir, T. N. Veziroglu, *Solar Energy.,* **2005**, 78, 647.
17. S. S. Penner, *Energy.,* **2006**, 31, 33.

18. B. C. R. Ewan, R. W. K. Allen, *Int. J. Hydrogen Energy.,* **2005**, 30, 809.
19. C. A. Linkous, *Hydrogen energy progress IX, Proceedings of the Ninth World Hydrogen Energy Conference. Paris (France),* **1992**, 419.
20. T. Pregger, D. Graf, W. Krewitt, C. Sattler, M. Roeb, S. Moller, *Int. J. Hydrogen Energy.,* **2009**, 34, 4256.
21. N. Nelson, A. B. Shem, *Nature Reviews.,* **2004**, 5, 971.
22. A. Fujishima, K. Honda, *Bull. Chem. Soc. Jpn*., **1971**, 44, 1148.
23. A. Fujishima, K. Honda, *Nature.,* **1972**, 238, 37.
24. S. P. Singh, S. C. Srivastava, K. D. Pandey, *International Journal of Hydrogen Energy.,* **1990**, 6, 403.
25. G. W. Crabtree, M. S. Dresselhaus, M. V. Buchanan, *Physics. Today.,* **2004**, 57, 39.
26. T. Kodama, T. Hasegawa, A. Nagasaki, *J. Sol. Energy Eng.,* **2009**, 131, 21008.
27. A. Steinfeld, *Sol. Energ.,* **2005**, 78, 603.
28. P. Loutzenhiser, M. Galvez, I. Hischier, A. Graf, A. Steinfeld, *Chem. Eng. Sci.,* **2010**, 65, 1855.
29. Annual Energy Outlook, US Dept of Energy, **2005**, Washington DC.
30. F. Rappaport and B. A. Diner, *Coord. Chem. Rev.,* **2008**, 252, 259.
31. Special section on "Sustainability and Energy", *Science.,* **2007**, 315, 781-813.
32. (a) N. Armaroli, V. Balzani, *Angew. Chem.,* **2007**, 119, 52.
33. V. Balzani, L. Moggi, M. F. Manfrin, F. Bolletta, M. Gleria, *Science.,* **1975**, 189, 852.
34. T. J. Meyer, *Acc. Chem. Res.,* **1989**, 22, 163.
35. P. V. Kamat, *J. Phys. Chem. C.,* **2007**, 111, 2834.
36. H. Akimoto, *Science.,* **2003**, 302, 1716.
37. C. K. Gratzel and M. Gratzel, *J. Am. Chem. Soc.,* **1979**, 101, 7741.
38. M. Terazima, K. Okamoto, N. Hirota, *J. Phys. Chem.,* **1993**, 97.
39. K. Chandrasekaran, D. G. Whitten, *J. Am. Chem. Soc.,* **1981**, 103, 7270.
40. F. H. Burstall, *J. Chem. Soc.,* **1936**, 173.
41. C. F. Liu, N. C. Liu, J. C. Bailar, *Inorg. Chem.,* **1964**, 3, 1085.
42. H. D. Gafney, A. W. Adamson, *J. Am. Chem. Soc.,* **1972**, 94, 8238.
43. R. C. Young, T. J. Meyer, D. G. Whitten, *J. Am. Chem. Soc.,* **1975**, 97, 4781.

---

44. T. J. Meyer, *Acc. Chem. Res.,* **1978**, 11, 94.
45. S. J. Valenty, G. L. Gaines, *J. Am. Chem. Soc.,* **1977**, 99, 1285.
46. A. Harriman, *J. Chem. Soc., Chem. Commun.,* **1977**, 777.
47. A. Moradpour, E. Amouyal, P. Keller, H. Kagan, *Nouv. J. Chem.,* **1979**, 2, 547.
48. G. M. Brown, S. F. Chan, C. Creutz, H. A. Schwarz, N. Sutin, *J. Am. Chem. Soc.,* **1979**, 101, 7638.
49. S. F. Chan, M. Chou, C. Creutz, T. Matsubara, N. Sutin, *J. Am. Chem. Soc.,* **1981**, 103, 369.
50. V. Balzani, *Tetrahedron.,* **1992**, 48, 10443.
51. A. Juris, V. Balzani, F. Barigelletti, S. Campagna, P. Belser and A. V. Zelewsky, *Coord. Chem. Rev.,* **1988**, 84, 85.
52. K. Kalyanasundaram, *Coord. Chem. Rev.,* **1982**, 46, 159.
53. M. N. Spallart, K. Kalyanasundaram, C. Gratzel, M. Gratzel, *Hel. Chim. Acta.,* **1980**, 63, 1111.
54. H. A. F. Wemer, R. Bauer, *J. Mol. Catal.,* **1994**, 88, 185.
55. P. P. lnfelta, *J. Photochem*., **1982**, 20, 181.
56. K. Kalyanasundaram, *Photochemistry of Polypyridine and Porphyrin Complexes*, Academic Press, New York, NY, **1992**, pp. 105–164.
57. P. J. Hay, *J. Phys. Chem. A.,* **2002**, 106, 1634.
58. J. I. Goldsmith, W. R. Hudson, M. S. Lowry, T. H. Anderson, S. Bernhard, *J. Am. Chem. Soc.*, **2005**, 127, 7502.
59. M. S. Lowry, J. I. Goldsmith, J. D. Slinker, R. Rohl, R. A. Pascal, G. G. Malliaras, S. Bernhard, *Chem. Mater.*, **2005**, 17, 5712.
60. N. Sutin, C. Creutz, E. Fujita, *Comments. Inorg. Chem.* **1997**, 19, 67.
61. S. Chan, M. Chou, C. Creutz, T. Matsubara, N. Sutin, *J. Am. Chem. Soc.,* **1981**, 103, 369.
62. E. D. Cline, S. E. Adamson, S. Bernhard, *Inorg. Chem.*, **2008**, 47, 10378.
63. M. Hambourger, M. Gervaldo, D. Svedruzic, P. W. King, D. Gust, M. Ghirardi, A. L. Moore, T. A. Moore, *J. Am. Chem. Soc.*, **2008**, 130, 2015.
64. I. Okura, *Coord. Chem. Rev.*, **1985**, 68, 53.
65. J. W. Peters, W. N. Lanzilotta, B. J. Lemon, L. C. Seefeldt, *Science*, **1998**, 282, 1853.

66. M. Frey, *Chem. Bio. Chem.*, **2002**, 3, 153.
67. Y. Na, M. Wang, J. Pan, P. Zhang, B. A. Kermark, L. Sun, *Inorg. Chem.*, **2008**, 47, 2805.
68. V. Balzani, G. Bergamini, F. Marchioni, P. Ceroni, *Coord. Chem. Rev.*, **2006**, 250, 1254.
69. C. Baffert, V. Artero, M. Fontecave, *Inorg. Chem.*, **2007**, 46, 1817.
70. P. Du, K. Knowles, R. Eisenberg, *J. Am. Chem. Soc.*, **2008**, 130,12576.
71. A. Fihri, V. Artero, A. Pereira, M. Fontecave, *Dalton Trans.*, **2008**, 5567.
72. L. L. Tinker, N. D. McDaniel, P. N. Curtin, C. K. Smith, M. J. Ireland, S. Bernhard, *Chem. Eur. J.*, **2007**, 13, 8726.
73. B. Probst, C. Kolano, P. Hamm, R. Alberto, *Inorg. Chem.*, **2009**, 48, 1836.
74. M. Elvington, J. Brown, S. M. Arachchige, K. J. Brewer, *J. Am.Chem. Soc.*, **2007**, 129, 10644.
75. H. Ozawa, M. Haga, K. Sakai, *J. Am. Chem. Soc.*, **2006**, 128, 4926.
76. S. Rau, B. Schafer, D. Gleich, E. Anders, M. Rudolph, M. Friedrich, H. Gorls, W. Henry, J. G. Vos, *Angew. Chem., Int. Ed.*, **2006**, 45, 6215.
77. P. Lei, M. Hedlund, R. Lomoth, H. Rensmo, O. Johansson, L. Hammarstrom, *J. Am. Chem. Soc.*, **2008**, 130, 26.
78. H. Cui, M. Wang, L. Duan, L. Sun, *J. Coord. Chem.*, **2008**, 61, 1856.
79. L. C. Song, M. Y. Tang, F. H. Su, Q. M. Hu, *Angew. Chem., Int. Ed.*, **2006**, 45, 1130.
80. X. Li, M. Wang, S. Zhang, J. Pan, Y. Na, J. Liu, B. A. Kermark, L. Sun, *J. Phys. Chem. B*, **2008**, 112, 8198.
81. A. Fihri, V. Artero, M. Razavet, C. Baffert, W. Leibl, M. Fontecave, *Angew. Chem., Int. Ed.*, **2008**, 47, 564.
82. J. Hawecker, J. M. Lehn, R. Ziessel, *New J. Chem.*, **1983**, 7, 271.
83. J. Rosenthal, J. Bachman, J. L. Dempsey, A. J. Esswein, T. G. Gray, J. M. Hodgkiss, D. R. Manke, T. D. Luckett, B. J. Pistorio, A. S. Veige, D. G. Nocera, *Coord. Chem. Rev.*, **2005**, 249, 1316.
84. A. F. Heyduk, D. G. Nocera, *Science*, **2001**, 293, 1639.
85. R. J. Watts, *Inorg. Chem.*, **1991**, 11, 303.
86. R. E. DeSimone, R. E. Drago, *Inorg. Chem.*, **1969**, 8, 2517.
87. B. Chiswell, S. E. Livingstone, *J. Inorg. Nucl. Chem.*, **1964**, 26, 47.

88. J. A. Broomhead, W. Grumley, *Inorg. Chem.*, **1971**, 10, 2002.
89. S. C. Rasmussen, M. M. Richter, E. Yi, H. Place, K. J. Brewer, *Inorg. Chem.*, **1990**, 29, 3926.
90. J. S. Bridgewater, L. M. Vogler, S. M. Molnar, K. J. Brewer, *Inorg. Chim. Acta.*, **1993**, 208, 179.
91. S. M. Molnar, G. Nallas, J. S. Bridgewater, K. J. Brewer, *J. Am. Chem. Soc.*, **1994**, 116, 5206.
92. G. N. A. Nallas, S. W. Jones, K. J. Brewer, *Inorg. Chem.,* **1996**, 35, 69747.
93. B. Martin, G. M. Waind, *J. Chem. Soc.*, **1958**, 4282.
94. C. M. Flynn, J. N. Demas, *J. Am. Chem. Soc.*, **1974**, 96, 1959.
95. J. L. Kahl, K. W. Hanck, M. K. DeArmond, *J. Phys. Chem.*, **1978**, 82, 540.
96. J. N. Demas, E. W. Harris, C. M. Flynn, D. Diemente, *J. Am.Chem. Soc.*, **1975**, 97, 3838.
97. R. J. Watts, J. S. Harrington, J. V. Houten, *J. Am. Chem. Soc.*, **1977**, 99, 2179.
98. W. A. Wickramasinghe, P. H. Bird, N. Serpone, *J. Chem. Soc., Chem. Commun.*, **1981**, 1284.
99. B. P. Sullivan, T. J. Meyer, *J. Chem. Soc. Chem. Commun.*, **1984**, 403.
100. S. Sprouse, K. A. King, P. J. Spellane, R. J. Watts, *J. Am. Chem. Soc.*, **1984**, 106, 6647.
101. M. Nonoyama, *Bull. Chem. Soc. Jpn.* **1974**, 47, 767.
102. A. S. Ionkin, W. J. Marshall, B. M. Fish, *Organometallics*, **2006**, 25, 1461.
103. F. O. Garces, R. J. Watts, *Inorg. Chem.*, **1990**, 29, 582.
104. I. M. Dixon, J. P. Collin, J. P. Sauvage, L. Flamigni, S. Encinas, F. Barigelletti, *Chem. Soc. Rev.,* **2000**, 29, 385.
105. M. A. Baldo, D. F. O'Brien, Y. You, A. Shoustikov, S. Sibley, M. E. Thompson, S. R. Forrest, *Nature,* **1998**, 395, 151.
106. M. S. Lowry, S. Bernhard, *Chem. Eur. J.,* **2006**, 12, 7970.
107. K. Goushi, R. Kwong, J. J. Brown, H. Sasabe, C. Adachi, *J. Appl. Phys.,* **2004**, 95, 7798.
108. E. Holder, B. M. W. Langeveld, U. S. Schubert, *Adv. Mater.,* **2005**, 17, 1109.
109. J. D. Slinker, A. A. Gorodetsky, M. S. Lowry, J. Wang, S. Parker, R. Rohl, S. Bernhard, G. G. Malliaras, *J. Am. Chem. Soc.,* **2004**, 126, 2763.
110. A. S. Ionkin, W. J. Marshall, D. C. Roe, Y. Wang, *Dalton Trans.,* **2006**, 2468.

---

111. K. A. King, P. J. Spellane, R. J. Watts, *J. Am. Chem. Soc.*, **1985**, 107, 1431.
112. K. Dedeian, P. I. Djurovich, F. O. Garces, G. Carlson, R. J. Watts, *Inorg. Chem.*, **1991**, 30, 1685.
113. P. I. Djurovich, A. L. Safir, N. L. Keder, R. J. Watts, *Inorg. Chem.*, **1992**, 31, 3195.
114. M. G. Colombo, T. C. Brunold, T. Riedener, H. U. Gudel, M. Fortsch, H. B. Burgi, *Inorg. Chem.*, **1994**, 33, 545.
115. Y. You, S. Y. Park, *J. Am. Chem. Soc.,* **2005**, 127, 12438.
116. S. Kappaun, S. Sax, S. Eder, K. C. Moller, K. Waich, F. Niedermair, R. Saf, K. Mereiter, J. Jacob, K. Mullen, E. J. W. List, C. Slugovc, *Chem. Mater.,* **2007**, 19, 1209.
117. S. Kappaun, S. Eder, S. Sax, K. Mereiter, E. J. W. List, C. Slugovc, *Eur. J. Inorg. Chem.* **2007**, 4207.
118. S. Lamansky, P. Djurovic, D. Murphy, F. A. Razzaq, R. Kwong, I. Tsyba, M. Bortz, B. Mui, R. Bau, M. E. Thompson, *Inorg. Chem.,* **2001**, 40, 1704.
119. S. Lamansky, P. Djurovich, D. Murphy, F. A. Razzaq, H. E. Lee, C. Adachi, P. E. Burrows, S. R. Forrest, M. E. Thompson, *J. Am. Chem. Soc.* **2001**, 123, 4304.
120. N. M. Hsu, W. R. Li, *Angew. Chem.,* **2006**, 118, 4244.
121. G. Morgan, F. H. Burstall, *J. Chem. Soc.*, **1937**, 1649.
122. L. M. Vogler, B. Scott, K. J. Brewer, *Inorg. Chem.*, **1993**, 32, 898.
123. N. P. Ayala, C. M. Flynn, L. A. Stacksteder, J. N. Demas, B. A. DeGraff, *J. Am. Chem. Soc.*, **1990**, 112, 3837.
124. J. P. Collin, I. M. Dixon, J. P. Sauvage, J. A. G. Williams, F. Barigelletti, L. Flamigni, *J. Am. Chem. Soc.*, **1999**, 121, 5009.
125. M. Licini, J. A. G. Williams, *Chem. Commun.*, **1999**, 1943.
126. P. Didier, I. Ortmans, A. K. D. Mesmaecker, R. J. Watts, *Inorg.Chem.*, **1993**, 32, 5239.
127. P. Didier, L. Jacquet, A. K. D. Mesmaecker, R. Hueber, A. V. Dorsselaer, *Inorg. Chem.*, **1992**, 31, 4803.
128. I. Ortmans, P. Didier, A. K. D. Mesmaecker, *Inorg. Chem.*, **1995**, 35, 3695.
129. J. H. V. Diemen, R. Hage, J. G. Haasnoot, H. E. B. Lempers, J. Reedijk, J. G. Vos, L. De Cola, F. Barigelletti, V. Balzani, *Inorg. Chem.*, **1992**, 31, 3518.

130. S. Serroni, A. Juris, S. Campagna, M. Venturi, G. Denti, V. Balzani, *J. Am. Chem. Soc.*, **1994**, 116, 9086.
131. F. Neve, A. Crispini, S. Campagna, S. Serroni, *Inorg. Chem.*, **1999**, 38, 2250.
132. T. Sajoto, P. I. Djurovich, A. Tamayo, M. Yousufuddin, R. Bau, M. E. Thompson, *Inorg. Chem.* **2005**, 44, 7992.
133. C. S. Chin, M. S. Eum, S. Y. Kim, C. Kim, S. K. Kang, *Eur. J. Inorg.Chem.,* **2007**, 372.
134. P. T. Chou, Y. Chi, *Chem. Eur. J.,* **2007**, 13, 380.
135. J. Li, P. I. Djurovich, B. D. Alleyne, M. Yousufuddin, N. N. Ho, J. C. Thomas, J. C. Peters, R. Bau, M. E. Thompson, *Inorg. Chem*., **2005**, 44, 1713.
136. T. Liu, B. H. Xia, X. Zhou, H. X. Zhang, Q. J. Pan, J. S. Gao, *Organometallics*, **2007**, 26, 143.
137. T. H. Kwon, H. S. Cho, M. K. Kim, J. W. Kim, J. J. Kim, K. H. Lee, S. J. Park, I. S. Shin, H. Kim, D. M. Shin, Y. K. Chung, J. I. Hong, *Organometallics,* **2005**, 24, 1578.
138. X. Yang, D. Neher, K. Mullen, U. Scherf, Eds.; Wiley-VCH: Weinheim, **2006**; p. 333.
139. M. A. Baldo, M. E. Thompson, S. R. Forrest, *Pure Appl. Chem.,* **1999**, 71, 2095.
140. J. A. G. Williams, S. Develay, D. L. Rochester, L. Murphy, *Coord. Chem. Rev.,* **2008**, 252, 2596.
141. M. A. Baldo, D. F. O'Brien, Y. You, A. Shoustikov, S. Sibley, M. E. Thompson, S. R. Forrest, *Nature*, **1998**, 395, 151.
142. M. K. Nazeeruddin, R. H. Baker, *J. Am. Chem. Soc.,* **2003**, 125, 8790.
143. G. J. Zhou, C. L. Ho, W. Y. Wong, Q. Wang, D. G. Ma, L. X. Wang, Z. Y. Lin, T. B. Marder, A. Beeby, *Adv. Funct. Mater.,* **2008**, 18, 499.
144. J. A. G. Williams, A. J. Wilkinson, V. L. Whittle, *Dalton Trans.,* **2008**, 2081.
145. Y. Chi, P. T. Chou, *Chem. Soc. Rev*., **2007**, 36, 1421.
147. P. P. Edwards, V. L. Kuznetsov, W. I. F. David, *Phil. Trans. R. Soc. A,* **2007**, 365, 1043.
148. J. Turner, G. Sverdrup, M. K. Mann, P. C. Maness, B. Kroposki, M. Ghirardi, R. J. Evans, D. Blake, *Int. J. Energy Res*., **2008**, 32, 379.
149. M. Roeb, M. Neises, N. Monnerie, C. Sattler, R. P. Paal, *Energy Environ. Sci.*, **2011**, 4, 2503.
150. A. Kudo, Y. Miseki, *Chem. Soc. Rev*., **2009**, 38, 253.

---

151. J. Barber, *Chem. Soc. Rev*., **2009**, 38, 185.
152. C. Konigstein, *Journal of Photochemistry and Photobiology A*., **1995**, 90, 141.
153. L. L. Tinker, N. D. McDaniel, S. Bernhard, *J. Mater. Chem.,* **2009**, 19, 3328.
154. J. Hawecker, J. M. Lehn, R. Ziessel, *New J. Chem*., **1983**, **7**, 271.
155. I. M. Dixon, J. P. Collin, J. P. Sauvage, L. Flamigni, *Inorganic Chemistry*, **2001**, 40, 5507.
156. L. Flamigni, J. P. Collin, J. P. Sauvage, *Acc. Chem. Res*., **2008**, 41, 857.
157. Y. Chi, P. T. Chou, *Chem. Soc. Rev*., **2010**, 39, 638.
158. P. T. Chou, Y. Chi, M. W. Chung, C. C. Lin, *Coord. Chem. Rev*., **2011**, 255, 2653.
159. Y. You, S. Y. Park, *Dalton Trans*., **2009**, 8, 1267.
160. C. H. Yang, Y. M. Cheng, Y. Chi, C. J. Hsu, F. C. Fang, K. T. Wong, P. T. Chou, C. H. Chang, M. H. Tsai, C. C. Wu, *Angew. Chem*., **2007**, 119, 2470.

Chapter 2

General introduction to synthesis, purification, physical techniques and measurements

The following chapter describes in detail the basic synthetic procedures that were followed throughout the course of this thesis. The instrumentation that was used in the characterisation of the complexes has been detailed. Also included are the methods by which data were analysed and conventions which were followed in the presentation of data throughout this thesis. For selected techniques a bief summary of theoretical basis is included.

2.1 General synthetic procedures and considerations

The reagents employed during the course of all experiments were purchased from Sigma-Aldrich and used without further purification. All solvents used for HPLC analysis are of HPLC grade and spectroscopic grade solvents were used for photophysical measurements. Deuteriated bipyridine ($d_8$bpy), phenanthroline ($d_8$phen), 4,4'-dimethyl-2,2'-bipyridyl (d_{12}dmbpy) and 4,4'-ditertiarybutyl-2,2'-bipyridyl (d_{24}dtbpy) were synthesised according to the procedure reported before.[1] The bridging ligands employed 2,2':6',2"-terpyridine (tpy) and 2,2'-bipyrimidine (bpm) were purchased from sigma aldrich and was used directly. The ligands 2,2'-bipyridyl (bpy), 1, 10-phenanthroline (phen), 4,4'-dimethyl-2,2'-bipyridyl (dmbpy), 4,4'-ditertiarybutyl-2,2'-bipyridyl (dtbpy), 4,4'-diphenyl-2,2'-bipyridyl (dpbpy) and 4,4'-diphenyl-1,10-phenanthroline (dpphen) were purchased from Sigma-Aldrich and used directly.

2.1.1 Deuteriation of ligands

The deuteriation of ligands was carried out in general purpose dissolution Bomb P/N 4744 from Scientific Medical Products, which included a Teflon cup and cover and was done in basic D_2O (1M NaOD/D_2O solution were prepared in situ by addition of 460 mg of sodium to 20 cm^3 of D_2O). After 3 days in the bomb, it was found that approximately 90 % atom deuteriation had been achieved. This percentage improved only slightly with increased reaction times. However, following a repeat of the procedure, i.e. another 3 days in the bomb with fresh reagents it was found that atom deuteriation of >99 % was achieved. The percentage of deuteriation was calculated by ^{1}H NMR spectroscopy. A known mass (and hence number of moles) of the non deuteriated ligand was dissolved in a known volume of solvent (d_6-dmso). The ratio of the peak integration of the ligand to the peak integration of the solvent was found. After obtaining a spectrum of the same amount of the deuteriated ligand in the same volume of solvent, a second ratio was obtained. Comparison of the ratios led to a measurement of the percentage of the atoms which have been successfully exchanged. The ^{1}H NMR spectra of the deuteriated 2,2'-bipyridyl ligand is shown in figure 2.1. The size of the solvent peak relative to the size of the 2,2'-bipyridyl ligand peaks should be noted. It is the ratio of the peak integration of these peaks that allow the second ratio to be calculated.

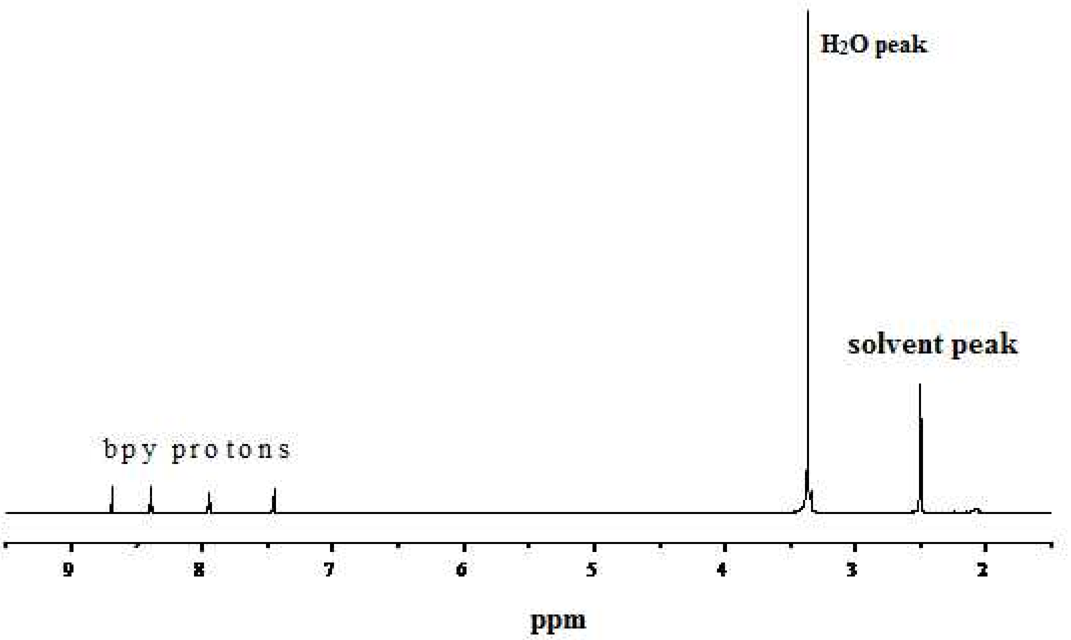

Figure 2.1 *^{1}H NMR of $d_8$bpy in d_6-dmso.*

2.1.1.1 Deuteriation of bpy, phen, dmbpy, dtbpy

Deuteriation of the ligands were done using basic D_2O (20 ml of 1M NaOD/D_2O) and carried out in a sealed steel container with a teflon liner at 200 ^{0}C for 6 days.[1,2] The percentage of H/D exchange and the percentage yield are summarised below.

[d_8]-2,2'-bipyridine (% H/D exchange = 99 %, % Yield = 90 %)
[d_8]-1,10-phenanthroline (% H/D exchange = 98 %, % Yield = 92 %)
[d_{12}]-4,4'-dimethyl-2,2'-bipyridyl (% H/D exchange = 98 %, % Yield = 96 %)
[d_{24}]-4,4'-ditertiarybutyl-2,2'-bipyridyl (% H/D exchange = 97 %, % Yield = 93 %)

2.1.2 Synthesis of ester substituted phenyl pyridine ligands

2.1.2.1 Synthesis of (ppy-COOH), 4-(pyridin-2-yl)benzoic acid

$AgNO_3$ (0.974 g, 5.7311 mmol) was taken in a 100 ml round bottom flask and stirred with 5 ml water at room temperature to which NaOH (0.447 g, 11.189 mmol) was added dissolved in 5 ml water. A brown semi-solid residue was formed. The reaction mixture was then placed in an ice bath to which 4-(pyridine-2-yl)benzaldehyde (0.500 g, 2.729 mmol) was weighed, powdered and added slowly part by part and kept for stirring at room temperature for 30 min. The black silver suspension was removed by suction filtration and was washed with several portions of hot water. The cold combined filtrate and washings were acidified with concentrated hydrochloric acid, the precipitate began to form at pH 7 and maximum precipitate was obtained at pH 4 which was vacuum filtrated and dried. (Yeild: 0.468 g, 94 %). ^{1}H NMR (400 MHz, DMSO), δ (ppm): 7.43 (t, 1H), 7.92 (t, 1H), 8.07-8.04 (m, 2H), 8.2 (d, 2H), 8.72 (d, 1H), 13.19 (s, 1H).

2.1.2.2 Synthesis of ppy-$COOCH_2CH_3$

4-(pyridin-2-yl)benzoic acid (0.114 g, 0.5722 mmol) was weighed in an R.B to which 2 ml of conc. H_2SO_4 and 30 ml Ethanol was added and refluxed at 90 ^{0}C overnight. The reaction mixture was poured into ice water and stirred to which 25 % NaOH (25 g in 100 ml) was added drop wise and the ester precipitated after the neutralisation was complete, filtered, washed with deionised water and dried. (Yield 0.103 g, 90.34 %). ^{1}H NMR (400 MHz, DMSO), δ (ppm): 1.35 (t, 3H), 4.35 (q, 2H), 7.43 (m, 1H), 7.94 (m, 1H), 8.08 (d, 1H), 8.25 (d, 1H), 8.72 (d, 1H).

2.1.2.3 Synthesis of ppy-$COOCH_3$

4-(pyridin-2-yl)benzoic acid (0.300 g, 0.0014 mmol) was weighed in an R.B to which 4 ml of conc. H_2SO_4 and 30 ml Methanol was added and refluxed at 90 ^{0}C overnight. The reaction mixture was poured into ice water and stirred to which 25 % NaOH (25 g in 100 ml) was added drop wise until the neutralisation was complete, which was then extracted with DCM and the solvents were removed to get the ester pure. Yield (0.245 g, 82 %). ^{1}H NMR (400 MHz, DMSO), δ (ppm): 3.89 (s, 3H), 7.44 (m, 1H), 7.95 (m, 1H), 8.08 (d, 1H), 8.25 (d, 1H), 8.727 (d, 1H).

2.1.3 Synthesis of Bridging Ligands

2.1.3.1 BPP (2-(6-(pyridin-2-yl)pyridin-3-yl)pyridine)

In a dried two neck round bottom flask 0.299 g (0.258 mmol) of $Pd(PPh_3)_4$ and 2 g (8.44 mmol) of 2,5-dibromopyridine was taken under nitrogen atmosphere. During the addition of 38.7 ml (16.8 mmol) of 2-pyridylzinc bromide to the reaction mixture, the temperature was kept at 0 ^{0}C. The reaction mixture was then stirred overnight at room temperature under nitrogen atmosphere. A white precipitate was formed. The reaction mixture was poured in a saturated aqueous solution of EDTA/Na_2CO_3 until the precipitate dissolves and yellow flakes come. The aqueous solution was then extracted with dichloromethane and dried over $MgSO_4$. The dichloromethane was dried in air and crude product was purified by alumina column using hexane/ethyl acetate (9:1). The second spot in TLC is the desired product. Yield (1.57 g, 6.75 mmol, 80 %). ^{1}H NMR (400 MHz, DMSO), δ (ppm): 7.2 (t, 1H), 7.3 (t, 1H), 7.78 (m, 2H), 7.8 (t, 1H), 8.44-8.37 (m, 2H), 8.5 (d, 1H), 8.7-8.65 (m, 2H), 9.3 (s, 1H). Elemental analysis for ligand BPP, $C_{15}H_{11}N_3$; (calculated) : C : 77.23, H : 4.75, N : 18.01; (found) : C : 77.25, H : 4.71, N : 17.98.

2.1.3.2 dpp (2,5-di(pyridin-2-yl)pyrazine)

Step 1. Synthesis of oxime

10 g acetylpyridine (82.54 mmol, M=121, 14 g/mol), 5.73 g hydroxylamine hydrochloride (82.54 mmol, M=69.49 g/mol) and 8 g potassium acetate (81.9 mmol, M=98.3 g/mol) were dissolved in 100 ml water and stirred for 30 minutes at 40 °C yielding white precipitate. After that the mixture was stirred for another 30 minutes at room temperature. The precipitate was filtered off, washed with water and recrystalised from an ethanol-water mixture (3:1) to give white crystals. Yield (9.1 g, 66.8 mmol, M=136.15 g/mol, 80 %), ^{1}H NMR (400 MHz, $CDCl_3$), δ (ppm): 2.43 (s, 3H), 7.29 (m, 1H), 7.71 (m, 1H), 7.84 (d, 1H), 8.65 (d, 1H), 9.91 (1H, s).

Step 2. Synthesis of Tosyl ester

10.798 g toluenesulphonylchloride (1.1 eq., 56.639 mmol, M=190.65 g/mol) was dissolved in 15 ml pyridine. After that 7.011 g acetylpyridine-oxime (51.49 mmol) was added slowly, forming a brownish gel. After stirring overnight at room temperature, the mixture was poured into ice water forming a white precipitate, which was filtered off, washed with water and recrystalised from an ethanol-water mixture (3:1). Yield (7.804 g, 26.91 mmol, M=290 g/mol, 52 %), ^{1}H NMR (400 MHz, $CDCl_3$), δ (ppm): 2.46 (s, 6H), 7.35 (m, 3H), 7.7 (m, 1H), 7.81 (d, 1H), 7.95 (d, 2H), 8.61 (d, 1H).

Step 3

The tosylester 7.804 g (26.91 mmol, M=290 g/mol) was dissolved in ethanol and reacted with freshly developed potassium ethanolate (1.58 g, 1.5 eq, 40.363 mmol solved in 150 ml ethanol). Potassium tosylate was filtered of and diethylether was added to the filtrate to get more tosylate, which was filtered off again. The filtrate was extracted with 2M HCl thrice. The aqueous phase was intermixed with NH_4OH in excess and stirred for 36 hours. The orange precipitate was filtered off and recrystalised from an ethanol-water mixture (3:1). Yield (449 mg, 1.917 mmol, M=234.26 g/mol, 17 %), ^{1}H NMR (400 MHz, $CDCl_3$), δ (ppm): 7.45 (t, 2H), 7.94 (t, 2H), 8.50 (d, 2H), 8.79 (d, 2H), 9.75 (s, 1H). Elemental analysis for ligand dpp, $C_{14}H_{10}N_4$; (calculated) : C : 71.78, H : 4.30, N : 23.92; (found) : C : 71.82, H : 4.29, N : 23.95.

2.1.4 Synthesis of cyclometallated iridium precursors

2.1.4.1 Synthesis of [Ir(ppy)$_2$Cl]$_2$

Iridium trichloride hydrate (1 g, 2.8 mmol) was combined with 2-phenylpyridine (1.76 g, 11.3 mmol), dissolved in a mixture of 2- methoxyethanol (75 ml) and water (25 ml), and refluxed for 24 h. The solution was cooled to room temperature, and the yellow precipitate was collected on a glass filter frit. The precipitate was washed with ethanol (60 ml) and acetone (60 ml) and then dissolved in dichloromethane (75 ml) and filtered. Toluene (25 ml) and hexane (10 ml) were added to the filtrate which was then reduced in volume, and cooled to give crystals of $[Ir(ppy)_2Cl]_2$. (Yield 1.12 g, 74 %). ^{1}H NMR (400 MHz, DMSO), δ (ppm): 5.64 (d, 1H), 6.23 (d, 1H), 6.67 (t, 1H), 6.74 (t, 1H), 6.82 (t, 1H), 6.88 (t, 1H), 7.43 (t, 1H), 7.55 (t, 1H), 7.71 (d, 1H), 7.77 (d, 1H), 7.99 (t, 1H), 8.07 (t, 1H), 8.16 (d, 1H), 8.24 (d, 1H), 9.51 (d, 1H), 9.78 (d, 1H). ^{1}H NMR (400 MHz, $CDCl_3$), δ (ppm): 5.89 (d, 1H), 6.53 (t, 1H), 6.74 (m, 2H), 7.45 (d, 1H), 7.70 (t, 1H), 7.84 (d, 1H), 9.20 (d, 1H). Elemental analysis for complex $[Ir(ppy)_2Cl]_2$, $C_{44}H_{32}Cl_2Ir_2N_4$; (calculated) : C : 49.29, H : 3.01, N : 5.23; (found) : C : 49.38, H : 3.00, N : 5.22.

2.1.4.2 Synthesis of [Ir(thpy)$_2$Cl]$_2$

Iridium trichloride hydrate (0.5 g, 1.4 mmol) was combined with thienylpyridine (0.9186 g, 5.6 mmol), dissolved in a mixture of 2- methoxyethanol (35 ml) and water (15 ml), and refluxed for 24 h. The solution was cooled to room temperature, and the brown precipitate was collected on a glass filter frit. The precipitate was washed with ethanol (60 ml) and acetone (60 ml) and then dissolved in dichloromethane (75 ml) and filtered. Toluene (25 ml) and hexane (10 ml) were added to the filtrate which was then reduced in volume, and cooled to give crystals of $[Ir(thpy)_2Cl]_2$. (Yield 0.59 g, 78 %). ^{1}H NMR (400 MHz, DMSO), δ (ppm): 5.64 (d, 1H), 6.11 (d, 1H), 7.22 (t, 1H), 7.32 (d, 1H), 7.35 (t, 1H), 7.51 (d, 1H), 7.63 (d, 1H), 7.74 (d, 1H), 7.88 (t, 1H), 7.94 (t, 1H), 9.30 (d, 1H), 9.63 (d, 1H). Elemental analysis for complex $[Ir(thpy)_2Cl]_2$,

$C_{36}H_{27}Cl_2Ir_2N_4S_4$; (calculated) : C : 39.34, H : 2.48, N : 5.10; (found) : C : 39.35, H : 2.12, N : 5.11.

2.1.4.3 Synthesis of [Ir(ppy-CHO)$_2$Cl]$_2$

Iridium trichloride hydrate (0.5 g, 1.4 mmol) was combined with 4-(pyridin-2-yl)benzaldehyde (0.9186 g, 5.6 mmol), dissolved in a mixture of 2-ethoxyethanol (35 ml) and water (15 ml), and refluxed for 24 h. The solution was cooled to room temperature, and the brown precipitate was collected on a glass filter frit. The precipitate was washed with ethanol (60 ml) and acetone (60 ml) and then dissolved in dichloromethane (75 ml) and filtered. Toluene (25 ml) and hexane (10 ml) were added to the filtrate which was then reduced in volume, and cooled to give crystals of [Ir(ppy-CHO)$_2$Cl]$_2$. (Yield 0.52 g, 72 %). ^{1}H NMR (400 MHz, DMSO), δ (ppm): 6.12 (d, 1H), 6.73 (d, 1H), 7.40 (d, 1H), 7.44 (d, 1H), 7.64 (t, 1H), 7.73 (t, 1H), 8.01 (d, 1H), 8.05 (d, 1H), 8.15 (t, 1H), 8.24 (t, 1H), 8.38 (d, 1H), 8.47 (d, 1H), 9.58 (d, 2H), 9.64 (s, 1H), 9.87 (d, 1H). Elemental analysis for complex [Ir(ppy-CHO)$_2$Cl]$_2$, $C_{48}H_{32}Cl_2Ir_2N_4O_4$; (calculated) : C : 48.69, H : 2.72, N : 4.73; (found) : C : 48.78, H : 2.41, N : 4.65.

2.1.4.4 Synthesis of [Ir(ppy-COOH)$_2$Cl]$_2$

Iridium trichloride hydrate (0.05 g, 0.14 mmol) was combined with 4-(pyridin-2-yl)benzoic acid (0.09186 g, 0.56 mmol), dissolved in a mixture of 2-ethoxyethanol (3.5 ml) and water (1.5 ml), and refluxed for 24 h. The solution was cooled to room temperature, and the brown precipitate was collected on a glass filter frit. The precipitate was washed with ethanol (30 ml) and acetone (30 ml) and then dissolved in dichloromethane (45 ml) and filtered. Toluene (15 ml) and hexane (5 ml) were added to the filtrate which was then reduced in volume, and cooled to give crystals of [Ir(ppy-COOH)$_2$Cl]$_2$. (Yield 0.112 g, 75 %). ^{1}H NMR (400 MHz, DMSO), δ (ppm): 6.28 (d, 1H), 6.84 (d, 1H), 7.40 (d, 1H), 7.44 (d, 1H), 7.58 (t, 1H), 7.66 (t, 1H), 7.85 (d, 1H), 7.92 (d, 1H), 8.08 (t, 1H), 8.18 (t, 1H), 8.30 (d, 1H), 8.30 (d, 1H), 9.54 (d, 1H), 9.83 (d, 1H), 12.52 (b, 2H). Elemental analysis for complex [Ir(ppy-COOH)$_2$Cl]$_2$, $C_{48}H_{32}Cl_2Ir_2N_4O_8$; (calculated) : C : 46.19, H : 2.58, N : 4.49; (found) : C : 46.35, H : 2.44, N : 4.53.

2.1.4.5 Synthesis of [Ir(ppy-COOCH$_3$)$_2$Cl]$_2$

Iridium trichloride hydrate (0.05 g, 0.14 mmol) was combined with methyl 4-(pyridin-2-yl)benzoate (0.09186 g, 0.56 mmol), dissolved in a mixture of 2-ethoxyethanol (3.5 ml) and water (1.5 ml), and refluxed for 24 h. The solution was cooled to room temperature, and the brown precipitate was collected on a glass filter frit. The precipitate was washed with ethanol (30 ml) and acetone (30 ml) and then dissolved in dichloromethane (45 ml) and filtered. Toluene (15 ml) and hexane (5 ml) were added to the filtrate which was then reduced in volume, and cooled to give crystals of [Ir(ppy-COOCH$_3$)$_2$Cl]$_2$. (Yield 0.112 g, 74 %). ^{1}H NMR (400 MHz, DMSO), δ (ppm): 3.63 (3H, s), 3.65 (3H, s), 6.28 (d, 1H), 6.86 (d, 1H), 7.42 (d, 1H), 7.45 (d, 1H), 7.61 (t, 1H), 7.71 (t, 1H), 7.89 (d, 1H), 7.95 (d, 1H), 8.13 (t, 1H), 8.22 (t, 1H), 8.33 (d, 1H), 8.42 (d, 1H), 9.56 (d, 1H), 9.85 (d, 1H). Elemental analysis for complex [Ir(ppy-COOCH$_3$)$_2$Cl]$_2$, $C_{52}H_{40}Cl_2Ir_2N_4O_8$; (calculated) : C : 47.89, H : 3.09, N : 4.30; (found) : C : 47.48, H : 3.11, N : 4.28.

2.1.4.6 Synthesis of [Ir(ppy)$_2$(CH$_3$CN)$_2$]CF$_3$SO$_3$

[Ir(ppy)$_2$Cl]$_2$ (0.0566 g, 0.05289 mmol) and CF_3SO_3Ag (0.0299 g, 0.11637 mmol were added to a 50ml RB to which 15ml ACN was added and stirred at ambient conditions (room temp) for 1 hour after which was filtered through a celite bed made in ACN, washed several times with ACN. The filtrate and washings were reduced to volume of 1ml to which diethyl ether was added resulting in the precipitation of the product which was vacuum filtered, washed with diethyl ether and pentane and dried to yield the desired product. (Yield: 0.048 g, 84 %). ^{1}H NMR (400 MHz, DMSO), δ (ppm): 6.12 (d, 1H), 6.75 (t, 1H), 6.90 (t, 1H), 7.41 (t, 1H), 7.62 (d, 1H), 7.93 (m, 2H), 9.15 (d, 1H). Elemental analysis for complex [Ir(ppy-COOCH$_3$)$_2$Cl]$_2$, $C_{26}H_{22}IrN_4$; (calculated) : C : 53.59, H : 3.81, N : 9.62; (found) : C : 53.72, H : 3.49, N : 9.85.

2.2 Results and Discussion

2.2.1 Ligand Preparation

Considering the synthesis of the ligand bpp (2-(6-(pyridin-2-yl)pyridin-3-yl)pyridine), the reaction was done between pyridyl zinc bromide and 2,5-dibromopyridine in a 2:1 molar ratio. The product was supposed to form by two catalytic cycle in the same reaction flask, in first catalytic cycle it forms 5-bromo bipyridine as the two position of 2,5-dibromo is more favourable to couple and in second catalytic cycle 5-bromo bipyridine acted as an aryl halide and it reacted with the excess pyridyl zinc bromide to form the final product. The synthetic reaction pathway is shown in figure 2.2. The ^{1}H NMR spectrum of the ligand bpp (2-(6-(pyridin-2-yl)pyridin-3-yl)pyridine) in d_6 DMSO is given in figure 2.4 (a)

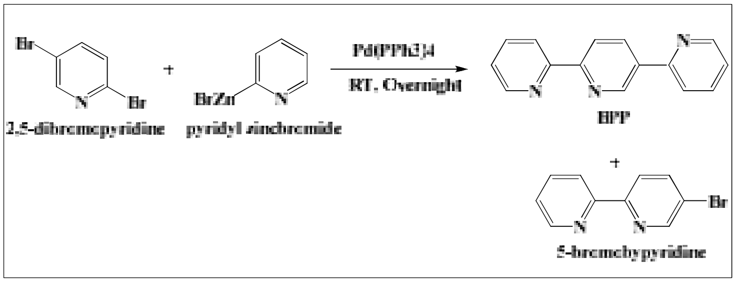

Figure 2.2 *General reaction pathway for the synthesis of BPP.*

Considering the synthesis of the ligand dpp (2,5-di(pyridin-2-yl)pyrazine) the published procedure consists of a three step reaction process,[3] starting with the preparation of the oxime, later on converting that to the tosyl ester and to the bridging ligand. The first two steps gave very high yields, but when coming on to the final step the yield was much reduced to less than 10 % which is similar to the ones reported. The procedure was modified by making changes in the final step, ie instead of stirring with NH_4OH, the ethanol solution after adding 2M HCl was left for two weeks which resulted in the precipitation of ligand as pure orange-red crystals with an increased yield of 17 %. The synthetic reaction scheme leading to the preparation of the ligand is shown in figure 2.3. The ^{1}H NMR spectrum of the ligand dpp (2,5-di(pyridin-2-yl)pyrazine) in d_6 DMSO is given in figure 2.4 (b)

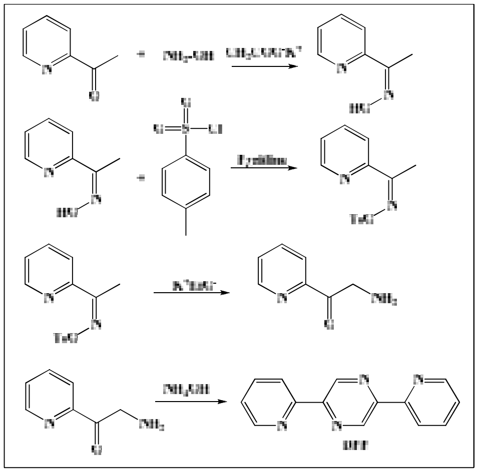

Figure 2.3 *General reaction pathway for the synthesis of dpp.*

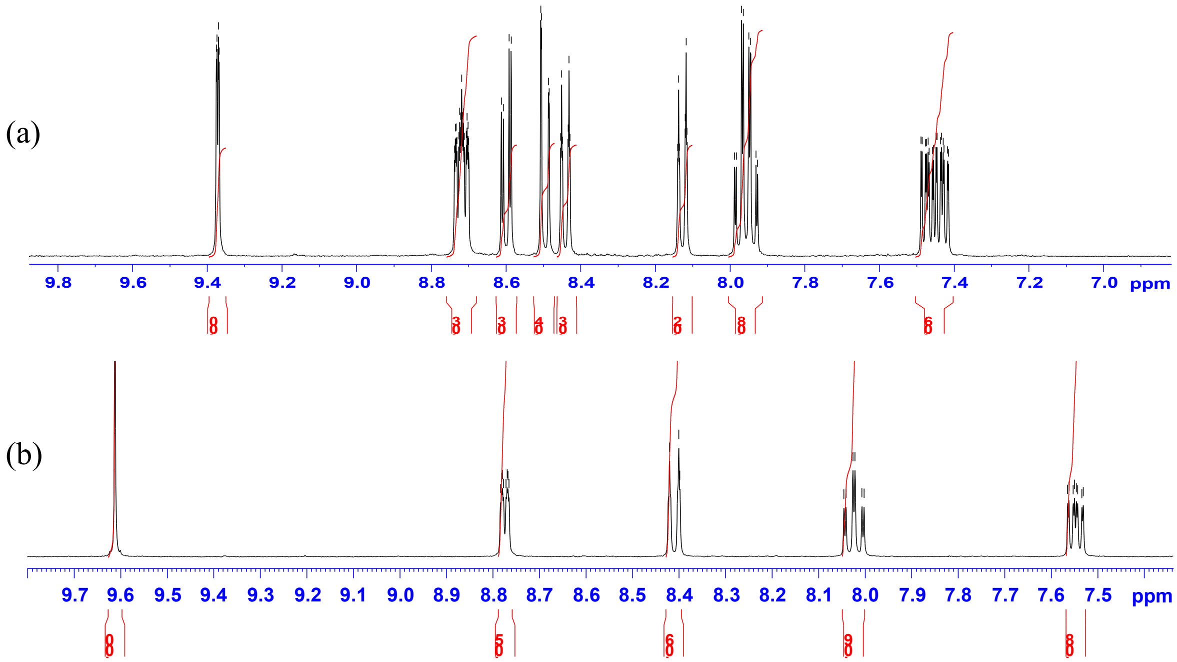

Figure 2.4 *^{1}H NMR Spectrum of bpp (a) and dpp (b) taken in d_6 DMSO.*

2.2.2 Cyclometallated iridium precursor synthesis

Iridium metal precursors with the cyclometallated ligands are all chloro bridged homo bimetallic dimers with general formulae $[Ir(L)_2Cl]_2$ where L is the cyclometallating ligand (eg: phenyl pyridine (ppy), thienyl pyridine (thpy), ppy-CHO, ppy-COOH, ppy-$COOCH_3$). The syntheses of these complexes were done following the reported procedure developed by Watts and co workers[4] as shown in figure 2.5, but necessary modifications have been done on the type of solvents, reaction temperature, reaction time and work up, based on different cyclometallated ligands. With phenyl pyridine the reaction was quite straight forward in ethoxyethanol and in methoxyethanol refluxed between 120 ^{0}C - 130 ^{0}C for 24 hours. The yellow precipitate formed at the end of the reaction is filtered and washed with diethyl ether and water many times, the nmr looks fine but the CHN was not fully correct, so the traditional Watts procedure of collecting the precipitate in a glass filter frit and washing it with ethanol and acetone first then dissolving the yellow precipitate left behind in DCM and precipitated by adding toluene and hexane was followed.[5] The reaction can also be successfully done in ethanol at normal reflux temperature.

Effort has been done to separate the tris iridium phenyl pyridine, [Ir(ppy)$_3$] in between the reaction, but was only partially successful.

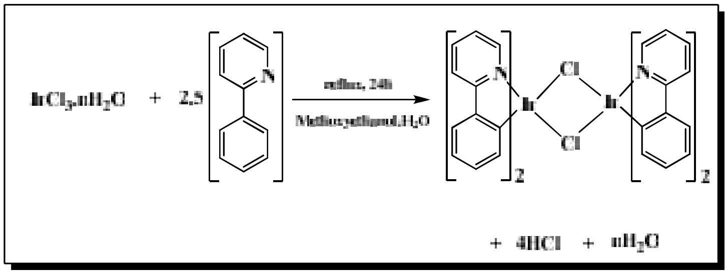

Figure 2.5 *Reaction scheme for the synthesis of cyclometallated iridium precursors taking the example of 2- phenylpyridine.*

These complexes were completely characterised using ^{1}H NMR, ^{13}C, COSY, HMQC, HMBC, mass spectrometry and elemental analysis. The 1D and 2D NMR data are given in appendix B. It was quite interesting to see the behaviour of this chloro bridged dimer complexes when their NMR was taken in different solvents. In $CDCl_3$ they give a neat spectrum of 8 proton signals coming from one phenyl pyridine, the same complex when taken nmr in DMSO gave 16 proton spectrum which suggests that the chloride bridge got ruptured and DMSO is coordinated in between resulting in the loss of symmetry of the entire complex, ie the two phenyl pyridine ligands are in two different planes and are different from one another. Similar behaviour is observed with other ligands. The NMR spectrums were shown in figure 2.6. In all these complexes, a doublet at about δ 5.9 and a triplet at δ 6.7 are assigned to the two protons of the phenyl ring ortho and meta to the metalated carbon atom, respectively. These assignments are consistent with previous assignments of high-field resonances in ortho-metalated bpy complexes.[5] Protons ortho and meta to the metalated C atom experience the largest shielding of any of the ligand protons.The nmr spectrum of complexes [Ir(thpy)$_2$Cl]$_2$ and [Ir(ppy-CHO)$_2$Cl]$_2$ in d$_6$ DMSO are given in appendix B.

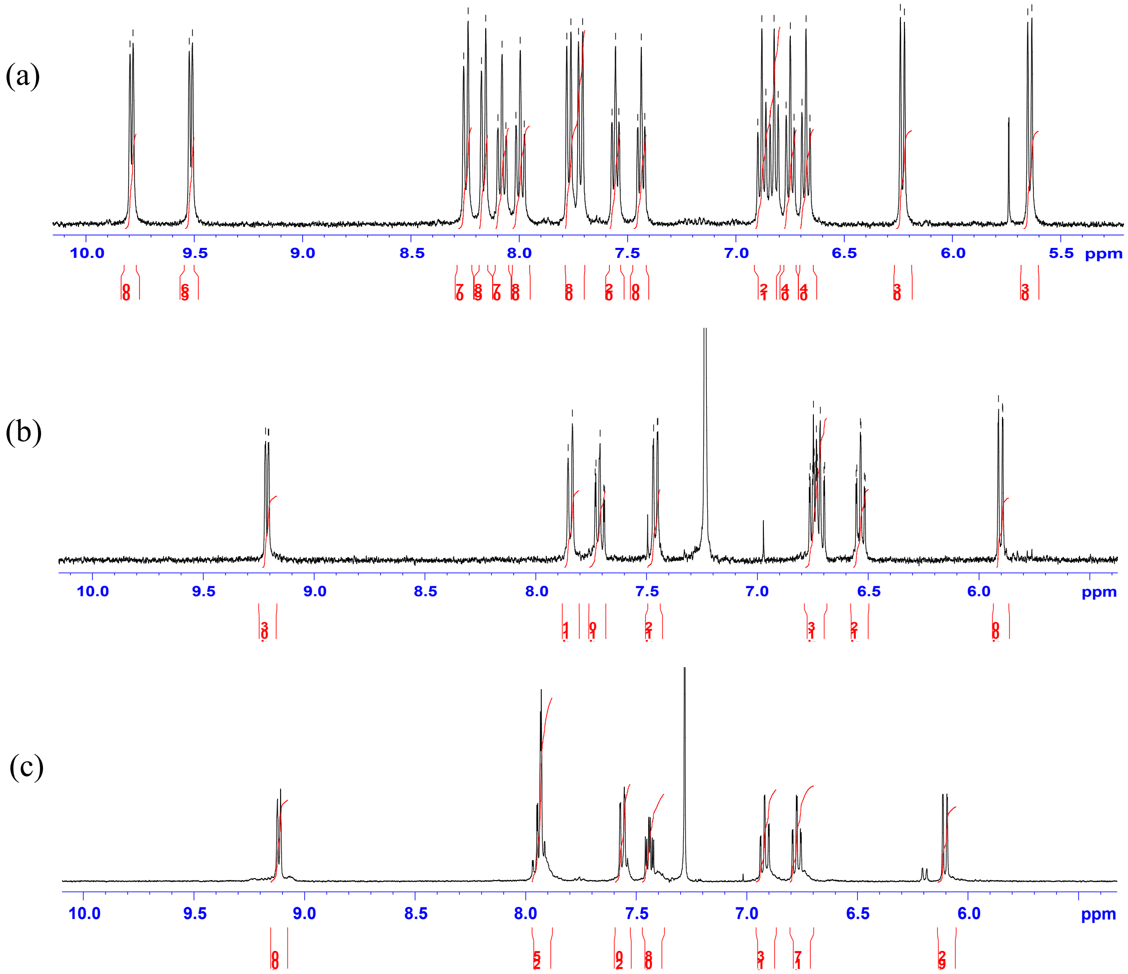

Figure 2.6 (a) *^{1}H NMR Spectrum of [Ir(ppy)$_2$Cl]$_2$ in d_6 DMSO.* ***(b)*** *^{1}H NMR Spectrum of [Ir(ppy)$_2$Cl]$_2$ in CDCl$_3$ and* ***(c)*** *^{1}H NMR Spectrum of [Ir(ppy)$_2$(ACN)$_2$] in d_6 DMSO.*

The actual aim consists of binding the entire photocatalytic system to the surface of a semiconductor and thereby replacing the sacrificial electron donor completely. For these type of systems to work properly the electron has to move from the semiconductor to the photocatalytic metal center for this the light absorbing unit (here the iridium center with the cyclometallated ligand) has to be attached to the surface of the semiconductor. For this some acid or ester functionality is required on the cyclometallated ligand by which the photo center can be easily binded to the surface. The phenyl pyridine ligand with carboxylic acid functionality was synthesised succesfully and protected by esterification into both ethyl and methyl esters. The ^{1}H

NMR and COSY data for these ligands are given in appendix B. The schematic representation of the synthetic scheme is given in figure 2.7 below.

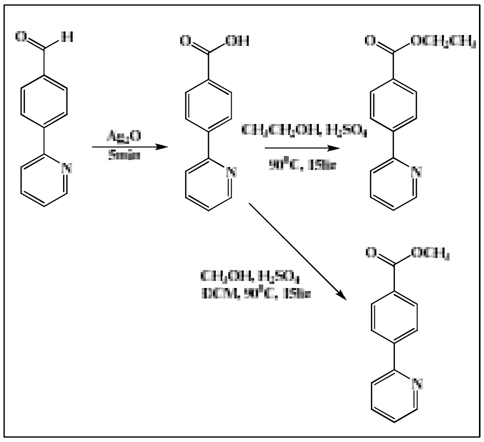

Figure 2.7 *General reaction pathways for the synthesis of ester phenyl pyridines.*

Also the reaction with the cyclometallating ligand ppy-COOH and its ethyl and methyl ester were not going satisfactionary in methoxyethanol but went fine in both ethanol and ethoxyethanol. In these cases the reaction went completely successful in pure ethanol itself since the acid and ester groups can be destroyed and a lot of side products are obtained when done in conventional solvents for this reactions. The NMR spectra for these complexes are shown in figure 2.12 and are discussed in chapter 3.

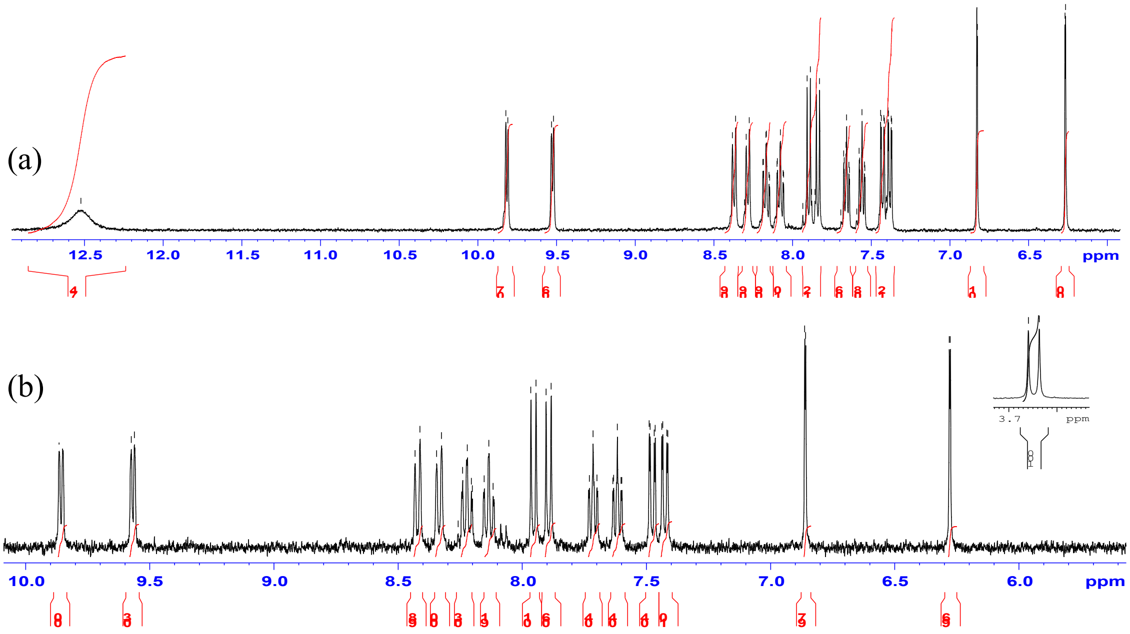

Figure 2.8 (a) *^{1}H NMR Spectrum of [Ir(COOH-ppy)$_2$Cl]$_2$ in d$_6$ DMSO.* ***(b)*** *^{1}H NMR Spectrum of [Ir(COOCH$_3$-ppy)$_2$Cl]$_2$ in d$_6$ DMSO.*

2.3 Chromatographic techniques

2.3.1 HPLC Measurements

High-Performance Liquid Chromatography (HPLC) was carried out using a Varian ProStar (model 335.71) photodiode array Detector, HPLC conjunction with Varian Star software, a Varian (model 210) pump, a 20 µl injector loop and a strong cation exchange Luna SCX 100A column (25 cm X 4.6 mm) provided by phenomenex . The column is packed with 5 µm particles and the operating pH range is between 2 and 8. The mobile phase for this work was 80:20 CH_3CN: H_2O: containing 0.1 M KNO_3. Filtered and degassed prior using the flow rate ranged 1.5 and 2 cm^3/min^{-1}. The monitoring wavelength used was 280 nm. The HPLC measurements were done with the help of Dr.Hamid M. Y Ahmed

2.3.2 Column Chromatography

Column chromatography was carried out on activated alumina (Al_2O_3, 150mesh) using acetonitrile or methanol as eluent or on silica gel (80/20, (v/v %) CH_3CN/H_2O). For the purification of $[Ir(bpy\text{-}N^\wedge N')_2(bpy\text{-}C^\wedge N')]^{2+}$, sephadex LH20 resin was used with methanol as solvent. Alumina and silica TLC plates used during the purification processes were purchased from Aldrich and used as received.

2.4 Nuclear Magnetic Resonance Spectroscopy

NMR spectroscopy is an invaluable tool not only in the identification of compounds but also in the monitoring of reactions and the determination of purity. It is used extensively throughout this thesis and where practical full assignment of ^1H and ^{13}C NMR spectra have been made using a combination of two dimensional techniques.[6]

2.4.1 ^1H, ^{13}C and ^1H COSY Spectroscopy

All ^1H NMR (400 MHz & 600 MHz), ^{13}C (100 MHz), COSY, HMQC, HMBC and DEPT-135 spectra were recorded on a Bruker AC400 (400 MHz) NMR spectrometer and Bruker Avance:3 (600 MHz) instrument. The chemical shifts were recorded relative to TMS and spectra were converted from their free induction decay (FID) profiles using XWIN-NMR software. All measurements were carried out in $(CD_3)_2SO$, $CDCl_3$ or $(CD_3)_2CO$ for ligands and CD_3CN or $(CD_3)_2CO$ for complexes. Peak positions are relative to residual solvent peaks. For ^1H COSY experiments 256 FID's, each of 8 scans, consisting of 1K data points were accumulated. After digital filtering using a sine bell squared function, the FID's were zero filed in the F1 dimension. Acquisition parameters were F1 = 500 Hz, F2 = 1000 Hz, $t_{1/2}$ = 0.001 s and the recycle delay was 1.5 s.

As an example of the potential of both 1D and 2D experiments in the elucidation of ^{1}H and ^{13}C NMR spectra, the following example is described in some detail. The compound 2-thiophen-2-yl-pyridine (thpy) contains a pyridyl and a thienyl moiety. The higher electron density of the pyridyl ring, and hence the larger ring current, results in a greater downfield shift of its resonances when compared with the thienyl proton resonances. The H6 resonance of the pyridyl ring is shifted downfield, with respect to the H4 and H5 protons, due to the proximity of the H6 with the electron withdrawing nitrogen atom of the pyridyl ring. ^{1}H COSY NMR spectroscopy (figure 2.12) shows as to the correlation between resonances using the "box" relationship. This allows for assignment of all peaks.

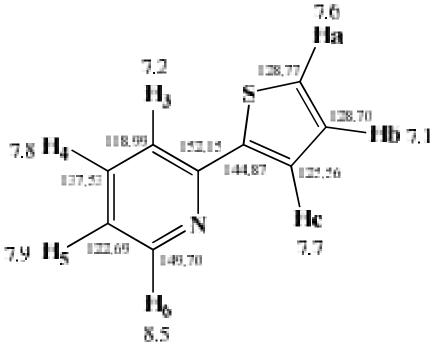

Figure 2.9 *Structure of pyth (2-Thiophen-2-yl-pyridine). δ in ppm*

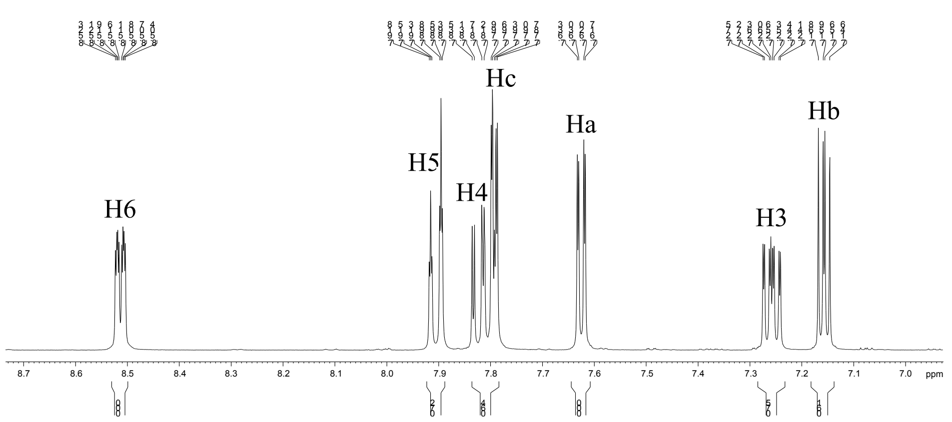

Figure 2.10 *^{1}H NMR spectra (400 MHz) of pyth in $(CD_3)_2SO$*

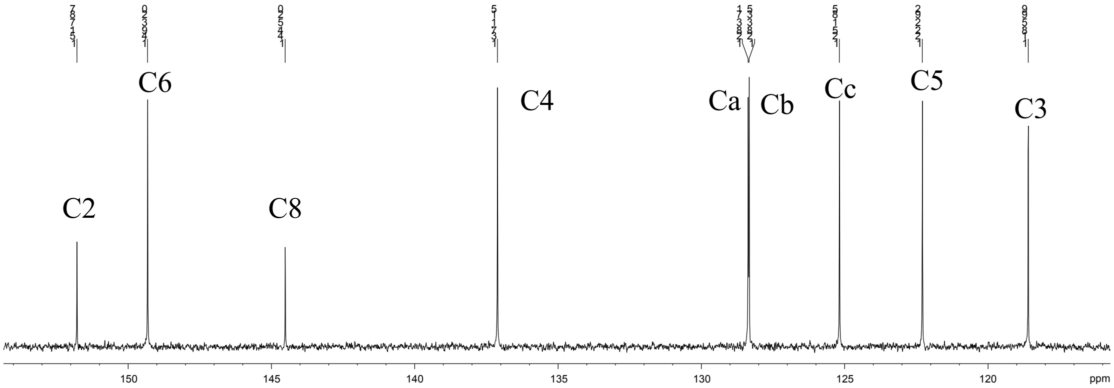

Figure 2.11 *^{13}C NMR spectra (400 MHz) of pyth in $(CD_3)_2SO$*

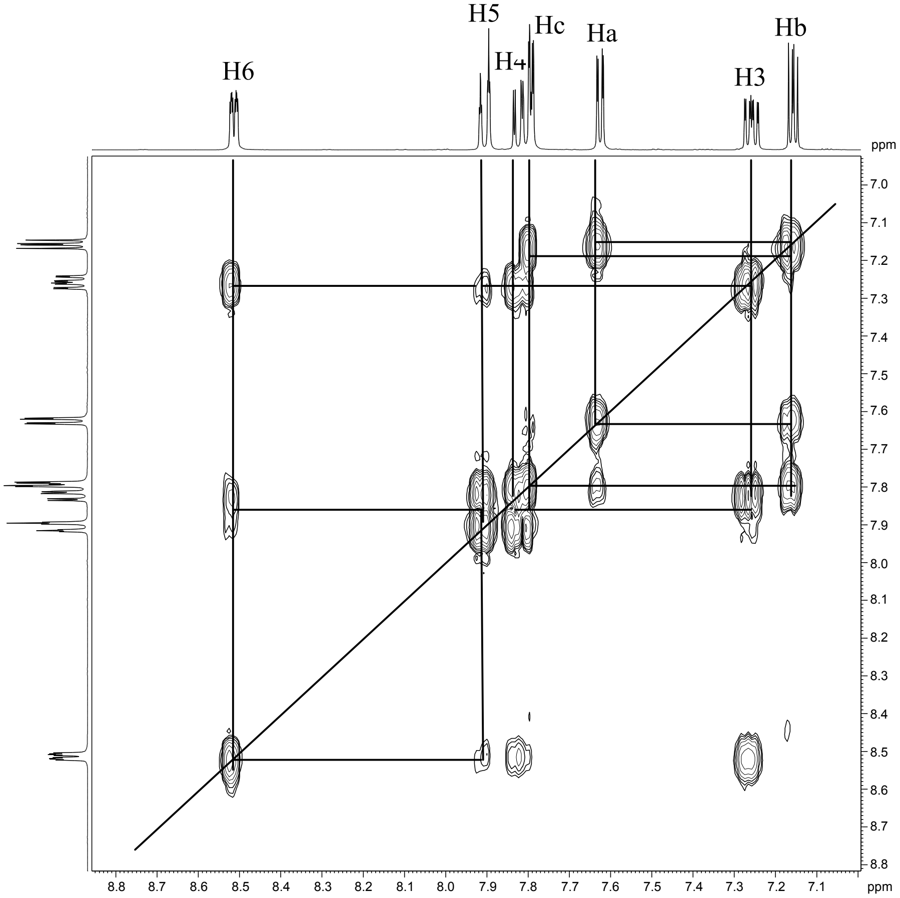

Figure 2.12 *^{1}H COSY NMR spectra (400 MHz) of pyth in $(CD_3)_2SO$*

2.5 Electronic Spectroscopy

Electronic spectroscopy is principally concerned with the absorption of electromagnetic radiation resulting in direct excitation of molecules to higher electronic energy states. Such transitions may, in the case of gaseous samples of simple molecules, result in very sharp well-defined spectra. However in condensed phases the bands observed are considerably broadened. This broadening arises primarily from three sources: doppler broadening, rotational energy level transitions and vibrational energy level transitions. Perturbation of energy levels by solvation adds to this broadening significantly.[7] A detailed discussion of these effects is beyond the scope of this thesis, however the area has been dealt with in detail by several authors.[8] Despite this electronic spectroscopy is an invaluable tool in the characterisation of the elctronic properties and excited state processes of molecules and, in the case of this thesis, of the iridium polypyridyl complexes.[9]

2.5.1 Absorption Spectroscopy

Absorption spectroscopy measures the transition of atoms and molecules between different electronic states. As the name suggests, the technique relates to the absorption by molecular species of light with wavelength between 200-800 nm. It is generally assumed that radiation in the infrared and microwave regions of the radiative spectrum are too low in energy to cause significant perturbations of the electronic structure of the species. The most important equation in absorption spectroscopy is the Beer-Lambert law, defined in equation 2.1 below.[10] It relates absorbance (the intensity of the light absorbed) to the path length of the light, l, and the concentration of the species in the solution, c.

$$Abs = log_{10}\left(\frac{I_0}{I_t}\right) = \epsilon cl \qquad \textbf{\textit{Equation 2.1}}$$

I_o and I_t are the incident and transmitted light intensities, respectively. ε is referred to as the molar extinction coefficient, and is a measure of the strength of the transition between the ground state and the excited state. A large value of ε indicates that the transition is almost fully allowed, such as the Metal to Ligand Charge Transfer (MLCT) process in $[Co(NH_3)_5Br]^{2+}$, where ε_{max} at 250nm = 20,000 $M^{-1}cm^{-1}$. In order to put this value in perspective, ϵ_{max} of the ligand field transition for the same complex at 550 nm is just 50 $M^{-1}cm^{-1}$ and is considered as a spin forbidden process.[10] The transition metal can sometimes affect the electronic structure, in such a way that certain transitions that are formally forbidden actually occur, with reasonably high molar extinction coefficients. In order for the measurement to be accurate, the absorbance should not be too low, as this makes it difficult to distinguish the actual peak from the baseline noise. However if the absorbance value is too high, this indicates that all the light has been absorbed by the sample and therefore the amount of light available for the measurement is not enough for a statistically accurate measurement to be made.

The UV measurements presented throughout this work were recorded on a Agilent 8453 UV-Vis Spectrophotometer, the spectra were obtained in the wavelength range 200 to 800 nm. Samples were measured in quartz cuvettes with a 1.0 cm path length. All the solvents were spectrometric grade and used without further purification.

2.5.2 Emission Spectroscopy

Emission spectroscopy is the investigation of the radiative relaxation processes which a complex may undergo during the transition between its excited state and its ground state. The excited state is formed via the absorption of light, followed by the relaxation to the thermally equilibrated (THEXI) state. The life time of the THEXI state can range from ns to ms, and its formation occurs on sub-nanoseconds timescale.[11] Steady state emission spectroscopy is used to investigate this steady state, via the intensity and energy of the emitted light.

It is important to note that sample preparation and concentration are just as important in emission spectroscopy as they are in UV-Vis absorption spectroscopy. Samples that are too highly concentrated have been observed to re-absorb the emitted light, leading to an overall decrease in the intensity of the emission. This is known as the inner filter effect. The other possibility is that samples that are too weakly concentrated have such low signal intensity that the signal to noise ratio becomes a major issue, and the error in the measurement becomes more apparent. Most of the samples for which the life time data was obtained were measured in four solvents, usually ACN, DCM, MeOH and $CHCl_3$. The reason for the use of these solvents was to investigate effect of solvent on the emission energy and intensity which helped us in assigning the various excited state from which emision occurs in the case of Ir (III) complexes. The solvent can sometimes play a key role in the stabilisation of the excited state of the complex, and this can affect the energy of the emission. The solvent generally affects the charge transfer states such as MLCT and LMCT to a greater degree than it affects the metal (d-d) and the ligand centered (π-π*) states. This is due to the large change in dipole upon the formation of the excited state,[12] which does not occur to the same amount in the MC and LC states, as the electron is not displaced as much.

All emission spectra were recorded using a Perkin Elmer LS50B Luminescence spectrophotometer, which was interfaced with an Elonex-466 PC via Windows 3.1 based fluorescence data manager software, FL Winlab, and a Varian UV Fluorimeter, using Cary UV software. Excitation and emission slit widths were usually set to 10 nm and 15 nm, but 5nm slits were also used, depending on the condition required. For low temperature measurements sample solutions in a pyrex tube were mounted in an Oxford Instruments Liquid Nitrogen PE1704 cryostat as shown in figure 2.13. An Oxford Instruments Intelligent Temperature Controller ITC 601 was used to adjust the temperature of the sample to the desired value. The excitation wavelength was 360 nm for both the room temperature and the low temperature measurements. Room temperature measurements were performed at 293K and low temperature measurements were carried out from 77 K to 280 K. The emission wavelength for the solution based samples varied with each sample, as required.

Figure 2.13 *Instrumental arrangement for measuring low temperature emission using cryostat*

2.5.3 Deaeration using freeze pump thaw method

Degassing is done very efficiently using the freeze pump thaw method using the apparatus shown in figure 2.14. The sample solution was first taken in a glass apparatus having a cuvette at one end and a glass bulb attached to it. The solution was kept in the glass bulb which is connected to the apparatus. A bowl of liquid N_2 was placed under the glass bulb in order to freeze the solution. The freeze pump thaw procedure was repeated 3 times, so that all dissolved gases were removed.

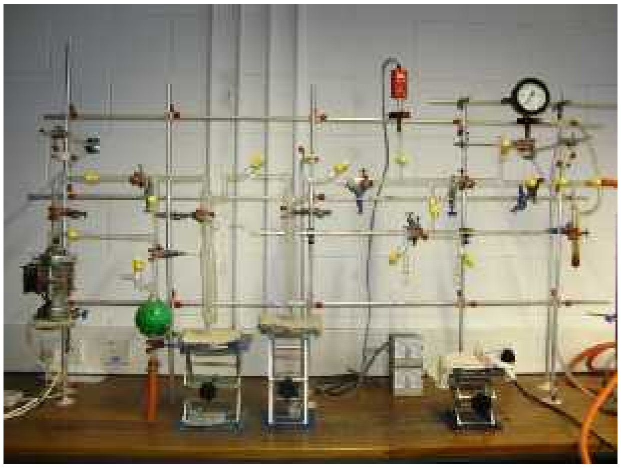

Figure 2.14 *Apparatus for freeze pump thaw method of deaeration*

2.5.4 Emission Quantum yield measurements

Quantum yield measurements were carried out by the optically dilute method[13] by comparison with $[Ru(bpy)_3](PF_6)_2$[14] in aerated/deaerated acetonitrile. Emission spectra were obtained at a wavelength where the absorption by $[Ru(bpy)_3](PF_6)_2$ and the sample under examination are equal. The area under the emission spectrum (A) of each sample was calculated using the spectrometer supplied software and the quantum yield was calculated from Equation 2.2:

$$\Phi_{unkown}/\Phi_{[Ru(bpy)_3](PF_6)_2} = A_{unkown}/A_{[Ru(bpy)_3](PF_6)_2} \qquad \textbf{Equation 2.2}$$

Where Φ is the quantum yield and A is the area under the emission spectrum. As all quantum yield measurements were carried out in acetonitrile, compensation for refractive indices is unnecessary.

Several factors must be accounted for in the determination of quantum yield values. Measurements must be carried out at the same temperature (preferably in a thermostatic bath when a large temperature dependence of emission intensity is observed). Quenching of emission is another problem and can arise from one or more sources eg: dissolved gasses $^3O_2$, electron transfer agents (eg. Methyl-viologen), concentration quenching (inner filter effects) and the presence of impurities such as water and protic solvents. Another common error is that of over concentrated samples. To avoid this, sample and standard are prepared in such a way that their optical densities at the overlapping point in absorption spectra should be approximately of 0.05.

2.6 Time Correlated Emission

This technique measures the lifetime of the excited state of the molecules. The method of operation of single photon counter (SPC) is discussed in detail below. Briefly the molecules are excited by N_2 flash lamp or an LED lamp of proper wavelength, and the emission of the sample is detected. The time difference between the emission of the initial lamp photon and the photon emitted by the excited state molecule is measured.

Time resolved emission measurements were performed on various Iridium and Ruthenium polypyridyl based complexes, bearing various conjugated polycyclic moieties, and modified pyridine ligands. These measurements were performed to compliment steady state measurements such as quantum yields and fluorescence, discussed in more detail in chapters 3, 4 and 5. The measurements are closely related and this relationship is described in equation 2.3 below.

$$I_{SS} = \int_0^{\infty} I_0 e^{-\frac{t}{\tau}} dt = I_0 \tau \qquad \textbf{\textit{Equation 2.3}}$$

where I_0 is the illumination intensity, τ is the lifetime of the excited state, and I_{SS} is the intensity of the steady state emission. It is possible to extract further information regarding the excited state processes of the system using time resolved emission techniques, as the lifetime and the number of decays are both valuable pieces of information. For low temperature (77 K) measurements sample solutions in a pyrex tube were mounted in an Oxford Instruments Liquid Nitrogen PE1704 cryostat. An Oxford Instruments Intelligent Temperature Controller ITC 601 was used to adjust the temperature of the sample to the desired value. The excitation wavelength was 360 nm. The emission wavelength for the solution based samples varied with each sample, as required.[15]

2.6.1 Time Correlated Single Photon Counting (TCSPC) Techniques, Nanosecond Time Resolved Single Photon Counting Measurements.

The life time measurements were carried out using an Edinburgh Instruments Single Photon Counter (TCSPC), with an LED excitation source of wavelength 360 nm as shown in figure 2.15 below. Spectrometric grade solvents were used for measurements. Deaeration was done using freeze-pump-thaw method.

Figure 2.15 *TCSPC apparatus used for the lifetime measurements*

A schematic diagram of the SPC system is shown in figure 2.16. The system is comprised of two main components, the excitation source and the detection system. The excitation source is an EPLED - 360 LED source.

The method of operation of Single Photon Counter is described as follows. A photon of light is emitted from a nano flash lamp and travels via an optical cable to the START detector. When this photon is detected by the START detector the TAC (Time to Analogue Converter) initiates a voltage ramp. Simultaneously, another photon passes the excitation monochromator, which is set to the appropriate excitation wavelength. This photon is then absorbed by the sample. The re-emitted photon then passes through the filter and also through an emission monochromator, which has been set to the desired emission wavelength of the sample.[10,13]

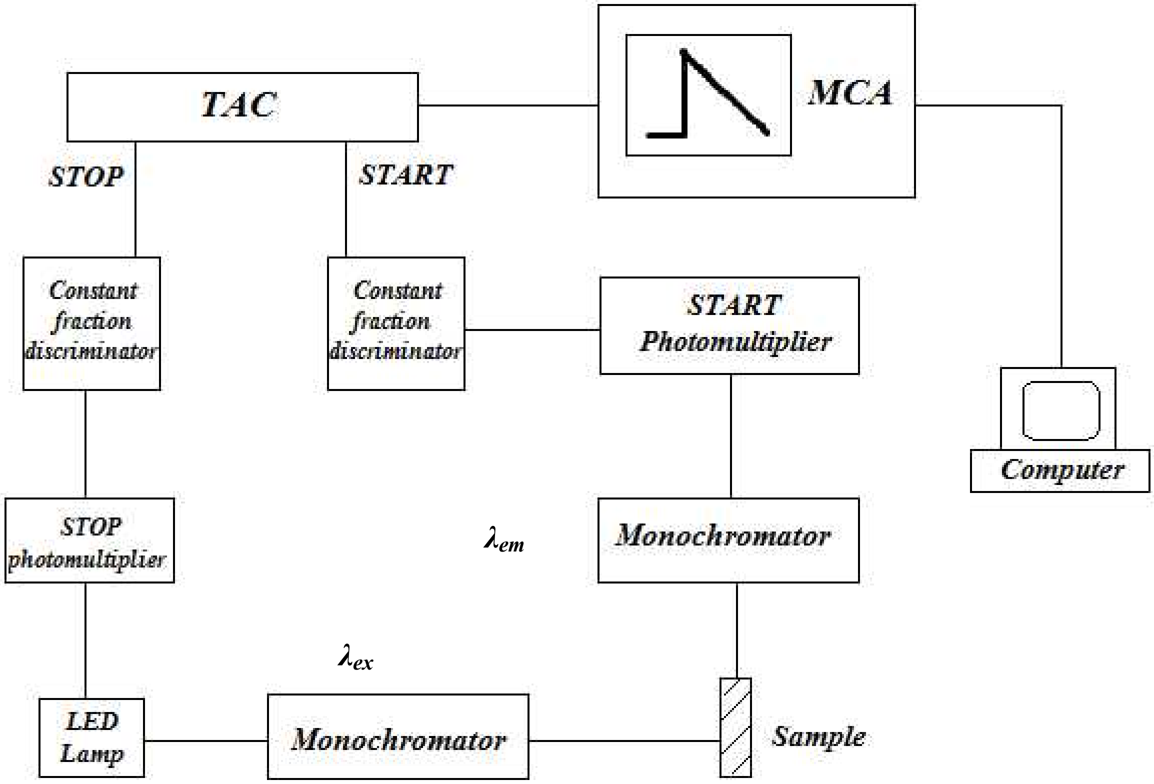

Figure 2.16 *Schematic diagram of TCSPC apparatus*

The voltage ramp is stopped when the STOP detector receives a photon of light from the sample. Both the START and the STOP detector contain signal amplifiers, which may be varied to adjust the sensitivity of the instrument. The signal amplifiers are related to the potential bias applied to the photomultiplier tubes, and therefore the lifetime of the tubes may be reduced if too high voltage is applied. The time range is split into 1024, 2048, and 4096 channels, depending on the settings chosen by the operator. Each of these channels is assigned a range of voltages corresponding to a certain time range. The Multi Channel Analyser (MCA) records the number of times a specific voltage is obtained in each of the channels. A spectrum of voltages and therefore time differences is produced by the MCA memory and the experiment is terminated when a sufficient number of counts are collected. The number of counts collected depends on a number of factors.

- The signal to noise ratio
- The number of decays in the sample
- The presence of scatter from the sample

It is sufficient in most experiments to obtain 1000 counts in order to get a good quality fit after data analysis, a process which will be discussed later. The detector contains a red sensitive S900-R photomultiplier. It has a working range of 160-870 nm, due to the quartz glass in its side window. This detector is generally operated within Peltier element cooled housing at 50 K below ambient temperature, so as to reduce dark counts. It is still necessary to perform some measurements in the dark, if emission arm filters are removed.

2.6.2 Analysis of TCSPC Data

There are two methods by which the data from the decay of the excited state, which is obtained from the lifetime measurement, can be analysed using the F900 program Version 6.24 namely, Reconvolution Fit and Tail Fit. Reconvolution Fit takes into account the finite nature of the excitation pulse, and the possibility that the sample decay is convoluted with the excitation pulse. The convolution integral (Equation 2.4) shows the mathematical relationship between the sample response function (X(t)), the instrument response function (E(t)) and the sample decay model (R(t)):[16]

$$X(t) = \int_0^t E(t)\, R(t - t')dt' \qquad \textbf{\textit{Equation 2.4}}$$

Reconvolution fit can be used to completely describe the data, apart from noise. It will fit the rise of the signal, the initial part of the decay, and the tail. The second data analysis method within the software is the tail fit. In this method X(t) is considered to be equal to R(t), and the instrument response is considered negligible. Since this is the case with most of the measurements described in this work, this is the method of analysis used unless otherwise stated. Once the method of fit has been chosen, the lifetime value is calculated by fitting the experimental decay to the equation 2.5;

$$R(t) = A + B_i e^{-\frac{t}{\tau i}}$$ ***Equation 2.5***

Where R(t) is the sample decay model, B_i is the pre-exponential factor, τ_i is the characteristic lifetime and A is an additional background. The Marquardt-Levenberg algorithms used to search for the best values of B_i and τ_i.[14,17,18] The quality of the life time data is assessed by two criteria, the reduced Chi-squared χ^2, and the nature of the residuals data. The χ^2 value is obtained by dividing the goodness of fit $\chi_g{}^2$, which itself is ultimately found by Marquardt-Levenberg algorithms, by the number of free parameters, n, (which is approximately the number of fitted points divided by the number of lifetime parameters used in the fit) and is shown in equation 2.6 below. The data follows a Poisson distribution, and therefore the χ^2 has a theoretical limit of 1.0. values above indicates a bad fit of the data and the values below 1.0 are the result of poor choice of the fitting range.[10,14] The F900 program also displays the residuals in the graph of residual value aganist time(ns). This is inspected visually to ensure that the residuals are more or less random in nature, and to ensure the absence of peaks or tails of peaks at the beginning of the trace. These peaks would suggest the presence of a very short lifetime, in addition to a longer decay, and can also indicate other processes such as energy transfer.

$$\chi 2 = \sum W_{k^2} \frac{[x_k - F_k]^2}{n}$$ ***Equation 2.6***

A common property found for many of the iridium (III) complexes examined in this thesis is that emission decays biexponentially and the long lived and short lived components behave differently. The percentage of the short lived and long lived components are clearly given for each decay. The χ^2 values, which are known as the fitting parameter, determine fine fit for the bi-exponential decay and are found to be ~1 and the average lifetime (τ_{av}) is calculated using the equation 2.7.[19]

$$\tau_{av} = \frac{\alpha_1\tau_1{}^2 + \alpha_2\tau_2{}^2}{\alpha_1\tau_1 + \alpha_2\tau_2}$$ ***Equation 2.7***

where $\boldsymbol{\alpha}_1$ and $\boldsymbol{\alpha}_2$ are the pre-exponential factors, which give the abundance of each emissive state and $\boldsymbol{\tau}_1$ and $\boldsymbol{\tau}_2$ are the lifetime values of the two emissive states. All the measurements were done at two different time ranges in order to make sure that the value for the lifetimes are accurate, all the datas for normal and deuteriated ones in different time ranges are plotted with the decay fit.

2.7 Laser flash photolysis for lifetime measurements

A schematic diagram of the laser flash photolysis instrumentation is given in figure 2.17. The excitation source is a neodymium yttrium aluminium garnet (Nd:YAG) laser, which operates at a frequency of 1064 nm. The host YAG crystals are implanted with Nd atoms of approximately one part per hundred. The main advantage of the YAG host material is its relatively high thermal conductivity which removes wasted heat, thus allowing these crystals to operate at high repetition rates of many pulses per second. Using non linear optics, the fundamental frequency of 1064 nm can be doubled, tripled or quadrupled to generate a second, third or fourth harmonic frequency at 532, 355 or 266 nm respectively. This allows specific excitation pathways within a system to be selected. Amplification of the laser power can be carried out by varying the voltage across an amplifier flash tube. At a frequency of 355 nm, the energy generated is typically 35 mJ per pulse and the lifetime of the laser pulse approximately 10 ns.

The circular laser pulse is diverted *via* a Pellin Broca prism through an optical trigger (which prepares the transient digitiser) onto the sample cuvette. The transient digitiser (a Hewlett Packard HP 54510A oscilloscope) detects the transient species. A Hamamatsu 5 stage photomultiplier operating at 850 V is situated at the exit slit of the monochromator. Following activation of the optical trigger the transient digitiser (oscilloscope) measures changes in the emission *via* a variable load transistor.

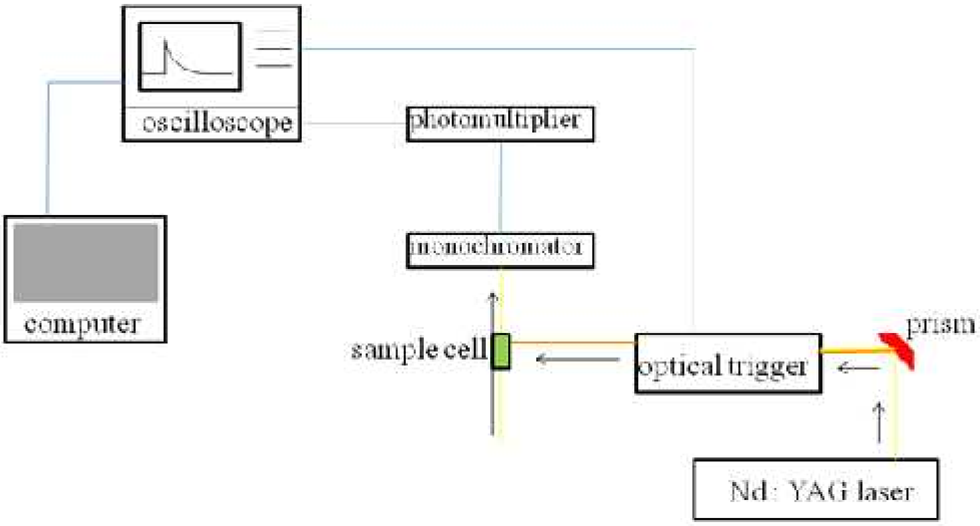

Figure 2.17 *Schematic diagram of laser flash photolysis instrumentation.*

2.8 Gas chromatography for measuring H_2 from Supramolecular Photocatalysts

2.8.1 Principles

Chromatography is a very important analytical tool because it allows the chemist to separate components in a mixture for subsequent use or quantification. Most samples that chemists want to analyze are mixtures. If the method of quantification is selective for a given component in the mixture, separation is not required. However, it is often the case that the detector is not specific enough, and a separation must first be performed. There are several types of chromatography depending on the type of sample involved. In this experiment, gas chromatography was used. The gas chromatograph makes it possible to separate the volatile components of a very small sample and to determine the amount of each component present. The essentials required for the method are an injection port through which samples are loaded, a "column" on which the components are separated, a regulated flow of a carrier gas which carries the sample through the instrument, a detector, and a data processor. In gas chromatography, the temperature of the injection port, column, and detector are controlled by thermostatic heaters.

2.8.2 Injection Port

The sample to be analyzed is loaded at the injection port via a gas tight syringe. The injection port is heated in order to volatilize the sample. Once in the gas phase, the sample is carried onto the column by the carrier gas, in our case nitrogen. The carrier gas is also called the mobile phase. The gas chromatographs are sensitive instruments. Typically samples of fifty micro litres or less are injected on the column.[20]

2.8.3 Column

The column is where the components of the sample are separated. The column contains the stationary phase. The gas chromatography columns are of two types - packed and capillary. Capillary columns are those in which the stationary phase is coated on the interior walls of a tubular column with a small inner diameter. The stationary phase in our column is a polysiloxane material. The basic structure of the polymeric molecules is shown below (figure 2.18), where n indicates a variable number of repeating units and R indicates an organic functional group. In our columns, 5 % of the "R's" are methyl groups (-CH_3) and 95 % of the "R's" are phenyl groups (-C_6H_5).[20]

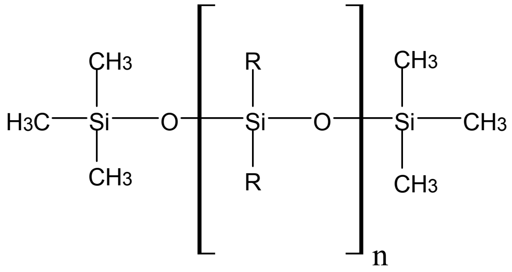

$$H_3C-Si(CH_3)_2-O-\left[Si(R)_2-O\right]_n-Si(CH_3)_2-CH_3$$

Figure 2.18 *Polysiloxine material used in our columns*

This polymeric liquid has a high boiling point that prevents it from evaporating off the column during the experiment.

The components in the sample get separated on the column because they take different amounts of time to travel through the column depending on how strongly they interact with the stationary phase. As the components move into the column from the injection port they dissolve in the stationary phase and are retained. Upon re-vaporization into the mobile phase they are carried further down the column. This process is repeated many times as the components migrate through the column. The components that interact more strongly with the stationary phase spend proportionally less time in the mobile phase and therefore move through the column more slowly. As described above, the rate at which compounds move through the column depends on the nature of the interaction between the compound and the stationary phase. Other variables that affect this rate are column temperature and carrier gas flow rate.

2.8.4 Detector

If the column conditions are chosen correctly, the components in the sample will exit the column and flow past the detector one at a time. There are several different types of detectors common to gas chromatography instruments. The choice of detector is determined by the general class of compounds being analyzed and the sensitivity required. Our gas chromatographs are equipped with thermal conductivity detector (TCD) and flame ionization detectors (FID). The FIDs, see figure 2.19 – are the most widely used detectors for organic samples. FIDs use an air/hydrogen flame to pyrolyze the effluent sample. The pyrolysis of the compounds in the flame creates ions. A voltage is applied across the flame and the resulting flow of ions is detected as a current. The number of ions produced, and therefore the resulting current, depends on the flame conditions and the identity of the molecule in question. In other words, the detector shows a different response to each compound. For this reason, separate calibrations were performed for each compound analyzed. The FID is extremely sensitive with a large dynamic range, its only disadvantage is that it destroys the sample.[20]

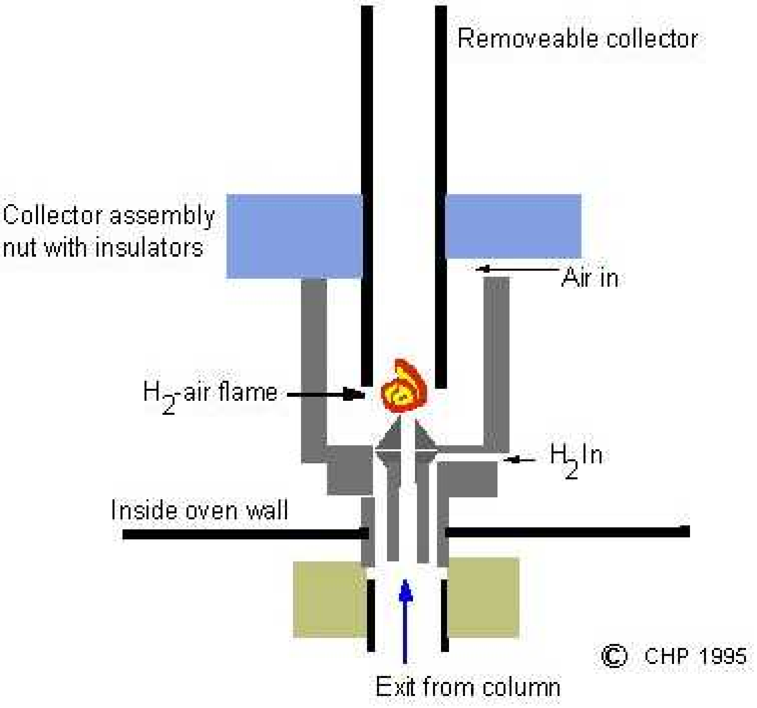

Figure 2.19 *Schematic of Flame Ionization Detector.*[20]

A TCD, see figure 2.20 consists of an electrically-heated wire or thermistor. The temperature of the sensing element depends on the thermal conductivity of the gas flowing around it. Changes in thermal conductivity, such as when organic molecules displace some of the carrier gas, cause a temperature rise in the element which is sensed as a change in resistance. The TCD is not as sensitive as other detectors but it is non-specific and non-destructive. Two pairs of TCDs are used in gas chromatographs. One pair is placed in the column effluent to detect the separated components as they leave the column, and another pair is placed before the injector or in a separate reference column. The resistances of the two sets of pairs are then arranged in a bridge circuit.

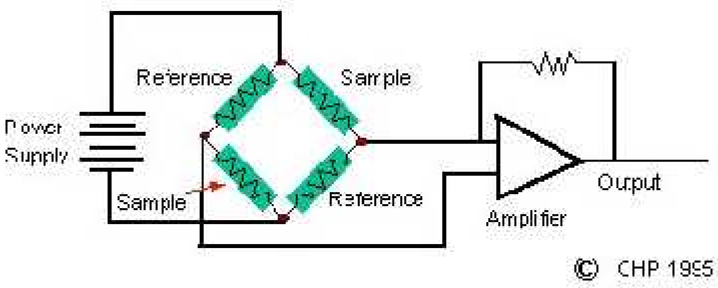

Figure 2.20 *Schematic of a bridge circuit for TCD detection.*[20]

The bridge circuit allows amplification of resistance changes due to analytes passing over the sample thermo conductors and does not amplify changes in resistance that both sets of detectors produce due to flow rate fluctuations.

2.8.5 Integrating Recorder

The output of the detector (converted from current to voltage) is sent to an integrating recorder that plots, stores, and analyzes the data. A typical chromatogram is shown in Figure 2.21. The detector voltage (y-axis) is plotted as a function of time (x-axis). Each peak corresponds to a separate component. The time it takes for a given peak to appear after injection is called the retention time. If the column conditions are kept constant, the retention time for each component is quite reproducible from one sample and injection to the next. The identity of each peak can be determined by injecting pure samples of the individual components of the mixture and noting their retention times. The voltage from the detector is proportional to the number of molecules passing through the detector at any given time.

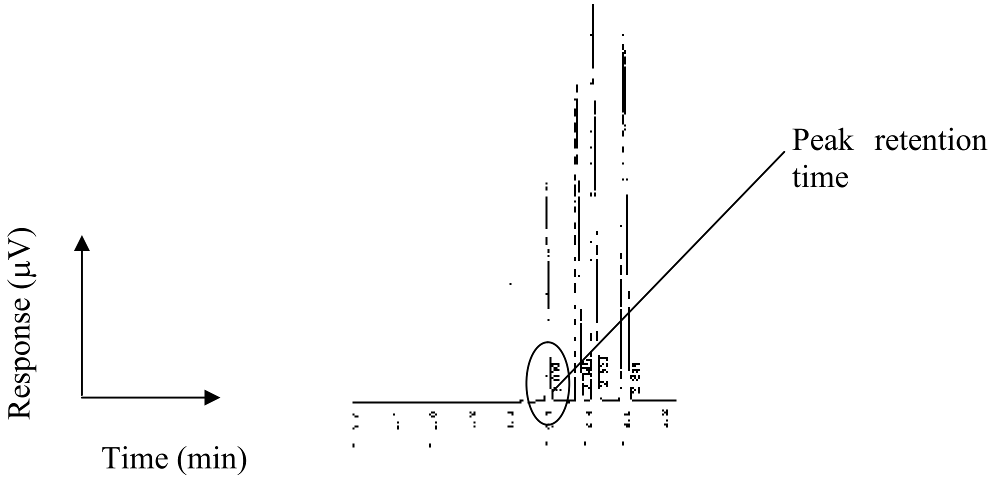

Figure 2.21 *Sample chromatogram* [20]

For well-separated peaks, the total number of molecules of each component reaching the detector is then proportional to the area under the peak. The recorder determines the area of each peak by integration and reports this in the results table. The proportionality factor between area and amount must be determined by a calibration experiment.[20]

2.8.6 TONs Calculations

TON for hydrogen and oxygen are calculated by the below mentioned equation,

$$\mathbf{TON} = \frac{\mathbf{[(vol.\ of\ gas)\ x\ atm.\ pressure\ x\ (ppm\ of\ gas\ /\ 10^{6})]\ /\ Gas\ constant\ x\ Temperature}}{\mathbf{Mass\ of\ complex\ /\ Mol.\ Weight\ of\ complex}}$$

Volume of the gas = in Litre,

Pressure = 1 atm,

Temperature = in Kelvin,

Gas constant = 0.082 L atm / K mol

Mass of the complex = gm,

Molecular weight = gm / mol.

The ppm of a particular gas is calculated by the area under the particular peak in the gas chromatogram in mVolt/sec. Then afterward area is changed to ppm by standard gas equation.

2.8.7 Photo catalytic experiments

The photo catalytic hydrogen production experiments were performed under argon atmosphere as follows. For the photolysis reaction in acetonitrile, the septa capped deoxygenated photolysis reaction vial (5ml full volume) containing 2 ml of the reaction solution containing the metal complexes (5x10^{-5}M), electron donor triethylamine (sacrificial agent) (16.6 % (v/v) and water (3.3% (v/v)) was used. The solutions were photolysed using blue light (470 nm) and UV light (350 nm) LED light array shown in figure 2.22. After 18 h photolysis time, the amount of hydrogen produced was measured by gas chromatography using gas tight syringe. Samples of the syringe (20 µL) were injected into a series CP-3800 Gas Chromatograph equipped with a 5 Å molecular sieves column and polymer supported silica column purchased from Varian Inc (UK) using ultra-high purity nitrogen as the carrier gas. The signals were amplified with a Varian Star Workstation chromatography Data system. The system was calibrated for hydrogen signal sensitivity by hydrogen standard measurements. The total amount of hydrogen produced in a photolysis experiment was obtained by the sum of hydrogen found in the gas phase as well as the hydrogen in the solution. The amount of hydrogen in the solution was calculated according to Henry's law using the reported solubility of hydrogen in acetonitrile as 1.78 x 10^{-4} (mole fraction). [21]

Figure 2.22 *This photography shows the reactor where the catalytic solutions were irradiated by blue LEDs (470 nm wavelength, 8000 mcd illumination capacity).*

2.9 Mass Spectrometry

Mass spectra were recorded with a Bruker-Esquire LC-00050 electrospray ionisation mass spectrometer at positive polarity with cap-exit voltage of 167 V. Spectra were recorded in the scan range of 50-2200 m/z with an acquisition time of between 300 and 900 µs. Each spectrum was recorded by summation of 20 scans. Spectra were collected by constant infusion of the analyte dissolved in acetonitrile, with a positive ion polarity. Samples were prepared by dissolving ~2 mg of sample in 1 mL of acetonitrile. 50 μL of this solution was then taken and diluted by the addition of 1ml of acetonitrile and this solution was then used to acquire the mass spectrum.

2.10 Elemental Analysis

Carbon, hydrogen and nitrogen (CHN) elemental analyses were carried out on an Exador Analytical CE440 by the Microanalytical Department, University College Dublin. The CHN analyzer used an Exador analytical CE440. It should be noted that when calculating the overall mass of deuteriated complexes the additional mass of the deuterium was included but when calculating the percentage of hydrogen and deuterium in the sample all protons and deuterons were treated as protons.

2.11 Bibliography

---

1. W.R. Browne, C. M. O'Connor, J. S. Killeen, A. L. Guckian, M. Burke, P. James, M. Burke and J.G. Vos, *Inorg. Chem.*, **2002**, 41, 4245.
2. W. R. Browne and J. G. Vos, *Coord. Chem. Rev.*, **2001**, 219, 761.
3. G. Denti, S. Campagna, L. Sabatino, S. Serroni, M. Ciano, V. Balzani, *Inorg. Chem.,* **1990**, 29, 4750.
4. S. Sprouse, K. A. King, P. J. Spellane and R. J. Watts, *J. Am. Chem. Soc.,* **1984**, 106, 6647.
5. P. J. Spellane, R. J. Watts, C. J. Curtis, *Inorg. Chem.,* **1983**, 22, 4060.
6. (a) G. Binsch and H. Kessler, *Angew. Chem., Int. Ed. Engl.,* **1980**, 19, 411 (b) R. W. King and K. R. Williams, *J. Chem. Ed.,* **1990**, 67, 101 (c) P. Crews, J. Rodriguez, *Organic Structural Analysis, Oxford University press*, Oxford, **1998**
7. A. B. P. Lever, Inorganic Electronic Spectroscopy, **1984**, page 863
8. (a) C. N. R. Rao, *"Ultraviolet and visible spectroscopy: chemical applications"*, Butterworth and Co. Ltd., UK, **1975** (b) R. J. H. Clark, T. Frost and M. A. Russell, ed., *"Techniques in visible and ultraviolet spectroscopy"*, Vol 4, Chapman and Hall, UK,

---

1993 (c) H-H. Perkampus, *"UV-VIS Spectroscopy and its applications"*, Springer Laboratory, Dusseldorf, **1992**

9. Y. You and S. Y. Park, *Dalton Trans.*, **2009**, 1267
10. G. B. Porter, *J. Chem Ed.,* **1983**, 60, 785
11. A. W. Adamson, *J. Chem. Ed*., **1983**, 60, 797
12. Edinburgh Instruments, nF900 Nanosecond Flash Lamp Operating Manual Issue 1, **2000**
13. Demas J. N. and Crosby G. A., *J. Phys. Chem*., **1971**, 75, 991
14. Nakamaru N., *Bull. Chem. Soc. Jpn*., **1982**, 55, 2697
15. Edinburgh Instruments, nF900 Nanosecond Flash Lamp Operating Manual Issue 2, **2000**
16. William Henry, Ph.D Thesis, Dublin City University, **2006**
17. Robert Groarke, PhD Thesis, Dublin City University, **2009**
18. I. Y. Phang, T. Liu, W. D. Zhang, H. Schonherr, G. J. Vancso, *Eur. Polymer J.,* 1, **2000**
19. J.R. Lakowicz, Principles of Fluorescence Spectroscopy, second ed., Kluwer Academic/Plenum Publishers, New York, 1999.
20. Varian cp-3800 gas chromatograph user manual, **2009**
21. R. M. Purwanto, R. V. Deshpande, C. Chaudhari and H. Delmas, *J. Chem. Eng. Data.,* **1996**, 41*,* 1414.

Chapter 3

Synthesis, characterisation, photophysics and photocatalysis of novel cyclometallated iridium (III) complexes

This chapter deals with the synthesis, characterisation, photophysics and photocatalysis of a range of mononuclear, homodinuclear and heterodinuclear cyclometallated iridium (III) complexes. All of these complexes proved to be potential candidates for H_2 generation. Intramolecular photocatalysis proved to be more effective than intermolecular photocatalysis and 470 nm irradiation produced more H_2 than 350 nm irradiation.

3.1 Introduction

The photoinduced cleavage of water using visible light is under intense investigation with the aim to develop an efficient method for converting solar radiation into a convenient and sustainable fuel. Out of the various methods available at present to harness renewable clean energy from sustainable sources, hydrogen is a promising candidate. Direct conversion of solar energy to chemical energy in the form of hydrogen is an attractive goal that can be accomplished by photosynthetic means from one of earth's most plentiful resources, water. Through the efficient spliting of water into hydrogen and oxygen, a major leap forward in our global energy situation can be achieved. As shown in figure 3.1 hydrogen and oxygen are produced using solar energy, and burnt them in heat engines, with useable heat released from the enthalpy of combustion, or in a fuel cell with electrical power generation.[1,3,8,15]

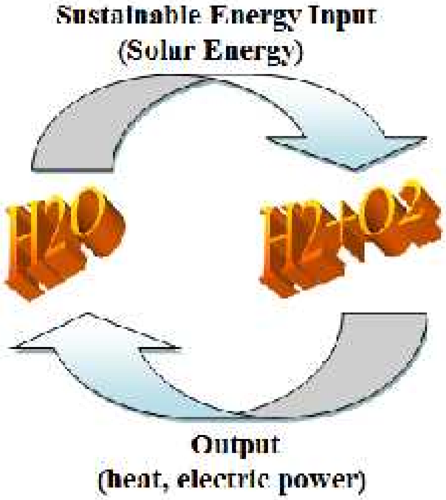

Figure 3.1 *The cycle of sustainable fuel production.*

There are numerous approaches to achieving this goal, including the use of photovoltaic cells to drive electrolysis,[1] semiconductor based charge separation techniques,[2,3] thermochemical disproportionation,[4] and the use of catalytic systems that include light harvesting transition metal complexes. Transition metal complexes have a distinct advantage over their semiconductor counterparts as their photophysical properties can be "tuned" through ligand modifications. Aided by this versatility, researchers have devised a variety of catalytic systems capable of performing the reduction half reaction of water cleavage, in which the excited state of the transition metal complex is quenched by charge transfer to an electron relay. Early work reports the successful use of $[Ru(bpy)_3]^{2+}$ (bpy-2,2'-bipyridine) as a photosensitiser, in combination with an electron relay species, and employing a platinum catalyst.[5,6] More recent variations involve the attachment of a photosensitiser to TiO_2

supported platinum particles,[7,8] as well as the use of different photosensitisers such as Zn^{II} porphyrins,[9,10,11] Mg chlorophyll-a from Spirulina, and cyclometallated $[Ir(C^\wedge N)_2\,(N^\wedge N)]^+$ complexes.[12,13]

3.1.1 Mononuclear iridium complexes for intermolecular photocatalytic H_2 generation

As a consequence of greater ligand field stabilisation energy (LFSE), the use of cyclometallated Ir (III) complexes avoids the thermal population and subsequent nonradiative decay from, the dissociative ^{3}MC state observed with tris diimine Ru (II) complexes.[14] In addition, the greater energetic requirements for the population of the ^{3}MC state allow a larger range of excited state energies by altering the ligand architecture.[15] The "tuning" of the $[Ir(C^\wedge N)_2(N^\wedge N)]^+$ complexe's excited state properties is further facilitated by the formation of a mixed excited triplet state associated with metal to ligand charge transfer (MLCT), ligand centered (LC) transitions and ligand to ligand centered transitions (LLCT) respectively.[16,17,18]

To facilitate the transfer of reducing equivalents, an electron relay such as methyl viologen is typically employed. The choice of an electron relay is generally crucial to the success of a system; a good relay oxidatively quenches the excited photosensitiser, thereby creating charge separation. Numerous relays have been used in place of methyl viologen, including a variety of quaternary bipyridines[19] as well as several cobalt[20,21,22] and rhodium[23,24,25] complexes. Other alternatives include bridged systems where a photosensitiser is covalently linked to hydrogen evolving metal complex.[26,27] Aside from net energy loss, the use of an electron relay allows charge separation at the expense of simplicity, which is compounded by the presence of a sacrificial electron donor that allows hydrogen evolution without concurrent water oxidation.

The first mononuclear iridium based intermolecular catalytic system described by Bernhard and co-workers that uses only a molecular photosensitiser (PS), colloidal metal catalyst, sacrificial reductant (SR), and visible light to evolve substantial amounts of hydrogen in the absence of an electron relay species is shown in figure 3.2 below.[12,13,82]

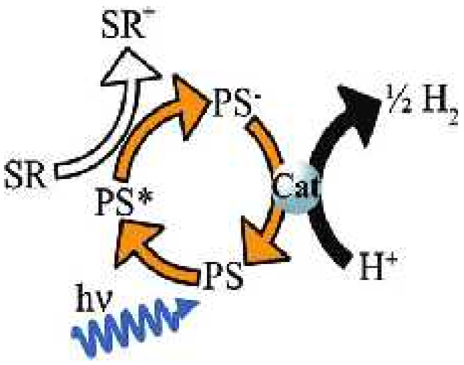

Figure 3.2 *General reaction pathways for mononuclear intermolecular catalytic systems.(PS-photosensitiser, SR-sacrificial reductant)*[12]

The systems that do not have an electron relay, while advantageous, are uncommon in the literature.[28] It has been reported previously that unlike $[Ru(bpy)_3]^{2+}$, heteroleptic cyclometallated iridium (III) complexes, such as the $[Ir(ppy)_2(bpy)]PF_6$ (ppy = 2-phenylpyridine) photosensitiser used are directly quenched by sacrificial electron donors like TEA and TEOA.[12] Bernhard and co-workers have found that quenching of the PS creates an activated reduced species capable of independently reducing protons or delivering reducing equivalents to a catalytic center to evolve hydrogen.[13,82] Such a system that avoids an electron relay is inherently simpler. In addition, energy losses and back reactions associated with the electron transfer to the relay are eliminated, while coupling of the PS to the water redox couple is facilitated.

3.1.2 Binuclear iridium complexes for intramolecular photocatalytic H_2 generation

The central processes in natural photosynthesis are light driven electron transfer from the special pair chromophores to the primary acceptor, and the subsequent charge separation to enable the reduction of substrates. The transfer of these design principles to artificial systems has led to the development of catalytic multicomponent systems for the photocatalytic H_2 production[6] and CO_2 reduction.[29] In these systems, active metal complexes and catalysts are used to facilitate directed photoinduced electron transfer. For example, Gratzel *et al.* showed that heterogeneous photocatalytic systems can be used for the generation of hydrogen,[30] and Currao *et al.* reported the photochemical[31] splitting of water with a system consisting of a photoactive silver/silver chloride anode and a silicon solar cell acting as a cathode. However, in these heterogeneous systems, the electron transfer processes depend on many interfacial parameters that are difficult to influence. Intermolecular systems, consisting of a photoactive Ru or Ir complex and an electron relay of Co or Pd complexes,[12,13] which generate H_2 have also been described in detail in chapter 1. Their effectiveness is limited by the instability of the reduced photocatalysts.

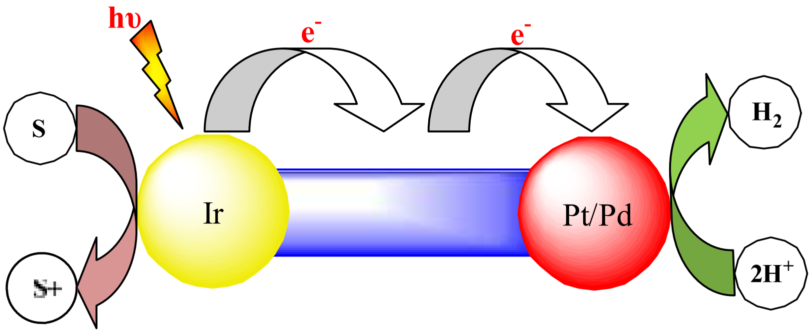

Figure 3.3 *General reaction pathway for a heterodinuclear intramolecular photocatalytic system, S = sacrificial agent.*

In an intramolecular photocatalyst it should be easier to control vectorial photoelectron transfer by precise tuning of the physical properties and orientation of the molecular components. If it were also possible to slow down charge recombination processes, efficient photocatalytic systems may become feasible. A range of intramolecular photocatalysts were reported in the literature but most of them use Ru metal center as the light absorbing unit, with only a few examples of Ir intramolecular systems reported so far, including the Ir-Co system by Fontecave[32,33,34] and the self assembled Ir-Co systems by Sakai[35] which are described in detail in chapter 1, in addition to other intramolecular systems reported. For the reported intramolecular iridium systems the efficiency is relatively low, with TON's less than 50. This shows the need for improved systems with this metal using different peripheral ligands, bridging ligands and catalytic centers. A series of heterodinuclear Ir-Pt/Pd systems with various peripheral ligands and bridging units were made. All of them proved to be more efficient in producing H_2 compared to the conventional Ru-Pt/Pd systems presently available.[27,38] The heterodinuclear Ir–Pt/Pd photocatalyst consists of the following three components as shown in figure 3.3.

- An iridium (III) fragment acting as the light absorber,[36]
- A $PtCl_2$/$PdCl_2$ unit which, when coordinated at the other end of the assembly, acts as a catalytic center,
- A bridging unit (bpp, dpp, tpy, bpm etc) connecting the two metal centers through a conjugated reducible π-electron system.[37]

In the first step of the photocatalytic process the iridium moiety is excited using both visible (470 nm) and UV (350 nm) light. To facilitate efficient electron transfer to the Pt/Pd center, the electron donor triethylamine (TEA) was utilised to re-reduce the photochemically formed Ir^{IV} center. The electron reaching the Pd/Pt catalytic center reduces the proton to form hydrogen (figure 3.3).

3.1.3 Role of bridging ligand

The ligand chosen to bridge the two metal centers is of vital importance because, as has been discussed previously, electronic communication is fundamental for the intramolecular photocatalyst to function properly. The ligands chosen here are (2-(6-(pyridin-2-yl)pyridin-3-yl)pyridine) (bpp) and 2,5-di(pyridin-2-yl)pyrazine (dpp), 2,2':6',2''-terpyridine (tpy) and 2,2'-bipyrimidine (bpm) as shown in figure 3.4 below. These ligands are good starting blocks as their electronic communication between different metal centres such as Ru-Pt/Pd, Ru-Os, Ru-Ru, has been extensively studied.[38,39,40]

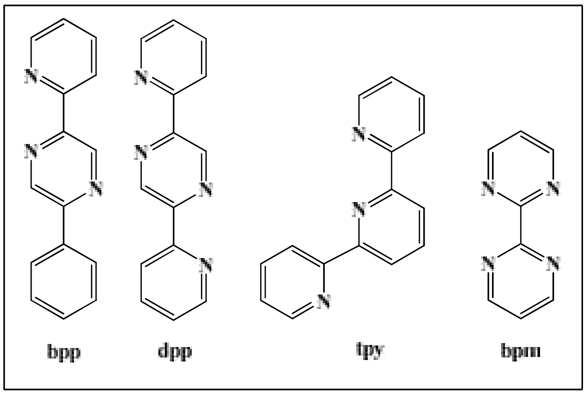

Figure 3.4 *Depicts the structures of the bridging ligands employed in this chapter.*

3.1.4 Iridium (III) polypyridine complexes as chemical and biological probes

In the past few years, a number of luminescent iridium (III) polypyridine complexes have been studied as molecular sensors as they usually display intense and long lived emission in the visible region and the emission energy can be controlled using various mono, bi and tridentate ligands, resulting in drastically different excited state characteristics.[41,42,43] The orgin of emission for common ruthenium (II), osmium (II) and rhenium (I) polypyridine complexes is confined to triplet metal to ligand charge transfer (^{3}MLCT) states.[44,45,46] However, whereas the emissive states of many iridium (III) polypyridine complexes are ^{3}MLCT and triplet intra ligand in character,[47,48] triplet states of ligand to ligand charge transfer (^{3}LLCT) and sigma bond to ligand charge transfer (^{3}SBLCT) have also been identified in some systems.[49,50,51]

In general, the triplet intra ligand emission for these Ir (III) complexes is more intense and longer lived than the ^{3}MLCT emission, and an interplay between these two states can result in pronounced changes in emission properties. Licini and Williams reported iridium (III) bis-terpyridine complexes, which display long lived pH sensitive luminescence.[56] The pyridine appended complex $[Ir(ttpy)(tpy–py)]^{3+}$ displays long lived triplet intra ligand ($\pi \rightarrow \pi^*$)(tpy) emission in aerated neutral aqueous solution, but both the lifetime and intensity are reduced by about 8 fold when the pH is lowered to 2. These significant changes have been attributed to the increasing ^{3}MLCT character in the excited state upon protonation of the appended pyridine nitrogen, which can promote deactivation and thereby shorten lifetimes and reduce intensities. In fact, the effects of the iridium (III) center on the spectroscopic properties of polypyridine ligands can be utilised in pH sensing. For example, the complex $[Ir(tpy\text{-}C_6H_4\text{-}OH)_2]^{3+}$ with pendant phenolic groups is pale yellow in aqueous solution at pH 6 but becomes deep orange upon increasing the pH to 10, and the electronic absorption spectra show a new low energy band at 468 nm upon deprotonation.

In another study by Williams and coworkers, a series of iridium (III) bis-terpyridine complexes $[Ir(tpy\text{-}R^1)(tpy\text{-}R^2)]^{3+}$ as shown in figure 3.5 below has been incorporated with pendant pyridyl groups at the 4'-positions of the terpyridine ligands.[52] In aqueous solution, the homoleptic complexes display structured emission bands resembling that of unsubstituted $[Ir(tpy)_2]^{3+}$, with emission lifetimes suggestive of triplet intra ligand state. The heteroleptic analogues give broader and red shifted emission bands, similar to that of $[Ir(ttpy)_2]^{3+}$, indicating that the emission originates primarily from a lower energy excited state associated with the 4'-tolyl-terpyridine ligand. The emission of most of the heteroleptic complexes is sensitive to the protonation state of the pendant pyridyl group.

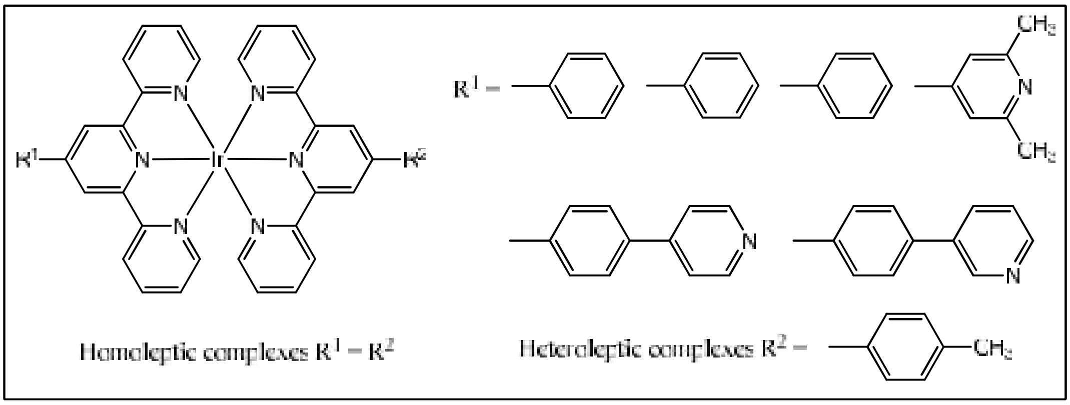

Figure 3.5 *Schematic representation of the iridium terpyridine complexes synthesised by Williams and coworkers.*[57]

Goodall and Williams have made use of the mixed ^{3}IL/^{3}MLCT emission properties of luminescent iridium (III) complexes for anion sensing.[53] The isomeric complexes $[Ir(ttpy)(tpy–py–Me)]^{4+}$ with a meta or para N-methylpyridinium substituent at the 4'-position of terpyridine display long lived emission in aqueous solution. The lower emission quantum yield and shorter lifetime of the para isomer is ascribed to the direct conjugation of the alkylated pyridine nitrogen with the terpyridine, which makes the ligand more electron deficient and hence lowers the energy of the ^{3}MLCT state, promoting mixing with the emissive triplet intra ligand state.

Complexes equipped with more than one reactive functional group may function as cross-linkers for biomolecules. For example, luminescent cyclometalated iridium (III) complexes containing two aldehyde groups $[Ir(pba)_2(N^\wedge N)]^+$ (N^N = bpy, phen, Me$_4$-phen, Ph$_2$-phen) (pba = ppy-CHO) have been synthesised and characterised.[54] The two aldehyde moieties are able to react with the primary amine of biomolecules to form stable secondary amines after reductive amination. L-Alanine and avidin, respectively, have been cross-linked by these complexes to form luminescent bioconjugates. The emissive states of the free complexes and cross-linked conjugates are ^{3}IL ($\pi \rightarrow \pi^*$) (pba) and ^{3}MLCT (dπ(Ir) - π^*(N^N)) in character, respectively. The structures of the complexes reported by Zhu and co-workers are given in figure 3.6 below.[55]

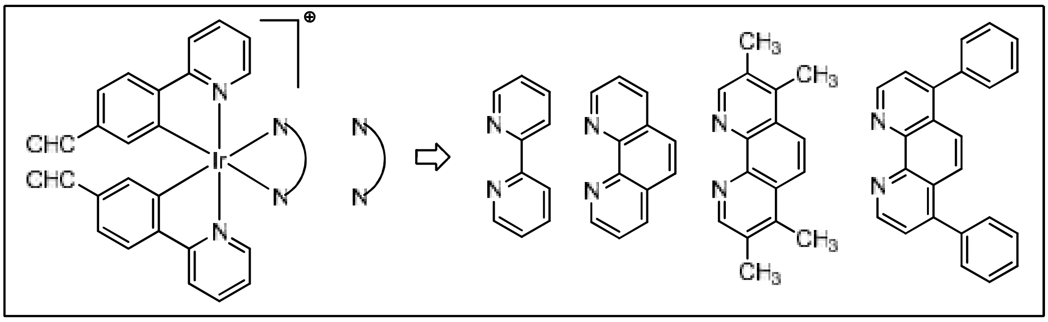

***Figure 3.6** Schematic representation of the iridium bipyridine complexes synthesised by Zhu and coworkers.*[59,60]

This chapter focuses on the synthesis and characterisation of a range of iridium precursor complexes, mononuclear iridium complexes, novel heterodinuclear Ir-Pt/Pd complexes and homodinuclear Ir-Ir complex. Detailed studies on the excited state photophysics were carried out. The lifetimes of all the complexes were measured using both TCSPC and laser flash photolysis and a comparative study of the results using both instruments gave a clear indication of the accuracy of the results obtained. Deuteriation was used as a tool to probe the excited states of some of the complexes. The effect of deuteriation on photocatalytic hydrogen generation was also studied, and this represents the first measurements with deuteriated analogues. This chapter also discusses different cyclometallated iridium photosensitiser units which were successfully employed for the catalytic generation of H_2 from H_2O by both intermolecular and intramolecular photocatalytic processes using visible light (470 nm) and UV light (350 nm). The Ir-Pt/Pd heterodinuclear systems discussed in this chapter are the only systems reported to date based on an iridium attached to either a Pt or Pd metal center. From all the results obtained it is clear that for good photocatalytic activity a range of conditions must be optimised, including the nature of peripheral ligands, bridging ligands, catalyst employed, concentration of the solution, excitation wavelength used etc. Maximum effort has been taken to optimise the conditions with different photocatalyts in order to get better results.

Schematic representation of the entire range of complexes discussed in this chapter is given in figure 3.7 below.

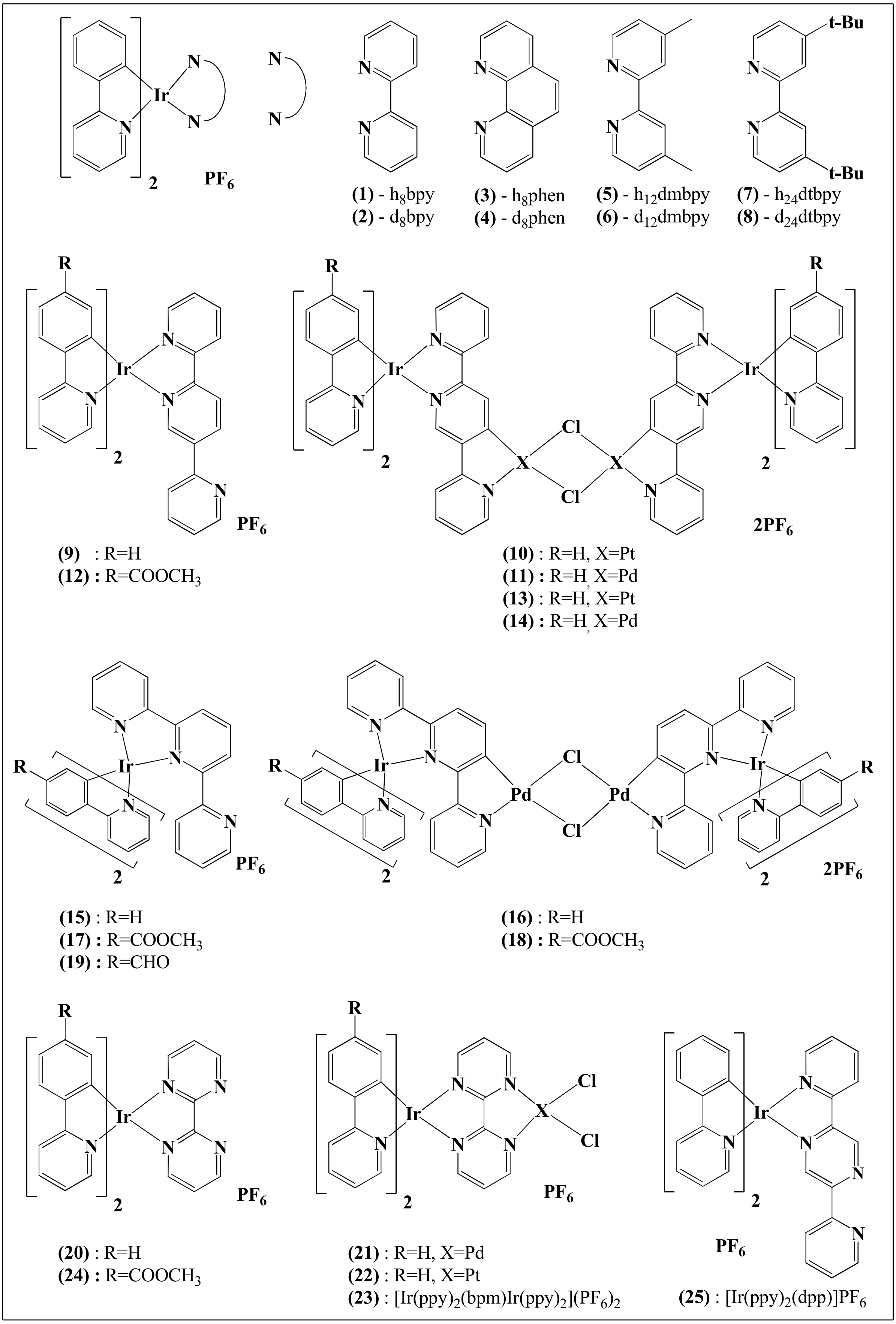

Figure 3.7 *Schematic representation of the complexes discussed in this chapter.*

3.2 Experimental

3.2.1 Synthesis of [Ir(ppy)$_2$(N^N)]PF$_6$ type complexes, [(N^N) → bpy, d$_8$bpy, phen, d$_8$phen, dmbpy, d$_{12}$dmbpy, dtbpy, d$_{24}$dtbpy]

The synthesis of the dichlorobridged Ir precursor complexes is given in chapter 2.

a) Method I

The dichlorobridged dimer (0.1 mmol) was treated with the appropriate neutral ligand (0.2 mmol) in ethylene glycol (5.0 ml) under reflux (150 ^{0}C) with constant stirring for 15 h. Upon cooling to room temperature, the mixture was transferred to a separating funnel with water (3×30 ml) and washed with diethyl ether (3×50 ml). The aqueous layer was heated to 70 ^{0}C for 5 min using a heat gun to remove residual organic solvents. The vessel was then placed on ice, and 10 ml of aqueous ammonium hexafluorophosphate solution (1.0 g in 10 ml of deionised water) was slowly added to the reaction mixture, yielding a coloured suspension. The precipitate was collected by vacuum filtration and allowed to air dry overnight. This product was recrystallised by acetonitrile : diethylether vapor diffusion and dried to yield the pure product, [Ir(C^N)$_2$(N^N)]PF$_6$ (Yield 70 - 80 %).

b) Method II

The dichlorobridged dimer (0.1 mmol) was reacted with the appropriate neutral ligand (0.22 mmol) in DCM : MeOH (2:1) under reflux (80 ^{0}C) with constant stirring for overnight. The reaction mixture was cooled, solvents were completly removed using a vacuum rotary evaporator. The yellow residue obtained was dissolved in water and filtered in order to remove any unreacted polypyridine ligand. To the filtrate a saturated aqueous KPF$_6$ solution was added resulting in the precipitation of the complex as yellow precipitate which was allowed to settle and filtered using vacuum suction and dried. The yellow residue obtained was then dissolved completely in acetone and reprecipitated by adding diethyl ether. This is filtered and recrystallised from acetone : H$_2$O to yield the pure complex, (Yield 70 - 80 %).

3.2.1.1 [Ir(ppy)$_2$(bpy)]PF$_6$ (1)

[Ir(ppy)$_2$Cl]$_2$ (0.050 g, 0.0407 mmol), 2,2'-bipyridyl (bpy) (0.0139 g, 0.0895 mmol), Yield (0.072 g, 0.0898 mmol, 75 %). ^{1}H NMR (400 MHz, DMSO), δ (ppm): 6.17 (d, 1H, 6' (ppy)), 6.89 (t, 1H, 5' (ppy)), 7.01 (t, 1H, 4' (ppy)), 7.14 (t, 1H, 4 (ppy)), 7.60 (d, 1H, 3 (ppy)), 7.68 (t, 1H, b (bpy)), 7.85 (d, 1H, a (bpy)), 7.92 (m, 2H, 5, 3' (ppy)), 8.26 (m, 2H, c (bpy), 6 (ppy)), 8.88 (d, 1H, d (bpy)). Elemental analysis for complex **(1)**, $C_{32}H_{24}F_6IrN_4P$; (calculated) : C :47.94, H :3.02, N :6.99; (found) : C :47.38, H :2.91, N :6.87.

3.2.1.2 [Ir(ppy)$_2$(d$_8$bpy)]PF$_6$ (2)

$[Ir(ppy)_2Cl]_2$ (0.050 g, 0.0407 mmol), deuteriated 2,2'-bipyridyl ($d_8$bpy) (0.0146 g, 0.0895 mmol), Yield (0.069 g, 0.08521 mmol, 72 %). ^{1}H NMR (400 MHz, DMSO), δ (ppm): 6.17 (d, 1H, 6' (ppy)), 6.89 (t, 1H, 5' (ppy)), 7.01 (t, 1H, 4' (ppy)), 7.14 (t, 1H, 4 (ppy)), 7.60 (d, 1H, 3 (ppy)), 7.68 (resd. s, b ($d_8$bpy)), 7.85 (resd. s, a ($d_8$bpy)), 7.92 (m, 2H, 5, 3' (ppy)), 8.26 (resd. s, c ($d_8$bpy) 1H, d, 6 (ppy)), 8.88 (resd. s, d ($d_8$bpy)). Elemental analysis for complex **(2)**, $C_{32}H_{16}D_8F_6IrN_4P$; (calculated) : C :47.42, H :2.96, N :6.91; (found) : C :47.12, H :2.95, N :6.64.

3.2.1.3 [Ir(ppy)$_2$(phen)]PF$_6$ (3)

$[Ir(ppy)_2Cl]_2$ (0.100 g, 0.0934 mmol), 1,10 phenanthroline (0.037 g, 0.2054 mmol), Yield (0.145 g, 0.1755 mmol, 69 %). ^{1}H NMR (400 MHz, DMSO), δ (ppm): 6.27 (d, 1H, 6' (ppy)), 6.95 (m, 2H, 4', 5' (ppy)), 7.04 (t, 1H, 4 (ppy)), 7.43 (d, 1H, 3' (ppy)), 7.85 (t, 1H, 5 (ppy)), 7.93 (d, 1H, 3 (ppy)), 8.03 (dd, 1H, b (phen)), 8.18 (d, 1H, a (phen)), 8.24 (d, 1H, 6 (ppy)), 8.37 (s, 1H, d (phen)), 8.88 (d, 1H, c (phen)). Elemental analysis for complex **(3)**, $C_{34}H_{24}F_6IrN_4P$; (calculated) : C :49.45, H :2.93, N :6.78; (found) : C :49.38, H :2.91, N :6.47.

3.2.1.4 [Ir(ppy)$_2$(d$_8$phen)]PF$_6$ (4)

$[Ir(ppy)_2Cl]_2$ (0.100 g, 0.0934 mmol), deuteriated 1,10 phenanthroline ($d_8$phen) (0.038 g, 0.2054 mmol), Yield (0.133 g, 0.1595 mmol, 62 %). ^{1}H NMR (400 MHz, DMSO), δ (ppm): 6.27 (d, 1H, 6' (ppy)), 6.95 (m, 2H, 4', 5' (ppy)), 7.04 (t, 1H, 4 (ppy)), 7.43 (d, 1H, 3' (ppy)), 7.85 (t, 1H, 5 (ppy)), 7.93 (d, 1H, 3 (ppy)), 8.03 (resd. s, b ($d_8$phen)), 8.18 (resd. s, a ($d_8$phen)), 8.24 (d, 1H, 6 (ppy)), 8.37 (resd. s, d ($d_8$phen)), 8.88 (resd. s, c ($d_8$phen)). Elemental analysis for complex **(4)**, $(C_{34}H_{16}D_8F_6IrN_4P)H_2O$; (calculated) : C :47.90, H :2.81, N :6.57; (found) : C :48.03, H :2.83, N :6.41.

3.2.1.5 [Ir(ppy)$_2$(dmbpy)]PF$_6$ (5)

$[Ir(ppy)_2Cl]_2$ (0.050 g, 0.0467 mmol), 4,4'-dimethyl-2,2'-bipyridine (dmbpy) (0.0172 g, 0.1027 mmol), Yield (0.060 g, 0.0723 mmol, 83 %). ^{1}H NMR (400 MHz, DMSO), δ (ppm): 3.32 (s, 3H), 6.17 (d, 1H, 6' (ppy)), 6.88 (t, 1H, 5' (ppy)), 7.00 (t, 1H, 4' (ppy)), 7.15 (t, 1H, 4 (ppy)), 7.50 (d, 1H, b (dmbpy)), 7.60 (d, 1H, 3 (ppy)), 7.66 (d, 1H, a (dmbpy)), 7.91 (m, 2H, 5, 3' (ppy)), 8.25 (d, 1H, 6 (ppy)), 8.74 (s, 1H, d (dmbpy)). Elemental analysis for complex **(5)**, ($C_{34}H_{28}F_6IrN_4P$); (calculated) : C :49.21, H :3.40, N :6.75; (found) : C :49.26, H :3.39, N :6.77.

3.2.1.6 [Ir(ppy)$_2$(d$_{12}$dmbpy)]PF$_6$.H$_2$O (6)

[Ir(ppy)$_2$Cl]$_2$ (0.050 g, 0.0467 mmol), 4,4'-dimethyl-2,2'-bipyridine (d$_{12}$dmbpy) (0.0201 g, 0.1027 mmol), Yield (0.051 g, 0.0605 mmol, 80 %). ^{1}H NMR (400 MHz, DMSO), δ (ppm): 3.32 (resd. s), 6.17 (d, 1H, 6' (ppy)), 6.88 (t, 1H, 5' (ppy)), 7.00 (t, 1H, 4' (ppy)), 7.15 (t, 1H, 4 (ppy)), 7.50 (resd. s, b (d$_{12}$tbpy)), 7.60 (d, 1H, 3 (ppy)), 7.66 (resd. s, a (d$_{12}$tbpy)), 7.91 (m, 2H, 5, 3' (ppy)), 8.25 (d, 1H, 6 (ppy)), 8.74 (resd. s, d (d$_{12}$tbpy)). Elemental analysis for complex **(6)**, ($C_{34}H_{16}D_{12}F_6IrN_4P$)$H_2O$; (calculated) : C :47.45, H :3.26, N :6.51; (found) : C :47.63, H :3.26, N :6.57.

3.2.1.7 [Ir(ppy)$_2$(dtbpy)]PF$_6$ (7)

[Ir(ppy)$_2$Cl]$_2$ (0.050 g, 0.0467 mmol), 4,4'-ditertiarybutyl-2,2'-bipyridine (dtbpy) (0.027 g, 0.1027 mmol), Yield (0.067 g, 0.0733 mmol, 75 %) ^{1}H NMR (400 MHz, DMSO), δ (ppm): 1.38 (s, 9H), 6.16 (d, 1H, 6' (ppy)), 6.89 (t, 1H, 5' (ppy)), 7.00 (t, 1H, 4' (ppy)), 7.17 (t, 1H, 4 (ppy)), 7.60 (d, 1H, b (dtbpy)), 7.70 (d, 1H, 3 (ppy)), 7.75 (d, 1H, a (dtbpy)), 7.93 (m, 2H, 5, 3' (ppy)), 8.26 (d, 1H, 6 (ppy)), 8.86 (s, 1H, d (dtbpy)). Elemental analysis for complex **(7)**, $C_{40}H_{40}F_6IrN_4P$; (calculated) : C :52.57, H :4.41, N :6.13; (found) : C :52.88, H :4.03, N :6.21.

3.2.1.7 [Ir(ppy)$_2$(d$_{24}$dtbpy)]PF$_6$.H$_2$O (8)

[Ir(ppy)$_2$Cl]$_2$ (0.050 g, 0.0467 mmol), deuteriated 4,4'-ditertiarybutyl-2,2'-bipyridine (d$_{24}$dtbpy) (0.030 g, 0.0934 mmol), Yield (0.058 g, 0.0618 mmol, 72 %) ^{1}H NMR (400 MHz, DMSO), δ (ppm): 1.38 (s, 9H), 6.16 (d, 1H, 6', (ppy)), 6.89 (t, 1H, 5' (ppy)), 7.00 (t, 1H, 4' (ppy)), 7.17 (t, 1H, 4 (ppy)), 7.60 (resd. s, b (d$_{24}$dtby)), 7.70 (d, 1H, 3 (ppy)), 7.75 (resd. s, a (d$_{24}$dtby)), 7.93 (m, 2H, 5, 3' (ppy)), 8.26 (d, 1H, 6 (ppy)), 8.86 (resd. s, d (d$_{24}$dtby)). Elemental analysis for complex **(8)**, ($C_{40}H_{16}D_{24}F_6IrN_4P$)$H_2O$; (calculated) : C :50.26, H :4.19, N :5.86; (found) : C :50.65, H :3.83, N :6.07.

3.2.2 Synthesis of mononuclear and heterodinuclear (Ir-Pt/Pd) cyclometallated iridium complexes with ligand bpp

3.2.2.1 Synthesis of [Ir(ppy)$_2$(bpp)]PF$_6$ (9)

The ligand bpp (0.050 g, 0.2146 mmol) was weighed and transferred to a 100 ml round bottom flask (R.B) to which 10 ml of solvent, DCM: EtOH (2:1) was added and stirred at 60 ^{0}C for 20 minutes. The dichlorobridged dimer, [Ir(ppy)$_2$Cl]$_2$ (0.115 g, 0.1072 mmol) dissolved in 20 ml of solvent was added slowly over an hour. The reaction was heated at reflux (90 ^{0}C) for 7 hours. The reaction mixture was cooled and the solvent was removed by vacuum rotary evaporation, 10 ml of deionised water was added and saturated aqueous NH$_4$PF$_6$ (1 g in 10 ml of deionised water) was added resulting in the precipitation of the product as [Ir(ppy)$_2$(bpp)]PF$_6$ which was recrystallised from acetone : H$_2$O (2:1), vacuum filtered and dried. Yield (0.149 g, 0.1695 mmol, 79 %). ^{1}H NMR (600 MHz, DMSO), δ (ppm): 6.21 (d, 1H, 6'' (ppy)), 6.25 (d, 1H, 6' (ppy)), 6.94 (m, 2H, 5', 5'' (ppy)), 7.05 (m, 2H, 4',4'' (ppy)), 7.16 (m, 2H, 5,5''' (ppy)), 7.43 (m, 1H, b (bpp)), 7.66 (d, 1H, 6 (ppy)), 7.71 (t, 1H, c (bpp)), 7.78 (d, 1H, 6''' (ppy)), 7.86 (d, 1H, d (bpp)), 7.90 (d, 1H, 3'' (ppy)), 7.94 (m, 4H, 4, 4''', 3' (ppy), e, f (bpp)), 8.27 (m, 3H, k (bpp), 3,3''' (ppy)), 8.55 (d, 1H, a (bpp)), 8.63 (s, 1H, g (bpp)), 8.85 (d, 1H, i (bpp)), 8.98 (d, 1H, j (bpp)), 8.99 (d, 1H, h (bpp)). Elemental analysis for complex **(9)**, (C$_{37}$H$_{27}$F$_6$IrN$_5$P); (calculated) : C : 50.57, H : 3.10, N : 7.97; (found) : C : 50.92, H : 3.10, N : 7.98.

3.2.2.2 Synthesis of [(ppy)$_2$Ir(bpp)PtCl]$_2$(PF$_6$)$_2$.H$_2$O (10)

Equimolar amounts of [Ir(ppy)$_2$(bpp)]PF$_6$ (0.05 g, 0.0689 mmol) and K$_2$PtCl$_4$ (0.023 g, 0.0689 mmol) were added together in an RB containing methanol (10 ml) and refluxed for 24 hours, the dimer complex precipitated from solution and was filtered, washed with diethyl ether, hexane and vacuum dried. The product was recrystallised from acetone: diethylether (2:1), vacuum filtered and dried. Yield (0.082 g, 0.0366 mmol, 54 %). ^{1}H NMR (600 MHz, DMSO), δ (ppm): 6.23 (d, 1H, 6'' (ppy)), 6.30 (d, 1H, 6' (ppy)), 6.91 (t, 1H, 5'' (ppy)), 7.03 (dd, 2H, 4'', 5' (ppy)), 7.11 (dd, 2H, 4', 5''' (ppy)), 7.18 (t, 2H, 5 (ppy)), 7.66 (d, 1H, 6 (ppy)), 7.73 (m, 2H, b, i (bpp)), 7.82 (s, 1H, g (bpp)), 7.88 (d, 1H, d (bpp)), 7.90 (d, 1H, a (bpp)), 7.94 (m, 5H, 4, 4''', 3', 3''' (ppy), c (bpp)), 8.25 (m, 5H), 8.24 (m, 3H, 3, 3''' (ppy)), 8.25 (m, 1H,), 8.34 (d, 1H, 6''' (ppy)), 9.51 (d, 1H, h (bpp)), 9.54 (s, 1H, e (bpp)). Elemental analysis for complex **(10)**, (C$_{74}$H$_{52}$Cl$_2$F$_{12}$Ir$_2$N$_{10}$P$_2$Pt$_2$)H$_2$O; (calculated) : C : 39.77, H : 2.44, N : 6.27; (found) : C : 39.47, H : 2.38, N : 6.09.

3.2.2.3 Synthesis of $[(ppy)_2Ir(bpp)PdCl]_2(PF_6)_2.3H_2O$ (11)

Equimolar amounts of $[Ir(ppy)_2(bpp)]PF_6$ (0.05 g, 0.0689 mmol) and $(NH_4)_2PdCl_4$ (0.015 g, 0.0689 mmol) were added together in an RB containing methanol (10 ml) and refluxed for 24 hours, the dimer complex was precipitated from solution and filtered, washed with diethyl ether, hexane and vacuum dried. The product was recrystallised from acetone : diethylether (2:1), vacuum filtered and dried. Yield (0.087 g, 0.0415 mmol, 62 %). ^{1}H NMR (600 MHz, DMSO), δ (ppm): 6.22 (d, 1H, 6'' (ppy)), 6.26 (d, 1H, 6' (ppy)), 6.88 (t, 1H, 5'' (ppy)), 6.94 (m, 2H, 5' (ppy), d (bpp)), 7.0 (t, 1H, 4'' (ppy)), 7.06 (t, 1H, 4' (ppy)), 7.15 (m, 2H, 5, 5''' (ppy)), 7.53 (t, 1H, c (bpp)), 7.63 (t, 2H, 4,4''' (ppy), 7.64 (s, 1H, g (bpp)), 7.80 (d, 1H, 3''' (ppy)), 7.85 (d, 1H, 3 (ppy)), 7.90 (m, 5H, 3', 3'', 6, 6''' (ppy), k (bpp)), 8.07 (t, 1H, b (bpp)), 8.23 (m, 3H, j, a, i (bpp)), 8.46 (d, 1H, h (bpp)), 9.09 (s, 1H, e (bpp)). Elemental analysis for complex **(11)**, $(C_{74}H_{52}Cl_2F_{12}Ir_2N_{10}P_2Pd_2)3H_2O$; (calculated) : C : 42.82, H : 2.72, N : 6.75; (found) : C : 42.31, H : 2.78, N : 6.45.

3.2.2.4 Synthesis of $[Ir(ppy\text{-}COOCH_3)_2(bpp)]PF_6.H_2O$ (12)

The ligand bpp (0.046 g, 0.1972 mmol) was weighed and transfered to a 100 ml round bottom flask (R.B) to which 10ml of solvent, DCM: EtOH (2:1) was added and stirred at 60 ^{0}C for 20 minutes to which the dichlorobridged dimer, $[Ir(ppy\text{-}COOCH_3)_2Cl]_2$ (0.1287 g, 0.0985 mmol) dissolved in 20 ml of solvent (DCM) was added slowly in about 3 hours. The reaction was heated at reflux (80 ^{0}C) overnight. The reaction mixture was cooled and solvents were all removed by vacuum rota evaporator, 10 ml of deionised water was added and saturated aqueous KPF_6 (1 g in 10 ml of deionised water) was added resulting in the precipitation of the product, filtered, washed with water and diethyl ether and was recrystallised from acetone : H_2O (2:1), vacuum filtered and dried. Yield (0.150 g, 0.1480 mmol, 77 %). ^{1}H NMR (600 MHz, DMSO), δ (ppm): 3.67 (s, 6H), 6.79 (d, 2H, 6'', 6' (ppy-OMe)),7.31 (m, 2H, 5''', 5 (ppy-OMe)), 7.40 (m, 1H, b (bpp)), 7.67 (m, 2H, 4''', 4' (ppy-OMe)), 7.73 (t, 1H, f (bpp)), 7.81 (d, 1H, 6 (ppy-OMe)), 7.88(d, 1H, g (bpp)), 7.92 (m, 3H, 6''' (ppy-OMe), d, c (bpp)), 8.053 (m, 4H, 4'', 4, 3'', 3' (ppy-OMe)), 8.31 (t, 1H, e (bpp)), 8.42 (m, 2H, 3''', 3 (ppy-OMe)), 8.50 (d, 1H, a (bpp)), 8.58 (s, 1H, k (bpp)), 8.88 (d, 1H, j (bpp)), 8.98 (m, 2H, i, h (bpp). Elemental analysis for complex **(12)**, $(C_{41}H_{31}F_6IrN_5O_4P)H_2O$; (calculated) : C : 48.62, H : 3.28, N : 6.91; (found) : C : 48.68, H : 3.10, N : 6.61.

3.2.2.5 Synthesis of [(ppy-COOCH$_3$)$_2$Ir(BPP)PtCl]$_2$(PF$_6$)$_2$.3H$_2$O (13)

Equimolar amounts of [Ir(ppy-COOCH$_3$)$_2$(bpp)]PF$_6$ (0.050 g, 0.05025 mmol) and K$_2$PtCl$_4$ (0.019 g, 0.04774 mmol) were added together in an RB containing methanol (10 ml) and refluxed for 48 hours, the dimer complex get precipitated out in solution and was filtered, washed with diethyl ether, hexane and vacuum dried. The product was recrystallised from acetone : diethylether (2:1), vacuum filtered and dried. Yield (0.081 g, 0.0323 mmol, 66 %). ^{1}H NMR (600 MHz, DMSO), δ (ppm): δ (ppm): 3.68 (d, 6H), 6.80 (s, 1H, 6'' (ppy-OMe)), 6.85 (s, 1H, 6' (ppy-OMe)), 7.17 (d, 1H), 7.31 (m, 2H, 4''', 4' (ppy-OMe)), 7.61 (dd, 2H), 7.66 (m, 3H), 7.73 (dd, 2H), 7.84 (s, 2H, g), 8.00 (d, 1H, 3' (ppy-OMe)), 8.05 (dd, 2H, 3''' (ppy-OMe)), 8.10 (m, 3H), 8.23 (t, 2H), 8.31 (dd, 2H), 8.37 (t, 2H), 9.49 (d, 1H, h (bpp)), 9.57 (s, 1H, e (bpp)). Elemental analysis for complex **(13)**, ($C_{82}H_{60}Cl_2F_{12}Ir_2N_{10}O_8P_2Pt_2$)3H$_2$O; (calculated) : C : 39.35, H : 2.66, N : 5.60; (found) : C : 39.89, H : 2.79, N : 5.10.

3.2.2.6 Synthesis of [(ppy-COOCH$_3$)$_2$Ir(bpp)PdCl]$_2$(PF$_6$)$_2$.5H$_2$O (14)

Equimolar amounts of [Ir(ppy-COOCH$_3$)$_2$(bpp)]PF$_6$ (0.05 g, 0.05025 mmol) and (NH$_4$)$_2$PdCl$_4$ (0.014 g, 0.04774 mmol) were added together in an RB containing methanol (10 ml) and refluxed for 48 hours, the dimer complex get precipitated out in solution and was filtered, washed with diethyl ether, hexane and vacuum dried. The product was recrystallised from acetone : diethylether (2:1) mixture first and then in acetone : water (2:1) mixture, vacuum filtered and dried. Yield (0.096 g, 0.0406 mmol, 84 %). ^{1}H NMR (600 MHz, DMSO), δ (ppm): 3.66 (d, 6H), 6.78 (s, 1H, 6'' (ppy-OMe)), 6.81 (s, 1H, 6' (ppy-OMe)), 7.02 (d, 1H, b (bpp)), 7.26 (m, 2H, 4''', 4' (ppy-OMe)), 7.53 (t, 1H, 3'' (ppy-OMe)), 7.59 (t, 1H, 3' (ppy-OMe)), 7.64 (m, 4H), 7.73 (d, 1H), 7.80 (d, 1H, f (bpp)), 7.93 (d, 1H, e (bpp)), 8.04 (m, 6H, 3''', 3 (ppy-OMe), g (bpp)), 8.23 (t, 1H), 8.40 (t, 2H), 8.47 (d, 1H, h (bpp)). Elemental analysis for complex **(14)**, ($C_{82}H_{60}Cl_2F_{12}Ir_2N_{10}O_8P_2Pd_2$)5H$_2$O; (calculated) : C : 41.70, H : 2.99, N : 5.93; (found) : C : 40.36, H : 2.86, N : 6.39.

3.2.3 Synthesis of mononuclear and heterodinuclear (Ir-Pd) cyclometallated iridium complexes with ligand tpy

3.2.3.1 Synthesis of [Ir(ppy)$_2$(tpy)]PF$_6$.CH$_2$Cl$_2$ (15)

The ligand tpy (0.044 g, 0.1869 mmol) was weighed and transfered to a 100 ml round bottom flask (R.B) to which 10 ml of solvent, DCM: EtOH (2:1) was added and stirred at 60 ^{0}C for 20 minutes to which the dichlorobridged dimer, [Ir(ppy)$_2$Cl]$_2$ (0.100 g, 0.0934 mmol) dissolved in 20 ml of solvent was added slowly in an hour. The reaction was refluxed (90 ^{0}C) for 7 hours. The reaction mixture was cooled and solvents were all removed by vacuum rotary evaporator, 10 ml of deionised water was added and saturated aqueous NH_4PF_6 (1 g in 10 ml of deionised water) was added resulting in the precipitation of the product which was recrystallised from acetone : H_2O (2:1), vacuum filtered and dried. Yield (0.120 g, 0.1245 mmol, 67 %). ^{1}H NMR (600 MHz, DMSO), δ (ppm): 5.39 (d, 1H, 6" (ppy)), 5.82 (d, 1H, 6' (ppy)), 6.30 (t, 1H, 5" (ppy)), 6.62 (t, 1H, 4" (ppy)), 6.78, (d, 1H, g (tpy)), 6.80 (t, 1H, 5' (ppy)), 6.99 (t,1H,f (tpy)), 7.03 (t, 1H),7.16 (t, 1H, b (tpy)), 7.25 (t, 1H), 7.35 (t, 1H, c (tpy)), 7.52 (d,1H, 3' (ppy)), 7.57(d, 1H, a (tpy)), 7.66 (m, 3H, 5, 5''' (ppy)), 7.87 (d, 1H, e (tpy)), 7.96 (t, 1H, c (tpy)), 8.03 (t, 1H, d (tpy)), 8.16 (d, 1H, d (tpy)), 8.19 (d, 1H), 8.29 (d, 1H, k (tpy)), 8.36 (m, 2H, 4''', 4 (ppy)), 8.85 (b, 1H, h (tpy)), 8.93 (t, 2H, 3''', 3 (ppy)). Elemental analysis for complex **(15)**, $(C_{37}H_{27}F_6IrN_5P)CH_2Cl_2$; (calculated) : C : 47.86, H : 3.03, N : 7.27; (found) : C : 48.00, H : 2.98, N : 7.34.

3.2.3.2 Synthesis of $[(ppy)_2Ir(tpy)PdCl]_2(PF_6)_2.H_2O.CH_2Cl_2$ (16)

Equimolar amounts of $[Ir(ppy)_2(tpy)]PF_6$ (0.06 g, 0.06827 mmol) and $(NH_4)_2PdCl_4$ (0.018 g, 0.06485 mmol) were added together in an RB containing methanol (10 ml) and refluxed for 24 hours, the dimer complex was precipitated from solution which was filtered, washed with diethyl ether, hexane and vacuum dried. The product was recrystallised firstly from DCM : hexane (5:2) and secondly from acetone : diethylether (2:1), vacuum filtered and dried. Yield (0.094 g, 0.0438 mmol, 62 %). ^{1}H NMR (600 MHz, DMSO), δ (ppm): 5.62 (d, 1H, 6" (ppy)), 6.22 (d, 1H, 6' (ppy)), 6.67 (t, 1H, 5" (ppy)), 6.74 (t, 1H, 5' (ppy)), 6.82 (t, 1H, 4" (ppy)), 6.87 (t, 1H, 4' (ppy)), 7.433 (t, 1H, 4''' (ppy)), 7.552 (t, 1H, 4 (ppy)), 7.71 (d, 1H, 3" (ppy)), 7.77 (d, 1H, 3' (ppy)), 7.87 (m, 2H, c (tpy)), 7.99 (t, 1H, 5''' (ppy)), 8.07 (t, 1H, 5 (ppy)), 8.16 (d, 1H, 6''' (ppy)), 8.24 (d, 1H, 6 (ppy)), 8.45 (m, 2H, b (tpy)), 8.62 (m, 5H), 8.72 (dd, 2H, e, d (tpy)), 9.51 (d, 1H, 3''' (ppy)), 9.78 (d, 1H, 3 (ppy)). Elemental analysis for complex **(16)**, $(C_{74}H_{52}Cl_2F_{12}Ir_2N_{10}P_2Pd_2)H_2O.CH_2Cl_2$; (calculated) : C : 40.98, H : 2.62, N : 6.29; (found) : C : 40.82, H : 2.44, N : 6.87.

3.2.3.3 Synthesis of $[Ir(ppy\text{-}COOCH_3)_2(tpy)]PF_6.CH_2Cl_2$ (17)

The ligand tpy (0.048 g, 0.2036 mmol) was weighed and transfered to a 100 ml round bottom flask (R.B) to which 10 ml of solvent, DCM: EtOH (2:1) was added and stirred at 60 ^{0}C for 20 minutes to which the dichlorobridged dimer, $[Ir(ppy\text{-}COOCH_3)_2Cl]_2$ (0.133 g, 0.1018 mmol) dissolved in 20 ml of solvent was added slowly in an hour. The reaction was refluxed (90 ^{0}C) for 7 hours. The reaction mixture was cooled and solvents were all removed by vacuum rota evaporator, 10 ml of deionised water was added and saturated aqueous NH_4PF_6 (1 g in 10 ml of deionised water) was added resulting in the precipitation of the product which was recrystallised from acetone : H_2O (2:1), vacuum filtered and dried. Yield (0.145 g, 0.1342 mmol, 66 %). ^{1}H NMR (600 MHz, DMSO), δ (ppm): 3.60 (s, 3H), 3.68 (s, 3H), 5.93 (s, 1H, 6' (ppy-OMe)), 6.79 (b, 1H, g (tpy)), 6.81 (m, 1H, 4'' (ppy-OMe)), 7.17, (m, 3H, 4', 3'', 4''' (ppy-OMe)), 7.43 (t, 1H, 4 (ppy-OMe)), 7.49 (d, 1H, a (tpy)), 7.59 (m, 5H, e, f (tpy), 6''', 6, 3' (ppy-OMe)), 7.99 (m, 2H, c, b (tpy)), 8.11 (t, 2H, 5''' (ppy-OMe), k (tpy)), 8.28 (d, 1H, d (tpy)), 8.36 (m, 3H, i, j (tpy), 5 (ppy-OMe)), 8.90 (m, 2H, 3''', 3 (ppy-OMe)), 9.05 (b, 1H, h (tpy)). Elemental analysis for complex **(17)**, ($C_{41}H_{31}F_6IrN_5O_4P$).CH_2Cl_2 ; (calculated) : C : 46.72, H : 3.08, N : 6.49; (found) : C : 46.55, H : 3.18, N : 6.36.

3.2.3.4 Synthesis of [(ppy-COOCH$_3$)$_2$Ir(tpy)PdCl]$_2$(PF$_6$)$_2$.H$_2$O.CH$_2$Cl$_2$ (18)

Equimolar amounts of [Ir(ppy-$COOCH_3$)$_2$(tpy)]PF_6 (0.07 g, 0.0702 mmol) and $(NH_4)_2PdCl_4$ (0.019 g, 0.0667 mmol) were added together in an RB containing methanol (10 ml) and refluxed for 48 hours, the dimer complex was precipitated from solution and was filtered, washed with diethyl ether, hexane and vacuum dried. The product was recrystallised firstly from DCM : hexane (5:2) and secondly from acetone : diethylether (2:1), vacuum filtered and dried. Yield (0.103 g, 0.0433 mmol, 63 %). ^{1}H NMR (600 MHz, DMSO), δ (ppm): 3.60 (s, 3H), 3.62 (s, 3H), 6.24 (s, 1H, 6'' (ppy-OMe)), 6.82 (s, 1H, 6' (ppy-OMe)), 7.39 (d, 1H, 4'' (ppy-OMe)), 7.44 (d, 1H, 4' (ppy-OMe)), 7.60 (t, 1H, 4''' (ppy-OMe)), 7.680 (t, 1H, 4 (ppy-OMe)), 7.88 (m, 4H, 3'',3' (ppy-OMe), c, f(tpy)), 8.12 (t, 1H, 5''' (ppy-OMe)), 8.19 (t, 1H, 5 (ppy-OMe)), 8.30 (d, 1H, 6''' (ppy-OMe)), 8.39 (d, 1H, 6 (ppy-OMe)), 8.45 (t, 1H, b (tpy)), 8.59 (m, 5H, a (tpy)), 8.74 (dd, 2H, d, e (tpy)), 9.52 (d, 1H, 3''' (ppy-OMe)), 9.83 (d, 1H, 3 (ppy-OMe)). Elemental analysis for complex **(18)**, ($C_{82}H_{60}Cl_2F_{12}Ir_2N_{10}O_8P_2Pd_2$) H_2O.CH_2Cl_2 ;(calculated): C : 41.02, H : 2.70, N : 5.70; (found) : C : 41.17, H : 2.65, N : 5.79.

3.2.3.5 Synthesis of [Ir(ppy-CHO)$_2$(tpy)]PF$_6$ (19)

The ligand tpy (0.039 g, 0.1686 mmol) was weighed and transfered to a 100 ml round bottom flask (R.B) to which 10 ml of solvent, DCM: EtOH (2:1) was added and stirred at 60 ^{0}C for 20 minutes to which the dichlorobridged dimer, [Ir(ppy-CHO)$_2$Cl]$_2$ (0.100 g, 0.0843 mmol) dissolved in 20 ml of solvent was added slowly in an hour. The reaction was refluxed (90 ^{0}C) for 7 hours. The reaction mixture was cooled and solvents were all removed by vacuum rota evaporator, 10 ml of deionised water was added and saturated aqueous NH_4PF_6 (1 g in 10 ml of deionised water) was added resulting in the precipitation of the product which was recrystallised from acetone : H_2O (2:1), vacuum filtered and dried. Yield (0.130 g, 0.1390 mmol, 83 %). ^1H NMR (600 MHz, DMSO), δ (ppm): 5.80 (s, 1H, 6'' (ppy-CHO)), 6.24 (s, 1H, 6' (ppy-CHO)), 6.71 (b, 1H, g (tpy)), 6.81 (m, 1H, 4 (ppy-CHO)), 7.08 (d, 1H, 4'' (ppy-CHO)), 7.17 (t, 1H, 3 (ppy-CHO)), 7.25 (t, 1H, 4''' (ppy-CHO)), 7.481 (m, 2H, b, (tpy) 4' (ppy-CHO)), 7.61 (m, 4H, e, f, c (tpy), 3''' (ppy-CHO)), 7.74 (d, 1H, 3'' (ppy-CHO)), 8.05 (t, 1H, 5''' (ppy-CHO)), 8.12 (m, 3H, a (tpy), 3', 5 (ppy-CHO)), 8.32 (m, 3H, d, k (tpy), 6''' (ppy-CHO)), 8.44 (d, 1H, 6 (ppy-CHO)), 8.92 (t, 2H, i, j (tpy)), 9.09 (b, 1H, h (tpy)), 9.42 (s, 1H,CHO), 9.585 (s, 1H, CHO). Elemental analysis for complex **(19)**, ($C_{39}H_{27}F_6IrN_5O_2P$) ;(calculated): C : 50.11, H : 2.91, N : 7.49; (found) : C : 49.88, H : 2.93, N : 7.21.

3.2.4 Synthesis of mononuclear and heterodinuclear (Ir-Pd) cyclometallated iridium complexes with ligand bpm

3.2.4.1 Synthesis of [Ir(ppy)$_2$(bpm)]PF$_6$.H$_2$O (20)

Bipyrimidine ligand (bpm) (0.0221 g, 0.1402 mmol) was weighed into a 100 ml R.B to which 20 ml of solvent, DCM: MeOH (2:1) was added and heated at 60 ^{0}C for 15 min at room temperature in N_2 atmosphere. The dichlorobridged dimer, $[Ir(ppy)_2Cl]_2$ (0.05 g, 0.04673 mmol) was dissolved in 20 ml of DCM and was added dropwise in 2 hours to the reaction mixture. The colour of the solution changes from yellow to wine red. The reaction mixture was refluxed (70 ^{0}C) for 6 hours, cooled to room temperature, solvents were all removed and the residue was dissolved in deionised water and filtered. To the filtrate 5 ml of saturated KPF_6 (1 g in 10 ml) was added and kept in fridge overnight resulting in the precipitation of a orange-yellow product which was recrystallised from acetone : H_2O (1:1), vacuum filtered, washed with diethyl ether and dried to get the product $[Ir(ppy)_2(bpm)].PF_6$ pure. Yield (0.062 g, 0.0754 mmol, 55 %). ^1H NMR (400 MHz, DMSO), δ (ppm): 6.14 (d, 1H, 6' (ppy)), 6.89 (t, 1H, 5' (ppy)), 7.02 (t, 1H, 4' (ppy)), 7.14 (t, 1H, 4 (ppy)), 7.91 (m, 4H, 3', 3, 5 (ppy), b (bpm)), 8.08 (d, 1H, a (bpm)), 8.26 (d, 1H, 6 (ppy)), 9.31 (d, 1H, c (bpm)). Elemental analysis for complex **(20)**, ($C_{30}H_{22}F_6IrN_6P$)H_2O ;(calculated): C : 43.85, H : 2.94, N : 10.23; (found) : C : 43.97, H : 2.79, N : 9.80.

3.2.4.2 Synthesis of [(ppy)$_2$Ir(bpm)PdCl$_2$]PF$_6$.2H$_2$O.CH$_2$Cl$_2$ (21)

[Ir(ppy)$_2$(bpm)]PF$_6$ (0.05 g, 0.0622 mmol) was heated with 1.2 equivalents of Pd(ACN)$_2$Cl$_2$ (0.019 g, 0.0746 mmol) in acetonitrile for 6 hours under reflux. In this process, the colour of the solution changed to dark green. After filtering the solution, the solvent was allowed to evaporate and to which acetone was added and the green precipitate was dissolved completely to which diethyl ether was added resulting in the precipitation of a green complex, which was recrystallised from DCM:Toluene (3:1) mixture, vacuum filtered and dried to get the pure product. Yield (0.055 g, 0.0499 mmol, 90 %). ^{1}H NMR (400 MHz, DMSO), δ (ppm): 6.05 (d, 1H, 6'' (ppy)), 6.11 (d, 1H, 6' (ppy)), 6.92 (m, 2H, 5'', 5' (ppy)), 7.04 (t, 1H, 4'' (ppy)), 7.093 (t, 2H, 4', 4''' (ppy)), 7.28 (t, 1H, 4 (ppy)), 7.96 (m, 6H, 3''', 3'', 3', 5''' (ppy), e, b (bpm)), 8.10 (t, 2H, 5, 3 (ppy)), 8.28 (m, 4H, f, a (bpm), 6''', 6 (ppy)), 9.30 (d, 1H, d (bpm)), 9.33 (d, 1H, c (bpm)). Elemental analysis for complex **(21)**, (C$_{30}$H$_{22}$Cl$_2$F$_6$IrN$_6$PPd) 2H$_2$O.CH$_2$Cl$_2$;(calculated): C : 33.79, H : 2.56, N : 7.63; (found) : C : 33.47, H : 2.20, N : 7.35.

3.2.4.3 Synthesis of [(ppy)$_2$Ir(bpm)PtCl$_2$]PF$_6$ (22)

[Ir(ppy)$_2$(bpm)]PF$_6$ (0.050g, 0.0622 mmol) was added to an RB dissolved in DCM. Pt(dmso)$_2$Cl$_2$ (0.0262g, 0.0622mmol) was also added dissolved in DCM. The mixture was refluxed for 24 hour, after which hexane was added resulting in precipitation of the product as grey powder, washed with diethyl ether and dried. Yield (0.036 g, 0.0336 mmol, 55 %). ^{1}H NMR (400 MHz, DMSO), δ (ppm): 6.06 (d, 1H), 6.16 (d, 1H), 6.91 (t, 2H), 7.04 (t, 2H), 7.17 (m, 2H), 7.95 (m, 4H), 8.11 (m, 2H), 8.27 (t, 2H), 8.34 (d, 1H), 9.34 (m, 2H), 9.70 (d, 1H), 9.78 (d, 1H). The CHN was out of range for this complex

3.2.4.4 Synthesis of [(ppy)$_2$Ir(bpm)Ir(ppy)$_2$](PF$_6$)$_2$ (23)

2,2' Bipyrimidine (bpm) (0.010 g, 0.0632 mmol) ligand was added to 10 ml of DCM: MeOH (2:1) mixture taken in an R.B and heated with continuous stirring for 15 minutes at 50 ^{0}C to which [Ir(ppy)$_2$Cl]$_2$ (0.0676 g, 0.0632 mmol) was added slowly and stirred at reflux for 7 hours after which the reaction mixture was cooled, filtered and aqueous KPF$_6$ was added to the filtrate resulting in the precipitation of the complex which was recrystallised from acetone : water (1:1) mixture and vacuum dried. Yield (0.013 g, 0.0089 mmol, 20 %). ^{1}H NMR (400 MHz, DMSO), δ (ppm): 6.10 (d, 1H, 6' (ppy)), 6.94 (m, 1H, 5' (ppy)), 7.05 (t, 1H, 4' (ppy)), 7.29 (t, 1H, 4 (ppy)), 7.919 (d, 1H, 3' (ppy)), 7.99 (t, 1H, 5 (ppy)), 8.12 (m, 2H, a (bpm), 3 (ppy)), 8.28 (m, 2H, b (bpm), 6 (ppy)). Elemental analysis for complex **(23)**, ($C_{52}H_{38}F_{12}Ir_2N_8P_2$); (calculated): C : 43.09, H : 2.64, N : 9.73; (found) : C : 43.97, H : 2.79, N : 9.80.

3.2.4.5 Synthesis of [Ir(ppy-COOCH$_3$)$_2$(bpm)]PF$_6$.CH$_2$Cl$_2$ (24)

[Ir(ppy-COOCH$_3$)$_2$Cl]$_2$ (0.030 g, 0.02297 mmol) dissolved in 20 ml DCM was added to a refluxing solution of bpm (0.0072 g, 0.04594 mmol) in a solvent mixture of DCM : MeOH (2:1) dropwise slowly taking around 2 hours. The reaction mixture was kept at reflux overnight. The solvents were removed, water was added, filtered and to the filtrate saturated aq KPF_6 was added resulting in the precipitation of the complex which was vacuum filtered , washed with water and diethyl ether and dried to obtain pure product. Yield (0.023 g, 0.0228 mmol, 90 %). ^{1}H NMR (400 MHz, DMSO), δ (ppm): 3.69 (s, 3H), 6.76 (s, 1H, 6' (ppy-OMe)), 7.32 (t, 1H, 4' (ppy-OMe)), 7.62 (dd, 1H,4 (ppy-OMe)), 7.87 (t, 1H, b (bpm)), 8.03 (d, 1H, 3' (ppy-OMe)), 8.12 (m, 3H, 3, 5 (ppy-OMe), a (bpm)), 8.44 (d, 1H, 6 (ppy-OMe)), 9.35 (d, 1H, c (bpm)). Elemental analysis for complex **(24)**, ($C_{34}H_{26}F_6IrN_6O_4P$)CH_2Cl_2; (calculated): C : 41.84, H : 2.81, N : 8.36; (found) : C : 41.70, H : 2.73, N : 8.05.

3.2.5 Synthesis of mononuclear cyclometallated iridium complexes with ligand dpp

3.2.5.1 Synthesis of [Ir(ppy)$_2$(dpp)]PF$_6$.2H$_2$O (25)

The ligand 2,5-dpp (0.064 g, 0.2733 mmol) was weighed and transfered to a 100 ml round bottom flask (R.B) to which 20ml of solvent, DCM: MeOH (2:1) was added and stirred at 70 ^{0}C for 20 minutes to which the Acetonitrile complex derived from dichlorobridged dimer [Ir(ppy)$_2$Cl]$_2$ (0.100g, 0.13665mmol) dissolved in 20 ml of solvent (DCM) was added slowly in about 4 hours dropwise. The reaction was heated in reflux (80 ^{0}C) overnight. The reaction mixture was cooled and solvents were all removed by vacuum rota evaporator, 10 ml of deionised water was added, filtered and to the filtrate saturated aqueous KPF_6 (1 g in 10 ml of deionised water) was added resulting in the precipitation of the product [Ir(ppy)$_2$(2,5-dpp)]PF$_6$, which was filtered , washed with water and diethyl ether and was recrystallised from acetone : H_2O (2:1), vacuum filtered and dried. Yield (0.078 g, 0.0851 mmol, 66 %). ^{1}H NMR (400 MHz, DMSO), δ (ppm): 6.315 (d, 1H, 6'' (ppy)), 6.371 (d, 1H, 6' (ppy)), 6.95 (m, 2H, 5'', 5' (ppy)), 7.07 (m, 4H, 4'', 4', 4''', 4 (ppy)), 7.49 (t, 1H, b (dpp)), 7.78 (t, 1H, 3''' (ppy)), 7.83 (d, 1H, 3 (ppy)), 7.94 (m, 5H, 6, 6''', 3'', 3' (ppy), d, c (dpp)), 8.13 (m, 2H, 5''' (ppy)), 8.23 (t, 2H, h (dpp)), 8.36 (t, 1H, c (dpp)), 8.42 (d,1H, g (dpp)), 8.54 (d, 1H, a (dpp)), 9.06 (d, 1H, j (dpp)), 9.10 (s, 1H, f (dpp)), 10.07 (s, 1H, e (dpp)). Elemental analysis for complex **(24)**, ($C_{36}H_{26}F_6IrN_6P$)2H_2O; (calculated): C : 47.21, H : 3.30, N : 9.18; (found) : C : 47.01, H : 2.90, N : 8.88.

3.3 Results and Discussion

3.3.1 Synthesis

For the synthesis of the iridium mononuclear complexes given in section 3.2.1, two different reaction methods were used and both of them worked well. One method involved refluxing the dichlorobridged dimer $[Ir(ppy)Cl]_2$ with the N^N ligands (bpy, $d_8$bpy, phen, $d_8$phen, dmbpy, d_{12}dmbpy, dtbpy, d_{24}dtbpy) in ethylene glycol at 150 ^{0}C, precipitation with KPF_6 and purification by recrystallisation. The second method involved refluxing $[Ir(ppy)Cl]_2$ with the N^N ligands in a DCM : EtOH (3:1) mixture, precipitation by KPF_6 and purification by recrystallisation from a acetone : water mixture. The synthesis of the mononuclear and heterodinuclear (Ir-Pt/Pd) iridium complexes with ligand bpp was explained in section 3.2.2. The synthesis of the mononuclear complexes were carried out in DCM : EtOH (3:1) mixture. Care was taken in adding the dichlorobridged dimer complex to the ligand (the precursor dissolved in the same solvent mixture was added dropwise in 2 hour time interval). For the heterodinuclear Ir-Pt complexes the mononuclear iridium complexes **(9)** and **(12)** were reacted with K_2PtCl_4 in methanol. This reaction has to be done carefully with a minimum amount of solvent and the reaction temperature of 105 ^{0}C has to be kept constant throughout the entire reaction. The reaction for **(10)** requires 24 h for completion and **(13)** requires 48 h after which the complex which forms is filtered, washed with excess methanol and recrystallised from an acetone : diethylether (2:1) mixture 2-3 times. The same method was used for the reaction of these monomers with $(NH_4)_2PdCl_4$.

The synthesis of the mononuclear and heterodinuclear (Ir-Pt/Pd) iridium complexes with the ligand tpy is given in section 3.2.3. The mononuclear complexes **(15)**, **(17)** and **(19)** were synthesised according to the same method as explained above. The reaction was carried out in a DCM : EtOH (3:1) mixture. Care was taken in the addition of the dichlorobridged dimer complex to the ligand. The product was recrystallised from an acetone : water (2:1) mixture. The reaction of these mononuclear complexes with K_2PtCl_4 was tried using a similar method as explained for complexes **(10)** and **(13)**. But unfortunately even by changing the reaction conditions (solvent, temperature and reaction time) the reaction did not work. One reason might be the steric strain as the tpy ligand has one pyridine ring attached to the 6 position of the middle pyridine ring which might be causing some problem for complexation of Pt. But both the monomers undergo reaction with $(NH_4)_2PdCl_4$ and it was possible to isolate the products completely pure. For complex **(16)** the reaction time was 24 h at a temperature of 105 ^{0}C whereas for complex **(18)** the reaction time was 48 h at a temperature of 105 ^{0}C.

The synthetic details of the mononuclear, homodinuclear (Ir-Ir) and heterodinuclear (Ir-Pd/Pt) iridium complexes **(20)**, **(21)**, **(22)**, **(23)** and **(24)** with the bpm ligand are shown in section 3.2.4. Synthesis of the mononuclear complexes **(20)** and **(24)** uses the same procedure as explained above for bpp and tpy ligands. The only change made was the solvent mixture, MeOH was used instead of EtOH. Care has to be taken in adding $[Ir(ppy)_2Cl]_2$ dissolved in DCM to the bpm ligand dissolved in a DCM : MeOH (2:1) solvent mixture as the possibility of dimer formation is very high for these complexes. For the Ir-Pd dinuclear complex **(21)** the the mononuclear complex **(20)** was reacted with $[Pd(ACN)_2Cl_2]$ in acetonitrile. The reaction was complete in 6 h following reflux at 70 ^{0}C. Precipitation by adding diethylether after dissolving in acetone resulted in a pure complex which was vacuum filtered and dried. For the Ir-Pt dinuclear complex **(22)** the mononuclear complex **(20)** was reacted with $[Pt(dmso)_2Cl_2]$ in DCM. The complex precipitated from solution and was vacuum filtered, dissolved in acetone and reprecipitated by adding hexane and diethylether. For the homodinuclear Ir-Ir complex **(23)** rather than taking 2 equivalents of the bridging ligand, a 1:1 mixture of the dichlorobridged precursor and bpm ligand was reacted in a DCM : MeOH (2:1) mixture, and heated at a reflux temperature (90 ^{0}C) for 7 hours after which solvents were removed and the residue was dissolved in water which was filterd to remove any excess bpm ligand. To the filtrate a saturated aq. KPF_6 solution was added resulting in precipitation of the PF_6^-complex which was then recrystallised from acetone : water (2:1) and dried. The synthesis of the mononuclear iridium complex with the ligand dpp is explained in section 3.2.5. The method used is exactly the same as that explained above for the other mononuclear complexes. Sufficient care has to taken while adding the dichlorobridged iridium precursor complex, slowly drop by drop in a time interval of 4 hour. After the reaction solvents were removed, dissolved in water and filtered to remove any excess amount of dpp and the complex is precipitated by counter ion exchange by adding saturated aq.KPF_6. The product was recrstallised from acetone : water and dried.

3.3.2 ^{1}H NMR spectroscopic charecterisation

The structure of complexes **(1)** to **(8)** with the ^{1}H NMR assignments is given in figure 3.8 below.

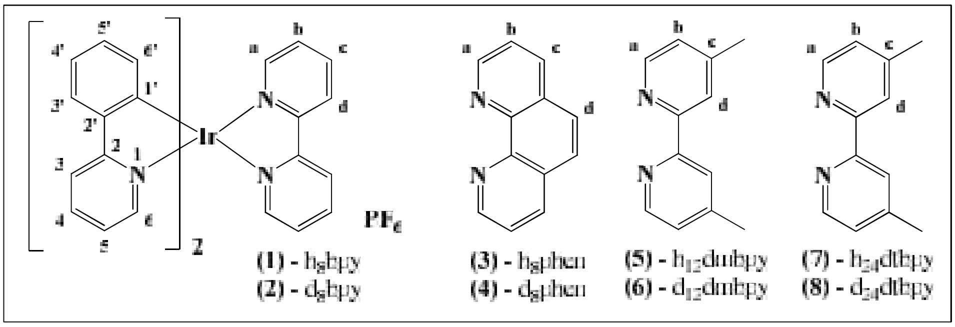

Figure 3.8 Structural representation with the ^{1}H NMR assignments for complexes (1) to (8).

The ^{1}H NMR spectra for complex [Ir(ppy)$_2$(bpy)]PF$_6$ **(1)** and [Ir(ppy)$_2$(d$_8$bpy)]PF$_6$ **(2)** along with the peak assignments are given in figure 3.9 below.

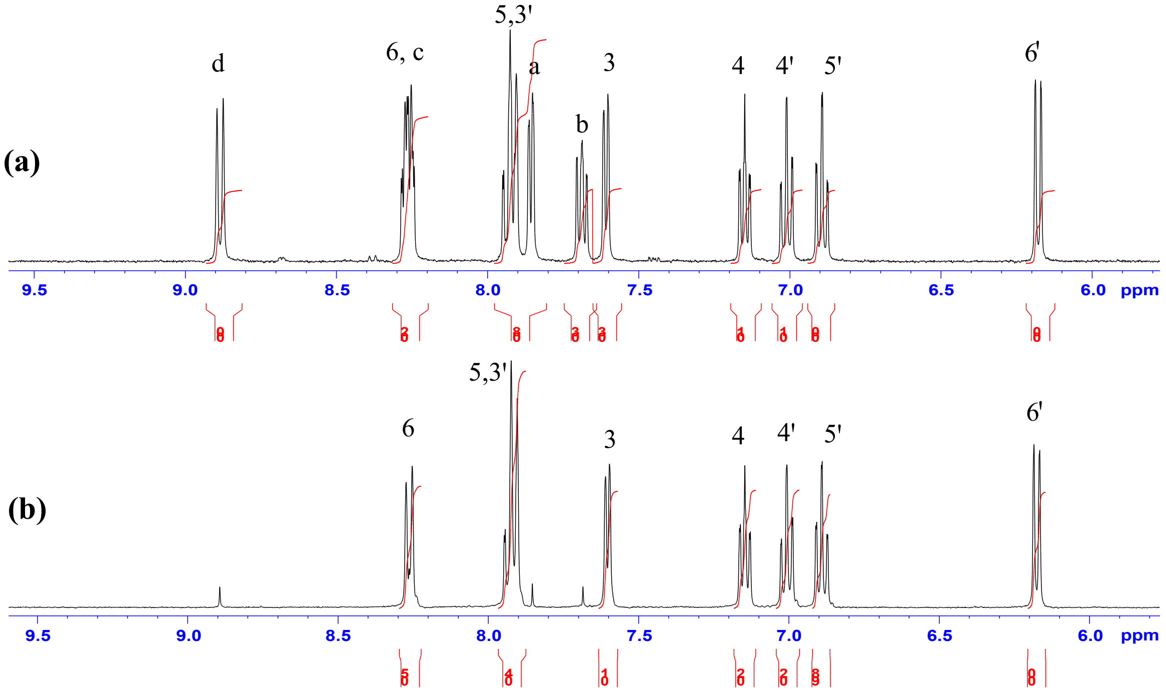

***Figure 3.9** ^{1}H NMR Spectrum of **(a)** [Ir(ppy)$_2$(bpy)]PF$_6$ **(1)** and **(b)** [Ir(ppy)$_2$(d$_8$bpy)]PF$_6$ **(2)** in d$_6$ dmso using 400 MHz instrument.*

From the above figure 3.9 it is quite clear that deuteriation of the bpy ligand results in the disappearence of NMR peaks (a, b, c and d) corresponding to the bpy ligand as shown in figure 3.8. Similarly the NMR spectra for complexes [Ir(ppy)$_2$(phen)]PF$_6$ **(3)** and

[Ir(ppy)$_2$(d$_8$phen)] PF$_6$ **(4)** are given in figure 3.10 below in which the peaks corresponding to the 1,10-phenanthroline (phen) ligand (a, b, c and d) as shown in figure 3.8 are clearly seen in the NMR for the protonated complex **(3)** (figure 3.10(a)) but are absent in the NMR for the deuteriated complex **(4)** (figure 3.10(b)). Detailed tabulated data with all the peaks are given in table 3.1.

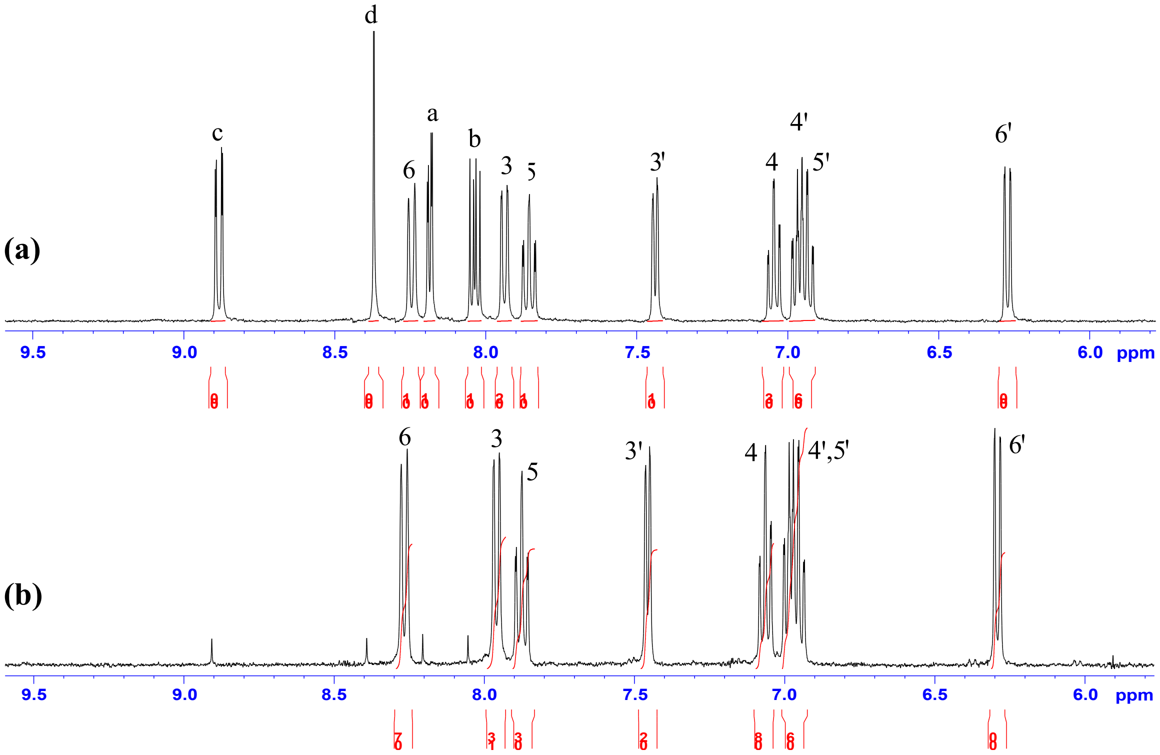

Figure 3.10 *^{1}H NMR Spectrum of **(a)** [Ir(ppy)$_2$(phen)]PF$_6$ **(3)** and **(b)** [Ir(ppy)$_2$(d$_8$phen)]PF$_6$ **(4)** in d$_6$ dmso.*

From the above figure it is evident that the doublet at δ 8.88 corresponding to proton c of the phen ligand (figure 3.8) seen in figure 3.10 (a) disappears for the deuteriated complex **(4)** as given in figure 3.10 (b). Similar is the case with protons numbered a, b and d, the peaks corresponding to these protons disappeared in the spectra for the deuteriated complexes.

The ^{1}H NMR spectra for complexes [Ir(ppy)$_2$(dmbpy)]PF$_6$ **(5)** and [Ir(ppy)$_2$(d$_{12}$dmbpy)]PF$_6$ **(6)** along with the peak assignments are given in figure 3.11 below. As given in figure 3.8 the peaks corresponding to the protons of the dmbpy ligand are a, b and d. Since the methyl group is substituted at position c in the dmbpy ligand, the peak corrsponding to c for complex **(1)** and **(2)** are absent in this case. From the figure 3.11 **(a)** and **(b)** it is clear that the peaks corresponding to protons a, b and d are absent in the deuteriated complex **(6)**. The NMR spectra for complexes [Ir(ppy)$_2$(dtbpy)]PF$_6$ **(7)** and [Ir(ppy)$_2$(d$_{24}$dtbpy)]PF$_6$ **(8)** are given in appendix B. The tabulated values for the ^{1}H NMR shifts for all these complexes are given in table 3.1 below.

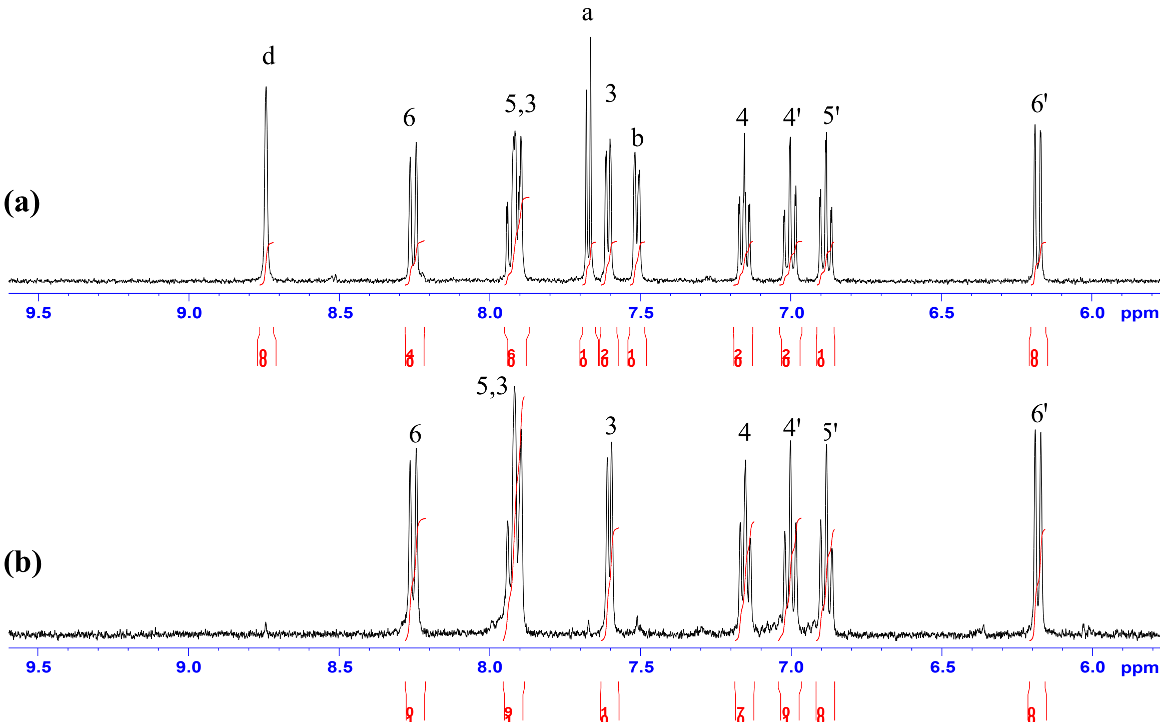

Figure 3.11 *^{1}H NMR Spectrum of **(a)** [Ir(ppy)$_2$(dmbpy)]PF$_6$ **(5)** and **(b)** [Ir(ppy)$_2$(d$_{12}$dmbpy)] PF$_6$ **(6)** in d$_6$ dmso.*

Complex	3'	4'	5'	6'	a	b	c	d
(1)	7.92	7.01	6.89	6.17	7.85	7.68	8.26	8.88
(2)	7.92	7.01	6.89	6.17	resd. s	resd. s	resd. s	resd. s
(3)	7.43	6.95	6.95	6.27	8.18	8.03	8.88	8.37
(4)	7.43	6.95	6.95	6.27	resd. s	resd. s	resd. s	resd. s
(5)	7.91	7.00	6.88	6.17	7.66	7.50	-	8.74
(6)	7.91	7.00	6.88	6.17	resd. s	resd. s	resd. s	resd. s
(7)	7.93	7.00	6.89	6.16	7.75	7.60	-	8.86
(8)	7.93	7.00	6.89	6.16	resd. s	resd. s	resd. s	resd. s

Table 3.1 *Tabulated ^{1}H NMR shift values for complexes **(1)** to **(8)** done in d$_6$ dmso.*

The structural representation along with the numbering of protons for mononuclear cyclometallated iridium complexes with ligands bpp, tpy, bpm and dpp are given in figure 3.12 below.

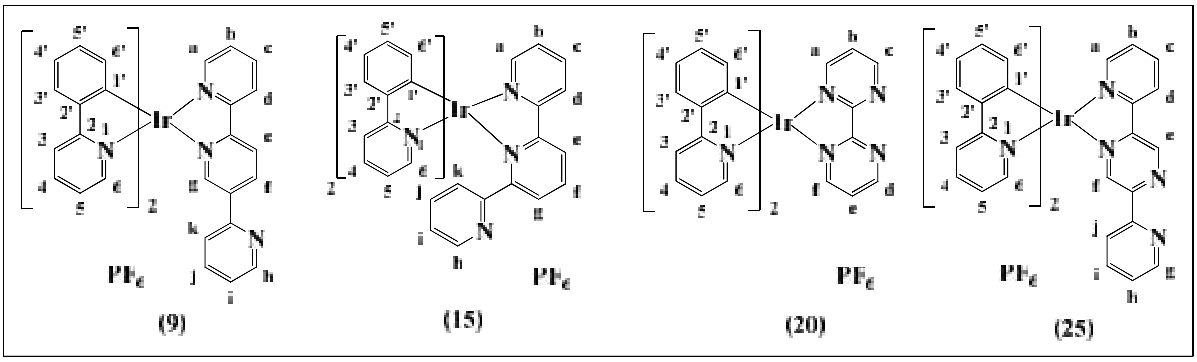

Figure 3.12 *Structural representation with the ^1H NMR assignments of cyclometallated iridium complexes with ligands bpp, tpy, bpm and dpp.*

The ^{1}H NMR spectra for complexes [Ir(ppy)$_2$(bpp)]PF$_6$ **(9)**, [Ir(ppy)$_2$(bpp)PtCl]$_2$(PF$_6$)$_2$ **(10)** and [Ir(ppy)$_2$(bpp)PdCl]$_2$(PF$_6$)$_2$ **(11)** are given in figure 3.13 below.

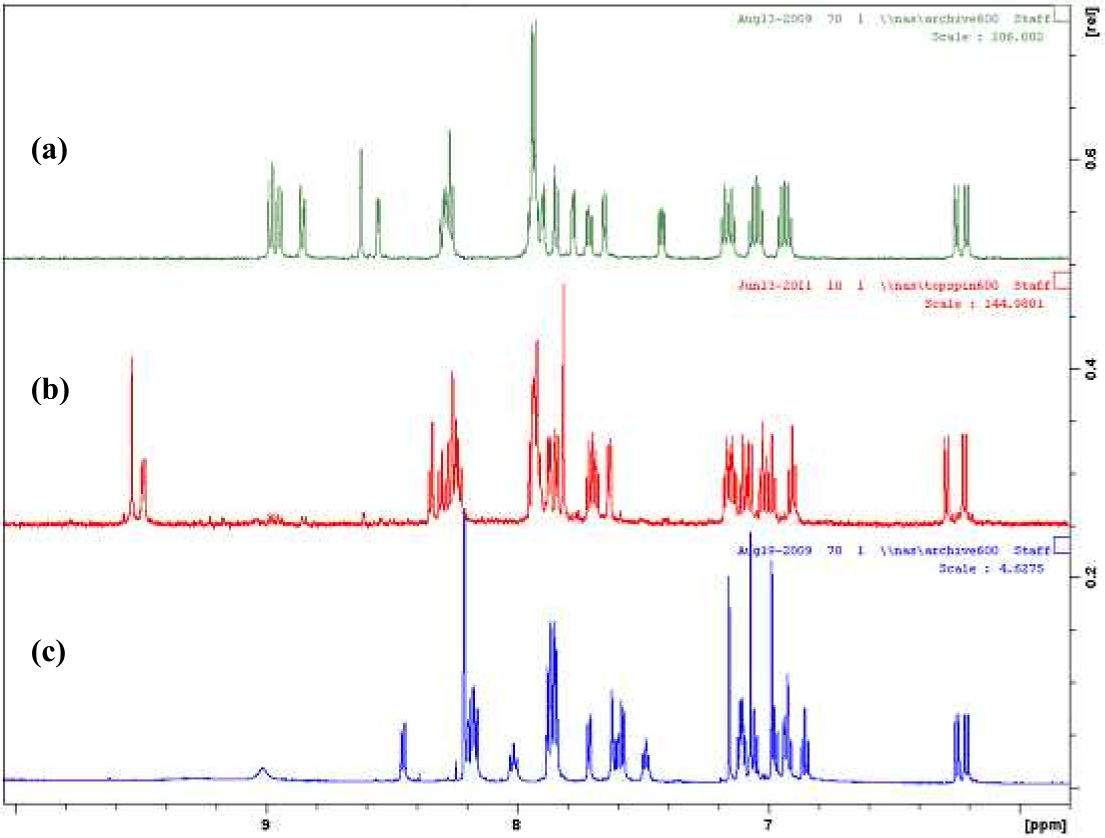

Figure 3.13 *^1H NMR Spectrum of **(a)** [Ir(ppy)$_2$(bpp)]PF$_6$ **(9)** and **(b)** [Ir(ppy)$_2$(bpp)PtCl]$_2$ (PF$_6$)$_2$ **(10)** and **(c)** [Ir(ppy)$_2$(bpp)PdCl]$_2$(PF$_6$)$_2$ **(11)** in d_6 DMSO.*

The NMR spectrum for all the three complexes are on the same scale in figure 3.13. From figure 3.13, if the ^{1}H NMR spectra of the monomer (green) is compared with the Ir-Pt dimer (red) and Ir-Pd dimer (blue) it is clear that there are prominent shifts in the δ values. Pt and

Pd are attached to the ligand in a cyclometallated way as given in figure 3.12. The ^{1}H NMR chemical shift values for some of the protons are given in table 3.2 below. For both dinuclear complexes the peak corresponding to proton f is absent, as the Pt or Pd binds at this position. Since both these metals cause shielding, the signals are shifted downfield for both the dimers. The proton NMR spectrum of the ester analogous complexes are given in appendix B where the substitution of ester group is at the 5' position.

Complex	6'	6	5'	5	a	e	f	h
(9)	6.25	7.66	6.94	7.16	8.55	7.94	7.94	8.99
(10)	6.30	7.66	7.03	7.18	7.90	9.54	_	9.51
(11)	6.26	7.90	6.96	7.15	8.23	9.09	_	8.46

Table 3.2 *Tabulated ^{1}H NMR shift values for complex* ***(9)****,* ***(10)*** *and* ***(11)*** *in d_6 dmso.*

The ^{1}H NMR spectra for complexes [Ir(ppy)$_2$(tpy)]PF$_6$ **(15)**, [Ir(ppy)$_2$(tpy)PdCl]$_2$(PF$_6$)$_2$ **(16)** [Ir(ppy-COOCH$_3$)$_2$(tpy)]PF$_6$ **(17)**, and [Ir(ppy-COOCH$_3$)$_2$(bpp)PdCl]$_2$(PF$_6$)$_2$ **(18)** are given in figure 3.14 below. The figure suggests that complexation of Pd leads to shifting of the NMR peaks for both **(15)** and ester containing complex **(17)**. Figure 3.14 (a) gives the NMR for the mononuclear complex [Ir(ppy)$_2$(tpy)]PF$_6$ **(15)**, the Pd dimer complex of [Ir(ppy)$_2$(tpy)PdCl]$_2$(PF$_6$)$_2$ **(16)** is given in figure 3.14 (b). By comparing these two NMR spectra, complexation with Pd resulted in a greater downfield shifts in NMR peaks. Important is the disappearence of peak corresponding to proton g for the dimer complex (figure 3.14 (b) and table 3.3). This is due to the complexation of Pd in a cyclometallated manner to the middle pyridine ring at position g. The peak for the proton at position h of the tpy ligand (figure 3.12 (a)) in the mononuclear complex at δ 8.85 ppm was shifted to 8.60 ppm as a result of complexation. The prominent shifts observed for some of the protons are given in table 3.3 below, the rest are included in appendix B. The NMR spectrum of the complex [Ir(ppy-COOCH$_3$)$_2$(tpy)]PF$_6$ **(17)** is given in figure 3.14 (c). Comparing this with the NMR spectra of complex **(20)** the effect of electron withdrawing ester groups is evident in the downfield shift of the protons. Also the ester group is substituted at the 5' position of ppy ligand therefore the peak at 5' postion is absent in both the monomer **(17)** and dimer **(18)**. The NMR spectra of the ester Ir-Pd dimer complex [Ir(ppy-COOCH$_3$)$_2$(bpp)PdCl]$_2$(PF$_6$)$_2$ **(18)** is given in figure 3.14 (d). By comparing figure 3.14 (c) and (d) the effect of Pd complexation is clear, there is a downfield shift in the NMR peaks. The peak corresponding to the proton at position g in the monomer is absent in the dimer complex as a result of cyclometallated binding to the Pd metal. Also the broad peak corresponding to proton h of the tpy ligand (figure 3.12) was shifted from δ 9.05 to δ 8.71 ppm. The NMR spectra for the aldehyde substituted complex [Ir(ppy-CHO)$_2$(tpy)]PF$_6$ **(19)** is given in appendix B. The proton NMR shifts for some of the main peaks for complexes **(15)**, **(16)**, **(17)**, **(18)** and **(19)** are given in table 3.3 below. NMR's were carried out in d$_6$ dmso.

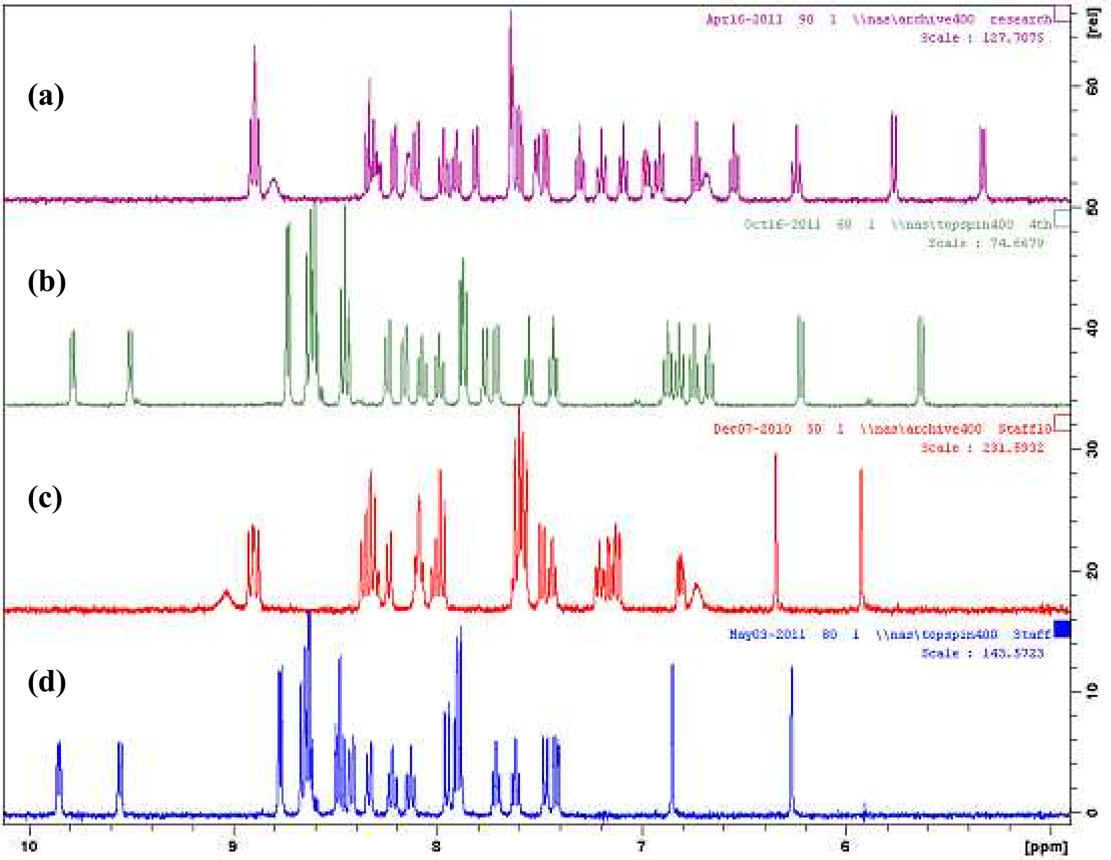

Figure 3.14 *^{1}H NMR Spectrum of* ***(a)*** *[Ir(ppy)$_2$(tpy)]PF$_6$* ***(15), (b)*** *[Ir(ppy)$_2$(tpy)PdCl]$_2$(PF$_6$)$_2$* ***(16), (c)*** *[Ir(ppy-COOCH$_3$)$_2$(tpy)]PF$_6$* ***(17)*** *and* ***(d)*** *[Ir(ppy-COOCH$_3$)$_2$(bpp)PdCl]$_2$(PF$_6$)$_2$* ***(18)*** *in d$_6$ DMSO.*

Complex	6'	5'	4'	3'	a	e	g	h
(15)	5.82	6.80	7.01	7.52	7.57	7.87	6.78	8.85
(16)	6.22	6.74	6.87	7.77	8.61	8.72	-	8.60
(17)	5.93	-	7.17	7.59	7.49	7.59	6.79	9.05
(18)	6.82	-	7.44	7.88	8.59	8.74	-	8.71
(19)	6.24	-	7.48	8.12	8.12	7.61	6.71	9.09

Table 3.3 *Tabulated ^{1}H NMR shift values for complex* ***(15)****,* ***(16)****,* ***(17)*** *and* ***(18)*** *in d$_6$ dmso.*

The ^{1}H NMR spectra for complexes [Ir(ppy)$_2$(bpm)]PF$_6$ **(20),** [Ir(ppy)$_2$(bpm)PdCl$_2$]PF$_6$ **(21),** [Ir(ppy)$_2$(bpm)Ir(ppy)$_2$](PF$_6$)$_2$ **(23)** and [Ir(ppy-COOCH$_3$)$_2$(bpm)]PF$_6$ **(24)** in d$_6$ dmso is given in figure 3.15 below.

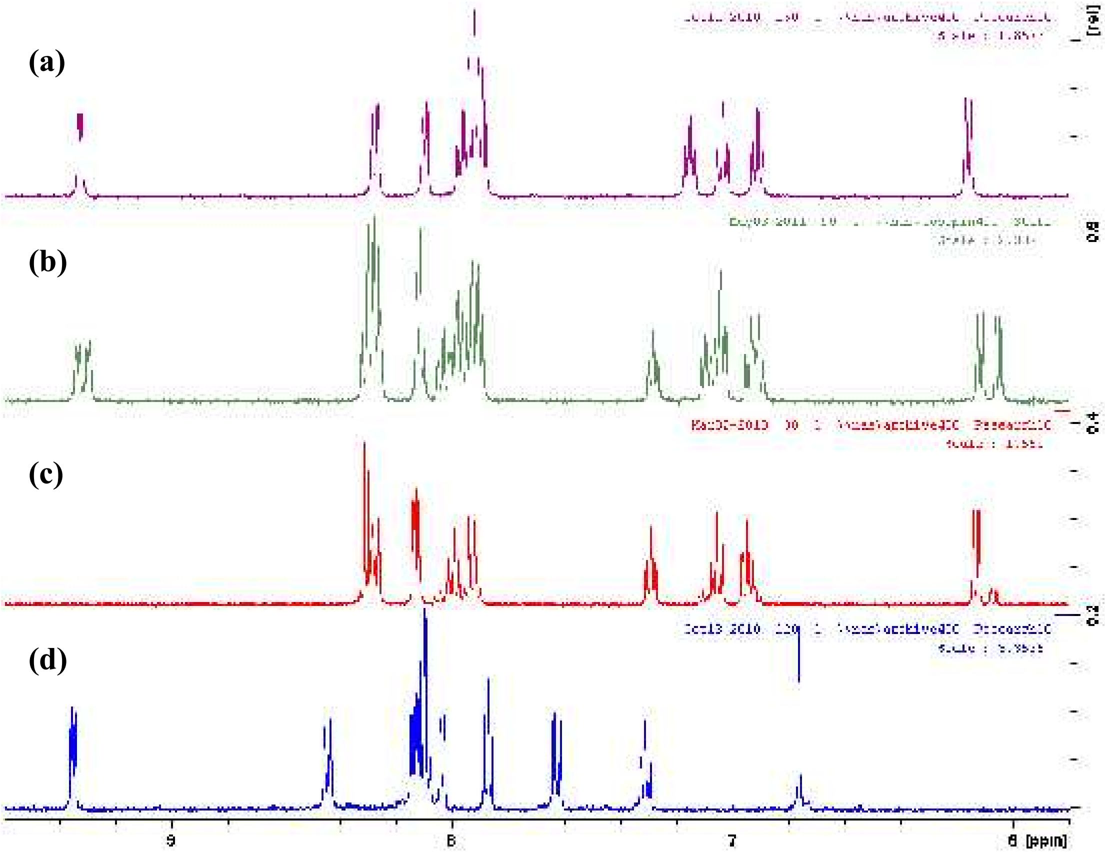

Figure 3.15 *^{1}H NMR spectra of **(a)** [Ir(ppy)$_2$(bpm)]PF$_6$ **(20), (b)** [Ir(ppy)$_2$(bpm)PdCl$_2$]PF$_6$ **(21), (c)** [Ir(ppy)$_2$(bpm)Ir(ppy)$_2$](PF$_6$)$_2$ **(23)** and **(d)** [Ir(ppy-COOCH$_3$)$_2$(bpm)]PF$_6$ **(24)** in d$_6$ dmso.*

The mononuclear complex [Ir(ppy)$_2$(bpm)]PF$_6$ **(20)** has an axis of symmetry. This is confirmed from the NMR as the total number of protons integrated was 11 confirming this. All the peaks is assigned as shown in the experimental section 3.2.4. Some of the main peaks with their chemical shift values are tabulated in table 3.4. The NMR spectra for the dinuclear complex [Ir(ppy)$_2$(bpm)PdCl$_2$]PF$_6$ **(21)** is given in figure 3.15 (b). Comparing this NMR spectrum (figure 3.15(b)) with the mononuclear complex (figure 3.15(a)) above it is clear that complexation with Pd results in loss of symmetry. It is interesting to compare these NMR with the NMR of the homodinuclear complex [Ir(ppy)$_2$(bpm)Ir(ppy)$_2$](PF$_6$)$_2$ **(23)** (figure 3.15(c)). The latter complex has two symmetry axis, as shown by the integration value for all the peaks given in figure 3.12 (c) which integrate for only 10 protons. The peak at the very high ppm value of δ 9.31 for the mononuclear complex is not seen in this homodinuclear complex as is evident by comparing the spectra (a) and (c) in the above figure. Finally the NMR spectra for the ester analogous complex [Ir(ppy-COOCH$_3$)$_2$(bpm)]PF$_6$ **(24)** is given in figure 3.12 (d). There is a considerable downfield shift as a result of substitution of the electron withdrawing group at the 5' position. Also the peak at δ 6.89 corresponding to the proton at 5' position for complex **(20)** is not present for complex **(24)** due to the ester substitution. Some of the prominent NMR shifts for the above mentioned complexes are tabulated in table 3.4 below. The NMR spectra for the Ir-Pt dinuclear complex $[Ir(ppy)_2(bpm)PtCl_2]PF_6$ **(22)** is given in appendix B.

Complex	6'	5'	4'	3'	a	b	c
(20)	6.14	6.89	7.02	7.91	8.08	7.91	9.31
(21)	6.11	6.92	7.093	7.96	8.28	7.96	9.33
(23)	6.10	6.94	7.05	7.92	8.12	8.28	-
(24)	6.76	-	7.32	8.03	8.12	7.87	9.35

***Table 3.4** Tabulated ^1H NMR shift values for complex **(20)**, **(21)**, **(23)** and **(24)** in d_6 dmso.*

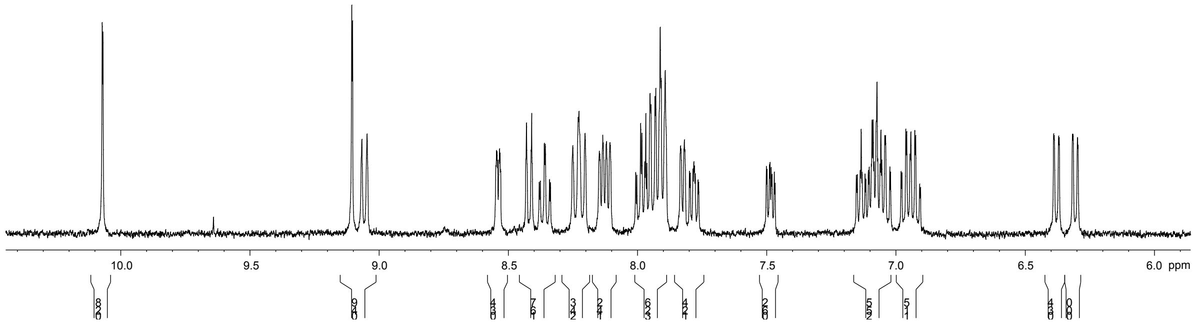

***Figure 3.16** ^1H NMR spectra of $[Ir(ppy)_2(2,5\text{-}dpp)]PF_6$ **(25)** in d_6 acetone.*

The ^1H NMR spectra for complex $[Ir(ppy)_2(2,5\text{-}dpp)]PF_6$ **(25)** measured in d_6 acetone is given in figure 3.16 above. Assignment of peaks are given in detail in the synthetic section 3.2.5.

3.3.3 Excited state photophysics

Cationic cyclometallated heteroleptic Ir (III) complexes have been studied in detail[56,57,58] of which the complex $[Ir(ppy\text{-}N^\wedge C)_2(bpy\text{-}N^\wedge N)]^+$ (where bpy is 2,2'-bipyridine and ppy is 2-phenylpyridine) is one of the standard complexes whose photophysics is well discussed.[59,60,61] Watts *et al.* observed dual emission with maxima at 520 and 560 nm for the mixed chelate/orthometallate complex, $[Ir(ppy)_2bpy]^+$, which they attribute to low lying $^3MLCT_{ppy}$ and $^3MLCT_{bpy}$ states.[62,63,64,65,66] These two states have an undifferentiated lifetime about 5.0 μs at 77 K and 0.35 μs in room temperature. Recently Chen *et al.* studied the emission mechanism for the above mentioned complex using time resolved spectroscopy, and according to them three basic transition processes are commonly encountered, namely ligand centred (LC) transitions, metal to ligand charge transfer transitions (MLCT), and ligand to ligand charge transfer (LLCT) transitions.[60,67,74]

3.3.3.1 Absorption measurements

The absorption spectra for complexes **(1)** to **(8)** measured in spectroscopic grade ACN at room temperature are given in figures 3.17 and 3.18. The bands were assigned by comparing the absorption spectra obtained in this study with the previous published results.[60-67]

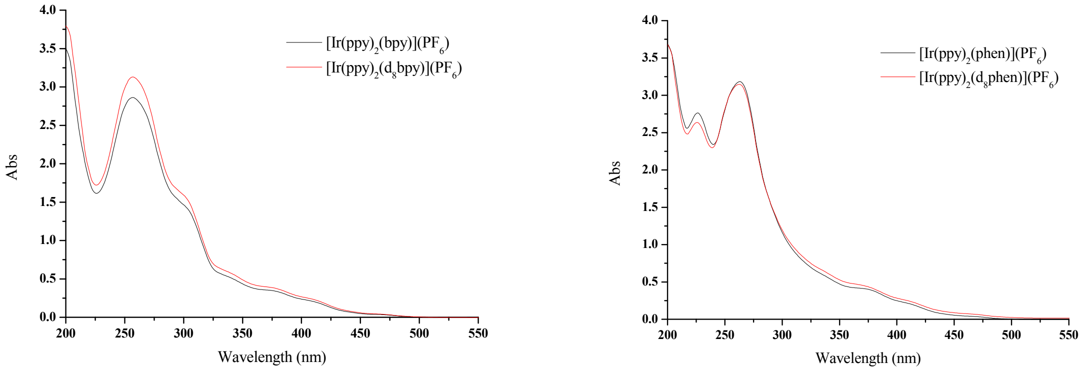

(a) **(b)**

Figure 3.17 ***(a)*** *Absorption spectra of $[Ir(ppy)_2(bpy)](PF_6)$* ***(1)*** *and $[Ir(ppy)_2(d_8bpy)](PF_6)$****(2)*** ***(b)*** *Absorption spectra of $[Ir(ppy)_2(phen)](PF_6)$* ***(3)*** *and $[Ir(ppy)_2(d_8phen)](PF_6)$* ***(4)****. All measurements were done in aerated ACN (298 K) at a conc. of 6×10^{-5}M*

The absorption features in the range of 250-350 nm are assigned to intra ligand charge transfer transitions which include ppy(π)→ppy(π*) and bpy(π)→bpy(π*) transitions. The absorption features between 350-400 nm are assigned to ligand to ligand charge transfer (LLCT) transitions ie. [ppy(π)→bpy(π*)]. The absorption bands in the range 400-500 nm are assigned to ^{1}MLCT and ^{3}MLCT transitions, with the lowest energy transition involving the substituted bpy ligand in all cases as expected. The deuteriation of the neutral chelating N^N ligand does not have any effect on the position of absorption bands as can be seen from the absorption spectra given above, both the protonated and deuteriated complexes showed similar absorption bands, and this is also observed for the other similar complexes. The absorption spectra for complexes **(5)** to **(8)** are given in figures 3.18 (a) and 3.18 (b).

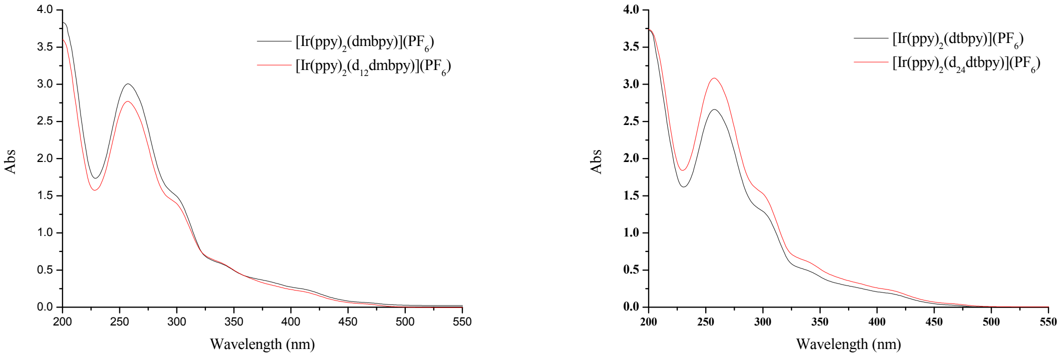

(a) **(b)**

Figure 3.18 (a) *Absorption spectra of [Ir(ppy)$_2$(dmbpy)](PF$_6$)* ***(5)*** *and [Ir(ppy)$_2$(d$_{12}$dmbpy)](PF$_6$)* ***(6) (b)*** *Absorption spectra of [Ir(ppy)$_2$(dtbpy)](PF$_6$)* ***(7)*** *and [Ir(ppy)$_2$(d$_{24}$dtbpy)](PF$_6$)* ***(8)****. All measurements were done in aerated ACN (298 K) at a conc. of 6×10^{-5}M*

The absorption properties of the complexes [Ir(ppy)$_2$(bpp)](PF$_6$) **(9)**, [Ir(ppy)$_2$(bpp)PtCl]$_2$(PF$_6$)$_2$ **(10)** and [Ir(ppy)$_2$(bpp)PdCl]$_2$(PF$_6$)$_2$ **(11)** are discussed in detail in chapter 4. The absorption spectra of the ester complexes [Ir(ppy-COOCH$_3$)$_2$(bpp)](PF$_6$) **(12)**, [Ir(ppy-COOCH$_3$)$_2$(bpp)PtCl]$_2$(PF$_6$)$_2$ **(13)** and [Ir(ppy-COOCH$_3$)$_2$(bpp)PdCl]$_2$(PF$_6$)$_2$ **(14)** are given in figure 3.19 below. Introduction of the electron withdrawing ester group on the peripheral cyclometallating ppy ligand results in a red shift for the absorption bands compared to the non ester complexes (figure 4.28, chapter 4).

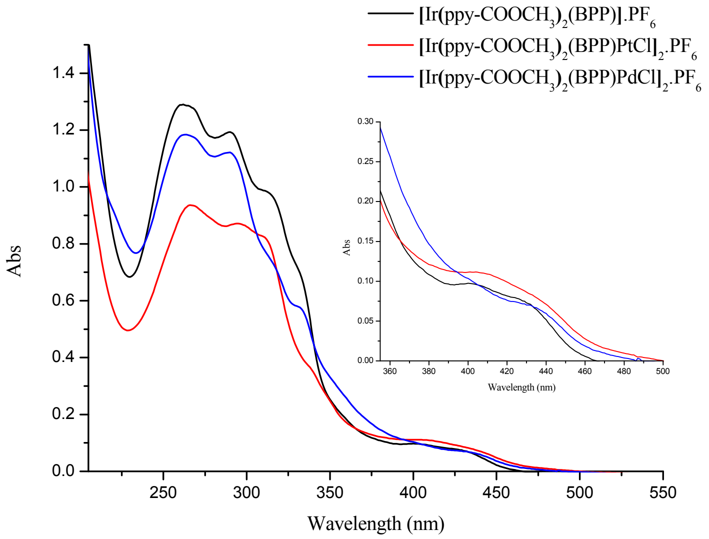

Figure 3.19 *Absorption spectra for complex [Ir(ppy-COOCH$_3$)$_2$(BPP)]$_2$(PF$_6$)* ***(12)*** *along with complex [Ir(ppy-COOCH$_3$)$_2$(BPP)PtCl]$_2$(PF$_6$)$_2$* ***(13)*** *and [Ir(ppy-COOCH$_3$)$_2$(BPP) PdCl]$_2$(PF$_6$)$_2$* ***(14)*** *measured in aerated ACN at room temperature (298 K) (concentration - 6×10^{-5}M). (MLCT region is expanded inside).*

Figure 3.19 shows that for the dinuclear complexes **(13)** and **(14)**, ^{3}MLCT absorption bands were red shifted (MLCT region is enlarged in the box inside graph) compared to the monomer complex **(12)**. This is attributed to the complexation of either Pt or Pd metal to the bpp ligand. The tabulated absorption data and extinction coefficients for all the three complexes measured in ACN are given in appendix B. The absorption spectra for complexes **(15)** to **(19)** are given in figure 3.20 (a) and 3.20 (b) below.

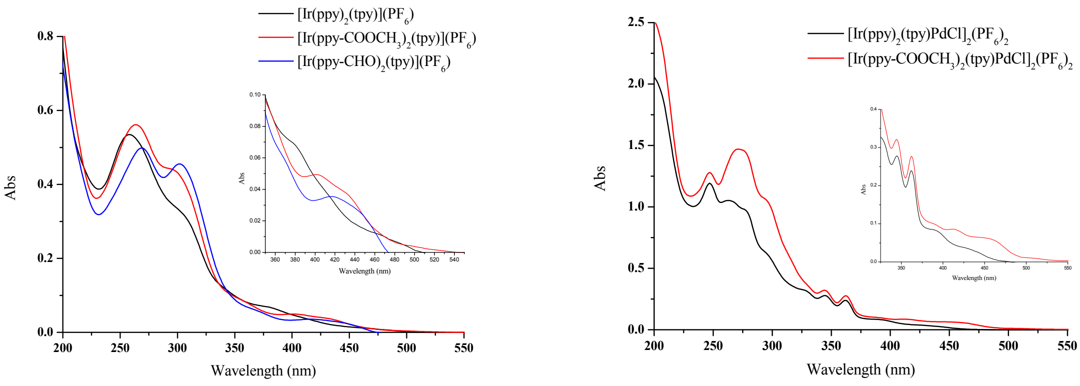

(a) **(b)**

Figure 3.20 (a) *Absorption spectra of [Ir(ppy)$_2$(tpy)](PF$_6$)* ***(15)****, [Ir(ppy-COOCH$_3$)$_2$(tpy)](PF$_6$)* ***(17)*** *and [Ir(ppy-CHO)$_2$(tpy)](PF$_6$)* ***(19) (b)*** *Absorption spectra of [Ir(ppy)$_2$(tpy)PdCl]$_2$(PF$_6$)$_2$* ***(16)*** *and [Ir(ppy-COOCH$_3$)$_2$(tpy)PdCl]$_2$(PF$_6$)$_2$* ***(18)****. All measurements were done in aerated ACN (298 K) at a conc. of 1×10^{-5}M, (MLCT region is expanded inside).*

From figure 3.20 (a) it is evident that substitution of the phenyl pyridine ligand with either an aldehyde or ester group resulted in changes in the absorption spectrum compared to the unsubstituted complex. For both the substituted ppy complexes **(17)** and **(19)**, a peak at around 320 nm is prominent which was reduced to a shoulder for the unsubstituted complex **(15)**. Comparing the absorption spectra (figure 3.20) with reported results[60-67] the band at 320 nm is tentatively assigned to an intraligand charge transfer transition (ILCT) based on the ppy ligands. Substitution of ppy by electron withdrawing groups (like CHO and $COOCH_3$) resulted in a prominent change to these absorption bands. Figure 3.20 (b) gives the absorption spectra of two Ir-Pd dimers [Ir(ppy)$_2$(tpy)PdCl]$_2$(PF$_6$)$_2$ **(16)** and [Ir(ppy-COOCH$_3$)$_2$(tpy) PdCl]$_2$(PF$_6$)$_2$ **(18)** with the ligand tpy. Comparing these absorption spectra with the monomers (figure 3.20 (a)) showed the difference in the bands both in the LC and MLCT regions as a result of Pd complexation. The absorption spectra for complexes **(20)**, **(21)** and **(22)** are given in appendix B.

3.3.3.2 Emission measurements

All of the iridium polypyridyl complexes reported here exhibit luminesence in the region of 500 nm - 650 nm at room temperature in acetonitrile solution. The lowest triplet state, which is responsible for phosphorescence emission for cyclometallating Ir (III) complexes according to Kasha's rule,[68,69] is either a ^{3}MLCT transition state or ^{3}LC transition state. Generally, phosphorescence originating from the LC transition state can be distinguished from that of the MLCT transition state in terms of spectral shape, phosphoresence lifetime (τ_p), rigidochromic and solvatochromic behaviours.[70] The low temperature emission spectra for these complexes are blue shifted in comparison to the room temperature emission which is a characteristic property for the emission from an MLCT excited state. The emission of the starting material, the iridium dichloro bridged dimer, $[Ir(ppy)_2Cl]_2$ was attributed to a metal to ligand charge transfer (MLCT) excited state formed by transfer of charge from Ir (III) to the cyclometallated ppy ligand ($MLCT_{ppy}$).[71,72] When the bridging chlorides of $[Ir(ppy)_2Cl]_2$ are replaced by a π acceptor neutral chelating (N^N) ligand like bpy, the Ir (III) metal center will become a poorer electron donor and the ($MLCT_{ppy}$) state will move up in energy.[71,72] Thus the emission will then takes place from the low lying ($MLCT_{N^\wedge N}$) excited state. Excited state absorption studies[69] of samples of $[Ir(ppy)_2(bpy)]^+$ and $[Ir(bzq)_2(bpy)]^+$ in fluid solutions at room temperature confirms emission from a $MLCT_{bpy}$ excited state which is the lowest excited state in room temperature solutions where equilibration of the two MLCT excited states occurs. In the present work a series of four similar complexes with the deuteriated (N^N) ligands were prepared, ($[Ir(ppy)_2(N^\wedge N)]PF_6$, where N^N ≡ $d_8$bpy, $d_8$phen, d_{12}dmbpy and d_{24}dtbpy) and the effect of deuteriation on the excited state properties were compared with the protonated complexes which provided further evidence for coupling between the ^{3}MLCT excited states present in these types of cyclometallated Ir (III) complexes.

The emission spectra for $[Ir(ppy)_2(bpy)]PF_6$ **(1)** and its deuteriated analogue $[Ir(ppy)_2(d_8bpy)]PF_6$ **(2)** are given in figure 3.21 (a). Both complexes showed a broad absorption band at 590 nm which is assigned to a ^{3}MLCT excited state, based on previous reports.[60-74] Figure 3.21 (b) shows the emission spectra for complexes $[Ir(ppy)_2(phen)]PF_6$ **(3)** and its deuteriated analogue $[Ir(ppy)_2(d_8phen)]PF_6$ **(4).** The emission spectra for complexes $[Ir(ppy)_2(dmbpy)]PF_6$ **(5)**, $[Ir(ppy)_2(dtbpy)]PF_6$ **(7)** and their deuteriated N^N analogous complexes **(6)** and **(8)** are given in appendix B.

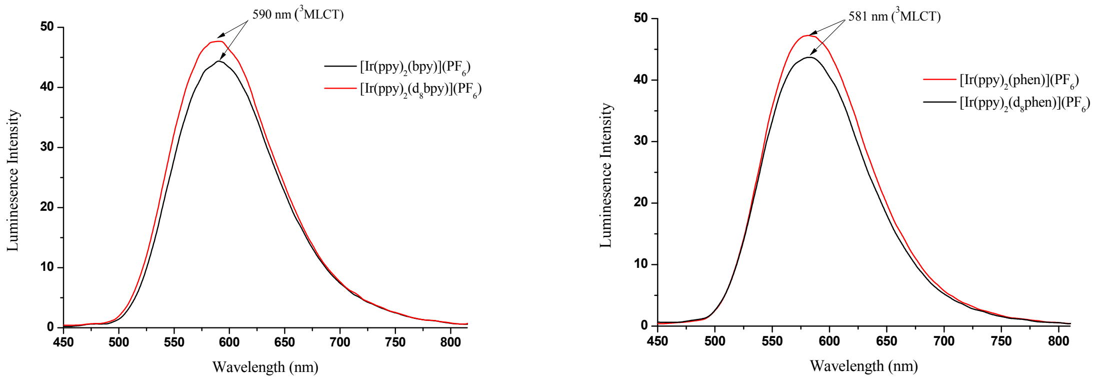

(a) **(b)**

Figure 3.21 (a) *Emission spectra for [Ir(ppy)$_2$(bpy)]PF$_6$* ***(1)*** *and [Ir(ppy)$_2$(d$_8$bpy)]PF$_6$* ***(2) (b)*** *Emission spectra for [Ir(ppy)$_2$(phen)]PF$_6$* ***(3)*** *and [Ir(ppy)$_2$(d$_8$phen)]PF$_6$* ***(4)****. All the measurements are done in aerated ACN at 298 K (Conc. 6×10^{-5}M).*

The emission spectra for the iridium mononuclear complex with the ligand bpp, [Ir(ppy)$_2$(bpp)]PF$_6$ **(9)** and the two heterodinuclear Ir-Pt and Ir-Pd dimers, [Ir(ppy)$_2$(bpp)PtCl]$_2$(PF$_6$)$_2$ **(10)** and [Ir(ppy)$_2$(bpp)PdCl]$_2$(PF$_6$)$_2$ **(11)** are given in figure 3.22 (a) below. The detailed excited state photophysical measurements including solvatochromic, rigidochromic and temperature dependent emission and lifetime measurements for these three complexes along with the assignments of the emission bands are studied in detail in chapter 4.

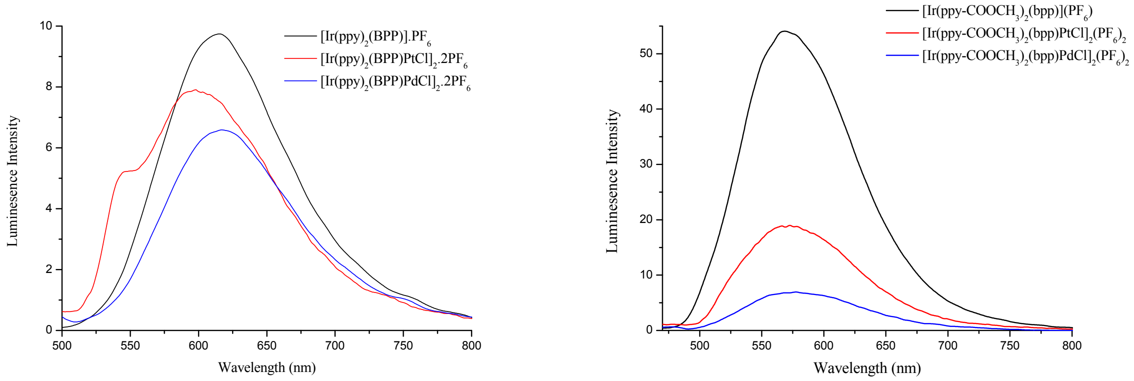

(a) **(b)**

Figure 3.22 (a) *Emission spectra for complexes [Ir(ppy)$_2$(BPP)]PF$_6$* ***(9)****, [Ir(ppy)$_2$(BPP)PtCl]$_2$(PF$_6$)$_2$* ***(10)*** *and [Ir(ppy)$_2$(BPP)PdCl]$_2$(PF$_6$)$_2$* ***(11)*** *in aerated ACN (1×10^{-5}M) at 298 K* ***(b)*** *Emission spectra for complexes [Ir(ppy-COOCH$_3$)$_2$(BPP)]PF$_6$* ***(12)****, [Ir(ppy-COOCH$_3$)$_2$(BPP)PtCl]$_2$(PF$_6$)$_2$* ***(13)*** *and [Ir(ppy-COOCH$_3$)$_2$(BPP)PdCl]$_2$(PF$_6$)$_2$* ***(14)*** *in aerated ACN (6×10^{-5}M) at 298 K.*

The emission spectra for the iridium ester complexes with the bpp ligand, [Ir(ppy-COOCH$_3$)$_2$(bpp)]PF$_6$ **(12)**, [Ir(ppy-COOCH$_3$)$_2$(bpp)PtCl]$_2$(PF$_6$)$_2$ **(13)** and [Ir(ppy-COOCH$_3$)$_2$(bpp)PdCl]$_2$(PF$_6$)$_2$ **(14)** are given in figure 3.22 (b). From the emission spectra it is clear that complexation with Pt and Pd centres resulted in a considerable decrease in the emission intensity. This shows the probability of charge reaching the Pt and Pd centres for the dimer complexes which are in thermal equilibrium with the ^{3}MC state at room temperature resulting in quenching of emission. A larger decrease in emission intensity was observed for the ester Ir-Pt and Ir-Pd complexes (figure 3.22 (b)) compared to the non ester complexes (figure 3.22 (a)). This may be due to the electron withdrawing ester groups on the peripheral phenylpyridine ring which results in an increase in the energy of the ^{3}MLCT excited states from which the charge is expected to be going to the Pt/Pd excited state. This increase in energy can be clearly seen by comparing the emission maxima for the non ester and ester analogues (for the ester analogues complexes there is prominent blue shift in the emission maxima compared to the non ester complexes). The emission maxima for the non ester mononuclear complex **(9)** at 617 nm (2.01 eV) was blue shifted to 568 nm (2.19 eV) in the ester complex **(12)**. Emission bands were observed at 605 nm (2.05 eV) and 546 nm (2.27 eV) for the Pt dimer complex **(10)**, and these were blue shifted to 573 nm (2.17 eV) and 530 nm (2.34 eV) for the ester analogue **(13)**. An emission band was observed at 615 nm (2.02 eV) for the Pd complex **(11)**, and this was blue shifted to 577 nm (2.15 eV) in the ester analogue **(14)**. Based on the detailed photophysical measurements carried out on the non ester complexes in chapter 4 along with published results,[60-74] the energy of the low lying ^{3}MLCT excited states in the ester complexes increases which leads to the thermal population of charge to the excited states of Pt/Pd metals thereby resulting in a more extensive quenching of emission compared to the non ester analogues. Further evidence in support of this explanation can be obtained from the photocatalytic H$_2$ production activity of these two different sets of complexes (non esters and esters). The ester complexes gave almost double the amount of hydrogen compared to the non ester complexes under similar conditions (section 3.3.3.2) which clearly shows that the lowest lying excited states for the ester complexes are more easily accessible to the Pt/Pd excited states at room temperature.

The 77 K emission curve for [Ir(ppy-COOCH$_3$)$_2$(bpp)]PF$_6$ **(12)** along with the 298 K emission is given in figure 3.23 below. The room temperature emission maxima at 568 nm is assigned to a ^{3}MLCT excited state. This assumption is made on the basis of the spectral shape (broadened spectrum), rigidochromic shift on going to 77 K (as shown in figure 3.23), lifetime value (118 ns) corresponding to the decay from a typical MLCT excited state and by comparing the results obtained for the analogous non ester complex **(9)** discussed in detail in section 4.2.2 of chapter 4. As discussed at the beginning of this section for complexes **(1)** to **(8)** the emission takes place from a lowest excited state which is an equilibrated state of ^{3}MLCT$_{ppy}$ and ^{3}MLCT$_{bpp}$ (due to the strong coupling between these low lying excited states).

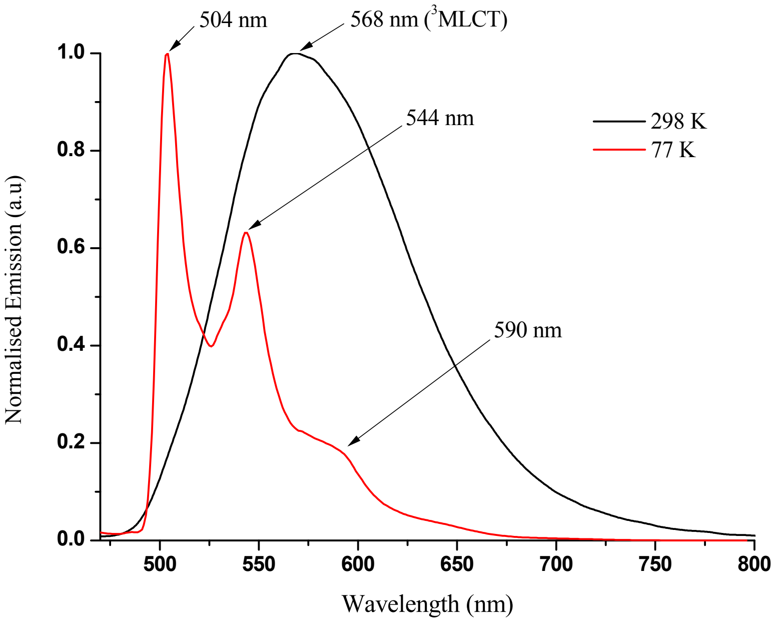

Figure 3.23 *Emission spectrum for [Ir(ppy-COOCH$_3$)$_2$(bpp)]PF$_6$* ***(12)*** *at 298 K (in aerated ACN) and 77 K (in 4:1 EtOH:MeOH glass)*

The 77 K emission spectra for complex **(12)** is structured with three prominent emission bands. Comparing this spectrum with the 77 K emission spectrum for the non ester complex **(9)** (figure 4.9 in chapter 4), the presence of the electron withdrawing ester group resulted in a blue shift of 36 nm (for complex 9 at 77 K the emission maxima was at 540 nm and was not structured). This clearly shows that ester substitution resulted in an increase in the energy of the excited state (energy increased by 0.16 eV). Due to the limitation of time it was not possible to complete the temperature dependent lifetime measurements for the ester complexes. So assignments of the peaks were made by comparing these values with the data of similar non ester complexes studied in detail in chapter 4 (sections 4.2.2, 4.3.2 and 4.4.2). The emission peak at 504 nm is assigned to a ^{3}LLCT excited state, and the emission peak at 544 nm to a mixed ^{3}LLCT/^{3}MLCT excited state and the lowest energy peak at 590 nm to a ^{3}MLCT excited state emission. However these are tentative assignments and further studies are required to confirm this assignment. The low temperature (77 K) emission spectra together with the room temperature emission spectra (298 K) for complexes $[Ir(ppy\text{-}COOCH_3)_2(bpp)PtCl]_2(PF_6)_2$ **(13)** and $[Ir(ppy\text{-}COOCH_3)_2(bpp)PdCl]_2 (PF_6)_2$ **(14)** are given in appendix B. Low temperature (77 K) emission curves for both complexes **(13)** and **(14)** showed a prominent blue shift in comparison to the non ester complexes **(10)** and **(11)**, due to the electron withdrawing ester group, which results in a shift of the excited states to higher energy.

The emission spectra for three cyclometallated iridium (III) complexes with the tpy ligand (2,2':6',2''-terpyridine) having two different electron withdrawing substituents ($COOCH_3$ and CHO) on the ppy ligand ($[Ir(ppy)_2(tpp)]PF_6$ **(15)**, $[Ir(ppy\text{-}COOCH_3)_2(tpp)]PF_6$ **(17)** and $[Ir(ppy\text{-}CHO)_2(tpp)]PF_6$ **(19)**) are shown in figure 3.24. It can be seen from the emission spectra that substitution by electron withdrawing groups resulted in a considerable increase in the energy of the lowest MLCT excited states as is evident from the extent of blue shift for complexes **(17)** and **(19)** compared to complex **(15)** (normalised emission spectra are given in inset).

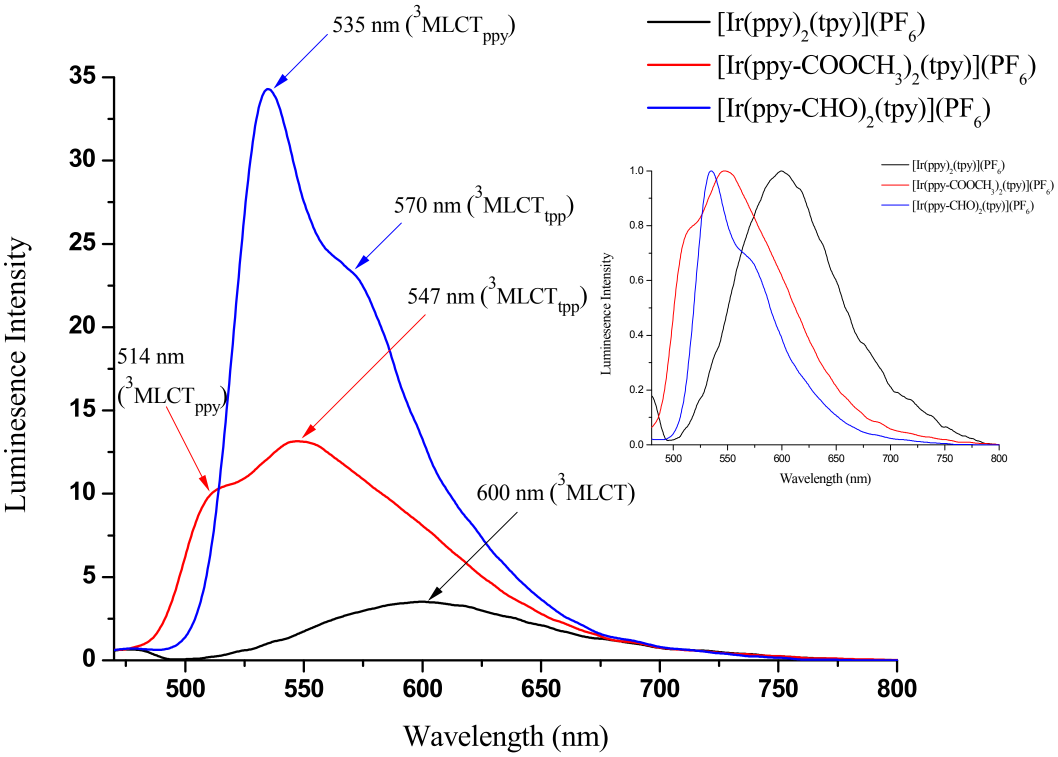

__Figure 3.24__ Emission spectrum for $[Ir(ppy)_2(tpy)]PF_6$ __(15)__, $[Ir(ppy\text{-}COOCH_3)_2(tpy)]PF_6$ __(17)__ and $[Ir(ppy\text{-}CHO)_2(tpy)]PF_6$ __(19)__ at 298 K in aerated ACN (Conc. 1×10^{-5}M).

For the unsubstituted complex **(15)**, the emission maximum at 600 nm (2.07eV) is assigned to a ^{3}MLCT excited state based on the emission data for the standard complex **(1)** given in figure 3.18 and with the published results.[60-74] The lifetime decay curve for complex **(15)** (appendix B) was single exponential with a value of 35 ns, characteristic of a decay from an MLCT excited state. Here as for complex **(1)** the two low lying ^{3}MLCT excited states (^{3}MLCT$_{ppy}$ and ^{3}MLCT$_{tpp}$) are strongly coupled and is difficult to differentiate between them. As explained at the beginning of this section, when the bridging chlorides of $[Ir(ppy)_2Cl]_2$ are replaced by a π acceptor neutral chelating (N^N) ligand like tpy, the Ir (III) metal center becomes a poorer electron donor and the (^{3}MLCT$_{ppy}$) state will move up in energy. This effect is enhanced by having elecron-withdrawing groups on the phenyl ring of the ppy ligand. Substitution of the ppy ligand by an ester group resulted in an increase in energy and also in splitting of the two low lying ^{3}MLCT excited states. The emission spectra has two bands, one at higher energy of 514 nm (2.41 eV) assigned to a ^{3}MLCT$_{ppy}$ excited state which showed an increase in energy of 0.34 eV. The lower energy band at 547 nm (2.27 eV) is assigned to a ^{3}MLCT$_{tpy}$ excited state which showed an increase in energy of 0.2 eV compared to the unsubstituted complex **(15)**. The aldehyde substituted complex **(19)** also showed a prominent increase in energy of the emission band and similar to the ester complex the electron withdrawing group substituted on the ppy ligand resulted in an increase in the ^{3}MLCT$_{ppy}$ state to a higher energy than the ^{3}MLCT$_{tpy}$ state. The emission band at 535 nm (2.32 eV) is assigned to a ^{3}MLCT$_{ppy}$ excited state and the emission band at 570 nm (2.18 eV) is assigned to a ^{3}MLCT$_{tpy}$ state. The former showed an increase in energy of 0.25 eV while the latter one showed an increase of 0.11 eV. All these assignments are based on results for the standard complex **(1)** and with the previous published results.[61-74]

Eventhough the lowest lying excited state for all the 3 complexes explained above with the tpy ligand (which can be considered as a substituted bipyridine ligand, having a pyridine substitution at the 6' position) is considered as a ^{3}MLCT$_{tpy}$ state in view of the low lying π* orbitals of the diimine ligand, however this state may be mixed (^{3}MLCT$_{tpy}$ and ^{3}MLCT$_{ppy}$) based on the results with a similar complex having a phenyl substituent on the 6' position of the bipyridine ligand.[73] The low reversibility of the oxidation waves of the complexes (appendix B) suggests the involvement of covalent Ir-C bond character in the HOMOs of the complexes. The possibility of a triplet σ bond to ligand ^{3}SBLCT [σ(Ir-C) → π*(diimine)] emissive state or simply ^{3}LLCT excited state thus cannot be totally ignored.[74,75,54] Confirming this hypothesis can only be made by carrying out further measurements like resonance Raman which are beyond the scope of this thesis and will be done in future.

It is interesting to note that the emission for the two Ir-Pd complexes with the tpy ligand, $[Ir(ppy)_2(tpy)PdCl]_2(PF_6)_2$ **(16)** and $[Ir(ppy\text{-}COOCH_3)_2(tpy)PdCl]_2(PF_6)_2$ **(18)** is completely quenched in comparison to the analogous complexes **(11)** and **(14)** containing the bpp ligand. Both these bridging ligands (bpp and tpy) can be considered as substituted bipyridines, bpp having a pyridine ring substituted at the 5' position and tpy having having a pyridine ring at the 6' position. The π^* level on the tpy ligand is at higher energy compared to that of the π^* level on bpp ligand. The reason for this is the lack of coplanarity of the pyridine ring with respect to the bipyridine due to steric hindrance when the pyridine ring is substituted at the 6' position which is explained for a similar complex having phenyl substitution at 6' position.[76] Due to this reason the low lying excited states are increased in energy (the mononuclear complex $[Ir(ppy)_2(tpy)]PF_6$ **(15)** has an energy of 0.06 eV higher than that of the corresponding bpp complex $[Ir(ppy)_2(bpp)]PF_6$ **(9)** as is clear from the emission spectra given in figures 3.22 and 3.24). This results in population of the Pd excited state at room temperature, and in quenching. For the Ir-Pd complex with the bpp ligand, substitution of the pyridine ring at the 5' position does not cause steric hindrance and the substituted pyridine ring will be coplanar to the bipyridine, which will result in extended π conjugation, this results in lowering of the energy of the excited states in comparison with complex containing the tpy ligand, thus emission at room temperature occurs from the lowest ^{3}MLCT excited states (explained in detail in chapter 4).

3.3.3.3 Lifetime measurements

Excited-state lifetimes of the complexes can provide evidence as to the nature of excited states of transition metal complexes. The instrumental procedures and conditions that were used to carry out the excited state lifetime measurements using TCSPC and laser flash photolysis were detailed in chapter 2. It should be noted that all excited state lifetimes reported here have an error of ± 5 % and two methods were used for analysing the quality of the data acquired a) χ^2 goodness of fit test and b) analysis of the residual plots. A χ^2 value as close as possible to 1 is ideal and all the data reported in this chapter have χ^2 value close to 1.

Based on the previous reports[64,77,78] for Ir (III) cyclometallated complexes, at room temperature (298 K) the excited states are in thermal equillibrium and the lifetimes will be in the nano second time range, decaying from the lowest excited state which is ^{3}MLCT in nature. It is very difficult to differentiate between the two ^{3}MLCT states (^{3}MLCT$_{(N^\wedge C)}$ and ^{3}MLCT$_{(N^\wedge N)}$) at room temperature. Detailed excited state photophysics of the complex [Ir(ppy)$_2$(bpy)](PF$_6$) and its analogous complexes having different substituents on the bipyridine (bpy) and phenyl pyridine (ppy) ligands have been already studied in detail[61-69] and it is concluded that at room temperature emission takes place from the lower energy ^{3}MLCT$_{bpy}$ excited state, but the possibility of emission occuring from an equillibrated ^{3}MLCT$_{ppy}$/^{3}MLCT$_{bpy}$ excited state cannot be ignored. In the present study a series of Ir (III) complexes, including deuteriated N^N ligands were synthesised and the emission lifetimes were measured for both the protonated and deuteriated complexes using TCSPC and laser flash photolysis, and the results are tabulated in table 3.5 below which shows good agreement between the two data sets.

Complex	Emission Wavelength λ_{em}, (nm)	Lifetime (TCSPC) (ns)	Lifetime (Laser) (ns)
[Ir(ppy)$_2$(bpy)](PF$_6$) **(1)**	590	64	64
[Ir(ppy)$_2$(d$_8$bpy)](PF$_6$) **(2)**	590	65	66
[Ir(ppy)$_2$(phen)](PF$_6$) **(3)**	581	58	58
[Ir(ppy)$_2$(d$_8$phen)](PF$_6$) **(4)**	581	57	57
[Ir(ppy)$_2$(dmbpy)](PF$_6$) **(5)**	572	60	61
[Ir(ppy)$_2$(d$_{12}$dmbpy)](PF$_6$) **(6)**	572	61	63
[Ir(ppy)$_2$(dtbpy)](PF$_6$) **(7)**	570	63	63
[Ir(ppy)$_2$(d$_{24}$dtbpy)](PF$_6$) **(8)**	570	64	63

Table 3.5 *Tabulated lifetime data for the complexes using TCSPC and laser flash photolysis. All the measurements were obtained in aerated ACN at room temperature (298 K).*

From the previous published results the lowest excited state for complexes of the type [Ir(N^C)$_2$(N^N)](PF$_6$) is always assigned to a ^{3}MLCT$_{N^\wedge N}$ excited state. Hence deuteriation of the N^N ligands should influence the lifetime of the excited state based on previous reports.[64,65,66]

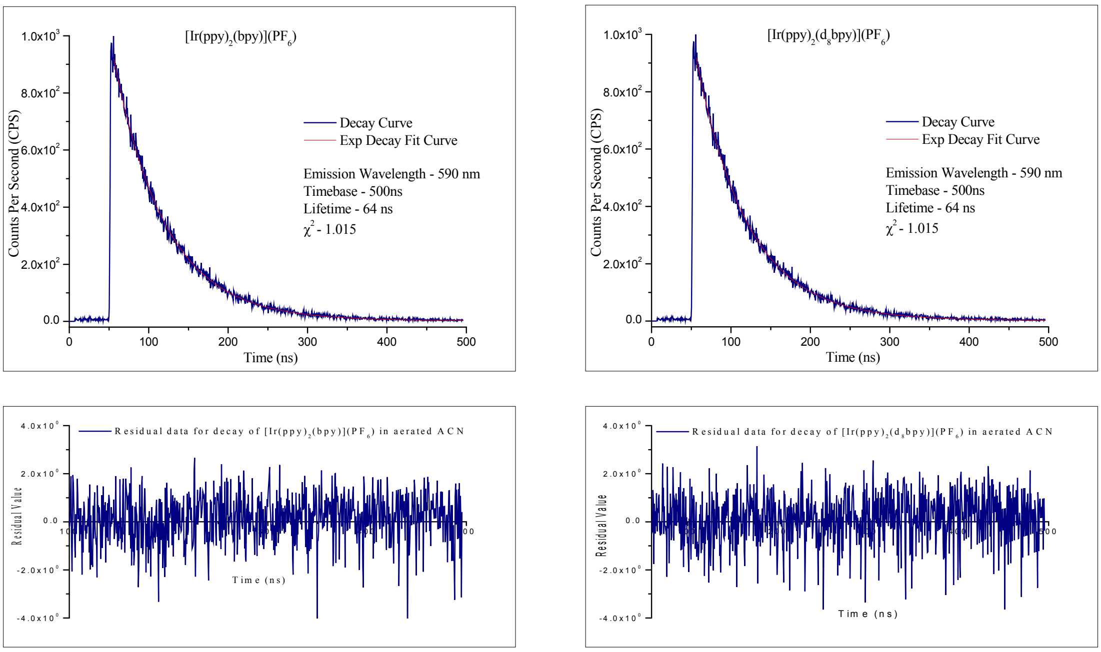

(a) **(b)**

Figure 3.25 ***(a)*** *Lifetime decay plots for complex [Ir(ppy)$_2$(bpy)](PF$_6$)* ***(1)*** ***(b)*** *Lifetime decay plots for complex [Ir(ppy)$_2$(d$_8$bpy)](PF$_6$)* ***(2)*** *measured in aerated ACN (298 K) using TCSPC.*

The emission decay curves along with the fit for [Ir(ppy)$_2$(bpy)](PF$_6$) **(1)** and [Ir(ppy)$_2$(d$_8$bpy)](PF$_6$) **(2)** measured at a timebase of 500 ns along with the residual plots are given in figures 3.25(a) and 3.25(b). Details regarding emission wavelength, timebase, lifetime and χ^2 value for each complex are given inside the plots itself. Interestingly in all the above cases deuteration of N^N ligands did not result in any change for the lifetime. This can be due to the strong coupling of the two close lying ^{3}MLCT excited states (^{3}MLCT$_{N^\wedge C}$ and ^{3}MLCT$_{N^\wedge N}$)[79] thereby the vibrational effects as a result of deuteration do not have any significant effect in these cyclometallated Ir (III) complexes. Such a deuteration effect study on these complexes has not been reported previously. The decay curves for the remaining complexes are given in table 3.5, and the residual plots are given in appendix B.

The detailed excited state lifetime measurements including solvent dependent and temperature dependent lifetimes for the three complexes, [Ir(ppy)$_2$(bpp)]PF$_6$ **(9)**, [Ir(ppy)$_2$(bpp)PtCl]$_2$(PF$_6$)$_2$ **(10)** and [Ir(ppy)$_2$(bpp)PdCl]$_2$(PF$_6$)$_2$ **(11)** are explained in detail in chapter 4. The lifetime data obtained for the methyl ester iridium (III) complexes containing the bpp ligand, [Ir(ppy-COOCH$_3$)$_2$(bpp)]PF$_6$ **(12)**, [Ir(ppy-COOCH$_3$)$_2$(bpp) PtCl]$_2$(PF$_6$)$_2$ **(13)**

and $[Ir(ppy\text{-}COOCH_3)_2(bpp)PdCl]_2(PF_6)_2$ **(14)** using both TCSPC and laser in aerated ACN at room temperature are given in table 3.6 below.

Complex	Emission Wavelength λ_{em}, (nm)	Lifetime (TCSPC) (ns)	Lifetime (Laser) (ns)
$[Ir(ppy\text{-}COOCH_3)_2(bpp)]PF_6$ **(12)**	568	118	120
$[Ir(ppy\text{-}COOCH_3)_2(bpp)PtCl]_2(PF_6)_2$ **(13)**	573	134	137
$[Ir(ppy\text{-}COOCH_3)_2(bpp)PdCl]_2(PF_6)_2$ **(14)**	577	τ_1 – 23 (67 %) τ_2 – 87 (33 %)	88

***Table 3.6** Tabulated lifetime data for the complexes measured with TCSPC and laser. All the measurements were obtained in aerated ACN at room temperature (298 K).*

From the above table it is evident that complexation of Pt to the mononuclear complex resulted in a slight increase in the emission lifetime as shown similarly by the non ester Ir-Pt complex **(10)**. The lifetime increased from 118 ns to 134 ns. The lifetime decay curve for both complexes, **(12)** and **(13)** was monoexponential as shown in figure 3.26 below. Interestingly for the Ir-Pd dimer complex **(14)** the lifetime decay curve was biexponential with one component of 23 ns (with a relative percentage of 67 %) and a long lived component having a relative percentage of 33 %. The average lifetime calculated gave a value of 87 ns which is almost half the lifetime of what was obtained for the monomer complex **(12)** clearly indicating quenching effect of the Pd center (figure 3.22(b)). This quenching effect for the ester Ir-Pd complex is much more prominent than for the Ir-Pt complex **(13)**. Further evidence in support of the above explained behaviour of the Ir-Pd ester complex is obtained from the photocatalytic H_2 production results explained in section 3.3.3. The ester Ir-Pd complex **(14)** produced more H_2 than the Ir-Pt complex **(13)** which supports the emission and lifetime quenching results (as the electron reaches the Pd center more efficiently than to the Pt center). But in the case of the non ester complexes, the Ir-Pt complex **(10)** is more efficient than the Ir-Pd complex **(11)** which is in agreement with the photophysical data. Details regarding this comparison are given in the next section.

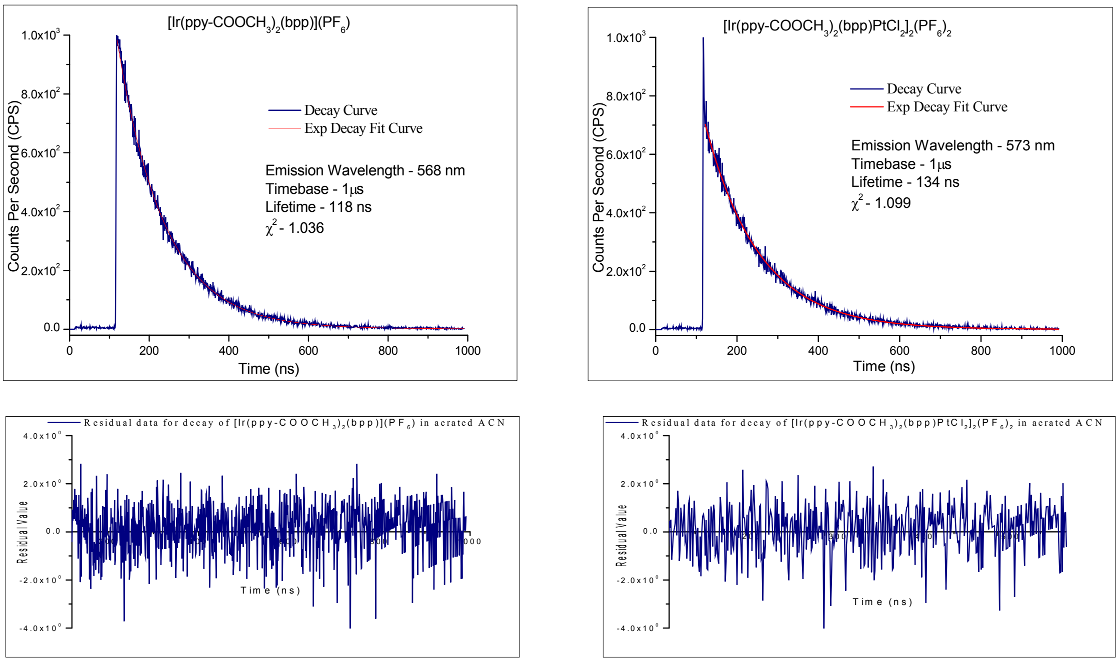

(a) **(b)**

Figure 3.26 (a) *Lifetime decay plots for complex [Ir(ppy-COOCH$_3$)$_2$(BPP)]PF$_6$* ***(12) (b)*** *Lifetime decay plots for complex [Ir(ppy-COOCH$_3$)$_2$(BPP)PtCl]$_2$(PF$_6$)$_2$* ***(13)*** *measured in aerated ACN (298 K) using TCSPC.*

The emission decay curves along with the fit for both [Ir(ppy-COOCH$_3$)$_2$(BPP)]PF$_6$ **(12)** and [Ir(ppy-COOCH$_3$)$_2$(BPP)PtCl]$_2$(PF$_6$)$_2$ **(13)** along with the residual plots are given in figures 3.26 (a) and 3.26 (b). The decay fit curves for the Ir-Pd complex **(14)** with the residual plots are given in appendix B.

The lifetime measurements for the three mononuclear complexes of iridium with the ligand tpy, [Ir(ppy)$_2$(tpy)]PF$_6$ **(15)**, [Ir(ppy-COOCH$_3$)$_2$(tpy)]PF$_6$ **(17)** and [Ir(ppy-CHO)$_2$(tpy)]PF$_6$ **(19)** measured using both TCSPC and laser flash photolysis are given in table 3.7 below. From the table it is clear that the lifetime values obtained using both instruments are comparable, showing the accuracy of the values obtained. The lifetime value for the Ir-Pd dimer complexes with the tpy ligands, [Ir(ppy)$_2$(tpy)PdCl]$_2$(PF$_6$)$_2$ **(15)** and [Ir(ppy-COOCH$_3$)$_2$(tpy)PdCl]$_2$(PF$_6$)$_2$ **(17)** could not be measured as the emission was completely quenched in both the cases following Pd coordination.

Complex	Emission Wavelength λ_{em}, (nm)	Lifetime (TCSPC) (ns)	Lifetime (Laser) (ns)
$[Ir(ppy)_2(tpy)]PF_6$ **(15)**	600	35	36
$[Ir(ppy\text{-}COOCH_3)_2(tpy)]PF_6$ **(17)**	514, 547	82, 81	83, 82
$[Ir(ppy\text{-}CHO)_2(tpy)]PF_6$ **(19)**	535, 570	341, 341	347, 348

***Table 3.7** Tabulated lifetime data for the complexes measured with TCSPC and laser. All the measurements were obtained in aerated ACN at room temperature (298 K).*

The unsubstituted ppy complex $[Ir(ppy)_2(tpy)]PF_6$ **(15)** gave a lifetime value of 35 ns. The substitution of ppy ligand with the electron withdrawing $COOCH_3$ and CHO groups resulted in an increase in the lifetime. For the ester complex **(17)** the lifetime increased to 82 ns from 35 ns. The lifetime for complex **(17)** was measured at two different emission wavelengths (514 nm and 547 nm) as given in the emission spectra for complex **(17)** (figure 3.24). The lifetime values at both these emission bands were equal which indicates a similarity in the nature of both excited states (ie ^{3}MLCT). Similar results were found for the aldehyde substituted complex **(19)**, the emission spectra (figure 3.24) showed two peaks, and the lifetime at both these emission wavelengths were exactly the same. For complex **(19)** substitution of CHO group to the ppy resulted in a 10 fold increase in the lifetime value (341 ns) compared to the mononuclear complex (35 ns). The increase in lifetime obtained for the substituted ppy complexes **(17)** and **(19)** can be explained by taking into consideration the emission spectra (figure 3.24). Substitution of these electron withdrawing groups resulted in an increase in the energy of the excited states compared to the unsubstituted complex as explained in section 3.3.2.2. This might be a reason for the longer lifetime values shown by the substituted ppy complexes which decays from a higher energy state with respect to the unsubstituted complex.

The emission decay curves along with the fit for $[Ir(ppy\text{-}CHO)_2(tpy)]PF_6$ **(19)** at two different emission wavelengths (535 nm and 570 nm) along with the residual plots are given in figures 3.27 (a) and 3.27 (b). The decay fit curves for the complexes **(15)** and **(17)** with the residual plots are given in appendix B.

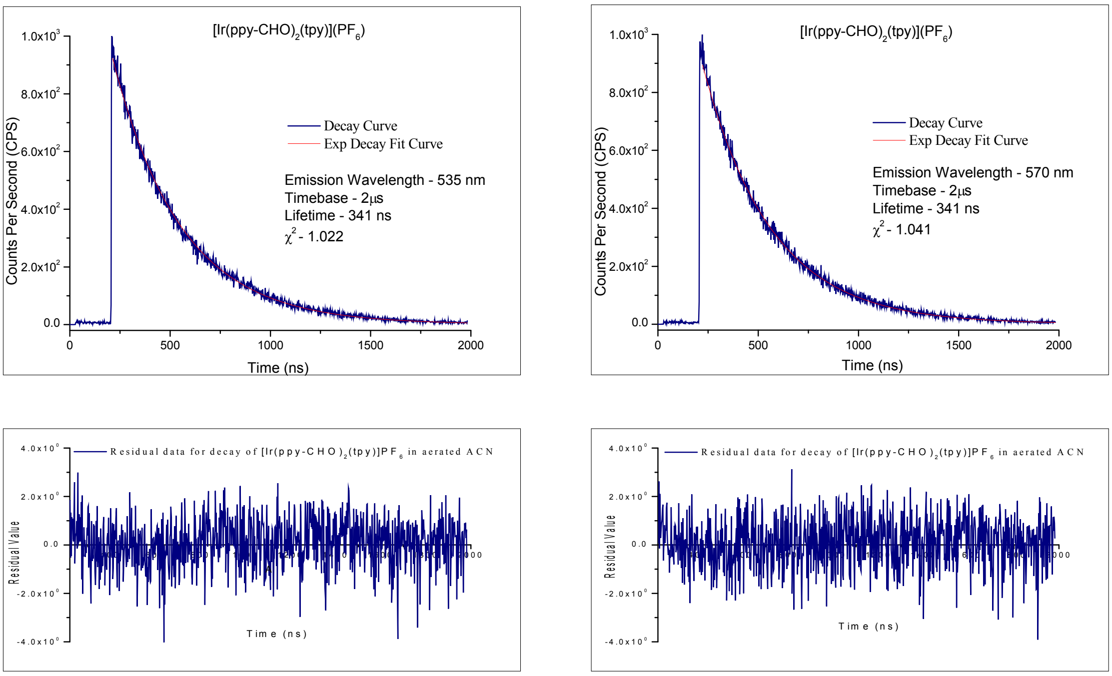

(a) **(b)**

Figure 3.27 *Lifetime decay plots for complex [Ir(ppy-CHO)$_2$(tpy)]PF$_6$* ***(19) (a)*** *at an emission wavelength of 535 nm* ***(b)*** *at an emission wavelength of 570 nm. All measurements were obtained in aerated ACN (298 K) using TCSPC.*

3.3.3.4 Effect of substitution on bpy and ppy ligands on emission energy of complex [Ir(ppy)$_2$(bpy)](PF$_6$)

In the previous sections 3.3.2.2 and 3.3.2.3 excited state photophysical measurements including absorption, emission and lifetime measurements of Ir (III) cyclometallated complexes has been explained on the basis of substitution to different bridging ligands and to other metal centres like Pt and Pd. In this section the dependence of emission data as a function of various substituents on bpy and ppy ligands is discussed. Given in figure 3.28 below are the different iridium complexes in this study.

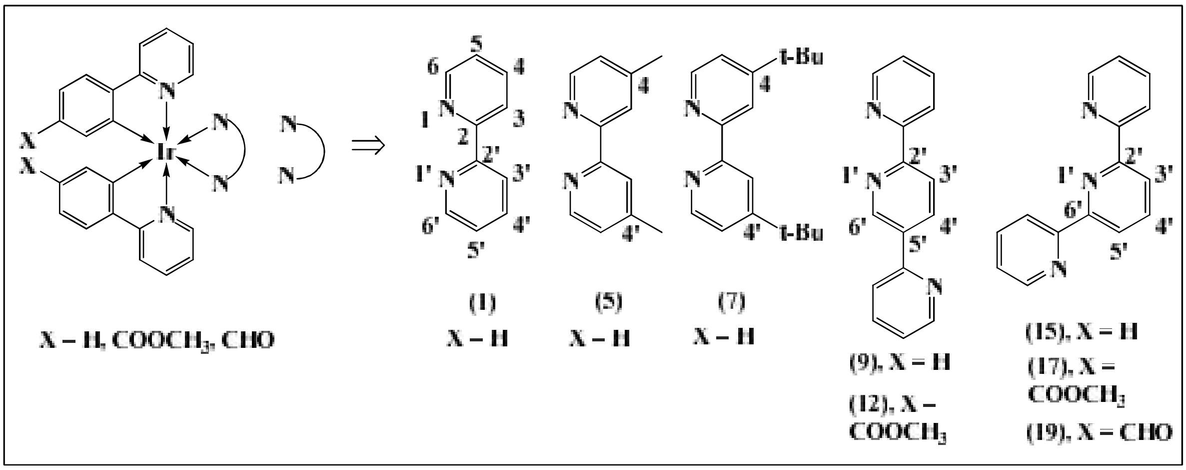

Figure 3.28 *Schematic representation of cyclometallated iridium (III) complexes having various substituted bpy as the chelating ligand*

The emission maxima for all these complexes together with the excited state energies in eV, and the corresponding lifetimes are tabulated in table 3.8 below.

Complex	Emission Wavelength, λ_{em}, (nm)	Energy (eV)	Lifetime (298 K) ns
$[Ir(ppy)_2(bpy)](PF_6)$ **(1)**	590	2.10	64
$[Ir(ppy)_2(dmbpy)](PF_6)$ **(5)**	572	2.17	60
$[Ir(ppy)_2(dtbpy)](PF_6)$ **(7)**	570	2.18	64
$[Ir(ppy)_2(bpp)](PF_6)$ **(9)**	617	2.01	72
$[Ir(ppy)_2(tpy)](PF_6)$ **(15)**	600	2.07	35
$[Ir(ppy\text{-}COOCH_3)_2(bpp)](PF_6)$ **(12)**	568	2.19	118
$[Ir(ppy\text{-}COOCH_3)_2(tpy)](PF_6)$ **(17)**	514, 547	2.41, 2.27	82, 81
$[Ir(ppy\text{-}CHO)_2(tpy)](PF_6)$ **(19)**	535, 570	2.32, 2.18	341, 341

Table 3.8 *Tabulated data for emission and lifetime measured in aerated ACN at room temperature*

From the above table 3.8, the variation in emission energy as a result of various substitutions on the bipyridine ligand and also on the nature of the cyclometallated phenyl pyridine (ppy) ligand are given. Substitution at 4 and 4' positions of bpy by methyl or tertiary butyl groups results in an increase in the emission energy from 2.10 eV to 2.17 eV for the dmbpy complex **(5)** and from 2.10 eV to 2.18 eV for the dtbpy complex **(7)** in agreement with the previously published results for the same complexes.[70,80,81] Complexes **(9)** and **(15)** are two isomers where the pyridyl substituent is bound at the 5' or 6' position of the coordinated bpy moiety. The substitution of the pyridine ring resulted in a decrease in the emission energy as can be seen from table 3.8. The emission energy for the unsubstituted bpy complex **(1)** at 2.10 eV, decreased to 2.01 eV for $[Ir(ppy)_2(bpp)](PF_6)$ **(9)** and to 2.07 eV for $[Ir(ppy)_2(tpy)](PF_6)$ **(15)**. This is due to the extended π conjugation present in both complex **(9)** and **(15)** which results in lowering of the energy of the π* orbital and consequently a decrease in the emission energy. From the above data it can be noted that the pyridine ring substitution at the 5' position in complex **(9)** resulted in a greater decrease in energy than substitution at 6' position for complex **(15)**. This might be due to some steric reasons for complex **(15)**, as the pyridine ring is not coplanar with the bipyridine ligand as can be seen from the structure itself given in figure 3.28 above. This lack of coplanarirty limits the extension in conjugation resulting in an increase of the π* energy level. Due to this reason not much change in the emission energy is seen between complex **(1)** and complex **(15)**. For complex **(9)**, the pyridine ring at 5' position, is coplanar with the bipyridine which results in extended π conjugation and thus lowering of the emission energy as given in table 3.8 above.

These results show that the effect of substitution of the cyclometallated ppy ligand resulted in greater changes to the emission energy than substituting the bipyridine ligands. By careful synthesis the emission may be tuned over the entire range of the visible spectrum which has further applications in the field of OLED's and other light emitting devices for which cyclometallated Ir (III) complexes are efficient.[55,61,65,77] All the above mentioned results are based on photophysical measurements. Nevertheless, more detailed studies such as MO calculations and resonance Raman spectroscopy are required to obtain a clearer picture of the excited state nature of these complexes.

3.3.4 Photocatalytic H_2 production experiments

Luminescent iridium (III) transition metal complexes are very appealing because of the synthetic modifications possible for the ligands, which allows manipulation of the photophysical and electrochemical properties of these complexes for various applications, including photocatalysis.[12,13,58,82] An examination of the various iridium photocatalysts reported now were given in the introduction chapter 1 (section 1.7.3). The details regarding the experimental conditions used for photocatalysis are given in chapter 2. Almost all of the cyclometallated iridium complexes reported in this chapter showed good photocatalytic activity. In this section the difference in photocatalytic properties between the iridium complexes as a function of the bridging ligands, bpp, tpy and bpm will be described. In some cases experiments were carried out at four different water percentages (0 %, 5 %, 10 % and 15 %), of which the 5 % composition was found to be the most effective for hydrogen production. The effect of ester groups on the photocatalytic activity was also considered. All the measurements were carried out at two different excitation wavelengths UV light (350 nm) and visible light (470 nm). Intramolecular photocatalysis were carried out using the novel Ir-Pt/Pd systems which are the first of its kind of heterodinuclear iridium complexes. Intermolecular experiments were carried out for all the mononuclear iridium complexes using two different catalysts [Pt(ACN)$_2$Cl$_2$] and [Pd(ACN)$_2$Cl$_2$]. In all the photocatalytic experiments carried out in this chapter TEA (triethylamine) was used as the sacrificial agent, ACN (acetonitrile) was used as the solvent and water as the proton donor.

3.3.4.1 Intermolecular photocatalysis of [Ir(ppy)$_2$(N^N)]PF$_6$ complexes.

The strong reducing strength of the excited state of iridium cyclometallated complexes enables effective catalysis of the reduction of H_2O to H_2. The [Ir(ppy)$_2$(bpy)] PF$_6$ complex and various analogues having substituents on both the ppy and bpy ligands have been studied by Bernhard and coworkers in the past few years.[12,13,58,82] In the present study photocatalysis was investigated for the above mentioned complexes by making changes to the structure of the photosensitiser and varying the conditions which include; (1) investigating the impact of synthetic modification on photosensitiser performance as a result of deuteriation of N^N ligand (2) using two different Pt and Pd catalyts [Pt(ACN)$_2$Cl$_2$] and [Pd(ACN)$_2$Cl$_2$] rather than the conventional K_2PtCl_4 and K_2PdCl_4 salts and (3) by the photocatalytic irradiation using two different wavelengths of light – visible light (470 nm) and UV light (350 nm).

Figure 3.29 given below gives an idea regarding the amount of H_2 formed expressed in TON's for the eight complexes, following irradiation under both visible light (470 nm) and UV light (350 nm). A set of 8 complexes with the cyclometallated ppy ligand were prepared, having protonated and deuteriated N^N ligands. The effect of deuteriated N^N analogues on photocatalysis has not previously been studied. Bernhard has shown that the use of bulkier N^N ligands minimises solvent access to the iridium center, which presumably stabilises the photosensitiser by hindering ligand substitution.[12,13,58,82] Figure 3.29 and table 3.9 shows that the amount of H_2 produced for the deuteriated N^N analogoues complexes of iridium were reduced considerably. Comparing this result obtained with the previous reports it is assumed that the deuteriated N^N ligands decompose more readily than the protonated complexes thus resulting in a decrease in the TON values.

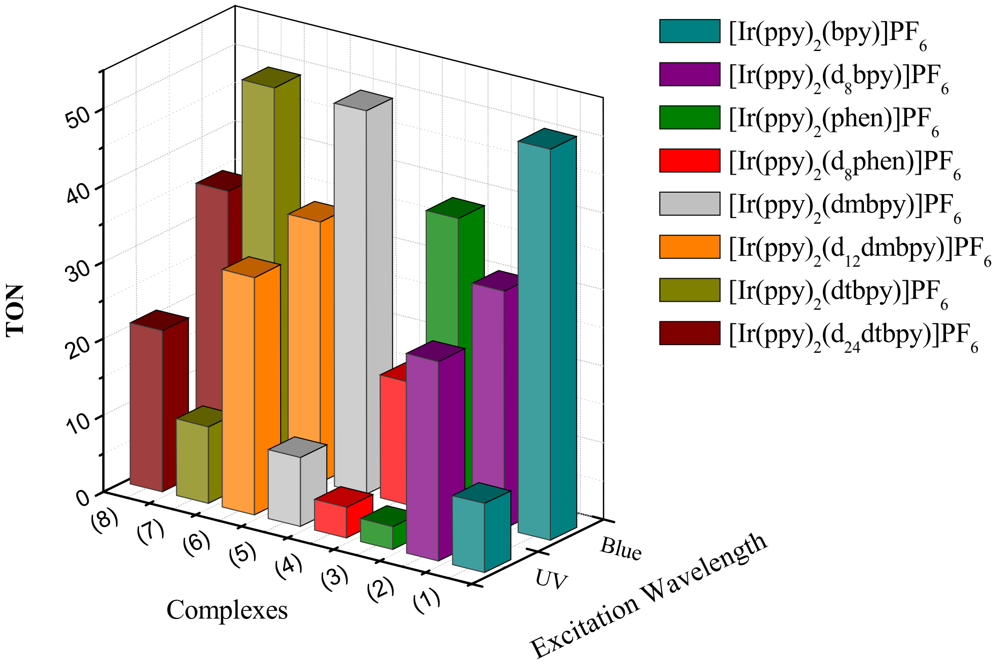

Figure 3.29 *Schematic representation of the photocatalytic TON values for complexes* ***(1)*** *to* ***(8)*** *obtained in ACN for both visible light (470 nm) and UV light (350 nm) irradiation. Irradiation time is 18h, sacrificial reagent used TEA, Conc. of PS and Pt catalyst is* 6×10^{-5}*M.*

The tabulated TON values for intermolecular photocatalysis with $[Pt(ACN)_2Cl_2]$ along with the areas obtained using gas chromatographic measurement for both visible light (470 nm) and UV light (350 nm) are tabulated in table 3.9 below. Previous reports of photocatalysis using conventional Pt and Pd salts ($K_2[PtCl_4]$ and $K_2[PdCl_4]$)[12,13] showed Pd catalysts to be more efficient than Pt catalysts. Interestingly when $[Pt(ACN)_2Cl_2]$ and $[Pd(ACN)_2Cl_2]$ complexes were used as catalysts, only Pt led to the production of hydrogen. The data presented shows that the nature of the catalyst plays a crucial role in determining the efficiency of the photocatalysis. It has been reported that molecular platinum and palladium species are reduced to form a colloidal catalyst under similar conditions to those applied in the present study.[12,13,20,21,32] However after 18h photolysis no precipitate was observed for Pt but when Pd was used as catalyst there was some precipitation (appendix B). This suggests aggregation of the Pd colloids at an earlier stage of photocatalysis resulting in decomposition of the Pd catalyst and decreasing the catalytic activity. Confirmation of this can only be made by carrying out SEM or TEM measurements.

Complex ($6x10^{-5}$ M) + $Pt(ACN)_2Cl_2$ ($6x10^{-5}$ M)	**H_2O %**	**470 nm**		**350 nm**	
		Area (mV/s)	**TON (average)**	**Area (mV/s)**	**TON (average)**
$[Ir(ppy)_2(bpy)](PF_6)$ **(1)**	5%	1) 88 2) 91 3) 85	51	1) 15 2) 17	9
$[Ir(ppy)_2(d_8bpy)](PF_6)$ **(2)**	5%	1) 58 2) 50 3) 52	31	1) 47 2) 45	26
$[Ir(ppy)_2(phen)](PF_6)$ **(3)**	5%	1) 70 2) 66 3) 66	39	1) 5 2) 7	3
$[Ir(ppy)_2(d_8phen)](PF_6)$ **(4)**	5%	1) 30 2) 25 3) 26	16	1) 7 2) 8	4
$[Ir(ppy)_2(dmbpy)](PF_6)$ **(5)**	5%	1) 86 2) 88 3) 85	50	1) 14 2) 16	9
$[Ir(ppy)_2(d_{12}dmbpy)](PF_6)$ **(6)**	5%	1) 57 2) 60 3) 62	34	1) 54 2) 55	31
$[Ir(ppy)_2(dtbpy)](PF_6)$ **(7)**	5%	1) 89 2) 84 3) 88	50	1) 16 2) 17	10
$[Ir(ppy)_2(d_{24}dtbpy)](PF_6)$ **(8)**	5%	1) 61 2) 59 3) 61	35	1) 37 2) 35	21

***Table 3.9** Tabulated TON values with their respective areas obtained from GC for complexes **(1)** to **(8)** (deuteriated ones are shown by shaded region).*

3.3.4.2 Intramolecular and intermolecular photocatalysis of iridium complexes with the bpp ligand

Photocatalysis of the six novel cyclometallated iridium complexes, $[Ir(ppy)_2(bpp)](PF_6)$ **(9)**, $[Ir(ppy)_2(bpp)PtCl]_2(PF_6)_2$ **(10)**, $[Ir(ppy)_2(bpp)PdCl]_2$ $(PF_6)_2$ **(11)**, $[Ir(ppy\text{-}COOCH_3)_2(bpp)]$ (PF_6) **(12)**, $[Ir(ppy\text{-}COOCH_3)_2(bpp)PtCl]_2(PF_6)_2$ **(13)** and $[Ir(ppy\text{-}COOCH_3)_2(bpp)PdCl]_2$ $(PF_6)_2$ **(14)** are discussed in this section. The intramolecular and intermolecular photocatalysis of complexes **(9)**, **(10)**, **(11)**, **(12)**, **(13)** and **(14)** were carried out with the help of Mr. Gurmeet Singh Bindra.

(a) Intramolecular photocatalysis using visible light (470 nm)

Many challenges exist in designing a complete homogeneous water splitting system. Once compatible PS and WRC components are found, the electron transfer processes must be perfected for optimal performance. The catalyst systems must efficiently quench the photoexcited PS complex, and a long lifetime for the charge separated state is required. The natural photosynthetic machinery fulfills these requirements by precise control of spatial organization, electronic coupling, and relative redox energies of the adjacent components, giving the systems directional charge transfer character. To accomplish these requirements in the laboratory, the components can be linked using multidentate bridging ligands that orchestrate electron transfer by providing optimal spatial separation and electronic coupling. A series of ruthenium intramolecular systems in which a Ru light absorbing unit is attached to different catalytic metals such as Pt, Pd, Co, Rh and Mn have been studied, and these systems showed good catalytic efficiency for H_2 production.[27,32,38] In the case of iridium complexes, most photocatalysis reported were intermolecular using mononuclear complexes. The only intramolecular photocatalysts reported to date are by Fontecave,[33,34] based on an Ir-Co system and Sakai used an Ir-Co self assembly system.[35] This shows the importance of the four novel Ir-Pt/Pd complexes discussed here.

The results obtained following 18 hours irradiation, using visible light for the four novel heterobimetallic Ir-Pt/Pd complexes, $[Ir(ppy)_2(bpp)PtCl]_2(PF_6)_2$ **(10)**, $[Ir(ppy)_2(bpp)PdCl]_2$ $(PF_6)_2$ **(11)**, $[Ir(ppy\text{-}COOCH_3)_2(bpp)PtCl]_2$ $(PF_6)_2$ **(13)** and $[Ir(ppy\text{-}COOCH_3)_2(bpp)PdCl]_2$ $(PF_6)_2$ **(14)** are given in figure 3.30, which gives a three dimensional plot of TON at four different percentages of H_2O.

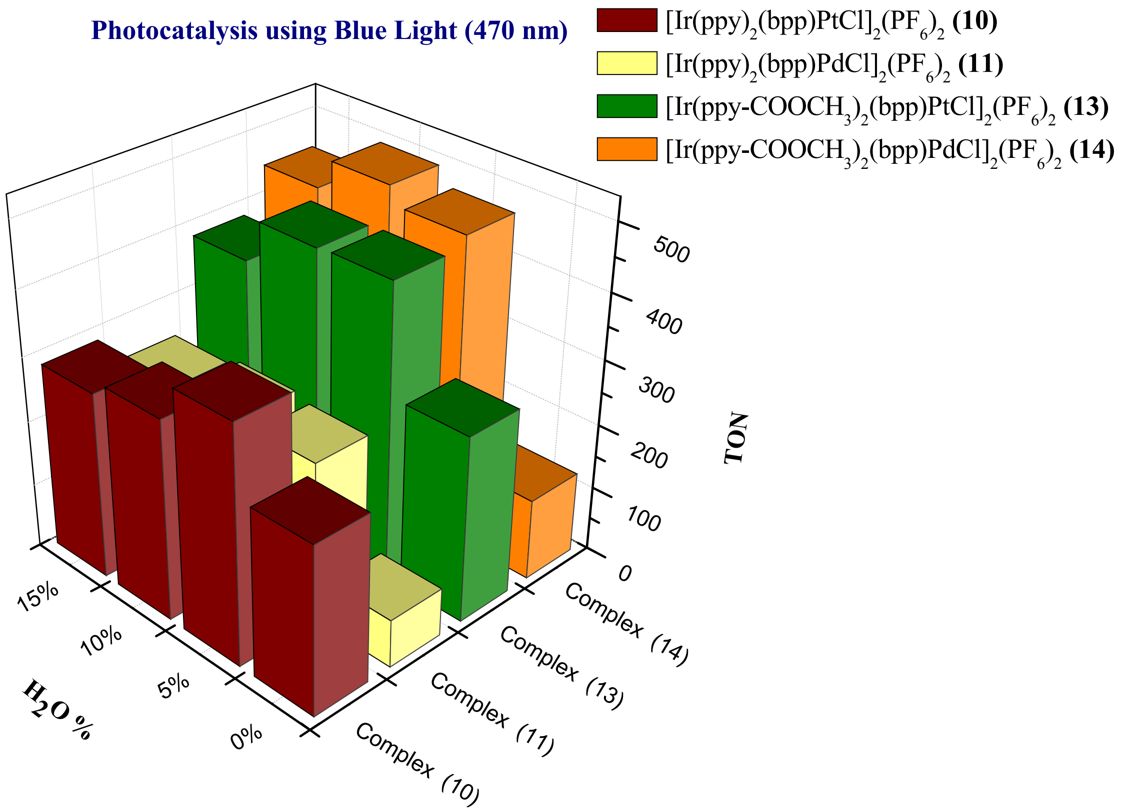

Figure 3.30 *Three dimensional representation of the photocatalytic TON values for H_2 production for complexes **(10)**, **(11)**, **(13)** and **(14)** in ACN using visible light (470 nm) irradiation. Irradiation time, 18h, sacrificial reagent used TEA, Conc. of PS and catalyst is 6×10^{-5}M.*

Photocatalysis was carried out using four different H_2O percentages (0 %, 5 %, 10 % and 15 %). For both non ester complexes **(10)** and **(11)**, the maximum yield of H_2 was obtained with 5 % H_2O. At greater percentages of water the TON for H_2 decreased slowly. Both complexes showed photocatalytic activity, at 0 % of water as shown in figure 3.30 (there is the possibility that H_2 may be formed by the decomposition of TEA as explained in chapter 1). On comparing the two non ester complexes $[Ir(ppy)_2(bpp)PtCl]_2(PF_6)_2$ **(10)** and $[Ir(ppy)_2(bpp)PdCl]_2(PF_6)_2$ **(11)**, the Ir-Pt complex **(10)** proved to be more efficient than the Ir-Pd complex **(11)**. A possible explanation for this behaviour is based on the photophysical measurements described in chapter 4. Compared to the mononuclear complex $[Ir(ppy)_2(bpp)](PF_6)$ **(9)** the energy of the low lying excited states are increased for both Ir-Pt **(10)** and Ir-Pd **(11)** complexes due to complexation of the iridium monomer with Pt/Pd. This is in the emission spectra given in figure 3.22. In the case of the Pt complex **(10)**, the energy of the $^3MLCT_{ppy}$ state increased by 0.26 eV, whereas for the Pd complex **(11)** there was only a slight increase of 0.01 eV. The net effect is that for the Ir-Pt complex the $^3MLCT_{ppy}$ excited state is increased in energy and populates the Pt excited state at room temperature thus resulting in more efficient photocatalysis. Such an increase in the energy of the excited state was not seen for the Ir-Pd complex **(11)**, which might be the reason for the decrease in catalytic efficiency compared to the Ir-Pt system. Further evidence in support of this hypothesis is obtained from the results shown in figure 3.22 for the analogous ester complexes (in which the photocatalytic activity almost doubled) and also by comparing TON to those obtained for the intermolecular photocatalytic experiments (figure 3.32) (which gave only half the value to that obtained by the intramolecular system).

The analogous ester complexes $[Ir(ppy\text{-}COOCH_3)_2(bpp)PtCl]_2\ (PF_6)_2$ **(13)** and $[Ir(ppy\text{-}COOCH_3)_2(bpp)PdCl]_2(PF_6)_2$ **(14)** showed significantly higher catalytic activity compared to the non ester analogous, as can be clearly seen from figure 3.22. The ester Pt complex **(13)** showed maximum catalytic activity in solutions containing 5 % and 10 % of H_2O. At higher percentages of water catalytic activity decreased. The ester Pd complex **(14)** showed maximum catalytic activity at 10 % H_2O. The ester complexes are much more efficient for H_2 formation than the non ester complexes. A possible explanation for this behaviour can be attributed to the photophysics explained in section 3.3.3.2. Substitution of peripheral phenyl pyridine ligand by ester groups resulted in an increase in the energy of the low lying excited states as demonstrated in the emission spectra (in figure 3.22). For the ester Pt complex **(13)** there was an increase of 0.12 eV in the energy of the lowest excited state compared to the non ester complex **(10)**. For the ester Pd complex **(14)** there was an increase of 0.13 eV in the energy of the lowest excited state compared to the non ester complex **(11)**. This increase in energy promotes electron transfer to the Pt or Pd centre more effectively, thus increasing the catalytic activity. The Pd ester complex, Ir-Pd complex **(14)** shows greater catalytic activity than the Ir-Pt complex **(13)**, the non ester Ir-Pt complex **(10)** was more photocatalytically efficient than Ir-Pd complex **(11)**. From the emission energies the two ester complexes showed almost the same energy as is evident in the emission spectra given in figure 3.22 (b). When emission spectra for complexes **(9)**-**(14)** are compared the Ir-Pd complex **(14)** showed more quenching, which suggests that electrons reach the Pd center more efficiently which results in a higher TON value. Further detailed studies are required to explain fully the possible mechanism for the results presented here. The detailed tabulated results for all these four complexes including the area obtained from GC are given in appendix B.

(b) Intramolecular photocatalysis using UV light (350 nm)

Intramolecular photocatalysis for the above mentioned four novel Ir-Pt/Pd complexes was also carried out using UV light (350 nm). All compounds have greater extinction coefficients at 350 nm (20-30 times) compared to 470 nm. The amount of H_2 produced was considerably less (in some cases no H_2 itself is produced) using this irradiation wavelength. A three dimensional reperesentation of the results for the four complexes, with four different percentages of H_2O are given in figure 3.31 below.

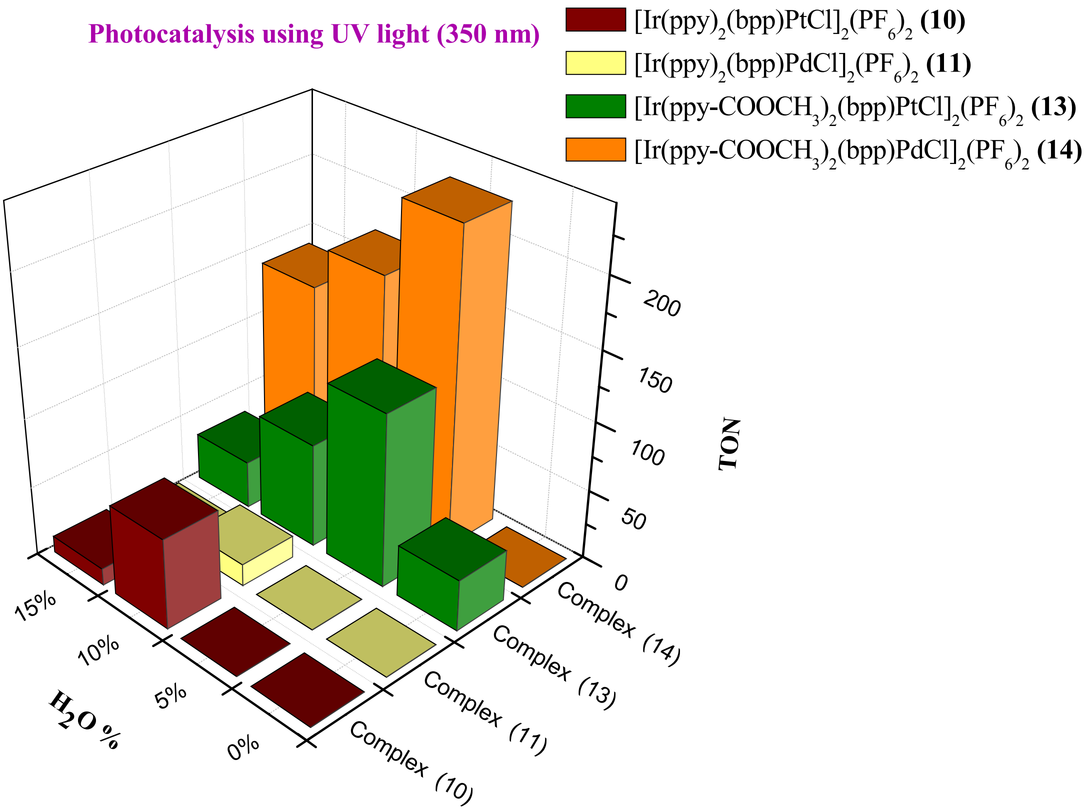

***Figure 3.31** Three dimensional representation of the photocatalytic TON values for complexes **(10)**, **(11)**, **(13)** and **(14)** in ACN using UV light (350 nm) irradiation. Irradiation time is 18h, sacrificial reagent used TEA, Conc. of PS and catalyst is 6×10^{-5}M.*

The above figure clearly shows a decrease in TON on moving to 350 nm from 470 nm (figure 3.31) irradiation for all complexes. Only complex **(13)** produced H_2 at 0 % H_2O. Complexes **(10)** and **(11)** produced small amount of H_2 at 10 % H_2O which is almost 1/5th of what was obtained under similar conditions using visible light (470 nm). Similarly to the studies carried out using visible light the Ir-Pt complex **(10)** was more efficient than Ir-Pd complex **(11)**. The ester complexes (**(13)** and **(14)**) show maximum efficiency at 5 % of H_2O and at higher concentrations of H_2O TON values decreased. Similarly to the behaviour observed using visible light, UV irradiation leads to greater catalytic activity for the ester Ir-Pd complex **(14)**. Visible light (470 nm) is far more efficient than the UV light (350 nm) and a possible explanation for this can be given on the basis of the excited state measurements. From the excited state studies carried out with these complexes, a low lying $^3MLCT_{ppy}$ state are thought to be responsible for populating the Pt and Pd excited states. For the ester complexes substitution of the peripheral ppy ligand by the electron withdrawing ester groups results in an increase in energy of the $^3MLCT_{ppy}$ excited state, as is evident by analysing the emission spectra of the non ester and ester complexes given in figure 3.22. The results for intermolecular photocatalysis for these four complexes, including the area obtained from GC are given in appendix B.

(c) Intermolecular photocatalysis using visible light (470 nm) and UV light (350 nm)

Intermolecular photocatalysis was carried out with the mononuclear complex $[Ir(ppy)_2(bpp)](PF_6)$ **(9)**, using both visible (470 nm) and UV light (350 nm), with two different percentages of H_2O (5 % and 10 %) in the presence of $[Pt(ACN)_2Cl_2]$ and $[Pd(ACN)_2Cl_2]$. The results obtained are shown in figure 3.32. The TONs are slightly higher for the solutions containing 5 % H_2O compared to those containing 10 % H_2O. Visible light (470 nm) produced more hydrogen than the UV light (350 nm) which is in agreement with the intramolecular photocatalysis.

When the TONs for H_2 production for complex **(9)** (figure 3.32) are compared to the two dimer complexes **(10)** and **(11)** (figure 3.30), using visible light intramolecular photocatalysis is more efficient than intermolecular photocatalysis. However, when UV light is used intermolecular photocatalysis is more efficient than the intramolecular photocatalysis (figure 3.31). The photophysical data may provide an explanation. In the case of intramolecular photocatalysis, low lying ^3MLCT states are populated and from here the excited state of Pt or Pd are populated at room temperature, when the system is in thermal equillibrium. From the absorption spectra it is quite clear that these ^3MLCT excited states show absorption bands in the range of 400 nm – 500 nm. Thus excitation of these systems using 470 nm results in direct population of the ^3MLCT levels from where an electron easily moves to Pt/Pd. But when the wavelength is changed to 350 nm the higher energy ligand to ligand charge transfer excited states (LLCT) are populated which for the heterobimetallic Ir-Pt/Pd complexes is much higher in energy than the excited Pt and Pd excited states so direct population of Pt/Pd excited states from this state is not as efficient as from the ^3MLCT states. This might be one possible explanation why intramolecular photocatalysis is more efficient using visible light compared to UV light.

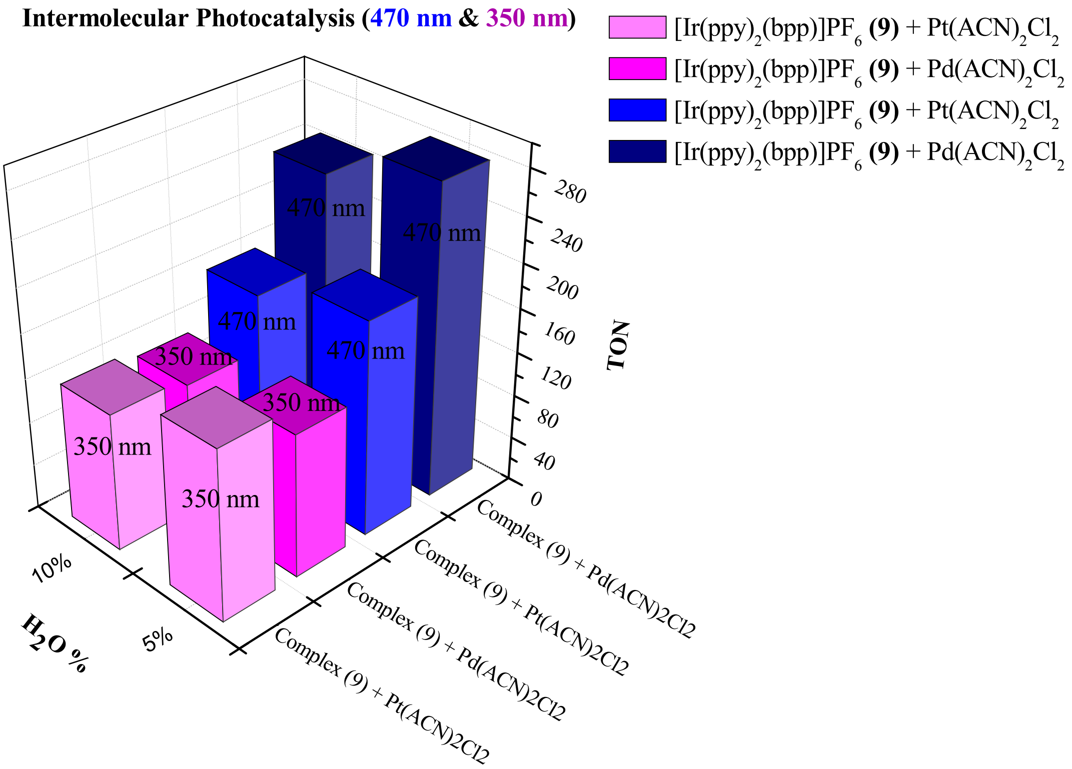

Figure 3.32 *Three dimensional representation of intermolecular photocatalytic TON values for complex* ***(9)*** *in ACN using visible light (470 nm) and UV light (350 nm). Irradiation time, 18h, sacrificial agent used, TEA, Conc. of PS and catalyst is* 6×10^{-5}*M.*

For the intermolecular systems studied here one possible electron transfer mechanism may be as follows: after excitation the electron moves from the ground state to singlet ligand centered excited states from where it decays to the triplet ligand to ligand excited state. For intermolecular photocatalysis this ^{3}LLCT state plays the major role in populating the Pt and Pd centers. This assumption was made on the basis that for intermolecular photocatalysis irradiation with 350 nm led to the formation of more H_2 than the intramolecular experiments. For these type of cyclometallated complexes the ^{3}LLCT absorption band is reported to occur at around 350 nm.[67] Further detailed studies are required to fully explain the differences observed. Based on the results presented here, these complexes may undergo photocatalysis through a reductive quenching mechanism as shown below.

$$\mathrm{PS} + h\nu \rightarrow \mathrm{PS}^* \tag{1}$$

$$\mathrm{PS}^* + \mathrm{SR} \rightarrow \mathrm{PS}^- + \mathrm{SR}^+ \tag{2}$$

$$\mathrm{PS}^- + \mathrm{H}^+ \rightarrow \mathrm{PS} + 1/2\mathrm{H}_2 \tag{3}$$

Interestingly the analogous non ester Ru complexes containing the bpp ligand which was synthesised within the group[82] gave lower amounts of H_2 than the iridium counterparts.

(d) Time dependent intramolecular and intermolecular photocatalysis using visible light

Time dependent intramolecular photocatalysis using visible light (470 nm) was carried out using $[Ir(ppy)_2(bpp)PtCl]_2(PF_6)_2$ **(10)** and $[Ir(ppy)_2(bpp)PdCl]_2(PF_6)_2$ **(11)**. Photocatalysis was performed in ACN, and using TEA as the sacrificial agent. The graphical representation of the TON's obtained every hour for a period of 8 hours is given in figure 3.33. From this figure it appears that initially the Ir-Pt complex **(10)** showed greater catalytic activity than the Ir-Pd complex **(11)**. The Ir-Pt complex **(10)** gave a TON value of 630 after 7 hours, and then begins to decrease (figure 3.33). After 18 h irradiation the TON value obtained is 364. This decrease in the amount of H_2 formed after 8h may possibly be due to leakage, or decomposition of the catalyst. For the Ir-Pd complex **(11)** no H_2 was produced up to 2h (figure 3.33) thereafter the amount of H_2 produced increases consistantly and reaches a TON value of 245 after 8h irradiation. As shown in figure 3.30, after 18h **(11)** a TON of 249 was observed. From these TON values it appears for the Ir-Pd complex the amount of H_2 produced remains constant after 8h irradiation.

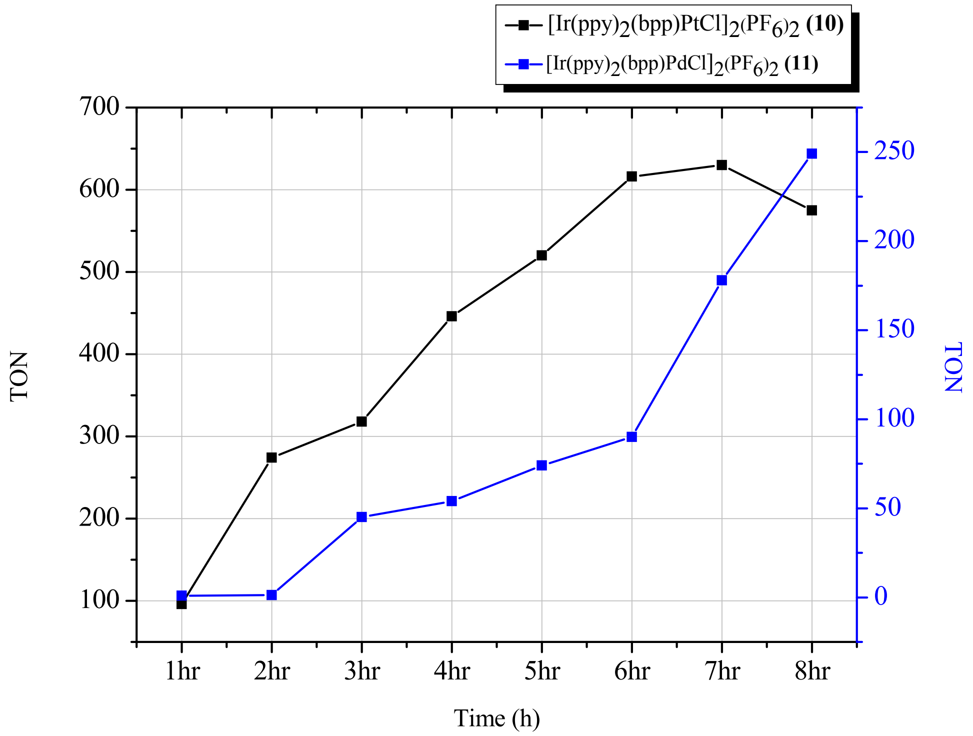

Figure 3.33 *Graphical representation of time dependent intramolecular photocatalysis using 470 nm visible light in 5 % H_2O ACN solution, sacrificial reagent used is TEA.*

Time dependent intermolecular photocatalysis were carried out with $[Ir(ppy)_2(bpp)](PF_6)$ **(9)** under similar conditions, but using two different catalysts $[Pt(ACN)_2Cl_2]$ and $[Pd(ACN)_2Cl_2]$. The graphical representation of the TON's obtained every hour for a period of 8 hours is given in figure 3.34. From the figure it is quite clear that in both cases the amount of H_2 produced increases constantly from 1h to 8h. Thus the photocatalysis is efficient, as both the PS and catalyst are not decomposing over this time period.

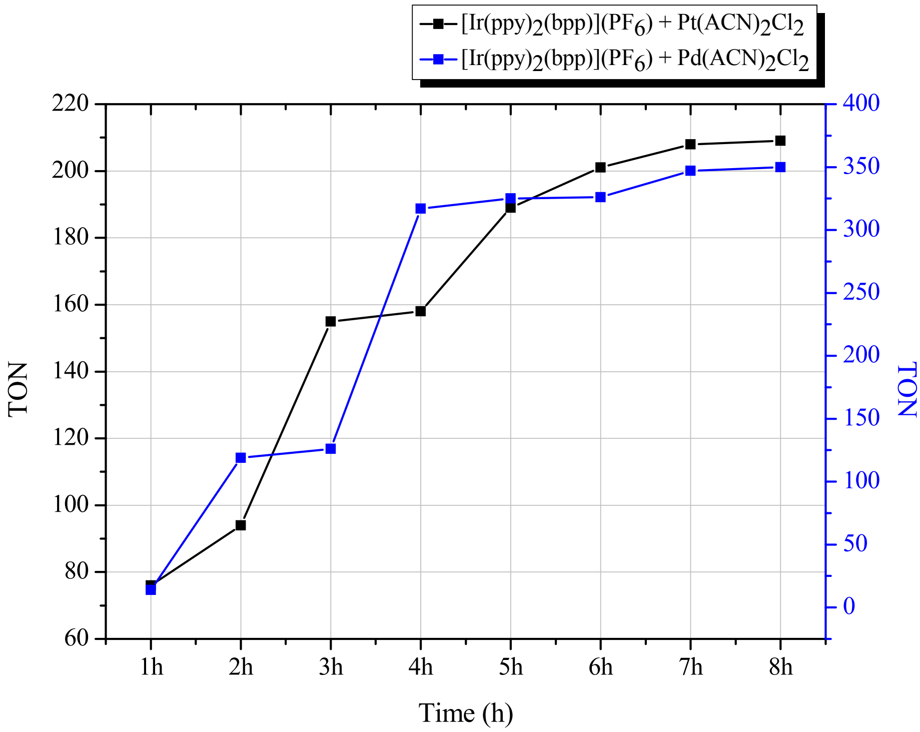

Figure 3.34 *Graphical representation of time dependent intramolecular photocatalysis using 470 nm light in a 5 %* H_2O *ACN solution, sacrificial reagent used is TEA.*

On comparing figures 3.33 and 3.34 it is clear that intramolecular photocatalysis is more efficient than intermolecular photocatalysis. Furthermore for the intramolecular photocatalytic experiments the Ir-Pt complex **(10)** showed better photocatalytic efficiency than the Ir-Pd complex **(11)**. In the case of the intermolecular photocatalytic experiments using $[Pt(ACN)_2Cl_2]$ and $[Pd(ACN)_2Cl_2]$ there was very little difference between the two catalytic centers (figure 3.34).

3.3.4.3 Intramolecular and intermolecular photocatalysis of iridium complexes with the tpy ligand using visible light (470 nm) and UV light (350 nm)

Photocatalysis of five novel cyclometallated iridium complexes containing the tpy (2,2':6',2''-terpyridine) ligand is discussed in this section. The three mononuclear complexes are

[Ir(ppy)$_2$(tpy)](PF$_6$) **(15)**, [Ir(ppy-COOCH$_3$)$_2$(tpy)](PF$_6$) **(17)**, [Ir(ppy-CHO)$_2$(bpp)PtCl]$_2$ (PF$_6$)$_2$ **(19)** and two dinuclear Ir-Pd complexes [Ir(ppy)$_2$(tpy)PdCl]$_2$(PF$_6$)$_2$ **(16)** and [Ir(ppy-COOCH$_3$)$_2$(tpy)PdCl]$_2$(PF$_6$)$_2$ **(18)**. Photocatalysis was carried out in ACN containing 5 % water and using TEA as the sacrificial agent. The results following 18 hours irradiation for both irradiation wavelengths are given in figure 3.35. It is interesting to note that both heterobimetallic dinuclear Ir-Pd complexes [Ir(ppy)$_2$(tpy)PdCl]$_2$(PF$_6$)$_2$ **(16)** and [Ir(ppy-COOCH$_3$)$_2$(tpy)PdCl]$_2$(PF$_6$)$_2$ **(18)** did not produce H$_2$. The results obtained however for the intermolecular photocatalytic experiments using complexes **(15)**, **(17)** and **(19)** in conjunction with [Pt(ACN)$_2$Cl$_2$] and [Pd(ACN)$_2$Cl$_2$] gave varied results.

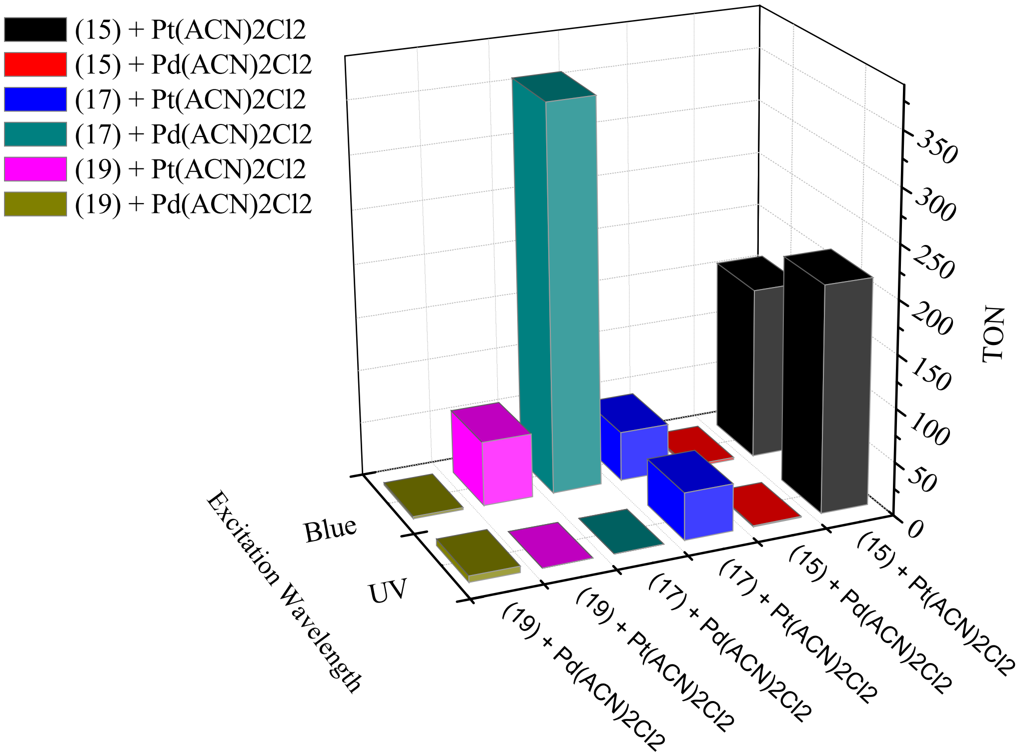

Figure 3.35 *Three dimensional representation of intermolecular photocatalytic TON values for complexes **(15)**, **(17)** and **(19)** in ACN using visible light (470 nm) and UV light (350 nm) irradiation. Irradiation time is 18h, sacrificial reagent used TEA, Conc. of PS and catalyst is* 6×10^{-5}*M.*

The unsubstituted ppy complex **(15)** formed H$_2$ only in the presence of [Pt(ACN)$_2$Cl$_2$] as catalyst and no H$_2$ when [Pd(ACN)$_2$Cl$_2$] was used. UV irradiation produced marginally more H$_2$ than the visible light. This is in contrast to the ester substituted complex **(17)**, which in the presence of [Pt(ACN)$_2$Cl$_2$] gave almost the same amount of H$_2$ for both visible and UV light irradiation. The use of [Pd(ACN)$_2$Cl$_2$] as catalyst, resulted in a very large TON when visible light was used but no H_2 was produced using UV light. The analogous non ester Ru mononuclear complexes[83] with the tpy ligand produced no hydrogen in the intermolecular photocatalytic experiments clearly indicating the higher efficiency of iridium metal photocatalyts. For the intramolecular systems, neither Ir nor Ru showed any H_2 production activity.[82]

3.3.4.4 Intramolecular and intermolecular photocatalysis of iridium complexes containing the bpm ligand using both visible (470 nm) and UV (350 nm) light

Photocatalysis of three novel cyclometallated iridium complexes containing the bpm ligand are discussed in this section. The complexes includes two mononuclear complexes $[Ir(ppy)_2(bpm)](PF_6)$ **(20)**, $[Ir(ppy\text{-}COOCH_3)_2(bpm)]$ (PF_6) **(24)** and one dinuclear Ir-Pd complex $[Ir(ppy)_2(bpm)PdCl_2](PF_6)$ **(21)**. The results obtained for both intermolecular and intramolecular photocatalysis using both visible (470 nm) and UV (350 nm) light in ACN solution containing 5 % H_2O, TEA, and either a Pd or Pt catalyst are given in table 3.10.

Complex (6x10^{-5} M)	**470 nm**	**350 nm**
	TON_{H2}	TON_{H2}
$[Ir(ppy)_2(bpm)](PF_6)$ **(20)** + $Pt(ACN)_2Cl_2$	20	8
$[Ir(ppy)_2(bpm)](PF_6)$ **(20)** + $Pd(ACN)_2Cl_2$	3	2
$[Ir(ppy)_2(bpm)PdCl_2](PF_6)$ **(21)**	39	7
$[Ir(ppy\text{-}COOCH_3)_2(bpm)](PF_6)$ **(24)** + $Pt(ACN)_2Cl_2$	3	5
$[Ir(ppy\text{-}COOCH_3)_2(bpm)](PF_6)$ **(24)** + $Pd(ACN)_2Cl_2$	3	5

Table 3.10 *Tabulated TON values for complexes* ***(20)****,* ***(21)*** *and* ***(24)*** *in ACN using using visible light (470 nm) and UV light (350 nm). Irradiation time is 18h, sacrificial reagent used TEA, Conc. of PS and catalyst is* 6×10^{-5}*M.*

The TON values obtained for these complexes are lower than the values obtained for the iridium complexes discussed in the last section. Interestingly the Ir-Pd dinuclear complex showed better photocatalytic activity than the intermolecular photocatalytic systems.

3.4 Conclusion

Iridium metal complexes have been extensively studied as chromophores for light to chemical energy conversion as they have large spin orbit coupling which results in long lived triplet excited states. In this chapter a range of mononuclear, homodinuclear and heterodinuclear cyclometallated iridium (III) complexes are studied including the detailed synthesis, characterisation, photophysics and photocatalysis. Novel iridium complexes containing either Pt or Pd metal centers, with three different bridging ligands (bpp, tpy and bpm) are reported. Deuteriation was used as a probe to study the nature of the lowest lying triplet excited states in iridium (III) complexes of the type $[Ir(N^{\wedge}C)_2(N^{\wedge}N)]PF_6$. By varying the substituents at the peripheral phenylpyridine ligand and also by substituting the neutral N^N bipyridine ligand of these complexes it was possible to tune the emission. It is quite clear from the emission spectra, that complexation with Pt or Pd results in decrease in intensity of emission.

Both intermolecular and intramolecular photocatalytic experiments were carried out in ACN using TEA as the sacrificial agent. Intramolecular photocatalysis proved to be more efficient than intermolecular photocatalysis. Also two different excitation wavelengths were used. The photocatalytic results showed that 470 nm irradiation produced more H_2 than the 350 nm which suggests that the low lying ^{3}MLCT excited states of iridium play a major role in populating the Pt/Pd excited states. Also the ester complexes were more efficient photocatalysts than the non ester analogues. A possible reason for this behaviour is attributed to an increase in the energy of the ^{3}MLCT states as a result of substitution with the electron withdrawing ester group on the peripheral ppy ligand. The ester complexes studied here will be bound to NiO surfaces thereby the use of sacrificial agents can be eliminated, thus making environment friendly photocatalytic systems for the production of hydrogen.

3.5 Bibliography

---

1. O. Khaselev, J. A. Turner, *Science,***1998**, 280, 425.
2. Z. Zou, J. Ye, K. Sayama, H. Arakawa, *Nature*, **2001**, 414, 625.
3. M. Gratzel, *Nature,* **2001**, 414, 338.
4. A. Steinfeld, *Solar Energy*, **2005**, 78, 603.
5. J. M. Lehn, J. P. Sauvage, *Nouv. J. Chim*, **1977**, 1, 449.
6. A. Moradpour, E. Amouyal, P. Keller, H. Kagan, *Nouv. J. Chim*, **1978**, 2, 547.

7. M. Gratzel, *Acc. Chem. Res,* **1981**, 14, 376.
8. D. Duonghong, E. Borgarello, M. Gratzel, *J. Am. Chem. Soc,* **1981**, 103, 4685.
9. J. R. Darwent, P. Douglas, A. Harriman, G. Porter, M. C. Richoux, *Coord. Chem. Rev*, **1982**, 44, 83.
10. L. Persaud, A. J. Bard, A. Campion, M. A. Fox, T. E. Mallouk, S. E. Webber, J. M. White, *J. Am. Chem. Soc*, **1987**, 109, 7309.
11. E. Adar, Y. Degani, Z. Goren, I. Willner, *J. Am. Chem. Soc*, **1986**, 108, 4696.
12. J. I. Goldsmith, W. R. Hudson, M. S. Lowry, T. H. Anderson, S. Bernhard, *J. Am. Chem. Soc*, **2005**, 127, 7502.
13. M. S. Lowry, J. I. Goldsmith, J. D. Slinker, R. Rohl, R. A. Pascal, G. G. Malliaras, S. Bernhard, *Chem. Mater*, **2005**, 17, 5712.
14. K. Kalyanasundaram, Photochemistry of Polypyridine and Porphyrin Complexes, *Academic Press, New York, NY*, **1992**, p. 105.
15. R. J. Watts, J. V. Houten, *J. Am. Chem. Soc*, **1974**, 96, 4334.
16. M. G. Colombo, A. Hauser, H. U. Gudel, *Inorg. Chem*, **1993**, 32, 3088.
17. M. G. Colombo, A. Hauser, H. U. Gudel, *Top. Curr. Chem*, **1994**, 171, 143.
18. P. J. Hay, *J. Phys. Chem. A*, **2002**, 106, 1634.
19. E. Amouyal, B. Zidler, P. Keller, A. Moradpour, *Chem. Phys. Lett*, **1980**, 74, 314.
20. C. V. Krishnan, N. Sutin, *J. Am. Chem. Soc*, **1981**, 103, 2141.
21. C. V. Krishnan, B. S. Brunschwig, C. Creutz, N. Sutin, *J. Am. Chem.Soc*, **1985**, 107, 2005.
22. J. Hawecker, J. M. Lehn, R. Ziessel, *Nouv. J. Chim*, **1983**, 7, 271.
23. G. M. Brown, S. F. Chan, C. Creutz, H. A. Schwarz, N. Sutin, *J. Am.Chem. Soc*, **1979**, 101, 7638.
24. S. F. Chan, M. Chou, C. Creutz, T. Matsubara, N. Sutin, *J. Am. Chem. Soc*, **1981**, 103, 369.
25. M. Kirch, J. M. Lehn, J. P. Sauvage, *Helv. Chim. Acta*, **1979**, 62, 1345.
26. H. Ozawa, M. Haga, K. Sakai, *J. Am. Chem. Soc*, **2006**, 128, 4926.
27. S. Rau, B. Schtfer, D. Gleich, E. Anders, M. Rudolph, M. Friedrich, H. Gerls, W. Henry, J. G. Vos, *Angew. Chem. Int. Ed*, **2006**, 45, 6215.
28. P. J. DeLaive, B. P. Sullivan, T. J. Meyer, D. G. Whitten, *J. Am. Chem. Soc*, **1979**, 101, 4007.
29. J. Hawecker, J. M. Lehn, R. Ziessel, *J. Chem. Soc. Chem.Commun*, **1983**, 536.

30. K. Kalyanasundaram, J. Kiwi, M. Gratzel, *Helv. Chim. Acta*, **1978**, 61, 2720.
31. A. Currao, V. R. Reddy, M. K. V. Veen, R. E. I. Schropp, G.Calzaferri, *Photochem. Photobiol. Sci*, **2004**, 3, 1017.
32. A. Fihri, V. Artero, M. Razavet, C. Baffert, W. Leibl and M. Fontecave, *Angew. Chem. Int. Ed.,* **2008**, 47, 564.
33. A. Fihri, V. Artero, A. Pereira and M. Fontecave, *Dalton Trans*., **2008**, 5567.
34. E. S. Andreiadis, M. C. Kerlidou, M. Fontecave and V. Artero, *Photochemistry and Photobiology*, **2011**, 87, 946.
35. S. Jasimuddin, T. Yamada, K. Fukuju, J. Otsaki, K. Sakai, *Chem. Commun.,* **2010**, 46, 8466.
36. B. Dietzek, W. Kiefer, J. Blumhoff, L. B. Mttcher, S. Rau, D. Walther, U. Uhlemann, M. Schmitt, J. Popp, *Chem. Eur. J*, **2006**, 12, 5105.
37. C. Chiorboli, M. A. J. Rodgers, F. Scandola, *J. Am. Chem. Soc*, **2003**, 125, 483.
38. G. S. Bindra, M. Shulz, A. Paul, S. Soman, R. Groarke, J. Inglis, M. T. Pryce, W. R. Browne, S. Rau, B. J. Maclean, J. G. Vos, *Dalton Trans.,* **2011**, 40, 10812.
39. M. Schulz, J. Hirschmann, A. Draksharapu, G. Singh Bindra, S. Soman, A. Paul, R. Groarke, M. T. Pryce, S. Rau, W. R. Browne and J. G. Vos, *Dalton Trans.,* **2011**, 40, 10545.
40. Losse, S, J. G. Vos and S. Rau, *Coord. Chem. Rev.,* **2010**, 254, 2492.
41. D. J. Hurley and Y. Tor, *J. Am. Chem. Soc.*, **2002**, 124, 3749.
42. K. K. W. Lo and K. H. K. Tsang, *Organometallics*, **2004**, 23, 3062.
43. V. L. Whittle and J. A. G. Williams, *Dalton Trans.,* **2009**, 3929.
44. V. Balzani and F. Scandola, *Supramolecular Photochemistry*, Ellis Horwood, New York, **1990**.
45. K. Kalyanasundaram, *Photochemistry of Polypyridine and Porphyrin Complexes*, Academic Press, San Diego, **1991**.
46. D. M. Roundhill, *Photochemistry and Photophysics of Metal Complexes*, Plenum Press, New York, **1994**.
47. I. V. Avilov, P. Minoofar, J. Cornil and L. De Cola, *J. Am. Chem.Soc.,* **2007**, 129, 8247.
48. J. P. Collin, I. M. Dixon, J. P. Sauvage, J. A. G. Williams, F. Barigelletti and L. Flamigni, *J. Am. Chem. Soc*., **1999**, 121, 5009.

49. M. Polson, S. Fracasso, V. Bertolasi, M. Ravaglia and F. Scandola, *Inorg. Chem.,* **2004**, 43, 1950.
50. E. I. Mayo, K. Kilsa , T. Tirrell, P. L. Djurovich, A. Tamayo, M. E. Thompson, N. S. Lewis and H. B. Gray, *Photochem. Photobiol. Sci*., **2006**, 5, 871.
51. M. Licini and J. A. G. Williams, *Chem. Commun*., **1999**, 1943.
52. K. J. Arm, W. Leslie and J. A. G. Williams, *Inorg. Chim. Acta*., **2006**, 359, 1222.
53. W. Goodall and J. A. G. Williams, J. Chem. Soc., *Dalton Trans*., **2000**, 2893.
54. K. K. W. Lo, C. K. Chung and N. Zhu, *Chem. Eur. J*., **2003**, 9, 475.
55. K. K. W. Lo, C. K. Chung and N. Zhu, *Chem. Eur. J*., **2006**, 12, 1500.
56. M. A. Baldo, M. E. Thompson, S. R. Forrest, *Nature*, **2000**, 403.
57. E. A. Plummer, J. W. Hofstraat, L. De Cola, *Dalton Trans.*, **2003**, 2080.
58. J. D. Slinker, A. A. Gorodetsky, M. S. Lowry, J. Wang, S. Parker, R. Rohl, S. Bernhard, G. G. Malliaras, *J. Am. Chem.Soc.,* **2004**, 126, 2763.
59. A. B. Tamayo, B. D. Alleyne, P. I. Djurovich, S. Lamansky, I. Tsyba, N. N. Ho, R. Bau, M. E. Thompson, *J. Am. Chem. Soc.,* **2003**, 125, 7377.
60. S. H. Wu, J. W. Ling, S. H. Lai, M. J. Huang, C. H. Cheng, I. C. Chen, *J. Phys. Chem. (A).,* **2010,** 114, 10339.
61. A. F. Rausch, M. E. Thompson, H. Yersin, *J. Phys. Chem. (A).,* **2009**, 113, 5927.
62. K. A. King, R. J. Watts, *J. Am. Chem. Soc*., **1987**, 109, 1589.
63. A. P. Wilde, R. J. Watts, *J. Phys. Chem.,* **1991**, 95, 622.
64. A. P. Wilde, K. A. King, R. J. Watts, *J. Phys. Chem.,* **1991**, 95, 629.
65. K. Ichimura, T. Kobayashi, K. A. King, R. J. Watts, *J. Phys.Chem.,* **1987**, 91, 6104.
66. F. O. Garces, K. A. King, R. J. Watts, *Inorg. Chem.,* **1988**, 27, 3464.
67. M. Polson, S. Fracasso, V. Bertolasi, M. Ravaglia and F. Scandola, *Inorg Chem.,* **2004**, 43, 1950.
68. M. Kasha, *Discussion of the faraday society*, **1950**, 9, 14.
69. T. Tsuboi and N. Aljaroudi, *Jpn. J. Appl. Phys., Part 1*, **2008**, 47, 1266.
70. S. Lamansky, P. Djurovich, D. Murphy, F. A. Razzaq, H. E. Lee, C. Adachi, P. E. Burrows, S. R. Forrest and M. E. Thompson, *J. Am.Chem. Soc*., **2001**, 123, 4304.
71. S. Sprouse, K. A. King, P. J. Spellane, R. J. Watts, *J. Am. Chem. Soc.,* **1984**, 106, 6647.
72. Y. Ohsawa, S. Sprouse, K. A. King, M. K. DeArmond, K. W. Hanck, R. J. Watts, *J.Phys. Chem.,* **1987**, 91, 1047.

---

73. M. Lepeltier, T. K. Lee, K. K. Lo, L. Toupet, H. L. Bozec, V. Guerchais, *Eur. J. Inorg. Chem.,* **2005**, 110.

74. S. Serroni, A. Juris, S. Campagna, M. Venturi, G. Denti, V. Balzani, *J. Am. Chem. Soc.,* **1994**, 116, 9086.

75. P. Didier, I. Ortmans, A. K. De Mesmaeker, R. J. Watts, *Inorg. Chem.* **1993**, 32, 5239.

76. F. Neve, A. Crispini, S. Campagna, S. Serroni, *Inorg. Chem.,* **1999**, 38*,* 2250.

77. D. D. Censo, S. Fantacci, F. D. Angelis, C. Klein, N. Evans, K. Kalyanasundaram, H. J. Bolink, M. Gratzel and M. K. Nazeeruddin, *Inorg. Chem.*, **2008**, 47, 980.

78. P. T. Chou, Y. I. Liu, H. W. Liu and W. S. Yu, *J. Am. Chem. Soc.*, **2001**, 123, 12119.

79. W. R. Browne and J. G. Vos, *Coord. Chem. Rev.*, **2001**, 219, 761

80. P. I. Djurovich, R. J. Watts, *Inorg. Chem.* **1993**, *32*, 4681.

81. B. Schmid, F. O. Garces, R. J. Watts, *Inorg. Chem.* **1994**, *33*, 9.

82. Gurmeet Singh Bindra, Ph.D Thesis , Dublin City University, **2011**

Chapter 4

Excited state photophysics of novel Ir-Pt/Pd complexes

This chapter deals with the solvent and temperature dependent excited state photophysics of three novel Ir (III) cyclometallated complexes, which includes the mononuclear $[Ir(ppy)_2(bpp)]PF_6$ and two heterodinuclear dimers - $[Ir(ppy)_2(bpp)PtCl]_2(PF_6)_2$ and $[Ir(ppy)_2(bpp)PdCl]_2(PF_6)_2$. Comparing the results obtained with those reported for other cyclometallated iridium (III) complexes yields an understanding of the possible electronic transitions taking place in these complexes.

4.1 General introduction to photophysics

Transition metal complexes have attracted a great deal of interest in recent years particularly due to their photochemical and photophysical properties.[1,2,3,17] The development of various bridging ligands has allowed for the creation of numerous polynuclear complexes which have been used in the study of electron transfer processes, in attempts to mimic photosynthesis and in the development of molecular devices.[4,33,48] If a photon of light, be it from the visible or the ultraviolet region, is absorbed by a metal complex, the metal complex will be transformed into an electronically excited state from where it will decay to the ground state by either radiative or by nonradiative means. Possible pathways are fluorescence or phosphorescence or a chemical pathway followed in which the complex is converted to products. It should be noted that fluorescence is the radiative deactivation pathway between states of the same multiplicity whereas phosphorescence involves states of different multiplicity.[5,6,63]

With respect to theoretical models, the first theory of electronic structure to be developed was crystal field theory. In crystal field theory a ligand lone pair is considered as a single point negative charge (or as the partial negative charge of an electric dipole) that repels electrons in the d orbitals of the central metal ion. Upon coordination, the energies of the d orbitals of the metal ion are raised but it should be noted that considering the geometry of the d orbitals of the central metal ion, those d orbitals that are directed toward the ligand (the e_g set) are repelled more than those directed in between the ligands (t_{2g} set).[7,8] This means that not all of the d electrons are destabilised to the same extent and this difference in the destabilisation energy, known as Δ_0 (where the subscript O stands for octahedral), gives rise to splitting of the d orbital energies. Whereas crystal field theory provides a simple and easy theory of electronic structure, ligand field theory focuses on the role of the d orbitals on the metal ion and their overlap with ligand orbitals.[7,8] When attempting to develop a composite electronic model to describe a complex using ligand field theory it is necessary to take all of the electrons involved in bonding, localised both on the metal ion and on the ligand into consideration in two separate sets. Based upon this it is then possible to combine the molecular orbital diagrams of both the metal and the ligand to create a model representative of the system as a whole.

4.1.1 Charge transfer in transition metal complexes

Symmetry selection rules state that for a transition to be "allowed" the electron that moves from an orbital that is even with respect to inversion through the center of symmetry, to an orbital that is uneven with respect to inversion (or vice versa). Since all d orbitals in an octahedral complex are even with respect to inversion d-d transitions are "forbidden". Under visible irradiation these complexes undergo strong metal to ligand charge transfer transitions (MLCT) and ligand centered (LC) transitions. In the case of transition metal complexes in addition to LC and MLCT, if the lowest unoccupied molecular orbital (LUMO) is located on the metal ion, the opposite charge transfer (LMCT) is also observed.[9,10]

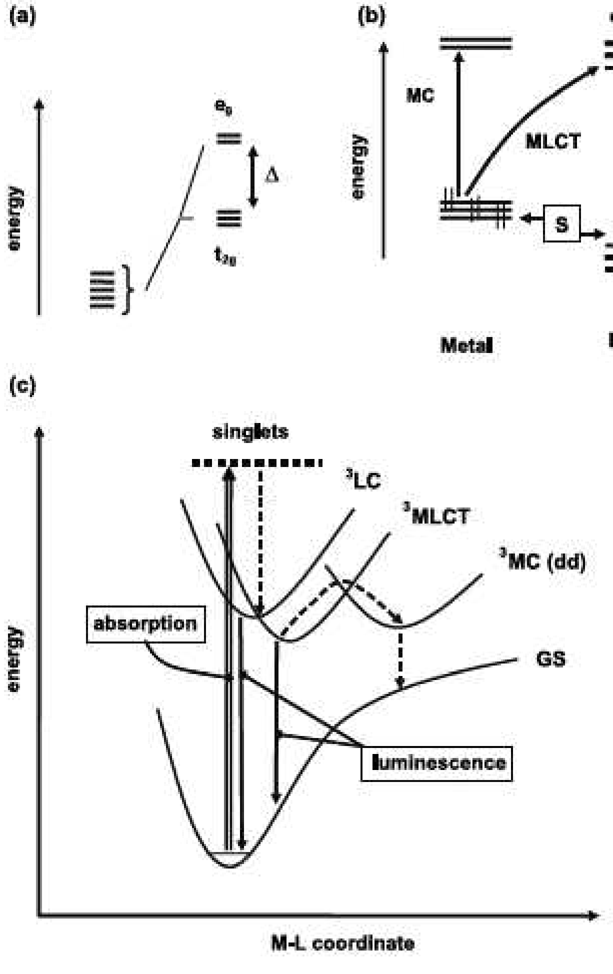

Figure 4.1 a) *d orbitals in octahedral field;* ***b)*** *orbital description of MC, MLCT and LC transitions, S is a substituent group capable of exerting electron withdrawing or releasing effects (resulting in stabilisation or destabilisation, respectively, of the energy level of the filled d and π orbitals);* ***c)*** *electronic transitions involving MC, MLCT and LC excited states.*[11]

The Ir (III) trication is a $5d^6$ center and the electronic properties of its polyimine complexes share several features with those of other well known octahedral complexes of Fe (II), Ru (II) and Os (II), whose metal centers are $3d^6$, $4d^6$, and $5d^6$ respectively. Figure 4.1 depicts useful orbital energy diagrams outlining possible electronic transitions taking place in polyimine complexes of such d^6 metal centers. As shown in figure 4.1 (a), the degenerate d orbitals of the Fe (II), Ru (II), Os (II) and Ir (III) cations are destabilised and split in an octahedral (O_h) ligand field, by an amount Δ_0. The amount of Δ_0 depends also on the field strength exerted by the ligands that can be ordered along a spectrochemical series. It is likely that in this series, a cyclometallated ligand like ppy occupies a position among those causing the strongest effect.[11]

It should be noted that in all cases discussed here, light absorption is associated with electronic transitions from the ground state (GS) to, mostly, singlet levels of various nature and electronic localisation, ligand centered (^{1}LC), ligand to ligand centered (^{1}LLCT) and metal to ligand centered (^{1}MLCT). In addition, ligand to metal centered transitions (^{1}LMCT) can in principle be involved. On the contrary, emission is always from triplet levels, such as ^{3}MLCT or ^{3}LC. Studies done by Scandola and coworkers[11,12] and Williams and coworkers[13,14,15] have shown that for the cyclometallated Ir (III) complexes there is a prominent contribution from the LLCT (ligand to ligand intermolecular charge transfer) states along with the MLCT excited states. All these transitions determine the photophysical properties of transition metal complexes and can be used for the interpretation of experimentally observed spectra or prediction of absorption and emission characteristics of novel compounds. Hence, this knowledge of the described processes is necessary to rationalize the impact of ligand modifications on the photophysical properties of phosphorescent dyes or to design highly efficient materials for various applications.

4.1.2 Excited state evolution

The fate of an excited species is usually depicted in a Jablonski diagram (figure 4.2). The kinetics of the different transitions illustrated in this picture are of major importance since any photochemical reaction will have to compete with these processes. The time for absorption is similar to the optical cycle of the incident light and is thus very short (few fs). The timescales for the different processes are given in figure 4.2. The values vary over several orders of magnitude and these differences give information about the photochemical behavior of the compounds.

Excited state deactivation can take place in a radiative or non-radiative way. In the latter case, vibrational relaxation not only depends upon the range of atoms but also upon the surrounding media (solvent, solid matrix) and ranges over a wide range of timescale.[4,5,16]

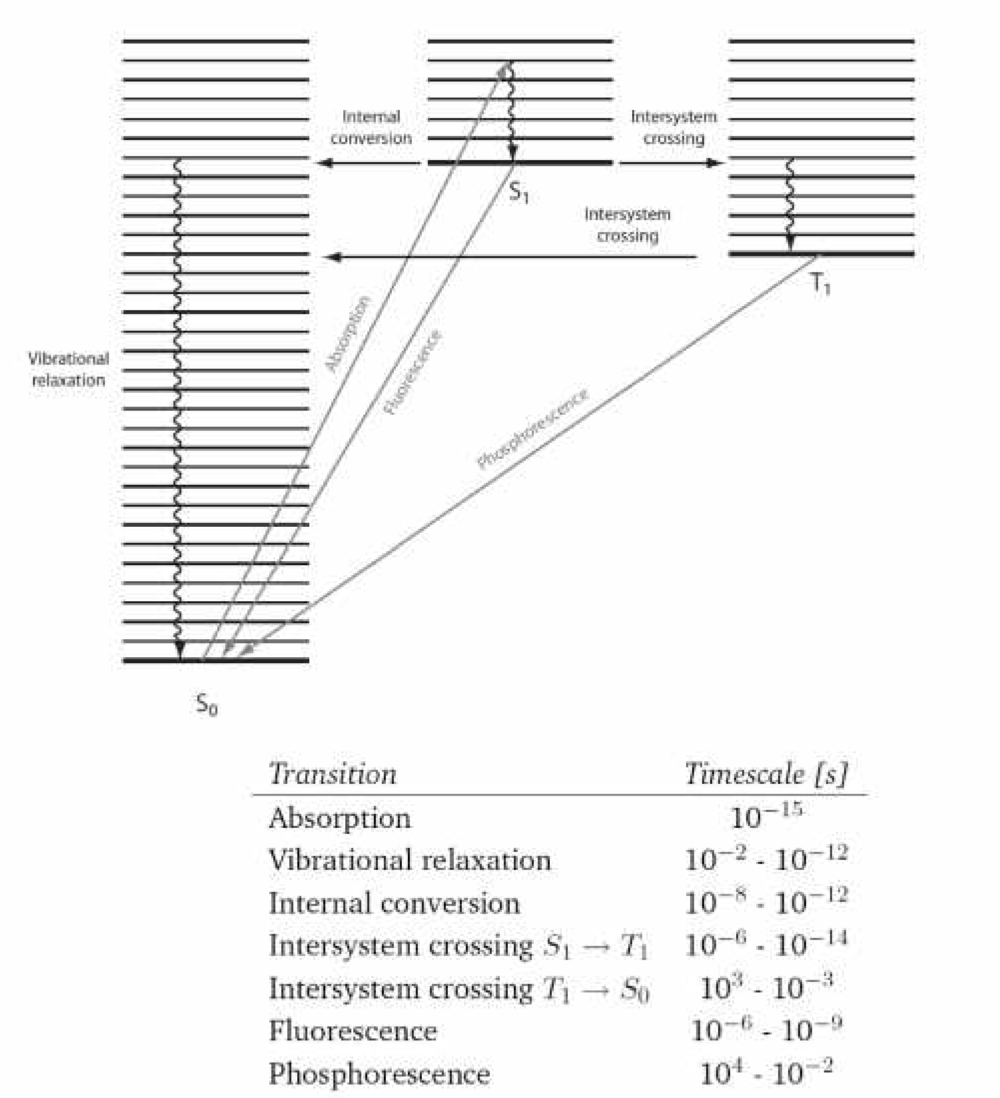

Transition	*Timescale [s]*
Absorption	10^{-15}
Vibrational relaxation	10^{-2} - 10^{-12}
Internal conversion	10^{-8} - 10^{-12}
Intersystem crossing $S_1 \rightarrow T_1$	10^{-6} - 10^{-14}
Intersystem crossing $T_1 \rightarrow S_0$	10^{3} - 10^{-3}
Fluorescence	10^{-6} - 10^{-9}
Phosphorescence	10^{4} - 10^{-2}

Figure 4.2 *Jablonski diagram with various timescales for excited state deactivation.*[5,9]

Radiative deactivation (fluorescence and phosphorescence) takes usually place from the lowest vibrational level (Kasha's rule).[17] The fluorescence spectrum is approximately the mirror image of the absorption spectrum. However, the emission peaks are usually shifted because of the vibrational relaxation in the singlet excited state (Stokes shift). The triplet state is normally energetically stabilized due to spin correlation and may be readily populated for systems where high spin orbit coupling is large.

4.1.3 Excited state photophysics of Ir (III) cyclometallated complexes

Potential applications as OLED's[18,19,20,21] and in flat panel displays[22] have led to a significant interest in iridium (III) complexes with cyclometallating ligands such as phenyl pyridine (ppy) and benzoquinoline (bzq).[23,24,25] The stronger σ-donor character of C^- relative to N results in several important differences between complexes with cyclometallating ligands and those of polypyridine ligands. One difference is the increased energy of the ^{3}MC states owing to the greater ligand field strengths of the cyclometallating ligands.[17,26] A second difference between cyclometallated complexes and the corresponding polypyridine complexes is that the strong donor properties of the cyclometallating ligands increase electron density on the metal center, resulting in lower energy MLCT states.[17,9,27] Consequently, the emissive state of many Ir (III) complexes with cyclometallating ligands is of ^{3}MLCT or mixed ^{3}LC/^{3}MLCT character.[1,28,29] Typically, the ^{3}MC ligand field states for these complexes are too high in energy to serve as an effective pathway for excited state deactivation. However, excited state deactivation through the above mentioned emissive states has been implicated in cases where the energy of the emissive state has been increased by ligand modification.[30] Even though reducing the ^{3}MLCT excited state energy does inhibit activated decay via the ^{3}MC states, the effect is offset by enhanced nonradiative relaxation directly from the ^{3}MLCT state. Longer lifetimes may still result due to the relative balance between the two deactivation pathways.[17,27,31]

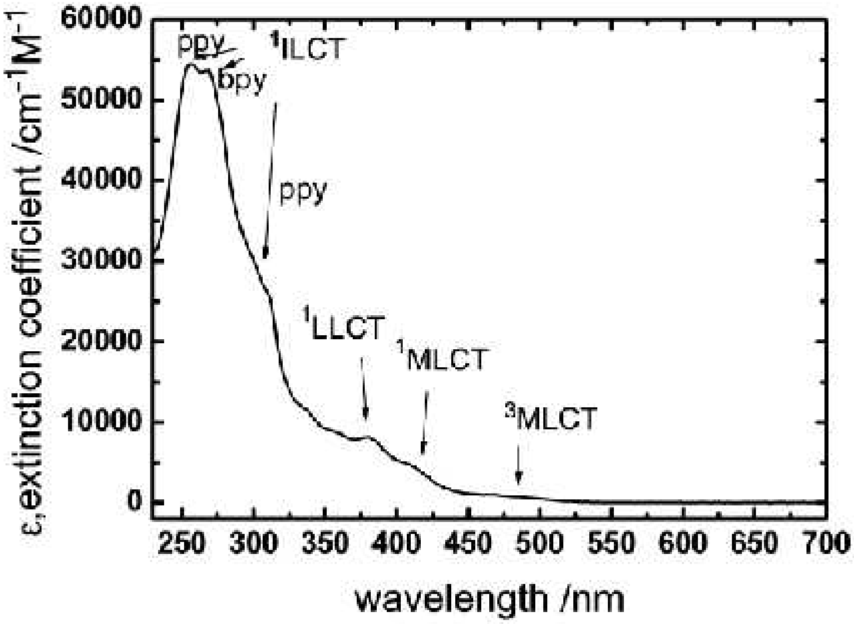

Figure 4.3 *Absorption spectrum of [Ir(ppy)$_2$bpy]$^+$ in dichloromethane.*[32]

The absorption spectra of the classical phosphorescent iridium (III) complex, $[Ir(ppy)_2(bpy)]^+$ displays absorption bands which include intra ligand charge transfer transitions (ILCT), ligand to ligand (inter ligand) charge transfer transitions (LLCT) and metal to ligand charge transfer (MLCT) transitions as shown in figure 4.3

For this compound literature data[33,34] suggests that, the bands with maxima in the 260-275 nm range receive larger contributions from ppy-centered transitions and absorption in the 275-300 nm range receives larger contributions from bpy-centered transitions. The absorption features in 350-400 nm are assigned as ligand to ligand charge transfer (LLCT) transitions. The absorption features in the range 400-450 nm are assigned to ^{1}MLCT and ^{3}MLCT transitions, with the lowest energy feature involving the substituted bpy ligand. After excitation of the iridium complex, the strong spin orbit coupling induced by the metal center gives the formally forbidden triplet to singlet ground state transition a significant allowedness.[35] Importantly the energies of the lowest excited states play a major role as they can be tuned by adjusting the metal and ligand orbitals through substituent effects or by changing the ligand structures. In other words, chemical modifications and alterations of the cyclometallating or ancillary ligands not only pave the way to efficient emission colour tuning but also provide the possibility of tuning the corresponding absorption characteristics towards particular needs. Extensive emission colour versatility has been achieved with iridium (III) luminophores applying the above described tuning procedures, giving materials with a broad range of excited state lifetimes and emission quantum yields.[36]

The lowest triplet state, which is responsible for phosphorescence emission for cyclometallating Ir (III) complexes according to Kasha's rule,[10,37] is either a ^{3}MLCT transition state or a ^{3}LC transition state. Generally, phosphorescence originating from the LC transition state can be distinguished from that of the MLCT transition state in terms of (1) spectral shape, (2) phosphoresence lifetime (τ_p), (3) rigidochromic and (4) solvatochromic behaviours:[38] (1) LC phosphorescence comprises prominent vibronic structures whereas a MLCT phosphorescence spectrum is structureless, (2) τ_p of LC phosphorescence is longer than that of MLCT phosphorescence, which reflects reduced metal contribution in the LC transition, (3) MLCT phosphorescence exhibits a hypsochromic shift when the medium becomes rigid (*e.g.* when solvent freezes or polymer hosts are left below T_g),[39] and (4) MLCT phosphorescence also exhibits a similar hypsochromic shift in non polar media.[40,41,42] Both (3) and (4) indicate a charge transfer (CT) character involved in the MLCT phosphorescence because the CT state energy is strongly affected by the arrangement of electric dipoles of surrounding media.[43,44] Apart from precisely judging which transition (MLCT or LC) state is more responsible for the observed phosphorescence, it may be the case that the phosphorescent state is a mixed state of MLCT and LC transition states.[45]

Recent studies[13-17] have shown that in addition to the above mentioned MLCT and LC states, ligand to ligand charge transfer (LLCT) also plays a prominent role in the excited state photophysics of cyclometallated Ir (III) complexes.[46,47,48] The LLCT proceeds from the occupied molecular orbitals of one type of ligand to the unoccupied molecular orbitals of other ligands. Confirmation of LLCT transitions is commonly hampered by the coexistence of other isoenergetic processes, such as d-d, MLCT (d-π*) and LC (π-π*) transitions. Nevertheless, for LLCT, the relocation of electron density across different ligands may be associated with large changes in dipole moment.[49,50] As a result, the contribution from LLCT transitions in the lowest lying excited state of luminescent transition metal complexes may be manifested by the associated solvent polarity dependent phosphorescence. The mixing of close lying, metal to ligand charge transfer transitions (MLCT) and ligand centred (LC) electronic transitions makes the fast singlet to triplet intersystem crossing feasible. Scandola reported[13,14] a bis-tridentate Ir (III) cyclometallated complex exhibiting a very small red shift of the emission band on passing from low to high temperature, assigning the emission to a ^{3}LLCT state. However, in their case the charge redistribution in the excited state compared to the ground state was also very small, due to the particular nature of the ligands involved. This suggests that whereas in general the extent of a red shift in emission for pure MLCT states is in some way similar in all the complexes, it can be quite different for LLCT emitters, strongly depending on the specific case. Cyclometallation has the effect of raising the energies of ligand field (d-d) excited states to very high levels due to the high position of the cyclometallating ligands in the spectrochemical series. Furthermore, the strong σ-donor abilities of these ligands tend to promote low energy MLCT excited states via enhancement of the ease of oxidation at the metal center.[51,52,53] This combination of effects leads to cyclometallated complexes, relative to their $[Ir(N^\wedge N)_2Cl_2]^+$ analogues, having low energy excited states well suited to participate in photoredox chemistry and show intense phosphorescence at room temperature.[54] A general proposed relaxation mechanism for the heteroleptic complex $[Ir(ppy)_2(bpy)]^+$ given by Chen and coworkers[32] is given in figure 4.4 below.

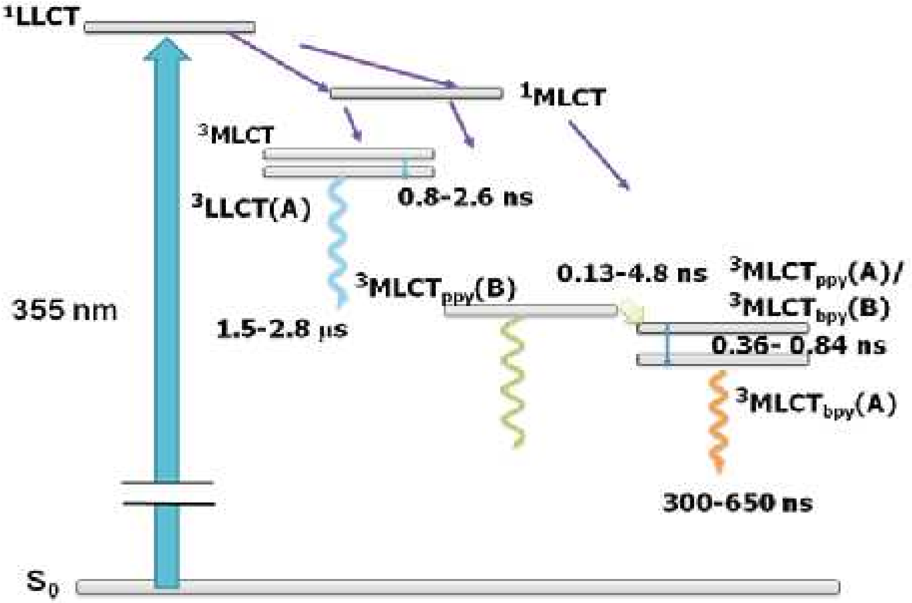

Figure 4.4 *Proposed relaxation mechanism of* $[Ir(ppy)_2bpy]^+$ *after radiation at 355 nm.*[32]

The mechanism of relaxation is explained as follows: after excitation, the ^{1}LLCT(A) (in parentheses showing the symmetry of the state) is accessed then rapidly relaxes to the triplet manifold, low lying states ^{3}LLCT, ^{3}MLCT$_{ppy}$, and ^{3}MLCT$_{bpy}$ possibly indirectly via the ^{1}MLCT states as displayed in figure 4.4. A portion relaxes to a ^{3}MLCT state and then to ^{3}LLCT(A); these two states are responsible for the blue emission band. A large portion goes to ^{3}MLCT states lying at lower energies. Under varied polarity of solvent, these states are shifted in energy and are consequently coupled differently; they emit green and orange light separately. Comparing the emission spectra at 77 K and near 290 K in various solvents, the ^{3}MLCT$_{bpy}$ has the greatest rigidochromic shift indicating the greatest variation of geometry. This state also has the greatest bathochromic shift in agreement with the results from the lifetime measurements.[32]

4.1.4 Excited state photophysics of cyclometallated Pt and Pd complexes

Cyclometallated complexes of the platinum and palladium group elements have been implicated as potential photosensitizers,[55,56] and in the present section effort has been done to study the relevant excited states properties of these complexes in order to compare them with the results of the novel Ir-Pt and Ir-Pd heterodinuclear complexes studied in detail in this chapter. The tendency of transition metal salts to undergo cyclometallation with heteroaromatic ligands such as 2-phenylpyridine (ppy) to give five membered metallocycles has been demonstrated with numerous metals, including Ir (III), Pt (II) and Pd (II).[26,29,57,58,59] These are mostly halo bridged dimers, although mononuclear cyclometallates of the form [M(C^N)LX] (M = Pt/Pd; C^N = cyclometallated ligand; L = neutral monodentate ligand such as pyridine and phosphines; X = halide) are also well documented.[60,61,62] A number of cyclometallated complexes of the platinum group metals are luminescent which is explained in detail in the recent review on luminesence of Pt (II) complexes by Williams and coworkers.[63] An interesting feature of square planar luminophores is a tendency to display multiple emissions attributed in part to the formation of ground state oligomers and excimers.[64,65]

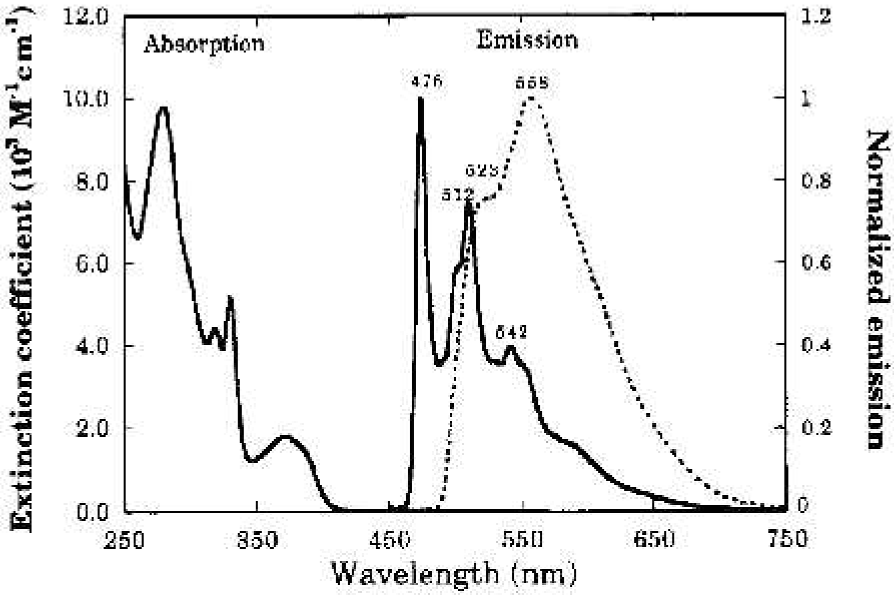

***Figure 4.5** Room temperature (298 K) absorption spectrum (left) of [Pt(ppy)(CO)Cl] in CH_2Cl_2 and the 77 K emission spectra (right) in dilute toluene glass (–) and in the solid state (---).*[66]

The UV/vis electronic absorption spectra for the Pt (II) cyclometallated complex, [Pt(ppy)(CO)Cl] are shown in figure 4.5. The absorption spectrum has intense bands in the UV region (375 nm) which have been assigned to metal to ligand charge transfer (MLCT) transitions, and the higher energy bands were assigned to ligand centered transitions.[66] This complex exhibits relatively long lived structured emissions in the solid state at ambient temperature and at 77 K in glassy toluene solutions (figure 4.5). These emissions are proposed to originate from ^{3}MLCT states. Structured emission spectra are commonly observed when the emitting states are LC or MLCT in character. The criteria generally used to differentiate between the two different excited states, are drawn from an evaluation of lifetime data and of solvent effects on the energies, structure, and emission maxima compared to those of the free ligand. The 30 μs lifetime for [Pt(ppy)(CO)Cl] in 77 K toluene glass is shorter than generally expected for LC emissions but somewhat longer than lifetimes usually associated with emissions from MLCT excited states in heavy metal complexes. This suggests that there may be some mixing of the LC and MLCT states as proposed for a Rh (III) 2-phenylpyridine complex[67] and in other cyclometallates.[68,69]

Photophysical descriptions of several palladium (II) cyclometallated azobenzene complexes[70] indicate that the photophysics of these systems is predominantly ligand localised in character. Luminescence lifetimes of these complexes are short in room temperature fluid solutions (<1 ns) and are characterised as singlet intraligand fluorescence emissions.[72] Photophysical studies involving rhodium (III), iridium (III), and platinum (II) complexes containing the orthometallating ligand ppy have been reported previously.[39,71,9] Since Pd (II), like Rh (III), is difficult to oxidize, one might expect to observe MLCT transitions in the absorption spectra of palladium ppy complexes while the emission may originate from ligand localised states. On the other hand, Pd (II) being a d^8 transition metal may alter the ground state energies enough that new MLCT states may be observed.[72]

Watts and coworkers have reported[72] four Pd (II) complexes, [Pd(ppy)Cl]$_2$, [Pd(ppy)(bpy)Cl], [Pd(ppy)(en)]Cl and [Pd(ppy)(CO)Cl], each of which contains the orthometallating ligand 2-phenylpyridinate (ppy). Absorption and low temperature emission data for these four palladium cyclometallates indicate large contributions to the excited states from transitions localized on the 2-phenylpyridine ligand. Absorption spectra at room temperature and emission spectra at 77 K for the dichloro bridged cyclometallated Pd complex, [Pd(ppy)Cl]$_2$ along with the lifetime values for the rest of the complexes reported by Watts are given in figure 4.6 below. The higher energy absorption transitions (240-340 nm) are intraligand π-π* transitions localised on the 2-phenylpyridine ligand. The low energy features observed in the absorption spectra are also assigned as ligand localised π-π* transitions of the 2-phenylpyridine ligand. These are excited states that are formed as a result of interaction between the π orbitals of the heterocyclic and aryl rings induced by the coplanarity imposed by orthometallation.[72]

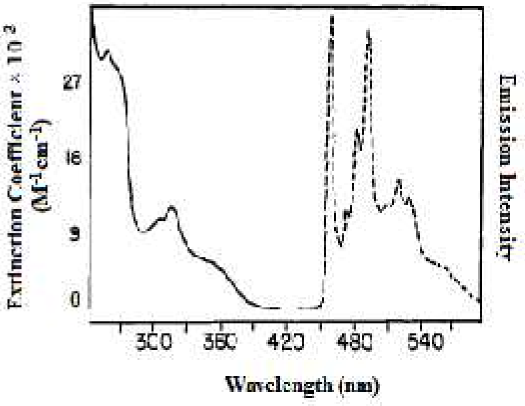

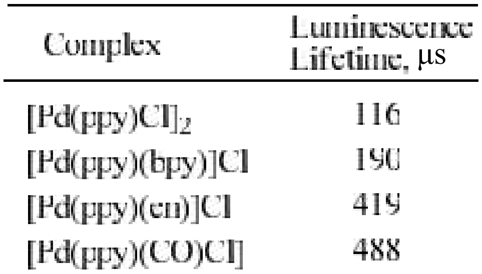

Complex	Luminescence Lifetime, μs
$[Pd(ppy)Cl]_2$	116
[Pd(ppy)(bpy)]Cl	190
[Pd(ppy)(en)]Cl	419
[Pd(ppy)(CO)Cl]	488

Figure 4.6 *Absorption (room temperature, 298 K) and 77 K emission spectra of* $[Pd(ppy)Cl]_2$.[72]

The luminescence lifetime trend for these complexes supports some MLCT contribution to the excited state. It is apparent from the 77 K emission spectra and the magnitude of the luminescent lifetimes of these complexes that the emitting state is principally a triplet state that corresponds in structure to the triplet emission of 2-phenylpyridine at low temperature. Comparison of these photophysical results to absorption and emission data for $[Pt(ppy)_2]$[66] also suggests that the four palladium complexes reported by Watts and coworkers have ligand centered excited states rather than the MLCT excited states observed in $[Pt(ppy)_2]$. The lifetimes of the palladium complexes relative to those of the platinum species coupled with the increased structure and energy of the emissions indicate a large contribution to the excited state from metal perturbed ligand centered states.

This chapter deals with the excited state photophysics including absorption, solvatochromic, rigidochromic, temperature dependent emission (298 K to 77 K) measurements and lifetimes (solvent dependent and temperature dependent) of three novel cyclometallated iridium (III) complexes (a) $[Ir(ppy)_2(bpp)]PF_6$ **(1)**, (b) $[Ir(ppy)_2(bpp)PtCl]_2(PF_6)_2$ **(2)** and

(c) $[Ir(ppy)_2(bpp)PdCl]_2(PF_6)_2$ **(3)** as shown in figure 4.7 below. Synthesis and characterisation of these three novel complexes are described in detail in chapter 3.

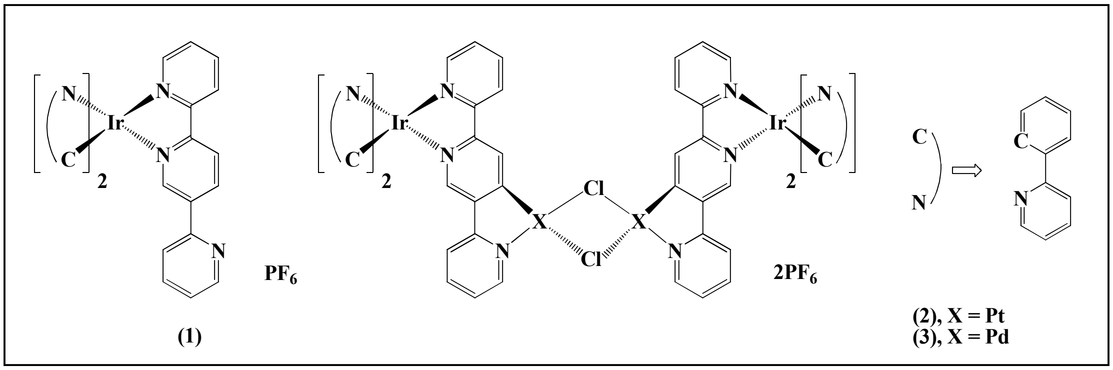

***Figure 4.7** Mononuclear iridium complex $[Ir(ppy)_2(bpp)]PF_6$ **(1)**, dinuclear iridium complexes $[Ir(ppy)_2bpp)PtCl]_2(PF_6)_2$ **(2)** and $[Ir(ppy)_2(bpp)PdCl]_2(PF_6)_2$ **(3)** having peripheral ligand phenyl pyridine (ppy).*

A wide variety of coordination complexes of the second and third row transition metals are now known to display dual emissions from thermally non equilibrated excited states in rigid media.[73,74,75,76,77] Several organometallic Ir (III) species containing coordinating ligands such as 2,2'-bipyridine (bpy) and 1,l0-phenanthroline (phen) in combination with ortho metallating ligands such as 2-phenylpyridine (ppy) and benzoquinoline (bzq) were also reported[78,10] to display dual emissions in rigid media. Dual emission from a bimetallic Pd(II)/Rh(III) orthometallated species has also been reported before.[79] Although dual emissions from thermally nonequilibrated excited states of coordination complexes in low temperature rigid glasses is now a well established phenomenon, it is by no means a common occurrence. The Ir (III) complexes studied in this chapter are the only heterodinuclear Ir-Pt/Pd systems reported now which shows the importance of understanding the excited state properties of these complexes. With the help of the photophysical measurements carried out it was possible to gain an insight into the electron transfer process in these novel heterodinuclear complexes. Complex **(2)** and complex **(3)** with a Pt and Pd metal center at the other end of the bridging ligand are efficient intramolecular photocatalyts as explained in chapter 3. Thus a clear understanding of the excited states helped to tune it in order to increase the efficiency of these photocatalyts.

4.2 Results and Discussion

4.2.1 Complex (1) : [Ir(ppy)$_2$(bpp)]PF$_6$

4.2.1.1 Absorption Properties

The absorption and emission properties of Ir (III) cyclometallated complexes have been outlined in section 4.1.5 but to summarise, these complexes typically have a ligand centered transition in the region 250 nm to 350 nm and MLCT transition in the region 350 nm to 450 nm. For Ir (III) complexes the ligand centered transitions can be either intraligand charge transfer transitions (ILCT), that is transitions ocurring on one cyclometallated ligand or can be interligand or ligand to ligand charge transfer transitions (LLCT), that is from the π orbital of one cyclometallated ligand to the π* orbital of another cyclometallated ligand. Also in most cases they have two MLCT states lying very close to each other. The first one is Ir to cyclometallated ligand charge transfer MLCT$_{(C\text{^}N)}$ transitions and the second is Ir to N^N chelating ligand charge transfer MLCT$_{(N\text{^}N)}$ transitions.[27-32] The absorption and emission measurements along with the lifetime measurements at both room temperature (298 K) and low temperature (77 K) in various solvents give an indication of the nature of the emitting states in these polypyridyl complexes. The UV spectra of complex [Ir(ppy)$_2$(bpp)]PF$_6$ is given in figure 4.8 below.

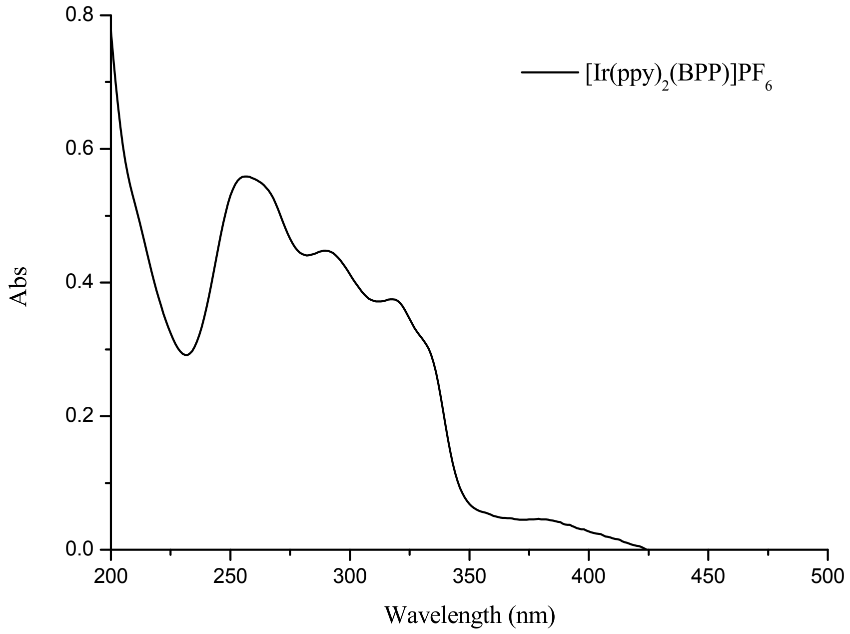

Figure 4.8 *Absorption spectrum for [Ir(ppy)$_2$(bpp)]PF$_6$ in aerated ACN (conc: 1×10^{-5}M).*

The visible electronic absorption spectra for complex **(1)** consists of a strong absorption band in the region 250 nm to 320 nm which are assigned to ligand centered (LC), ppy(π)→ppy(π*) transitions of which the lower energy bands near to 320 nm can be assigned to bpp(π)→bpp(π*) ligand centered transitions. The bands around 350 nm may be due to interligand ppy(π)→bpp(π*) charge transfer transitions (LLCT). The bands in the region 370 nm to 430 nm are assigned to MLCT transitions. There may be two MLCT bands, $\mathrm{MLCT}_{(ppy)}$ (Ir to ppy charge transfer) and $\mathrm{MLCT}_{(bpp)}$ (Ir to bpp charge transfer) having similar energies however it is difficult to differentiate between them based on earlier reports of Ir (III) cyclometallated complexes.[23-32]

4.2.1.2 Emission properties

All of the iridium polypyridyl complexes reported here exhibit intense luminesence between 500 nm - 650 nm at room temperature in acetonitrile solution. The excitation wavelength used was 420 nm which is considered to be a ^{3}MLCT transition as explained before.[32] The low temperature emission spectra for all these complexes are blue shifted in comparison to the room temperature emission which is a characteristic property for emission from an MLCT excited state.

As already stated above cyclometallation has the effect of raising the energies of ligand field (d-d) excited states to high levels due to the higher position of the cyclometallating ligands in the spectrochemical series. If the emitting states (either LLCT or MLCT) and MC states lie too close in energy, they can thermally equilibrate, thereby quenching the emission through fast radiationless decay through the MC states.[31,32,80] Furthermore, the strong σ-donor abilities of these cyclometallated ligands tend to lower the energy of metal to ligand charge transfer (MLCT) excited states via enhancement of the ease of oxidation at the metal center.[35,36,37,81] When the bridging chlorides of $[\mathrm{Ir(ppy)_2Cl}]_2$ are replaced by a π acceptor ligand such as bpp the Ir (III) metal center becomes a poorer electron donor and the MLCT_{ppy} state moves up in energy, compared to the MLCT_{bpp} state. The room temperature (298 K) and low temperature (77 K) emission spectra for complex $[\mathrm{Ir(ppy)_2(bpp)}]\mathrm{PF_6}$ are given in figure 4.9 below.

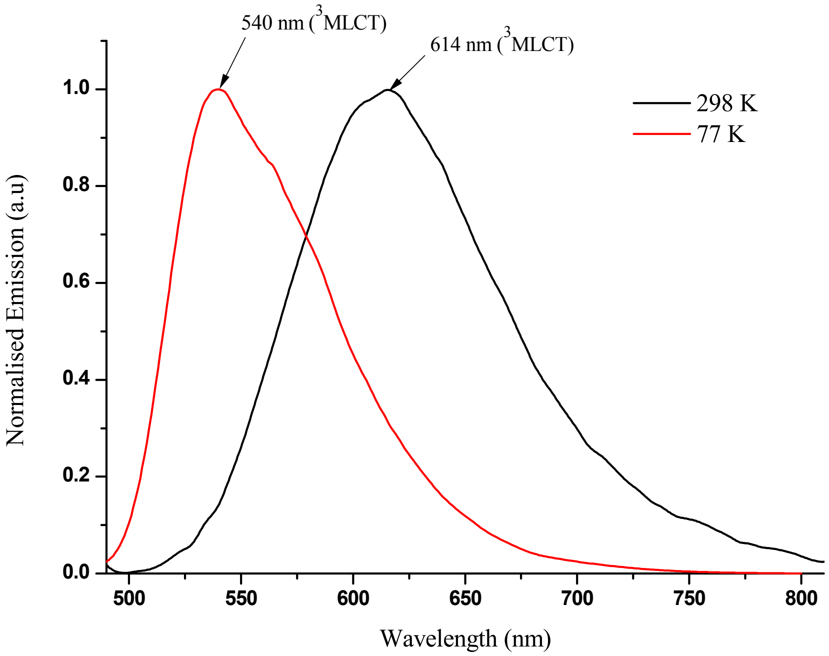

Figure 4.9 *Emission spectrum for [Ir(ppy)$_2$(bpp)]PF$_6$ at 298 K (in aerated ACN) and 77 K (in 4:1 EtOH:MeOH glass)*

From figure 4.9 the emission at both 298 K (614 nm) and 77 K (540 nm) is assigned to an MLCT excited state. Assignment of the lowest energy component in the emission to a MLCT excited state is based upon previous publications[39-45] and a number of other considerations which include spectral shape, phosphoresence lifetime (τ_p), rigidochromic and solvatochromic behaviour.[22] As in the room temperature spectrum, the emission spectrum of complex **(1)** at 77 K is broad and structureless. This rules out an LC nature of the emission (which would induce prominent vibrational structure)[82] and is consistent with the charge transfer nature of the excited state. It has already been noticed that cyclometallated complexes with trans Ir-C bonds (e.g., mer-[Ir(ppy)$_3$]) tend to give structureless emissions, probably because of the large excited state distortion brought about by this geometric arrangement.[13] The blue shift of the low temperature (77 K) spectrum is qualitatively consistent with a ^{3}MLCT assignment, for solvent reorganisation is fast in fluid solution at room temperature and it stabilises the MLCT states before emission takes place. This process is hampered at 77 K in a rigid matrix, and under these conditions emission occurs at higher energy. The extent of the blue shift is related to the degree of real charge separation, that is, how much the charge distribution is different between ground and excited states. For typical MLCT emitters, like the well known $[Ru(bpy)_3]^{2+}$ complex and analogous compounds, such a blue shift is usually in the range of 1000-2000 cm^{-1}, and it is also in the same range for Ir (III) cyclometalated compounds, which are reported to be pure MLCT emitters.[83,84,51]

Further evidence to support the assignment of the excited state is obtained from the concentration dependent and solvent dependent studies on $[Ir(ppy)_2(bpp)]PF_6$ **(1)** provided in figure 4.10 (a) and 4.10 (b). The concentration dependent emission spectra for complex **(1)** does not show any change in structure on going from low to high concentrations other than the normal increase in intensity of emission.

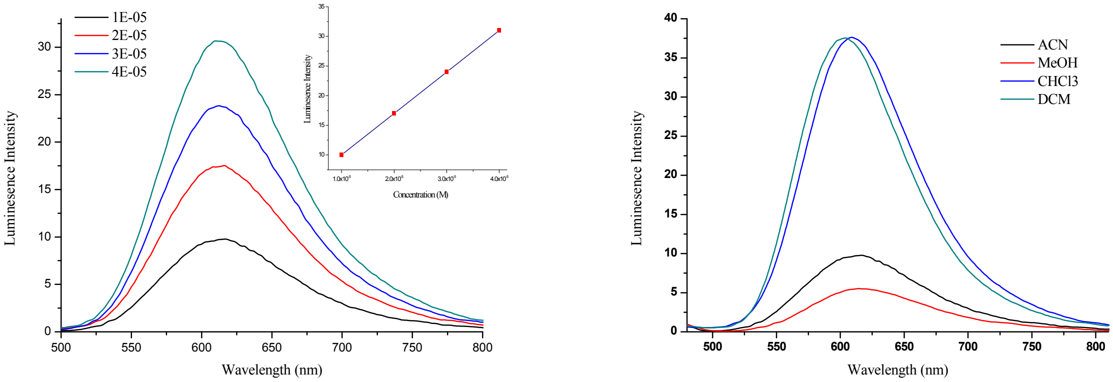

(a) **(b)**

Figure 4.10 ***(a)*** *Concentration dependent emission for complex* ***(1)*** *in ACN and* ***(b)*** *solvent dependent emission for complex 1 in four different solvents having conc.* 1×10^{-5}*M.*

Solvatochromism is a potentially important probe in assessing charge distributions in both ground and excited states.[85] Normally MLCT phosphorescence should exhibit a hypsochromic shift on moving from polar to non polar solvents.[40,41] From figure 4.10 (b) and the tabulated values of emission in table 4.1, it is clear that the band maxima for $[Ir(ppy)_2(bpp)]PF_6$ showed a hypsochromic shift (blue shift) on moving from polar to non polar solvents which supports the assignment of a ^{3}MLCT state. It can also be seen that the emission intensity for the complex in non polar solvents ($CHCl_3$ and DCM) is found to be almost three times higher than in polar solvents. This can be due to the fact that the ground and excited state dipoles orginating in cyclometallated iridium complexes are stabilised in non polar solvents, which results in an emission in higher intensity, and this was seen for the tris cyclometallated species, fac $[Ir(ppy)_3]$.[86,35,39]

The deaerated emission plots for complex $[Ir(ppy)_2(bpp)]PF_6$ in four different solvents are given in figure 4.11 below. Deaeration experiments were performed using the freeze pump thaw method (explained in chapter 2).

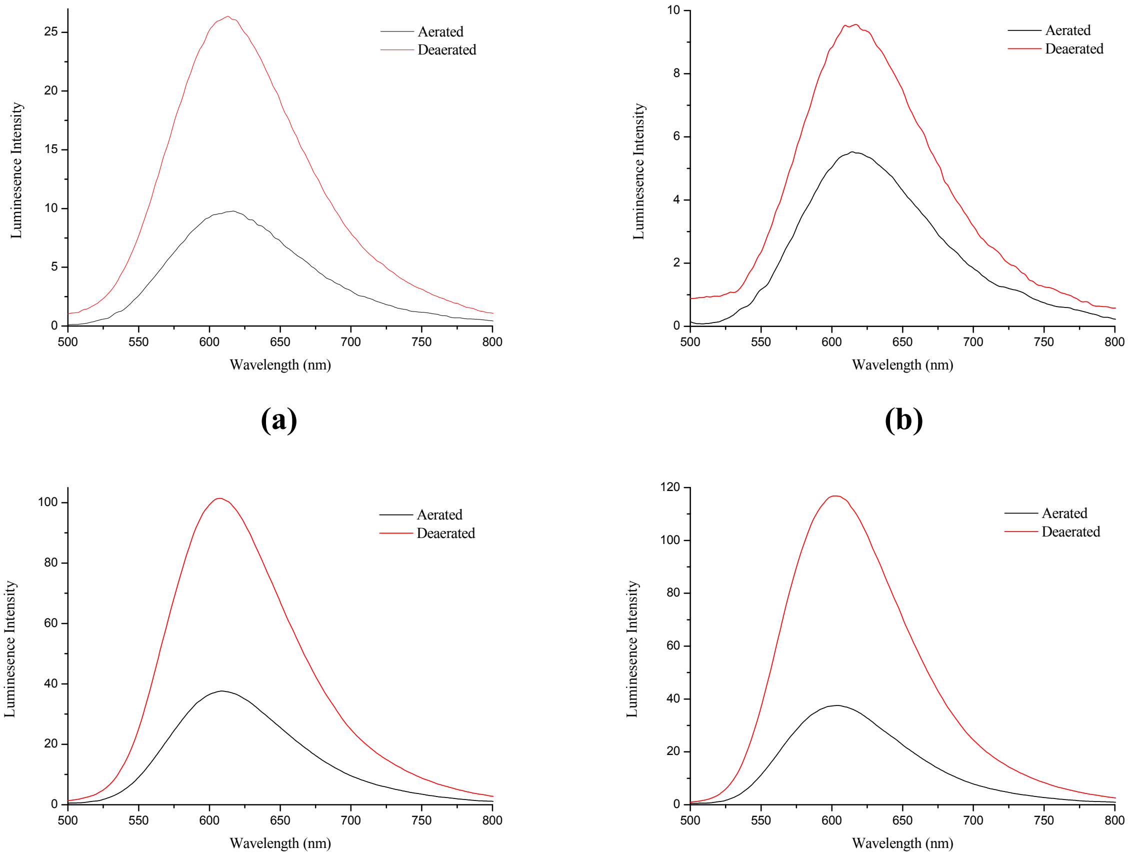

(a) **(b)**

(c) **(d)**

Figure 4.11 *Aerated and deaerated emission spectra of complex* ***(1)*** *in* ***(a)*** *ACN (1×10^{-5}M),* ***(b)*** *MeOH (1×10^{-5}M),* ***(c)*** *$CHCl_3$ (1×10^{-5}M) and* ***(d)*** *DCM (1×10^{-5}M).*

In all the four cases deaeration resulted in an increase in the intensity of emission to more than double due to the removal of oxygen which quenches the emission in aerated solutions. Along with all the above mentioned considerations one of the most important measurements that gives evidence to the nature of the lowest excited state (to be either LC or MLCT) is the solvent dependent lifetime measurements carried out at room temperature (298 K), and the low temperature lifetime measurements (77 K) which are explained in detail below.

4.2.1.3 Solvent dependent lifetime measurements

Based on the previous reports[32,39-45] for Ir (III) cyclometallated complexes, at room temperature (298 K) the ^{3}MLCT excited states are in thermal equillibrium and the lifetime will be in the nano second time range. It is difficult to differentiate between the ^{3}MLCT$_{(N\hat{}C)}$ and ^{3}MLCT$_{(N\hat{}N)}$ states at room temperature, but at 77 K when there is no thermal equillibrium the decay can occur from different low lying excited states which can be ^{3}MLCT states, ^{3}LLCT states or a mix of both. If the excited state is an MLCT state as the solvent polarity decreases the emission lifetime should increase as given for complex **(1)** in figure 4.12 below.

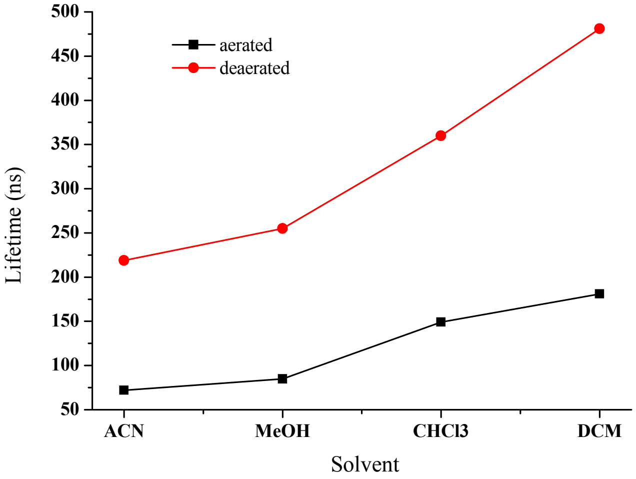

Figure 4.12 *Solvent dependent lifetime for complex* ***(1)*** *in four different solvents under aerated and deaerated conditions (Conc. in all the four solvents is* 1×10^{-5}*M).*

Figure 4.12 clearly shows that as the solvent changes from a polar solvent to a non polar solvent there is a continuous increase in the lifetime and this effect is more prominent in the deaerated case since no gases are present in the deaerated sample so quenching caused by oxygen and other gases are completely removed resulting in a much longer lifetime values. In both cases (aerated and deaerated) the lifetime values of complex **(1)** in non polar solvents ($CHCl_3$ and DCM) are higher than in the case of polar solvents (ACN and MeOH). This supports the data given for solvent dependent emission measurements for complex **(1)** in figure 4.10 (b) where the emission for complex **(1)** in non polar solvents ($CHCl_3$ and DCM) is almost 3 times higher than in polar solvents (ACN and MeOH). As explained before this can be due to the reason that the excited state metal centered dipoles are better stabilised by the non polar solvents, and have longer lifetimes than in polar solvents. The tabulated result with the values are given in table 4.1 below.

Solvent (polarity)	Aerated/ Deaerated	Emission Wavelength, λ_{em}, (nm)	Timebase (ns)	Lifetime ns, (χ^2)
ACN (5.8)	Aerated	617	500	72 (1.072)
	Deaerated	617	500	219 (0.989)
MeOH (5.1)	Aerated	615	500	85 (1.049)
	Deaerated	615	500	255 (1.035)
$CHCl_3$ (4.1)	Aerated	609	1000	149 (1.063)
	Deaerated	609	1000	360 (1.021)
DCM (3.1)	Aerated	604	500	181 (1.073)
	Deaerated	604	1000	481 (1.030)

Table 4.1 *Solvent dependent lifetime values for complex* ***(1)*** *measured using TCSPC under aerated and deaerated (shaded) condition (Conc. in all four solvents is* 1×10^{-5}*M,* λ_{ex} *= 360 nm).*

For complex **(1)** the lifetime decay curve obtained in aerated ACN at a time base of 500 ns is given in figure 4.13 (a). From the decay curve it is clear that the decay is monoexponential (the decay was obtained at an emission wavelength of 617 nm as given in table 4.1). The lifetime of 72 ns is assigned to a decay from a ^{3}MLCT excited state based on the previous considerations and published results for similar complexes.[39-45, 87] The χ^2 value for the fit is 1.072 indicating close fit to experimental data and the residual plot curve given in figure 4.13 (a) also shows the perfection of the fit. The lifetime decay curve obtained in deaerated ACN at a time base of 500 ns is given in figure 4.13 (b). From the decay curve it is clear that the decay is monoexponential. The χ^2 value for the fit is 0.989 indicating close fit to experimental data and the residual plot curve given in figure 4.13 (b) also shows the perfection of the fit.

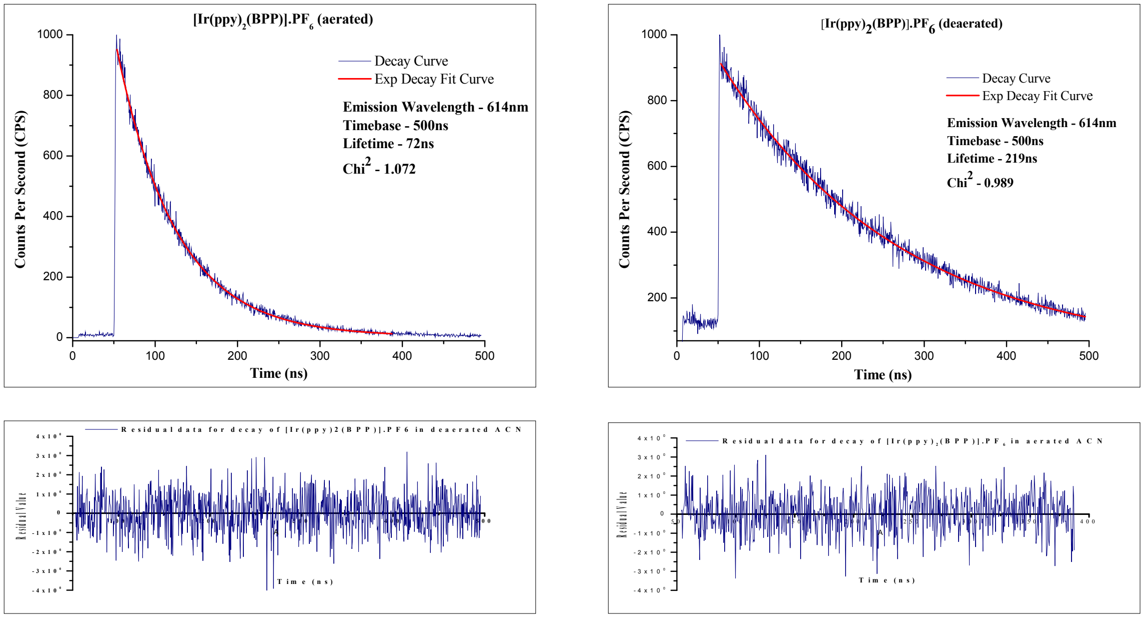

(a) **(b)**

Figure 4.13 *Lifetime decay plots for complex [Ir(ppy)$_2$(bpp)]PF$_6$ (1) in* ***(a)*** *aerated ACN and* ***(b)*** *deaerated ACN measured at room temperature (298 K) using TCSPC.*

The decay curves for complex **(1)** in the remaining solvents are given in appendix C, all of which show a single exponential decay. Based on the above considerations given in sections 4.2.1.2 and 4.2.1.3 the lowest excited state from which the emission occurs can be assigned to be a ^{3}MLCT state. The low temperature lifetime measurement along with the temperature dependent emission and lifetimes from 77 K to 290 K in every 10 K difference for [Ir(ppy)$_2$(bpp)]PF$_6$ is explained in detail in the section 4.2.1.4 below which gives an idea of the variation in the nature of the excited state as a function of temperature.

4.2.1.4 Temperature dependent emission and lifetime measurements

The instrumental procedures and conditions that were used to carry out the temperature dependent excited state emission and lifetime measurements using a cryostat have been detailed in chapter 2. The temperature dependent emission for [Ir(ppy)$_2$(bpp)]PF$_6$ in a temperature range of 77 K to 120 K is given in figure 4.14 and the emission in a temperature range of 150 K to 220 K is given in figure 4.15.

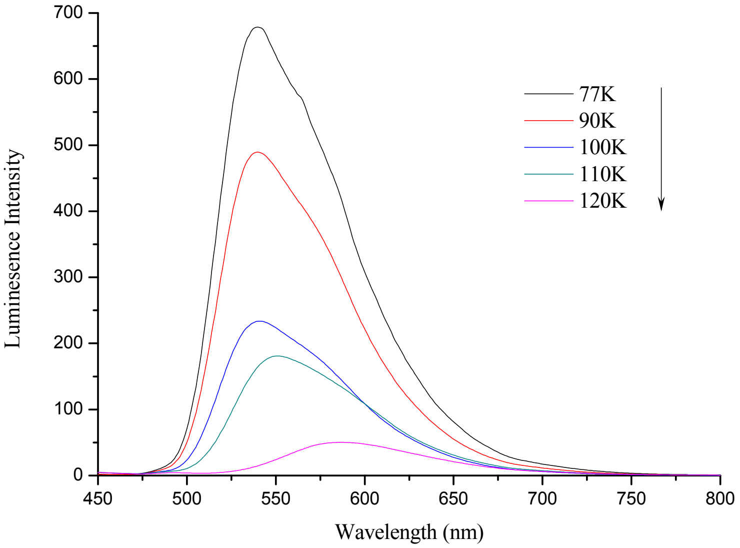

Figure 4.14 *Temperature dependent emission spectra for [Ir(ppy)$_2$(bpp)]PF$_6$ from 77 K to 120 K measured in EtOH: MeOH (4:1) glass.*

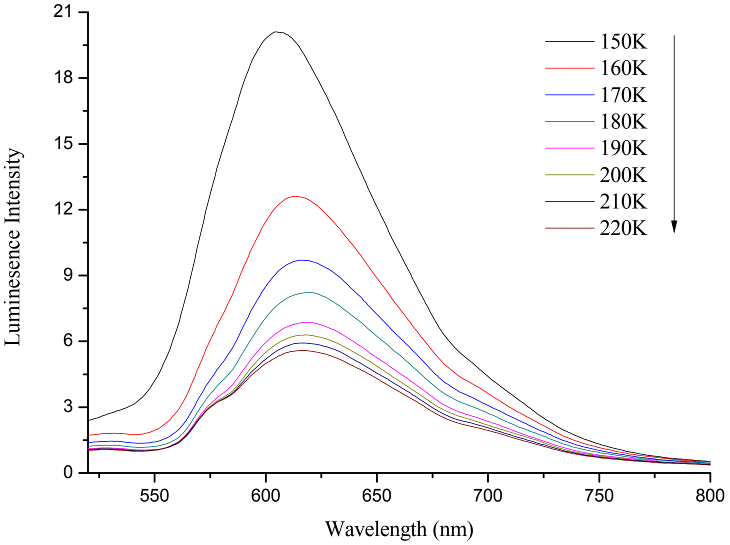

Figure 4.15 *Temperature dependent emission spectra for [Ir(ppy)$_2$(bpp)]PF$_6$ from 150 K to 220 K measured in EtOH: MeOH (4:1) glass.*

From both figures 4.14 and 4.15 it is evident that there is a blue shift in the emission maximum on going to low temperature which is based on the consideration that MLCT phosphorescence exhibits a hypsochromic shift when the medium becomes rigid (especially when the solvent freezes below T_g = 125 K).[39] The explanation for this blue shift on going from room temperature fluid solution (298 K) to a low temperature (77 K) rigid matrix is explained in section 4.2.1.2. Solvent reorganisation is fast in fluid solution at room temperature and it stabilises the metal centered charge transfer states before emission takes place. This process is hampered at 77 K in a rigid matrix, and under these conditions emission occurs from higher energy.[53,81,84] This change is more prominent below the glass transition temperature (T_g), which can be seen from figure 4.14 and also the variation in lifetime occuring around T_g as shown in figure 4.16.

The lifetime values for complex **(1)** as a function of temperature (77 K to 298 K) are given in figure 4.16 which shows that as the temperature decreases the lifetime increases. This can be explained by considering the difference in the nature of the sample at 298 K, and at 77 K glass and also the changes taking place in the energy of the excited states from which the emission takes place as the temperature decreases. In the solution state the molecules are free to move and will collide with each other resulting in the exchange of energy and sufficient quenching will be there also from the dissolved gasses such as oxygen, but at 77 K in EtOH:MeOH glass the molecules are not able to move and the quenching due to collisions and also due to other gases which are present at 298 K can be completely eliminated thereby higher emission and lifetime values were obtained compared to those obtained at room temperature in solution. Also from the temperature dependent emission spectra (figures 4.14 and 4.15) it is clear that as the temperature decreases the excited state moves to higher energies (ie blue shift occurs) thereby the lifetime decay from these higher lying states at those lower temperature should be higher than the decay lifetime at 298 K where the emission takes place from lower lying excited states. The tabulated data for the lifetimes are given in table 4.2 below.

Temperature (K)	Lifetime, τ (ns)	Temperature (K)	Lifetime, τ (ns)	Temperature (K)	Lifetime, τ (ns)
77	3830	140	530	220	113
90	3120	150	336	240	95
100	2810	160	246	260	79
110	1560	170	213	280	64
120	1430	180	181	293	60
130	737	200	152		

Table 4.2 *Tabulated temperature dependent lifetime data (shaded columns) for complex* ***(1)****.*

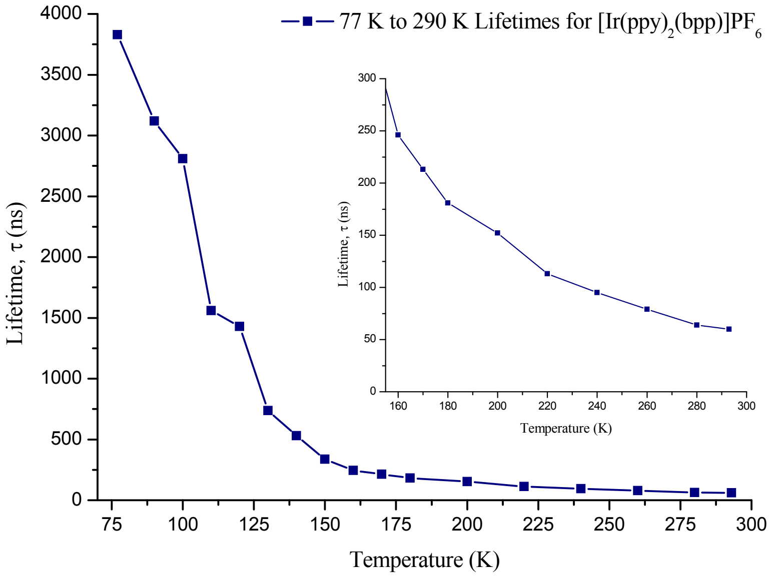

Figure 4.16 *Temperature dependent lifetime plot for [Ir(ppy)*$_2$*(bpp)]PF*$_6$ ***(1)*** *from 77 K to 290 K measured in EtOH: MeOH (4:1) glass.*

On the basis of all results discussed above in sections 4.2.1.2, 4.2.1.3 and 4.2.1.4 and in comparison with published reports on similar complexes,[27-45] the emission of the lowest excited state for complex [Ir(ppy)$_2$(BPP)]PF$_6$ at 298 K is assigned to a ^{3}MLCT state. Assignment of the lowest excited state as an MLCT state is confirmed by various considerations which include spectral shape, phosphoresence lifetime (τ_p), rigidochromic and solvatochromic behaviours. The monoexponential decay for this complex at 298 K led us into the preliminary assumption that there is no mixing of the ^{3}MLCT$_{ppy}$ and ^{3}MLCT$_{bpp}$ states at room temperature (298 K), but based on the previous reports,[26,27] when the bridging chlorides of the starting material, iridium dichloro bridged dimer, [Ir(ppy)$_2$Cl]$_2$ is replaced by a π acceptor ligand like bpp, the Ir (III) metal center will become a poorer electron donor and the (MLCT$_{ppy}$) state will move up in energy. Thus the possibility of emission occuring from a low lying (MLCT$_{bpp}$) excited state cannot be ignored. This can be confirmed by doing wavelength dependent emission and further studies, which are outside the scope of this thesis. At 77 K, considering the emission curves explained in sections 4.2.1.2 and 4.2.1.4 it was concluded that the emission is from a ^{3}MLCT excited state but based on the recent reports of the excited state photophysics of Ir (III) complexes[13-17] and the closeness of the emission lifetime below T_g (1.4 μs - 3.8 μs) to the published results, the possibility of emission from a ^{3}LLCT state also cannot be ignored. However more advanced techniques such as resonance Raman and computational methods are required. Based on the results obtained in all of our measurements a general schematic representation of the energy levels and possible electronic transitions for complex $[Ir(ppy)_2(bpp)]PF_6$ is given in figure 4.17 below.

The proposed mechanism for relaxation is as follows: after excitation, the ^{1}LLCT$_{(ppy \rightarrow bpp)}$ state is accessed then rapidly relaxes to the ^{1}MLCT through internal conversion (IC), inter system crossing (ISC) takes place from there to ^{3}LLCT$_{(ppy \rightarrow bpp)}$ state. Internal coversion follows this, resulting in the relaxation to the ^{3}MLCT$_{(ppy)}$ and ^{3}MLCT$_{(bpp)}$ excited states with the lower one being ^{3}MLCT$_{(bpp)}$ state from which emission takes place. There is also a possibility of populating the lowest excited states ^{3}LLCT$_{(ppy \rightarrow bpp)}$, ^{3}MLCT$_{(ppy)}$, and ^{3}MLCT$_{(bpp)}$ indirectly via the ^{1}MLCT states.

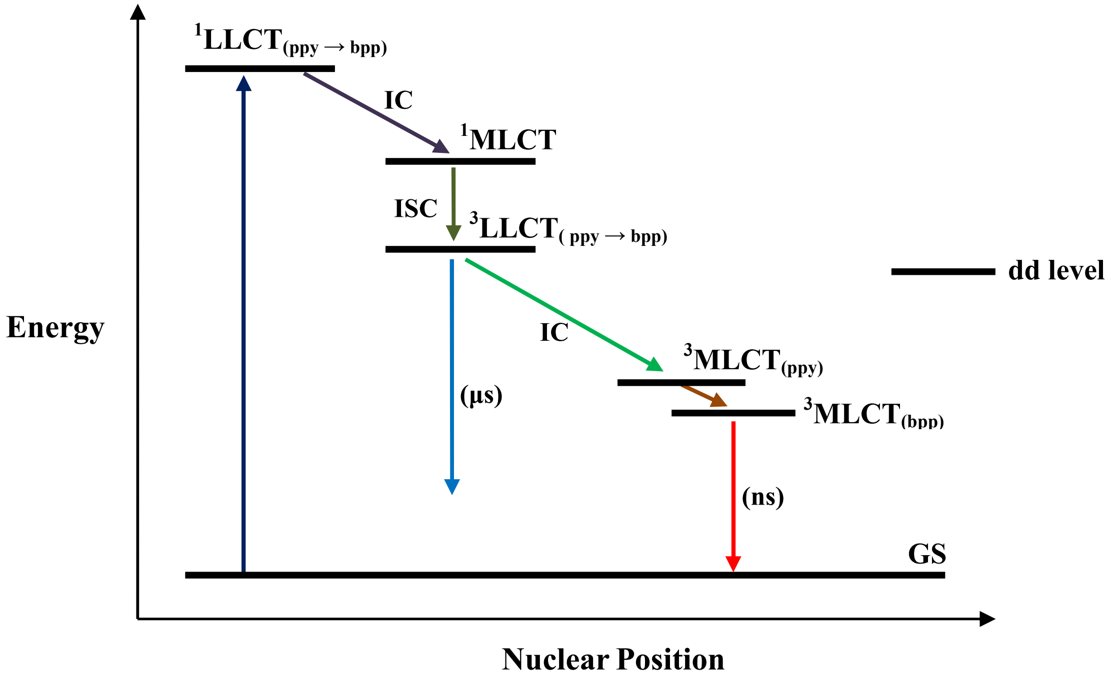

Figure 4.17 *Schematic representation of the energy levels and possible electronic transition for complex* $[Ir(ppy)_2(bpp)]PF_6$ *(IC-internal conversion, ISC-intersystem crossing).*

4.2.2 Complex (2) : [Ir(ppy)$_2$(bpp)PtCl]$_2$(PF$_6$)$_2$

4.2.2.1 Absorption properties

The visible electronic absorption spectra for the Ir-Pt dimer complex [Ir(ppy)$_2$(bpp)PtCl]$_2$(PF$_6$)$_2$ along with the absorption spectra for the Ir monomer complex [Ir(ppy)$_2$(bpp)]PF$_6$ are given in figure 4.18 below. It can be seen from the absorption spectra that complexation of Pt resulted in shifting of the absorption bands to lower energy (red shift) compared to the mononuclear complex. The assignments of the absorption bands were made by comparing the results with the spectrum of complex **(1)** and the reported spectra[27-32] given in section 4.1.5.

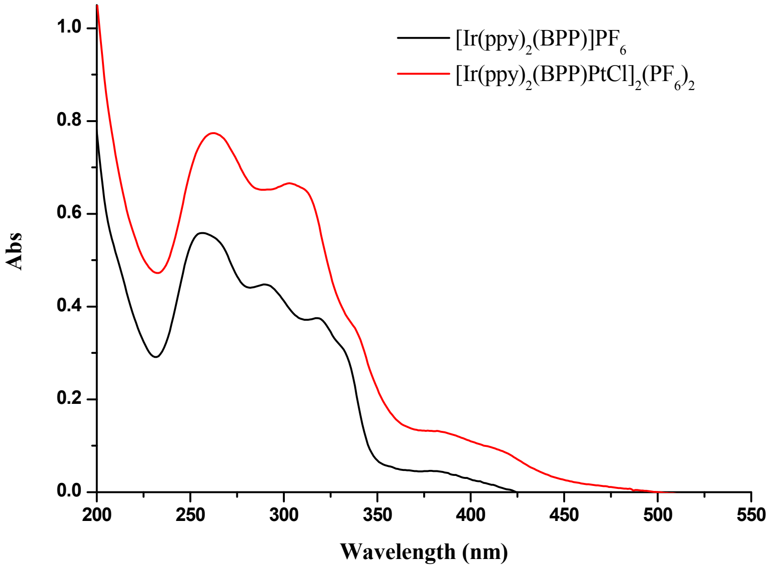

Figure 4.18 *Absorption spectra for complex [Ir(ppy)$_2$(bpp)PtCl]$_2$(PF$_6$)$_2$ (—) along with complex 1 (—) in aerated ACN (1×10^{-5}M).*

From the above figure 4.18 it can be seen that the shifts for the ligand centered bpp(π)→bpp(π*) transitions are more prominent than the ligand centered ppy(π)→ppy(π*) transitions. This is attributed to the fact that the Pt metal is directly complexed to the bpp ligand which can result in an energy change of the excited state based on the bpp ligand resulting in a shift of the absorption bands. Complexation with Pt resulted in a red shift for the LLCT$_{ppy \to bpp}$ band at 350 nm for the Ir mononuclear complex **(1)** to 370 nm in the Ir-Pt dimer complex **(2)**. Both the MLCT excited states also showed a red shift on complexation with Pt as the bands around 370 nm and 420 nm for MLCT$_{(ppy)}$ and MLCT$_{(bpp)}$ in complex **(1)** were red shifted to 420 nm and

470 nm in complex **(2)**. The absorption spectra of the cyclometallated Pt complexes have intense bands in the near UV region (375 nm) (figure 4.5) which have been assigned as metal to ligand charge transfer (MLCT) transitions.[66]

4.2.2.2 Emission properties

The room temperature (298 K) and low temperature (77 K) emission spectra for complex $[Ir(ppy)_2(bpp)PtCl]_2(PF_6)_2$ are given in figure 4.19 below. The emission spectra is structured at both room temperature (298 K) and low temperature (77 K), with the latter having more prominent structured bands than the former.

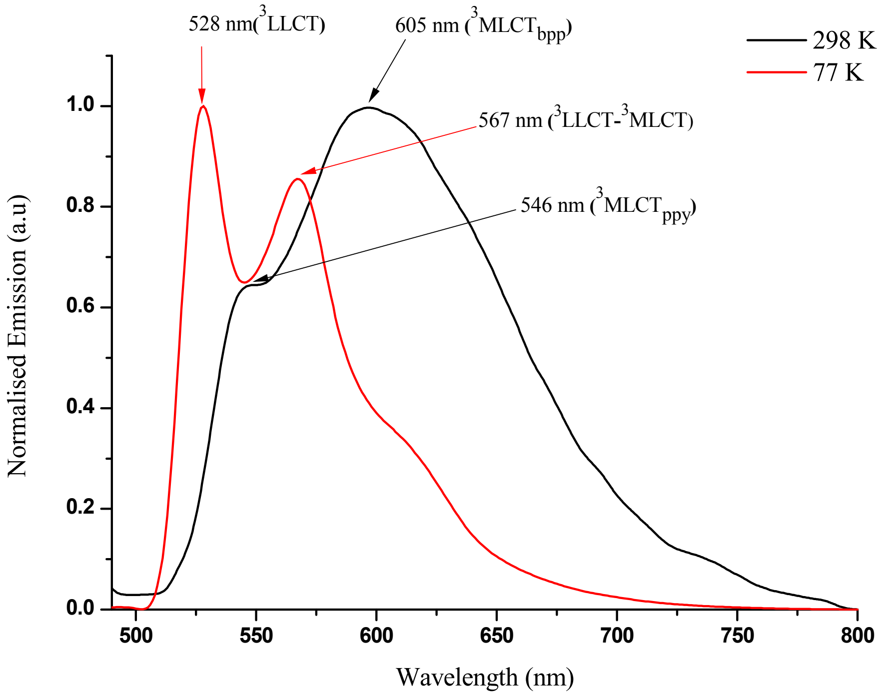

Figure 4.19 *Emission spectra for complex $[Ir(ppy)_2(bpp)PtCl]_2(PF_6)_2$ at 298 K (—) measured in aearated ACN and 77 K (—) measured in EtOH:MeOH (4:1) glass.*

Assignment of excited states in the emission spectrum at both temperatures is based upon previous publications[39-45] and a number of other considerations as discussed with the Ir monomer complex **(1)** in section 4.2.1, which includes spectral shape, rigidochromic and solvatochromic emission behaviours,[22] phosphorescence lifetime (τ_p) (77 K and 298 K) and effect of solvent polarity and temperature dependent lifetimes. The room temperature emissions (at 546 nm and 605 nm) are assigned to be from ^{3}MLCT excited states. This assignment is confirmed by carrying out detailed lifetime measurements in four different solvents of varying polarities as explained in section 4.2.2.3. As explained for complex **(1)**, when the bridging chlorides of $[Ir(ppy)_2Cl]_2$ are replaced by a π acceptor ligand such as bpp the Ir (III) metal center will become a poorer electron donor and the $MLCT_{ppy}$ state will move up in energy compared to the $MLCT_{bpp}$ state. From the emission spectra (figure 4.9) and lifetime measurements (table 4.1) for the mononuclear complex **(1)** it is difficult to differentiate between these two close lying ^{3}MLCT excited states. For complex **(2)**, Pt coordination resulted in a sufficient increase in the energy of the excited states, together with splitting of the emission band as can be clearly seen from the emission spectra (figure 4.19, black line). Based on the above consideration the emission band at 546 nm is assigned to a $^3MLCT_{ppy}$ excited state and the emission at lower energy to a $^3MLCT_{bpp}$ excited state.

For the 77 K emission spectra the peak at 528 nm is assigned to a ^{3}LLCT excited state and the emission at 567 nm is assigned to a mixed ^{3}LLCT-^{3}MLCT excited state. These assignments are made based on the previous references for Ir (III) cyclometallated complexes[39-45] and from the temperature dependent emission and lifetime data explained in section 4.2.2.4. The rigidochromic shift for the emission band at 528 nm is higher than that normally seen for pure MLCT emitters. This may indicate that this is not a pure MLCT state, but rather an LLCT (ppy to bpy) triplet state in which the donor orbital is the ppy centered one. A relatively large inner and outer reorganisation is expected to take place in such an excited state, and this would justify the large blue shift going from high to low temperature.[89] Further evidence in support of the assignment of excited state to a ^{3}MLCT state at room temperature (298 K) is obtained from the concentration dependent and solvent dependent studies carried out with complex $[Ir(ppy)_2(bpp)PtCl]_2(PF_6)_2$ as given below in figures 4.20(a) and 4.20(b).

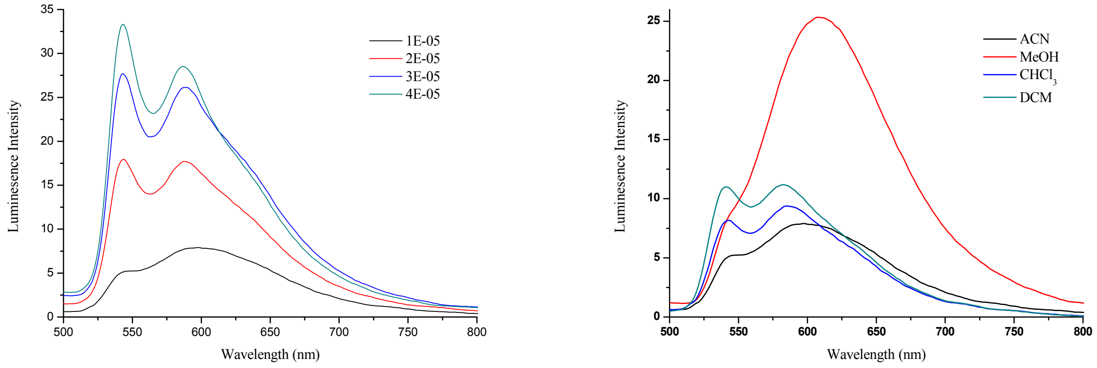

(a) **(b)**

Figure 4.20 ***(a)*** *Concentration dependent emission and* ***(b)*** *solvent dependent emission for complex [Ir(ppy)$_2$(bpp)PtCl]$_2$(PF$_6$)$_2$ in four different solvents having conc. 1×10^{-5}M.*

Solvatochromism is a potentially important probe in assessing charge distributions in both ground and excited states.[85] Normally MLCT phosphorescence should exhibit a hypsochromic shift on moving from polar to non polar solvents.[40,41] The normalised emission spectrum for complex **(2)** is given in figure 4.21 below.

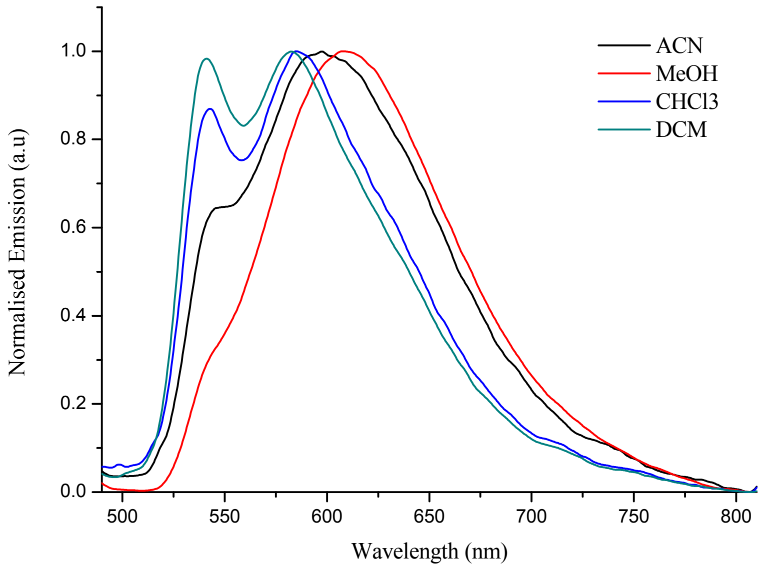

Figure 4.21 *Solvent dependent normalised emission spectrum for complex [Ir(ppy)$_2$(bpp)PtCl]$_2$ (PF$_6$)$_2$ in four different solvents having conc. 1×10^{-5}M.*

The peak at lower energy underwent a hypsochromic shift on moving from polar to non polar solvents but the shift was less prominent for the higher energy peak. Based on the assignments given before for the higher energy excited state to a $MLCT_{ppy}$ state, one explanation for the smaller blue shift for this state which can be due to extensive mixing of the metal and ligand orbitals for $MLCT_{ppy}$ as a result of the the strong σ-donor character of the ppy ligand that leads to less charge transfer character in the electronic transition and hence a decrease in the solvatochromic behavior of the transition.[85] The tabulated emission values in four different solvents are given in table 4.3. Along with all the above mentioned considerations one important measurement that provides evidence on the nature of the lowest excited state is the solvent dependent lifetime measurements at room temperature (298 K) and temperature dependent lifetime measurements which are explained in detail in the following sections.

4.2.2.3 Solvent dependent lifetime measurements

The solvent dependent lifetime measurements support the assignments of the excited states described in the previous sections. Based on published reports[39-45] for Ir (III) cyclometallated complexes and by comparing these results obtained with the iridium mononuclear complex **(1)** (explained in section 4.2.1), the lowest excited states for $[Ir(ppy)_2(bpp)PtCl]_2(PF_6)_2$ at 298 K are assigned to ^3MLCT excited states. If the excited state is an MLCT state as the solvent polarity decreases the emission lifetime should increase since the MLCT states for Ir (III) cyclometallated complexes are destabilised to a greater extent in non polar solvents than in polar solvents.[85,88] The results obtained for solvent dependent lifetime measurements for $[Ir(ppy)_2(bpp)PtCl]_2(PF_6)_2$ in four solvents with varying polarity are tabulated in table 4.3 below.

From the solvent dependent emission spectra (figure 4.21), it is clear that the emission for complex **(2)** is structured in all the four solvents studied at room temperature (298 K). So the lifetime was measured at two different emission maxima in all four solvents and the decay obtained was biexponential in all cases. The average lifetime for each different emission wavelength was calculated using the equation 2.7 explained in chapter 2, by considering their relative percentage as given in table 4.3 below. From table 4.3 it is clear that as the solvent polarity decreases the lifetime for both the peaks increases which supports the assignment that both the emitting states (one at higher energy and the other at lower energy) for complex **(2)** at room temperature (298 K) are ^{3}MLCT in nature. The above mentioned statement is much more clearer from the solvent dependent average lifetime plot for complex **(2)** given in figure 4.22.

Solvent (polarity)	Emission Wavelength, λ_{em}	Timebase (ns)	Lifetime (ns), (χ^2)	Relative %	Avg.lifetime τ_{av}, ns
ACN (5.8)	546	500	$\tau_1 - 5$	39.75	69
			$\tau_2 - 72$	60.25	
			$\chi^2 - 1.119$		
	605	500	$\tau_1 - 5$	15.15	76
			$\tau_2 - 77$	84.85	
			$\chi^2 - 1.017$		
MeOH (5.1)	545	500	$\tau_1 - 14$	16.19	75
			$\tau_2 - 77$	83.81	
			$\chi^2 - 1.133$		
	608	500	$\tau_1 - 27$	11.39	81
			$\tau_2 - 83$	88.61	
			$\chi^2 - 1.085$		
$CHCl_3$ (4.1)	543	500	$\tau_1 - 7$	36.84	190
			$\tau_2 - 194$	63.16	
			$\chi^2 - 1.045$		
	585	500	$\tau_1 - 7$	10.01	220
			$\tau_2 - 221$	89.99	
			$\chi^2 - 1.017$		
DCM (3.1)	541	500	$\tau_1 - 8$	54.67	195
			$\tau_2 - 204$	45.33	
			$\chi^2 - 1.001$		
	583	500	$\tau_1 - 8$	19.26	245
			$\tau_2 - 247$	80.74	
			$\chi^2 - 1.006$		

Table 4.3 *Solvent dependent lifetime values for complex* $[Ir(ppy)_2(bpp)PtCl]_2(PF_6)_2$ *measured using TCSPC at 298 K (Conc. in all four solvents is* 1×10^{-5}*M).*

Based on the nature of the Ir (III) cyclometallated complexes studied previously[23-32] the emission band observed at higher energy is assigned to ^{3}MLCT$_{ppy}$ excited state and ^{3}MLCT$_{bpp}$ excited state occupies a position lower in energy than the former. Based on this assumption the emission lifetime for the ^{3}MLCT$_{ppy}$ should be higher than that from ^{3}MLCT$_{bpp}$ excited state. From the lifetime values given in table 4.3 and the solvent dependent lifetime plot for the two different excited state emissions given in figure 4.22 below it is clear that the lifetime value for the decay from ^{3}MLCT$_{bpp}$ excited state is higher than the decay from ^{3}MLCT$_{ppy}$ excited state.

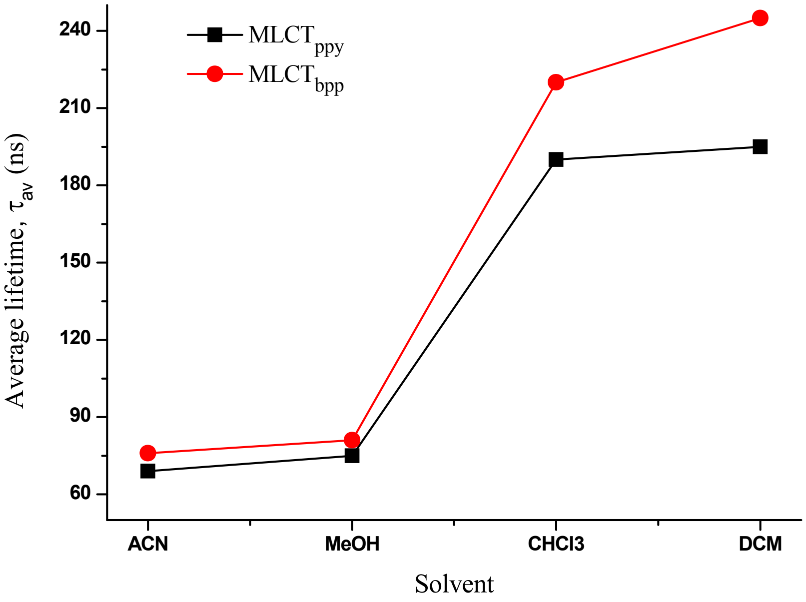

Figure 4.22 *Solvent dependent lifetime for complex [Ir(ppy)$_2$(bpp)PtCl]$_2$(PF$_6$)$_2$ measured at two different emission maxima using TCSPC at 298 K (Conc. in all four solvents is 1×10^{-5}M).*

This behaviour shown by [Ir(ppy)$_2$(bpp)PtCl]$_2$(PF$_6$)$_2$ is due to complexation of Pt to one end of the bridging ligand in a cyclometallated manner. As explained in the introduction, based on the published results[55-69] normally cyclometallated Pt (II) complexes like Pt(N^C)Cl$_2$ do not emit at room temperature. This is attributed to the relatively small energy gap between the lowest lying ^{3}MLCT state and the upper lying ^{3}MC state. At room temperature (298 K), when the system is in thermal equillibrium population of the ^{3}MC state occurs resulting in quenching of the emission. Based on this consideration, for complex **(2)** the emission from Pt based excited states are not seen at room temperature. The excited state for cyclometallated Pt (II) complexes is assigned to a mixed (MLCT/LC$_{Pt}$) excited state, $d_{Pt}/\pi_{(N^C)} \rightarrow \pi^*_{(N^C)}$ based on previous reports.[61,62,63] Electrochemical measurements and DFT calculations, suggest that the HOMO level in these complexes comprise contributions from both Pt and ligand orbitals while the LUMO is largely localised on the N^C ligand.[88] Based on the above mentioned considerations for [Ir(ppy)$_2$(bpp)PtCl]$_2$(PF$_6$)$_2$ the ^{3}MLCT$_{ppy}$ excited state is expected to have an energy very close to Pt excited state. A portion of the charge is transferred from the ^{3}MLCT$_{ppy}$ excited state to the Pt based excited state at room temperature when the system is in thermal equillibrium, which then relaxes to the ^{3}MC state. This results in a decrease in lifetime for the ^{3}MLCT$_{ppy}$ excited state in comparison to the ^{3}MLCT$_{bpp}$ excited state. Temperature dependent emission and lifetime measurements discussed in section 4.2.2.4 gives a much more clearer picture regarding this electron transfer process. In order to get an exact picture regarding the position of different excited states further measurements like the transient absorption and excitation wavelength dependent lifetimes must be carried out, which are beyond the scope of this thesis.

The lifetime decay curves for complex $[Ir(ppy)_2(bpp)PtCl]_2(PF_6)_2$ measured in aerated ACN at two different emission wavelengths (546 nm and 605 nm) are given in figure 4.23 (a) and 4.23 (b). From the decay curves it is clear that the decay is biexponential at both wavelengths. At an emission wavelength of 546 nm, both the lifetime values (τ_1 and τ_2) are assigned to a ^{3}MLCT excited state. The short lived component has a lifetime of 5 ns (τ_1) which contributes 40 % and the longer lived component has a lifetime of 72 ns (τ_2) which contributes 60 %. The χ^2 value for the fit is 1.119 indicating close fit to experimental data and the residual plot curve also shows the perfection of the fit. Similarly the decay curve obtained at an emission wavelength of 605 nm is also biexponential as given in figure 4.24 (b). The short lived component has a lifetime of 5 ns (τ_1) which contributes 15 %, the long lived component having a lifetime of 77 ns (τ_2) which contributes 85 %. The χ^2 value for the fit is 1.017 indicating close fit to experimental data and the residual plot curve also shows the perfection of the fit.

The decay curves for complex **(2)** in the remaining solvents are given in appendix C, all of which have a biexponential decay. Also the deaerated emission decay lifetimes are also measured for complex **(2)** in four different solvents which gave a similar trend to those explained for the aerated samples. Based on the above (sections 4.2.2.2 and 4.2.2.3) the lowest excited state from which the emission occurs at 298 K is assigned to a ^{3}MLCT state, and more specifically ^{3}MLCT$_{bpp}$ state. The temperature dependent emission and lifetimes from 77 K to 290 K for $[Ir(ppy)_2(bpp)PtCl]_2(PF_6)_2$ are explained in detail in the following section.

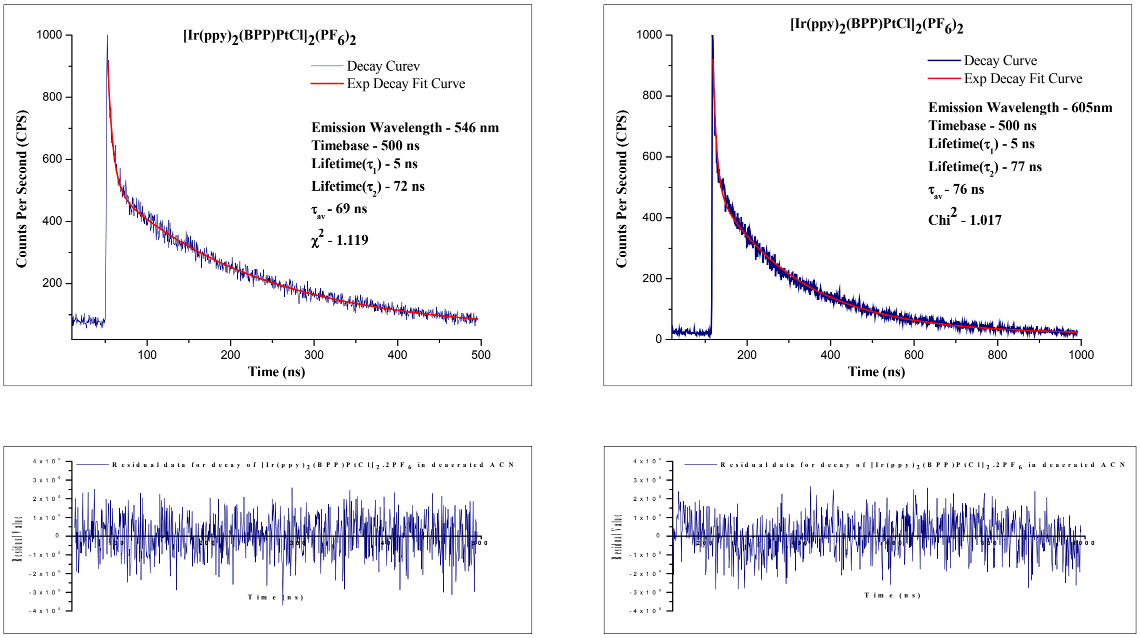

(a) **(b)**

Figure 4.23 *Lifetime decay plots for complex [Ir(ppy)$_2$(bpp)PtCl]$_2$(PF$_6$)$_2$ in aerated ACN **(a)** at an emission wavelength (λ_{em}) of 546 nm and **(b)** λ_{em} of 605 nm.*

4.2.2.4 Temperature dependent emission and lifetime measurements

The temperature dependent emission spectra for [Ir(ppy)$_2$(bpp)PtCl]$_2$(PF$_6$)$_2$ **(2)** in a temperature range of 77 K to 280 K in every 10 K difference of temperature are given in figures 4.24 (a) and 4.24 (b) below.

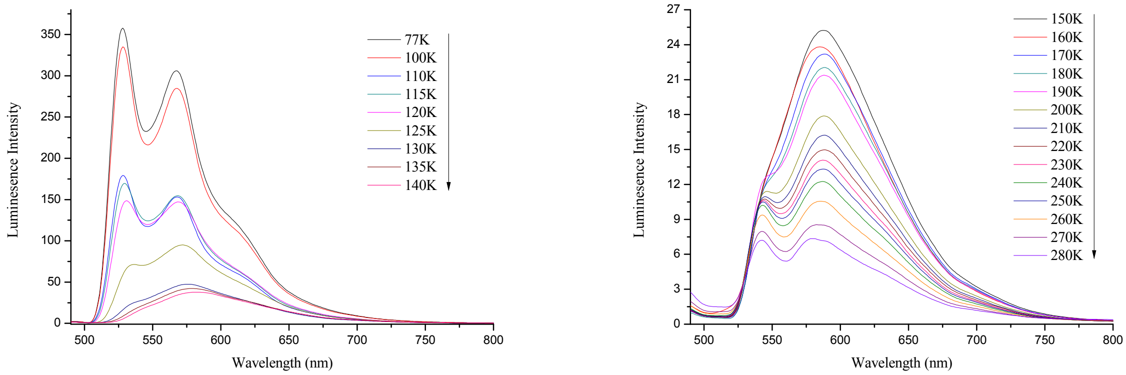

(a) **(b)**

Figure 4.24 *Temperature dependent emission spectrum for complex 2 **(a)** from 77 K to 140 K **(b)** from 150 K to 280 K, measured in EtOH: MeOH (4:1) glass.*

From both figures it is evident that there is a prominent blue shift (an increase in energy of the excited states) in the emission maximum on going to low temperatures which is based on the assumption that MLCT phosphorescence exhibits a hypsochromic shift when the medium becomes rigid (especially below T_g).[39] A possible explanation given on the basis of the measurements done with complex **(2)** on the change in emission spectra with changes in temperature can be explained as follows. At room temperature there are two prominent peaks in the emission spectra for complex **(2)**. The assignments for these peaks are given by comparing the results obtained, to those with the previously published results of Ir (III) cyclometallated complexes.[39-45] On this basis the emission maxima at higher energy is assigned to a ^{3}MLCT$_{ppy}$ excited state and the emission maxima at lower energy is assigned to a ^{3}MLCT$_{bpp}$ excited state. As the temperature decreases the intensity of the emission band at higher energy (^{3}MLCT$_{ppy}$) decreases and the emission band at lower energy (^{3}MLCT$_{bpp}$) grows in intensity. At around 200 K the intensity for the lower energy emission band is twice that of the higher energy one. As the temperature again decreases the emission band at higher energy becomes almost a shoulder and it disappears completely at 140 K. At this temperature emission only from the lower energy ^{3}MLCT$_{bpp}$ excited state was observed as shown in figures 4.24 (a). The explanation for this behaviour is given by considering the ^{3}MLCT/LC$_{Pt}$ excited state of Pt. As the temperature decreases the peak at 546 nm corresponding to the ^{3}MLCT$_{ppy}$ excited state is blue shifted that is to higher energy. This results in the ^{3}MLCT$_{ppy}$ excited state moving closer to the ^{3}MLCT/LC$_{Pt}$ excited state. This ^{3}MLCT/LC$_{Pt}$ excited state which has an energy state close to the ^{3}MC state resulting in quenching of emission intensity and also the phosphoresence lifetime as temperature decreases.

Change in the emission spectra in the glass transition temperature range of 120 K to 130 K at every 1 K difference are given in figure 4.25 below which shows that at the glass transition temperature one higher energy emission band again started to grow but is slightly blue shifted compared to the emission maxima at room temperature.

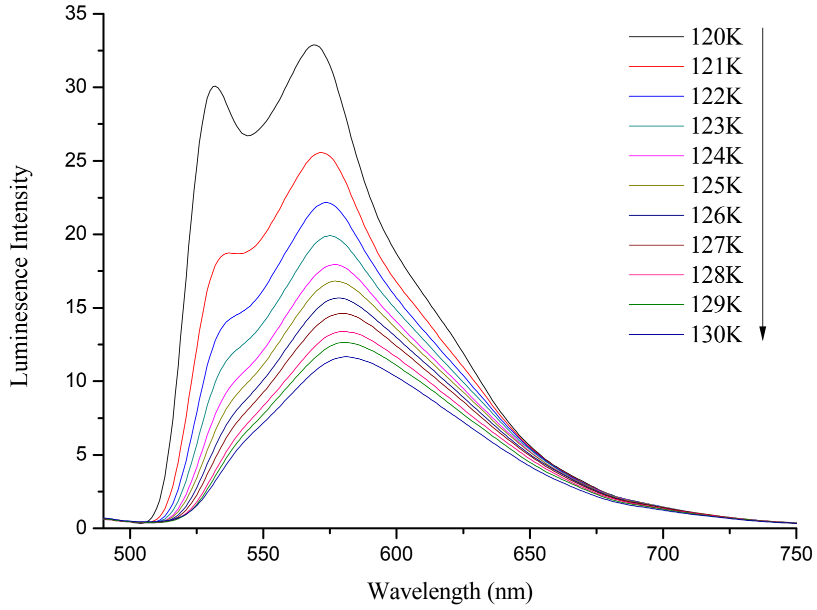

Figure 4.25 *Temperature dependent emission spectrum for complex 2 for each 1 K increase of temperature from 120 K to 130 K measured in EtOH: MeOH (4:1) glass.*

The intensity of this high energy band at ~528 nm increases in intensity as the temperature falls below the glass transition temperature. At 77 K the intensity of this emission band is higher than the nearby low energy band as shown in figure 4.24 (a). The lifetime decay curve at this emission wavelength was monoexponential (3.3 µs), and suggests a decay from the ^{3}LLCT excited state as reported previously.[14-16,32] The emission maxima at 567 nm is assigned to a mixed ^{3}LLCT/^{3}MLCT excited state as the lifetime decay curve was biexponential at this emission wavelength with a long lived component of 3.1 µs similar to that of ^{3}LLCT emission, and a short lived component of 635 ns as observed from the decay in pure ^{3}MLCT excited states. The lifetime decay values are tabulated in table 4.4 and the detailed values at every 10 K difference of temperature from 77 K to 290 K are given in appendix C. Also below the glass transition temperature there was one shoulder at 620 nm which was not seen at higher temperatures. Based on the previous data and explanations this is assigned to a low lying ^{3}MLCT state but due to the very low counts obtained at that emission wavelength the exact lifetime, was not determined. Further advanced measurements are rquired in order to confirm this and also the proper energy gap of each excited state.

Temperature dependent lifetime measurements carried out on complex 2 provided supporting data for the assignments made as discussed with temperature dependent emission on the change in energy of excited states as a function of temperature. Lifetimes were measured for the higher energy emission maxima and lower energy emission maxima as shown in the temperature dependent emission data plots in figure 4.24 for the entire range of temperature from 77 K to 290 K at every 10 K difference. All the decay curves obtained were dual exponential having a short lived component and a long lived component. The higher energy bands around 528 nm in the temperature range 77 K to 120 K, showed only monoexponential decays with a lifetime in the range of 1.9 μs to 3.3 μs clearly demonstrating a similarity with the ^{3}LLCT decay as per previous reports.[14-16,32] The plot for the average lifetime (τ_{av}) for both these high energy and low energy emission maxima as a function of temperature for the entire temperature range is given in figure 4.26 below.

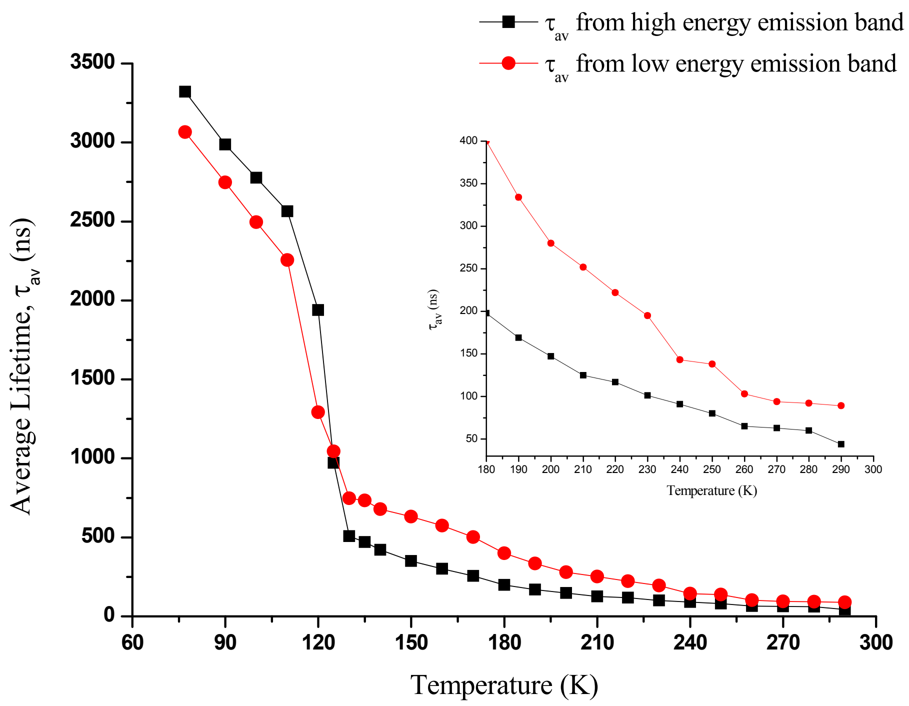

Figure 4.26 *Average lifetime as a function of temperature for complex 2 for each 10 K increase of temperature from 120 K to 130 K measured in EtOH:MeOH (4:1) glass.*

From figure 4.26 it is evident that at 77 K, the lifetime decay from the higher energy emission band dominates over the lifetime from the lower energy emission band, but as the temperature increases and reaches the glass transition temperature T_g, the lifetime values for both the emission maxima showed almost the same lifetimes and as the temperature increased further the lifetime value from the lower energy emission band showed a longer lifetime than the lifetime from the higher energy emission band. This can be explained by taking into account the cyclometallated Pt coordination at one end of the complex. Based on the previous reports,[55-69] cyclometallated Pt complexes do not emit at room temperature as the energy of the ^{3}MLCT/LC$_{Pt}$ state is very close to the ^{3}MC state. This ^{3}MLCT/LC$_{Pt}$ state is expected to have an energy in between the ^{3}LLCT and ^{3}MLCT states of iridium. After the glass transition temperature when the system reaches a solution state there is the possibility of populating the ^{3}MLCT/LC$_{Pt}$ excited state from the ^{3}MLCT$_{ppy}$ excited state through non radiative transitions. This will result in the decrease in the emission lifetimes of the decay from the ^{3}MLCT states of higher energy as the temperature increases above T_g. Also at low temperatures these cyclometalated Pt complexes show intense emission bands at higher energies in the range of 470 nm – 520 nm, so there is the possibility of higher emission bands being based on Pt. However this can be clearly ruled out by analysing the emission decay curves and lifetime values in the temperature range of 77 K to 120 K for the higher energy emission band. The decays were all monoexponential as discussed before with lifetimes in the range 1.9 – 3.3 μs which is much less than what is expected for an emission from a ^{3}MLCT/LC$_{Pt}$ excited state (30 μs) based on the reported publications.[66] Table 4.4 below gives the lifetime data with relative percentage and average lifetime at selected temperatures.

Temperature (K)	Emission Wavelength, λ_{em}, (nm)	Lifetime (ns), (χ^2)	Relative %	Avg.lifetime τ_{av}, ns
77K	527	$\tau = 3322$	100	3322
		$\chi^2 = 1.012$		
	567	$\tau_1 = 635$	11.57	3066
		$\tau_2 = 3130$	88.43	
		$\chi^2 = 1.035$		
125K	534	$\tau_1 = 106.20$	20.11	972
		$\tau_2 = 994.77$	79.89	
		$\chi^2 = 1.098$		
	572	$\tau_1 = 283.20$	21.83	1044
		$\tau_2 = 1099$	78.17	
		$\chi^2 = 1.138$		
200K	543	$\tau_1 = 34.89$	42.78	147
		$\tau_2 = 164.18$	57.22	
		$\chi^2 = 1.097$		
	589	$\tau_1 = 69.41$	25.70	280
		$\tau_2 = 296.89$	74.30	
		$\chi^2 = 1.111$		
290	543	$\tau_1 = 12.21$	24.71	44
		$\tau_2 = 46.96$	75.29	
		$\chi^2 = 1.105$		
	587	$\tau_1 = 21.22$	25.84	89
		$\tau_2 = 94.21$	74.16	
		$\chi^2 = 1.107$		

Table 4.4 *Tabulated data for the lifetimes for* $[Ir(ppy)_2(bpp)PtCl]_2(PF_6)_2$ *(2) in selected tempertaures measured in EtOH:MeOH (4:1) glass.*

Considering all these aspects a schematic representation for the possible transitions for $[Ir(ppy)_2(bpp)PtCl]_2(PF_6)_2$ is given in figure 4.27. The proposed mechanism for relaxation is as follows: after excitation, the $^1LLCT_{(ppy\rightarrow bpp)}$ state is accessed then rapidly relaxes to the ^1MLCT through internal conversion (IC), then inter system crossing (ISC) takes place to the $^3LLCT_{(ppy\rightarrow bpp)}$ state. Internal coversion follows this resulting in the relaxation to the $^3MLCT_{(ppy)}$ and $^3MLCT_{(bpp)}$ excited states (the lower being the $^3MLCT_{(bpp)}$). At room temperature (298 K) emission takes place from $^3MLCT_{(ppy)}$ and $^3MLCT_{(bpp)}$ excited states but as the temperature decreases to 77 K emission from $^3LLCT_{(ppy\rightarrow bpp)}$ state becomes prominent. At lower temperatures, below T_g, mixing of the LLCT and MLCT states can take place based on the results obtained for the temperature dependent lifetime measurements but further detailed measurements are recommended.

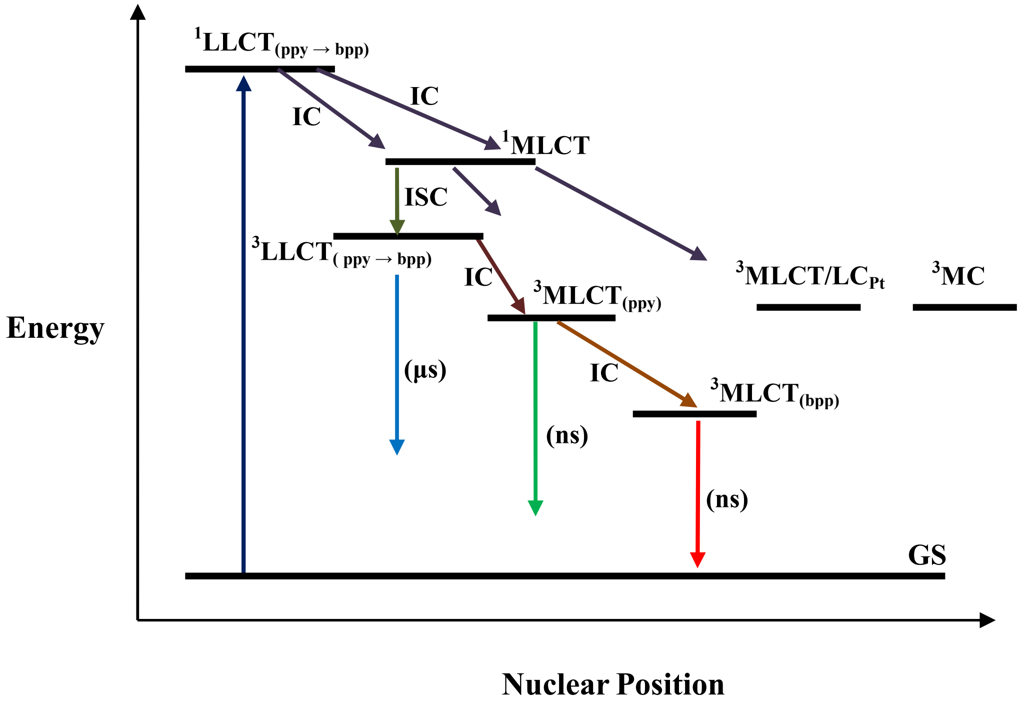

Figure 4.27 *Schematic representation of the energy levels and possible electronic transition for complex [Ir(ppy)$_2$(BPP)PtCl]$_2$(PF$_6$)$_2$ (2) (IC-internal conversion, ISC-intersystem crossing).*

4.2.3 Complex (3) : $[Ir(ppy)_2(bpp)PdCl]_2(PF_6)_2$

4.2.3.1 Absorption properties

The visible electronic absorption spectra for the Ir-Pd dimer complex $[Ir(ppy)_2(bpp)PdCl]_2(PF_6)_2$ along with the absorption spectra for Ir-Pt dimer, $[Ir(ppy)_2(bpp)PtCl]_2(PF_6)_2$ and the mononuclear complex $[Ir(ppy)_2(bpp)]PF_6$ are given in figure 4.28. It can be seen from the absorption spectra that complexation of Pd results in a shift of the absorption bands for complex **(3)** to lower energy (red shift) compared to the mononuclear complex. The shift in absorption bands is similar to that of the Ir-Pt complex **(2)**.

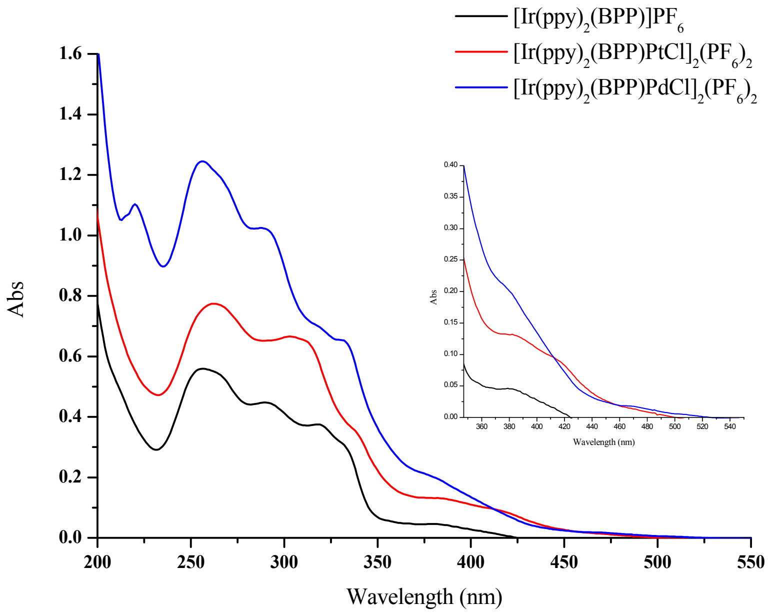

Figure 4.28 *Absorption spectra for complex $[Ir(ppy)_2(bpp)PdCl]_2(PF_6)_2$ along with complex complex $[Ir(ppy)_2(bpp)]PF_6$ and complex $[Ir(ppy)_2(bpp)PtCl]_2(PF_6)_2$ measured in aerated ACN at room temperature (298 K) (concentration - 1×10^{-5}M).*

The absorption spectra for $[Ir(ppy)_2(bpp)PdCl]_2(PF_6)_2$ consists of strong absorption bands in the region of 250 nm to 350 nm which are assigned as intraligand charge transfer transitions ($ILCT_{ppy}$), ppy(π)→ppy(π*) of which the lower energy bands close to 340 nm are assigned to bpp(π)→bpp(π*) intraligand charge transfer transitions ($ILCT_{bpp}$). The bands at 370 nm are attributed to interligand ppy(π)→bpp(π*) charge transfer transitions ($LLCT_{ppy\rightarrow bpp}$). The bands in the region of 400 nm to 500 nm are assigned to ^{3}MLCT transitions. It is possible that two MLCT bands, $MLCT_{(ppy)}$ (Ir to ppy charge transfer) and $MLCT_{(bpp)}$ (Ir to bpp charge transfer) have almost similar energies based on similar reported complexes.[23-32] The assignments were made by comparing the results with the spectrum of complex **(1)**, complex **(2)** and the reported publications[23-42] explained in section 4.1.5.

From figure 4.28 it is apparent that for the dimer complex **(3)**, the red shift for $ILCT_{bpp}$ transitions are more prominent than the $ILCT_{ppy}$ transitions. This is attributed to the fact that the Pd metal is directly complexed to one end of bpp ligand which can result in a greater perturbation of the excited state based on the bpp ligand ($ILCT_{bpp}$), resulting in a shifting of the absorption band as explained similarly for Ir-Pt dimer complex **(2)** in section 4.3.2.1. Similar is the case with $LLCT_{ppy \rightarrow bpp}$ transition, following complexation of the Pd a red shift for the $LLCT_{ppy \rightarrow bpp}$ band to 370 nm in Ir-Pd dimer complex **(3)** as opposed to 350 nm for the Ir monomer complex **(1)**. Both the MLCT transitions showed red shift on complexation with Pd as the bands at 370 nm and 420 nm for $MLCT_{(ppy)}$ and $MLCT_{(bpp)}$ in complex **(1)** were red shifted to 420 nm and 470 nm in complex **(3)**. The tabulated absorption data and extinction coefficients for all the three complexes measured in aerated ACN are given in table 1 in appendix C. The high energy and low energy bands in the room temperature absorption spectra of cyclometallated Pd complexes have been assigned as intraligand π-π* transitions.[72] Based on this consideration, complex **(3)** is expected to have a π-π* intraligand transitions in 250 nm to 450 nm range.

4.2.3.2 Emission properties

The room temperature (298 K) and low temperature (77 K) emission spectra for $[Ir(ppy)_2(bpp)PdCl]_2(PF_6)_2$ are given in figure 4.29. From the emission spectra it is clear that there is only one emission maximum at room temperature and low temperature. The emission observed for the Ir-Pt complex discussed in section 4.2.2.2 exhibits a difference in energy between the two low lying ^{3}MLCT excited states, whereas for the Ir-Pd complex **(3)** no splitting of the ^{3}MLCT states were seen in the emission spectra, thus it appears that the effect of Pd (II) metal centre on the ^{3}MLCT excited states is less than that for Pt (II) centre.

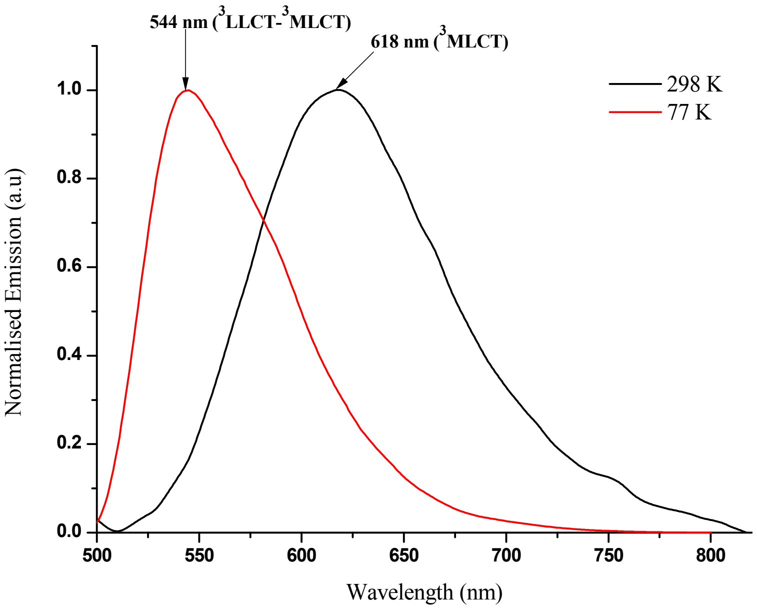

Figure 4.29 *Emission spectra for complex [Ir(ppy)$_2$(bpp)PdCl]$_2$(PF$_6$)$_2$ (3) at 298 K (—) measured in aearated ACN and 77 K (—) measured in EtOH:MeOH (4:1) glass.*

Assignment of the excited state in the emission spectra at both temperatures were based on previous publications[39-45] and by comparison with the Ir monomer (complex **(1)**) and Ir-Pt dimer (complex **(2)**) discussed in sections 4.2.1.2 and 4.2.2.2, and also spectral shape, rigidochromic and solvatochromic emission behaviours,[22] phosphoresence lifetime (τ_p) (77 K and 298 K) measurements and effect of solvent polarity on lifetimes. At room temperature (298 K) there is only one emission maxima at 618 nm which is assigned to emission from ^{3}MLCT excited state. The lifetime measurements showed that the decay at this wavelength is dual exponential in character with a short lived component of 3 ns and a long lived component of 73 ns. The measurements were made in aerated ACN at room temperatue, the tabulated results are given in table 4.5. For the Ir-Pd complex **(3)**, the Pd metal does not appear to influence the ^{3}MLCT excited states to the same extent as seen for the Ir-Pt complex **(2)**, therefore for the Ir-Pd complex **(3)**, both the ^{3}MLCT excited states may lie very close in energy giving emission from a mixed ^{3}MLCT$_{ppy}$/^{3}MLCT$_{bpp}$ state. The blue shift of the emission spectra on going from room temperature (298 K) to low temperature (77 K) is typical of MLCT states. The room temperature (298 K) emission band at 618 nm is rigidochromically shifted to 544 nm at 77 K as shown in figure 4.29. The difference in energy between the two peaks is characteristic of an MLCT excited state. Further measurements carried out at 77 K suggests that the emission at 544 nm takes place from a mixed ^{3}LLCT/^{3}MLCT excited state which is explained in detail in section 4.2.3.4.

Further support for assignment of the excited state (^{3}MLCT at room temperature) is obtained from the concentration dependent and solvent dependent studies carried out with complex $[Ir(ppy)_2(bpp)PdCl]_2(PF_6)_2$ as given below in figures 4.30 (a) and 4.30 (b).

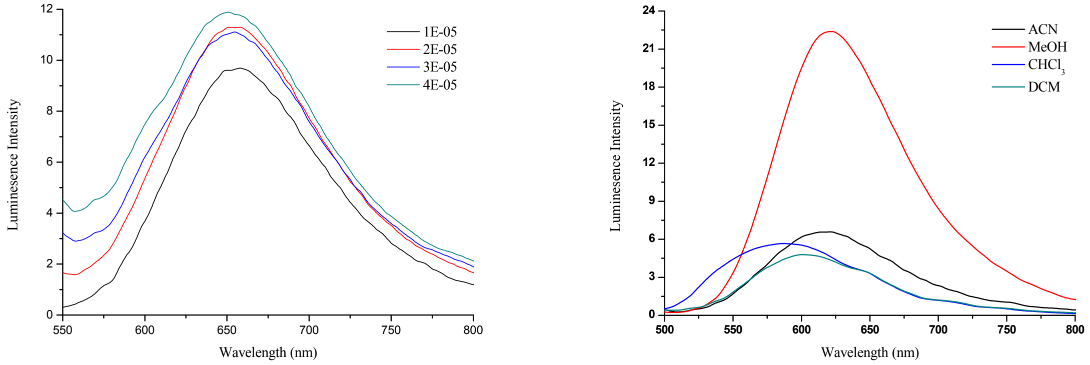

(a) **(b)**

Figure 4.30 *(**a**) Concentration dependent emission and (**b**) solvent dependent emission for complex $[Ir(ppy)_2(bpp)PdCl]_2(PF_6)_2$ (3) in four different solvents having conc. 1×10^{-5}M.*

Solvatochromism is a potentially important probe in assessing charge distribution in both ground and excited states.[85] It can be seen from figure 4.30 (b) that the emission is influenced by polarity of the solvent. Normally MLCT phosphorescence should exhibit a hypsochromic shift on moving from polar to non polar solvents.[85,86] For complex **(3)** as the solvent polarity decreases there is blue shift as given in table 4.5 but the results are not consistent, as the emission in $CHCl_3$ (587 nm) is blue shifted to a greater extent compared to the less polar solvent DCM (601 nm). Also the emission in MeOH (622 nm) is red shifted more so than the ACN (615 nm).

4.2.3.3 Solvent dependent lifetime measurements

The solvent dependent lifetime measurements further supports the assignments of the excited states described in previous sections. Based on the published reports[39-45] for Ir (III) cyclometallated complexes and by comparing the results obtained with those for the iridium monomer complex **(1)** and Ir-Pt dimer complex **(2)**, explained in sections 4.2.1 and 4.2.2, the lowest excited state for complex **(3)** at 298 K is attributed to a ^{3}MLCT excited state. The solvent-dependent lifetime measurements explained in this section provide supporting evidence for this assignment. If the excited state is an MLCT state as the solvent polarity decreases the emission lifetime should increase since the MLCT states for Ir (III) cyclometalated complexes are stabilised to a greater extent in non polar solvents than in polar solvents.[85,88] The graphical plot of avarage lifetime (both aerated and deaerated) in four different solvents is given in figure 4.32 below which shows the solvent effect much more clearly.

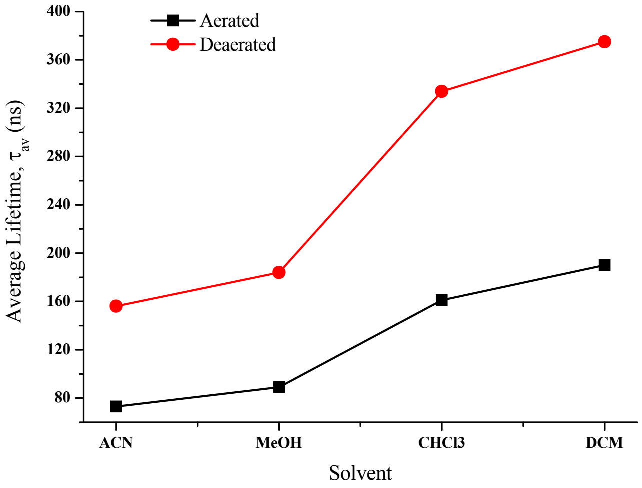

Figure 4.32 *Solvent dependent lifetime measurement for complex* ***(3)*** *(aerated and deaerated) measured at room temperature (298 K) and having a concentration of* 1×10^{-5}*M.*

From the above figure it is clear that as the solvent polarity decreases the lifetime increases for both aerated and deaerated sample characteristic of the emission from a ^{3}MLCT excited state. The entire data for the decay with the emission wavelength at which the decay was measured, relative percentage of each component and the average lifetime calculated are given in table 4.5 below.

Solvent (polarity)	Aerated/ Deaerated	Emission Wavelength, λ_{em}, (nm)	Timebase (ns)	Lifetime (ns), (χ^2)	Relative %	Avg. lifetime τ_{av}, ns
ACN (5.8)	Aerated	615	500	$\tau_1 - 3$	3.21	73
				$\tau_2 - 73$	96.79	
				$\chi^2 - 1.043$		
	Deaerated	615	500	$\tau_1 - 3$	1.32	156
				$\tau_2 - 156$	98.68	
				$\chi^2 - 1.012$		
MeOH (5.1)	Aerated	622	500	$\tau_1 - 89$	100	89
				$\chi^2 - 1.008$		
	Deaerated	622	500	$\tau_1 - 184$	100	184
				$\chi^2 - 1.050$		
$CHCl_3$ (4.1)	Aerated	587	500	$\tau_1 - 19$	3.84	161
				$\tau_2 - 162$	96.16	
				$\chi^2 - 1.001$		
	Deaerated	587	500	$\tau_1 - 33$	4.15	334
				$\tau_2 - 335$	95.85	
				$\chi^2 - 1.031$		
DCM (3.1)	Aerated	601	500	$\tau_1 - 190$	100	190
				$\chi^2 - 1.032$		
	Deaerated	601	500	$\tau_1 - 375$	100	375
				$\chi^2 - 1.052$		

***Table 4.5** Tabulated results for the solvent dependent lifetime measurement for complex **(3)** in both aerated and deaerated ACN measured at room temperature (298 K) and having a concentration of 1×10^{-5}M (shaded region corresponds to deaerated measurements).*

The emission decay for complex **(3)** in solvents ACN and $CHCl_3$ showed dual exponential behaviour in aerated and deaerated (shaded portion) conditions as given in table 4.5. For ACN the short lived component (τ_1) has a value of 3 ns and the long lived component (τ_2) has a lifetime of 73 ns The long lived component contributes 98 % of the decay observed. Changing the solvent polarity effects both components (τ_1 and τ_2) equally as shown in table 4.5. Both τ_1 and τ_2 values increased as the solvent was changed from the ACN (polarity - 5.8) to $CHCl_3$ (polarity - 4.1). τ_1 increased from 3 ns to 19 ns and τ_2 increased from 73 ns to 162 ns in aerated ACN. The same trend was seen in the measurements done in deaerated ACN as given by the shaded portion in table 4.5. Interestingly the lifetime measurements carried out in MeOH and DCM showed only single exponential decay with lifetimes of 89 ns (MeOH) and 190 ns (DCM) in aerated samples and 184 ns (MeOH) and 375 ns (DCM) in deaerated samples (shaded portions). These results support the assignment of the lowest excited state at room temperature (298 K) to a ^{3}MLCT state.

The lifetime decay curves for complex **(3)** measured in aerated ACN are given in figure 4.33 (a) and 4.33 (b). From the decay curves it is clear that the decay is biexponential. At an emission wavelength of 618 nm both lifetime values (τ_1 and τ_2) are assigned to ^{3}MLCT excited state. The short lived component has a lifetime of 3 ns (τ_1) and the long lived component has a lifetime of 73 ns (τ_2) which contributes 97 %. The χ^2 value for the fit is 1.043 indicating close fit to experimental data and the residual plot curve given in figure 4.33 (a) also shows the fit.

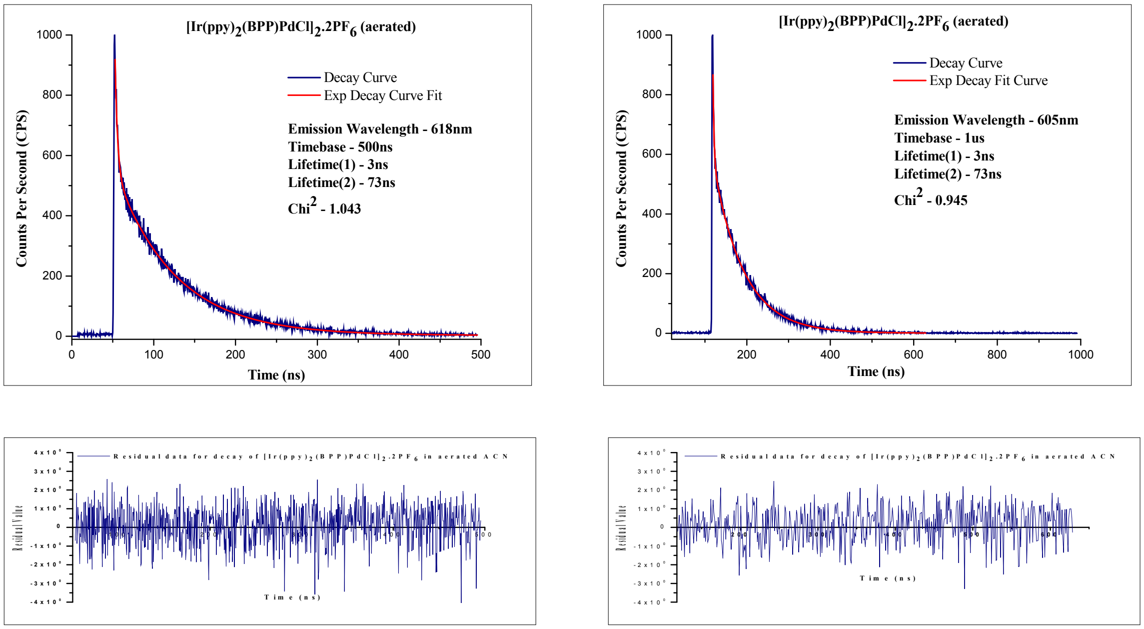

(a) **(b)**

Figure 4.33 *Lifetime decay plots for complex* $[Ir(ppy)_2(bpp)PdCl]_2(PF_6)_2$ *(3) in aerated ACN at timebase of* ***(a)*** *500 ns and* ***(b)*** *1 µs measured at room temperature (298K).*

The decay curves for complex **(3)** in the remaining solvents under aerated and deaerated conditions are given in appendix C. Based on all the above considerations given in sections 4.2.3.2 and 4.2.3.3 the lowest excited state from which the emission occurs at 298 K is assigned to a ^{3}MLCT state.

4.2.3.4 Temperature dependent emission and lifetime measurements

The temperature dependent emission spectra for $[Ir(ppy)_2(bpp)PdCl]_2(PF_6)_2$ in the temperature range 77 K to 290 K for every 10 K difference is given in figures 4.34, 4.35 (a) and 4.35 (b). From these figures blue shift in the emission maximum on going to low temperatures was observed which is based on the assumption that MLCT phosphorescence exhibits a hypsochromic shift when the medium becomes rigid.[23]

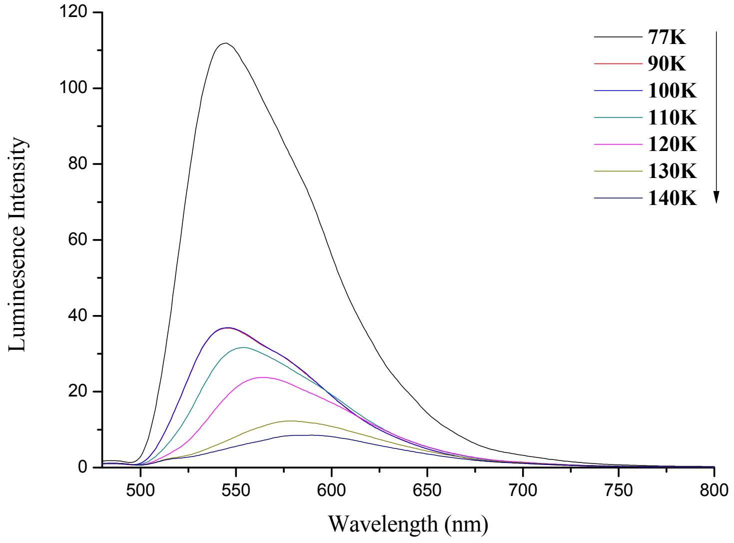

Figure 4.34 *Temperature dependent emission spectrum for* $[Ir(ppy)_2(bpp)PdCl]_2(PF_6)_2$ *from 77 K to 140 K measured in EtOH: MeOH (4:1) glass.*

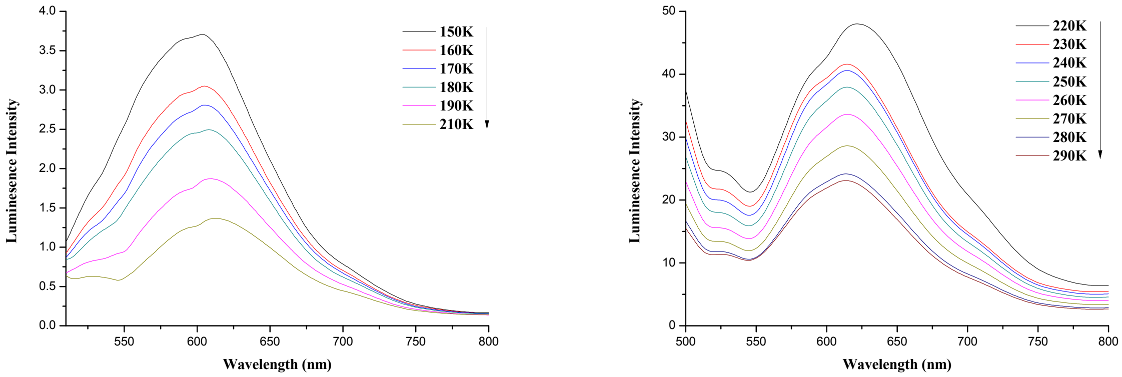

(a) **(b)**

Figure 4.35 *Temperature dependent emission spectrum for* $[Ir(ppy)_2(bpp)PdCl]_2(PF_6)_2$ ***(a)*** *from 150 K to 210 K* ***(b)*** *from 220 K to 290 K, measured in EtOH: MeOH (4:1) glass.*

The explanation for this blue shift on going from room temperature (298 K) to low temperature (77 K) in a rigid matrix was explained in section 4.2.3.2. From the emission plots over the entire temperature range there is no evidence for a decay from two different excited states as seen for the Ir-Pt dimer complex **(2)**. Also from the nature of the emission spectra (broadened emission), it is possible that the emission is from a ^{3}MLCT excited state. Further evidence is provided by the lifetime measurements. Considering the emission decay lifetimes at each of these emission maxima, decay curves obtained were all dual exponential. A few of the selected values are given in table 4.6 and the rest are given in appendix C.

As the temperature decreases from room temperature (298 K) to low temperature (77 K) the lifetimes increased as shown in figure 4.36, which gives a plot of average lifetime (τ_{av}) as a function of temperature from 77 K to 290 K.

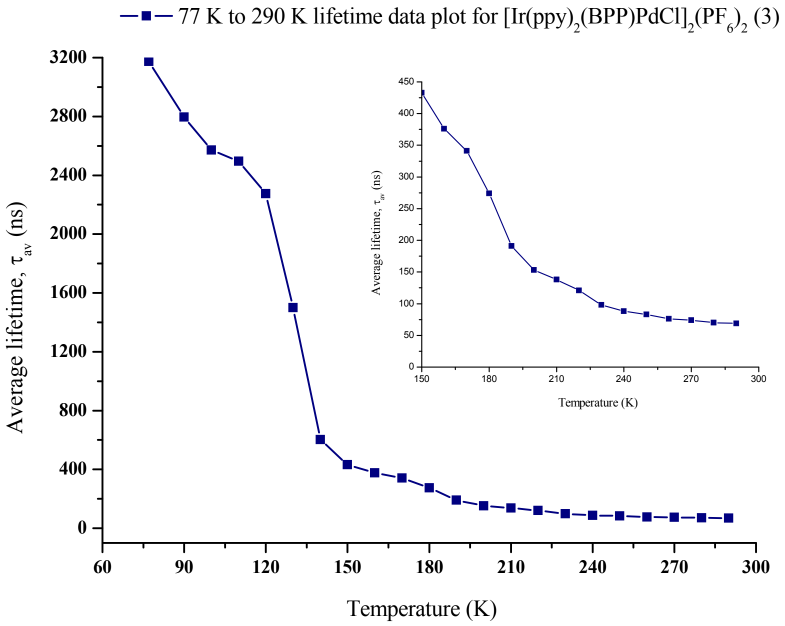

Figure 4.36 *Average lifetime as a function of temperature for complex [Ir(ppy)$_2$(bpp)PdCl]$_2$(PF$_6$)$_2$ (3) for each 10 K increase of temperature from 120 K to 130 K measured in EtOH:MeOH (4:1) glass.*

The lifetime increases slowly as the temperature decreases and as temperature reaches the glass transition temperature (T_g) there is a notable increase in the lifetime value as seen in the graph. The lifetime decay curve for all of these temperatures showed dual exponential decays with a short lived (τ_1) and long lived (τ_2) component. The tabulated data for some of the selected temperatures are given in table 4.6 below. The entire tabulated data including the emission wavelength, lifetimes (τ_1 and τ_2), their relative percentage and the average lifetime obtained are given in appendix C.

Temperature (K)	Emission Wavelength, λ_{em}, (nm)	Lifetime (ns), (χ^2)	Relative %	Avg.lifetime τ_{av}, ns
77 K	544	τ_1= 455	4.64	3174
		τ_2= 3193	95.36	
		χ^2= 1.059		
120 K	564	τ_1= 144.35	2.78	2275
		τ_2= 2279	97.22	
		χ^2= 1.001		
130 K	579	τ_1= 128.49	2.67	1500
		τ_2= 1503	97.33	
		χ^2= 1.057		
140 K	587	τ_1= 122.12	32.05	603
		τ_2= 646.24	67.95	
		χ^2= 1.114		
200 K	609	τ_1= 9.03	0.81	153
		τ_2= 152.63	99.19	
		χ^2= 1.084		
250 K	615	τ_1= 0.539	0.19	83
		τ_2= 82.54	99.81	
		χ^2= 1.079		
290 K	615	τ_1= 0.56	2.05	69
		τ_2= 69.63	97.95	
		χ^2= 1.007		

Table 4.6 *Tabulated data for the temperature dependent lifetime measurement done for complex* $[Ir(ppy)_2(bpp)PdCl]_2(PF_6)_2$ *in a temperature range of 77 K to 290 K in (4:1) EtOH:MeOH glass.*

By analysing the emission spectra (broadened emission) and each of the lifetime values, and comparing these results with those previously reported results for iridium (III) cyclometallated complexes it is clear that all the emission lifetimes recorded above the glass transition temperature (T_g) occurs from ^{3}MLCT excited states. As the temperature reaches the the glass transition temperature (T_g) (125 K, λ_{em}-564 nm), the value for τ_1 is 144 ns suggesting the decay to be from a ^{3}MLCT excited state and the value obtained for τ_2 is 2279 ns, suggesting the decay is from a ^{3}LLCT excited state. At 77 K (λ_{em}-564 nm) the short lived component (τ_1) is 455 ns characteristic of ^{3}MLCT state decay and the value for the long lived component (τ_2) is 3193 ns, characteristic of a ^{3}LLCT state, based on previous reports.[11,12,32] The variation of τ_1 and τ_2 as a function of temperature from 77 K to 290 K at 10 K intervals is shown in figure 4.37.

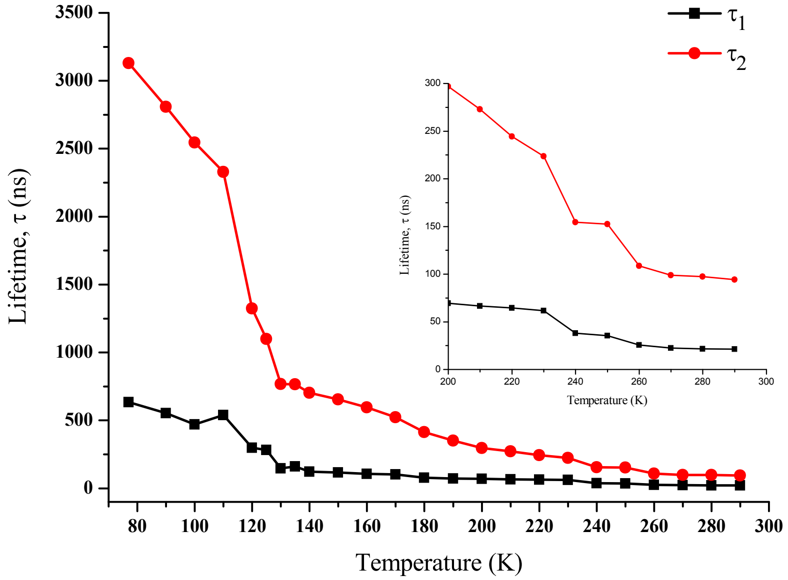

Figure 4.37 *Variation of τ_1 and τ_2 as a function of temperature for complex [Ir(ppy)$_2$(bpp)PdCl]$_2$(PF$_6$)$_2$ in a temperature range of 77 K to 290 K in (4:1) EtOH:MeOH glass.*

These assumptions are all made on the basis of comparing the lifetime data obtained, with the results for complex **(1)**, complex **(2)** and with previously reported publications for cyclometallated iridium (III) complexes.[23-45] Further studies using a wavelength dependent emission lifetime, different excitation wavelength in order to populate each of these excited states seperately, transient absorption measurements and advanced techniques like computational methods etc are required for conformation of the hypothesis presented here.

On the basis of all these assumptions a proposed schematic representation for the possible transition for complex [Ir(ppy)$_2$(bpp)PdCl]$_2$(PF$_6$)$_2$ is given in figure 4.38. The mechanism for relaxation is proposed as follows: after excitation, the ^{1}LLCT$_{(ppy\rightarrow bpp)}$ state is populated, then this rapidly relaxes to the ^{1}MLCT through internal conversion (IC), inter system crossing (ISC) takes place to the ^{3}LLCT$_{(ppy\rightarrow bpp)}$ state. Internal coversion follows this resulting in the relaxation to the ^{3}MLCT$_{(ppy)}$ and ^{3}MLCT$_{(bpp)}$ excited states, with the lower one being the ^{3}MLCT$_{(bpp)}$. At room temperature (298 K) emission takes place from ^{3}MLCT$_{(ppy)}$ and ^{3}MLCT$_{(bpp)}$ excited states but as the temperature decreases to 77 K emission from ^{3}LLCT$_{(ppy\rightarrow bpp)}$ state also occurs.

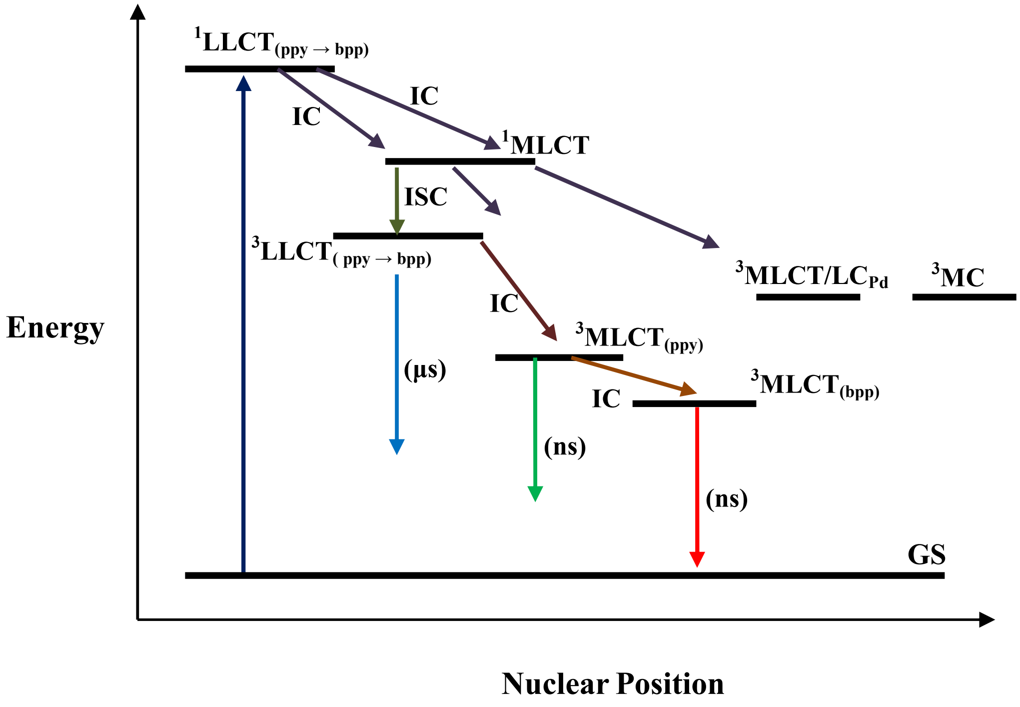

Figure 4.38 *Schematic representation of the energy levels and possible electronic transition for complex* $[Ir(ppy)_2(BPP)PdCl]_2(PF_6)_2$ *(IC-internal conversion, ISC-intersystem crossing).*

4.3 Conclusion

Detailed solvent dependent and temperature dependent excited state photophysics of three novel iridium complexes $[Ir(ppy)_2(bpp)]PF_6$ (complex 1), $[Ir(ppy)_2(bpp)PtCl]_2(PF_6)_2$ (complex 2) and $[Ir(ppy)_2(bpp)PdCl]_2(PF_6)_2$ (complex 3) were caried out. The results were compared with reported publications on cyclometallated Ir (III) complexes.[23-47] Coordination of Pt resulted in an increase in the energy (increase in energy can be clearly seen from the emission spectra with the blue shift of the band) of the ^{3}MLCT$_{ppy}$ excited state to a position where it can easily populate the excited state of Pt (MLCT/LC$_{Pt}$). Thus the electron in the ^{3}MLCT$_{ppy}$ easily moves on to the Pt excited state and this increases as the temperature decreases as can be clearly seen from a decrease in the emission intensity and lifetime value for the high energy $^3MLCT_{ppy}$ excited state when lowering of temperature (figure 4.24 and figure 4.26). Thus the $^3MLCT_{ppy}$ excited state plays a key role in populating the Pt excited state in heterodinuclear complex $[Ir(ppy)_2(bpp)PtCl]_2(PF_6)_2$. Supporting evidence for this electron transfer process is obtained from the photocatalytic results reported for these three complexes in chapter 3. Photocatalysis of complex 2 with UV light (λ_{ex} – 350 nm) and visible light (λ_{ex} – 470 nm) demonstrate the role of $^3MLCT_{ppy}$ excited state. H_2 production following 350 nm excitation was almost zero compared to the excitation at 470 nm. In the former case the ligand centered charge transfer bands were excited which do not play any prominent role in the electron transfer process to the Pt (II) excited state. But in the second case excitation at 470 nm results in direct population of $^3MLCT_{ppy}$ state from which the charge moves to the Pt (II) excited state and results in more efficient catalytic H_2 production.

For $[Ir(ppy)_2(bpp)PdCl]_2(PF_6)_2$, the results obtained indicate that there is little change in the energy of the ^3MLCT excited states as seen for $[Ir(ppy)_2(bpp)PtCl]_2(PF_6)_2$. Therefore for complex **(3)** the electron decays from ^1LLCT to ^1MLCT state from where it reaches the $^3MLCT_{ppy}$ and $^3MLCT_{bpp}$ excited state via the ^3LLCT excited state and decays to the ground state from the low lying ^3MLCT excited state (figure 4.27). Thus for the Ir-Pd complex **(3)** as the excited state of the Pd lies above the ^3MLCT state there is very little possibility of populating the Pd excited state through ^3MLCT excited states. Due to this reason the Ir-Pd system has less catalytic H_2 generation efficiency compared to the Ir-Pt complex. For the Ir-Pd complex 470 nm irradiation gave better TON values than 350 nm irradiation. This demonstrates the importance of the ^3MLCT excited state for the Ir-Pd system also. Further support of the influence of the $^3MLCT_{ppy}$ is obtained from the analysis of the photocatalytic results of the ester substituted Ir-Pt, Ir-Pd complexes with the non ester derivatives. The ester complexes gave almost double the amount H_2 as did the non ester derivatives. Here the electron withdrawing ester groups on the peripheral ppy ligand results in an increase in energy of the $^3MLCT_{ppy}$ excited state, occupying a position from where the Pt/Pd excited state can be easily populated at room temperature.

The excited state photophysical measurements carried out with these complexes gave an idea regarding the possible electronic transition in the novel Ir-Pt, Ir-Pd intramolecular photocatalytic systems. Varying the substituents on peripheral ppy ligands and also by using different bridges it is possible to tune the excited state, which results in more H_2 than the conventional intermolecular photocatalytic systems.

4.4 Bibliography

---

1. T. Hofbeck and H. Yersin, *Inorg. Chem.,* **2010**, 49, 9290.
2. C. Wu, H. F. Chen, K. T. Wong and M. E. Thompson, *J. Am. Chem. Soc.,* **2010**, 132, 3133.
3. A. A. Rachford, R. Ziessel, T. Bura, P. Retailleau and F. N. Castellano, *Inorg. Chem.,* **2010**, 49, 3730.
4. V. Balzani, A. Juris, M. Venturi, S. Campagna, S. Serroni, *Chem.Soc. Rev.*, 1996, 96, 759.
5. J. R. Lakowicz, *Principles of Fluorescence Spectroscopy*, 1984, Plenum Press, New York.
6. D. F. Schriver, P. W. Atkins, C. H. Langford, *Inorg. Chem.*, *Second Edition*, **1994,** Oxford University Press, New York.
7. F. A. Cotton, G. Wilkinson, P. L. Gaus, *Basic Inorg. Chem., 3rd Ed.*, **1995**, Wiley & Sons Inc., New York.
8. D. F. Schriver, P. W. Atkins, C. H. Langford, *Inorg. Chem.*, *Second Edition*, **1994,** Oxford University Press, New York.
9. V. Balzani and S. Campagna, *Photochemistry and photophysics of coordination compounds II*, Springer, **2010.**
10. K. Kalyanasundaram and M. Gratzel, *Photosensitisation and photocatalysis using inorganic and organometallic compounds*, Springer, **1993**, vol 14.
11. M. Polson, S. Fracasso, V. Bertolasi, M. Ravaglia and F. Scandola, *Inorg Chem.,* **2004**, 43, 1950.
12. M. Polson, M. Ravaglia, S. Fracasso, M. Garavelli, F. Scandola, *Inorg. Chem.,* **2005**, 44, 1282.
13. A. J. Wilkinson, H. Puschmann, J. A. K. Howard, C. E. Foster, J. A. G. Williams, *Inorg. Chem.,* **2006**, 45, 8685.
14. V. L. Whittle and J. A. G. Williams, *Inorg. Chem.,* **2008**, 47, 6596.

15. J. A. G. Williams, *Chem. Soc. Rev.,* **2009**, 38, 1783.
16. V. Balzani, G. Bergamini, S. Campagna and F. Puntoriero, *Photochemistry and photophysics of coordination compounds I*, Springer, **2007.**
17. M. Kasha, *Discussion of the faraday society*, **1950**, 9, 14.
18. C. H. Yang, S. W. Li, Y. Chi, Y. M. Cheng, Y. S. Yeh, P. T. Chou, G. H. Lee, C. H. Wang, C. F. Shu, *Inorg. Chem.,* **2005**, 44, 7770.
19. T. Sajoto, P. I. Djurovich, A. Tamayo, M. Yousufuddin, R. Bau, M. E. Thompson, *Inorg. Chem.,* **2005**, 44, 7992.
20. C. S. K. Mak, A. Hayer, S. I. Pascu, S. E. Watkins, A. B. Holmes, A. Köhler, R. H. Friend, *Chem. Commun.*, **2005**, 4708.
21. H. Jang, C. H. Shin, N. G. Kim, K. Y. Hwang, Y. Do, *Synth. Met.,* **2005**, 154, 157.
22. P. T. Chou, Y. Chi, *Chem. Eur. J.,* **2007**, 13, 380.
23. R. Ragni, E. A. Plummer, K. Brunner, J. W. Hofstraat, F. Babudri, G. M. Farinola, F. Naso, L. De Cola, *J. Mater. Chem.,* **2006**, 16, 1161.
24. C. S. Chin, M. S. Eum, S. Y. Kim, C. Kim, S. K. Kang, *Eur. J. Inorg.Chem.,* **2007**, 372.
25. S. C. Lo, C. P. Shipley, R. N. Bera, R. E. Harding, A. R. Cowley, P. L. Burn, I. D. W. Samuel, *Chem. Mater.,* **2006**, 18, 5119.
26. S. Sprouse, K. A. King, P. J. Spellane, R. J. Watts, *J. Am. Chem. Soc.,* **1984**, 106, 6647.
27. Y. Ohsawa, S. Sprouse, K. A. King, M. K. DeArmond, K. W. Hanck, R. J. Watts, *J.Phys. Chem.,* **1987**, 91, 1047.
28. L. Flamigni, A. Barbieri, C. Sabatini, B. Ventura, F. Barigelletti, *Top. Curr. Chem.,* **2007**, 281, 143.
29. J. P. Collin, I. M. Dixon, J. P. Sauvage, J. A. G. Williams, F. Barigelletti, L. Flamigni, *J. Am. Chem. Soc.,* **1999**, 121, 5009.
30. A. F. Rausch, M. E. Thompson, H. Yersin, *J. Phys. Chem. (A).,* **2009**, 113, 5927.
31. G. Treboux, J. Mizukami, M. Yabe, S. Nakamura, *Chem. Lett.,* **2007**, 36, 1344.
32. S. H. Wu, J. W. Ling, S. H. Lai, M. J. Huang, C. H. Cheng, I. C. Chen, *J. Phys. Chem. (A).,* **2010,** 114, 10339.
33. A. Juris, V. Balzani, F. Barigelletti, S. Campagna, P. Belser, A. V. Zelewsky, *Coord. Chem. Rev.,* **1988**, 84, 85.

---

34. M. Maestri, V. Balzani, C. D. Cornioley, A. V. Zelewsky, *Adv. Photochem*., **1992**, 17, 1.
35. X. Yang, D. Neher, K. Müllen, U. Scherf, Eds.; Wiley-VCH: Weinheim, **2006**; p. 333.
36. M. S. Lowry, S. Bernhard, *Chem. Eur. J.,* **2006**, 12, 7970.
37. T. Tsuboi and N. Aljaroudi, *Jpn. J. Appl. Phys., Part 1*, **2008**, 47, 1266.
38. S. Lamansky, P. Djurovich, D. Murphy, F. A. Razzaq, H. E. Lee, C. Adachi, P. E. Burrows, S. R. Forrest and M. E. Thompson, *J. Am.Chem. Soc.*, **2001**, 123, 4304.
39. A. Tsuboyama, H. Iwawaki, M. Furugori, T. Mukaide, J. Kamatani, S. Igawa, T. Moriyama, S. Miura, T. Takiguchi, S. Okada, M. Hoshino and K. Ueno, *J. Am. Chem. Soc.*, **2003**, 125, 12971.
40. K. K. W. Lo, C. K. Chung, T. K. M. Lee, L. K. Lui, K. H. K. Tsang and N. Zhu, *Inorg. Chem.*, **2003**, 42, 6886.
41. K. Dedeian, J. Shi, E. Forsythe, D. C. Morton and P. Y. Zavalij, *Inorg.Chem.*, **2007**, 46, 1603.
42. D. D. Censo, S. Fantacci, F. D. Angelis, C. Klein, N. Evans, K. Kalyanasundaram, H. J. Bolink, M. Gratzel and M. K. Nazeeruddin, *Inorg. Chem.*, **2008**, 47, 980.
43. P. T. Chou, Y. I. Liu, H. W. Liu and W. S. Yu, *J. Am. Chem. Soc.*, **2001**, 123, 12119.
44. J. W. Seo, S. Kimand, S. Y. Park, *J. Am. Chem. Soc.*, **2004**, 126, 11154.
45. J. Li, P. I. Djurovich, B. D. Alleyne, M. Yousufuddin, N. N. Ho, J. C. Thomas, J. C. Peters, R. Bau and M. E. Thompson, *Inorg. Chem.*, **2005**, 44, 1713.
46. A. Vogler, H. Kunkely, *Coord. Chem. Rev.,* **2000**, 200, 991.
47. A. Vogler, H. Kunkely, *Top. Curr. Chem.,* **2001**, 213, 143.
48. D. J. Stufkens, A. J. Vlcek, *Coord. Chem. Rev.,* **1998**, 177, 127.
49. G. Zhou, W. Y. Wong, S. Y. Poon, C. Ye, Z. Lin, *Adv. Funct. Mater.,* **2009**, 19, 531.
50. S. W. Li, Y. M. Cheng, Y. S. Yeh, C. C. Hsu, P. T. Chou, S. M. Peng, G. H. Lee, Y. L. Tung, P. C. Wu, Y. Chi, F. I. Wu, C. F. Shu, *Chem. Eur. J.,* **2005**, 11, 6347.
51. K. A. King, M. F. Finlayson, P. J. Spellane, R. J. Watts, Sci.Pap. *Inst. Phys. Chem. Res.,* **1984**, 78, 97.
52. M. Maestri, D. Sandrini, V. Balzani, L. Chassot, P. Jolliet, A. V. Zelewsky, *Chem. Phys. Lett.,* **1985**, 122, 375.
53. E. C. Constable, J. M. Holmes, *J. Organomet. Chem.,* **1986**, 301, 203.

54. J. C. Ostrowski, M. R. Robinson, A. J. Heeger, G. C. Bazan, *Chem. Commun.,* **2002**, 784.
55. K. A. King, P. J. Spellane, R. J. Watts, *J. Am. Chem. Soc.,* **1985**, 107, 1431.
56. V. Balzani, F. Bolleta, M. Ciano, M. Maestri, *J. Chem. Educ.* **1983**, 60, 447.
57. A. Kasahara, *Bull. Chem. Soc. Jpn.* **1968**, 41, 1272.
58. B. N. Cockbum, D. V. Howe, T. Keating, B. F. G. Johnson, J. Lewis, *J. Chem. Soc., Dalton Trans.* **1973**, 404.
59. G. B. Caygill, P. J. Steel, *J. Organomet. Chem.,* **1987**, 327, 115.
60. D. L. Weaver, *Inorg. Chem.,* **1970**, 9, 2250.
61. M. A. Gutierrez, G. R. Newkome, J. Selbin, *J. Organomet. Chem.* **1980**, 202, 341.
62. J. M. Vila, M. Gayoso, M. T. Pereira, A. Romar, J. J. Fernandez, M. T. Pett, *J. Organomet Chem.* **1991**, 401, 385
63. J. A. G. Williams, S. Develay, D. L. Rochester, L. Murphy, *Coord. Chem. Rev.,* **2008**, 252, 2596.
64. M. Maestri, D. Sandrini, A. V. Zelewsky, C. D. Cornioley, *Inorg. Chem.,* **1991**, 30, 2476.
65. K. T. Wan, C. M. Che, K. C. Cho, *J. Chem. Soc., Dalton Trans.,* **1991**, 1077.
66. M. M. Mdleleni, J. S. Bridgewater, R. J. Watts, P. C. Ford, *Inorg. Chem.,* **1995**, 34, 2335.
67. M. Maestri, D. Sandrini, V. Balzani, U. Maeder, A. V. Zelewsky, *Inorg. Chem.,* **1987,** 2 6, 1323.
68. A. Zilian, U. Maeder, H. U. Gddel, *J. Am. Chem. Soc.* **1989,** 111, 3855
69. M. G. Colombo, A. Hauser, H. U. Gudel, *Inorg. Chem.* **1993**, 32, 3088.
70. Y. Wakatsuki, H. Yamazaki, P. A. Grutsch, M. Santhanam, C. J. Kutal, *J. Am. Chem. Soc.,***1985**, 107, 8153.
71. L. Chassot, E. Miiller, A. V. Zelewsky, *Inorg. Chem.,* **1984**, 23, 4249.
72. C. A. Craig and R. J. Watts, *Inorg. Chem.,* **1989**, 28, 311
73. M. K. DeArmond, C. M. Carlin, C. M. *Coord. Chem. Rev.,* **1981**, 36, 325.
74. R. J. Watts, *J. Am. Chem. Soc.,* **1974**, 96*,* 6186.
75. R. J. Watts and J. V. Houten, *J. Am. Chem. Soc.,* **1978**, 100, 1718.
76. P. Belser, A. V. Zelewsky, A. Juris, F. Barigelletti, V. Balzani, *Chem. Phys. Lett.,* **1984**, 104, 100.

77. M. Nishizawa, T. M. Suzuki, S. Sprouse, R. J. Watts, P. C. Ford, *Inorg. Chem.,* **1984**, 23, 1837
78. K. A. King and R. J. Watts, *J . Am. Chem. Soc.,* **1987**, 109, 1589.
79. H. Yersin and A. Vogler, *Photochemistry and Photophysics of Coordination Compounds;* Eds.; Springer-Verlag: Berlin, **1987**; p 135.
80. T. K. Aldridge, E. M. Stacy, D. R. McMillin, *Inorg. Chem*. **1994**, 33, 722.
81. H. Yessin, D. Donges, *Top. Curr. Chem.,* **2001**, 214, 81.
82. J. W. Seo, S. Kim and S. Y. Park, *J. Am. Chem. Soc.*, **2004**, 126, 11154
83. E. A. Plummer, J. W. Hofstraat, L. De Cola, *Dalton Trans*. **2003**, 2080.
84. P. Didier, L. Ortmans, A. K. D. Mesmaeker, R. J. Watts, *Inorg. Chem.*, **1993**, 32, 5239.
85. A. P. Wilde and R. J. Watts, *J. Phys. Chem.* **1991**, 95, 622-629
86. K. Ichimura, T. Kobayashi, K. A. King, R. J. Watts, *J. Phys. Chem.,* **1987**, 91, 6104.
87. A. P. Wilde, K. A. King and R. J. Watts, *The Journal of Physical Chemistry,* **1991,** 95.
88. J. Brooks,Y. Babayan, S. Lamansky, P. I. Djurovich, I. Tsyba, R. Bau, M. E.Thompson, *Inorg. Chem.,* **2002**, 41, 3055.

Chapter 5

Synthesis, characterisation and physical properties of Ir (III) complexes based on N-N bound polypyridyl ligands

A rapid and efficient synthetic route for the preparation of heteroleptic [Ir(polypyridyl-N,N')$_3$]$^{3+}$ type complexes is reported. In the first step [Ir(bpy-N,N)$_2$Cl$_2$]$^+$ type precursors such as [Ir(bpy)$_2$Cl$_2$]$^+$, [Ir(phen)$_2$Cl$_2$]$^+$, [Ir(dmbpy)$_2$Cl$_2$]$^+$, [Ir(dtbpy)$_2$Cl$_2$]$^+$ and their deuteriated analogous are prepared. The formation of the orthometallated complex, [Ir(bpy-N,N')$_2$(bpy-C,N')]$^{2+}$ is also reported. The ratio between this cyclometallated species and the main product [Ir(bpy)$_2$Cl$_2$]$^+$ is affected by deuteriation of the bpy ligand. The reaction pathway for the formation of these polypyridyl systems has been investigated using time dependent NMR and HPLC analysis. The removal of chlorides from these complexes were successfully carried out resulting in the formation of triflate intermediates and heteroleptic [Ir(polypyridyl-N,N')$_3$]$^{3+}$ complexes.

5.1 Introduction

For the last number of years interest in the design of molecular assemblies for application in sensing,[1] molecular electronics,[2] photocatalysis,[3] solar cells[4] and light emitting diodes has continuously increased.[5,6] Many of the approaches taken were based on metal polypyridyl ligands such as 2,2'-bipyridine (bpy) and 1,10-phenanthroline (phen).[7] This approach has been very successful in particular for Ru, Os, Rh and Re metal complexes, however for iridium (III) complexes a different route has been developed based on cyclometallating ligands such as phenyl pyridines and pyridine triazoles.[8] Polypyridyl ligands such as bpy, phen and others have only seldom been investigated and little work has been reported during the past 20 years on the chemistry of $[Ir(bpy)_2Cl_2]^+$ and other similar compounds.[9,10] From the early 1970's many attempts were made to develop efficient high yield synthetic pathways for the preparation of N-N bound polypyridyl complexes. In general it proved difficult to even prepare complexes such as $[Ir(bpy)_2Cl_2]^+$ while the use of such precursors for the preparation of heteroleptic compounds of the type $[Ir(bpy)_2(L\text{-}L)]^+$ has not been developed. The main factors that prevented its investigation is the multi step synthetic procedures reported before[11] resulting in low yields combined with the formation of a series of side products.[12,13,14,15] The ligand 2,2'-bipyridine (bpy) has been used extensively due to its rigidity which leads to a high preference for the bidentate binding mode and ease with which it chelates most transition metal ions.[12] Iridium (III) complexes of 2,2'-bipyridine (bpy) are difficult to prepare and purify [16] compared to the isoelectronic and isostructural analogues of Ru^{II} and Os^{II} due to its unexplored reaction mechanism and kinetically sluggish substitution rates.[17,18,19,20,21,22]

5.1.1 *Photophysical properties of iridium (III) bis polypyridyl and tris polypyridyl complexes - $[Ir(L)_2(X)_2]^+$ and $[Ir(L)_3]^{3+}$, L = bpy/phen, X = Cl, Br, I*

Almost all of the reported publications on $[Ir(polypyridyl)_2Cl_2]^+$ and $[Ir(polypyridyl)_3]^{3+}$ complexes came in the period of 1960-1980, most of which are included in this chapter.[10-54] However the synthesis of these complexes was tedious and involved elaborate work up procedures. This resulted in complexes with small amounts of impurities and the photophysical data obtained from these systems are sometimes questionable. By developing an efficient synthetic procedure and obtaining these complexes in 100 % purity, the excited state photophysics of these complexes can be investigated in more detail. A brief description of the excited state photophysics of iridium (III) polypyridyl complexes is summarised below. These results and explanations were used to determine excited states of the analogous complexes reported in sections 5.3.5, 5.3.6, 5.3.7 and 5.3.8.

The ligands 2,2'-bipyridine and 1,10-phenanthroline form complexes with a large number of transition metals. In particular, the luminescence of the bis and tris complexes of 2,2'-bipyridine and 1,10-phenanthroline with ruthenium (II) have been extensively studied.[23,24,25] The luminescence in these complexes was said to arise primarily from a spin-forbidden triplet charge transfer (d-π*) transition. Although much less work has been done on the iridium (III) complexes of these ligands, the luminescence spectra of $[Ir(phen)_2Cl_2]^+$ and $[Ir(bpy)_2Cl_2]^+$,[10,21(b)] have been reported. The emission of the former ion at 77 K has been assigned by Crosby to a mixture of charge-transfer (d-π*) and ligand centered (π-π*) transitions.[10] Measurements of the quantum yield and lifetime of the luminescence of the phenanthroline complex at 77 K revealed that emission occurs with a high efficiency and the radiative lifetime is 14 µs.[26] DeArmond and Hil1s [21(b)] suggested that these emissions could be labeled as “delocalized molecular’’ due to large mixing of d and π orbitals. The absorption spectrum of $[Ir(bpy)_2C1_2]^+$ is dominated by Ir (III) to bpy charge transfer bands (d-π*) in the visible region and internal bpy bands (π-π*) in the ultraviolet region.[21(b),10] It is noteworthy that the band around 400-450 nm also has been reported in the absorption spectra of $[Ir(bpy)_3]^{3+}$ where it has been assigned as a intra ligand ^{3}π-π* transition.[27] The water coordinated complexes $[Ir(bpy)_2(H_2O)Cl]^{2+}$ and $[Ir(bpy)_2(H_2O)_2]^{3+}$ also show absorption bands around 360 nm and 352 nm which are also assigned as d-π* transitions and their progressive movement to shorter wavelengths illustrates the influence of the π-donating Cl^- ligand on the energy of d-π* states.[21(b)] The interpretation of the absorption spectra of the hydroxo complexes is based upon the same principles that was applied to the aquo complexes with the following exception; the OH^- ligand is a better π donor than $C1^-$, and should therefore lower the energy of the d-π* bands.[28] This influence is apparent in the movement of the 380 nm d-π* absorption band of $[Ir(bpy)_2Cl_2]^+$ to 386 nm in $[Ir(bpy)_2(OH)Cl]^+$ and to 400 nm in $[Ir(bpy)_2(OH)_2]^+$.[29] These bands are extremely broad and tail beyond 500 nm.[29]

The photophysics of the complex [Ir(bpy)$_2$Cl$_2$]$^+$ has been studied at 77 K in rigid glasses.[10,21(b)] Due to the failure of the system to attain thermal equilibrium between the excited d-π* and π-π* states, luminescence properties are associated primarily with emissions from the higher energy d-π* states. The emission of [Ir(bpy)$_3$]$^{3+}$ in ethanol : methanol (4:1) glass at 77 K, has been assigned as an intra ligand π-π* transition from a ^{3}π-π* state of bidentate bpy[27] as shown in figure 5.1 below, whereas the 77 K emission of [Ir(bpy)$_2$C1$_2$]$^+$ has been assigned to a combination of π-π* and d-π* states, and illustrates that two π donating C1$^-$ ligands lower the energy of d-π* levels below the π-π* states. This effect of π donating ligands on the luminescence is further illustrated by the chlorohydroxo and dihydroxo complexes.[12] The large red shifts and broadening of the emissions of these complexes relative to the chloroaquo and diaquo complexes suggest that both emissions are due to d-π* states which are largely influenced by the strong π donating effect of OH$^-$ in the coordination sphere of iridium (III). The emission maximum of [Ir(bpy)$_2$(OH)Cl]$^+$ is shifted from 530 nm in ethanol : methanol (4:1) glass at 77 K to 510 nm in methanol : water at 77 K. A shift from 550 to 540 nm is also found in [Ir(bpy)$_2$(OH)$_2$]$^+$ as expected for d-π* emissions. The emissions of the diaquo complexes are very similar to the emission of [Ir(bpy)$_3$]$^{3+}$ in ethanol : methanol at 77 K, which has been assigned as an intra ligand transition from a ^{3}π-π* of bidentate bpy.[27]

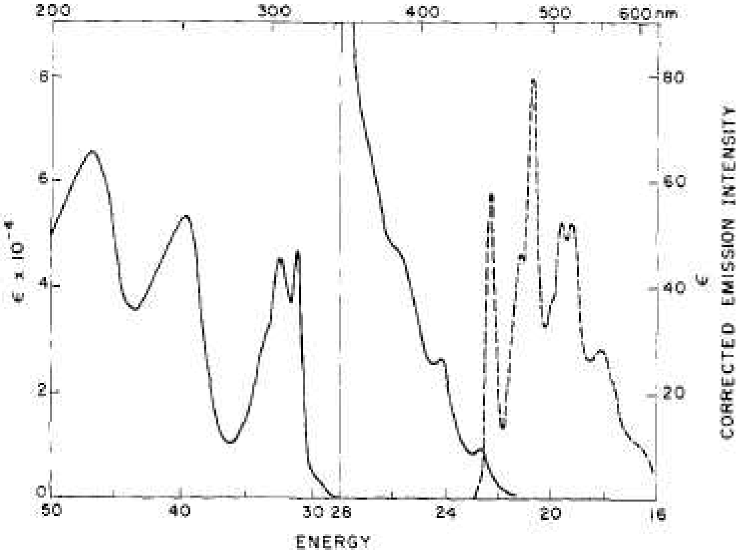

Figure 5.1 *Absorption and luminescence (77 K in ethanol : methanol glass) spectra of [Ir(bpy)$_3$]$^{3+}$* [27]

The emission of [Ir(phen)$_2$Cl$_2$]$^+$ was assigned to a predominantly d-π* state with some π-π* character.[21(d)] As the solvent polarity is increased, the lower level d-π* state is raised in energy closer to the π-π* state; the decreased energy gap increases mixing of the π-π* state into the emitting d-π* state, which increases the ligand character of the emission of [Ir(phen)$_2$Cl$_2$]$^+$ in polar solvents.[30] [Ir(bpy)$_3$]$^{3+}$ and [Ir(phen)$_3$]$^{3+}$ complexes are found to have photoproperties that indicate the existence of several closely spaced low lying excited states of different orbital percentage.[31] Examples of various ordering of metal centered (d-d), ligand centered (π-π*), and metal to ligand charge transfer (d-π*) excited states are found among complexes of Ru(II),[32,33] Rh(III),[34,35] Fe(II),[36,37] Os(II),[38,39] and Ir(III).[27,12,40,19]

The room temperature (298 K) absorption spectrum of [Ir(phen)$_3$]$^{3+}$ consists of three major peaks that are assigned to π-π* transitions by analogy with the [Rh(phen)$_3$]$^{3+}$ spectra.[41] Similar assignments have been made for [Ir(bpy)$_3$]$^{3+}$.[27] The emission is predominantly π-π* phosphorescence.[41] There is no overlap between the absorption and emission spectra. The emission shapes are essentially insensitive to different solvents.[27(a)] The 77 K emission spectrum of [Ir(phen)$_3$]$^{3+}$ is also assigned as π-π* phosphorescence The much longer room temperature lifetime in polar solvents (80 μs in H_2O for [Ir(phen)$_3$]$^{3+}$ compared to 3.7 μs in MeCN) is explained by an increase in energy of the d-π* level relative to the π-π* level as the polarity of the solvent increases. Less contribution of the shorter lived d-π* state with the predominantly longer lived π-π* level increases the lifetime of [Ir(phen)$_3$]$^{3+}$ in polar solvents. This is similar to the solvent dependencies reported earlier by Watts.[30] The low temperature (77 K) emission spectrum of [Ir(phen)$_3$]$^{3+}$ in 4:1 methanol:water published by DeGraff et. *al* is given in figure 5.2 below.

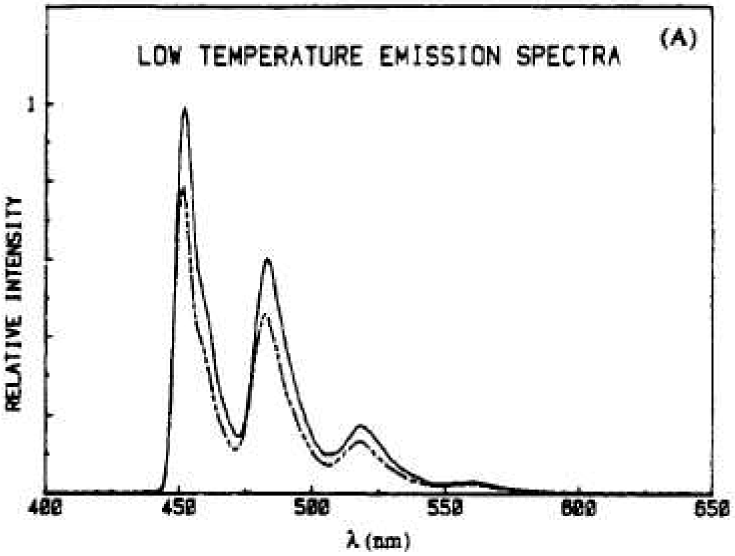

Figure 5.2 *Low temperature emission spectrum of [Ir(phen)$_3$](ClO$_4$)$_3$ in 4:1 MeOH:H$_2$O* [42]

In many ways, the photochemistry and photophysics of [Ir(bpy)$_2$Cl$_2$]$^+$ appear to be analogous to those of [Ir(phen)$_2$Cl$_2$]$^+$, where more detailed photochemical studies[20(a),43] have been performed. Chloride photoaquation of the latter complex has been attributed[47] to a π-π* excited state, and although some debate concerning the energy of this state relative to the d-π* state has occured,[16,44] studies[45,46] showed that the π-π* state is the lower of the two. The marked similarity between the photophysical and photochemical properties of [Ir(bpy)$_2$Cl$_2$]$^+$ and [Ir(phen)$_2$Cl$_2$]$^+$ indicate that chloride photosolvation in the former arises from a π-π* excited state just as it does in the latter.[47]

The effect of phenyl substituted 2,2'-bipyridine (dpbpy) and 1,10-phenanthroline (dpphen) ligands in iridium (III) complexes excited state photophysics at 77 K was also studied in detail by Watts and Crossby.[10,47] The energy of the lowest lying ligand triplet state is red shifted by the introduction of the phenyl substituents. Watts suggested that the energy of emitting state of [Ir(dpphen)$_2$Cl$_2$]$^+$ lies much lower than that of the [Ir(phen)$_2$Cl$_2$]$^+$ complex and this difference is greater than the energy difference of the emitting states of [Ir(dpbpy)$_2$Cl$_2$]$^+$ and [Ir(bpy)$_2$Cl$_2$]$^+$ complexes. He suggested therefore a higher red shift in emission of the former case to be twice that of the latter.[51] He suggested the occurrence of a strong (d-π*)-(π-π*) configurational interaction for the complex [Ir(dpphen)$_2$Cl$_2$]$^+$. The luminescence of [Ir(dpbpy)$_2$Cl$_2$]$^+$ was assigned to a normal d-π* transition, but for [Ir(dpphen)$_2$Cl$_2$]$^+$ they were not able to give a proper assignment due to close proximity of the d-π* state with the π-π* state, which can result in an inversion at 77 K.[51]

In studies of light emission from heterobischelated complexes of iridium (III) with phen, bpy, and 5,6-dimethyl-l,10-phenanthroline (5,6-mephen), Watts[48] established that multiple emissions from thermally nonequilibrated states occur in [Ir(phen)(5,6-mephen)Cl$_2$]Cl. However, the very slight deviation from exponential luminescence decay which was observed for [Ir(phen)(bpy)Cl$_2$]Cl, indicates that the electronic excited states of this complex may be close to thermal equilibration. These results suggest that π-π* and d-π* states may be sufficiently uncoupled to emit independently, but that two d-π* states are coupled strongly enough to approach thermal equilibration.[49] Studies of heteroleptic complexes of Ru (II) appear to confirm the conclusion that d-π* states undergo rapid thermal equilibration.[50] Finally in 1977 Balzani's group re-examined the photophysics of phen derivatives[16] and concluded that due to the complex synthetic procedures, very small amounts of by-products which are very difficult to eliminate resulted in a dual emission for all these systems at 77 K. This really shows the importance of measuring the excited state photophysics of all these iridium (III) polypyridyl complexes again which are 100 % pure by confirmation using NMR, CHN and HPLC, showing that other than the main product no by-products are present in any of these complexes.

5.1.2 Applications of Ir (III) polypyridyl complexes

5.1.2.1 Phosphorescent Ir (III) complexes in OLED applications

During the last two decades, extensive research effort has been focused on the synthesis and photochemical properties of cyclometalated 4d^6 and 5d^6 complexes.[51,52,53] The major interest behind these studies is not only to understand the fundamental mechanism associated with the electron transfer processes but also to apply this knowledge to a variety of applications.[54,55,56,57] In particular, iridium complexes have been investigated thoroughly because they can be used as phosphorescent molecules in the organic light emitting diodes (OLEDs).[58,59,60] They possess high luminescence efficiencies as well as long lived excited states mainly due to the strong spin-orbit coupling of the iridium (III).[61,62] The interest in phosphorescent iridium (III) complexes is growing rapidly, however, the most outstanding characteristic of this class of complexes might be the variability of the electro optical properties. Their metal ligand based luminescence provides the opportunity to tune the emission colour over the whole visible spectrum by varying the attached ligands.[63,64] All these criteria make iridium (III) complexes highly appealing as phosphors in multicolor OLEDs.

While common light emitting diodes (LEDs) produce light by electroluminescence of III–V group mixed crystal inorganic semiconductors, organic LEDs (OLEDs) generate light from organic or organometallic molecules.[64] These devices generally have a multilayer architecture where a thin film of one or more light emitting materials is sandwiched between two electrodes, one of which must be transparent to light. Additional layers (e.g. ETL(electron transporting layer), HBL(hole blocking layer), HIL(hole injection layer), HTL(hole transporting layer)) assist charge injection and transport from the electrodes to the light emitting film, improving significantly the device performances. Upon application of a bias voltage to the electrodes, electrons and holes are injected into the organic stack. They migrate through the respective charge transporting layers and recombine in the emitting molecules, forming excited states (excitons) that can generate light by radiative decay.

The most prominent coordination motifs are cyclometallating ligands, available in a wide range. Triscyclometallated homo and heteroleptic complexes, as well as bis-cyclometallated ones, are the most common phosphorescent iridium (III) species.[68] A variety of so called ancillary ligands gives additional possibilities to define structure and to tune the properties. Neutral and charged complexes are accessible, and the ligand design spans from small modifications and functionalizations over dendritic layouts to polymeric assemblies.[65] In particular, polymers containing iridium (III) complexes are gaining interest, with features of both phosphor and polymer matrix combined within one material.

5.1.2.2 Phosphorescent Ir (III) complexes in oxygen sensing

The long-lived triplet excited state of luminescent iridium (III) complexes enables the efficient transfer of energy to the triplet ground state of molecular oxygen, resulting in luminescence quenching and the generation of singlet oxygen.[66] This feature of iridium (III) luminophores can be utilized as a sensitive oxygen probe in, e.g., medicinal, chemical or environmental sensors.[55,67,68] An experimental array for the measurement of oxygen concentration with respect to medicinal applications, i.e., for intraocular measurements, was recently introduced by Nazeeruddin and co-workers.[69]

Since the oxygen concentration is in general related to sudden changes in the luminescence of the iridium (III) complex, new materials with high quantum yields and long excited-state lifetimes (i.e., up to several microseconds) for reliable, sensitive detection are the focus of current research.[60] Among others, mixed-ligand iridium (III) complexes are highly promising candidates, due to their well-tunable excited state properties, high durability, and stability towards the generated singlet oxygen. However, for successful development of solid state iridium (III) containing sensors, the compatibility of the luminescent dye with the polymer matrix represents a crucial requirement.[70]

Beyond the development of novel luminescent probes for molecular oxygen, highly sensitive systems based on iridium (III) complexes for the sensing of various anions,[71] amino acids,[72] and alkali[73] as well as heavy transition metal cations[74] has been introduced in recent years.

5.1.2.3 Cationic Iridium (III) Complexes in Bioanalytical Applications

Besides the previously discussed chemosensory applications, their electrochemical and photophysical properties have been made iridium (III) complexes also highly promising candidates as labeling reagents and probes in biological systems.[75] Sensitive, time resolved detection is enabled due to their intense emission and excited state lifetimes. For applications as labeling compounds for luminescence imaging in biomaterials, charged iridium (III) complexes can be bound covalently[76] or non-covalently, e.g., by DNA or protein intercalation,[77] to biological substrates. Generally, the bound complexes exhibit luminescence properties that significantly differ from that of the free substrate, due to changes in rigidity and hydrophobicity of the surroundings.[78] Therefore, the facile monitoring of bioconjunction reactions or the investigation of binding affinities can be conducted utilizing such luminescent iridium (III) complexes.

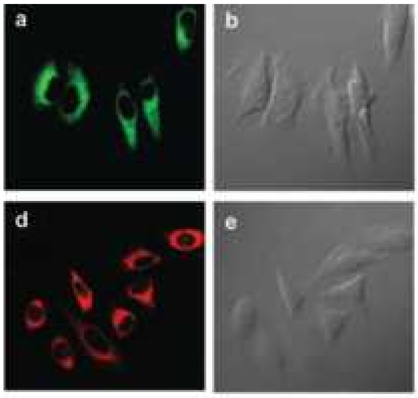

Figure 5.3 *Confocal luminescence (a,d) and brightfield images (b,e) of living HeLa cells incubated with 20 mM of a green (top) or red iridium(III) emitter (bottom) in DMSO/phosphate buffer solution.*[79]

The exceeding potential of charged phosphorescent iridium (III) complexes in modern biomedical research is highlighted by the first example of bioimaging of living cells using such complexes. *Yu et. al.* successfully introduced phosphorescent complexes into the cytoplasm of cervical cancer cells (HeLa) and observed low cytotoxicity and reduced photobleaching, compared to conventional dyes (figure 5.3).[79]

5.1.2.4 Iridium (III) N^N polypyridyl complexes for intermolecular photocatalytic H_2 generation

Various types of transition metal complexes (e.g., based on Rh^I, Ru^{II}, Ir^{III} or Pt^{II}) have been employed as photosensitizers,[80,81,82] but heteroleptic cyclometallated iridium (III) complexes have gained attraction in this field due to their highly tunable photophysical properties. Bernhard and co-workers have introduced iridium (III) based sensitizers featuring remarkable improvements in the production of molecular hydrogen, compared to previously investigated Ru (II) based systems.[3,99,103] But up to now iridium N^N polypyridyl complexes of the type reported in this chapter have not been used for hydrogen generation. This is the first report based on intermolecular photocatalysis using visible light (470 nm) and UV light (350 nm) for iridium (III) N^N polypyridyl complexes and very good Turn Over Numbers (TON's) were obtained than the conventional cyclometallated systems, thereby making these complexes potentially important candidates for future research.

In this chapter novel high yield synthetic method for making [Ir(polypyridyl)$_2$Cl$_2$]PF$_6$ complexes and their deuteriated analogues in high purity are discussed. Successfull removal of chlorides was achieved from these complexes novel tris heteroleptic complexes were synthesised through triflate intermediates which are also discussed in the synthetic section. The characterisation of these complexes was achieved using 1D and 2D NMR spectroscopy, mass spectrometry, CHN analysis and HPLC measurements. The time dependent HPLC and NMR analysis of the reaction of these complexes provided possible reaction intermediates and side products. Detailed photophysics of all these complexes were studied which include absorption, emission (298 K and 77 K) and lifetimes (298 K and 77 K) which helped to assign the excited states for these complexes and to explain the dual emission properties of these complexes at 77 K. The photocatalytic H_2 production experiments for these complexes, carried out at two different excitation wavelength (470 nm and 350 nm) is discussed in the last section. This is the first report based on report of H_2 production from iridium (III) N^N polypyridyl complexes.

5.2 Experimental

5.2.1 Synthesis of [Ir(bpy)$_2$Cl$_2$]PF$_6$ (I) and [Ir(bpy-N,N')$_2$(bpy-C,N')](PF$_6$)$_2$ (II)

Iridium trichloride hydrate (0.10 g, 0.3349 mmol) was reacted with 2,2'-bipyridyl (bpy) (0.105 g, 0.6696 mmol) dissolved in 1 cm^3 of glycerol. The reaction was heated to reflux temperature (300 ^{0}C) for 25 minutes when the colour of the solution has changed from red to straw yellow. The solution was cooled to room temperature and 5 cm^3 of water was added. The mixture was filtered and washed with 5 ml of diethyl ether. To the filtrate 10 ml of saturated NaCl solution was added yielding [Ir(bpy)$_2$Cl$_2$]Cl which was filtered and dried. The complex was then dissolved completely in water to which saturated aqueous KPF$_6$ was added resulting in the precipitation of complex **I**, which was filtered, washed with 20 cm^3 of deionised water and dried. Complex **I** was then dissolved in a minimal amount of acetone and reprecipitated by adding excess diethyl ether and hexane, the precipitated complex was vacuum filtered, washed with diethyl ether and hexane. This procedure was repeated 3-4 times in order to remove any traces of glycerol. (Yield: 0.12 g, 0.1665 mmol, 70 %). ^{1}H NMR (400 MHz, DMSO), δ (ppm): 7.51 (t, 1H, H5'), 7.83 (d, 1H, H6'), 8.12 (t, 1H, H5), 8.20 (t, 1H, H4'), 8.52 (t, 1H, H4), 8.82 (d, 1H, H3'), 8.93 (d, 1H, H3), 9.65 (d, 1H, H6). ^{13}C (100 MHz, DMSO), δ (ppm): 125.1, 128.7, 140.8, 141.4, 151, 157.6. m/z expected: 575.49, obtained: 575.03. Elemental analysis for complex I, $C_{20}H_{16}Cl_2F_6IrN_4P$; (calculated) : C :33.34, H :2.24, N :7.78; (found) : C :33.29, H :2.13, N :7.37

The filtrate obtained after precipitating out [Ir(bpy)$_2$Cl$_2$]Cl was concentrated, dried and stirred with 20 cm^3 of DCM, filtered and the process is repeated until all of excess bipyridine and any remaining fraction **I** are removed. The yellow residue was dried and 20 cm^3 of dry methanol was added. The solution was then stirred, filtered, concentrated and chromatographed on Sephadex (LH : 20) using ethanol to yield [Ir(bpy-N,N')$_2$(bpy-C,N')](Cl)$_2$ in pure form. The complex was then dissolved completely in water to which saturated aqueous KPF$_6$ was added resulting in the precipitation of complex **II**, which was vacuum filtered, washed with deionised water and dried. (Yield: 0.015 g, 0.0157 mmol, 5 %). ^{1}H NMR (400 MHz, DMSO), δ (ppm): 9.04 (d, 1H, D3), 9.01 (d, 1H, C3'), 8.96 (m, 2H, E3', F3'), 8.45 (m, 3H, C4', E4', F4), 8.42 (d, 1H, A6), 8.38 (m, 2H, B3', B4'), 8.21 (t, 1H, D4), 8.01 (d, 1H, D6), 7.91 (d, 1H, D5), 7.90 (d, 1H, C6'), 7.81 (m, 2H, E6', F6), 7.72 (d, 1H, B6'), 7.67 (m, 3H, C5', E5', F5), 7.48 (t, 1H, B5'), 7.08 (m, 1H, A5), 6.58 (d, 1H, A4).

5.2.2 Synthesis of [Ir(d$_8$bpy)$_2$Cl$_2$]PF$_6$ (III) and [Ir^{III}(d$_8$bpy-N,N')$_2$(d$_8$bpy-C,N')](PF$_6$)$_2$ (IV)

These compounds were obtained using the method outlined above. Iridium trichloride hydrate (0.10 g, 0.3349 mmol) was combined with deuteriated 2,2'-bipyridyl (d$_8$bpy) (0.1153 g, 0.6696 mmol) and dissolved in 1 cm^3 of glycerol. (Yield: 0.15 g, 0.2037 mmol, 80 %). ^{1}H NMR (400 MHz, DMSO), δ (ppm): 7.51 (resid. s, H5'), 7.83 (resid. s, H6'), 8.12 (resid. s, H5), 8.20 (resid. s, H4'), 8.52 (resid. s, H4), 8.82 (resid. s, H3'), 8.93 (resid. s, H3), 9.65 (resid. s, H6). Elemental analysis for complex **III**, $C_{20}D_{16}C_{l2}F_6IrN_4P$; (calculated) : C :32.58, H :2.17, N :7.60; (found) ; C :32.75, H :2.14, N :7.77.

The filtrate obtained after precipitating out [Ir(d$_8$bpy)$_2$Cl$_2$]Cl was concentrated, dried and stirred with 20 cm^3 of DCM, filtered and the process is repeated until all of excess bipyridine and any remaining fraction III are removed. The yellow residue was dried and 20 cm^3 of dry methanol was added. The solution was then stirred, filtered, concentrated and chromatographed on Sephadex (LH: 20) using ethanol to yield [Ir(d$_8$bpy-N,N')$_2$(d$_8$bpy-C,N')](Cl)$_2$ in pure form. The complex was then dissolved completely in water to which saturated aqueous KPF$_6$ was added resulting in the precipitation of complex **IV**, which was vacuum filtered, washed with deionised water and dried. (Yield: 0.010 g, 0.0102 mmol, 3 %). ^{1}H NMR (400 MHz, DMSO), δ (ppm): 9.04 (resid. s, D3), 9.01 (resid. s, C3'), 8.96 (resid. s, E3', F3'), 8.45 (resid. s, C4', E4', F4), 8.42 (resid. s, A6), 8.38 (resid. s, B3', B4'), 8.21 (resid. s, D4), 8.01 (resid. s, D6), 7.91 (resid. s, D5), 7.90 (resid. s, C6'), 7.81 (resid. s, E6', F6), 7.72 (resid. s, B6'), 7.67 (resid. s, C5', E5', F5), 7.48 (resid. s, B5'), 7.08 (resid. s, A5), 6.58 (resid. s, A4).

5.2.3 Synthesis of [Ir(phen)$_2$Cl$_2$]PF$_6$ (V)

Iridium trichloride hydrate (0.10 g, 0.2836 mmol) was combined with two equivalents of 1, 10-phenanthroline (phen) (0.102 g, 0.567 mmol) dissolved in 1 cm^3 of glycerol. The reaction mixture was heated at reflux (300 ^{0}C) for 25 minutes until the colour of the solution changes from red to straw yellow. The solution was cooled to room temperature and 5 cm^3 of deionised water was added. The mixture was filtered and saturated aqueous KPF$_6$ was added resulting in the precipitation of complex **V**, which was vacuum filtered, washed with 20 cm^3 of deionised water and dried. Complex **V** was then dissolved in minimal amount of acetone and reprecipitated by adding excess diethyl ether and hexane, the precipitated complex was vacuum filtered, washed with diethyl ether and hexane. This procedure was repeated 3-4 times inorder to remove any traces of glycerol. (Yield: 0.160 g, 0.2082 mmol, 90 %). ^{1}H NMR (400 MHz, DMSO), δ (ppm): 7.69 (m, 1H, H8), 8.08 (d, 1H, H9), 8.38 (d, 1H, H6), 8.49 (m, 2H, H4, H5), 8.76 (d, 1H, H7), 9.16 (d, 1H, H3), 9.94 (d, 1H, H2). Elemental analysis for complex **V**, $C_{24}H_{16}Cl_2F_6IrN_4P$; (calculated); C :37.51, H :2.10, N :7.29; (found); C :37.52, H :2.10, N :7.27

5.2.4 Synthesis of [Ir(d$_8$phen)$_2$Cl$_2$]PF$_6$ (VI)

Iridium trichloride hydrate (0.10 g, 0.2836 mmol) was combined with two equivalents of deuteriated 1,10-phenanthroline (d$_8$phen) (0.106 g, 0.567 mmol) dissolved in 1 cm^3 of glycerol. The reaction mixture was heated at reflux (300 ^{0}C) for 25 minutes until the colour of the solution changes from red to straw yellow. The solution was cooled to room temperature and 5 cm^3 of deionised water was added. The mixture was filtered and saturated aqueous KPF$_6$ was added resulting in the precipitation of complex **VI**, which was vacuum filtered, washed with 20 cm^3 of deionised water and dried. Complex **VI** was then dissolved in minimal amount of acetone and reprecipitated by adding excess diethyl ether and hexane, the precipitated complex was vacuum filtered, washed with diethyl ether and hexane. This procedure was repeated 3-4 times inorder to remove any traces of glycerol. (Yield: 0.210 g, 0.2677 mmol, 95 %). ^{1}H NMR (400 MHz, DMSO), δ (ppm): 7.69 (resid. s, H8), 8.08 (resid. s, H9), 8.38 (resid. s, H6), 8.49 (resid. s, H4, H5), 8.76 (resid. s, H7), 9.16 (resid. s, H3), 9.94 (resid. s, H2). Elemental analysis for complex **VI**, $C_{24}D_{16}Cl_2F_6IrN_4P$; (calculated); C :36.74, H :2.05, N :7.14; (found); C :36.91, H :1.80, N :7.47

5.2.5 *Synthesis of [Ir(dmbpy)$_2$Cl$_2$]PF$_6$ (VII)*

Iridium trichloride hydrate (0.10 g, 0.2836 mmol) was combined with two equivalents of 4,4'-dimethyl-2,2'-bipyridyl (dmbpy) (0.1045 g, 0.5672 mmol) dissolved in 1 cm^3 of glycerol. The reaction mixture was heated at reflux (300 ^{0}C) for 10 minutes, cooled and the turbid yellow solution was filtered, washed with 10 cm^3 of deionised water and to the filtrate saturated aqueous KPF$_6$ was added resulting in the precipitation of complex **VII**, which was vacuum filtered, washed with 20 cm^3 of deionised water and dried. Complex **VII** was then dissolved in minimal amount of acetone and reprecipitated by adding excess diethyl ether and hexane, the precipitated complex was vacuum filtered, washed with diethyl ether and hexane. This procedure was repeated 3-4 times inorder to remove any traces of glycerol. (Yield: 0.21 g, 0.2704 mmol, 95 %). ^{1}H NMR (400 MHz, DMSO), δ (ppm): 2.56 (s, 3H), 2.76 (s, 3H), 7.32 (dd, 1H, H5'), 7.59 (d, 1H, H6'), 7.93 (dd, 1H, H5), 8.66 (s, 1H, H3'), 8.76 (s, 1H, H3), 9.42 (d, 1H, H6). Elemental analysis for complex **VII**, $C_{24}H_{24}Cl_2F_6IrN_4P$; (calculated) : C :37.12, H :3.12, N :7.21; (found) : C :36.79, H :2.87, N :6.99.

5.2.6 *Synthesis of [Ir(d$_{12}$dmbpy)$_2$Cl$_2$]PF$_6$ (VIII)*

Iridium trichloride hydrate (0.10 g, 0.2836 mmol) was combined with two equivalents of deuteriated 4,4'-dimethyl-2,2'-bipyridyl (d$_{12}$dmbpy) (0.111 g, 0.5672 mmol) dissolved in 1 cm^3 of glycerol. The reaction mixture was heated at reflux (300 ^{0}C) for 10 minutes, cooled and the turbid yellow solution was filtered, washed with 10 cm^3 of deionised water and to the filtrate saturated aqueous KPF$_6$ was added resulting in the precipitation of complex **VIII**, which was vacuum filtered, washed with 20 cm^3 of deionised water and dried. Complex **VIII** was then dissolved in minimal amount of acetone and reprecipitated by adding excess diethyl ether and hexane, the precipitated complex was vacuum filtered, washed with diethyl ether and hexane.

This procedure was repeated 3-4 times inorder to remove any traces of glycerol. (Yield: 0.26 g, 0.3248 mmol, 98 %). ^{1}H NMR (400 MHz, DMSO), δ (ppm): 2.56 (resid. s, 3H), 2.76 (resid. s, 3H), 7.32 (resid. s, H5'), 7.59 (resid. s, H6'), 7.93 (resid. s, H5), 8.66 (resid. s, H3'), 8.76 (resid. s, H3), 9.42 (resid. s, H6). Elemental analysis for complex **VIII**, $C_{24}D_{24}Cl_2F_6IrN_4P$; (calculated) : C :36.00, H :3.02, N :7.00; (found) : C :36.38, H :2.77, N :7.29.

5.2.7 Synthesis of [Ir(dtbpy)$_2$Cl$_2$]PF$_6$ (IX)

Iridium trichloride hydrate (0.10 g, 0.2836 mmol) was combined with two equivalents of 4,4'-di tertiarybutyl-2,2'-bipyridyl (dtbpy) (0.1522 g, 0.5672 mmol) dissolved in 1 cm^3 of glycerol. The reaction mixture was heated at reflux (300 ^{0}C) for 10 minutes, cooled and some amount of unreacted ligand was filtered. To the filtrate, deionised water was added to which saturated aqueous KPF_6 was added resulting in the precipitation of complex **IX**, which was vacuum filtered, washed with 20 cm^3 of deionised water and dried. Complex **IX** was then dissolved in minimal amount of acetone and reprecipitated by adding excess diethyl ether and hexane, the precipitated complex was vacuum filtered, washed with diethyl ether and hexane. This procedure was repeated 3-4 times inorder to remove any traces of glycerol. (Yield: 0.16 g, 0.1693 mmol, 72 %). ^{1}H NMR (400 MHz, DMSO), δ (ppm): 1.36 (s, 9H), 1.543 (s, 9H), 7.48 (dd, 1H, H5'), 7.62 (d, 1H, H6'), 8.09 (dd, 1H, H5), 8.83 (s, 1H, H3'), 8.93 (s, 1H, H3), 9.48 (d, 1H, H6). Elemental analysis for complex **IX**, $C_{36}H_{48}Cl_2F_6IrN_4P$; (calculated) : C :45.76, H :5.12, N :5.93; (found) : C :45.32, H :5.05, N :5.70

5.2.8 Synthesis of [Ir(d$_{24}$dtbpy)$_2$Cl$_2$]PF$_6$ (X)

Iridium trichloride hydrate (0.10 g, 0.2836 mmol) was combined with two equivalents of deuteriated 4,4'-ditertiarybutyl-2,2'-bipyridyl (d$_{24}$dtbpy) (0.165 g, 0.5672 mmol) dissolved in 1 cm^3 of glycerol. The reaction mixture was heated at reflux (300 ^{0}C) for 10 minutes, cooled and some amount of unreacted ligand was filtered. To the filtrate, deionised water was added to which saturated aqueous KPF_6 was added resulting in the precipitation of complex **IX**, which was vacuum filtered, washed with 20 cm^3 of deionised water and dried. Complex **IX** was then dissolved in minimal amount of acetone and reprecipitated by adding excess diethyl ether and hexane, the precipitated complex was vacuum filtered, washed with diethyl ether and hexane. This procedure was repeated 3-4 times inorder to remove any traces of glycerol. (Yield: 0.81 g, 0.1822 mmol, 80 %). ^{1}H NMR (400 MHz, DMSO), δ (ppm): 1.36 (resid. s), 1.54 (resid. s), 7.48 (resid. s, H5'), 7.62 (resid. s, H6'), 8.09 (resid. s, H5), 8.83 (resid. s, H3'), 8.93 (resid. s, H3), 9.48 (resid. s, H6). Elemental analysis for complex **X**, $C_{36}D_{48}Cl_2F_6IrN_4P.2H_2O$; (calculated) : C :41.98, H :5.05, N :5.44; (found) : C :42.32, H :5.17, N :5.70

5.2.9 Synthesis of [Ir(dpbpy)$_2$Cl$_2$]PF$_6$ (XI)

Iridium trichloride hydrate (0.20 g, 0.5672 mmol) was combined with two equivalents of 4,4'-diphenyl-2,2'-bipyridine (dpbpy) ligand (0.3495 g, 1.1345 mmol) dissolved in 1 cm^3 of glycerol. The reaction mixture was heated at reflux (300 ^{0}C) for 20 minutes, cooled and some amount of unreacted ligand was filtered. To the filtrate, deionised water was added to which saturated aqueous KPF_6 was added resulting in the precipitation of complex **XI**, which was vacuum filtered, washed with 20 cm^3 of deionised water and dried. Complex **XI** was then dissolved in minimal amount of acetone and reprecipitated by adding excess diethyl ether and hexane, the precipitated complex was vacuum filtered, washed with diethyl ether and hexane. This procedure was repeated 3-4 times inorder to remove any traces of glycerol. (Yield: 0.45 g, 0.4390 mmol, 77 %). ^{1}H NMR (400 MHz, DMSO), δ (ppm): 7.65 (m, 6H, Ph(A)), 7.75 (d, 2H, Ph(B)), 7.80 (t, 2H, Ph(B)), 7.92 (d, 2H, H3', Ph(B)), 8.25 (d, 1H, H3), 8.37 (m, 2H, H5, H5'), 8.55 (d, 1H, H6'), 10.11 (d, 1H, H6). Elemental analysis for complex **XI**, $C_{44}H_{32}Cl_2F_6IrN_4P$; (calculated) : C :51.57, H :3.15, N :5.47; (found) : C :51.48, H :3.19, N :5.42

5.2.10 Synthesis of [Ir(dpphen)$_2$Cl$_2$]PF$_6$ (XII)

Iridium trichloride hydrate (0.20 g, 0.5672 mmol) was combined with two equivalents of 4,4'-diphenyl-1,10-phenanthroline (dpphen) ligand (0.3768 g, 1.1345 mmol) dissolved in 1 cm^3 of glycerol. The reaction mixture was heated at reflux (300 ^{0}C) for 20 minutes, cooled and some amount of unreacted ligand was filtered. To the filtrate, deionised water was added to which saturated aqueous KPF_6 was added resulting in the precipitation of complex **XII**, which was vacuum filtered, washed with 20 cm^3 of deionised water and dried. Complex **XII** was then dissolved in minimal amount of acetone and reprecipitated by adding excess diethyl ether and hexane, the precipitated complex was vacuum filtered, washed with diethyl ether and hexane. This procedure was repeated 3-4 times inorder to remove any traces of glycerol. (Yield: 0.48 g, 0.4474 mmol, 78 %). ^{1}H NMR (400 MHz, DMSO), δ (ppm): 7.63 (m, 6H, Ph(A)), 7.74 (d, 2H, Ph(B)), 7.79 (t, 2H, Ph(B)), 7.90 (d, 2H, H8, Ph(B)), 8.24 (d, 1H, H9), 8.36 (m, 2H, H5, H6), 8.54 (d, 1H, H3), 10.10 (d, 1H, H2).. Elemental analysis for complex **XII**, $C_{48}H_{32}Cl_2F_6IrN_4P$; (calculated) : C :53.74, H :3.01, N :5.22; (found) : C :53.49, H :3.03, N :4.95

5.2.11 Synthesis of [Ir(bpy)$_2$(OSO$_2$CF$_3$)$_2$]CF$_3$SO$_3$ (XIII)

1,2 dichlorobenzene (15 cm^3) was added to a 2 necked round bottom flask. Nitrogen was bubbled through the solution for 30 min after which [Ir(bpy)$_2$Cl$_2$]PF$_6$ (0.156 g, 0.2165 mmol) was added and stirred in N_2 for 15 min to which 0.47 cm^3 of neat triflouromethanesulphonic acid was added and stirred for 3 hr at 200 ^{0}C . The reaction mixture was cooled and diethyl ether was added resulting in the precipitation of the product which was filtered and washed with diethyl ether to get the product in full purity. (Yield: 0.178 g, 0.1870 mmol, 85 %). ^{1}H NMR (400 MHz, DMSO), δ (ppm): 7.52 (t, 1H, H5'), 7.69 (d, 1H, H6'), 8.23 (t, 1H, H5), 8.34 (t, 1H, H4'), 8.67 (t, 1H, H4), 8.83 (d, 1H, H3'), 9.02 (m, 2H, H6, H3). Elemental Analysis for complex **XIII**, $C_{23}H_{16}F_9IrN_4O_9S_3$: (calculated) : C :29.02, H :1.69, N :5.89; (found) :C :28.62, H :1.52, N :5.54

5.2.12 Synthesis of [Ir(phen)$_2$(OSO$_2$CF$_3$)$_2$]CF$_3$SO$_3$ (XIV)

1,2 dichlorobenzene (10 cm^3) was taken in a 2 necked round bottom flask. N_2 was bubbled through the solution for 30 min. [Ir(phen)$_2$Cl$_2$]PF$_6$ (0.05 g, 0.0650mmol) was added and stirred in N_2 for 15 min to which 0.17 cm^3 of neat triflouromethanesulphonic acid was added and stirred for 2 hr at 200 ^{0}C . The reaction mixture was cooled and diethyl ether was added resulting in the precipitation of the product which was filtered and washed with diethyl ether to get the product in full purity. (Yield: 0.065 g, 0.0650 mmol, 98 %). ^{1}H NMR (400 MHz, DMSO), δ (ppm): 7.72 (m, 1H, H8), 7.98 (d, 1H, H9), 8.41 (d, 1H, H6), 8.57 (d, 1H, H4), 8.70 (m, 1H, H5), 8.80 (d, 1H, H7), 9.34 (d, 1H, H3), 9.43 (d, 1H, H2). Elemental Analysis for complex **XIV**, $C_{27}H_{16}F_9IrN_4O_9S_3.H_2O$; (calculated) : C :31.86, H :1.78, N :5.50; (found) : C :31.42, H :1.55, N :5.87.

5.2.13 Synthesis of [Ir(dmbpy)$_2$(OSO$_2$CF$_3$)$_2$]CF$_3$SO$_3$ (XV)

1,2 dichlorobenzene (10 cm^3) was taken in a 2 necked round bottom flask. N2 was bubbled through the solution for 30 min. [Ir(dmbpy)$_2$Cl$_2$]PF$_6$ (0.102 g, 0.1314 mmol) was added and stirred in N_2 for 15 min to which 0.23 cm^3 of neat triflouromethanesulphonic acid was added and stirred for 2 hr at 200 ^{0}C . The reaction mixture was cooled and diethyl ether was added resulting in the precipitation of the product which was filtered and washed with diethyl ether to get the product in full purity. (Yield: 0.108 g, 0.1072 mmol, 82 %). ^{1}H NMR (400 MHz, DMSO), δ (ppm): 2.61 (s, 3H), 2.79 (s, 3H), 7.32 (d, 1H, H5'), 7.45 (d, 1H, H6'), 8.16 (d, 1H, H5), 8.68 (s, 1H, H3'), 8.79 (d, 1H, H6), 8.85 (s, 1H, H3). Elemental Analysis for complex **XV**, $C_{27}H_{24}F_9IrN_4O_9S_3.H_2O$; (calculated) : C :31.61, H :2.55, N :5.46; (found) : C :31.23, H :2.26, N :5.20

5.2.14 Synthesis of [Ir(dmbpy)$_2$(HPhpytr)](CF$_3$SO$_3$)$_3$ (XVI)

1,2 dichlorobenzene (15 cm^3) was taken in a 2 necked round bottom flask. Nitrogen was bubbled through the solution for 30 min to which the ligand Hphpytr (0.0482 g, 0.2183 mmol) was added and stirred in N_2 for 15 min to which [Ir(bpy)$_2$(OSO$_2$CF$_3$)$_2$]CF$_3$SO$_3$ (0.110 g, 0.1091 mmol) was added & refluxed overnight at 210 ^{0}C . The reaction mixture was cooled and diethyl ether was added resulting in the precipitation of the product which was filtered, washed with diethyl ether and recrystalised from acetone: water (1:1) mixture to get the product in full purity. (Yield: 0.248 g, 0.2016 mmol, 82 %). ^{1}H NMR (400 MHz, DMSO), δ (ppm): 2.62 (dd, 6H), 2.66 (dd, 6H), 7.37 (m, 3H), 7.45 (d, 1H), 7.50 (d, 1H, H6'), 7.52 (dd, 1H, H5'), 7.57 (dd, 1H), 7.61 (m, 2H, H5, H6), 7.75 (m, 3H), 7.86 (m, 2H, H5'', H6''), 7.91 (d, 1H), 8.31 (m, 2H, H5''', H6'''), 8.82 (s, 1H, H3'), 8.84 (s, 1H, H3), 8.88 (s, 1H, H3''), 8.90 (s, 1H, H3'''). Elemental Analysis for complex **XVI**, $C_{40}H_{35}F_9IrN_8O_9S_3$; (calculated) : C :39.02, H :2.87, N :9.10; (found) : C :39.07, H :2.83, N :9.01

5.3 Results and Discussion

5.3.1 Synthetic Considerations

[Ir(bpy)$_3$]$^{3+}$ has been prepared by reaction of iridium sulphates with bpy in a halide free medium.[27] It is considerably more difficult to bind three bpy's to iridium (III) than it is to other metal ions.[83] The synthesis for *cis*-[Ir(phen)$_2$Cl$_2$]Cl was first described in 1964 by *Chiswell et al.*,[9] which was prepared in 27 % yield by heating K_3IrCl_6 with 1,10-phenanthroline at 220 °C for 14 h. In 1971 Broomhead *et al.* reported a different synthesis.[84] These early examples reflect the synthetic difficulties usually encountered when preparing simple iridium (III) complexes. Our work focuses firstly on the preparation of [Ir(bpy)$_2$Cl$_2$]$^+$ (**I**), [Ir(phen)$_2$Cl$_2$]$^+$ (**V**), [Ir(dmbpy)$_2$Cl$_2$]$^+$

(**VII**), $[Ir(dtbpy)_2Cl_2]^+$ (**IX**) complexes and their deuteriated analogous in high purity and yield. Studies were carried out on the effect of deuteriation on formation of $[Ir(bpy\text{-}N,N')_2(bpy\text{-}C,N')]^{2+}$ (**II**) along with $[Ir(bpy)_2Cl_2]^+$ (**I**). Secondly the removal of inner sphere chlorides from these complexes forming stable triflate intermediates and coordination of new ligands there by opens a new synthetic route towards novel homoleptic and heteroleptic tris iridium (III) polypyridyls.

A series of experiments aimed at developing an efficient high yield synthetic method for $[Ir(bpy)_2Cl_2]PF_6$ has been carried out. In these studies a variety of solvents including ethylene glycol, ethanol, methoxyethanol, ethanol : H_2O (1:1) were investigated. In addition the reaction times were varied systematically from 25 min to 3 days. Reaction was also carried out in the temperature range 150 ^{0}C and 310 ^{0}C. The best results were obtained by heating $IrCl_3.3H_2O$ with bpy in glycerol at reflux temperature for 25 minutes at 300 ^{0}C. By increasing the reaction temperature and by using a short reaction time the formation of intermediate species and the trans isomer were suppressed. With this method the reaction time is reduced considerably and $[Ir(bpy\text{-}N,N')_2Cl_2]^+$ (**I**) was obtained in high purity and in a good yield without the employment of further purification methods such as column chromatography. The method employed has a yield higher than the microwave synthetic method reported recently.[85] A second product, $[Ir(bpy\text{-}N,N')_2(bpy\text{-}C,N')]^{2+}$ (**II**), could be obtained from the reaction mixture by working up the remaining reaction mixture. For the synthesis of the heteroleptic iridium complex (**XVI**) the solvent and reaction temperature play a crucial role, the reaction was attempted in various solvents but 1,2 dichlorobenzene at a refluxing temperature of 210 ^{0}C was successful. The schematic representation of the general synthetic method followed by taking 2,2'-bipyridyl (bpy) and 4,4'-dimethyl-2,2'-bipyridine (dmbpy) as the polypyridyl ligands are given in figure 5.4.

$$IrCl_3.3H_2O + \text{2,2'-bipyridyl} \xrightarrow[300^oC]{\text{Glycerol, 25min}} \underset{\mathbf{I}}{[Ir^{III}(bpy\text{-}N,N')_2Cl_2]^+} + \underset{\mathbf{II}}{[Ir^{III}(bpy\text{-}N,N')_2(bpy\text{-}C,N')^-]^{2+}}$$

$$\underset{\mathbf{I}}{[Ir^{III}(bpy\text{-}N,N')_2Cl_2]^+} \xrightarrow[\text{1,2-dichlorobenzene, }200^oC]{CF_3SO_3H\text{, 2h}} \underset{\mathbf{XIII}}{[Ir^{III}(bpy\text{-}N,N')_2(CF_3SO_3)_2]^+(CF_3SO_3)}$$

$$\underset{\mathbf{XV}}{[Ir^{III}(dmbpy)_2(CF_3SO_3)_2](CF_3SO_3)} + HPhpytr \xrightarrow[\text{1,2-dichlorobenzene}]{12h,\ 210^oC} \underset{\mathbf{XVI}}{[Ir^{III}(dmbpy)_2(HPhpytr)](CF_3SO_3)_3}$$

***Figure 5.4** Schematic representation of the synthetic method followed.*

Attempts to precipitate the complex (**I**) directly at the end of the reaction mixture by adding PF$_6$ salts resulted in a mixture of complexes (**I**) and (**II**) which was very difficult to purify afterwards. So the method described here involves the initial precipitation of the complex as its chloride salt, followed by precipitation of (**I**) by PF$_6$ was very efficient in getting the complexes with maximum purity. [Ir(phen)$_2$Cl$_2$]PF$_6$, [Ir(dmbpy)$_2$Cl$_2$]PF$_6$ and [Ir(dtbpy)$_2$Cl$_2$]PF$_6$ were also obtained in good yield. It is worth noting that cyclometallation is not possible for these ligands, since the H4 hydrogen atom has been substituted and only a single product is obtained, simplifying the synthesis and increasing the yield. The structural representation of the complexes are given in figure 5.5.

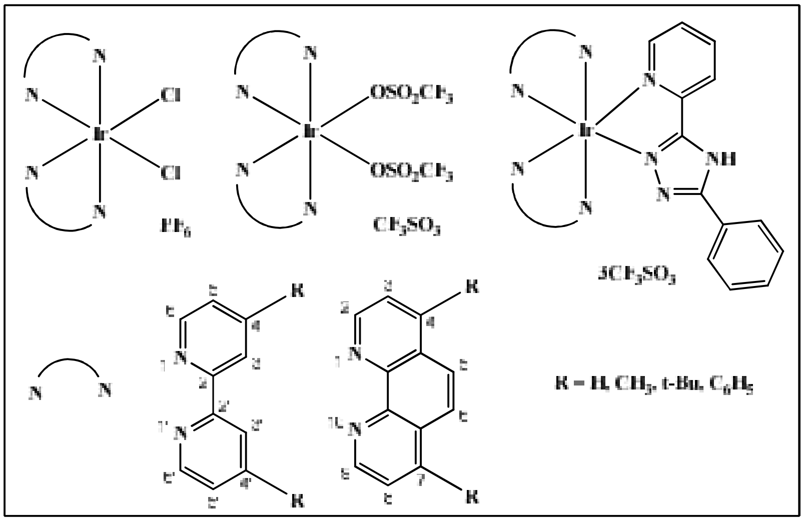

Figure 5.5 *Structural representations of complexes*

Past studies have shown that the inner sphere chlorides are strongly coordinated to the Ir metal and that harsh conditions and chlorinated solvents were needed to remove these chlorides. Meyer has reported[17] this previously. His method involes firstly removing the outer sphere chloride, purifying the resultant product and then reacting with 20 times molar excess of CF$_3$SO$_3$H forming the triflate intermediate. Formation of the triflate intermediate was achieved in a single step by using the PF$_6$ analogue of the precursor and heating in reflux temperature for 5h with triflic acid and precipitating by adding diethyl ether. The product was recrystallised from acetone : diethyl ether. In the next step the triflate intermediate was heated at reflux temperature with the polypyridyl ligand in 1,2 dichlorobenzene at 200 ^{0}C and the product was precipitated by adding anhydrous diethyl ether. The product was washed thoroughly with diethyl ether and hexane and recrystallised from acetone: water mixture.

5.3.2 Characterisation - ^{1}H NMR spectroscopy

The general numbering scheme for (**I**) and (**II**) is shown in figure 5.6 below. The ^{1}H NMR spectra of the reaction mixture taken directly from the preparation of complex [Ir(bpy)$_2$Cl$_2$]PF$_6$ (**I**) on completion of the reaction (after 25 min) along with the purified complexes are given in figure 5.7(A). By comparing the NMR spectrum of the mixture with those obtained for (**I**) and (**II**) (figure 5.7(B) and (C)) it can concluded that apart from these two compounds no side products were obtained. The ^{13}C NMR spectrum of **I** is given in Figure 5.7(D). The bis bipyridyl complex showed ten distinct carbons in the ^{13}C NMR spectrum.

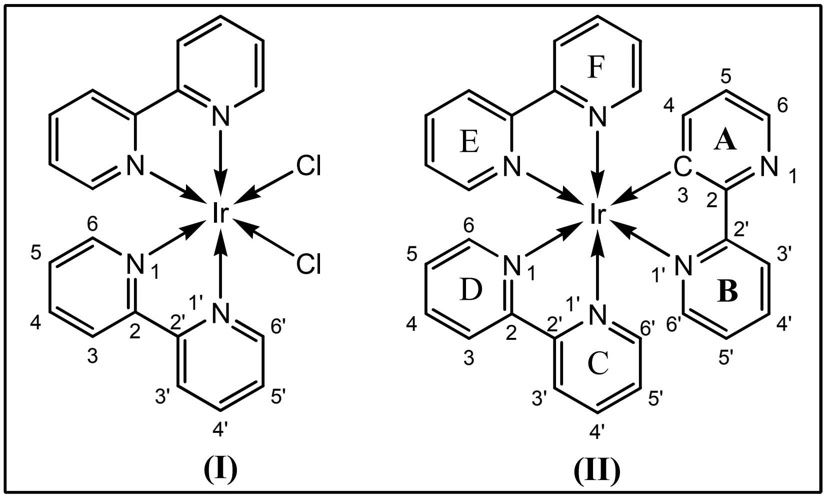

***Figure 5.6** General numbering schemes for the complexes*

As shown in Figure 5.7(B) the spectrum of the iridium complex (**I**) shows the presence of two different types of bpy rings, in agreement with a cis arrangement of the bpy ligands and the presence of chloride ligands, similar to that observed for the analogous [Ru(bpy)$_2$Cl$_2$] complexes.[23,86] The ^{1}H NMR spectrum of (**II**) (Figure 5.7 C) includes a doublet at δ 6.58 ppm that integrates for 1 proton and this can be assigned to the H4 proton of the C-bonded ring from the COSY measurements and also considering the fact that the H4 proton is situated immediately above the pyridyl ring of an adjacent ligand and therefore will experience a high ring-current shielding which has been shown before for similar complexes using X-Ray diffraction methods.[26] The shift is 2 ppm upfield from the position of the H4 protons in the [Ir(bpy-N,N')$_3$]$^{2+}$

complex.[87] The two distinct high-field multiplets (δ 6.58 ppm and δ 7.08 ppm) are coupled and to the resonance at δ 8.42 ppm. These three resonances are not coupled to any other resonances, and each of the three integrates to one proton. These three correspond to protons A4, A5, and A6. A similar upfield shift of ~2 ppm was also observed in the $[Pt(bpy\text{-}N,N')_2]^{2+}$ NMR spectrum where, on going from square-planar to a cis conformation, half of the H6 protons become shielded by an adjacent aromatic ring.[88] The proton NMR shift for complexes (**I**), (**VII**), (**IX**), (**XIII**) and (**XV**) in d_6 DMSO is given in table 5.1.

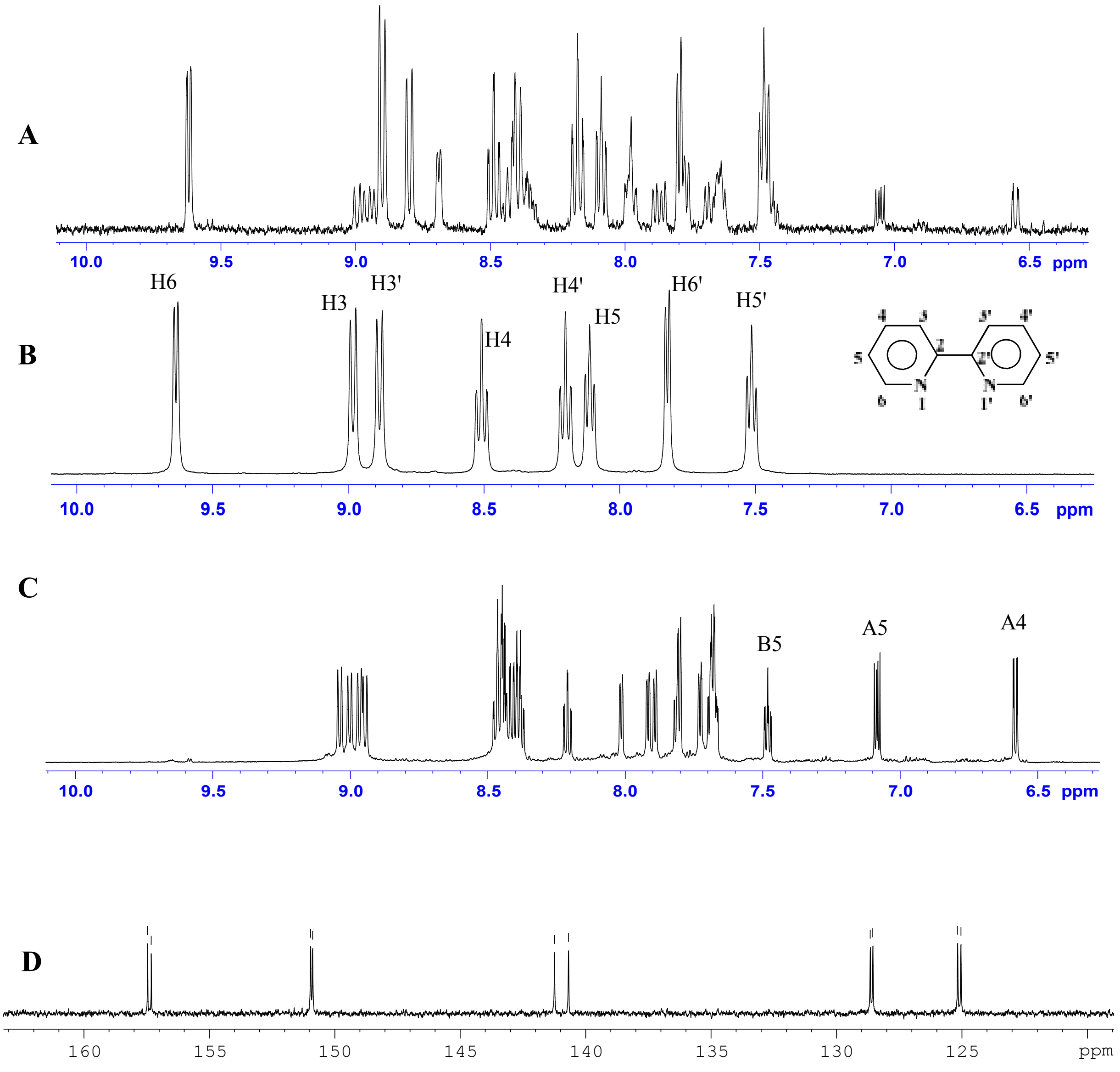

Figure 5.7 *^{1}H NMR spectra* ***(A)*** *directly taken from the reaction mixture for $h_8$bpy containing complex* ***(I)*** *and* ***(II)****,* ***(B)*** *$[Ir(bpy)_2Cl_2]^+$**(I)**,* ***(C)*** *$[Ir(bpy\text{-}N,N')_2(bpy\text{-}C,N')]^{2+}$**(II)**,* ***(D)*** *^{13}C NMR of $[Ir(bpy)_2Cl_2]^+$**(I)** carried out in d_6 DMSO.*

For complexes (**V**), (**VII**) and (**IX**) it was confirmed from NMR spectra and hplc traces that the orthometallated tris complex as similar to bpy is not formed due to the steric hindrance caused by the bulky methyl and tertiary butyl groups present on the C4 position of bipyridine ring and for phenanthroline there is no free rotation possible. The ^{1}H NMR spectrum of (**V**), (**VII**) and (**IX**) are given in figure 5.8. The ^{13}C spectrum for (**V**) and (**VII**) are given in figure 5.8 (D) and figure 5.8 (E). For complex (**V**) a total of 8 distinct protons are observed whose splitting patterns can be clearly identified from the spectra and the peaks are also assigned on the basis of the COSY spectrum given in figure S8 in appendix D. Similarly for complex (**VII**) the CH$_3$ group on ring B gives a 3 proton singlet observed at δ 2.53 ppm. Also the singlet for the CH$_3$ group on ring A is at δ 2.74 ppm.

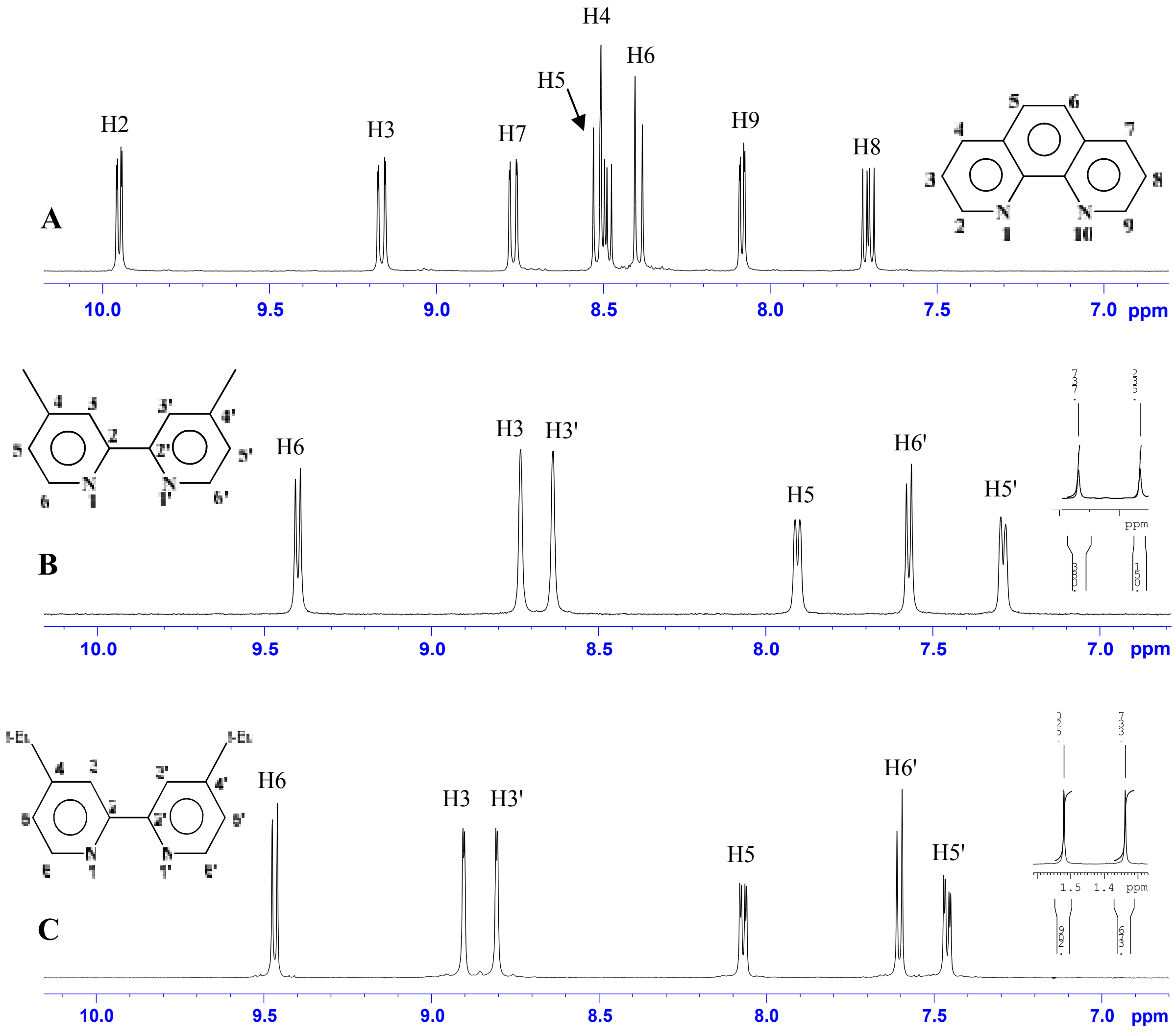

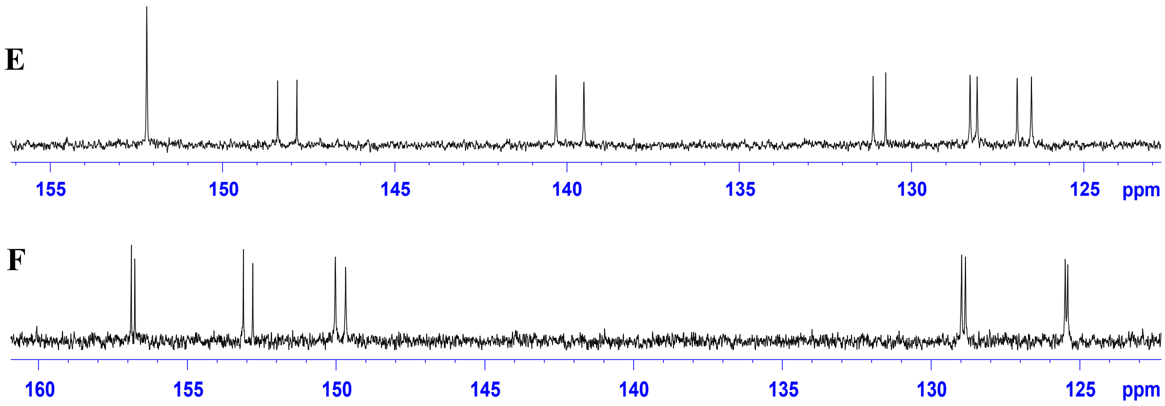

Figure 5.8 *^{1}H NMR spectra of **(A)** [Ir(phen)$_2$Cl$_2$]PF$_6$ (V), **(B)** [Ir(dmbpy)$_2$Cl$_2$]PF$_6$ **(VII)**, **(C)** [Ir(dtbpy)$_2$Cl$_2$]PF$_6$ **(IX)**, **(D)** ^{13}C NMR of [Ir(phen)$_2$Cl$_2$]PF$_6$ (V), **(E)** ^{13}C NMR of [Ir(dmbpy)$_2$Cl$_2$]PF$_6$ **(VII)** carried out in d$_6$ DMSO.*

Considering the NMR of (**IX**), 3 CH$_3$ groups on ring B are equivalent giving a 9 proton singlet at δ 1.35 ppm and the 3 equivalent CH$_3$ groups on ring A gives a 9 proton singlet at δ 1.53 ppm. The rest of the peaks for (**V**), (**VII**) and (**IX**) are assigned in accordance with the ^{13}C, COSY, HMQC and HMBC spectra which are given in appendix D.

The chemical shifts of protons in [Ir(bpy)$_2$Cl$_2$]PF$_6$, the substituted bipyridyl complexes, (**VII**), (**IX**) and triflate complexes are given in the table 5.1 below

Complex	H3	H4	H5	H6	H3'	H4'	H5'	H6'
[Ir(bpy)$_2$Cl$_2$]PF$_6$ **(I)**	8.93	8.52	8.12	9.65	8.82	8.20	7.51	7.83
[Ir(dmbpy)$_2$Cl$_2$]PF$_6$ **(VII)**	8.76	-	7.93	9.42	8.66	-	7.32	7.59
[Ir(dtbpy)$_2$Cl$_2$]PF$_6$ **(IX)**	8.92	-	8.09	9.48	8.83	-	7.48	7.62
[Ir(bpy)$_2$(OSO$_2$CF$_3$)$_2$]CF$_3$SO$_3$ **(XIII)**	9.02	8.67	8.23	9.02	8.83	8.34	7.52	7.69
[Ir(dmbpy)$_2$(OSO$_2$CF$_3$)$_2$]CF$_3$SO$_3$ **(XV)**	8.85	-	8.16	8.79	8.68	-	7.32	7.45

Table 5.1 *^{1}H NMR shift for complexes (**I**), (**VII**), (**IX**), (**XIII**) and (**XV**) in d$_6$ dmso.*

From the table given above it is clear about the shifting of the proton peaks as a result of substitution of the 4 and 10 positions of bpy by methyl and tertiary butyl groups as the shifting of H3 and H5 protons are much higher than others for (**VII**) and (**IX**) compared to (**I**). The removal of the inner sphere chlorides by triflate groups results in considerable shifts to the proton peaks.

In this case the H6 and H12 protons are influenced more, for (**XIII**), the H6 proton shifts upfield to 9.02 ppm from 9.65 ppm and the H12 proton also undergoes an upfield shift to 7.69 ppm from 7.83 ppm compared with complex (**I**). Similarly, the H6 proton for (**XV**) shifts to 8.79 ppm from 9.42 ppm and H12 shifted to 7.45 ppm.

The ^{1}H NMR spectrum of the three triflate complexes (**XIII**), (**XIV**) and (**XV**) are given in figure 5.9 below.

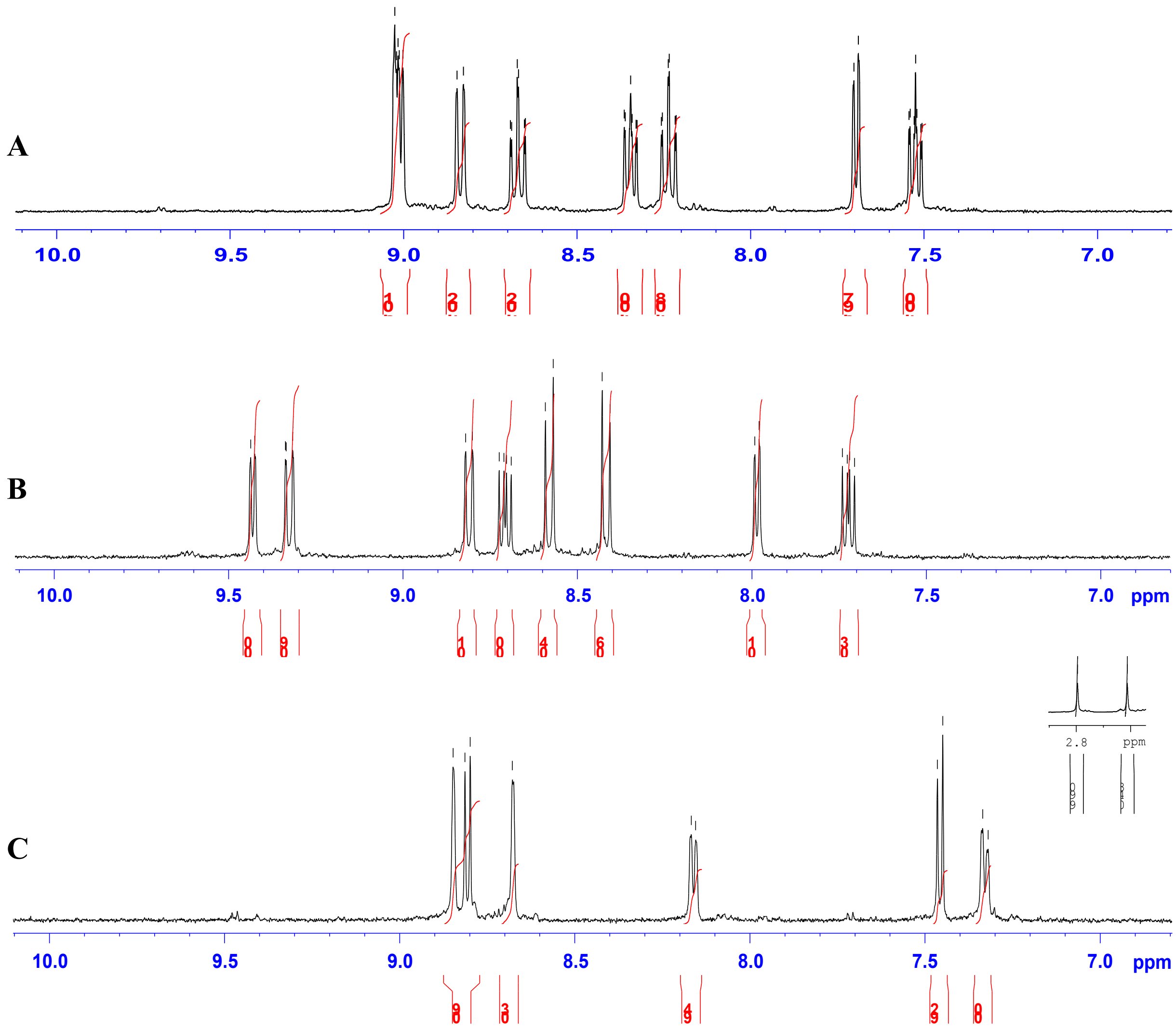

Figure 5.9 *^{1}H NMR spectra of **(A)** [Ir(bpy)$_2$(CF$_3$SO$_3$)$_2$]CF$_3$SO$_3$, **(B)**[Ir(phen)$_2$(CF$_3$SO$_3$)$_2$] CF$_3$SO$_3$ and **(C)** [Ir(dmbpy)$_2$(CF$_3$SO$_3$)$_2$]CF$_3$SO$_3$ carried out in d$_6$ DMSO.*

The ^{1}H NMR chemical shifts for the complex [Ir(phen)$_2$Cl$_2$]PF$_6$ **(V)** and the triflate complex [Ir(phen)$_2$(OSO$_2$CF$_3$)$_2$]CF$_3$SO$_3$ **(XIV)** are given in table 5.2. Substitution of the inner sphere chlorides with the triflate groups result in significant change in chemical shifts which can be clearly seen from the table 5.2 below.

Complex	H2	H3	H4	H5	H6	H7	H8	H9
[Ir(phen)$_2$Cl$_2$]PF$_6$ **(V)**	9.94	9.15	8.49	8.48	8.37	8.76	7.69	8.07
[Ir(phen)$_2$(OSO$_2$CF$_3$)$_2$]CF$_3$SO$_3$ **(XIV)**	9.42	9.33	8.57	8.70	8.40	8.80	7.72	7.97

Table 5.2 *^{1}H NMR shift for complexes V and XIV in d_6 dmso.*

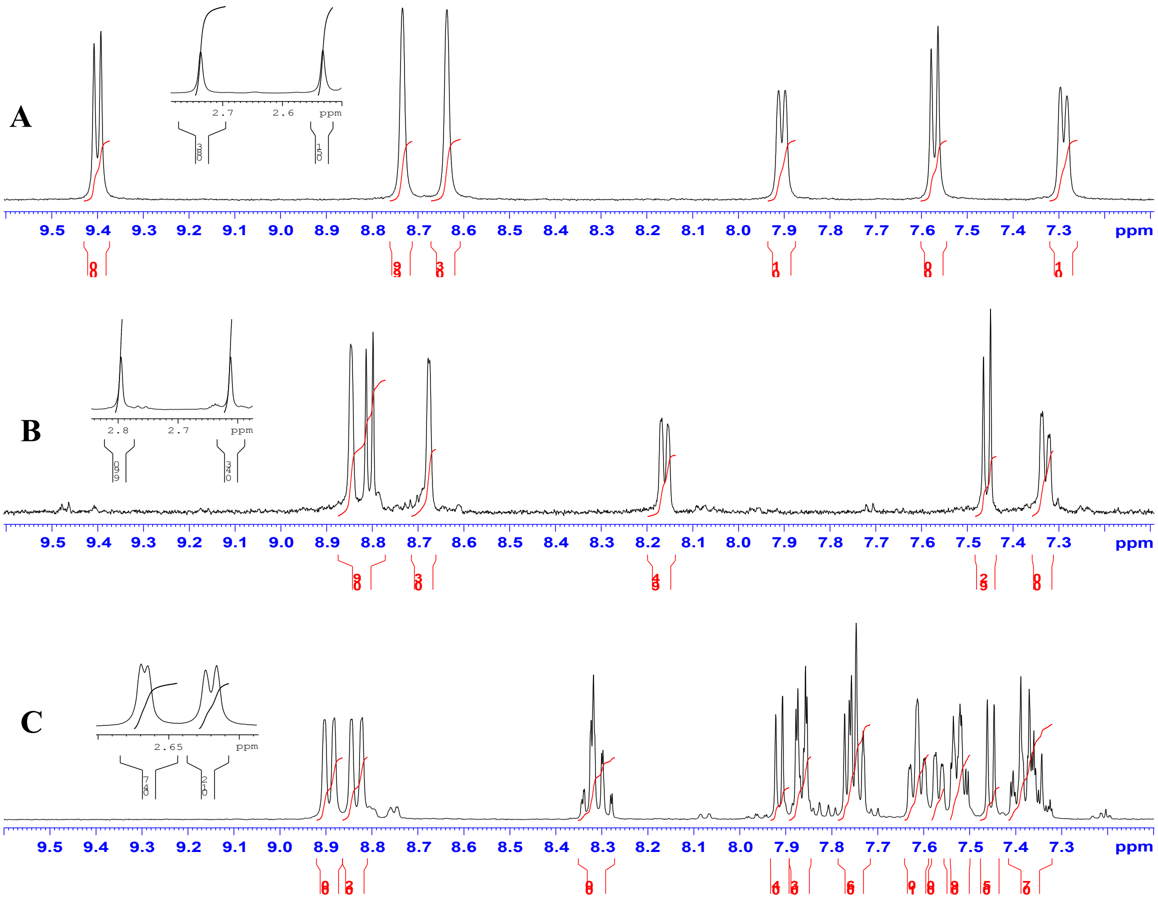

Figure 5.10 *^{1}H NMR spectra of **(A)** [Ir(dmbpy)$_2$Cl$_2$]PF$_6$ **(VII)**, **(B)**[Ir(dmbpy)$_2$(CF$_3$SO$_3$)$_2$] CF$_3$SO$_3$ **(XV)**, **(C)** [Ir(dmbpy)$_2$(HPhpytr)](CF$_3$SO$_3$)$_3$ **(XVI)**, carried out in d_6 DMSO.*

The ^{1}H NMR spectrum of complexes (**VII**), (**XV**) and (**XVI**) are shown in figure 5.10 above. For complex (**VII**) the CH$_3$ group on ring B gives a 3 proton singlet at δ 2.53 ppm. Also the 3 proton singlet of the CH_3 group on ring A is at δ 2.74 ppm. There is a noticable shift in the proton signals on moving from complex (**VII**) to (**XVI**). The H6 proton at δ 9.42 ppm in (**VII**) underwent a upfield shift to δ 8.79 ppm due to the presence of the strong electron withdrawing CF_3SO_3 group. The H5 proton in (**VII**) at δ 7.93 ppm was shifted upfield to δ 8.16 ppm. The complexation to the triazole ligand resulted in further more shifting as can be clearly seen from figure 5.10.

5.3.3 HPLC Measurements

HPLC of the sample taken directly from the reaction mixture for $[Ir(bpy)_2Cl_2]PF_6$ indicates three peaks (figure 5.11a). Peak 1 with a retention time of 1.69 min, peak 2 with 2.33 min and peak 3 having a retention time of 10.44 min. The peak area counts obtained for the 2nd and 3rd peaks indicate that the 3rd peak is 34 % of that of the 2nd one. Peak 2 showed an absorption maxima at 282 nm and third peak showed an absorption maxima of 277 nm. By running $h_8$bpy in the HPLC one peak was obtained with a retention time of 1.69 min which clearly indicates that the first peak is unreacted bpy. The second peak corresponds to $[Ir(bpy)_2Cl_2]PF_6$ which is confirmed by NMR, absorption and emission spectroscopy. HPLC of the purified fraction 1 (figure 5.11b) indicates only one peak with a retention time of 2.33 min, and an absorption maximum at 282 nm corresponding to $[Ir(bpy)_2Cl_2]PF_6$. The third peak having a retention time of 10.44 min is $[Ir(bpy\text{-}N,N')_2(bpy\text{-}C,N')]^{2+}$ (fraction 2) confirmed by NMR.

HPLC of the sample taken directly from the reaction mixture for $[Ir(d_8bpy)_2Cl_2]PF_6$ indicates three peaks (figure 5.11c). The first peak has a retention time of 1.67 min corresponding to the unreacted bpy, the second peak at 2.28 min corresponds to $[Ir(d_8bpy)_2Cl_2]PF_6$ (fraction 1) and the third peak having a retention time of 10.71 min is that of $[Ir(d_8bpy\text{-}N,N')_2(d_8bpy\text{-}C,N')]^{2+}$ (fraction 2). The peak area counts obtained for the 2nd and 3rd peaks indicate that the 3rd peak is 25 % of that of the 2nd one. Peak 2 showed absorption maxima of 282 nm and peak 3 showed absorption maxima of 276 nm. HPLC of the purified fraction 1 (Figure 5.11d) indicates only one peak with retention time 2.28 min, an absorption maxima of 283 nm, corresponding to $[Ir(d_8bpy)_2Cl_2]PF_6$.

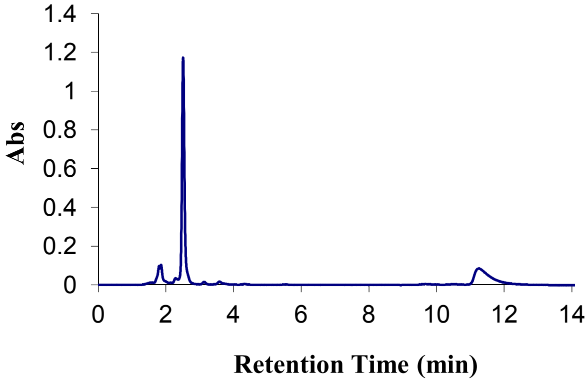

Fig 5.11a. *HPLC plot of [Ir(bpy)$_2$Cl$_2$]$^+$ directly from reaction mixture.*

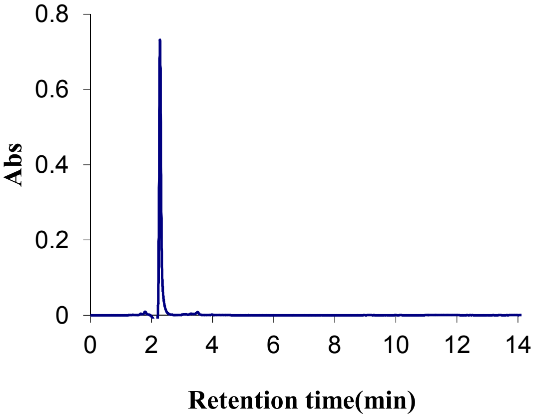

Fig 5.11b. *HPLC plot of purified [Ir(bpy)$_2$Cl$_2$]$^+$*

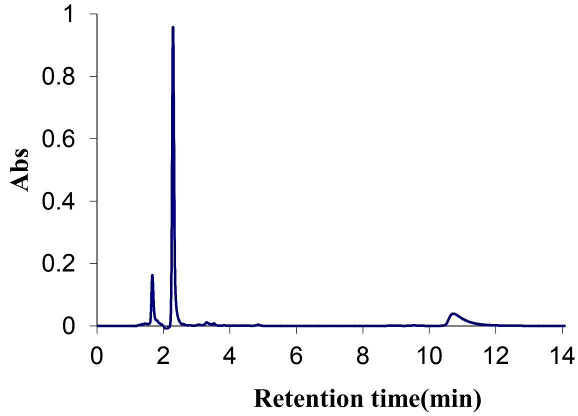

Fig 5.11c. *HPLC plot of [Ir(d$_8$bpy)$_2$Cl$_2$]$^+$ directly from reaction mixture.*

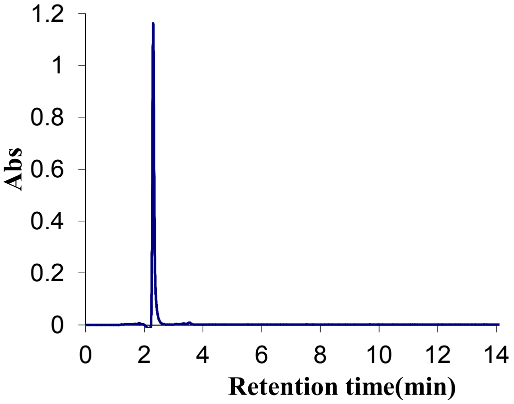

Fig 5.11d. *HPLC plot of purified [Ir(d$_8$bpy)$_2$Cl$_2$]$^+$*

5.3.4 Time Dependent Study of the reaction mechanism of IrCl$_3$ with h$_8$ bpy using HPLC and NMR

In the course of the reaction of IrCl$_3$ with 2,2'-bipyridine at 300 ^{0}C the formation of two products [Ir(bpy)$_2$Cl$_2$]$^+$ and [Ir(bpy-N,N')$_2$(bpy-C,N')]$^{2+}$ was observed. To obtain further information concerning the reaction pathway as a function of time, HPLC (figure 5.12) and NMR (figure 5.13) data were obtained at 5 min intervals from the reaction mixture starting from 5 min up to 25 min which provides a good insight into the progress of the reaction. The HPLC data are clearly indicative of the formation of different species and by comparing with the NMR spectrum for the same time intervals the formation of both complexes (**I**) and (**II**) start at 15 min. This can be clearly distinguished from the peaks obtained for the NMR spectrum. By comparing Figure

5.12c and Figure 5.12d with Figure 5.13c and Figure 5.13d confirms the formation of the orthometallated species.

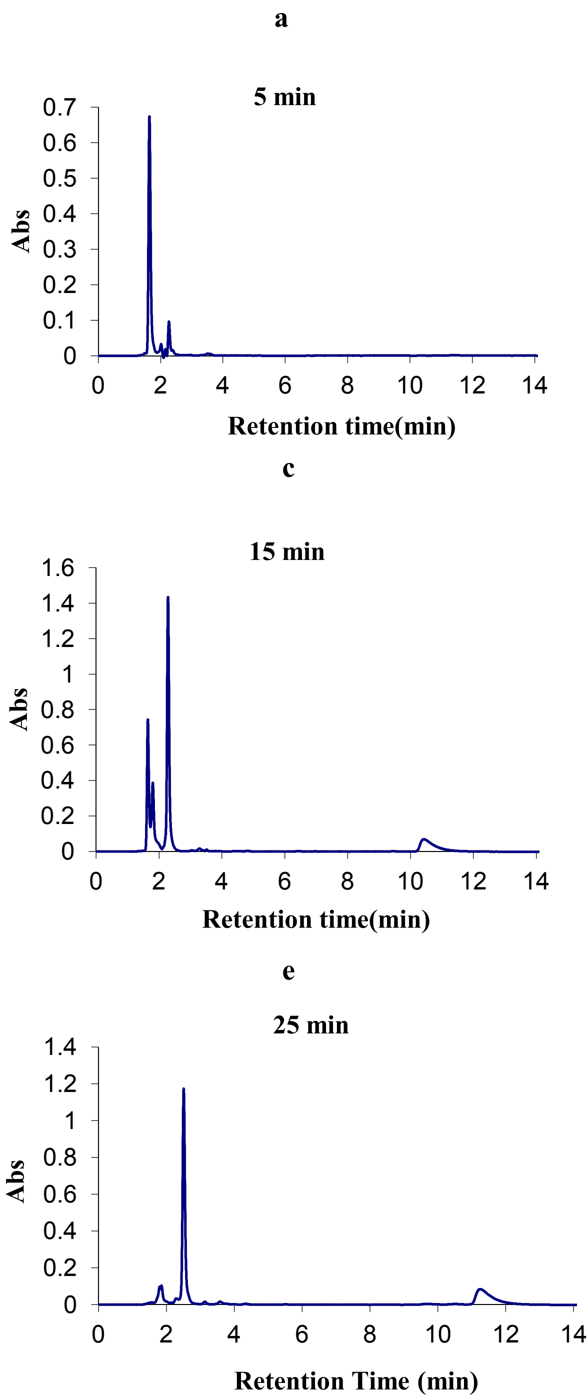

Figure 5.12 *Time dependent HPLC data for reaction of IrCl$_3$ with h$_8$bpy at different time intervals ranging from 5 min to 25 min. a) 5 min b) 10 min c)15 min d) 20 min e) 25 min.*

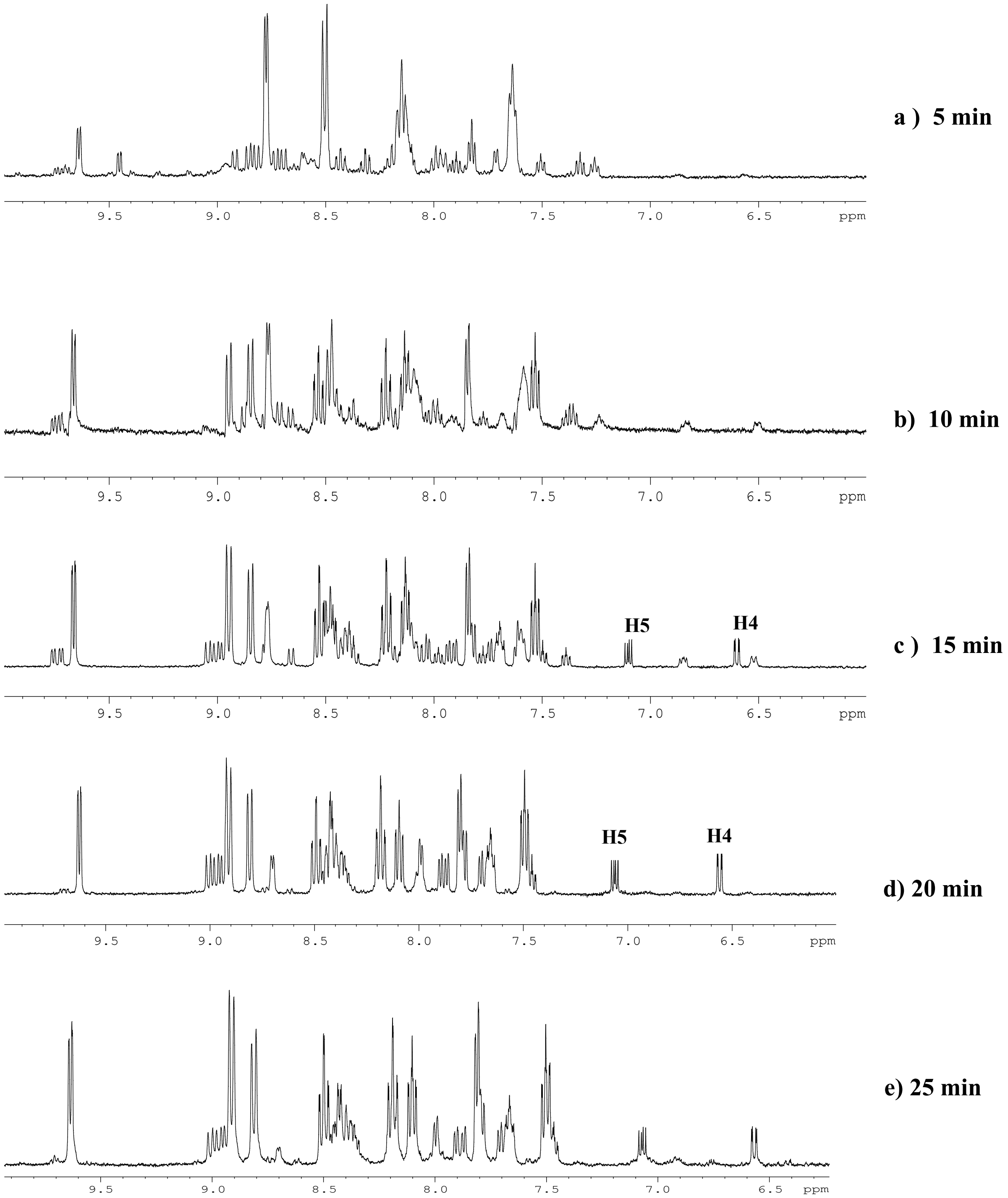

Figure 5.13 *Time dependent NMR data for the reaction of IrCl$_3$ with h$_8$bpy at different time intervals ranging from 5 min to 25 min. a) 5 min b) 10 min c) 15 min d) 20 min. e)25 min.*

From Figure 5.12 (a) two peaks were identified with retention times of 1.69 min and 2.33 min. These samples were injected 5 min after the start of the reaction. The former peak is assigned to bpy and latter to $[Ir(bpy)_2Cl_2]^+$ (**I**). The ^{1}H NMR spectra shown in Figure 5.13 supports the identity of both peaks. After 10 min the intensity of 2nd peak has increased showing that more of complex **I** is formed by the reaction of starting materials, and the first peak has become more structured possibly because of the formation of an intermediate chloro bridged iridium dimer in which one bpy is complexed to each Ir metal which undergoes cyclometallation,[89] which is evident from the doublet at δ 6.5, multiplet at δ 6.85 ppm and δ 9.75 ppm given in Figure 5.13(b). After 15 min the first peak in HPLC at 1.69 min splits into two, corresponding to the unreacted bpy and the intermediate species. In Figure 5.12(c) the upcoming 3rd peak at retention time 10.44 min corresponds to $[Ir(bpy\text{-}N,N')_2(bpy\text{-}C,N')]^{2+}$ (**II**) evident from the δ 6.58 ppm H4 proton doublet and δ 7.08 ppm multiplet. At 20 min most of the intermediates get converted into complex (**II**) which is evident from HPLC Figure 5.12(d) and NMR Figure 5.13(d), as the peaks at δ values 6.5 ppm, 6.85 ppm and 9.75 ppm have disappeared on going from 15 min to 20 min. At 25 min almost all of the bipyridine has reacted and are left with the final two products. The study was continued up to 1.5 hours which showed that most of the metal was charred at this high temperature resulting in a decreased yield of 30 %. No side products are formed, as found in the conventional reaction of Ir metal with bpy, by employing a higher temperature which resulted in the formation of only two products at the end of the reaction as shown in figures 5.12 and 5.13.

The deuteriation effect study provided promising results on the formation of complex (**II**) through an intermediate species. The use of deuteriated bpy ($d_8$bpy), results in a reduced yield of complex (**II**) due to the greater bond strength of C-D bond over the C-H bond. The ratio of (**I**) and (**II**) for $h_8$bpy and $d_8$bpy tabulated using HPLC and NMR are given in Table 5.3. The ratio of the two products can be obtained both from the ^{1}H NMR as well as the HPLC data. For $h_8$bpy NMR analysis indicates that the ratio of **I:II** is 67:33, with HPLC ratio of 66:34 is obtained. For the deuteriated analogues a ratio of 75:25 is determined from HPLC. This is in agreement with the increased bond strength of C-D bond over the C-H bond.

	HPLC		**^{1}H NMR**	
	I	**II**	**I**	**II**
h8	66	34	67	33
d8	75	25	NA	NA

Table 5.3 *Ratio of the two products obtained in two different cases calculated from HPLC and NMR data.*

5.3.5 Absorption Properties

The absorption and emission properties of iridium (III) bis polypyridyl and tris polypyridyl complexes were outlined in section 5.1.1 but to summarise, the tris polypyridyl complexes typically have a lowest excited state which is classified as being associated with a ligand localised π-π* transition.[27,31,41] The UV absorption spectra of the complexes $[Ir(phen)_3]^{3+}$ and $[Ir(bpy)_3]^{3+}$ are both π-π* in nature and do not exhibit any clear evidence for d-π* and d-d bands.[31] In the case of bis polypyridyl complexes the energy gap between the π-π* state and d-π* state is small. At room temperature emission is seen from the lowest lying π-π* state with a slight contribution from the d-π* state. The absorption and emission measurements coupled with the lifetime measurements carried out at both room temperature (298 K) and low temperature (77 K) give a clear indication of the nature of the emitting states in these polypyridyl complexes. The UV spectra of complex $[Ir(bpy)_2Cl_2]PF_6$ along with its deuteriated analogue and 2,2'-bipyridine (bpy) which are typical of the spectra obtained for the iridium (III) dichloride complexes discussed in this chapter, are given in figure 5.14 below.

The absorption spectra of (**I**) and (**III**) clearly show a red shift compared to the absorption spectrum of the free ligand as a consequence of complex formation. The visible absorption spectrum of $[Ir(bpy)_2Cl_2]PF_6$ (**I**) consists of a weak band at 380 nm which has been assigned as a metal to ligand charge transfer d-π* transition. The absorption features in the range of 250-300 nm in these type of polypyridyl complexes are probably due to π-π* transitions. The assignments are made by comparing the results with the reported publications[20,21] explained in section 5.1.1.

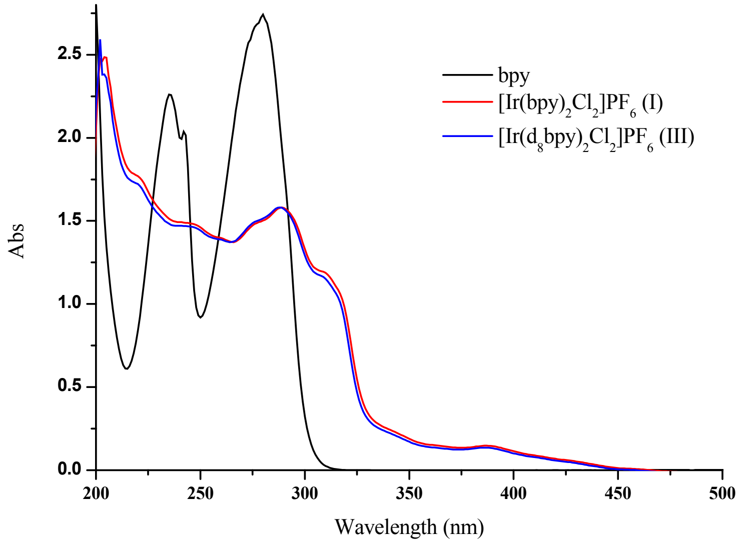

***Figure 5.14** Absorption spectra of complexes **(I)** and **(III)** along with bpy obtained in spectroscopic grade ACN (Conc. 1×10^{-4} mol L^{-1}).*

The absorption data for complexes I, II, III and IV are tabulated in table 5.4 below.

Complex	**Absorption λ_{abs} (nm)** **ε ($LM^{-1}cm^{-1}$)x 10^3**
[Ir(h$_8$bpy)$_2$Cl$_2$]PF$_6$ (**I**)	239(17.90),280(17.99), 302(1.52),380(1.73)
[Ir(h$_8$bpy-N,N')$_2$(h$_8$bpy-C,N')](PF$_6$)$_2$ (**II**)	296(1.68), 310(1.50), 357(1.74)
[Ir(d$_8$bpy)$_2$Cl$_2$]PF$_6$ (**III**)	239(18.12),280(18.67),302(1.15),380(1.62)
[Ir(d$_8$bpy-N,N')$_2$(d$_8$bpy-C,N')](PF$_6$)$_2$ (**IV**)	304(1.77), 310(1.74), 350(1.50)

***Table 5.4** Absorption and extinction coefficients for complexes **(I)**, **(II)**, **(III)** and **(IV)** measured at 298 K in spectroscopic grade acetonitrile.*

Figure 5.15 shows the absorption spectra of [Ir(phen)$_2$Cl$_2$]PF$_6$ (**V**) and [Ir(dpphen)$_2$Cl$_2$]PF$_6$ (**XII**). The absorption bands at 265 nm and 275 nm for complex [Ir(phen)$_2$Cl$_2$]PF$_6$ (**V**) have been assigned as phen(π)→phen(π*) transitions.[20,21] These bands are red shifted compared to the absorption spectra of the free ligand as a result of complex formation. Also two bands, one at 338 nm, and the second at 390 nm, seen in the absorption spectra of complex (**V**) are assigned to a d-π* transition.

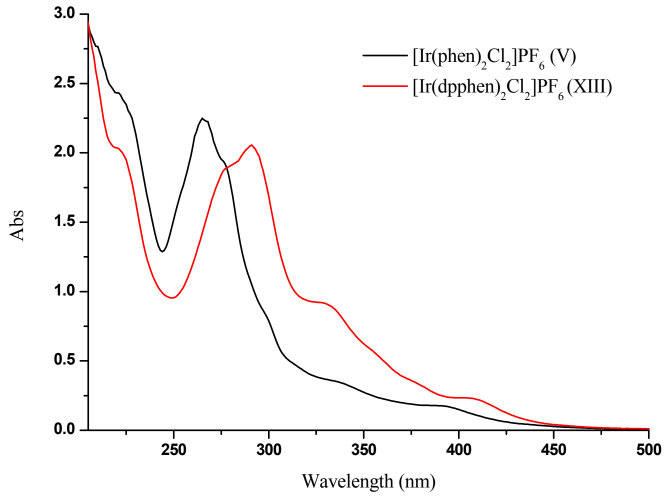

Figure 5.15 *Absorption spectra of complexes* ***(V)*** *and* ***(XIII)*** *taken in spectroscopic grade ACN (Conc. 1×10^{-4} mol L^{-1}).*

For the complex [Ir(dpphen)$_2$Cl$_2$]PF$_6$ (**XII**) the bands at 290 nm and 330 nm are assigned as dpphen(π)→dpphen(π*) transitions. For (**XII**) the band due to d-π* transition is at the lower energy of 405 nm. The introduction of electron withdrawing diphenyl groups at 4 and 7 positions resulted in a red shift in the absorption spectra of (**XII**) compared to (**V**). The assignments are made by a comparison of the absorption spectra of [Ir(bpy)$_2$Cl$_2$]PF$_6$ (**I**) in figure 5.14 and the previous references.[20-30]

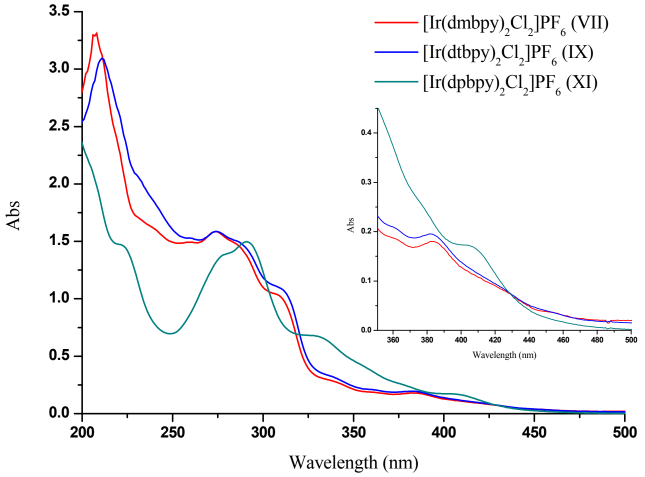

Figure 5.16 *Absorption spectra of complexes* ***(VII)****,* ***(IX)*** *and* ***(XI)*** *taken in spectroscopic grade ACN (Conc. 1×10^{-4} mol L^{-1}).*

The effect of substitution on the absorption spectra of iridium polypyridyl complexes becomes clearer from the data given in figure 5.16 which shows the absorption spectra of complexes (**VII**), (**IX**) and (**XI**). By comparing the absorption spectra in figures 5.14 and 5.15, the absorption bands for these complexes are also assigned as π-π* in the UV region and d-π* bands in the visible region. Complex (**VII**) has a methyl group at the 4 and 4' position and complex (**IX**) has a tertiary butyl group at the 4 and 4' position of the bipyridine. Interestingly from the spectra given above substitution of the bipyridine ligand with electron donating groups resulted in a slight blue shift of the bands in the UV region. The band at 280 nm which is due to bpy(π)→bpy(π*) transitions (figure 5.12) was slightly blue shifted to 275 nm, due to dmbpy(π)→dmbpy(π*) transitions in (**VII**) and 274 nm which is due to a dtbpy(π)→dtbpy(π*) transition. The rest of the spectrum does not undergo any change as a result of the substitution. For complex (**XI**) which has a phenyl group at the 4 and 4' positions, resulted in a considerable red shift in the spectrum as can be seen from the graphs above. The π→π* transitions at 280 nm and 302 nm in (**I**) was considerably red shifted to 290 nm and 330 nm. The d-π* band at 380 nm in (**I**) also red shifted to 405 nm in (**XI**). The tabulated data for the absorption and extinction coefficients are given in Table 5.5

Complex	**Absorption λ_{abs} (nm)** **ε (LM^{-1}cm^{-1})x 10^3**
[Ir(phen)$_2$Cl$_2$]PF$_6$ **(V)**	265(39.85),275(34.86), 338(5.87),390(2.74)
[Ir(d$_8$phen)$_2$Cl$_2$]PF$_6$ **(VI)**	265(37.12),275(32.43), 338(4.16),390(1.02)
[Ir(dmbpy)$_2$Cl$_2$]PF$_6$ **(VII)**	275(13.67),311(8.73), 341(2.38),385(1.39)
[Ir(d$_{12}$dmbpy)$_2$Cl$_2$]PF$_6$ **(VIII)**	275(12.36),311(7.85), 341(1.12),385(1.01)
[Ir(dtbpy)$_2$Cl$_2$]PF$_6$ **(IX)**	274(23.52),308(15.44), 340(3.98),383(2.22)
[Ir(d$_{24}$dtbpy)$_2$Cl$_2$]PF$_6$ **(X)**	274(22.32),308(14.19), 340(2.15),383(1.06)
[Ir(dpbpy)$_2$Cl$_2$]PF$_6$ **(XI)**	290(14.95),330(6.74),405(1.72)
[Ir(dpphen)$_2$Cl$_2$]PF$_6$ **(XII)**	290(20.49),330(9.13),405(2.33)

Table 5.5 *Absorption and extinction coefficients of complexes measured at 298K in spectroscopic grade acetonitrile.*

There is no change in the absorption spectra as a result of deuteriation which can be clearly seen from the absorption spectra of the deuteriated analogoues of bpy, dmbpy and dtbpy given in appendix D. The absorption spectra of the deuteriated analogues of bpy, dmbpy and dtbpy gave exactly the same spectra as those of their proton counterparts.

The triflate intermediate species show considerable change in the absorption spectra as a result of substitution of the inner sphere chlorides with the strong electron donating triflate groups. In figure 5.17 the band at 311 nm in complex (**VII**) which has been assigned to a dmbpy(π)→dmbpy(π*) transition, split, to give two bands at 302 nm and 313 nm in (**XVI**) which both are assigned as π-π* transitions by comparison with the spectra of similar complexes (in figure 5.14). The substitution of Cl$^-$ with the strong electron donating triflate group inside the co-ordination sphere can result in an increase in crystal field parameter, Δ_0, resulting in the increase in energy of d-π* bands as reported before.[29] This resulted in a blue shift in the absorption spectra of the triflate complex (**XV**) compared to the chloride complex (**VII**). The absorption spectra of the complexes along with the extinction coefficients are given in table 5.6

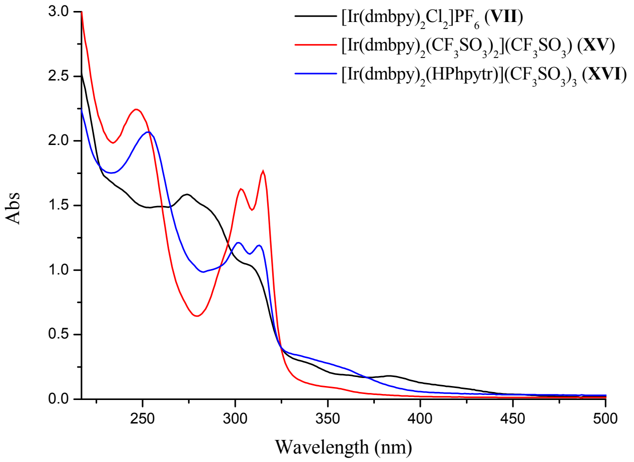

Figure 5.17 *Absorption spectra of complexes (**VII**), (**XV**) and (**XVI**) in spectrometric grade ACN (Conc. 1×10^{-4} moles/lit).*

Complex	**Absorption λ_{abs} (nm)** **ε (LM^{-1}cm^{-1})x 10^3**
[Ir(bpy)$_2$(OSO$_2$CF$_3$)$_2$]CF$_3$SO$_3$ (**XIII**)	252 (20.36), 307 (16.20), 316 (4.78), 355 (1.32)
[Ir(dmbpy)$_2$(OSO$_2$CF$_3$)$_2$]CF$_3$SO$_3$ (**XV**)	247 (24.25), 303 (7.73), 315 (8.64), 355 (0.62)
[Ir(dmbpy)$_2$(HPhpytr)](CF$_3$SO$_3$)$_3$ (**XVI**)	253 (29.43), 302 (5.01), 313 (4.92), 355 (1.03)

Table 5.6 *Absorption and extinction coefficients of complexes XIII, XV and XVI measured at 298 K in spectrometric grade acetonitrile.*

5.3.6 Emission Measurements

Compared to ruthenium complexes of the type $[Ru(L)_3]^{2+}$, where L = 2,2'-bipyridine or 1,10-phenanthroline whose electronic properties result from metal to ligand (d-π*) transitions, for $[Ir(L)_3]^{3+}$ complexes, the lowest excited state is classified as a ligand localised π-π^* transition at both room temperature (298 K) and low temperature (77 K).[90] But for $[Ir(L)_2Cl_2]^+$ complexes, where L = 2,2'-bipyridine or 1,10-phenanthroline, the energy gap between π-π* and d-π* states is small and under thermally equilibrated conditions the mixing of states can take place and the emission can be from both. Previous results suggested that at room temperature (298 K) emission takes place from an equilibrated (π-π*)-(d-π*) excited state for these complexes.[10,20,21,47] The photophysical properties of iridium (III) bis heteroleptic complexes can be quite intricate with dual emissions being distinctly possible. Crosby *et al.* and Watts *et al.*[53,54] observed multiple emissions for bisheteroleptic iridium (III) complexes [Ir(phen)(5,6-dmphen)Cl$_2$]Cl and [Ir(phen)(4,7-dmphen)Cl$_2$]Cl, and these multiple emissions are assigned as from thermally nonequilibrated states of d-π* and π-π*.[52,91] Almost all of the complexes detailed in this chapter exhibited multiple emissions at 77 K. This can be explained much more clearly by considering the lifetime results obtained for these complexes and their deuteriated analogoues at 298 K and 77 K, which is explained in detail in sections 5.3.7 and 5.3.8.

All of the iridium polypyridyl complexes reported here exhibit luminesence between 450-550 nm at room temperature in acetonitrile solution. The excitation wavelength for almost all of the compounds was recorded at 380 nm which is considered to be a d-π* transition as explained before.[52] The low temperature emission spectra for all the complexes are blue shifted in comparison to the room temperature emission. At low temperature the system forms a glass in which there will not be any movement possible for the molecules present in the system, so the quenching occuring as a result of molecular collisons is eliminated, resulting in increased intensity of emission. The dual emission can originate from a mixture of structural isomers or from a ground-state association process, and emission originating from a second nonequilibrated electronic excited state. The absence of evidence of impurities in NMR, CHN and HPLC analysis and adherence of solutions to Beer-Lambert's law over the concentration range studied, suggests that dual emission of these complexes is not due to any impurities but rather due to emission from an nonequilibrated excited state. For all of these complexes the emission maximum is independent of the excitation wavelength.

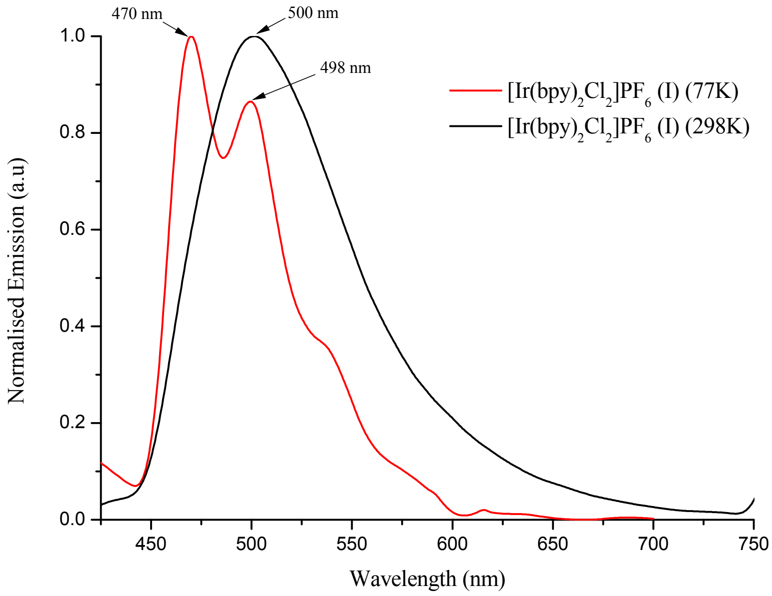

Figure 5.18 *Normalised emission spectra of complex I at 298 K (—) measured in spec grade ACN and 77 K (—) measured in EtOH : MeOH (4:1) glass.* λ_{ex}*=380 nm.*

Figure 5.18 given above shows the emission spectra of complex [Ir(bpy)$_2$Cl$_2$]PF$_6$ (**I**) at room temperature (298 K) and low temperature (77 K). This is taken as the standard for comparing the results obtained for the analogous complexes in this chapter as the assignment of the excited state for this complex was studied in detail by Watts and Crosby.[10,20,21,47] By comparison with the reported publications for this complex as given in section 5.1.1, the room temperature emission at 500 nm is assigned to a mixed (π-π*)-(d-π*) excited state. The lifetime measurements carried out using TCSPC showed a biexponential decay curve at room temperature with one component having a longer lifetime in the range of 300-500 ns which is attributed to a decay from a π-π* excited state, and this long lived component almost doubled as a result of deuteriation of the polypyridyl ligand (table 5.9). The second component is short lived with a lifetime <10 ns and may possibly be emission from a d-π* state which lies very close to the π-π* state. Deuteriation of the polypyridyl ligand does not have much influence on this short lived component (table 5.9). Even though the π-π* and d-π* state exist in very close proximity, the π-π* state has slightly lower energy than the d-π* state on the basis of the deuteriation effect study on lifetimes of these complexes explained in section 5.3.7. The low temperature emission (77 K) spectra for [Ir(bpy)$_2$Cl$_2$]PF$_6$ (**I**) is blue shifted and showed two bands at 470 nm and 498 nm. The lifetime was measured at these two different wavelengths using laser flash photolysis (table 5.15 of section 5.3.8) and for both of them the decay obtained was monoexponential. The lifetimes obtained from both excitation wavelengths were similar (11 μs) from which it is assumed that the nature of the excited state for both these emission bands at 77 K to be quite similar.

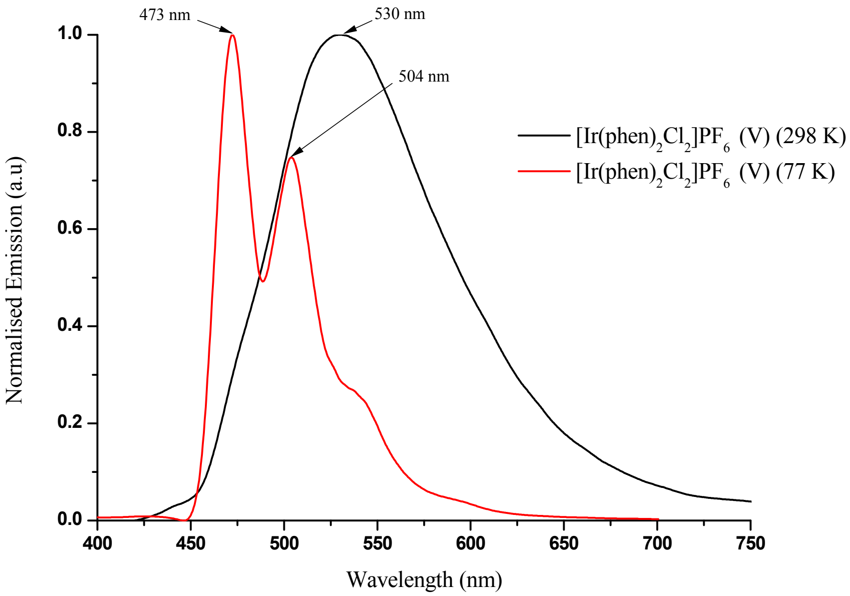

Figure 5.19 *Normalised emission spectra of complex V at 298 K (——) measured in spectroscopic grade ACN and 77 K (——) measured in EtOH : MeOH (4:1) glass. λ_{ex}=380 nm.*

The room temperature (298 K) and low temperature (77 K) emission spectra for [Ir(phen)$_2$Cl$_2$]PF$_6$ (**V**) are given in figure 5.19 above. The emission spectra are compared with the results obtained for complex (**I**) in figure 5.18 along with the lifetime measurements at 298 K and 77 K which helped in assigning the excited state of this complex. The band at 530 nm observed in room temperature measurement is assigned to an emission from the mixed (π-π*)-(d-π*) excited state as it is clear from the lifetime measurements, having a dual exponential decay with a short lived and long lived components (table 5.10). The low temperature emission gives two bands one at 473 nm and the second band at 504 nm. The lifetime measurements at these wavelengths gave similar lifetimes so it is assumed to be from excited states of similar nature. The lifetime results at 298 K and 77 K are explained in detail in sections 5.3.7 and 5.3.8. The room temperature (298 K) and low temperature (77 K) emission of the deuteriated analogues of the complexes (**I**) and (**V**), [Ir(d$_8$bpy)$_2$Cl$_2$]PF$_6$ (**III**) and [Ir(d$_8$phen)$_2$Cl$_2$]PF$_6$ (**VI**) along with complexes [Ir(dmbpy)$_2$Cl$_2$]PF$_6$ (**VII**) and [Ir(dtbpy)$_2$Cl$_2$]PF$_6$ (**IX**) and their deuteriated analogous [Ir(d$_{12}$dmbpy)$_2$Cl$_2$]PF$_6$ (**VIII**) and [Ir(d$_{24}$dtbpy)$_2$Cl$_2$]PF$_6$ (**X**) are given in appendix D.

The emission of these polypyridyl complexes can be influenced by the introduction of various electron donating and electron withdrawing groups thereby tuning the emission spectrum.[49,100] The emisson spectrum for [Ir(bpy)$_2$Cl$_2$]PF$_6$ and the corresponding polypyridyl complexes with various substitution on the 4 and 4' carbon atoms are given in figure 5.20 (a) below. Complexes (**VII**) and (**IX**) have electron dontaing methyl groups and tertiary butyl groups as the substituents. Substitution by methyl group doesn't have an impact on the emission band as there is no change in the emission wavelength. For complex (**IX**) which has a more efficient electron donating tertiary butyl group, a slight red shift was observed.[49] Interestingly substitution of the electron withdrawing phenyl groups on 4 and 4' position of bpy resulted in considerable red shift in emission spectrum as the band at 500 nm for complex (**I**) was red red shifted to 520 nm, which is just the reverse of the result obtained in the case of phenyl substitution of 1,10-phenanthroline. For [Ir(dpphen)$_2$Cl$_2$]PF$_6$ a slight blue shift of 10 nm in emission was observed.[10]

The room temperature emission spectra for the novel Ir (III) tris heteroleptic triazole complex [Ir(dmbpy)$_2$(Hphpytr)](CF$_3$SO$_3$)$_3$ (**XVI**) is given in figure 5.20(b). This complex is the first example of a heteroleptic tris Ir (III) complex, with a triazole ligand. The emission spectra of the complex (**XVI**) shows a main peak at 495 nm, and a shoulder at 470 nm which was absent in the case of the other bis(polypyridyl)$_2$Cl$_2$ complexes. The lifetime was measured at these two emission wavelengths (table 5.14), and data showed that the decay was biexponential in both the cases with a short and a long lived component. Based on this result the decay is attributed to a mixed (π-π*)-(d-π*) excited state.

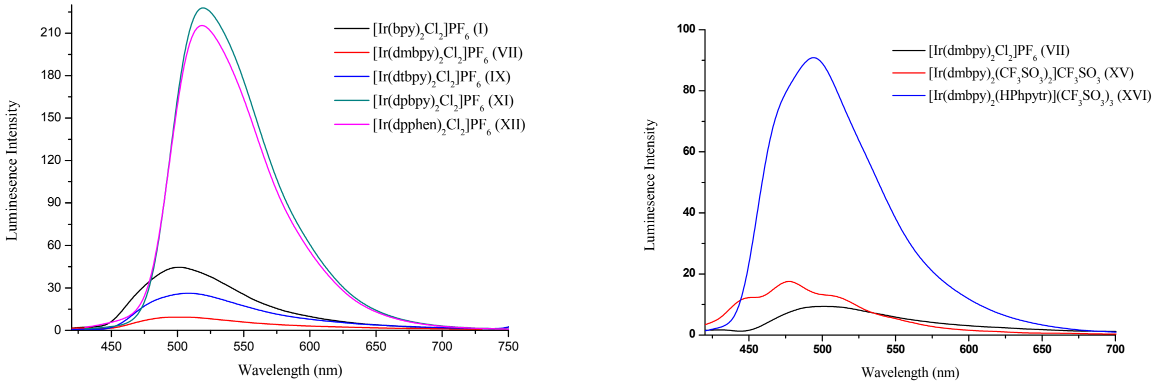

(a) **(b)**

Figure 5.20 (a) *Emission spectra of complexes I, VII, IX, XI and XII in spec grade ACN, (Conc. 1×10^{-4} moles/lit), λ_{ex}=380 nm* ***(b)*** *Emission spectra of complexes VII, XV and XVI in spec grade ACN, (Conc. 1×10^{-4} moles/lit), λ_{ex}=380 nm.*

The emission data for all the complexes described in this section at both room (298 K) and low temperature (77 K) are tabulated, along with the quantum yields in tables 5.7 and 5.8 below. The quantum yields obtained for these complexes are comparatively less than the cyclometallated Ir (III) complexes.[51,60] It was anticipated that the deuteriated analogous would have a higher quantum yield than the protonated complexes, but from the result given in table 5.7, quantum yields for the deuteriated analogous are less than the protonated complexes. Further detailed measurements are required in order to provide an explanation for this behaviour. Interestingly the tris heteroleptic complex (**XVI**) showed a quantum yield much higher than its precursor complex (**VII**). The emission spectra for these two complexes, given in figure 5.20 (b) demonstrates that the tris heteroleptic complex has an intensity 10 times greater than the precursor complex at the same concentration. This shows the importance of synthesising analogous tris complexes with different triazole ligands, as it improves the quantum yields for these complexes which makes their potential application in organic light emitting diodes (OLED's) more likely.[65] The wavelength dependent emission spectrum for all these complexes were carried out by considering different bands in the absorption spectra which is given in appendix D. The results show that emission is independent of the excitation wavelength.

Complex	Emission (298K) λ_{max} (nm)	Emission (77K) λ_{max} (nm)	Quantum Yield
[Ir(h$_8$bpy)$_2$Cl$_2$]PF$_6$ **(I)**	500	470, 498	0.057
[Ir(d$_8$bpy)$_2$Cl$_2$]PF$_6$ **(III)**	500	470, 498	0.052
[Ir(phen)$_2$Cl$_2$]PF$_6$ **(V)**	530	473, 504	0.047
[Ir(d$_8$phen)$_2$Cl$_2$]PF$_6$ **(VI)**	530	473, 504	0.039
[Ir(dmbpy)$_2$Cl$_2$]PF$_6$ **(VII)**	502	470, 502	0.019
[Ir(d$_{12}$dmbpy)$_2$Cl$_2$]PF$_6$ **(VIII)**	502	470, 502	0.011
[Ir(dtbpy)$_2$Cl$_2$]PF$_6$ **(IX)**	508	468, 490	0.030
[Ir(d$_{24}$dtbpy)$_2$Cl$_2$]PF$_6$ **(X)**	508	468, 490	0.021

Table 5.7 *Emission (298 K measured in spec grade ACN and 77 K measured in EtOH : MeOH (4:1) glass. λ_{ex}=380 nm) and quantum yield (298 K) measured in spec grade ACN using [Ru(bpy)$_3$]$^{2+}$ [92] as a standard, all samples had the same absorbance.*

Complex	Emission (298K) λ_{max} (nm)	Quantum Yield
[Ir(dpbpy)$_2$Cl$_2$]PF$_6$ **(XI)**	520	0.195
[Ir(dpphen)$_2$Cl$_2$]PF$_6$ **(XII)**	520	0.194
[Ir(dmbpy)$_2$(OSO$_2$CF$_3$)$_2$]CF$_3$SO$_3$ **(XV)**	450,477,505	-
[Ir(dmbpy)$_2$(HPhpytr)](CF$_3$SO$_3$)$_3$ **(XVI)**	470,495	0.310

Table 5.8 *Emission and quantum yield of complexes **(XI)**, **(XII)**, **(XV)** and **(XVI)** measured at 298K in spectroscopic grade ACN (λ_{ex}=380 nm).*

5.3.7 Life Time Measurements using TCSPC

The instrumentational procedures and conditions that were used to carry out the excited state lifetime measurements using TCSPC have been detailed in Chapter 2. Using TCSPC it is possible to measure excited state lifetimes in the region 1 ns to 10 μs, and laser flash photolysis was used for measuring lifetimes above 10 μs. It should be noted that all the excited state lifetimes reported here are ± 5 % and that two methods were used for analysing the quality of the data acquired a) χ^2 goodness of fit test and b) analysis of the residuals plot. A χ^2 value as close as possible to 1 is ideal and χ^2 values between 1 and 1.1 were obtained for all the data reported in this chapter. When the samples were initially measured all showed some multi-exponential behaviour. In order to verify this, the lifetimes were measured in two different time ranges for each complex and the results obtained were comparable at these two different time ranges for each of the complexes. All the measurements were also carried out with a laser (λ_{ex} = 355 nm) at 298 K and the results obtained were quite similar to the values obtained using TCSPC. A difference of ±20 ns between both methods were observed. All the 77 K measurements were done using the laser flash photolysis.

The application of deuteriation has been discussed in Chapter 2 and also in this chapter in relation to its contribution in assigning ^{1}H NMR spectra. Deuteriation is a useful tool in photophysical studies[86] in order to assign the lowest excited states from which emission takes place. Deuteriation has the effect of reducing both the amplitude and the frequency of vibrational modes and as a result C-D vibrations occur at lower frequency and amplitude than the equivalent C-H vibrations. Thus the vibrational overlap between two states will be diminished for the same energy gap and as non-radiative deactivation is less effective in the deuteriated case it results in an increase in the observed lifetime of the electronically excited state.[86] It has been shown that this observation may be used for the determination of the location of the excited state in iridium (III) complexes previously studied by Watts.[30]

From the absorption spectra for the [Ir(polypyridyl)$_2$Cl$_2$]$^+$ complexes it is clear that two absorption bands, π-π* bands in the UV region and d-π* bands in the visible region were observed of which the former one dominates with a much higher extinction coefficient than the latter as per the studies and measurements done with these complexes described in section 5.3.5. From the emission measurements performed on these complexes, which was explained in detail in section 5.3.6, at room temperature (298 K) only one emission maximum was observed. This was assigned to originate in a mixed (π-π*)-(d-π*) excited state. The luminesence lifetime decay was biexponential for all the polypyridyl complexes studied with the longer lifetime (τ_2) assigned to emission from a π-π* excited state and the shorter lifetime (τ_1), orginates from a d-π* excited state which exist in close proximity to the π-π* state. The lifetime of the deuteriated analogoues of these [Ir(polypyridyl)$_2$Cl$_2$]$^+$ complexes showed a prominent increase in the longer lifetime (τ_2), which is almost doubled but no change for the shorter lifetime (τ_1). This is due to the fact that deuteriation increases the lifetime of the ligand centered π-π* state but does not affect the lifetime of the d-π* state. Eventhough both π-π* and d-π* excited states lies very close in energy, the lowest lying excited state is the π-π* state from which emission was observed at 298 K.

For the [Ir(bpy)$_2$Cl$_2$]PF$_6$ (**I**) complex the lifetime decay curve obtained is given in figure 5.21 (a). From the decay curve recorded at 495 nm, it is clear that the decay is biexponential. The short lived component has a lifetime of 5 ns (τ_1) which contributes 3 % and is assigned to a decay from a d-π* excited state. The long lived component has a lifetime of 353 ns (τ_2) which contributes 97 % and is assigned to a decay from a π-π* excited state. The χ^2 value for the fit is 1.010 indicating close fit to experimental data and the residual plot curve given in figure 5.21 (a) also shows the perfection of the fit. The average lifetime (τ_{av}) calculated is 353 ns.

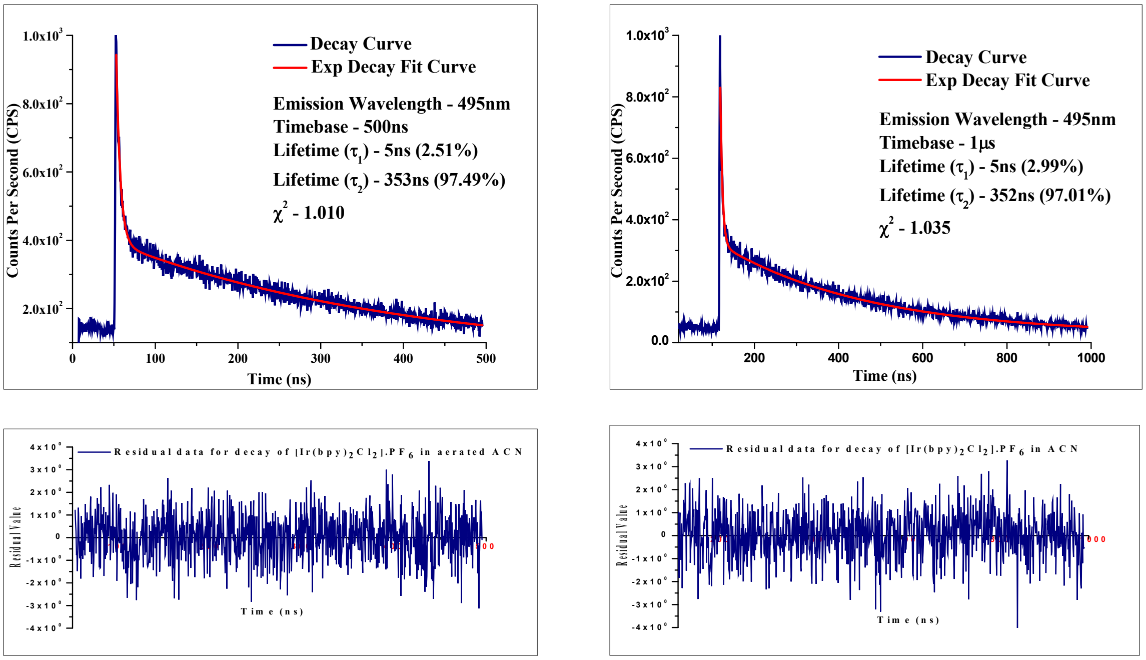

(a) **(b)**

Figure 5.21 *Lifetime decay plots for complex [Ir(bpy)$_2$Cl$_2$]PF$_6$ (**I**) **(a)** at a time range of 500 ns **(b)** at a time range of 1 μs in aerated spec grade ACN (298K).*

The effect of deuteriation on the excited state lifetime especially on the long lived π-π* excited state can be clearly seen from the decay curve for [Ir(d$_8$bpy)$_2$Cl$_2$]PF$_6$ (**III**) (figure 5.22 (a)). From the decay curve recorded at 495 nm it is clear that the decay is biexponential. The short lived component has a lifetime of 7 ns (τ_1) which contributes <1 % and is assigned to a d-π* excited state as this value did not change substantially from the protonated one which gave a lifetime of 5 ns. The long lived component has a lifetime of 691 ns (τ_2) which contribute 99 % and is assigned to a decay from π-π* excited state based on the results obtained for the π-π* excited state decay for the protonated analogue which was 353 ns. The χ^2 value for the fit is 1.083. The lifetime decay curve obtained for [Ir(d$_8$bpy)$_2$Cl$_2$]PF$_6$ (**III**) is given in Figure 5.22 (b).

The data including the short lived and long lived lifetimes, their relative percentages and the average lifetime are given in table 5.9. The deuteriation effect on the excited state lifetimes is evident from this table. Deuteriation of the peripheral bipyridine ligand resulted in almost doubling of the lifetime of the complex which shows that the lowest lying excited state for the complex is π-π* state at room temperature.

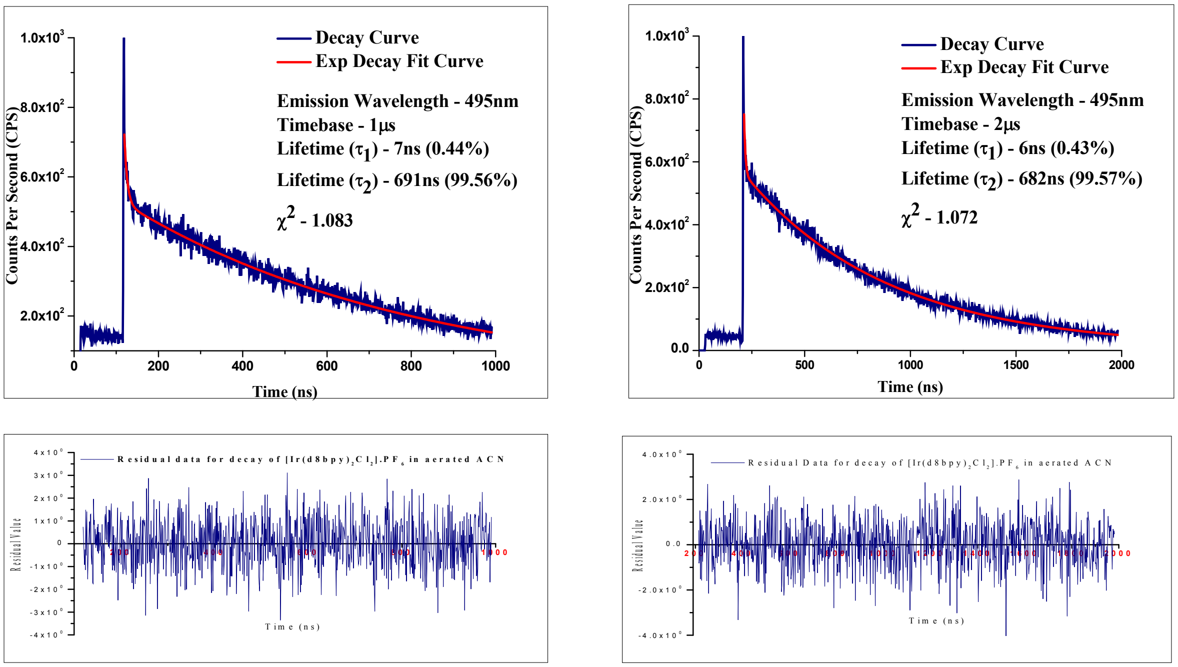

(a) **(b)**

Figure: 5.22 *Lifetime decay plots for complex [Ir(d$_8$bpy)$_2$Cl$_2$]PF$_6$ **(III)** **(a)** at a time range of 1 μs **(b)** at a time range of 2 μs in aerated spec grade ACN solution (298K).*

Complex	Wavelength, λ_{em}	Timebase (ns)	Lifetime (ns)	Relative %	Avg. Lifetime,ns
[Ir(bpy)$_2$Cl$_2$]PF$_6$ **(I)**	500	500	$\tau_1 - 5$	3	τ_{av} - 353
			$\tau_2 - 353$	97	
			$\chi^2 - 1.010$		
[Ir(d$_8$bpy)$_2$Cl$_2$]PF$_6$ **(III)**	500	1000	$\tau_1 - 7$	0.4	τ_{av} - 691
			$\tau_2 - 691$	99	
			$\chi^2 - 1.083$		

Table 5.9 *Tabulated lifetiemes and their relative percentage for complexes **(I)** and **(III)** at various time bases.*

The luminesence decay lifetimes for complexes [Ir(phen)$_2$Cl$_2$]PF$_6$, [Ir(dmbpy)$_2$Cl$_2$]PF$_6$, [Ir(dtbpy)$_2$Cl$_2$]PF$_6$ and their deuteriated analogoues [Ir(d$_8$phen)$_2$Cl$_2$]PF$_6$, [Ir(d$_{12}$dmbpy)$_2$Cl$_2$]PF$_6$, [Ir(d$_{24}$dtbpy)$_2$Cl$_2$]PF$_6$ were all measured at room temperature (298 K) using TCSPC. The results were analysed by taking into consideration the data obtained for complex [Ir(bpy)$_2$Cl$_2$]PF$_6$ and its deuteriated analogoue described in detail above (figure 5.21, 5.22 and table 5.9). The decay curves given in figure 5.23 shows that all of these complexes are biexponential with a shorter lifetime assigned to a d-π* excited state and the long lived component orginating from the π-π* excited state. Further support of the assignment is obtained from the deuteriation effect shown by all these complexes. The long lived lifetime almost doubled upon deuteriation which clearly shows that the lowest lying excited state is the π-π* state, the short component does not show any difference, thus indicating the possibility of a decay from d-π* excited state. All data including the short lived and long lived lifetimes, their relative percentages and the average lifetimes for all these complexes are given in tables 5.10, 5.11 and 5.12.

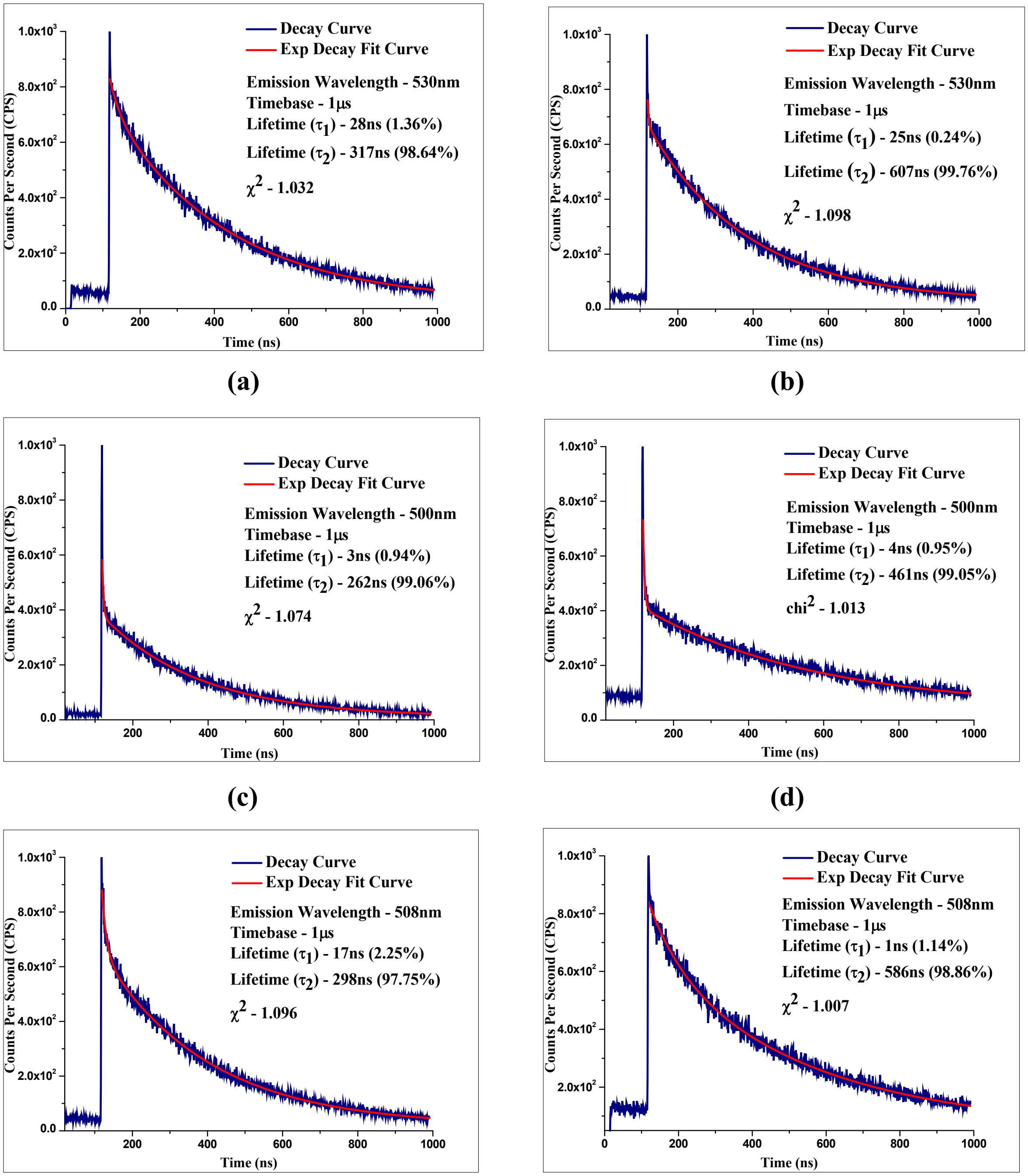

(a) (b)

(c) (d)

(e) (f)

Figure: 5.23 ***(a)*** *Lifetime decay plot for complex [Ir(phen)$_2$Cl$_2$]PF$_6$ (V) at a time range of 1 μs* ***(b)*** *Lifetime decay plot for complex [Ir(d$_8$phen)$_2$Cl$_2$]PF$_6$ (VI) at a time range of 1 μs* ***(c)*** *Lifetime decay plot for complex [Ir(dmbpy)$_2$Cl$_2$]PF$_6$ (VII) at a time range of 1 μs* ***(d)*** *Lifetime decay plot for complex [Ir(d$_{12}$dmbpy)$_2$Cl$_2$]PF$_6$ (VIII) at a time range of 1 μs* ***(e)*** *Lifetime decay plot for complex [Ir(dtbpy)$_2$Cl$_2$]PF$_6$ (IX) at a time range of 1 μs* ***(f)*** *Lifetime decay plot for complex [Ir(d$_{24}$dtbpy)$_2$Cl$_2$]PF$_6$ (X) at a time range of 1 μs. All measurements were done in aerated spec grade ACN solution (298K).*

Complex	Wavelength λ_{em}	Timebase (ns)	Lifetime (ns)	Relative %	Avg. Lifetime,ns
$[Ir(phen)_2Cl_2]PF_6$ **(V)**	530	500	$\tau_1 - 17$	0.9	τ_{av} - 292
			$\tau_2 - 292$	99	
			$\chi^2 - 1.083$		
$[Ir(d_8phen)_2Cl_2]PF_6$ **(VI)**		2000	$\tau_1 - 27$	0.3	τ_{av} - 614
			$\tau_2 - 614$	99	
			$\chi^2 - 1.014$		

Table 5.10 *Tabulated lifetiemes and their relative percentage for complexes (**V**) and (**VI**) measured in spec grade ACN at room temperature (298 K).*

Complex	Wavelength, λ_{em}	Timebase (ns)	Lifetime (ns)	Relative %	Avg. Lifetime,ns
$[Ir(dmbpy)_2Cl_2]PF_6$ **(VII)**	500	500	$\tau_1 - 2$	0.8	τ_{av} - 241
			$\tau_2 - 241$	99	
			$\chi^2 - 1.018$		
$[Ir(d_{12}dmbpy)_2Cl_2]PF_6$ **(VIII)**		1000	$\tau_1 - 4$	0.9	τ_{av} - 461
			$\tau_2 - 461$	99	
			$\chi^2 - 1.013$		

Table 5.11 *Tabulated lifetiemes and their relative percentage for complexes (**VII**) and (**VIII**) measured in spec grade ACN at room temperature (298 K).*

Complex	Wavelength, λ_{em}	Timebase (ns)	Lifetime (ns)	Relative %	Avg. Lifetime,ns
$[Ir(dtbpy)_2Cl_2]PF_6$ **(IX)**	508	500	$\tau_1 - 12$	2	τ_{av} - 284
			$\tau_2 - 284$	98	
			$\chi^2 - 1.000$		
$[Ir(d_{24}dtbpy)_2Cl_2]PF_6$ **(X)**		2000	$\tau_1 - 1$	2	τ_{av} - 592
			$\tau_2 - 592$	98	
			$\chi^2 - 1.023$		

Table 5.12 *Tabulated lifetiemes and their relative percentage for complexes (**IX**) and (**X**) measured in spec grade ACN at room temperature (298 K).*

The room temperature (298 K) decay curve for complexes $[Ir(dpbpy)_2Cl_2]PF_6$ and $[Ir(dpphen)_2Cl_2]PF_6$ are given in figure 5.24. Both the complexes showed biexponential decays with the shorter component arising from the d-π* excited state and the longer component arising from π-π* excited state, based on prior studies.

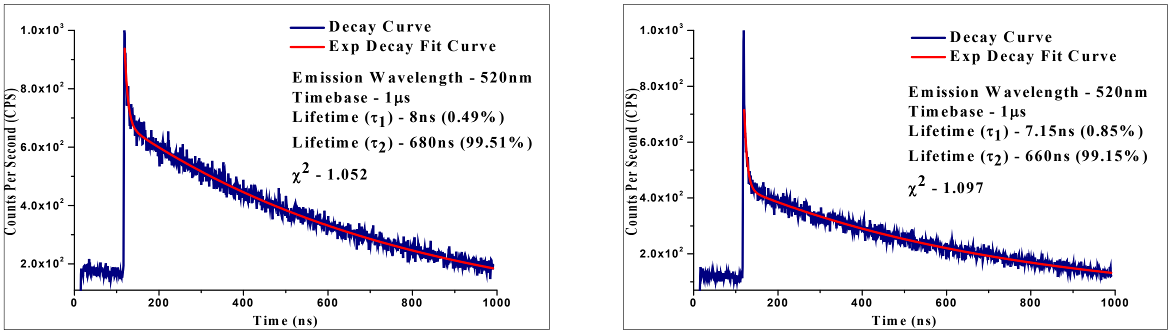

(a) **(b)**

Figure: 5.24 (a) *Lifetime decay plot for complex $[Ir(dpbpy)_2Cl_2]PF_6$* ***(XI)*** *at a time range of 1 µs* ***(b)*** *Lifetime decay plot for complex $[Ir(dpphen)_2Cl_2]PF_6$* ***(XII)*** *at a time range of 1 µs, both are measured in spec grade aerated ACN solution (298K).*

Complex	Wavelength, λ_{em}	Timebase (ns)	Lifetime (ns)	Relative %	Avg. Lifetime,ns
$[Ir(dpbpy)_2Cl_2]PF_6$ **(XI)**	520	1000	τ_1 – 8	0.5	τ_{av} – 680
			τ_2 – 680	99	
			χ^2 – 1.052		
		2000	τ_1 – 7	1	τ_{av} - 698
			τ_2 – 698	99	
			χ^2 – 1.048		

Table 5.13 *Tabulated lifetiemes and their relative percentage for complex* ***(XI)*** *measured in spectroscopic grade ACN at room temperature (298 K).*

For $[Ir(dmbpy)_2(HPhpytr)](CF_3SO_3)_3$ (**XVI**) the lifetime decay curves obtained at two different emission wavelengths, 470 and 495 nm are given in figure 5.25 (a) and 5.25 (b) below. From the decay curve it is clear that both the decays are biexponential. Figure 5.25 (a) gives the lifetime deacay curve at 470 nm. The short lived component has a lifetime of 44 ns (τ_1) which contributes 7 % , the long lived component has a lifetime of 343 ns (τ_2) which contributes 93 %. The χ^2 value for the fit is 1.001 indicating close fit to experimental data. The lifetime decay curve obtained at 495 nm at a time base of 1 µs is given in figure 5.25 (b). From the decay curve it is clear that the decay is biexponential. The decay was obtained at an emission wavelength of 495 nm. The short lived component is having a lifetime of 48 ns (τ_1) which contributes 10 % , the long lived component is having a lifetime of 338 ns (τ_2) which contributes 90 %.

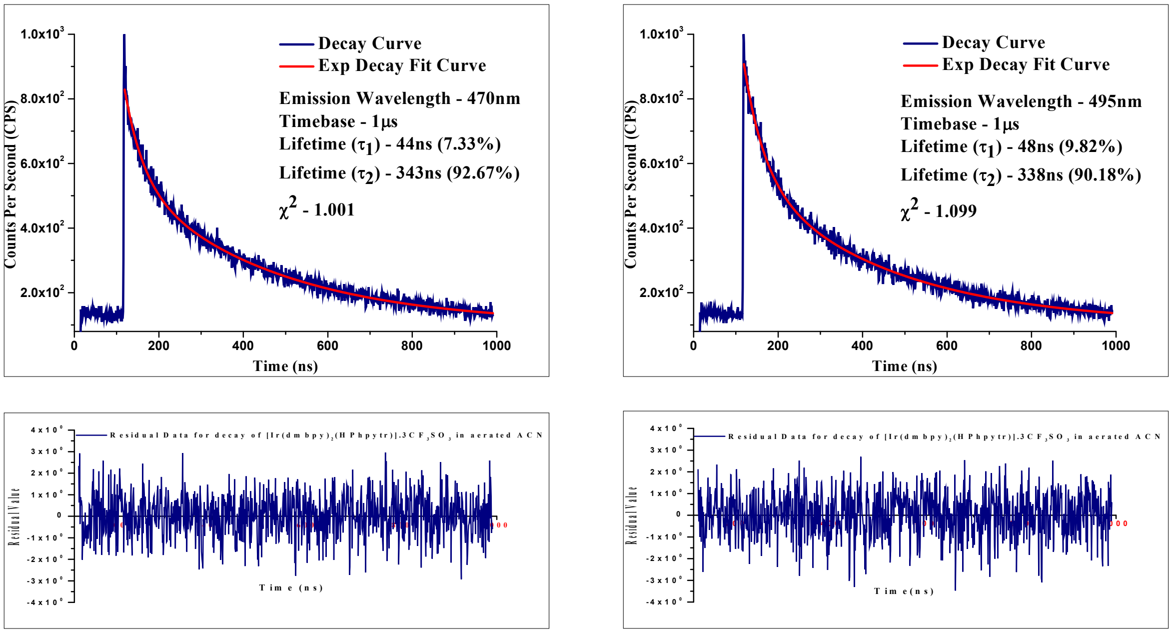

(a) **(b)**

Figure: 5.25 *Lifetime decay plots for complex [Ir(dmbpy)$_2$(HPhpytr)](CF$_3$SO$_3$)$_3$ (XVI)* ***(a)*** *at a wavelength of 470 nm* ***(b)*** *at a wavelength of 495 nm in aerated spec grade ACN solution (298K).*

Complex	Wavelength, λ_{em}	Timebase (ns)	Lifetime (ns)	Relative %	Avg. Lifetime,ns
[Ir(dmbpy)$_2$(Hphpytr)] (CF$_3$SO$_3$)$_3$	470	1000	$\tau_1 - 44$	7	τ_{av} - 340
			$\tau_2 - 343$	93	
			$\chi^2 - 1.001$		
	495	1000	$\tau_1 - 48$	10	τ_{av} - 334
			$\tau_2 - 338$	90	
			$\chi^2 - 1.099$		

Table 5.14 *Tabulated lifetiemes and their relative percentage for complex XVI at various time bases*

5.3.8 Lifetime measurements using laser flash photolysis

The excited state properties of the iridium (III) polypyridyl complexes were measured at 298 K and 77 K using laser flash photolysis and the results are shown in Tables 5.1. The data were plotted and analysed with the aid of the software provided in the instrument and in some cases using sigma plot 8 software. The graphs along with the errors calculated for all the samples are given in appendix D. The measurements at 298 K for all the complexes measured with TCSPC was again repeated using the laser flash photolysis at 355 nm and the results obtained were found to be in good agreement with the results obtained with the former which shows the accuracy of the results reported for lifetimes in this chapter. The low temperature (77 K) lifetimes are measured in EtOH : MeOH (4:1) glasses.

From the emission measurements carried out for all the iridium (III) polypyridyl complexes described in this chapter the lowest excited state at 298 K is tentatively assigned to a mixed ^{3}(d-π*)-^{3}(π-π*) excited state based on the results obtained from emission and lifetime measurements at 298 K. The emission curves at 77 K given in section 5.3.6 indicate the possibility of a dual emission. It can be seen that all the low temperature emission (77 K) curves are structured having more that one emission maxima. The lifetimes were measured at these two different emission maxima and in all the polypyridyl complexes studied in this chapter the lifetime of these two different emission maxima at 77 K had a difference of 1µs-3µs as shown in table 5.15. By comparing the emission curves and lifetime measurements done at 77 K with the reported photophysical data[10,20,21,23] of similar complexes assignments were made for the excited states. The long lived lifetime is expected to arise from a π-π* excited state. In order to prove this, the effect of deuteriation on the excited state lifetimes at 77 K for these Ir (III) polypyridyl complexes was determined. The deuteriation study on the excited state photophysics of Ru (II) complexes was extensively studied detail in the group[86] which gave the basic platform to extend the concepts in assigning the excited state of Ir (III) complexes.[20d] The deuteriated analogues of all these polypyridyl complexes gave lifetimes greater than the protonated analogous, but the increase in lifetime at 77 K is not sufficient (1µs-2µs) in order to assign the emission to be from a pure π-π* excited state. Also if it is from a pure π-π* excited state the lifetime should be in the range of 80-100 µs as shown by the tris polypyridyl complexes based on previous reports.[27,31,41] The lifetime value for all of these complexes came in the range of 10-15 µs which shows the mixing of the metal centered d-π* state and ligand centered π-π* state. Based on the results obtained emission is assigned to occur from a mixed ^{3}(d-π*)-^{3}(π-π*) excited state. Further detailed measurements including solvent dependent and temperature dependent photophysical measurements along with resonance Raman should be carried out in order to give a clear conformation regarding the assignments which will be studied in future. The excited state decay curve for [Ir(d$_8$bpy)$_2$Cl$_2$]PF$_6$ (**III**) along with the fit curve and the measured errors are given in figure 5.26 below. The rest of the decay curves are given in appendix D.

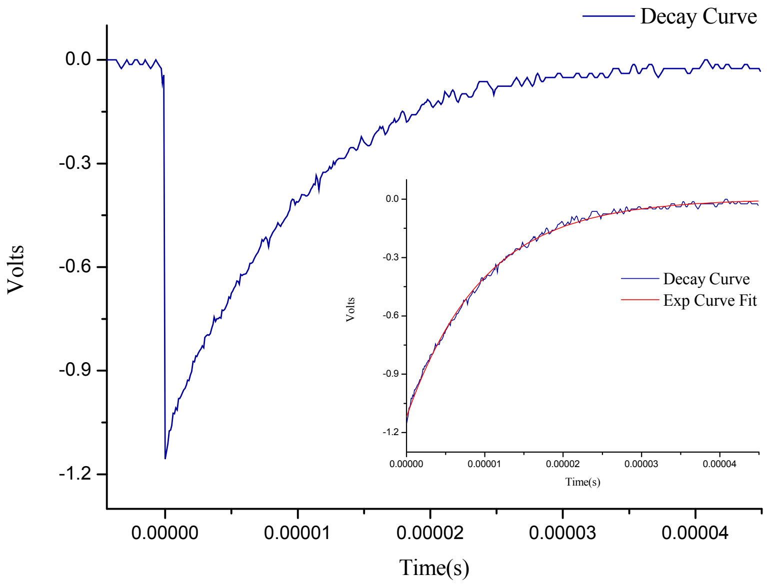

Figure 5.26 *Low temperature (77 K) excited state lifetime plot, non linear fitted curve, lifetime and error calculated for [Ir(bpy)$_2$Cl$_2$]PF$_6$ (I) in spectroscopic grade EtOH:MeOH (4:1) glass. Excitation wavelength, λ_{ex} = 355 nm*

Complex	Lifetime (298K), ns	Lifetime (77K)(λ_{em}) µs
[Ir(bpy)$_2$Cl$_2$]PF$_6$ **(I)**	390	10.61(470), 11.26 (498)
[Ir(d$_8$bpy)$_2$Cl$_2$]PF$_6$ **(III)**	730	10.94(470), 13.79(498)
[Ir(phen)$_2$Cl$_2$]PF$_6$ **(V)**	363	13.12(473), 16.52(504)
[Ir(d$_8$phen)$_2$Cl$_2$]PF$_6$ **(VI)**	654	14.29(473), 17.96(504)
[Ir(dmbpy)$_2$Cl$_2$]PF$_6$ **(VII)**	277	10.93(470), 12.45(502)
[Ir(d$_{12}$dmbpy)$_2$Cl$_2$]PF$_6$ **(VII)**	530	12.27(470), 13.98(502)
[Ir(dtbpy)$_2$Cl$_2$]PF$_6$ **(IX)**	330	6.4(468), 7.08(490)
[Ir(d$_{24}$dtbpy)$_2$Cl$_2$]PF$_6$ **(IX)**	603	8.88(468), 11.22(490)

Table 5.15 *Lifetimes at 298 K are measured in spectroscopic grade ACN and 77 K are measured in spectroscopic grade EtOH:MeOH (4:1) glass. Excitation wavelength λ_{ex} = 355 nm.*

5.3.9 Intermolecular photocatalysis of [Ir(polypyridyl)$_2$Cl$_2$]$^+$ complexes using Visible light (470 nm) and UV Light (350 nm)

Photoreduction of water into H_2 based on solar energy conversion is of great importance in view of generating alternative energy sources to meet the rising global energy demand. It has been known since the late 1970s that tris (2,2'-bipyridine) ruthenium (II) and its derivatives possess the excited states thermodynamically capable of reducing water into H_2 in the presence of a sacrificial electron donor, an electron mediator and a suitable catalyst.[93,94] Intermolecular photocatalyts with cyclometallated iridium complexes such as [Ir(C^N)$_2$(N^N)]$^+$ are studied to a greater extent.[3,95] As a consequence of greater ligand-field stabilization energy (LFSE), the use of cyclometalated iridium (III) complexes avoids the thermal population of, and subsequent non radiative decay from, the dissociative ^{3}MC state observed with tris diimine Ru (II) complexes.[96] In addition, the greater energetic requirements for the population of the ^{3}MC state allow a larger range of excited state energies by altering the ligand architecture.[97] Detailed references are given in chapter 1 and intermolecular photocatalysis of cyclometallated iridium (III) complexes are reported in chapter 3. There are no reports in the literature where N^N polypyridyl iridium (III) complexes such as [Ir(polypyridyl-N,N')$_2$Cl$_2$]$^+$ were used for intermolecular photocatalytic H_2 genaration using both visible (470 nm) or UV (350 nm) light. These complexes proved to be much more efficient than the traditional cyclometallated complexes giving very good TON's. The intermolecular photocatalysis were all done at 5 % H_2O using [Pt(ACN)$_2$Cl$_2$] and [Pd(ACN)$_2$Cl$_2$] as the catalysts. Triethylamine (TEA) was used as the sacrificial agent in all these measurements. The details regarding the photocatalytic measurements are discussed in detail in chapter 2. The intermolecular photocatalysis done for [Ir(bpy)$_2$Cl$_2$]PF$_6$ (**I**) and its deuteriated analogue [Ir(d$_8$bpy)$_2$Cl$_2$]PF$_6$ (**III**) using both visible and UV light are tabulated in tables 5.16 and 5.17. The results obtained are compared with the standard complex [Ir(ppy)$_2$(bpy)]PF$_6$ in both visible and UV light. In both the cases it can be seen that the N^N polypyridyl complex [Ir(bpy)$_2$Cl$_2$]PF$_6$ (**I**) and its deuteriated analogue (**III**) proved to be more efficient than the cyclometallated iridium (**III**) complex.

Complex ($6x10^{-5}$ M) + [Pt(ACN)$_2$Cl$_2$],($6x10^{-5}$ M)	**H_2O %**	**Area (mV/sec)**	**TON (average)**
[Ir(ppy)$_2$(bpy)]PF$_6$	5%	1) 88 2) 91 3) 85	51
[Ir(bpy)$_2$Cl$_2$]PF$_6$ **(I)**	5%	1) 132 2) 147 3) 138	80
[Ir(d$_8$bpy)$_2$Cl$_2$]PF$_6$ **(III)**	5%	1) 50 2) 48 3) 48	28

Table 5.16 *Tabulated data for intermolecular photocatalysis using visible light (470 nm) of complexes* ***(I)*** *and* ***(III)*** *in ACN, sacrificial agent used is TEA (2.15 M), irradiation time - 18h.*

Complex ($6x10^{-5}$ M) + [Pt(ACN)$_2$Cl$_2$]($6x10^{-5}$ M)	**H_2O %**	**Area (mV/sec)**	**TON (average)**
[Ir(ppy)$_2$(bpy)]PF$_6$	5%	1) 15 2) 17	9
[Ir(bpy)$_2$Cl$_2$]PF$_6$ **(I)**	5%	1) 48 2) 45	27
[Ir(d$_8$bpy)$_2$Cl$_2$]PF$_6$ **(III)**	5%	1) 28 2) 24	15

Table 5.17 *Tabulated data for intermolecular photocatalysis using UV light (350 nm) of complex* ***(I)*** *and* ***(III)*** *in ACN, sacrificial agent used is TEA (2.15 M), irradiation time – 18h.*

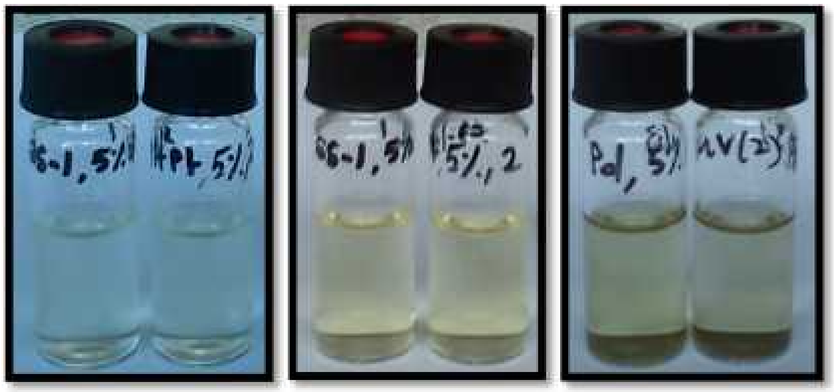

(a) **(b)** **(c)**

Figure 5.27 ***(a)*** *Photocatalytic solution of complex* ***(I)*** *before irradiation* ***(b)*** *Photocatalytic solution for complex* ***(I)*** *after 18h irradiation using visible light (470 nm).(catalyst – [Pt(ACN)$_2$Cl$_2$])* ***(c)*** *Photocatalytic solution for complex* ***(I)*** *after irradiation using visible light (470 nm).(catalyst – [Pd(ACN)$_2$Cl$_2$]).*

From table 5.16 complex (**I**) has a TON of 80 and complex (**III**) has a TON of 28, deuteriation thus resulted in a decrease of the amount of H_2 produced. The results are quite similar in the case of UV light irradiation, with complex (**I**) a TON of 27 and complex (**III**) shows a TON of 15, so a decrease in the amount of H_2 produced was observed using higher energy UV light. Another important difference is that the results clearly show that similarly to the cyclometallated complexes described in chapter 3 these complexes also show a notable decrease in the TON's on moving from visible light (470 nm) to UV light (350 nm) which suggest that apart from the π-π* transitions d-π* transitions play a major role in photocatalysis in these type of complexes. Figure 5.27 (a) shows the photocatalytic solution for complex (**I**) in 5 % H_2O in ACN before irradiation and figure 5.27 (b) the solutions with [Pt(ACN)$_2$Cl$_2$] as the catalyst after 18h irradiation using visible light (470 nm). The colour of the solution changed after 18h irradiation from colourless to pale yellow. There was no visible precipitate present in the solution containing [Pt(ACN)$_2$Cl$_2$] as the catalyst. But when [Pd(ACN)$_2$Cl$_2$] was used instead of Pt after 18h irradiation a large amount of black precipitate was formed at the bottom of vials, but there was no hydrogen formed when [Pd(ACN)$_2$Cl$_2$] was used as the catalyst. From these results it was assumed that in the case of Pt some colloidal Pt may have formed[98] which was not visible, and promoted the catalytic activity. For Pd these colloidals aggregate to form particles which accumulates at the bottom. In all of the polypyridyl complexes described in this chapter the results are similiar. Other than the novel tris heteroleptic complex [Ir(dmbpy)$_2$(HPhpytr)](CF$_3$SO$_3$)$_3$ (**XVI**) all others gave zero TON when [Pd(ACN)$_2$Cl$_2$] was used as the catalyst. The photocatalytic results for the novel complex (**XVI**) is described in detail at the end of this section. The TON values obtained using both irradiation wavelengths for all the complexes along with their corresponding peak areas obtained from GC are tabulated in table 5.18. All the results are compared with the standard complex [Ir(ppy)$_2$(bpy)]PF$_6$ which was also measured under similar conditions and the results shows the efficiency of N^N polypyridyl Ir (III) complexes compared to the cyclometallated complex. This is important since the N^N polypyridyl Ir (III) complexes similar to the Ir (III) cyclometallated complexes described in detail in chapter 3 has not yet been synthesised. The results shown below indicates that these N^N polypyridyl ligands if complexed to our bridging ligands might produce more H_2 than the corresponding cyclometallated systems.

Complex ($6x10^{-5}$ M) + $Pt(ACN)_2Cl_2$ ($6x10^{-5}$ M)	**H_2O %**	**470 nm**		**350 nm**	
		Area (mV/s)	**TON (average)**	**Area (mV/s)**	**TON (average)**
[Ir(ppy)$_2$(bpy)]PF$_6$	5%	1) 88 2) 91 3) 85	51	1) 15 2) 17	9
[Ir(phen)$_2$Cl$_2$]PF$_6$ **(V)**	5%	1) 17 2) 15 3) 18	10	1) 10 2) 11	6
[Ir(d$_8$phen)$_2$Cl$_2$]PF$_6$ **(VI)**	5%	1) 12 2) 12 3) 13	7	1) 5 2) 7	3
[Ir(dmbpy)$_2$Cl$_2$]PF$_6$ **(VII)**	5%	1) 60 2) 62 3) 56	34	1) 11 2) 10	6
[Ir(d$_{12}$dmbpy)$_2$Cl$_2$]PF$_6$ **(VIII)**	5%	1) 150 2) 157 3) 153	88	1) 33 2) 35	20
[Ir(dtbpy)$_2$Cl$_2$]PF$_6$ **(IX)**	5%	1) 312 2) 307 3) 306	177	1) 22 2) 25	14
[Ir(d$_{24}$dtbpy)$_2$Cl$_2$]PF$_6$ **(X)**	5%	1) 333 2) 339 3) 331	192	1) 76 2) 74	44
[Ir(dpbpy)$_2$Cl$_2$]PF$_6$ **(XI)**	5%	1) 143 2) 155 3) 156	87	1) 17 2) 16	10
[Ir(dpphen)$_2$Cl$_2$]PF$_6$ **(XII)**	5%	1) 481 2) 456 3) 489	273	1) 15 2) 19	10

Table 5.18 *Tabulated data for intermolecular photocatalysis using Visible light (470 nm) and UV light (350 nm) in ACN, sacrificial agent used is TEA (2.15M), irradiation time - 18h.*

Table 5.18 shows that complex [Ir(dpbpy)$_2$Cl$_2$]PF$_6$ (**XI**) has a TON of 87 and complex [Ir(dpphen)$_2$Cl$_2$]PF$_6$ (**XII**) has a TON of 273. These results indicate that the substitution of an electron withdrawing phenyl group on the 4 and 4' positions of bpy did not make a difference in the amount of H_2 produced as the TON increased to 87 for complex (**XI**) from 78 as obtained for complex [Ir(bpy)$_2$Cl$_2$]PF$_6$ (**I**) under similar conditions. For complex (**XII**) substitution of the electron withdrawing phenyl group at 4 and 7 positions resulted in an increase in the amount of hydrogen produced as the TON increased to 273 for complex (**XII**) from only a TON of 10 for the unsubstituted phenanthroline complex [Ir(phen)$_2$Cl$_2$]PF$_6$ (**V**) (table 5.18). These results suggest that the substitution with an electron withdrawing group has a larger effect for both phenanthroline and bipyridine ligands. Comparing complexes (**I**), (**VII**) and (**IX**) in which the last two have electron donating dimethyl and ditertiary butyl groups on 4 and 4' positions of bipyridine, complex (**VII**) there is a decrease in TON to 34 from 80 but for complex (**IX**) there is doubling of TON to 177 from 80. For UV irradiation there is a decrease in TON for both substituted complexes compared to (**I**), where the TON decreased from 27 to 6 in case the of (**VII**) and 14 in the case of (**IX**). But interestingly for the deuteriated analogues of these complexes both the substituted deuteriated complexes (**VIII**) and (**X**) produced more H_2 than the deuteriated unsubstituted counterpart (**III**) as can be seen from tables 5.16, 5.17 and 5.18. No hydrogen was obtained for all these complexes when photocatalysis was carried out using [Pd(ACN)$_2$Cl$_2$] under similar conditions. The figures before irradiation and after irradiation for all these complexes are given in appendix D.

The intermolecular photocatalytic results for the novel green emitting heteroleptic iridium complex [Ir(dmbpy)$_2$(Hphpytr)](CF$_3$SO$_3$)$_3$ (**XVI**) in both visible and UV light at two different percentages of water using [Pt(ACN)$_2$Cl$_2$] as catalyst are tabulated in tables 5.19 and 5.20. Complex (**XVI**) shows a TON of 403 using 5 % water as shown in table 5.27, which is the highest amount of H_2 produced by a N^N polypyridyl Ir (III) complex upto now, and shows that the introduction of a triazole ligand to the iridium metal leads to increased H_2 production. The precursor complex [Ir(dmbpy)$_2$Cl$_2$]PF$_6$ (**VII**) shows a TON of 34 under the similar condition (table 5.18) so there is almost 10 fold increase in the amount of H_2 produced on complexing with the triazole ligand. For the UV irradiation experiments the increase in H_2 formation for the heteroleptic complex (**XVI**) is almost 25 times that of the precursor bis chloride complex (**VII**), as the TON increased from 6 to 149. Using both visible and UV light, and 5 % of water proved to be the optimum condition for photocatalytic activity. For complex (**XVI**) under visible light irradiation, moving to 10 % water resulted in a TON of 239 which is almost half the value of the result obtained at 5 % water. Similarly to the case with UV light irradiation, the TON decreased to 130 from 149 as the H_2O percentage was increased from 5 % to 10 %. As seen in the case of other polypyridyl complexes the heteroleptic tris iridium (III) complex also showed a prominent decrease in the TON on going from visible light to UV light. A solution of complex (**XVI**) and [Pt(ACN)$_2$Cl$_2$], before irradiation and after 18h visible light irradiation, is given in figure 5.28. The colourless solution before irradiation changed to pale yellow coloured solution following irradiation.

Complex (6x10^{-5} M) + [Pt(ACN)$_2$Cl$_2$] (6x10^{-5} M)	**H$_2$O %**	**Area (mV/sec)**	**H$_2$ (ml)**	**TON (average)**
[Ir(dmbpy)$_2$(HPhpytr)] (CF$_3$SO$_3$)$_3$ (**XVI**)	5%	697	0.5879	403
		702	0.5921	
		705	0.5947	
	10%	435	0.3669	239
		395	0.3332	
		415	0.3501	

Table 5.19 *Tabulated data for intermolecular photocatalysis using visible light (470 nm) for complex (**XVI**) in ACN at 5 % and 10 % H$_2$O, sacrificial agent used is TEA (2.15 M), irradiation time - 18h.*

Complex (6x10^{-5} M) + [Pt(ACN)$_2$Cl$_2$] (6x10^{-5} M)	**H$_2$O %**	**Area (mV/sec)**	**H$_2$ (ml)**	**TON (average)**
[Ir(dmbpy)$_2$(HPhpytr)] (CF$_3$SO$_3$)$_3$ (**XVI**)	5%	261	0.2202	149
		258	0.2176	
	10%	230	0.1940	130
		223	0.1881	

Table 5.20 *Tabulated data for intermolecular photocatalysis using UV light (350 nm) of complex (**XVI**) in ACN at 5 % and 10 % H$_2$O, sacrificial agent used is TEA (2.15 M), irradiation time - 18h.*

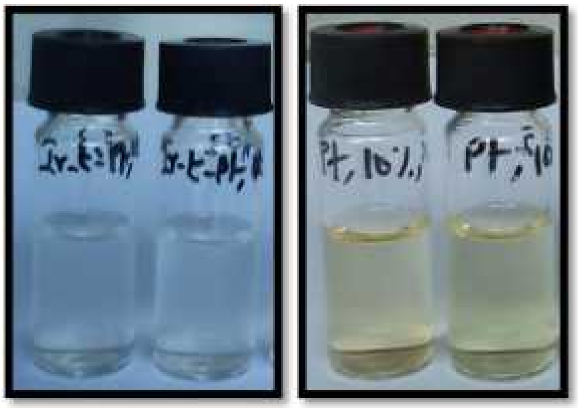

(a) **(b)**

Figure 5.28 (a) *Photocatalytic solution of complex **(XVI)** before irradiation **(b)** Photocatalytic solution for complex **(XVI)** after 18h irradiation using visible light (470 nm).(catalyst – [Pt(ACN)$_2$Cl$_2$])*

One of the biggest difference showed by this new heteroleptic complex is the catalysis experiments with [Pd(ACN)$_2$Cl$_2$]. All the iridium (III) polypyridyl complexes reported in this chapter except complex [Ir(dmbpy)$_2$(HPhpytr)](CF$_3$SO$_3$)$_3$ (**XVI**) gave no hydrogen when [Pd(ACN)$_2$Cl$_2$] was used as the catalyst. But complex (**XVI**) gave good results with respect to others, but comparitively less than what was obtained with the same complex using a Pt catalyst. The results are tabulated in table 5.21 and 5.22 below. Complex (**XVI**) gave a TON of 226 at 5 % water as shown in table 5.21, which is half the amount of H$_2$ produced using Pt as the catalyst mentioned above. The precursor complex [Ir(dmbpy)$_2$Cl$_2$]PF$_6$ (**VII**) did not produce hydrogen under similar conditions so there is almost 200 fold increase in the amount of H$_2$ produced on complexing with the triazole ligand. Using UV irradiation there is also an increase in the amount of H$_2$ formed. The TON increased from 0 to 70 at 5 % water and from 0 to 2 at 10 % water. Using both blue and UV light, 5% of water proved to be the optimum condition for photocatalytic activity using [Pd(ACN)$_2$Cl$_2$] as catalyst. As seen in the case of other polypyridyl complexes and the above mentioned photocatalysis with the Pt catalyst the heteroleptic iridium complex also showed a notable decrease in the TON on going from visible light to UV light in this case also.

Complex ($6x10^{-5}$ M) + [Pd(ACN)$_2$Cl$_2$] ($6x10^{-5}$ M)	**H_2O %**	**Area (mV/sec)**	**H_2 (ml)**	**TON (average)**
[Ir(dmbpy)$_2$(HPhpytr)] 3CF$_3$SO$_3$ (XVI)	5%	396	0.3340	226
		399	0.3366	
		382	0.3222	
	10%	231	0.1948	127
		210	0.1771	
		223	0.1881	

***Table 5.21** Tabulated data for intermolecular photocatalysis using visible light (470 nm) for complex (**XVI**) in ACN at 5 % and 10 % H_2O, sacrificial agent used is TEA (2.15 M), irradiation time - 18h.*

Complex ($6x10^{-5}$ M) + [Pd(ACN)$_2$Cl$_2$] ($6x10^{-5}$ M)	**H_2O %**	**Area (mV/sec)**	**H_2 (ml)**	**TON (average)**
[Ir(dmbpy)$_2$(HPhpytr)]. 3CF$_3$SO$_3$ (XVI)	5%	123	0.1038	70
		120	0.1012	
	10%	3.32	0.0028	2
		3.01	0.0025	

***Table 5.22** Tabulated data for intermolecular photocatalysis using UV light (350 nm) of complex (**XVI**) in ACN at 5 % and 10 % H_2O, sacrificial agent used is TEA (2.15 M), irradiation time - 18h.*

A photocatalytic solution of complex (**XVI**) and [Pd(ACN)$_2$Cl$_2$] before irradiation and after 18 h visible light irradiation is given in figure 5.29 where it appears that the colourless solution before irradiation changed to pale yellow after irradiation. Comparing figures 5.28 and 5.29 it can be seen that the latter one has a black precipitate at the bottom of the vial after 18h irradiation which is absent in the former. A similar precipitate was seen for all other polypyridyl complexes but none of them gave any hydrogen with Pd.

(a) **(b)**

Figure 5.29 ***(a)*** *Photocatalytic solution of complex* ***(XVI)*** *before irradiation* ***(b)*** *Photocatalytic solution for complex* ***(XVI)*** *after 18h irradiation using visible light (470 nm).(catalyst – [Pd(ACN)$_2$Cl$_2$]).*

5.4 Conclusion

In conclusion a series of iridium polypyridyl complexes having the general formulae [Ir(polypyridyl-N,N')$_2$Cl$_2$](PF$_6$) along with their deuteriated analogues have been successfully synthesised in high yield. The removal of chlorides from these complexes was achieved successfully using a much shorter and efficient synthetic procedure. The formation of [Ir(bpy-N,N')$_2$Cl$_2$]$^+$ and [Ir(bpy-N,N')$_2$(bpy-C,N')]$^{2+}$ has been confirmed by ^{1}H NMR, ^{13}C, HPLC, UV-Vis and emission studies. The possible mechanistic significance of C coordination for reactions of iridium (III) bipyridine complexes and the ratio of normal and orthometallated complex formed was investigated. The time dependent HPLC and NMR data gave promising results as to the mechanistic pathway for the synthesis of these complexes.

Excited state photophysics for these complexes were studied in detail which includes absorption, emission (298 K and 77 K), quantum yields and lifetimes (298 K and 77 K). Lifetime measurements were carried out on two different instruments and the results obtained were comparable. The deuteriation effect study proved to be very promising as it helped in the identification of the lowest energy excited states in these systems and interestingly at low temperatures (77 K) all of them showed dual emission which was tentatively assigned to orginate from a mixed (d-π*)-(π-π*) state which are very close in energy. The emission wavelength observed suggests that these materials may be developed in particular for the preparation of OLED materials. By varying the polypyridyl systems either by substituting the bipyridine or phenanthroline with electron withdrawing or electron releasing groups, emission can be tuned through the entire range of visible spectrum, and all of them show long lived excited states.

Combining these two properties, together with the synthetic method, these complexes were synthesised in high purity and good yield in a very short reaction opening up new applications for these complexes.

The removal of chlorides from these complexes was achieved successfully using a much shorter and efficient synthetic procedure. The coordination of the triflate intermediates to triazolyl pyridine ligands has not yet been done, which will tell us the importance of the new novel green emitting [Ir(dmbpy)$_2$(HPhpytr)](CF$_3$SO$_3$)$_3$ complex. This complex proved to be a very efficient intermolecular photocatalyst giving a TON of 400 following 18h irradiation time using a 470 nm light source compared to its analogous phenyl pyridine derivative which produced no hydrogen. Further studies by varying the conditions are under investigation. Transition metal complexes containing ligands with extended π-systems (eg., pyridine, bipyridine) have generated tremendous interest because of their potential to participate as photocatalysts in solar driven artificial photoconversion processes.[3,99] Iridium complexes reported here are all potential candidates for intermolecular photocatalytic hydrogen generation showing higher efficiency than the corresponding cyclometallated analogues, which can be extended in future to intramolecular multimetallic systems thereby producing even higher TON's.

5.5 Bibliography

---

1. Y. Shen and B. P. Sullivan, *J. Chem. Educ.*, **1997**, 74, 685
2. C. Joachim, J. K. Gimzewski and A. Aviram, *Nature.*, **2000**, 408, 541
3. J. I. Goldsmith, W. R. Hudson, M. S. Lowry, T. H. Anderson and S. Bernhard, *J. Am. Chem. Soc.*, **2005**, 127, 7502
4. A. S. Polo, M. K. Itokazu and N. Y. M. Iha, *Coordination Chemistry Reviews.*, **2004**, 248, 1343
5. I. M. Dixon, J. P. Collin, J. P. Sauvage, L. Flamigni, S. Encinas and F. Barigelletti, *Chem. Soc. Rev.*, **2000**, 29, 385
6. S. J. Liu, Q. Zhao, Q. L. Fan and W. Huang, *Eur. J. Inorg. Chem.,* **2008**, 13, 2177
7. A. B. Tamayo, S. Garon, T. Sajoto, P. I. Djurovich, I. M. Tsyba, R. Bau and M. E. Thompson, *Inorganic Chemistry.*, **2005**, 44, 8723

8. C. S. K. Mak, A. Hayer, S. I. Pascu, S. E. Watkins, A. B. Holmes, A. Kohler and R. H. Friend, *Chem.Commun.*, **2005**, 37, 4708
9. B. Chisweli and S. E. Livingstone, *J. Inorg. Nucl.Chem.,* **1964**, 26, 47
10. R. J. Watts and G. A. Crosby, *J. Am. Chem. Soc.,* **1971**, 93, 3184
11. G. Nord, A. C. Hazell, R. G. Hazell and O Farver, *Inorg. Chem.*, **1983**, 22, 3429
12. R. J. Watts, J. S. Harrington and J. V. Houten, *J. Am.Chem. Soc.*, **1977**, 99, 2179
13. R. D. Gillard, R. J. Lancashire and P. A. Williams, *J.Chem. Soc.*, *Dalton Trans*, **1979**, 193, 3429
14. W. A. Wickramasinghe, P. H. Bird and N. Serpone, *J. Chem.Soc., Chem.Commun.*, **1981,** 24, 1284
15. R. J. Watts and P. J. Spellane, *Inorg.Chem.*, **1981**, 20, 3561
16. R. Ballardini, G. Varani, L. Moggi, V. Balzani, *J. Am.Chem.Soc.,* **1977***,* 99, 6881
17. B. P. Sullivan, T. J. Meyer, *J. Chem. Soc., Chem.Commun.* **1984***,* 403
18. J. L. Kahl, K. W. Hanck, K. DeArmond, *J. Phys.Chem.,* **1979**, 83, 2606
19. J. L. Kahl, K. W. Hanck, K. DeArmond, *J. Phys.Chem.,* **1978**, 82, 540
20. (a) M. M. Muir, W. L. Luang, *Inorg.Chem.,* **1973**, 12, 1930 (b) J. A. Broomhead, W. Grumley, *Inorg.Chem.,* **1971**, 10, 2002 (c) L. H. Berka, G. E. Philippon, ***J.*** *Inorg. Nucl. Chem.* **1970**, 32, 3355 (d) B. Divisia, P. C. Ford, R. J. Watts, *J. Am. Chem. Soc.,* **1980**, 102, 7264
21. (a) R. J. Watts, S. Efrima, H. Metrin, *J. Am. Chem. Soc.,* **1979**, 101, 2742 (b) M. K. DeArmond, J. E. Hills, *J. Chem. Phys.,* **1971**, 54, 2247 (c) Y. Ohashi, T. Kobayashi, *Bull. Chem. Soc. Jpn.,* **1979**, 52, 2214 (d) T. L. Cremers, G. A. Crosby, *Chem. Phys. Lett.,* **1980**, 73, 541
22. (a) P. A. Marnot, R. R. Ruppert, J. Sauvage, *Nouv. J. Chim.,* **1981**, 5, 543 (b) J. Hawecker, J. M. Lehn, R. J. Ziessel, *Chem. Soc., Chem. Commun.* **1983**, 531
23. G. A. Crosby, *J. Chem. Phys.,* **1967**, 64, 160
24. D. M. Klassen and G. A. Crosby, *J. Chem. Phys.,* **1968**, 48, 1853
25. F. E. Lytle and D. M. Hercules, *J. Am. Chem. Soc.,* **1969**, 91**,** 253
26. G. A. Crosby and D. H. W**.** Carstens in "Molecular Luminescence," E. C. Lim, Ed., W. A. Benjamin, New York**,** N. Y., **1969**, p 309.

27. C. M. Flynn and J. N. Demas, *J. Am. Chem. Soc.,* **1974**, 96, 1959; **1975**, 97, 1988
28. J. S. Harrington and R. J. Watts, Abstracts, *Pacific Conference on Chemistry and Spectroscopy, North Hollywood, Calif.,* Oct **1975,** Abstract 91, p 56
29. R. D. Gillard, R. J Lancashire and P. A. Williams, *J. C. S Dalton.,* **1978**, 190
30. R. J. Watts, *Inorg. Chem.,* **1981**, 20, 2302
31. P. C. Ford, *Rev. Chem. Intermed.,* **1979**, 2, 267
32. T. J. Meyer, *Acc. Chem. Res.,* **1978**, *11,* 94
33. K. Kalyanasundaram, *Coord. Chem. Rev.,* **1982**, 46, 159
34. F. Bolleta, A. Rosi, F. Barigellatti, S. Dellonte, V. Balzani., *Gazr.Chim.Iral.,* **1981**, 111, 155
35. M. Nishizawa, T. M. Suzuki, S. Sprouse, R. J. Watts, P. C. Ford, *Inorg. Chem.,* **1984**, 23, 1837
36. A. D. Kirk, P. E. Hoggard, G. B. Porter, M. G. Rockley, M. W. Windsor, *Chem. Phys. Lett.,* **1976**, 37, 199
37. C. Creutz, M. Chou, T. L. Netzel, M. Okumura, N. Sutin, *J. Am. Chem. Soc.,* **1980**, 102, 1309
38. G. A Crosby, D. M. Klassen, S. L. Sabath., *Mol. Cryst.,* **1966**, 1, 453
39. J. M. Dernas, G. A. Crosby, *J. Am. Chem. Soc.,* **1971**, 93, 2841
40. R. J. Watts, J. S. Hamngton, J. V. Houten, *Adu. Chem. Ser.,* **1978**, 168, 57
41. K. Sone, P. Krumholz, H. Stammreich, *J. Am. Chem. Soc.,* **1955**, 77, 777
42. N. P. Ayala, C. M. Flynn, L. Sacksteder, J. N. Demas and B. A. DeGraff, *J. Am. Chem. Soc.,* **1990**, 112, 3837
43. R. Ballardini, G. Varani, L. Moggi, V. Balzani, K. R. Olson, F. Scandola, M. Z. Hoffman, *J. Am. Chem. Soc.,* **1975**, 97, 728
44. R. J. Watts, T. P. White, B. G. Griffith, *J. Am. Chem. Soc.,* **1975**, 97, 6914
45. R. J. Watts, D. Missimer, *J. Am. Chem. Soc.,* **1978**, 100, 5350
46. M. K. DeArmond, W. L. Huang, C. M. Carlin, *Inorg. Chem.,* **1979**, 18, 3388
47. R. J. Watts and G. A. Crossby, *J. Am. Chem. Soc.,* **1972**, 94, 2606
48. R. J. Watts, *J. Am. Chem. Soc.,* **1974**, 96, 6186
49. K. A. King and R. J. Watts, *J. Am. Chem. Soc.,* **1987**, 109, 1589

50. G. A. Crosby, K. W. Hipps and W. H. Elfring, *J. Am. Chem. Soc.,* **1974**, 96, 629
51. J. Brooks, Y. Babayan, S. Lamansky, P. I. Djurovich, I. Tsyba, R. Bau and M. E. Thompson, *Inorg. Chem.*, **2002**, 41, 3055
52. B. Higgins, B. A. DeGraff and J. N. Demas, *Inorg. Chem.*, **2005**, 44, 6662
53. P. T. Chou and Y. Chi, *Chem. Eur. J.*, **2007**, 13, 380
54. K. A. King, P. J. Spellane and R. J. Watts, *J. Am. Chem. Soc.*, **1985**, 107, 1431
55. M. C. DeRosa, D. J. Hodgson, G. D. Enright, B. Dawson, C. E. B. Evans and R. J. Crutchley, *J. Am. Chem. Soc.*, **2004**, 126, 7619
56. M. S. Lowry and S. Bernhard, *Chem.Eur. J.*, **2006**, 12, 7970
57. K. K. W. Lo and J. S. Y. Lau, *Inorg. Chem.*, **2007**, 46, 700
58. M. A. Baldo, D. F. O'Brien, Y. You, A. Shoustikov, S. Sibley, M. E. Thompson and S. R. Forrest, *Nature.,* **1998**, 395, 151
59. M. K. Nazeeruddin, R. H. Baker, D. Berner, S. Rivier, L. Zuppiroli and M. Graetzel, *J. Am. Chem. Soc.*, **2003**, 125, 8790
60. S. Lamansky, P. Djurovich, D. Murphy, F. A. Razzaq, H. E. Lee, C. Adachi, P. E. Burrows, S. R. Forrest and M. E. Thompson, *J. Am. Chem. Soc.*, **2001**, 123, 4304
61. F. O. Garces, K. A. King and R. J. Watts, *Inorg. Chem.*, **1988**, 27, 3464
62. H. Yersin, *Top. Curr. Chem.*, **2004**, 241, 1
63. M. G. Colombo, A. Hauser and H. U. Gudel, *Inorg. Chem.*, **1993**, 32, 3088
64. J. A. G. Williams, *Platinum Metals Rev.,* **2007**, 51, 85
65. M. Sudhakar, P. I. Djurovich, T. E. H. Esch and M. E. Thompson, *J. Am. Chem. Soc.,* **2003**, 125, 7796
66. M. C. DeRosa, P. J. Mosher, C. E. B. Evans, R. J. Crutchley, *Macromol. Symp.*, **2003**, 196, 235
67. A. M. Borisov, I. Klimant, *Anal. Chem.,* **2007**, 79, 7501
68. J. F. Sanchez, R. Cannas, S. Spichiger, R. Steiger, U. E. S. Keller, *Anal. Chim. Acta.,* **2006**, 566, 271
69. O. Ergeneman, G. Dogangil, M. P. Kummer, J. J. Abbot, M. K. Nazeeruddin, B. J. Bradley, *IEEE Sensors J.,* **2008**, 8, 29
70. J. M. B. Anslow, J. P. Hubner, B. F. Carroll, K. S. Schanze, *Langmuir.*, **2000**, 16, 9137

71. W. Goodall, J. A. G. Williams, *J. Chem. Soc, Dalton Trans.,* **2000**, 2893
72. H. L. Chen, Q. Zhao, F. Y. Li, Y. B. Wu, H. Yang, T. Yi, C. H. Huang, *Inorg. Chem.,* **2007**, 46, 11075
73. M. L. Ho, F.M. Hwang, P. N. Chen, Y.H. Hu, Y. M. Chen, K. S. Chen, G. H. Lee, Y. Chi, P. T. Chou, *Org. Biomol. Chem.,* **2006**, 4, 98
74. Q. Zhao, S. J. Liu, F. Y. Li, T. Yi, C. H. Huang, *Dalton Trans.,* **2008**, 3836
75. K. K. W. Lo, C. K. Chung, N. Zhu, *Chem. Eur. J.,* **2006**, 12, 1500
76. K. K. W. Lo, K. Y. Zhang, S. K. Leung, M. C. Tang, *Angew. Chem. Int. Ed.,* **2008**, 47, 2213
77. D. L. Ma, W. L. Wong, W. H. Chung, F. Y. Chan, P. K. So, T. S. Lai, Z. Y. Zhou, Y. C. Leung, K. Y. Wong, *Angew. Chem. Int. Ed.,* **2008**, 47, 3735
78. K. K. W. Lo, C. K. Chung, T. K. M. Lee, L. H. Lui, K. H. K. Tsang, N. Zhu, *Inorg. Chem.,* **2003**, 42, 6886
79. M. Yu, Q. Zhao, L. Shi, F. Li, Z. Zhou, H. Yang, T. Yi, C. Huang, *Chem. Commun.,* **2008**, 2115
80. M. Elvington, J. Brown, S. M. Arachchige, K. J. Brewer, *J. Am. Chem. Soc.,* **2007**, 129, 10644
81. S. Rau, B. Schafer, D. Gleich, E. Anders, M. Rudolph, M. Friedrich, H. Gorls, W. Henry, J. G. Vos, *Angew. Chem. Int. Ed.,* **2006**, 45, 6215
82. P. Du, J. Schneider, P. Jarosz, R. Eisenberg, *J. Am. Chem. Soc.,* **2006**, 128, 7726
83. N. Yoshikawa, T. M. Inoue, *Chem Lett*., **2000**, 1206
84. J. A. Broomhead, W. Grumley, *J. Chem. Soc., Chem. Commun*, **1968**, 1211
85. N. Yoshikawa, J. Sakamoto, T. M. Inoue, H. Takashima, K. Tsukahara, N. Kanehisa, Y. Kai, *Analytical Sciences.,* **2004**, 20, 711
86. V. T. Coombe, G. A. Heath, A. J. MacKenzie, *Inorg Chem.,* **1984**, 23, 3423
87. J. L. Kahl, K. Hanck, K. DeArmond, *J. Inorg. Nucl. Chem.,* **1979**, 41, 495
88. O. Farver, O. Monsted, G. Nord, *J. Am. Chem. Soc.,* **1979**, 201, 6118
89. F. O. Garces, R. J. Watts, *Inorg. Chem*., **1990**, 29, 582
90. V. Balzani and A. Juris, *Coord. Chem. Rev.*, **2001**, 211, 97

91. R. J. Watts, M. J. Brown, B. G. Griffith, J. S. Harrington, *J. Am. Chem. Soc*., **1975**, 97, 6030
92. J. V. Casper and T. J. Meyer, *Inorg. Chem.,* **1983**, 22, 2444
93. J. M. Lehn and J. P. Sauvage, *Nouv. J. Chim.,* **1977**, 1, 449
94. G. M. Brown, B. S. Brunschwig, C. Creutz, J. F. Endicott and N. Sutin, *J. Am. Chem. Soc.,* **1979**, 101, 1298
95. M. S. Lowry, J. I. Goldsmith, J. D. Slinker, R. Rohl, R. A. Pascal, G. G. Malliaras, S. Bernhard, *Chem. Mater.,* **2005**, 17, 5712
96. K. Kalyanasundaram, *Photochemistry of Polypyridine and Porphyrin Complexes*, Academic Press, New York, NY, **1992**, p. 105
97. R. J. Watts, J. V. Houten, *J. Am. Chem. Soc.,* **1974**, 96, 4334
98. T. M. McCormick, B. D. Calitree, A. Orchard, N. D. Kraut, F. V. Bright, M. R. Detty and R. Eisenberg, *J. Am. Chem. Soc.,* **2010**, 132, 15480
99. E. D. Cline, S. E. Adamson, S. Bernhard, *Inorg. Chem*., **2008**, 47, 10378

Chapter 6

Conclusion and Future Work

Having detailed the results of the synthesis and characterisation of a series of novel Ir (III) mononuclear and novel heterodinuclear Ir-Pt/Pd complexes using cyclometallated and N^N polypyridyl ligands in previous chapters it is the aim of the following chapter to take all of the results obtained into consideration and to relate the behaviour exhibited by these complexes to the photophysics and photocatalytic behaviour and provide some suggestions for future experiments that could be carried out.

6.1 Concluding remarks

This thesis focuses on the synthesis and various physical properties of iridium (III) transition metal complexes. Two different types of complexes were discussed in detail in the thesis. Firstly iridum (III) metal complexes with cyclometallating ligands of the type $[Ir(N\hat{}C)_2(N\hat{}N)]^+$ where N^C represents cyclometallating ligands like ppy, ppy-$COOCH_3$, thpy, etc and N^N represents neutral chelating ligands like bpy, bpp, tpy, bpm, dpp etc. Secondly iridium (III) complexes of the type $[Ir(N\hat{}N)_2Cl_2]^+$ and $[Ir(N\hat{}N)_3]^{3+}$ where N^N denotes neutral chelating ligands like bpy, phen, dmbpy etc. In both of the above cases synthesis, characterisation, photophysical measurements and photocatalysis were studied in detail.

Deuteriation along with the detailed photophysical measurements were used as a tool to probe the excited states of many of these iridium (III) complexes which were not studied before. New heterodinuclear Ir-Pt/Pd complexes were reported with various bridging ligands that are photocatalytically very efficient for H_2 generation. The solvent and temperature dependent excited state measurements provided an insight into the possible electron transfer processes taking place in these systems.

In chapter 1, a brief summary on iridium (III) transition metal complexes along with its application in various fields of chemistry were presented, including reference to the photocatalytic H_2 production systems. The entire chapter is divided into different sections. The chapter starts with explaining the various methods and approaches currently available for H_2 production along with a range of general storage, distribution and utilisation techniques. This is followed by a short discussion on natural photosynthetic systems and artificial photosynthetic systems. The latter one includes both intermolecular and intramolecular photocatalytic hydrogen production systems using transition metal complexes. Efforts were made to include the maximum number of references on both intermolecular and intramolecular photocatalytic systems in this section, but it is not fully complete as in this field a huge amount of research is presently going on. From these sections it is quite clear that in the past few years most of the work has been devoted to ruthenium based photosensitisers but little work has been done on iridium based systems, especially intramolecular photocatalytic systems. The next section of the chapter gives a brief description of the various types of iridium (III) polyamine complexes, followed by a brief description of the photophysical properties and its applications in OLED devices. In chapter 2, a summary of the standard synthetic procedures and physical measurements are presented. Wherever it was required a brief discussion of the basis of the techniques employed and of problems encountered was included.

Chapter 3 deals with the synthesis, characterisation, photophysics and photocatalysis of some standard cyclometallated iridium (III) complexes and novel complexes with bridging ligands bpp, tpy, bpm, and dpp. A small library of 25 cyclometallated iridium (III) complexes were presented in this chapter. The characterisations of all these complexes were done in full with the help of 1D and 2D NMR spectroscopy. Deuteriation was used in spectroscopic characterisation and to probe the excited state electronic structure. Deuteriation studies included absorption, emission and lifetimes of cyclometallated iridium (III) complexes of the type $[Ir(N^{\wedge}C)_2(N^{\wedge}N)]^+$, where deuteriation was carried on N^N neutral ligands. These types of deuteriated iridium (III) complexes have not previously been reported. Studies and measurements showed that iridium metal complexes can act as excellent catalytic systems for photogeneration of H_2 having efficiencies much higher than the other metals such as ruthenium. For intramolecular catalytic hydrogen generation, an efficient light absorbing unit, and bridging ligand which can transfer electrons to the catalyst from the light absorbing unit are required together with an efficient metal catalyst that can use the electrons in order to reduce water to produce H_2. A series of iridium cyclometallated precursors were synthesised for using as photosensitisers.

The first of its kind of heterodinuclear Ir-Pt/Pd photocatalytic system is reported in this thesis. And interestingly these complexes have their second metal (Pt/Pd) attached to the bridging ligand in a cyclometallated manner. Basic photophysical measurements including absorption, emission and lifetimes for all these complexes were done, which showed that with this entire range of cyclometallated iridium (III) complexes it was possible to tune the emission over the entire range of visible spectrum by varying the substituent's on the peripheral ligands, and the neutral chelating ligands. This has potential application for OLED devices which were not discussed in this chapter and. All of the complexes presented in this chapter are promising candidates for photocatalytic H_2 production, and gave good TON which are comparatively much higher than that produced by the analogous ruthenium complexes. Both intermolecular and intramolecular photocatalysis produced H_2, but intramolecular photocatalysis proved to be more efficient than the intermolecular ones. Of the intramolecular systems, the Ir-Pt systems showed better catalytic activity than the Ir-Pd systems which are given a possible explanation on the basis of the photophysical measurements. Time dependent photocatalysis gave an idea of the efficiency of these novel photocatalyts. Also the ester complexes produced almost double the H_2 than the non ester complexes in solution. The aim is to finally bind these complexes to NiO surfaces thereby completely avoiding the use of sacrificial agents like TEA, which clearly shows the potential of these complexes. One of the interesting studies presented is a comparison of photocatalysis using visible (470 nm) and UV light (350 nm). The higher efficiency of 470 nm excitation, in conjunction with the photophysical data suggests that the ^{3}MLCT state plays a crucial role in intramolecular photocatalysis of Ir-Pt/Pd heterodinuclear complexes.

Chapter 4 deals with the detailed solvent and temperature dependent excited state photophysics of three novel cyclometallated iridium (III) complexes; $[Ir(ppy)_2(bpp)](PF_6)$, $[Ir(ppy)_2(bpp)PtCl]_2(PF_6)_2$ and $[Ir(ppy)_2(bpp)PdCl]_2(PF_6)_2$. As the photophysics of the complexes presented here (heterodinuclear Ir-Pt/Pd complexes) have not been reported previously all the assumptions on the excited state assignments are based on the preliminary photophysical measurements including concentration dependent, solvatochromic and temperature dependent photophysics. Further detailed excited state experiments such as resonance raman, transient absorption and DFT calculations have to employed in order to gain a complete understanding of the nature of excited states which is beyond the scope of this. Varying the substituent's on the peripheral ppy ligands and by using different bridges it was possible to tune the excited state thereby influencing the pathway for the electron to reach the Pt/Pd centre, and gave more hydrogen.

Chapter 5 focuses on the iridium polypyridyl complexes having the general formula $[Ir(N^\wedge N)_2Cl_2]PF_6$ where N^N represents neutral chelating ligands like bpy, phen, dmbpy etc. Over the last 30 years very little work has been done on the chemistry of $Ir(polypyridyl)_2Cl_2$ type complexes. The main drawback included tedious work up procedures along with the lack of knowledge on the actual synthetic reaction mechanism of the reaction. A novel synthetic method for preparing these complexes in high purity and yield is very short time without the use of any columns and days long workups has been developed. The ligands that were used for preparing the complexes include 2,2'-bipyridine, 1,10 phenathroline, 4,4'-dimethyl-2,2'-bipyridine, 4,4'-ditertiarybutyl-2,2'-bipyridine and the deuteriated analogues of these ligands. The mechanism of the reaction was confirmed using a time dependent NMR and HPLC study. Purification and characterisation of the products showed the different pathways and side products involved in the reaction. However it was possible to control the formation of the desired product inorder to get the primary product in good yield and purity by tuning the solvent and reaction temperature.

Detailed excited state photophysical measurements including absorption, emission, quantum yields and lifetimes for these complexes are included. The deuteriation effect on the excited state photophysics at room temperature (298 K) and low temperature (77 K) helped in identifying the lowest excited states of these complexes. The emission wavelengths observed suggests the possibility of using these complexes for OLED devices. The inner sphere chlorides were removed successfully by a short and efficient synthetic method which has opened an entirely new insight into the application of these complexes in various fields of chemistry. Success was obtained in developing the first tris heteroleptic polypyridyl complex with the triazole ligand which showed green emission, and good photocatalytic activity for hydrogen production (TON of 400).

No reports are present in the literature on the photocatalytic hydrogen production activity of simple $[Ir(N^\wedge N)_2Cl_2]PF_6$ complexes. Intermolecular photocatalysis was carried out for a range of these complexes using two different catalysts namely $Pt(ACN)_2Cl_2$ and $Pd(ACN)_2Cl_2$. The results were quite interesting, with most giving very good turn over number over 18 hour irradiation, in acetonitrile using TEA as sacrificial agent. Two different irradiation wavelengths were used; visible (470 nm) and UV light (350 nm). The visible light irradiation experiments gave more hydrogen than the UV light, similarly to the cyclometallated iridium (III) complexes. The use of $Pt(ACN)_2Cl_2$ as catalysts produced more hydrogen than $Pd(ACN)_2Cl_2$. Comparing the intermolecular photocatalytic results obtained for these complexes with the standard cyclometallated iridium (III) complexes it is clear that these systems are more efficient than the conventional cyclometallated iridium (III) complexes for photocatalytic hydrogen generation. By developing an efficient and simple method for the synthesis of these complexes followed by the success in removal of inner sphere chlorides has opened up an entirely new field itself in chemistry which has far reaching potential applications in various fields such as photocatalytic hydrogen generation, OLEDs etc.

6.2 Future Work

The main areas of future work recommended are as follows.

Chapter 3. For all the complexes discussed in this chapter three different peripheral ligands were used (ppy, ppy-$COOCH_3$ and ppy-CHO). The library should be extended by employing a range of different substituted and unsubstituted cyclometallating ligands. Also the mononuclear complex with dpp has been synthesised succesfully with which the dinuclear Ir-Pt/Pd complexes can be synthesised. This is expected to show much higher photocatalytic activity than the ruthenium analogous. The Ir-Pt complexes synthesised can be used as potential candidates in anticancer therapies which has been proved before using cyclometallated Pt complexes. All of the iridium complexes synthesised can be used on OLED devices also and also some of the ester complexes as dyes in dye sensitised solar cells (DSSC's). Much more detailed photophysics including the solvatochromic and rigidochromic measurements along with the resonance raman and computational methods (DFT) should be done in order to gain a clear picture of the excited states of these systems. From the photocatalysis point of view all the experiments reported here were carried in one solvent (ACN) and at one particular concentration. Different solvents and different concentrations should be employed, also different sacrificial agents should be tried. The time dependent photocatalysis for the remaining molecules should be completed. One of the most important steps is binding the ester analogous iridium photocatalyts to the NiO sufaces as shown in figure below.

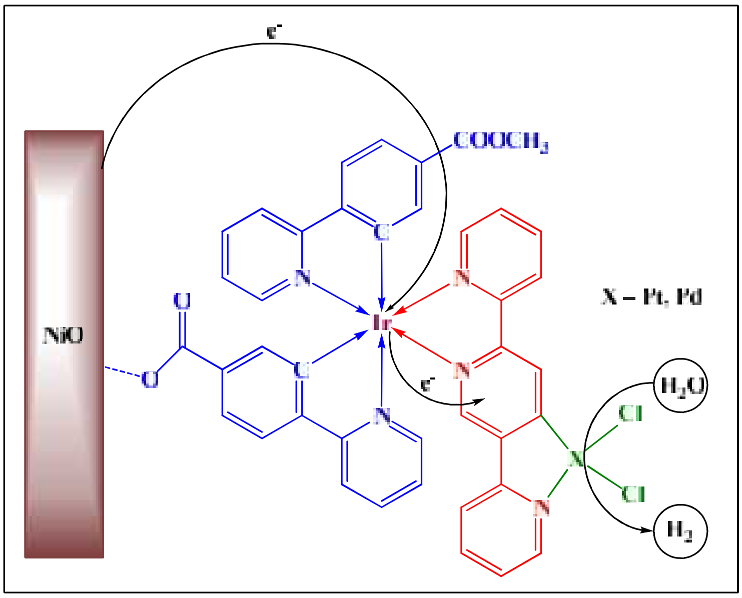

Figure: Possible electron transfer mechanism in novel Ir-Pt complex binded to NiO surface

A range of cyclometallated iridium complexes with some of the triazole ligands have been synthesised succesfully and are given in appendix E. Further studies such as detailed excited state photophysics and photocatalysis of these systems should be carried out, and the synthesis of a dinuclear system has to be attempted.

Chapter 4. Solvatochromic, rigidochromic and temperature dependent photophysics must be completed and, further detailed studies of excited state including temperature dependent resonance raman, DFT calculaions, transient absorption spectroscopy etc this will confirm the electronic transitions predicted here for the novel Ir-Pt/Pd complexes explained in this chapter. Also the similar studies should be extended to the analogous ester complexes which will give a clear picture regarding the effect of substitution on the excited state photophysics and therby its influence on the photocatalysis.

Chapter 5. A new efficient and high yield synthesis of Ir(polypyridyl)$_2$Cl$_2$ complexes and successful removal of inner sphere chlorides has opened up an entirely new area. For the novel heteroleptic complex [Ir(dmbpy)$_2$(Hphpytr)](CF$_3$SO$_3$)$_3$ dmbpy was used as the peripheral ligand. Using the same triazole ligand and by changing the peripheral ligands using other starting materials like, bpy, phen, dtbpy and their deuteriated analogous an entire range of complexes can be synthesised thereby tuning the visible spectrum which will lead to the compounds having potential applications in OLED's, and as efficient photocatalyts. Similar to the cyclometallated complexes these polypyridyl precursor complexes can be efficienly complexed to various bridging ligands (bpp, tpy, bpm, dpp etc) thereby synthesising mononuclear, homodinuclear (Ir-Ir) and heterodinuclear complexes (Ir-Pt/Pd). Preliminary photocatalytic results showed that the precursor complexes are much more efficient than the convential cyclometallated complexes. By analysing all these results, intramolecular complexes made using these N^N polypyridyl peripheral ligands were expected to show greater photocatalytic activity. The potential of these complexes are really huge as they can be used for multidisciplinary applications such as OLED's, bioimaging, photocatalysis etc.

Altogether a basic platform has been built up for the iridium (III) transition metal complexes, but further research has to carried out in order to extend the application of these complexes.

Appendix A

Publications

1) *"Photoinduced ligand isomerisation in a pyrazine-containing ruthenium polypyridyl complex"*
Sabine Horn, Hamid M. Y. Ahmed, Helen P Hughes**, Suraj Soman**, Wesley R. Browne and Johannes G. Vos, *Photochemical & Photobiological Sciences*., **2010**, 9, 985-990.

2) *"Reinvestigating 2,5-di(pyridin-2-yl)pyrazine ruthenium complexes: selective deuteration and Raman spectroscopy as tools to probe ground and excited-state electronic structure in homo- and heterobimetallic complexes"*
Martin Schulz, Johannes Hirschmann, Appu Draksharapu, Gurmeet Singh Bindra, **Suraj Soman**, Avishek Paul, Robert Groarke, Mary. T. Pryce, Sven Rau, Wesley R. Browne and Johannes. G. Vos, *Dalton Trans.*, **2011**, 40, 10545–10552.

3) *"The effect of peripheral bipyridine ligands on the photocatalytic hydrogen production activity of Ru/Pd catalysts"*
Gurmeet Singh Bindra, Martin Schulz, Avishek Paul, **Suraj Soman**, Robert Groarke, Jane Inglis, Mary T. Pryce, Wesley R. Browne, Sven Rau, Brian J. Maclean and Johannes G. Vos, *Dalton Trans.*, **2011**, 40, 10812–10814.

4) *"Novel iridium-Pt/Pd complexes for photocatalytic hydrogen generation from water using blue light (470nm) and UV light (350nm)"*
Suraj Soman, Gurmeet Singh Bindra, Jane Inglis, Avishek Paul, Martin Schulz, Mary T. Pryce and Johannes G. Vos, (manuscript under preperation)

5) *"High yield synthesis for the preparation of heteroleptic Ir (III) polypyridyl complexes"*
Suraj Soman, Hamid M. Y. Ahmed, Laura Cleary, Gurmeet Singh Bindra, Wesley R. Browne, Mary T. Pryce, Johannes G. Vos, (manuscript under preparation)

6) *"Effect of peripheral ligand and bridging ligands on intermolecular and intramolecular photocatalytic H_2 generation for novel Ir (III) complexes"*
Suraj Soman, Gurmeet Singh Bindra, Mary T. Pryce, Johannes G. Vos, (manuscript under preparation)

7) *"Novel Ru (II) complexes with bpp ligand as efficient H_2 generation photocatalysts"*
Gurmeet Singh Bindra, **Suraj Soman**, Martin Schulz, Mary T. Pryce, Johannes G. Vos, (manuscript under preparation)

Posters Presented

1) *Development of a New Synthetic Strategy for getting $[Ir^{III}(bpy\text{-}N,N')_2Cl_2]^+$ in High Purity and Yield and the Study of Deuteriation Effect on the Formation of $[Ir^{III}(bpy\text{-}N,N')_2(bpy\text{-}C,N')^-]^{2+}$ Complexes*
<u>Suraj Soman</u>, Hamid Younis, Mary T. Pryce, Wesley R. Browne and Johannes G. Vos, 10th Annual Symposium on Supramolecular Chemistry in Ireland held on 9th July **2009** in Trinity College Dublin, Ireland (Also presented at Annual Conference of SCI in Ireland held in Dublin City University, Ireland on 15th April **2010**).

2) *Harvesting Solar Energy for the generation of H_2*
<u>Suraj Soman</u>, Gurmeet Singh Bindra, Avishek Paul, Danilo Dini, Mary T. Pryce and Johannes G. Vos, **2010** Annual EPA Conference held at Cork Park, Dublin, Ireland.

3) *Novel Iridium-Pt/Pd Photocatalyts for Intramolecular & Intermolecular Catalytic H_2 Generation from H_2O*
<u>Suraj Soman</u>, Gurmeet Singh Bindra, Avishek Paul, Martin Schulz, Mary T. Pryce and Johannes G. Vos, Photochemistry and Photochemical Techniques 16-18th May **2011**, University College Dublin, Trinity College Dublin, Ireland.

4) *Temperature dependent and solvent dependent photophysics of novel Ir-Pt/Pd dinuclear complexes*
<u>Suraj Soman</u>, Robert Goarke, Gurmeet Singh Bindra, Jane Inglis, Mary T. Pryce and Johannes G. Vos, Photochemistry and Photochemical Techniques 16-18th May **2011**, UCD, Ireland (also presented in International Symposia on Advancing the Chemical Sciences: Challenges in Renewable Energy (ISACS4), MIT, Boston, USA, **2011** July).

5) *Novel Iridium-Pt/Pd Photocatalyts for Intramolecular & Intermolecular Catalytic H_2 Generation from H_2O using Blue Light (470nm) & UV Light (350nm)*
<u>Suraj Soman</u>, Gurmeet Singh Bindra, Jane Inglis, Avishek Paul, Martin Schulz, Mary T. Pryce and Johannes G. Vos, International Symposia on Advancing the Chemical Sciences: Challenges in Renewable Energy (ISACS4), MIT, Boston, USA, **2011** July.

6) *Effect of metal centers on spectroscopic and catalytic properties of metal complexes*
<u>Robert Groarke</u>, **Suraj Soman**, Gurmeet Singh Bindra, Martin Schulz, Mary T. Pryce and Jonannes G. Vos, 19th International Symposium on the Photophysics and Photochemistry of Coordination Compounds, Strasbourg, France, **2011** July.

Oral Presentation

1) *"The design of new photocatalytic systems for the generation of hydrogen from water using solar energy"*
   Suraj Soman, Annual Conference of SCI in Ireland held in Dublin City University, Ireland on 15th April **2010**.

2) *"H_2 – Fuel for the future"*
   Suraj Soman, presented in Prof. Sven Rau's group during the photocatalytic meeting at University of Nuremberg, Germany in July **2010**.

3) *"Novel Ir-Pt/Pd Photocatalyts for Intramolecular & Intermolecular Catalytic H_2 Generation from H_2O"*
   Suraj Soman, Photochemistry and Photochemical Techniques held in University College Dublin, Ireland on 17th May **2011**.

Appendix B

Supplimentary data from chapter 2 and chapter 3

Synthesis of bridging ligands

The ligands Hpztr, Hpytr, Hbpt and Hbpzt were prepared as previously reported by Hage.[1]

1) Synthesis of Hpztr (3-(pyrazin-2-yl)-1,2-4-triazole)

To a mixture of 5 g (0.048 mol) of molten 2-cyanopyrazine with an equimolar amount of 2.33 cm^3 hydrazine hydrate, 20 cm^3 of ethanol was added. The solution was stirred at room temperature and the yellow crystals that formed where filtered. The pyrazylamidrazone (3.74 g, 0.0267 mol) was dissolved in a 10 fold excess of formic acid while keeping the temperature below 10 ^{0}C. The mixture was stirred at room temperature for 3 hours. After subsequent heating to dryness the ligand precipated and was then recrystallised from ethanol. Yield (2.5 g, 39 %). ^{1}H NMR (400 MHz, DMSO), δ (ppm): 7.43 (dd), 7.88 (s), 8.02 (dd), 8.20 (d), 8.79 (d).

2) Synthesis of Hpytr (2-(4H-[1,2,4]-triazole-3-yl)-pyridine)

To 15 cm^3 (0.26 mol) hydrazine hydrate 20 g (0.19 mol) 2-cyanopyridine was added. The mixture was stirred at room temperature for 2 hours and then left at 4 ^{0}C for 1hr. The intermediate, 2-pyridylamidrazone, was filtered and washed with diethyl ether. 2-pyridylamidrazone was dissolved in concentrated formic acid and heated until only a small amount of solvent was left. The crude product was recrystallised from an ethanol / water mixture (pH 7). Yield (20.3 g, 61 %). ^{1}H NMR (400 MHz, DMSO), δ (ppm): 7.50 (dd, 1H), 7.98 (dd, 14Hz, 1H), 8.15 (d, 1H), 8.75 (d, 1H).

3) Synthesis of Hbpt (3,5-Bis(pyridin-2-yl)-1,2,4-triazole)

(a) (3,5-bis(pyridin-2-yl)-4-amino-1,2,4-triazole)

A mixture of 2-cyanopyridine (8.112 g, 78 mmol) and hydrazine hydrate (5 g, 156 mmol) were heated at 100 ^{0}C for 4.5 hour. The orange precipitate that formed was filtered, washed with cold EtOH (10 cm^3) and diethyl ether (100 cm^3). The orange 3,5-bis(pyridin-2-yl)-4-amino-1,2,4-triazole was dissolved in 2M HCl (120 cm^3)and boiled for 30 min. The solution was allowed to cool to room temperature and then made alkaline by the addition of ammonia. The solution was cooled to +4 ^{0}C for 1 hour and then filtered. The tan precipitate was washed with alkaline H_2O and recrystalised from hot EtOH. Yield (3.98 g, 17.5 mmol, 45 %. ^{1}H NMR (400 MHz, DMSO), δ (ppm): 8.20 (d), 7.43 (t), 7.88 (s), 8.02 (t), 8.79 (d).

(b) *(3,5-Bis(pyridin-2-yl)-1,2,4-triazole)*

The tan 3,5-bis (pyridin-2-yl)-4-amino-1,2,4-triazole (3.5 g, 15.7 mmol) was dissolved in boiling 5M nitric acid (17.5 cm^3). The solution was cooled to 0 ^{0}C and an aqueous sodium nitrite solution (10.5 g in 17.5 cm^3) was slowly added dropwise with stirring until no further brown fumes were released. This solution was then boiled for 5 min and cooled to room temperature. The white product, which crashed out, was washed with alkaline H_2O and cold EtOH. The product was then recrystalised from EtOH. Yield (3.0 g, 13.5 mmol, 85 %). ^{1}H NMR (400 MHz, DMSO), δ (ppm): 7.52 (2H, t), 8.05 (2H, t), 8.22 (2H, d), 8.73 (2H, d).

4) Synthesis of Hbpzt (3,5-bis(pyrazin-2-yl)-1,2,4-triazole)

2-Pyrazinecarboxylic acid (8.0 g, 65 mmol) and conc. H_2SO_4 (2 ml) were heated at reflux in EtOH for 3 h. Sodium carbonate was added to neutralize the H_2SO_4 after which excess hydrazine hydrate (5.05 g, 101 mmol) was added. The solution was stirred at 0 ^{0}C for 3 h. The precipitate was filtered and washed with cold EtOH. 2-Cyanopyrazine (4.2 g, 40 mmol) was converted to 2-pyrazylmethylimidate by heating it at reflux with Na metal in MeOH for 3 h. The hydrazide from above was added and the solution heated for an additional 1 h. The yellow precipitate was filtered and washed with cold EtOH. 3,5-Bis(pyrazin-2-yl)-1,2,4-triazole was obtained by heating the pyrazine-2-carboxylic acid N'-(imino-pyrazin-2-yl-methyl)-hydrazide at reflux in ethylene glycol for 1 h. The product was then recrystallised from ethanol. Yield (6.0 g, 27 mmol, 42 %). ^{1}H NMR(400 MHz, DMSO), δ (ppm): 8.78 (d), 8.81 (d), 9.35 (s).

Synthesis of mononuclear iridium complexes

5) Synthesis of $[Ir(thpy)_2(bpp)]PF_6$

The ligand BPP (0.0340 g, 0.1459 mmol) was weighed and transfered to a 100 ml round bottom flask (R.B) to which 5 ml of solvent, DCM: EtOH (2:1) was added and stirred at 60 ^{0}C for 20 minutes to which the dichlorobridged dimer, $[Ir(thpy)_2Cl]_2$ (0.080 g, 0.0729 mmol) dissolved in 15 ml of solvent was added slowly in an hour. The reaction was heated in reflux (90 ^{0}C) for 7 hours. The reaction mixture was cooled and solvents were all removed by vacuum rota evaporator, 10 ml of deionised water was added and saturated aqueous NH_4PF_6 (1 g in 10 ml of deionised water) was added resulting in the precipitation of the product as $[Ir(ppy)_2(BPP)].PF_6$ which was recrystalised from Acetone:Toluene:Hexane (2:1:1), vacuum filtered, washed with diethyl ether and dried. Yield (0.109 g, 71 %). ^{1}H NMR (400 MHz, DMSO), δ (ppm): 6.193 (1H, d), 6.225 (1H, d), 6.957 (2H, m), 7.446 (1H, t), 7.552 (1H, d), 7.69 (3H, m), 7.777 (5H, m), 7.850 (1H, d), 7.932 (2H, m), 8.288 (1H, t), 8.561 (1H, d), 8.605 (1H, d), 8.869 (1H, d), 8.951 (2H, m). CHN for [Ir(thpy)$_2$(bpp)]PF$_6$, Calcd: C, 44.49; H, 2.60; N, 7.86., Found: C, 44.38; H, 2.29; N, 6.09.

6) Synthesis of [Ir(ppy)$_2$(pztr)]PF$_6$

The dichlorobridged dimer, [Ir(ppy)$_2$Cl]$_2$ (0.1 g, 0.0860 mmol) and the corresponding pyrazinetriazole ligand, Hpztr (0.0278 g, 0.1893 mmol) were refluxed in 9 ml of CH$_2$Cl$_2$ and 3 ml of EtOH for 16 hour under nitrogen atmosphere. Upon completion of the reaction (confirmed by TLC), all solvents were removed under reduced pressure and the resulting yellow-brown solid was chromatographed on silica gel using CH$_2$Cl$_2$:EtOH (10:1) mixture as eluent and recrystalised from acetone: water (1:1) mixture to get the complex [Ir(ppy)$_2$(pztr)].PF$_6$ pure. Yield (0.042 g, 27 %). ^{1}H NMR (400 MHz, DMSO), δ (ppm): 6.15 (d, 1H), 6.23 (d, 1H), 6.77 (t, 1H), 6.85 (t, 1H), 6.87 (t, 1H), 6.95 (t, 1H), 7.08 (t, 1H), 7.16 (t, 1H), 7.36 (s, 1H), 7.54 (d, 1H), 7.57 (d, 1H), 7.75 (d, 1H), 7.81 (d, 1H), 7.86 (m, 3H), 8.17 (m, 2H), 8.53 (d, 1H), 9.42 (d, 1H).

7) Synthesis of [Ir(ppy)$_2$(pytr)]PF$_6$

A solution of the dichloro-bridged starting material [Ir(ppy)$_2$Cl]$_2$ (0.128 g, 0.12 mmol) in dichloromethane/ethanol (2:1 v/v) was added slowly to a solution of Hpytr (0.035 g, 0.24 mmol) in the same solvents. The total amount of solvent was 25 mL in which the reaction mixture was reuxed for 5 hours. After allowing the mixture to cool down the solvent was removed under reduced pressure and the product remaining in the RB was dissolved in acetone. A product precipitated overnight which was green-yellow of color with a total yield of 82 %. Two isomers formed, which was confirmed by both NMR and HPLC analysis. ^{1}H NMR (DMSO-d6, 400 MHz) δ (ppm): 8.72 (s, pytr), 8.66 (s, pytr), 8.45 (m, pytr), 8.23 (m, pytr and ppy), 7.92 (m, ppy), 7.81 (d, ppy), 7.71 (m, pytr and ppy), 7.64 (m, pytr and ppy), 7.59 (m, pytr and ppy), 7.16 (m, ppy), 7.03-6.78 (m, ppy), 6.20 (d, ppy), 6.14 (d, ppy).

Novel Neutral Iridium Complexes

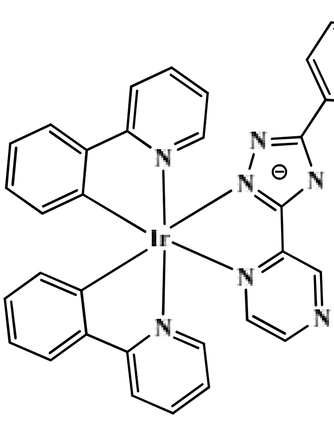
(8)

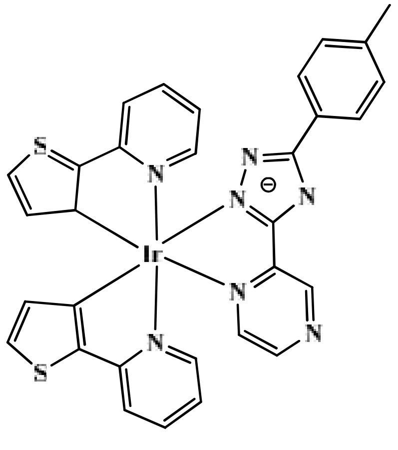
(9)

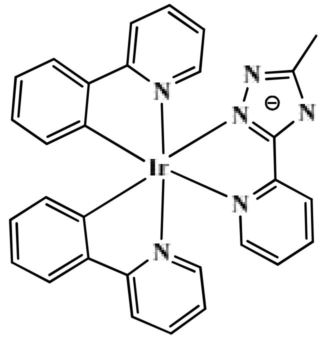
(10)

8) Synthesis of [Ir(ppy)$_2$(MePhpztr)]

A solution of the dichloro-bridged starting material [Ir(ppy)$_2$Cl]$_2$ (0.218 g, 0.2 mmol) in dichloromethane/ethanol (2:1 v/v) was added slowly to a solution of HMePhpztr (0.1 g, 0.4 mmol) in the same solvents. The total amount of solvent was 40 mL in which the reaction mixture was refluxed for five hours. After allowing the mixture to cool down the solvent was removed under reduced pressure and the product remaining in the RB was filtered and washed with acetone and water. The final product was yellow in color with a total yield of 26 %. ^{1}H NMR (DMSO-d6, 400 MHz) δ (ppm): 9.37 (1H, s), 8.56 (1H, s), 8.21 (2H, t), 7.87 (6H, m), 7.77 (1H, d), 7.59 (2H, m), 7.19 (3H, m), 7.11 (1H, t), 6.99 (1H, t), 6.92 (2H, m), 6.79 (1H, t), 6.21 (1H, d), 6.17 (1H, d). Elemental analysis, Ir(ppy)2(MePhpztr) exp. (calc.): C 55.11 (57.05) H 3.69 (3.56) N 11.88 (13.31).

9) Synthesis of [Ir(thpy)$_2$(MePhpztr)]

A solution of the dichloro-bridged starting material [Ir(ppy)$_2$Cl]$_2$ (0.117 g, 0.1 mmol) in dichloromethane/ethanol (2:1 v/v) was added slowly to a solution of HMePhpztr (0.05 g, 0.2 mmol) in the same solvents. The total amount of solvent was 40 mL in which the reaction mixture was refluxed for 5 hours. After allowing the mixture to cool down the solvent was removed under reduced pressure and the solid remaining in the RB was partially dissolved in water. This was filtered, but turned out to contaminated. The remaining precipitate in the RB was washed with acetone and diethyl ether. This final product was orange of color with a total yield of 8 %. ^{1}H NMR (DMSO-d6, 400 MHz) δ (ppm): 9.31 (1H, s), 8.56 (1H, s), 7.84 (2H, d), 7.71 (2H, m), 7.61 (4H, m), 7.55 (1H, d), 7.46 (2H, m), 7.15 (2H, d), 6.98 (1H, t), 6.86 (1H, t), 6.13 (1H, s), 6.08 (1H, s).

10) Synthesis of [Ir(ppy)$_2$(Mepytr)]

The ligand (0.05g, 0.314129 mmol) was first weighed and transferred into an RB which contains the solvent DCM:EtOH (2:1) & is heated for about 20-30 minutes. The metal [Ir(ppy)2Cl]2 (0.168g, 0.15706 mmol) dissolved in 20 ml of DCM was added dropwise to the reaction mixture in an hour and the entire system was refluxed for 6 hours. After which the solvents were removed completly and water was added resulting in the precipitation of the product which was filtered and washed with water and diethyl ether and recrystalised from acetone : water to get it completly pure. Yield: 0.147g, 71%

Synthesis of homodinuclear (Ir-Ir) and heterodinuclear (Ir-Ru) Complexes

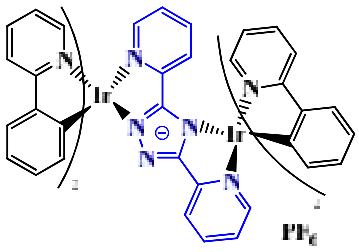

{[Ir(ppy)$_2$]$_2$(bpt)}PF$_6$ **(11)**

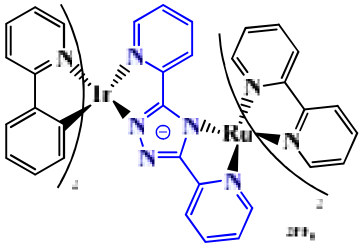

[(bpy)$_2$Ru(bpt)Ir(ppy)$_2$]PF$_6$ **(12)**

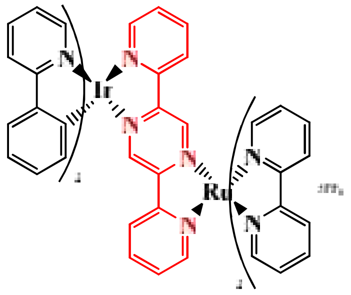

[Ir(ppy)$_2$(dpp)Ru(bpy)$_2$]3PF$_6$ **(13)**

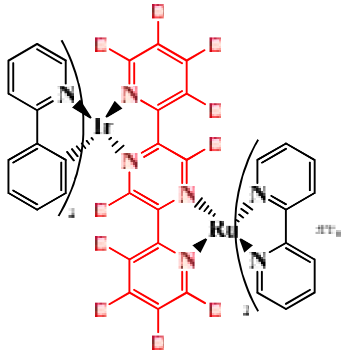

[Ir(ppy)$_2$(d$_{10}$-dpp)Ru(bpy)$_2$]3PF$_6$ **(14)**

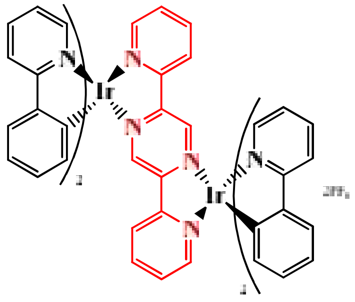

[Ir(ppy)$_2$(dpp)Ru(bpy)$_2$]2PF$_6$ **(15)**

11) Synthesis of [(ppy)$_2$Ir(bpt)Ir(ppy)$_2$]PF$_6$

A 0.25 mmol sample of [Ir(ppy)$_2$Cl]$_2$ and 0.4 mmol of Hbpt were heated at reflux for 6h in 50 ml of CH$_2$C1$_2$/EtOH (2:l v/v). After being cooled to room temperature, the solution was evaporated to 10 ml and added to an excess of aqueous NH$_4$PF$_6$. The crude product was filtered off and recrystalised from water/acetone (1: l v/v). CHN for {[Ir(ppy)$_2$]$_2$(bpt)}.PF$_6$.acetone Calcd: C, 49.68; H, 3.15; N, 8.84. Found: C, 49.40; H,3.33; N, 8.91.

12) Synthesis of [(bpy)$_2$Ru(bpt)Ir(ppy)$_2$]PF$_6$

A 0.25 mmol sample of [Ru(bpy)2(bpt)]$^+$ was dissolved in 50 ml of 2-methoxyethanol. A 0.25 mmol sample of [Ir(ppy)$_2$C1]$_2$ was added, and the mixture was heated to reflux for 48 h. After being cooled to room temperature, the volume of the filtered solution was reduced by evaporation to 25 %. The solution was then added to an excess of aqueous NH$_4$PF$_6$. The precipitate was filtered off, dissolved in acetone and purified by column chromatography (neutral EtOH as eluent; height of 20 cm; width of column, 2 cm). The product was recrystalised from water/acetone (1:l v/v). CHN for [(bpy)$_2$Ru(bpt)Ir(ppy)$_2$]PF$_6$.H$_2$O Calcd : C, 44.91; H, 2.91; N, 10.67. Found : C, 44.69; H, 2.69; N, 10.40.

13) Synthesis of [(bpy)$_2$Ru(dpp)Ir(ppy)$_2$]3PF$_6$

[Ru(bpy)$_2$(dpp)]2PF$_6$ (0.0151 g, 0.000023297 mmol) was taken in a 50 ml R.B to which 5 ml of the solvent was added and refluxed at 80 ^{0}C to which [Ir(ppy)$_2$Cl]$_2$ (0.0115 g, 0.00001164 mmol), dissolved in 5ml of solvent was added. The reaction mixture was refluxed then for 6 hours, cooled, solvent was removed, dissolved in water and aqueous KPF$_6$ was added in order to precipitate the product, which is vacuum dried and recrystalised from acetone: water (1:1) and then with acetone: toluene (1:1) mixture. Yield: 0.020 g

14) Synthesis of [(bpy)$_2$Ru(d$_{10}$-dpp)Ir(ppy)$_2$]3PF$_6$

[Ru(bpy)$_2$(d$_{10}$-dpp)]2PF$_6$ (0.0151 g, 0.000023297 mmol) was taken in a 50 ml R.B to which 5 ml of the solvent was added and refluxed at 80 ^{0}C to which [Ir(ppy)$_2$Cl]$_2$ (0.012 g, 0.00001164 mmol), dissolved in 5ml of solvent was added. The reaction mixture was refluxed then for 6 hours, cooled, solvent was removed, dissolved in water and aqueous KPF$_6$ was added in order to precipitate the product, which is vacuum dried and recrystalised from acetone: water (1:1) and then with acetone: toluene (1:1) mixture. Yield: 0.018 g

15) Synthesis of $[(ppy)_2Ir(dpp)Ir(ppy)_2]3PF_6$

dpp (0.0328 g, 0.0001401 mmol) was taken in an R.B to which 20 ml of DCM: MeOH (1:1) was added and refluxed at 60 ^{0}C for 15 min in N_2 atmosphere. $[Ir(ppy)_2Cl]_2$ (0.05 g, 0.00004672 mmol) was dissolved in 20 ml DCM and added slowly, dropwise in 30 minutes and the entire solution was refluxed for 7 hours. The solvent was all removed then, dissolved in water, filtered and aqueous KPF_6 was added resulting in the precipitation of the product which was recrystalised from acetone: water (1:1) mixture, vacuum filtered and dried to get the pure product. Yield: 0.043 g

^{1}H NMR Spectra

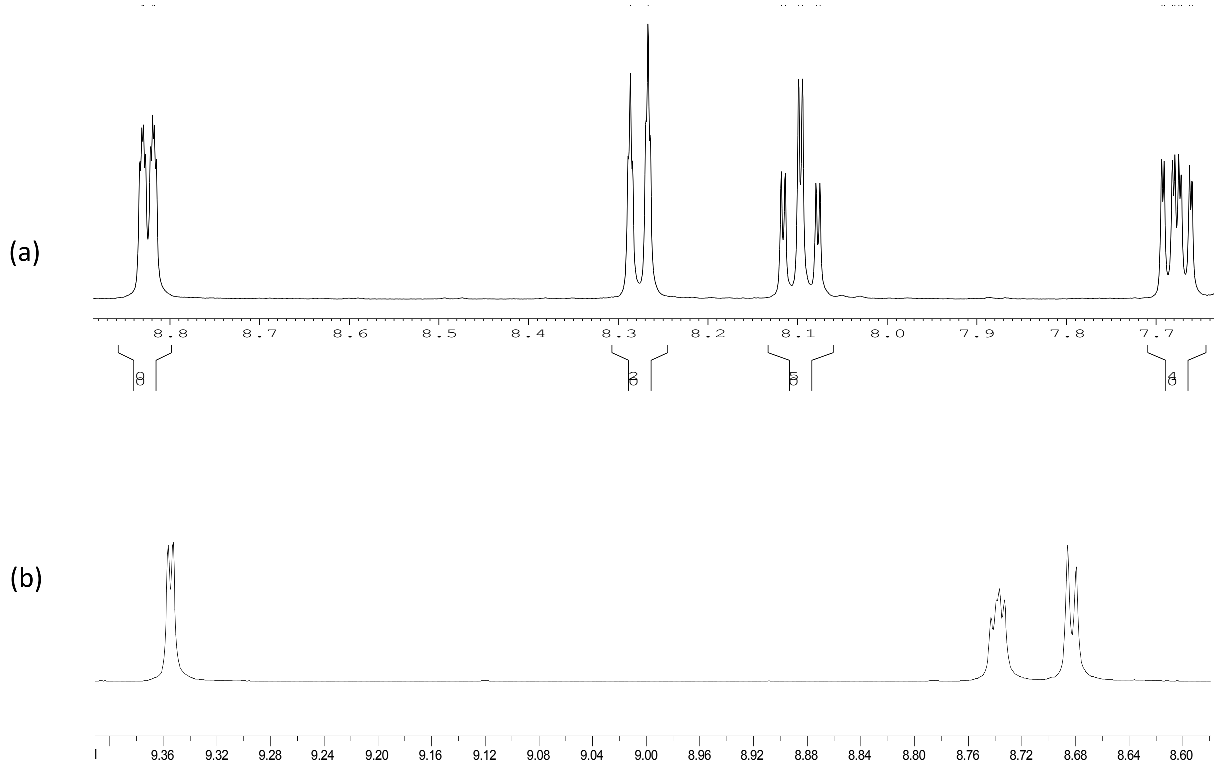

Figure A1. *^{1}H NMR Spectrum of Hbpt (a) and Hbpzt (b) taken in d_6 DMSO.*

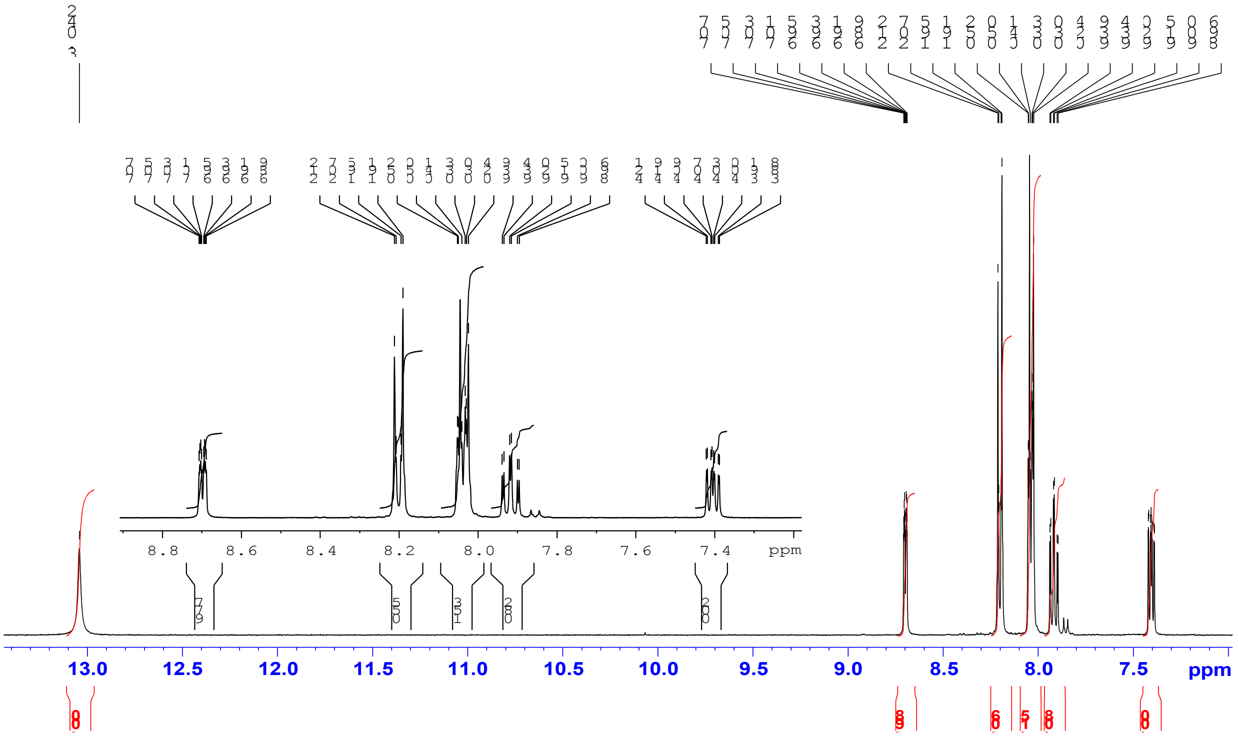

Figure A2. *^{1}H NMR spectrum of ppy-COOH in d_6 DMSO.*

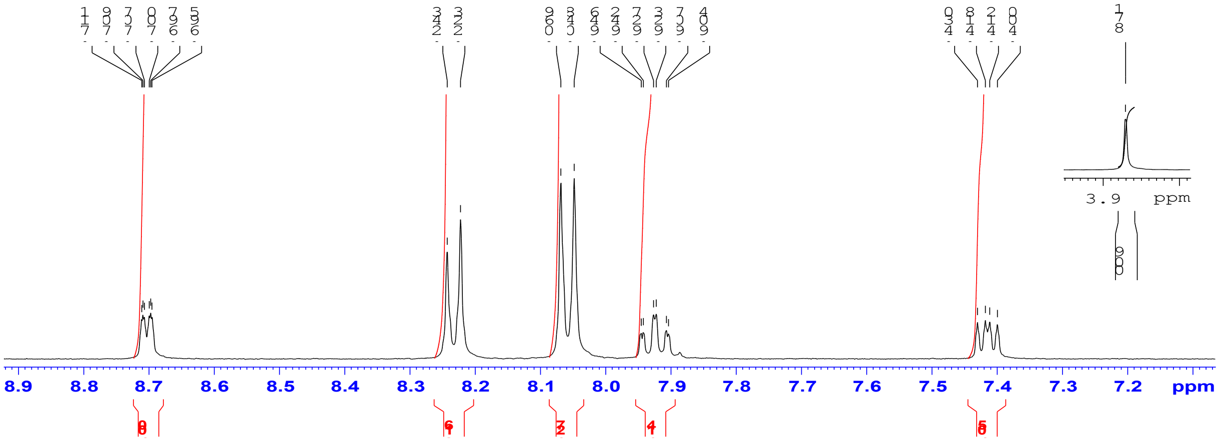

Figure A3. *^{1}H NMR spectrum of ppy-COOCH$_3$ in d_6 DMSO*

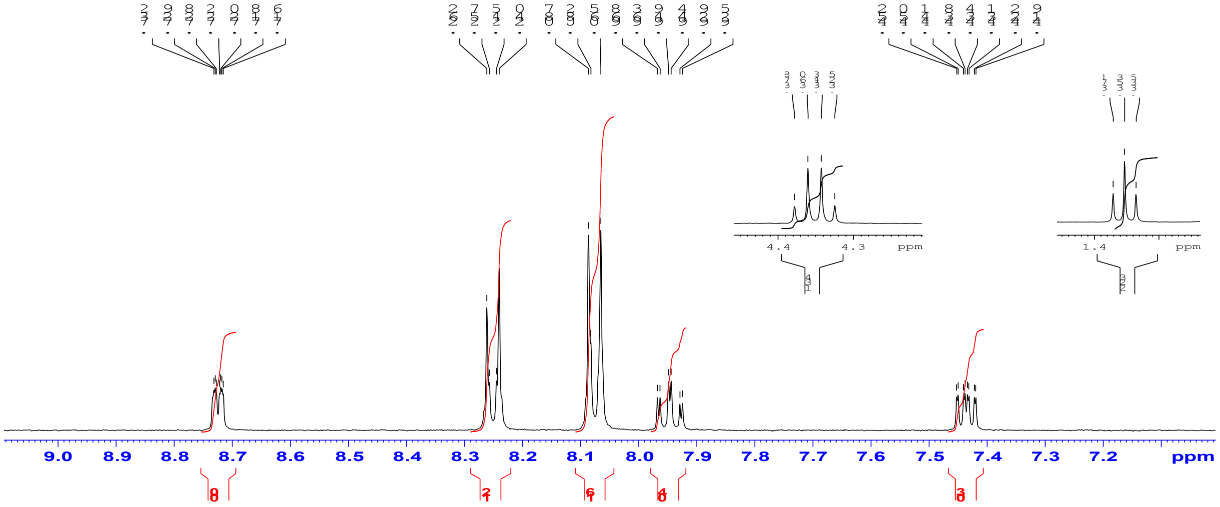

Figure A4. *^{1}H NMR spectrum of ppy-COOCH$_2$CH$_3$ in d$_6$ DMSO*

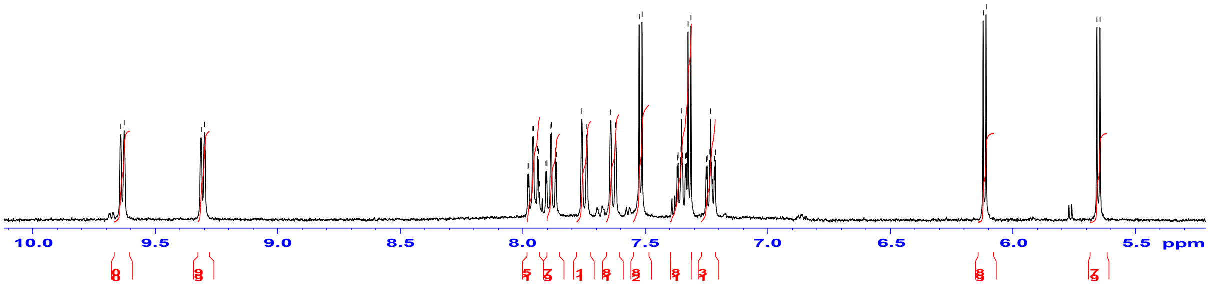

Figure A5. *^{1}H NMR spectrum of [Ir(thpy)$_2$Cl]$_2$ in d$_6$ DMSO*

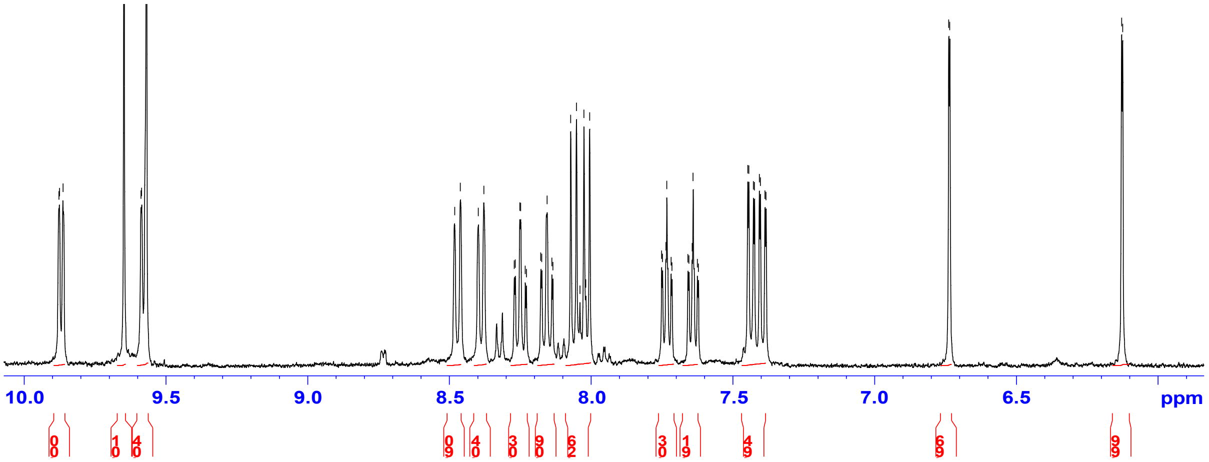

Figure A6. *^{1}H NMR spectrum of [Ir(CHO-ppy)$_2$Cl]$_2$ in d$_6$ DMSO*

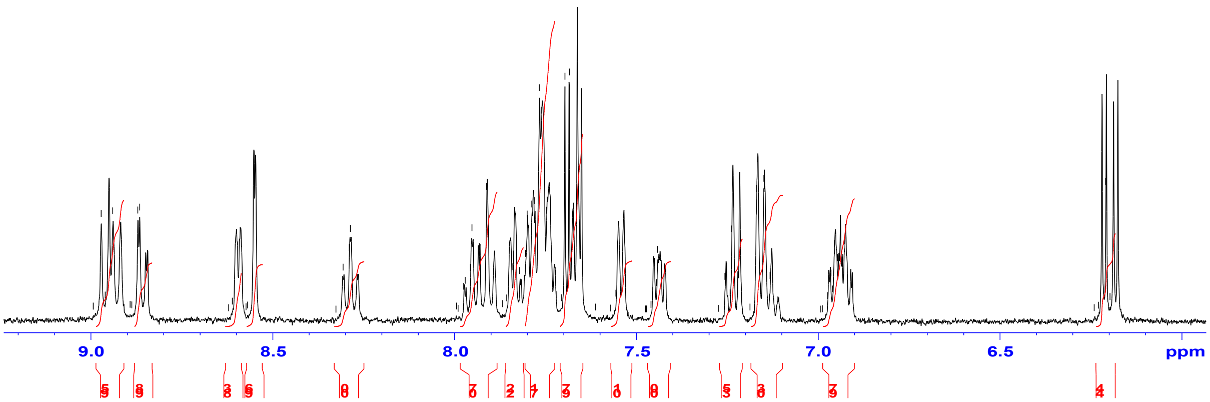

Figure A7. *^{1}H NMR spectrum of [Ir(thpy)$_2$(bpp)]PF$_6$ in d$_6$ DMSO*

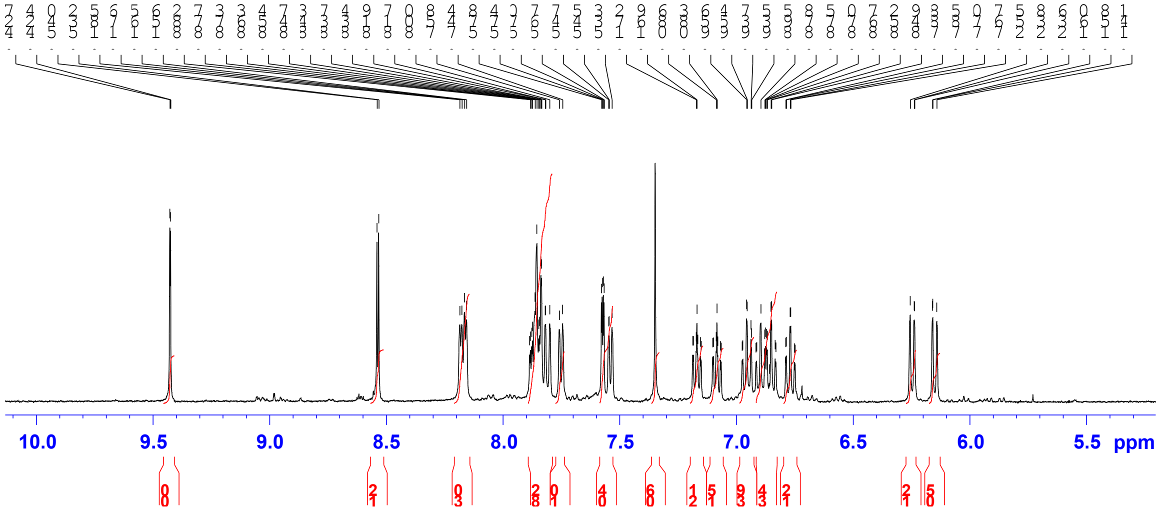

Figure A8. *^{1}H NMR spectrum of [Ir(ppy)$_2$(pztr)]PF$_6$ in d$_6$ DMSO*

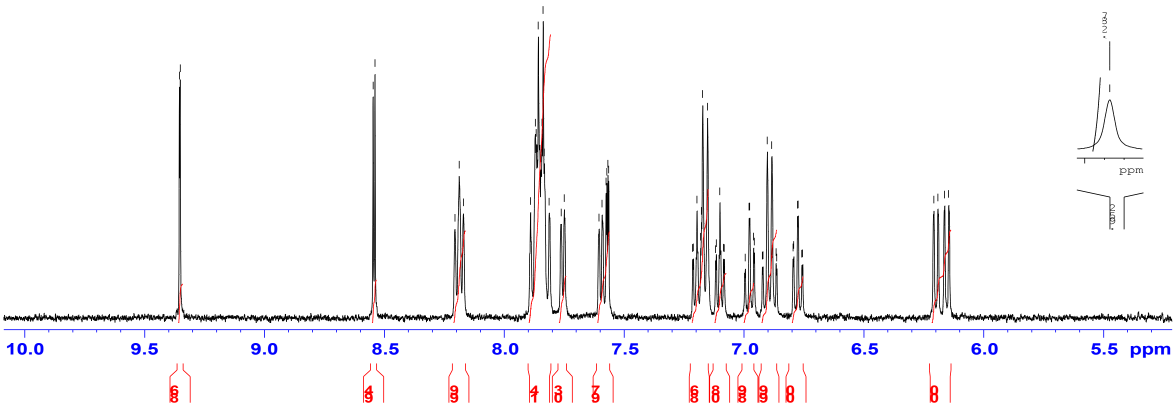

Figure A9. *^{1}H NMR spectrum of [Ir(ppy)$_2$(MePhpztr)] in d_6 DMSO*

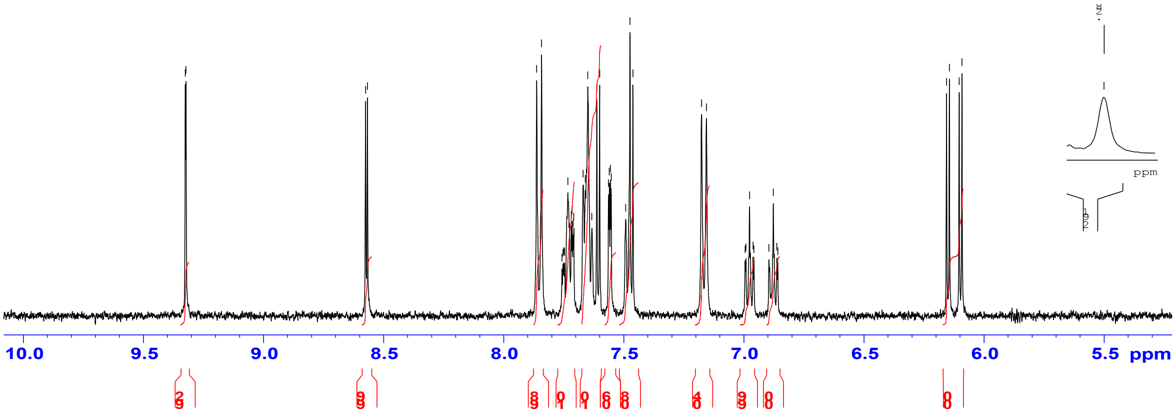

Figure A10. *^{1}H NMR spectrum of [Ir(thpy)$_2$(MePhpztr)] in d_6 DMSO*

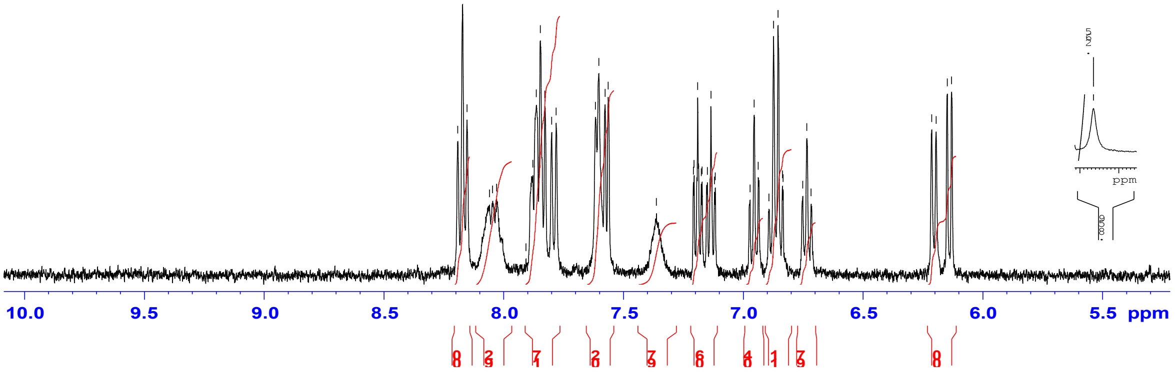

Figure A11. *^{1}H NMR spectrum of [Ir(ppy)$_2$(Mepytr)] in d_6 DMSO*

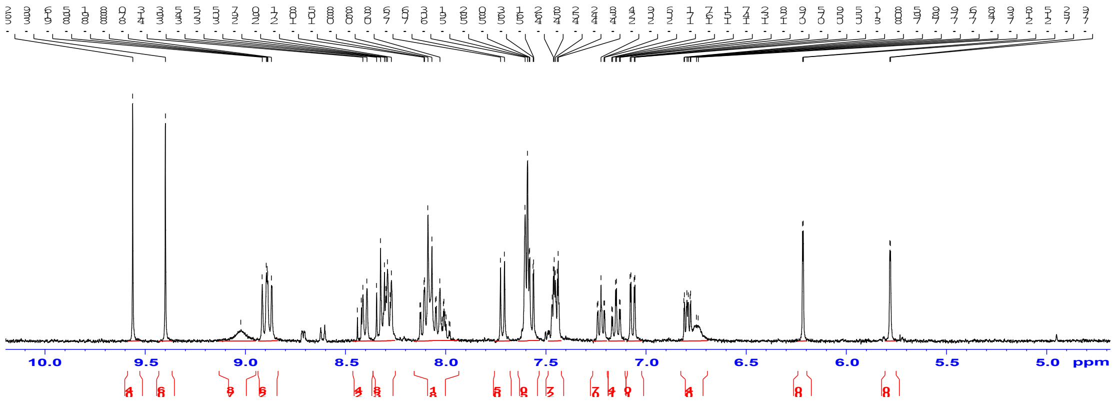

Figure A12. *^{1}H NMR spectrum of [Ir(CHO-ppy)$_2$(tpy)]PF$_6$ in d$_6$ DMSO*

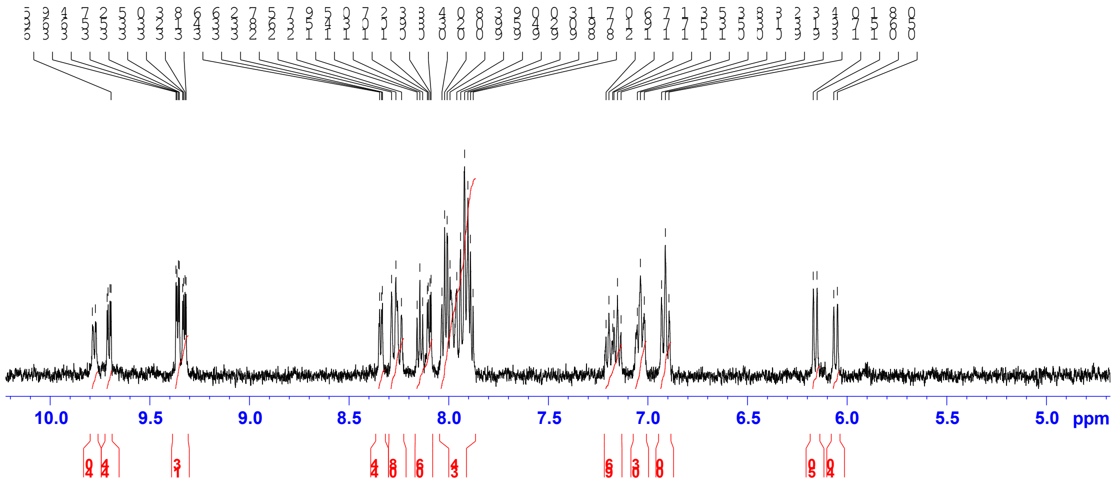

Figure A13. *^{1}H NMR spectrum of [Ir(ppy)$_2$(bpm)PtCl$_2$]PF$_6$ in d$_6$ DMSO*

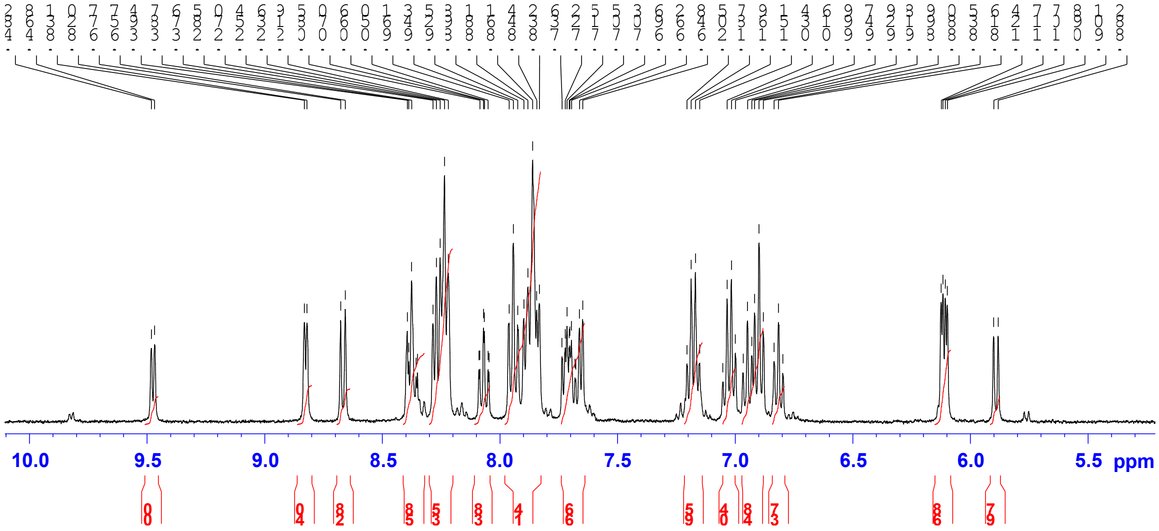

Figure A14. *^{1}H NMR spectrum of [Ir(ppy)$_2$(bpt)Ir(ppy)$_2$]PF$_6$ in d$_6$ DMSO*

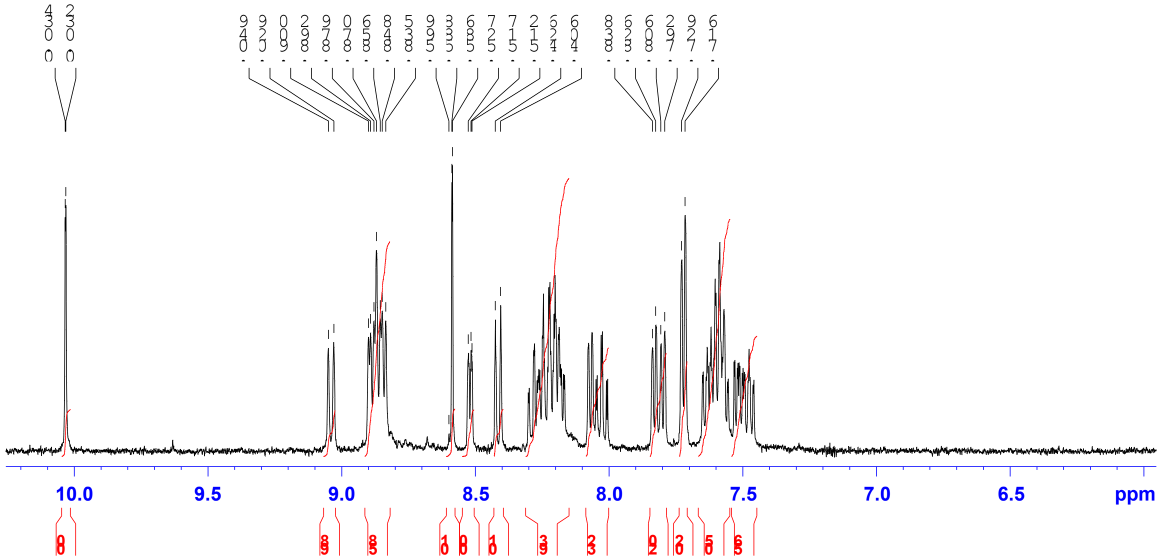

Figure A15. *^{1}H NMR spectrum of [(bpy)$_2$Ru(dpp)]2PF$_6$ in d$_6$ DMSO*

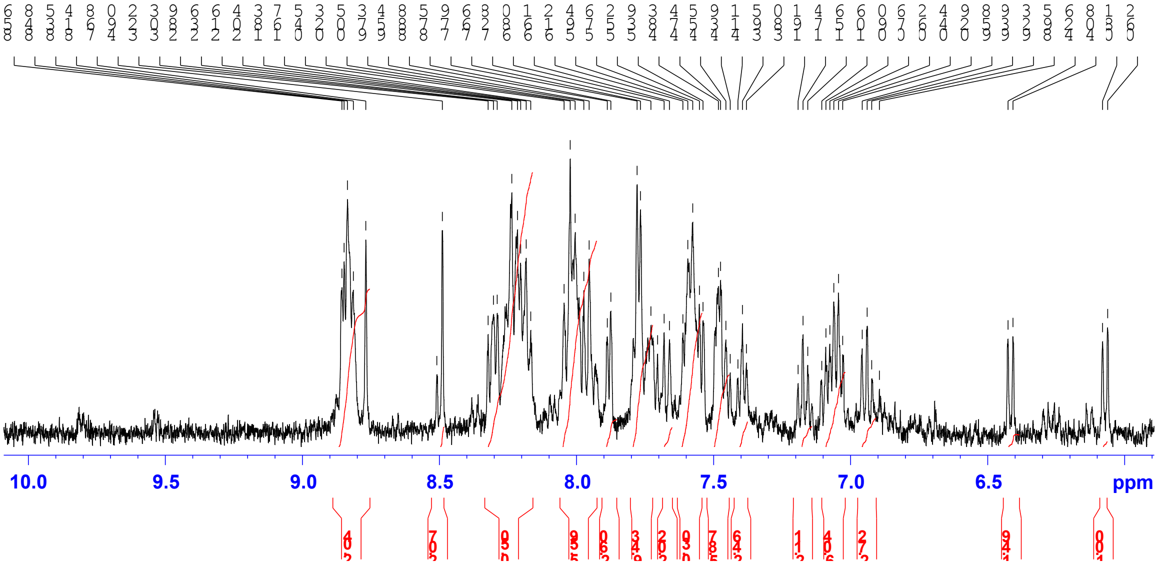

Figure A16. *^{1}H NMR spectrum of [(bpy)$_2$Ru(dpp)Ir(ppy)$_2$]3PF$_6$ in d$_6$ DMSO*

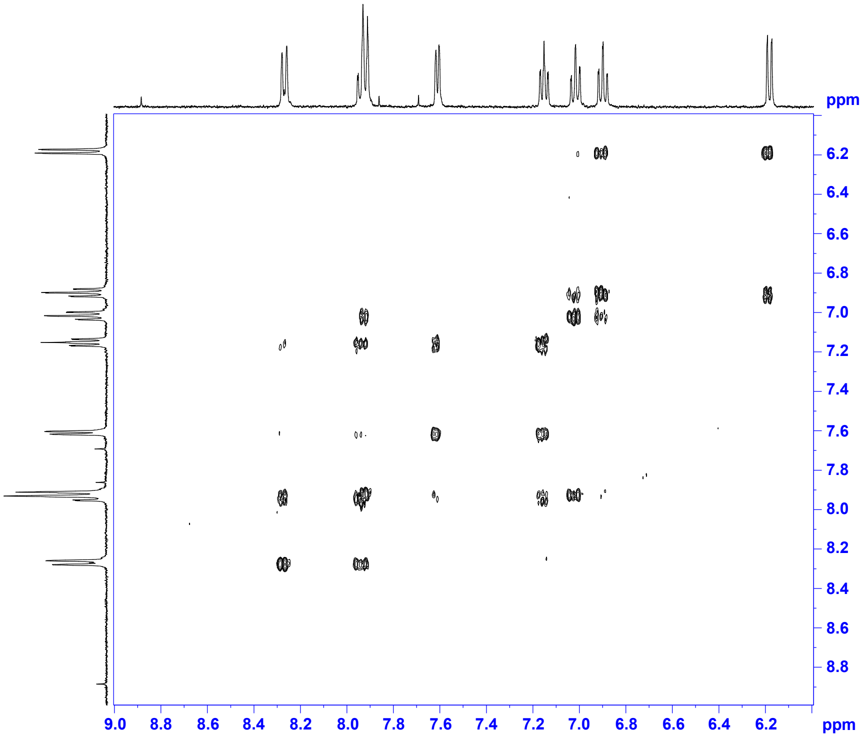

Figure A17. *^{1}H NMR spectrum of [Ir(ppy)$_2$(d$_8$bpy)]PF$_6$ in d$_6$ DMSO*

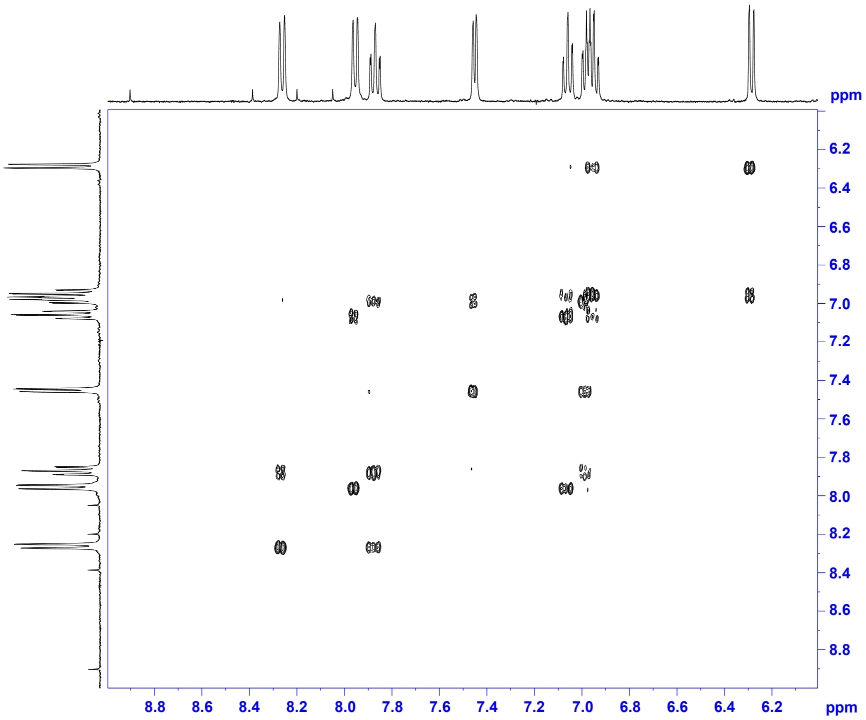

Figure A18. *^{1}H NMR spectrum of [Ir(ppy)$_2$(d$_8$phen)]PF$_6$ in d$_6$ DMSO*

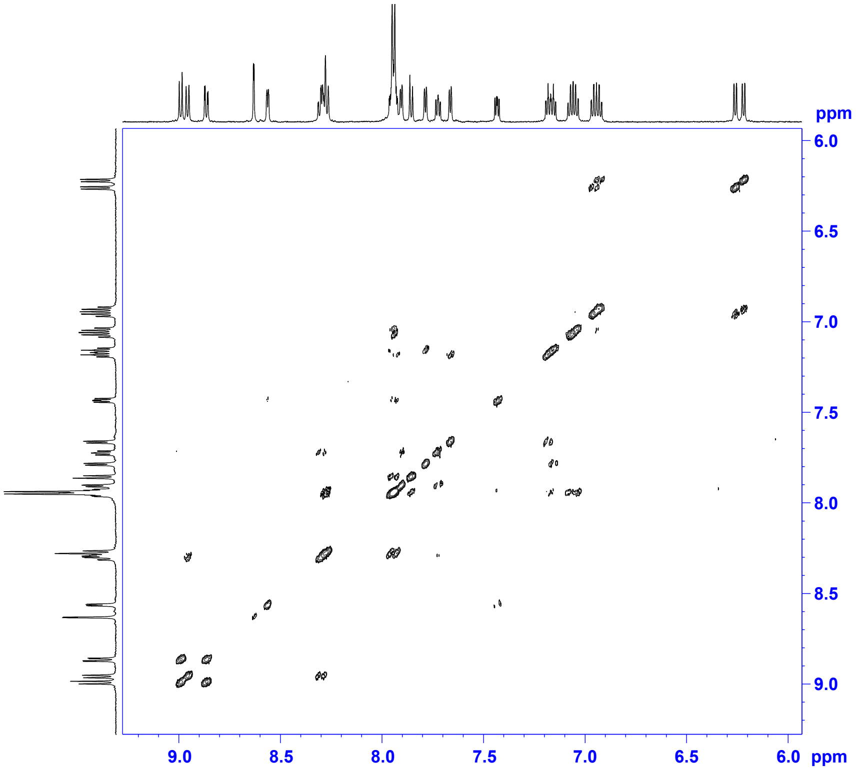

Figure A19. *^{1}H NMR spectrum of [Ir(ppy)$_2$(bpp)]PF$_6$ in d_6 DMSO*

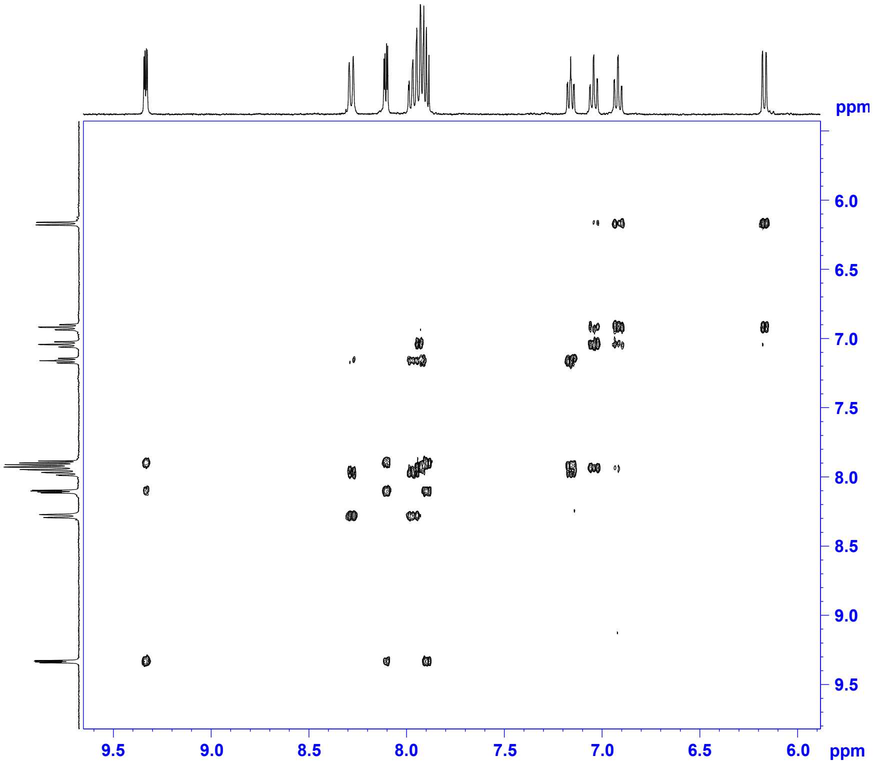

Figure A20. *^{1}H NMR spectrum of [Ir(ppy)$_2$(bpm)]PF$_6$ in d_6 DMSO*

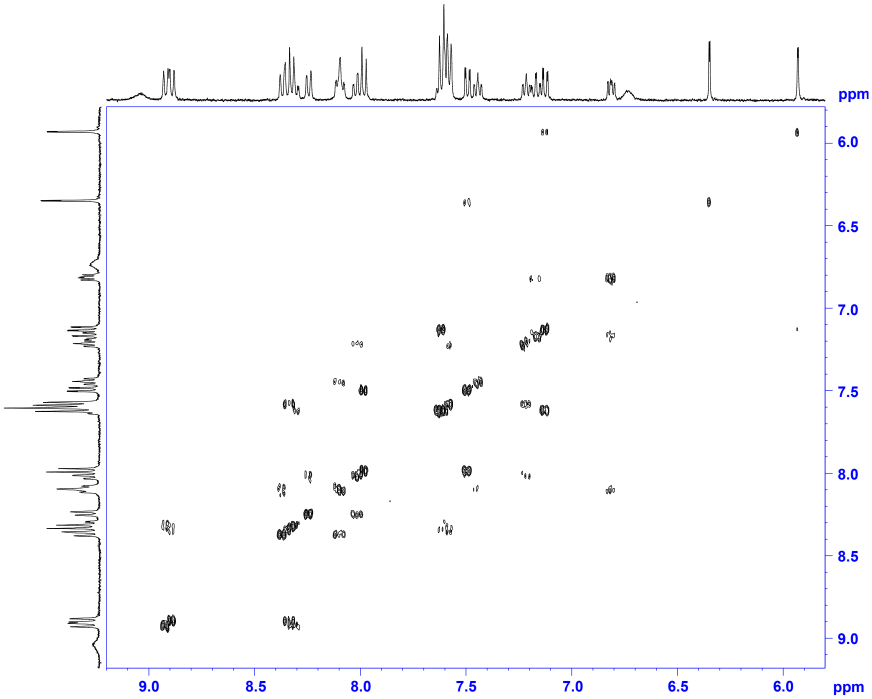

Figure A21. *^{1}H NMR spectrum of [Ir(ppy-COOCH$_3$)$_2$(terpy)]PF$_6$ in d$_6$ DMSO*

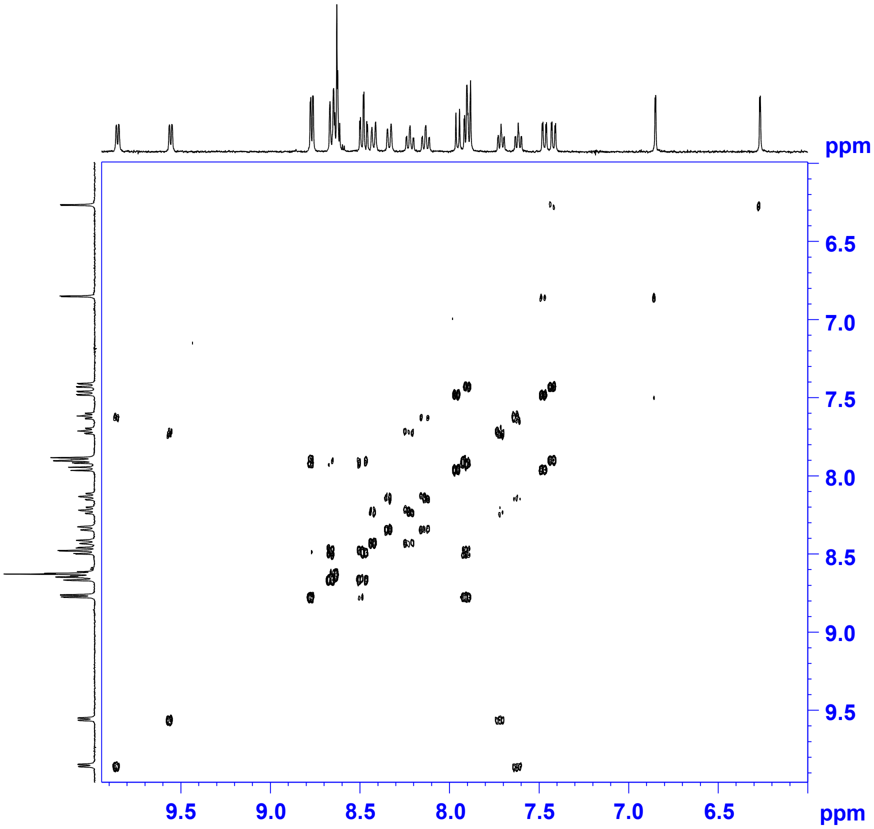

Figure A22. *^{1}H NMR spectrum of [Ir(ppy-COOCH$_3$)$_2$(terpy)PdCl$_2$]2PF$_6$ in d$_6$ DMSO*

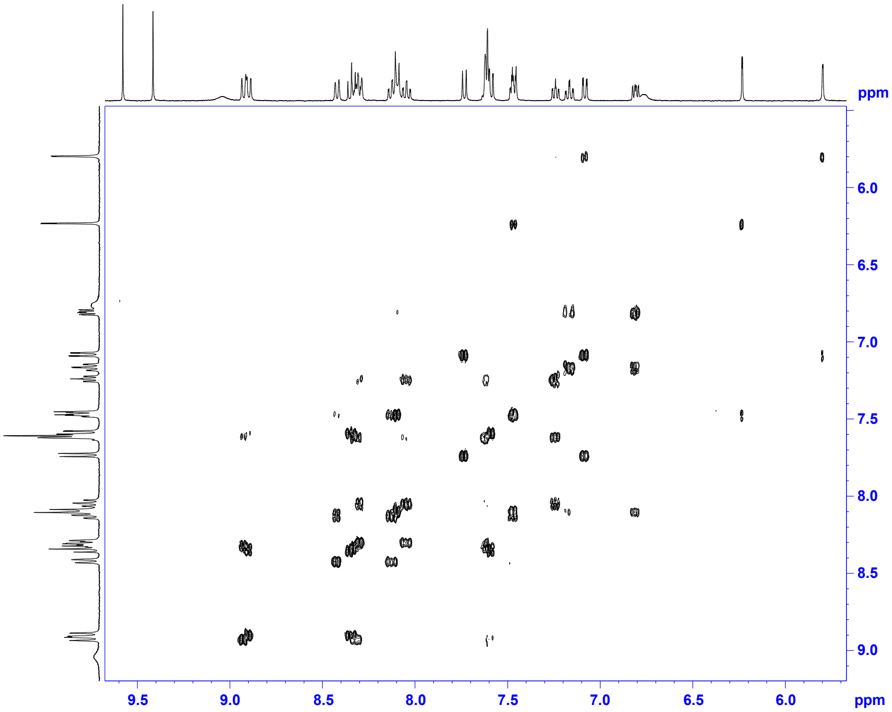

Figure A23. *^1H NMR spectrum of $[Ir(ppy\text{-}CHO)_2(terpy)]PF_6$ in d_6 DMSO*

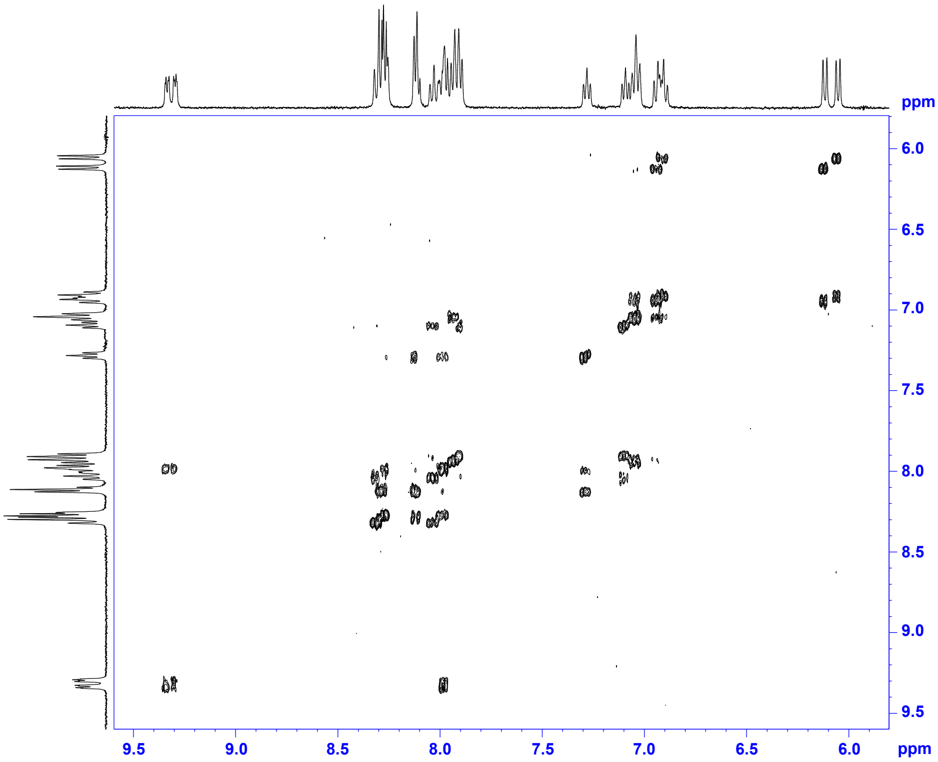

Figure A24. *^1H NMR spectrum of $[Ir(ppy)_2(bpm)PdCl_2]\,2PF_6$ in d_6 DMSO*

Complex	3	4	5	6
(1)	7.60	7.14	7.92	8.26
(2)	7.60	7.14	7.92	8.26
(3)	7.93	7.04	7.85	8.24
(4)	7.93	7.04	7.85	8.24
(5)	7.60	7.15	7.91	8.25
(6)	7.60	7.15	7.91	8.25
(7)	7.70	7.17	7.93	8.26
(8)	7.70	7.17	7.93	8.26

Table 3.1 *Tabulated ^{1}H NMR shift values for complexes (1) to (8) done in d_6 dmso.*

Complex	6"	6'''	5"	5'''	4"	4'''	d	b	c	k	i	j
(9)	6.21	7.78	6.94	7.16	7.05	7.94	7.86	7.43	7.71	8.27	8.85	8.98
(10)	6.23	8.34	6.91	7.11	7.94	7.94	7.88	7.81	7.94	8.58	7.73	8.45
(11)	6.22	7.90	6.88	7.15	7.0	7.63	6.94	8.07	7.53	7.90	8.23	8.23

Table B1 *Tabulated ^{1}H NMR shift values for complex **(9)**, **(10)** and **(11)** in d_6 dmso.*

Complex	6"	5"	4"	3"	5'''	4'''	3'''	c	d	k	f
(15)	5.82	6.80	7.01	7.52	7.66	8.36	8.93	7.35	8.03	8.29	6.99
(16)	6.22	6.74	6.87	7.77	7.99	7.43	9.51	7.87	8.72	-	-
(17)	5.93	-	7.17	7.59	8.11	7.17	8.90	7.99	8.28	8.11	7.59
(18)	6.82	-	7.44	7.88	8.12	7.60	9.52	7.88	8.74	-	7.88
(19)	6.24	-	7.48	8.12	8.05	7.25	7.61	7.61	8.32	8.32	7.61

Table B2 *Tabulated ^{1}H NMR shift values for complex **(15)**, **(16)**, **(17)** and **(18)** in d_6 dmso.*

Complex	6	5	4	3	d	e	f
(20)	8.26	7.91	7.14	7.91	-	-	-
(21)	8.28	8.10	7.28	8.10	9.30	7.96	8.28
(23)	8.28	7.99	7.29	8.12	-	-	-
(24)	8.44	8.12	7.62	8.12	-	-	-

Table B3 *Tabulated ^{1}H NMR shift values for complex **(20)**, **(21)**, **(23)** and **(24)** in d_6 dmso.*

Photophysics

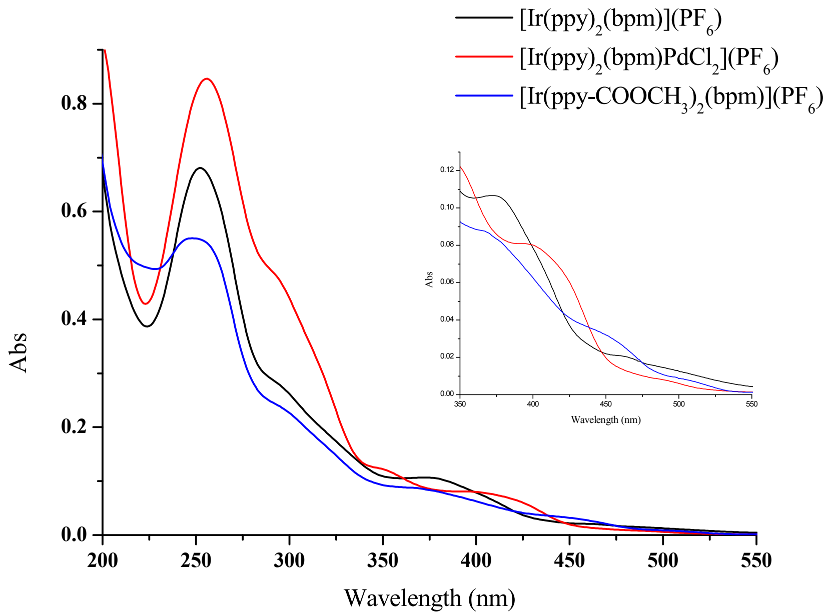

Figure A25. *Absorption spectra for complex [Ir(ppy)$_2$(bpm)](PF$_6$) (20) along with complex [Ir(ppy)$_2$(bpm)PdCl$_2$](PF$_6$) (21) and [Ir(ppy-COOCH$_3$)$_2$(bpm)](PF$_6$) (21) measured in aerated ACN at room temperature (298 K) (concentration - 6×10^{-5}M). (MLCT region is expanded inside).*

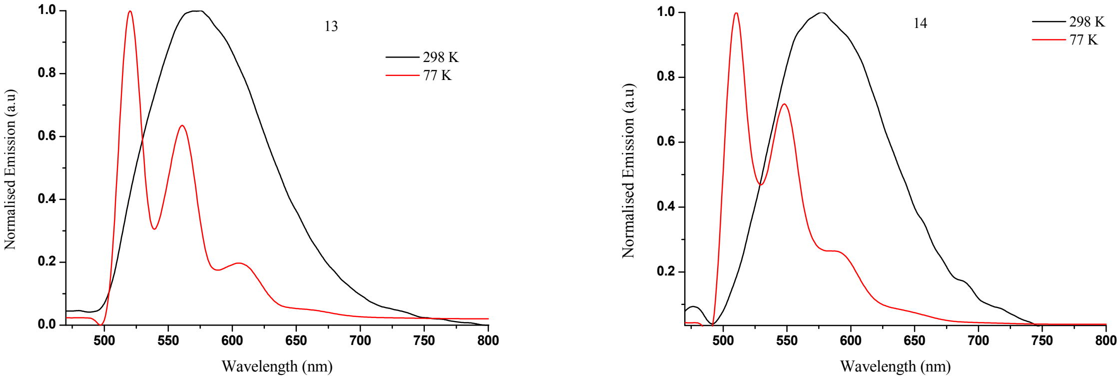

(a)

(b)

Figure A26 (a) *Emission spectrum for [Ir(ppy-COOCH$_3$)$_2$(BPP)PtCl]$_2$(PF$_6$)$_2$* ***(****13) at 298 K (in aerated ACN) and 77 K (in 4:1 EtOH:MeOH glass)* ***(b)*** *Emission spectrum for [Ir(ppy-COOCH$_3$)$_2$(BPP)PdCl]$_2$(PF$_6$)$_2$* ***(****14) at 298 K (in aerated ACN) and 77 K (in 4:1 EtOH:MeOH glass)*

Absorption data with extinction coefficients for complexes discussed in chapter 3

Complex	**Absorption λ_{abs} (nm)** **ε ($LM^{-1}cm^{-1}$)x 10^3**
$[Ir(ppy)_2(bpy)](PF_6)$ **(1)**	257 (47698), 300 (23947), 350 (7263), 410 (3437), 470 (548)
$[Ir(ppy)_2(d_8bpy)](PF_6)$ **(2)**	257 (52181), 300 (26523), 350 (8141), 410 (3895), 470 (3888)
$[Ir(ppy)_2(phen)](PF_6)$ **(3)**	263 (53053), 350 (7874), 470 (581)
$[Ir(ppy)_2(d_8phen)](PF_6)$ **(4)**	263 (52427), 350 (8788), 470 (1070)
$[Ir(ppy)_2(dmbpy)](PF_6)$ **(5)**	257 (50096), 300 (24864), 350 (8248), 410 (4115), 470 (968)
$[Ir(ppy)_2(d_{12}dmbpy)](PF_6)$ **(6)**	257 (46167), 300 (23211), 350 (8323), 410 (3556), 470 (629)
$[Ir(ppy)_2(dtbpy)](PF_6)$ **(7)**	257 (44337), 300 (21504), 350 (6851), 410 (3135), 470 (394)
$[Ir(ppy)_2(d_{24}dtbpy)](PF_6)$ **(8)**	257 (51390), 300 (25466), 350 (51535), 410 (3918), 470 (704)

***Table B4**. Absorption data with extinction coefficient values for complexes **(1)** to **(8)** measured in ACN*

Complex	**Absorption λ_{abs} (nm)** **ε ($LM^{-1}cm^{-1}$)x 10^3**
$[Ir(ppy)_2(tpy)]PF_6$ **(15)**	257 (53445), 350 (9866), 470 (996)
$[Ir(ppy)_2(tpy)PdCl]_2(PF_6)_2$ **(16)**	265 (104933), 350 (23492), 470 (290)
$[Ir(ppy\text{-}COOCH_3)_2(tpy)]PF_6$ **(17)**	264 (56141), 300 (43173), 350 (9646), 470 (993)
$[Ir(ppy\text{-}COOCH_3)_2(tpy)PdCl]_2(PF_6)_2$ **(18)**	270 (146928), 350 (26570), 470 (4500)
$[Ir(ppy\text{-}CHO)_2(tpy)]PF_6$ **(19)**	270 (49780), 303 (45466), 350 (8847), 470 (264)

***Table B5**. Absorption data with extinction coefficient values for complexes **(15)** to **(19)** measured in ACN*

Complex	**Absorption λ_{abs} (nm)** **ε ($LM^{-1}cm^{-1}$)x 10^3**
$[Ir(ppy)_2(bpm)]PF_6$ **(20)**	252 (68098), 350 (10914), 470 (1874)
$[Ir(ppy)_2(bpm)PdCl_2]PF_6$ **(21)**	256 (84616), 350 (12226), 470 (1119)
$[Ir(ppy\text{-}COOCH_3)_2(bpm)]PF_6$ **(24)**	250 (54990), 350 (9269), 470 (2058)

***Table B6**. Absorption data with extinction coefficient values for complexes **(20), (21) & (24)** measured in ACN*

The molar extension coefficient (ε) for all the iridium complexes has been calculated by the method as follows. Four to five different concentrations of a particular complex is prepared and absorption spectra is measured, the concentration is kept in such a way as all of them obey beer lamberts law (O.D kept below 1). In cases where there is huge difference between the absorbance of visible and UV regions are seen ε was calculated separately at different sets of concentrations for UV and visible regions in those cases. After that absorbance at a particular wavelength was plotted against different concentration and the linear fit of the data gave us the slope which is the molar extinction coefficient data. An example of the absorption against the concentration for [Ir(ppy)$_2$(bpy)](PF$_6$) at two different wavelengths are shows in figure below. The rest of all are obtained using the same method.

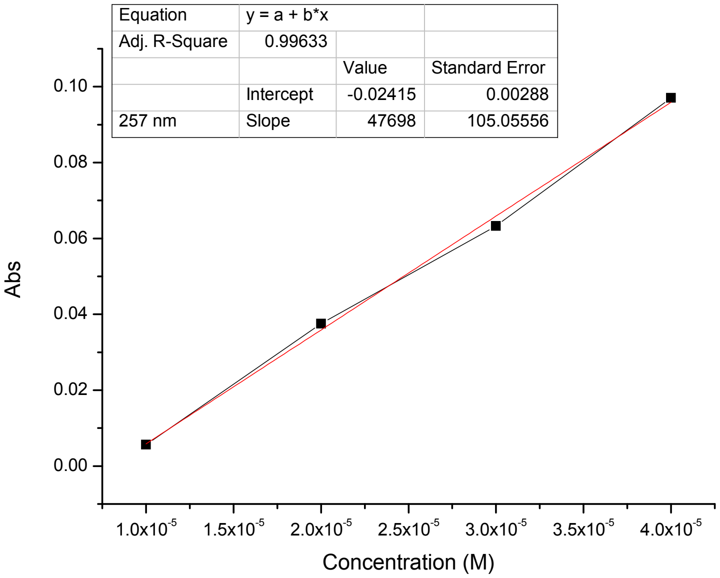

Figure : Absorbance, concentration and molar extintction coefficient for [Ir(ppy)$_2$(bpy)](PF$_6$) at 257 nm.

Lifetime decay curves and residual plots

The lifetime decay plots for all of the complexes discussed in chapter 3 along with the decay fit curve and the corresponding residual plots are given in figures below. All the measurements were done in spectroscopic grade ACN at room temperature (298 K). The complete details regarding emission wavelength, time base, lifetime value and χ^2 value which determines the perfection of fit are given inside each of the graphs.

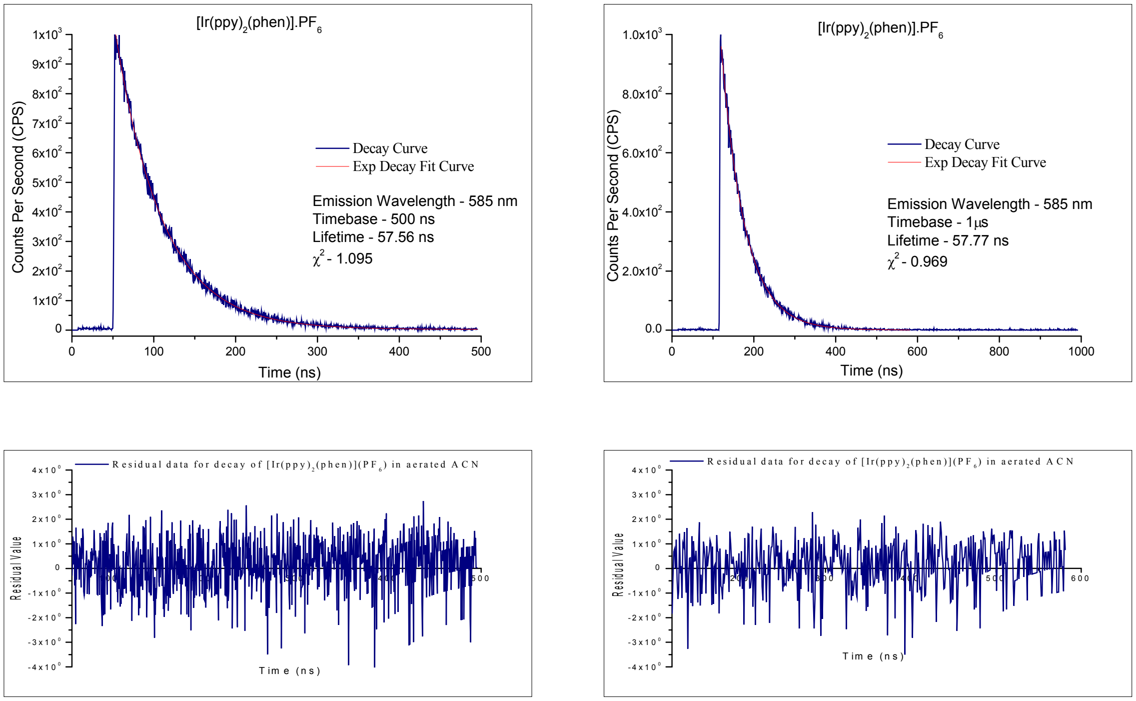

Figure A27. Lifetime values with decay plots for $[Ir(ppy)_2(phen)]PF_6$ in aerated ACN at 298 K.

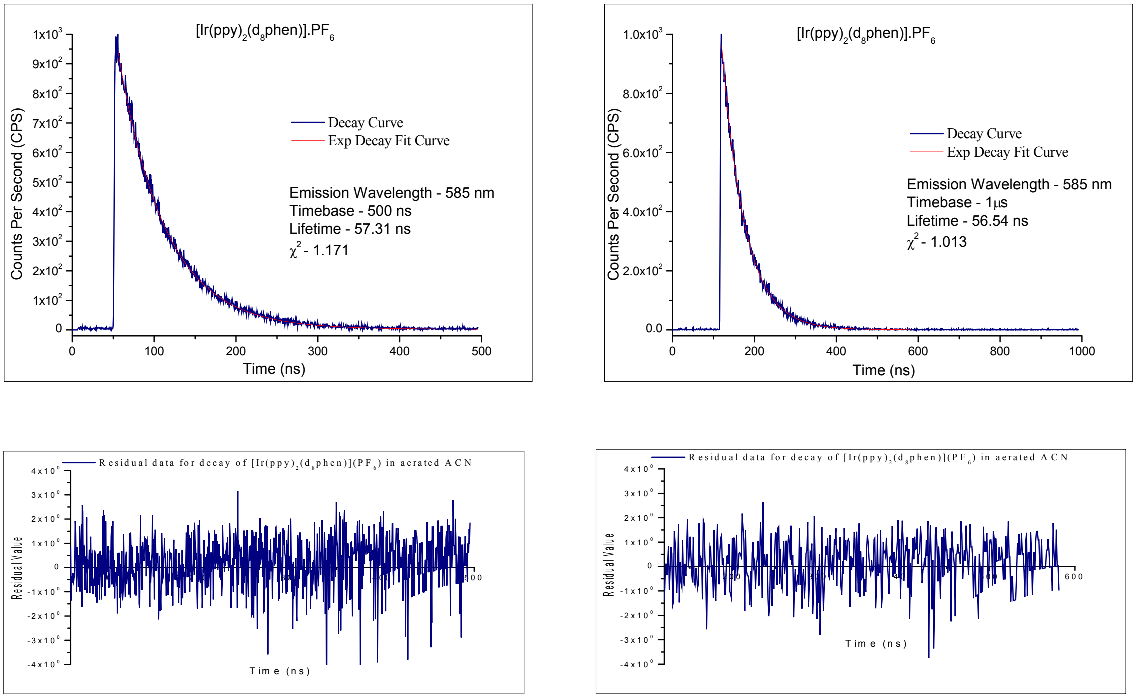

Figure A28. Lifetime values with decay plots for $[Ir(ppy)_2(d_8phen)]PF_6$ in aerated ACN at 298K.

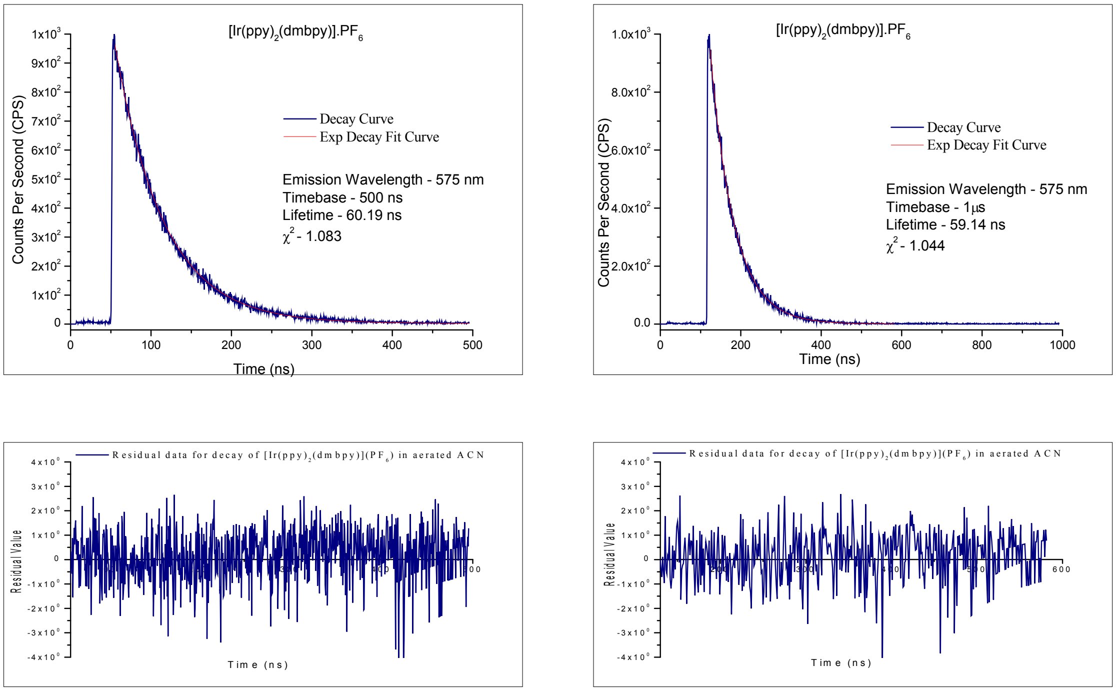

Figure A29. Lifetime values with decay plots for[Ir(ppy)$_2$(dmbpy)]PF$_6$ in aerated ACN at 298K.

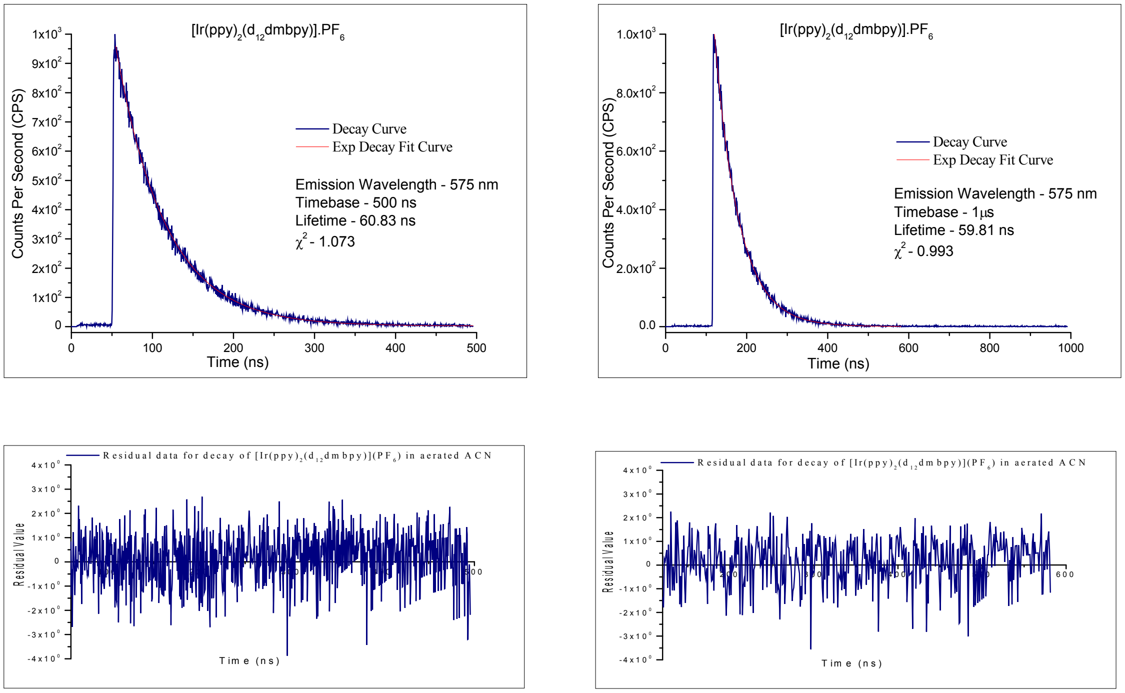

Figure A30. Lifetime values with decay plots for[Ir(ppy)$_2$(d$_{12}$dmbpy)]PF$_6$ in aerated ACN at 298K.

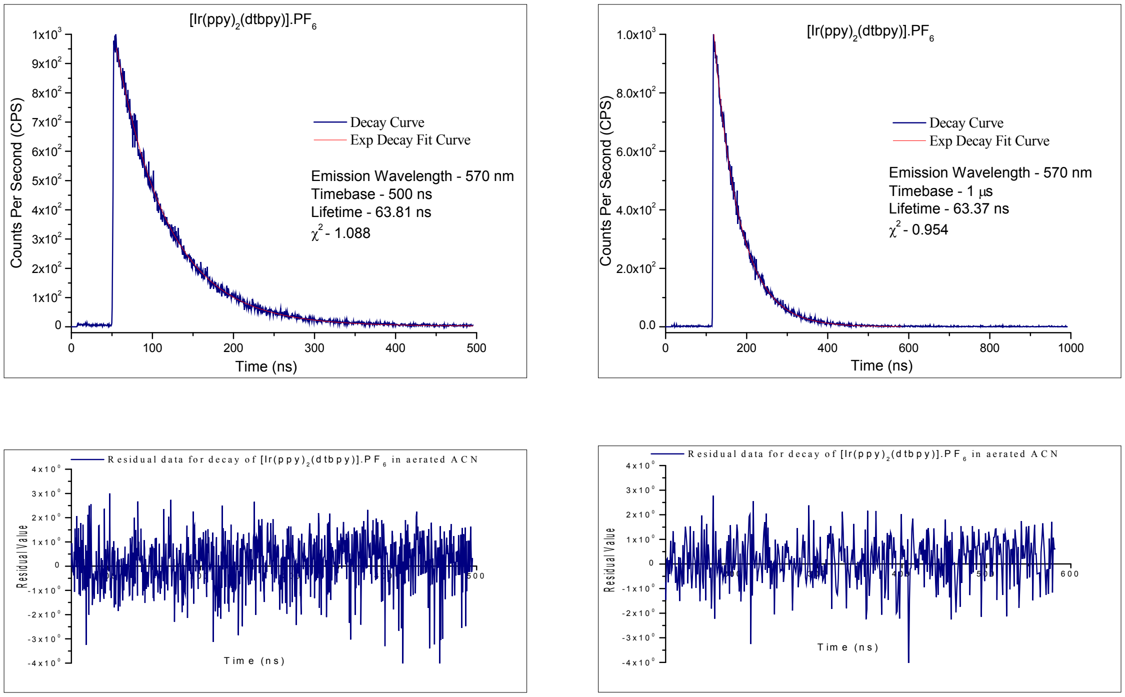

Figure A31. *Lifetime values with decay plots for[Ir(ppy)*$_2$*(dtbpy)]PF*$_6$ *in aerated ACN at 298K.*

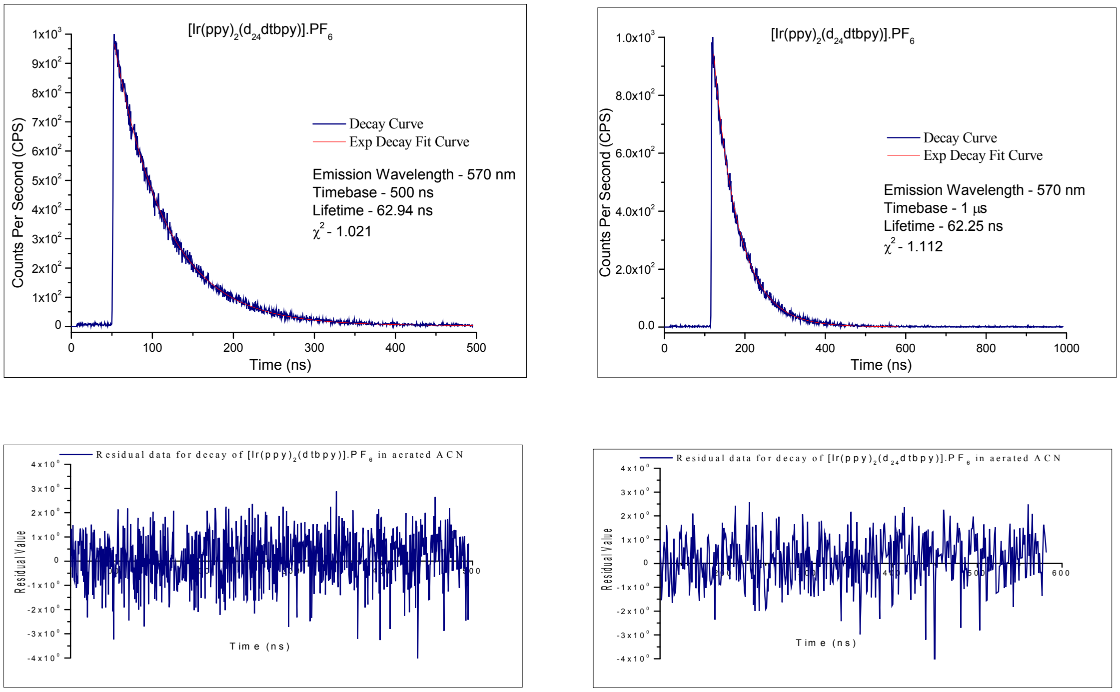

Figure A32. *Lifetime values with decay plots for[Ir(ppy)*$_2$*(d*$_{24}$*dtbpy)]PF*$_6$ *in aerated ACN at 298K.*

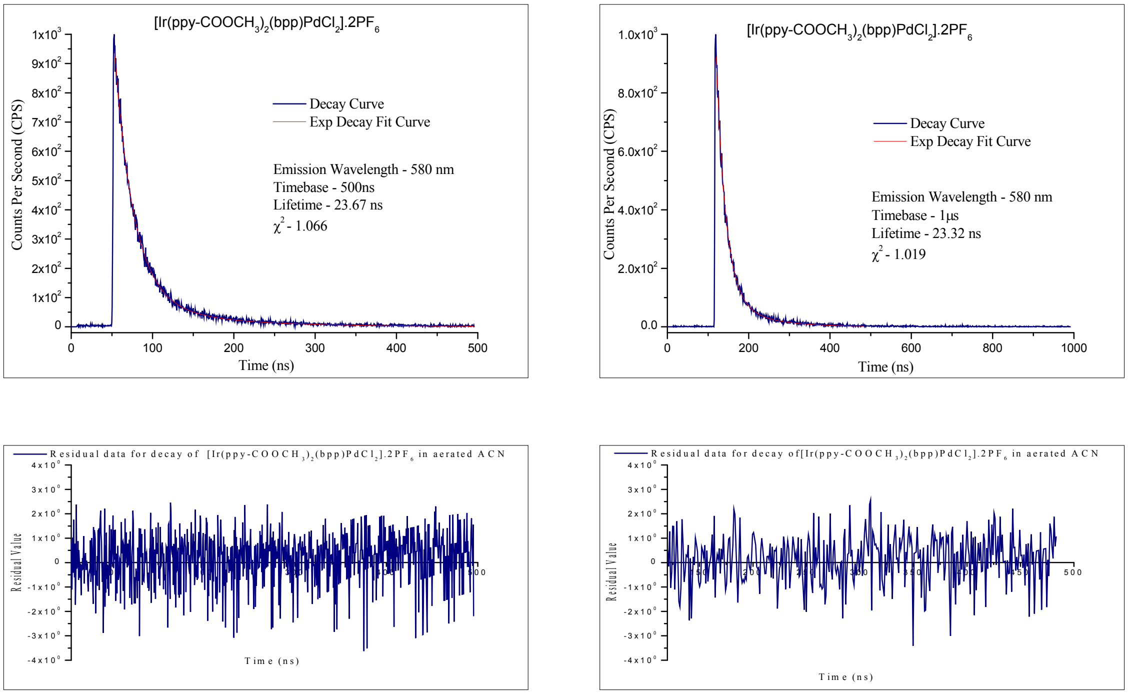

Figure A33. *Lifetime values with decay plots for[Ir(ppy-COOCH$_3$)$_2$(bpp)PdCl$_2$]PF$_6$ in aerated ACN at 298K.*

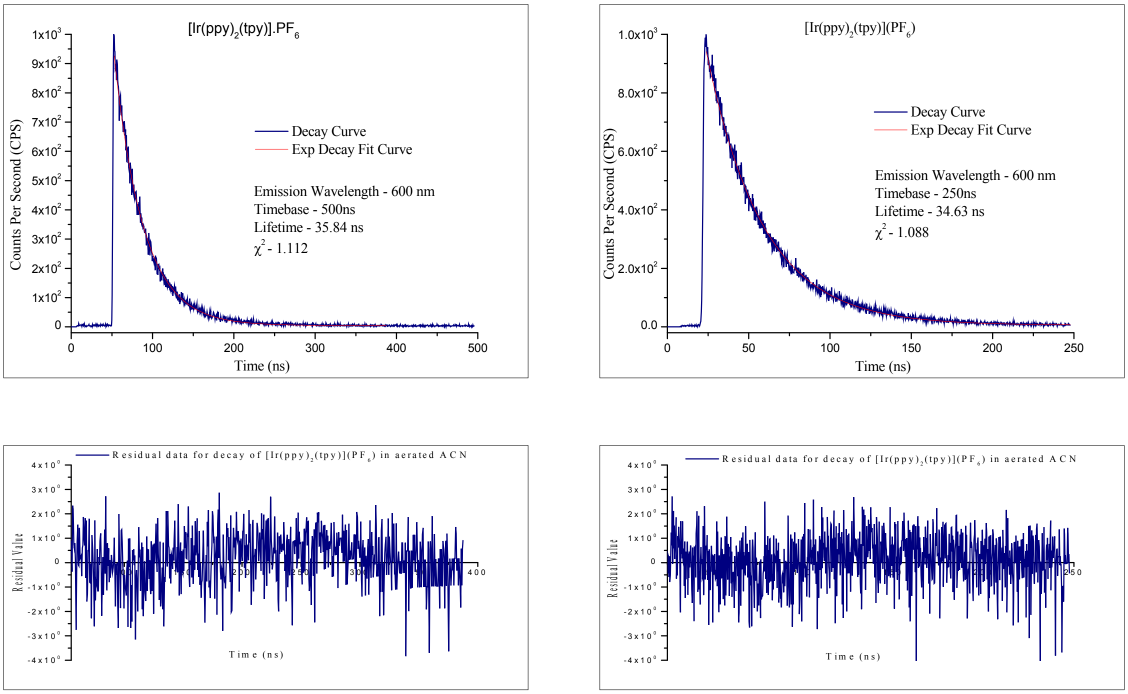

Figure A34. *Lifetime values with decay plots for[Ir(ppy)$_2$(tpy)]PF$_6$ in aerated ACN at 298K.*

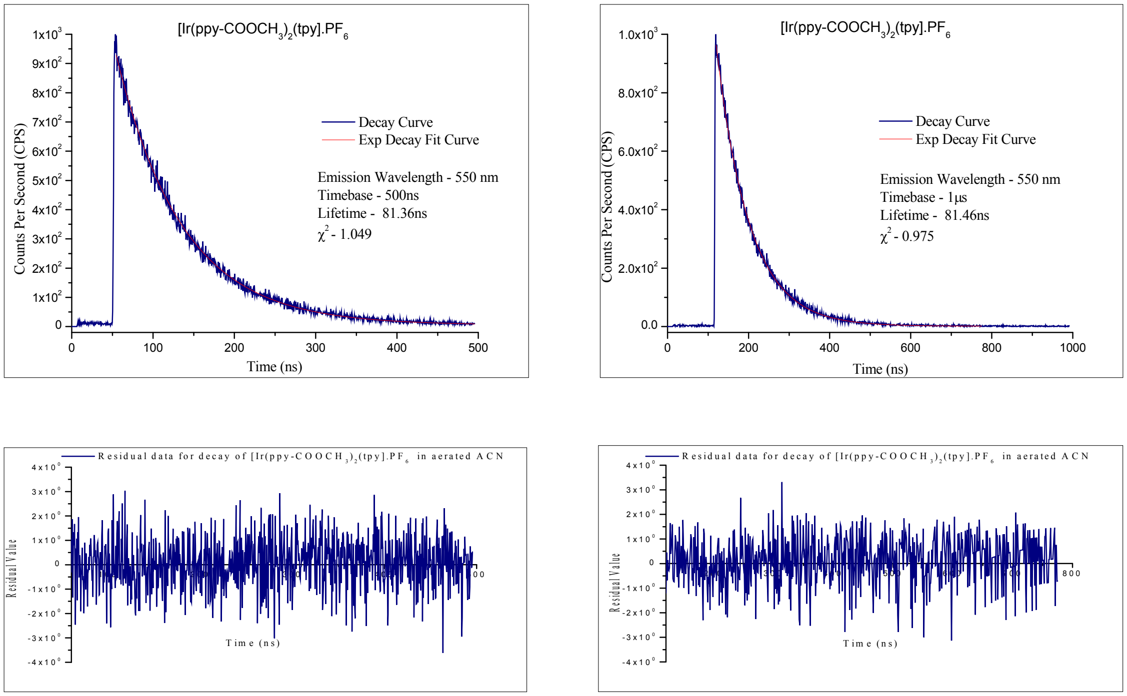

Figure A35. *Lifetime values with decay plots for[Ir(ppy-COOCH$_3$)$_2$(tpy)]PF$_6$ in aerated ACN at 298K.(λ_{em} = 550 nm)*

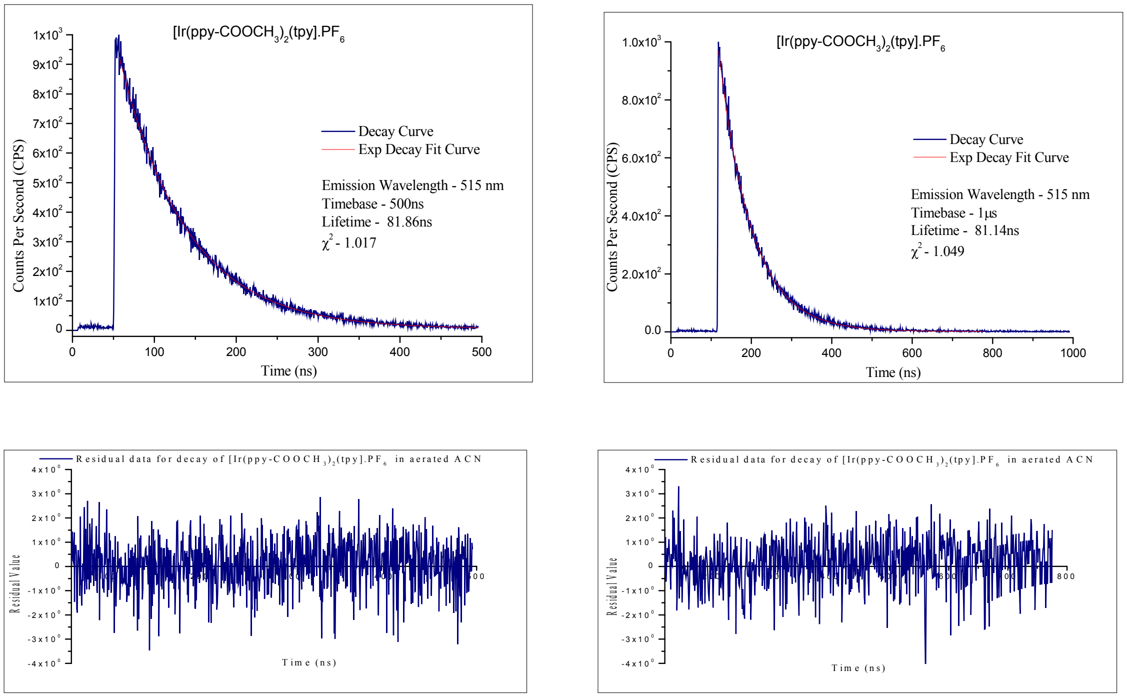

Figure A36. *Lifetime values with decay plots for[Ir(ppy-COOCH$_3$)$_2$(tpy)]PF$_6$ in aerated ACN at 298K. (λ_{em} = 515 nm)*

Electrochemistry of complexes discussed in chapter 3 - All the measurements were completly done and tabulated by Jane Inglis

Complex	**$E_{1/2\ ox.}$ (V)**	**Epa-Epc (mV)**	**$E_{1/2red.}$ (V)**	**Epc-Epa (mV)**
$[Ir(ppy)_2(bpp)](PF_6)$ **(9)**	+1.33	70	-1.21, -1.73, -2.27	60, 70, 70
$[Ir(ppy)_2(bpp)PtCl]_2(PF_6)_2$ **(10)**	+1.89		-0.94(irr), -1.35, -1.82	80, 100
$[Ir(ppy)_2(bpp)PdCl]_2(PF_6)_2$ **(11)**	+1.43 (irr), +1.92	130	-0.89, -1.33, -1.78	60, 140
$[Ir(ppy\text{-}COOCH_3)_2(bpp)]$ (PF_6), **(12)**	+1.56	95	-1.16, -1.70, -1.86, -1.99	70, 90, 70, 110
$[Ir(ppy\text{-}COOCH_3)_2(bpp)$ $PtCl]_2(PF_6)_2$ **(13)**	+1.49	70	-1.29, -1.68, -1.87, -2.08	60, 60, 60, 85
$[Ir(ppy)_2(tpy)](PF_6)$ **(15)**	+1.35, +1.49	Irreversible 100	-1.35, -1.98, -2.17	60, 70, 150
$[Ir(ppy)_2(tpy)PdCl]_2(PF_6)_2$ **(16)**	+1.05 +1.44 +1.94	60 60 Irreversible	-0.78 -1.38 -2.04 -2.30	100 Irreversible 75 75
$[Ir(ppy\text{-}COOCH_3)_2(tpy)]$ (PF_6), **(17)**	+1.53 +1.62 +1.94	Irreversible 85 100	-0.85 -1.30 -1.78 -2.02	Irreversible 60 70 120
$[Ir(ppy\text{-}COOCH_3)_2(tpy)$ $PdCl]_2(PF_6)_2$, **(18)**	+1.17 +1.58	70 70	-0.76 -1.76 -1.89 -2.09	Irreversible 90 70 100
$[Ir(CHO\text{-}ppy)_2(tpy)](PF_6)$ **(19)**	+1.51 +1.73 +1.96	Irreversible 90 110	-0.83 -1.29 -1.57 -1.78 -2.02	Irreversible 60 60 100 150

[Ir(ppy)$_2$(bpm)](PF$_6$) **(20)**	+1.39	80	-0.98 -1.66 -2.05 -2.20	60 60 140 160
[Ir(ppy)$_2$(bpm)PdCl$_2$](PF$_6$) **(21)**	+ 1.55	95	-0.36 -0.71 -1.06 -1.79 -2.02 -2.16	50 Irreversible 65 80 120 70
[Ir(ppy-COOCH$_3$)$_2$(bpm)] (PF$_6$), **(24)**	+ 1.58	100	-0.85 -0.95 -1.62 -1.82 -1.96 -2.28	Irreversible 50 50 60 100 70
[Ir(ppy)$_2$(dpp)](PF$_6$) **(25)**	+ 1.40	60	-0.94 -1.58 -2.24	60 60 110

---

[1] R. Hage, *Ruthenium and osmium complexes containing triazole ligands: syntheses, structures, electrochemical and photophysical properties*, Ph.D. Dissertation, Leiden University, The Netherlands, **1991.**

Appendix C

Supplimentary data from chapter 4

Photophysics

Complex	**Absorption λ_{abs} (nm) ε($LM^{-1}cm^{-1}$)**	**Emission, λ_{max} (nm), λ_{ex} (420nm)**		**Quantum Yield ϕ_F**	**Avg. Lifetime τ_{av}, (ns) 298 K**
		298K Aerated	77K (nm)		
(a)	256(56197), 291(45699), 318(37498), 350(6848), 420(563), 470(0)	614	540	0.219	72
(b)	262(74679), 303(68770), 350(34111), 420(9210), 470(1973)	546, 605	528, 567	0.052	69, 76
(c)	256(116297), 287(99499), 350(35839), 420(8266), 470(1841)	618	544	0.048	73

Table S1. *Photophysical properties of the complexes [Ir(ppy)$_2$(bpp)]PF$_6$* ***(a)****, [Ir(ppy)$_2$(bpp) PtCl]$_2$(PF$_6$)$_2$* ***(b)*** *and [Ir(ppy)$_2$(bpp)PdCl]$_2$(PF$_6$)$_2$* ***(c)***

The molar extension coefficient (ε) for all the iridium complexes has been calculated by the method as follows. Four to five different concentrations of a particular complex is prepared and absorption spectra is measured, the concentration is kept in such a way as all of them obey beer lamberts law (O.D kept below 1). In cases where there is huge difference between the absorbance of visible and UV regions are seen ε was calculated separately at different sets of concentrations for UV and visible regions in those cases. After that absorbance at a particular wavelength was plotted against different concentration and the linear fit of the data gave us the slope which is the molar extinction coefficient data. Some of them are given below the rest are done in the same way

Linear Fit data at four different conc. used for calculating extinction coefficient

Complex **(b)** : $[Ir(ppy)_2(bpp)PtCl]_2(PF_6)_2$

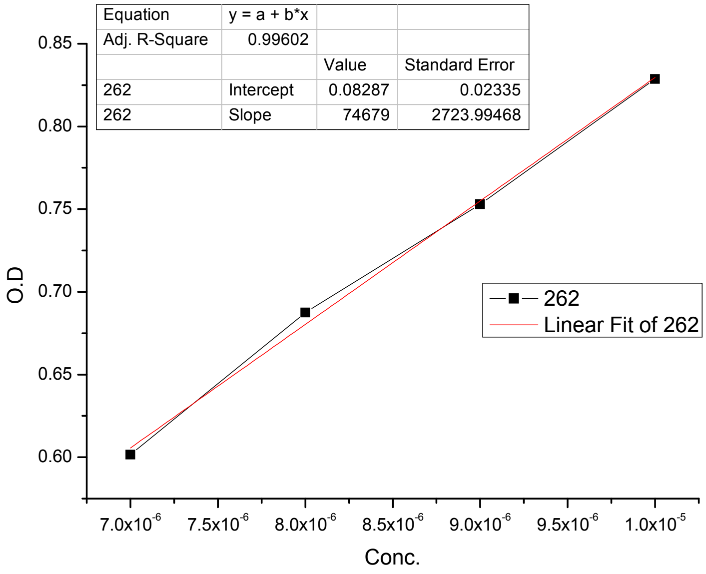

Equation	y = a + b*x		
Adj. R-Square	0.99602		
		Value	Standard Error
262	Intercept	0.08287	0.02335
262	Slope	74679	2723.99468

Linear fit at 4 different conc. for complex **(b)** at a wavelength of **262 nm**

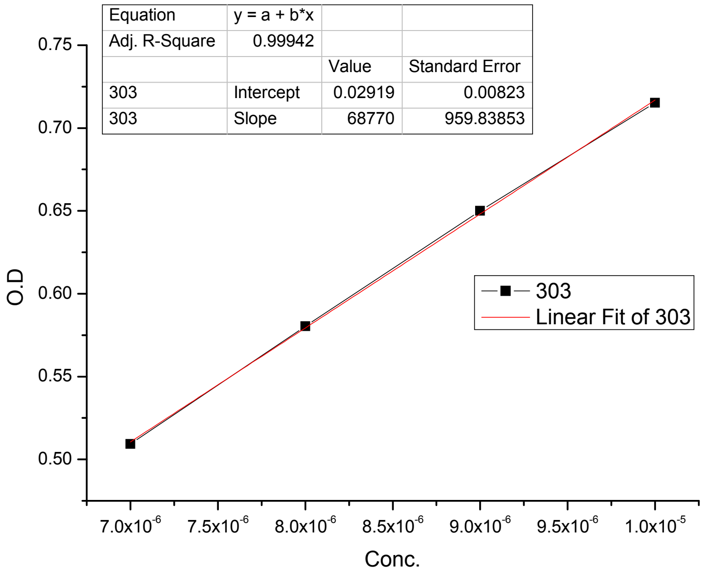

Equation	y = a + b*x		
Adj. R-Square	0.99942		
		Value	Standard Error
303	Intercept	0.02919	0.00823
303	Slope	68770	959.83853

Linear fit at 4 different conc. for complex **(b)** at a wavelength of **303 nm**

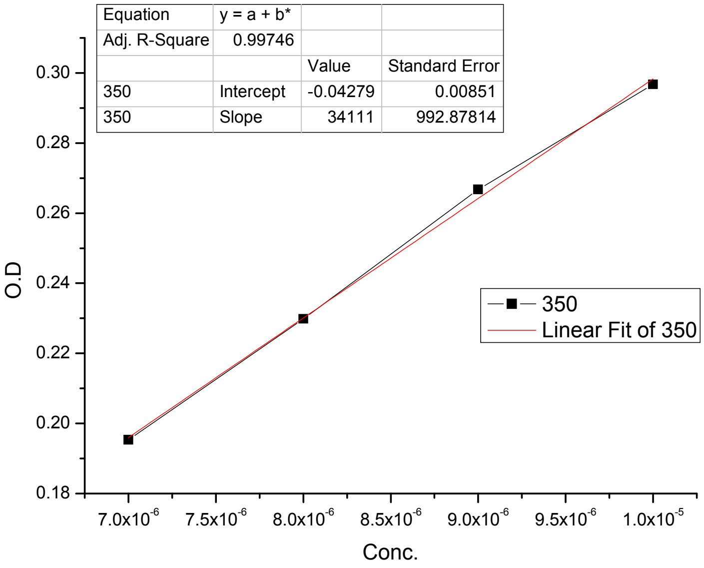

Linear fit at 4 different conc. for complex **(b)** at a wavelength of **350 nm**

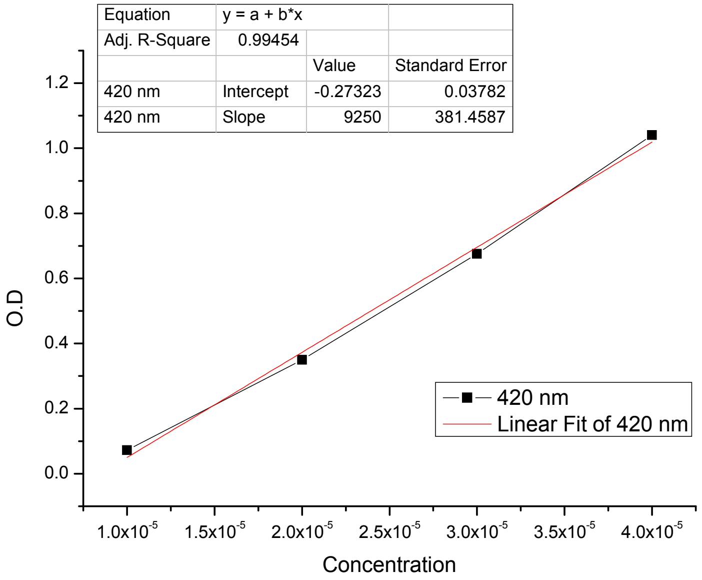

Linear fit at 4 different conc. for complex **(b)** at a wavelength of **420 nm**

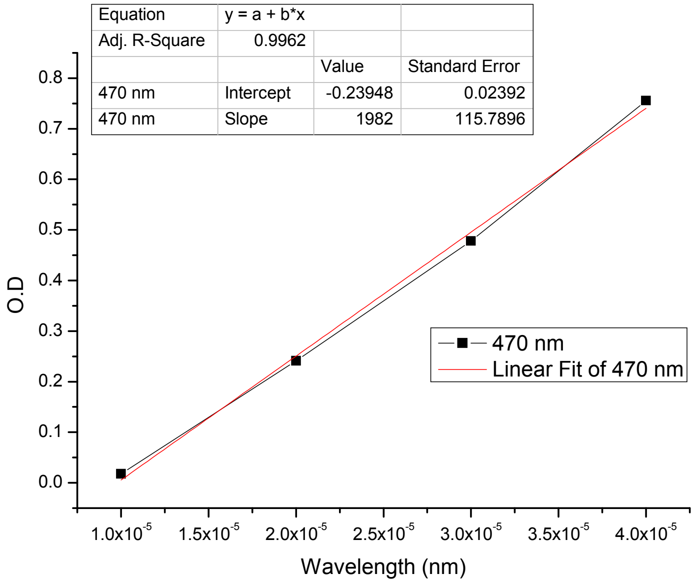

Linear fit at 4 different conc. for complex **(b)** at a wavelength of **470 nm**

Complex **(c)** : $[Ir(ppy)_2(bpp)PdCl]_2(PF_6)_2$

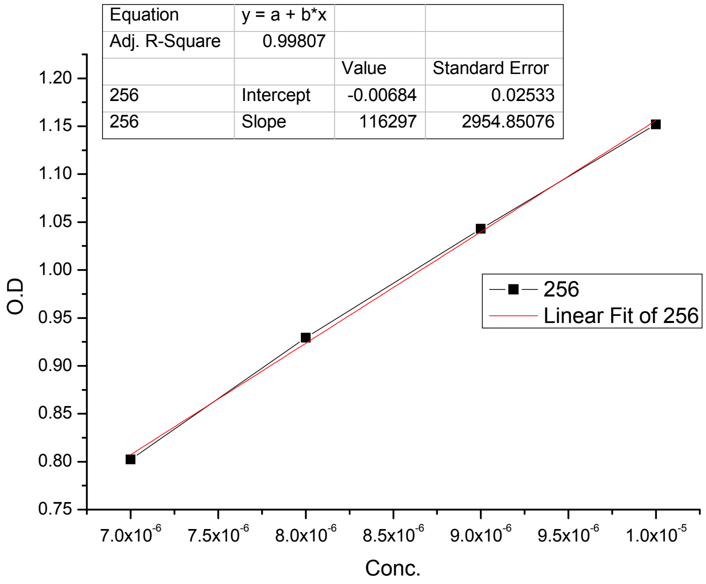

Linear fit at 4 different conc. for complex **(c)** at a wavelength of **256 nm**

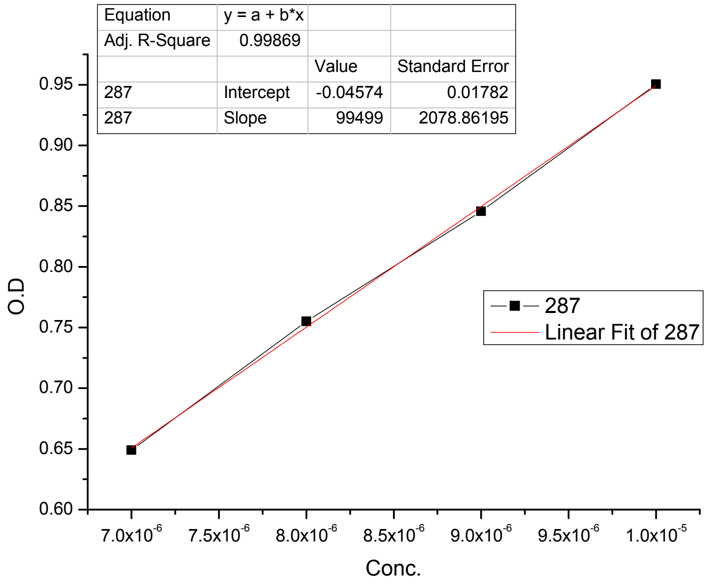

Equation	y = a + b*x		
Adj. R-Square	0.99869		
		Value	Standard Error
287	Intercept	-0.04574	0.01782
287	Slope	99499	2078.86195

Linear fit at 4 different conc. for complex **(c)** at a wavelength of **287 nm**

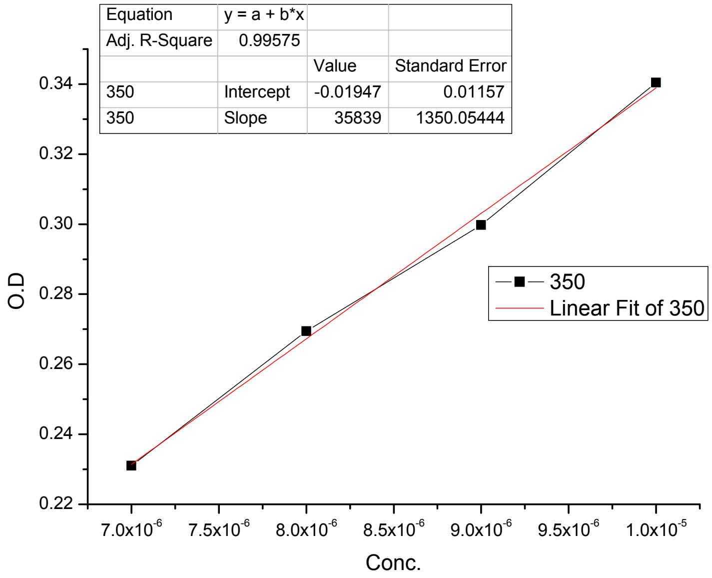

Equation	y = a + b*x		
Adj. R-Square	0.99575		
		Value	Standard Error
350	Intercept	-0.01947	0.01157
350	Slope	35839	1350.05444

Linear fit at 4 different conc. for complex **(c)** at a wavelength of **350 nm**

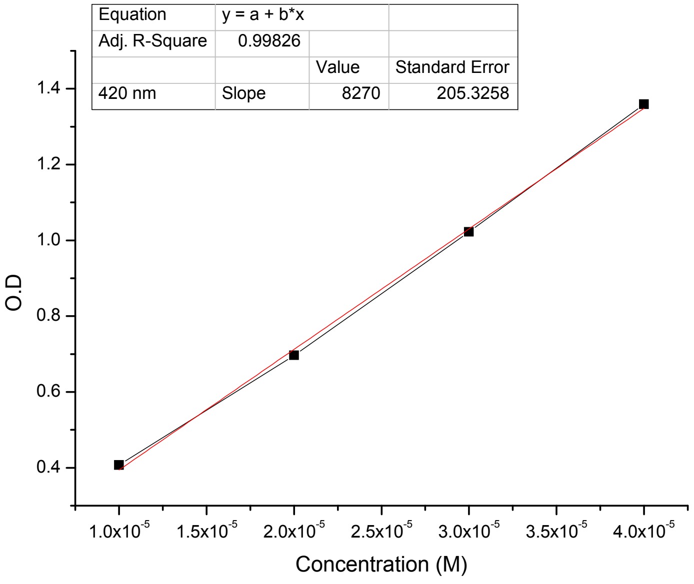

Linear fit at 4 different conc. for complex **(c)** at a wavelength of **420 nm**

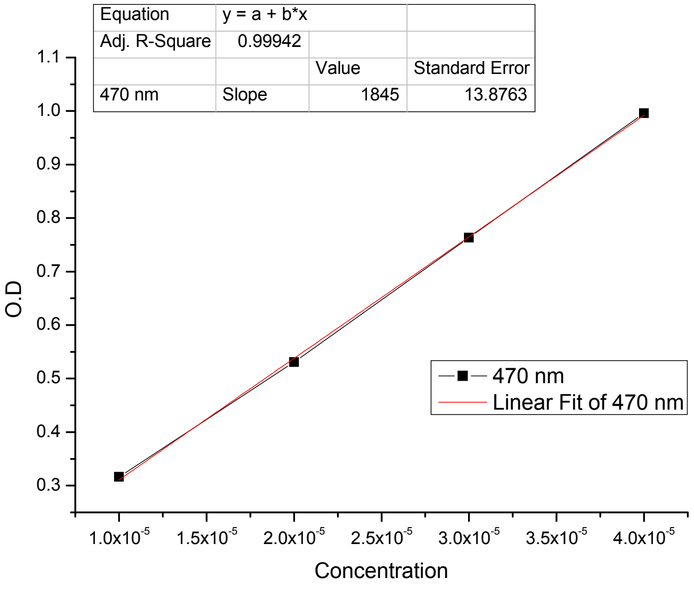

Linear fit at 4 different conc. for complex **(c)** at a wavelength of **470 nm**

Complex 1 : $[Ir(ppy)_2(BPP)]PF_6$ Photophysics

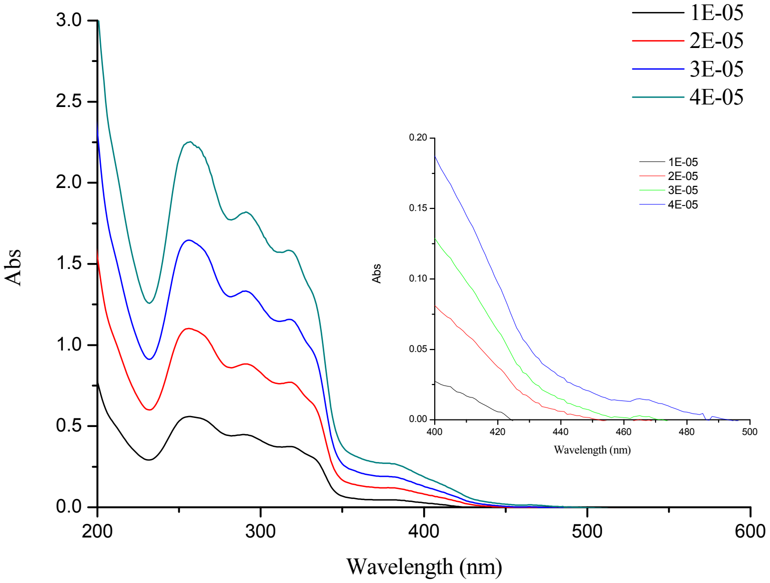

Figure C1. *Conc. dependent absorption spectrum for complex 1*

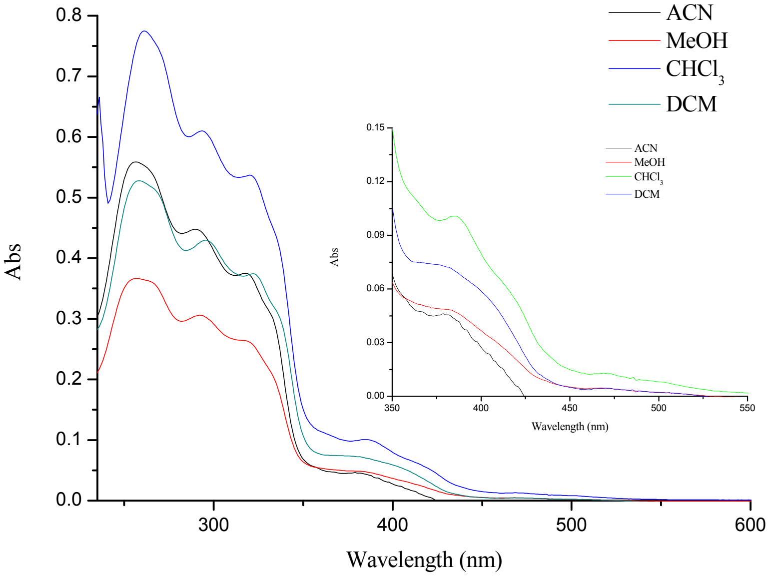

Figure C2. *Solvent dependant absorption spectrum for complex 1 (conc: 1E-05)*

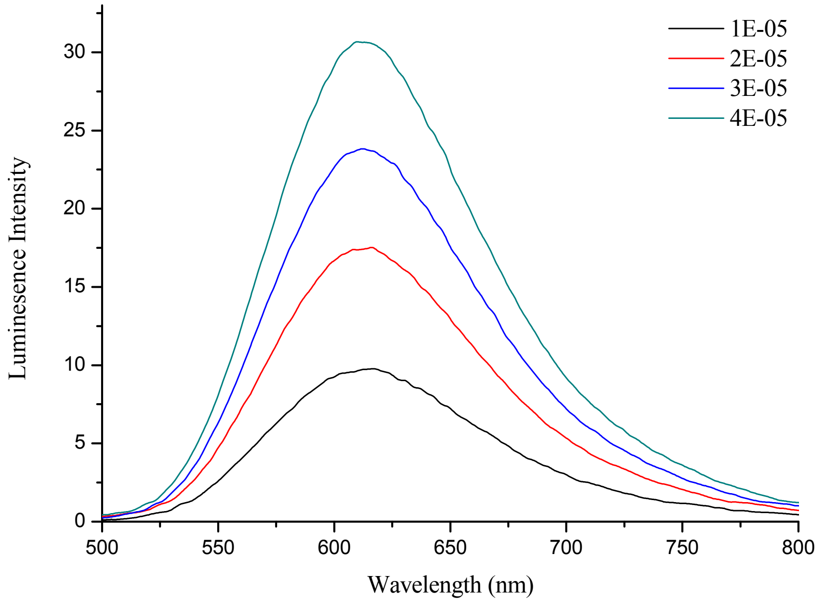

Figure C3. *Conc dependant emission in ACN*

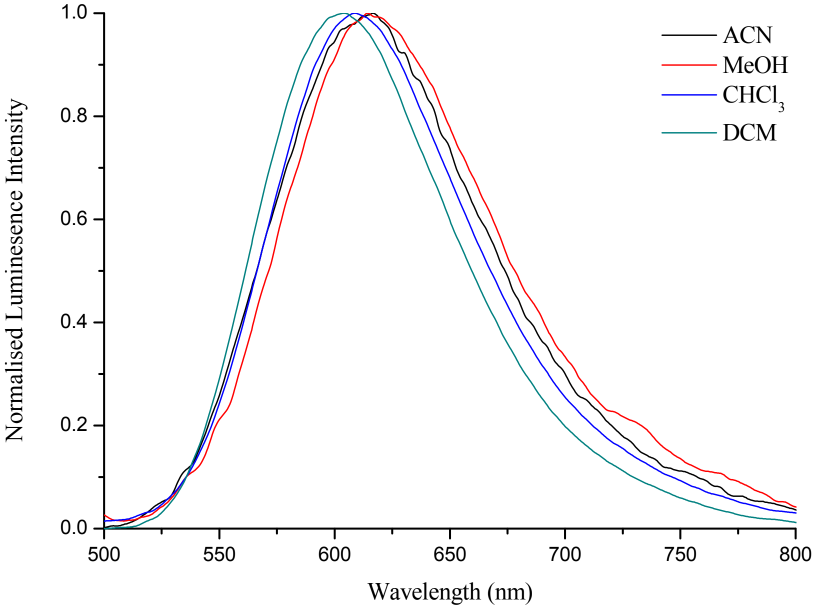

Figure C4. *Solvent dependant emission (Conc. 1E-05)*

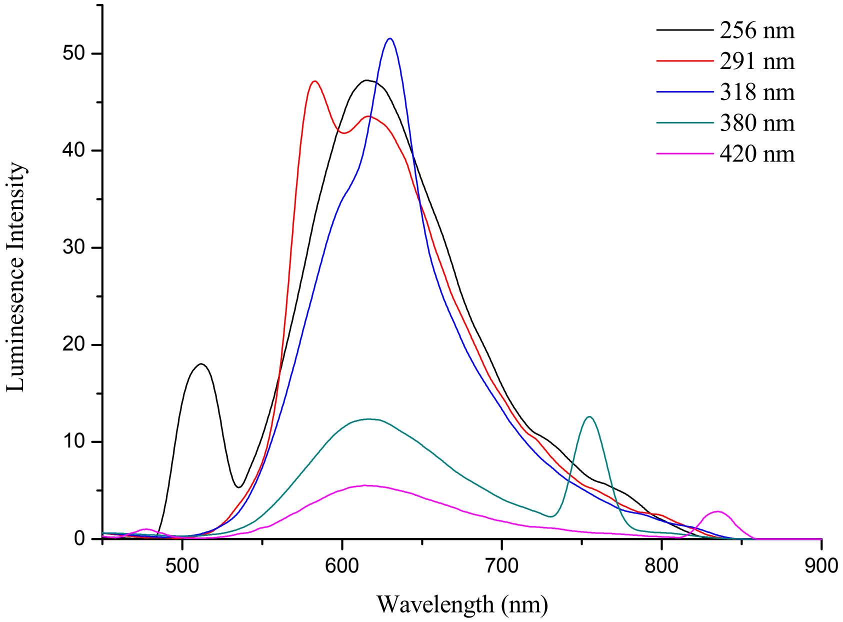

Figure C5. *Excitation wavelength dependant emission in MeOH (Conc. 1E-05)*

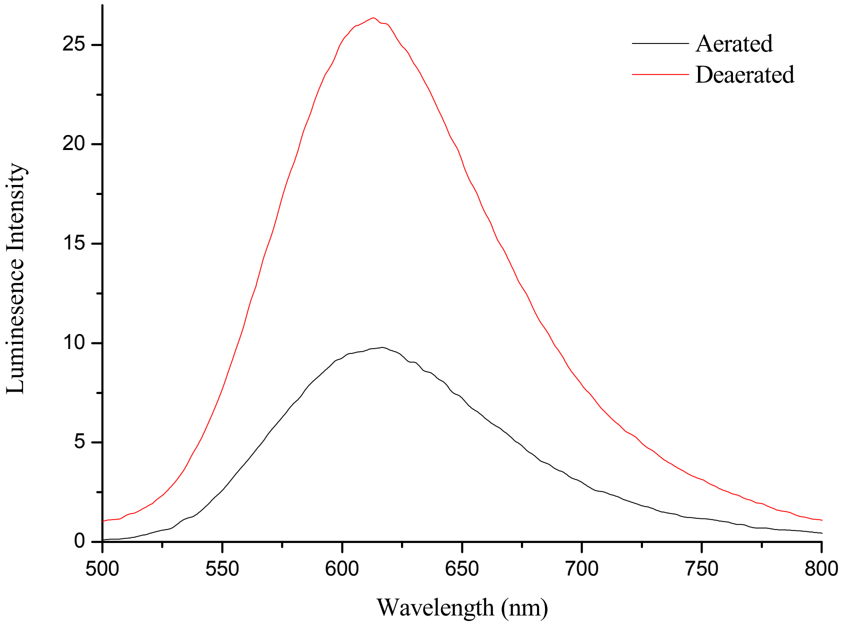

Figure C6*. aerated & deaerated emission of complex 1 in ACN (1E-05)*

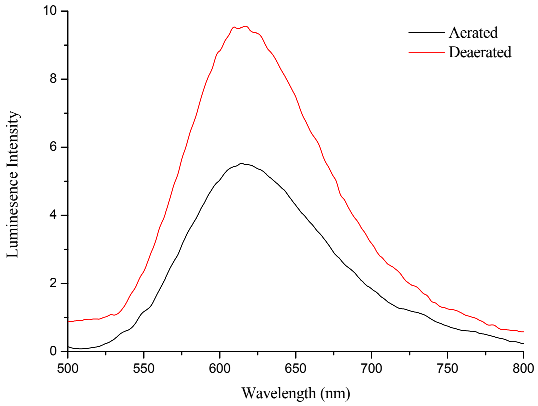

***Figure C7**. aerated & deaerated emission of complex 1 in MeOH (1E-05)*

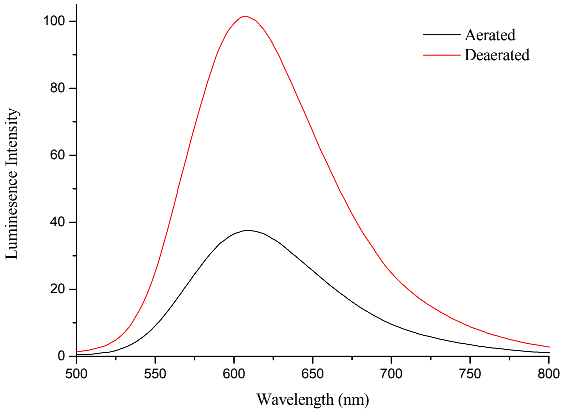

Figure C8. aerated & deaerated emission of complex 1 in $CHCl_3$ (1E-05)

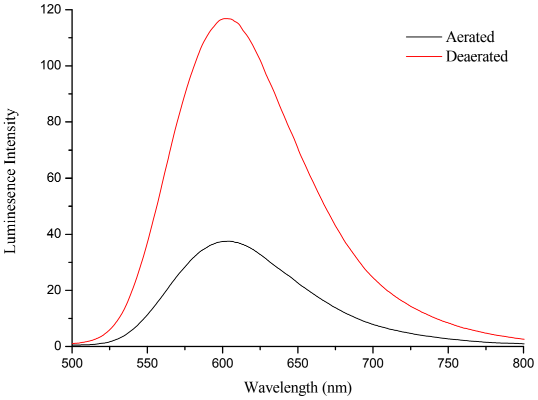

***Figure C9**. aerated & deaerated emission of complex 1 in DCM (1E-05)*

Complex 2 : $[Ir(ppy)_2(BPP)PtCl]_2(PF_6)_2$ Photophysics

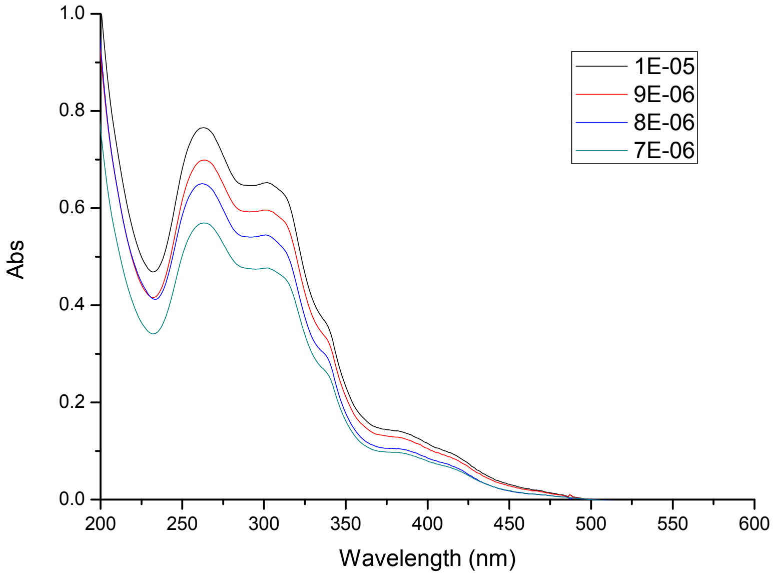

Figure C10. *Conc. Dependant abs for complex 2 in ACN*

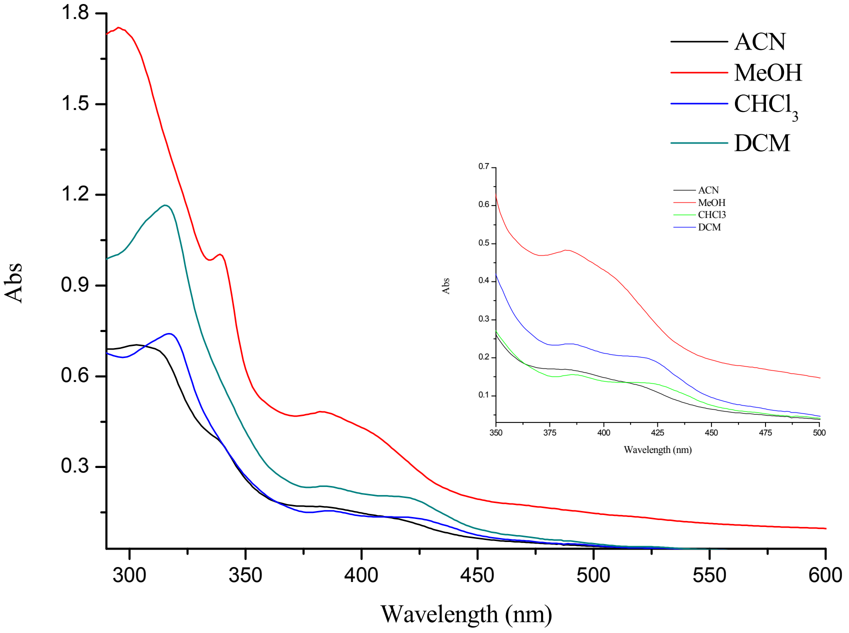

Figure C11. *Solvent Dependant abs for complex 2 (1E-05)*

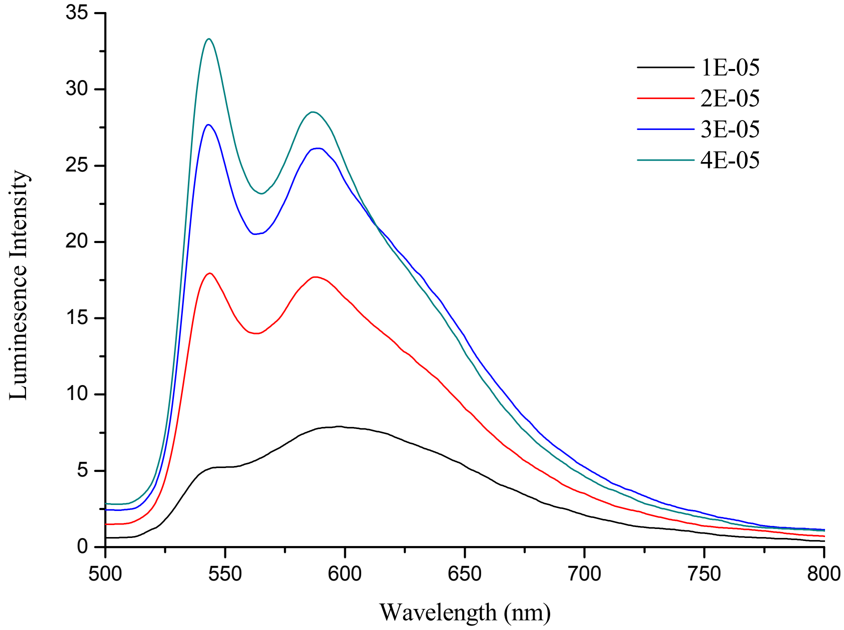

***Figure C12**. Conc. Dependant emission for complex 2*

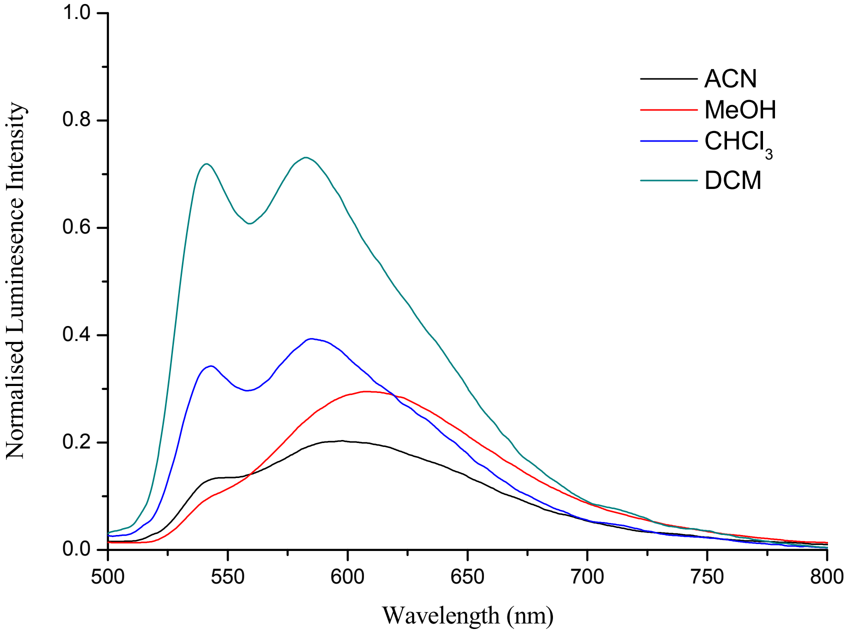

***Figure C13**. Solvent Dependant emission for complex 2 (Conc. 1E-05)*

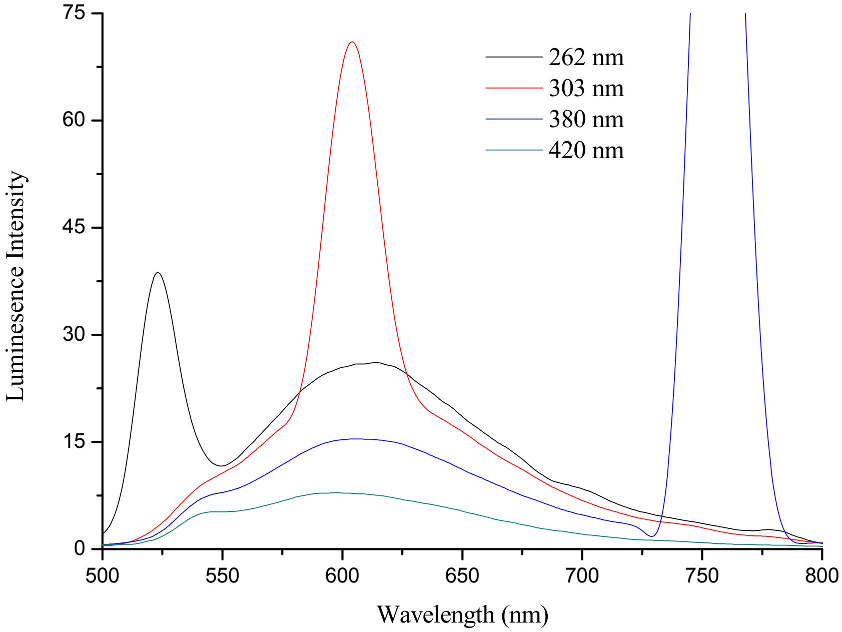

Figure C14. *Excitation wavelength Dependant emission for complex 2 in ACN (Conc.1E-05)*

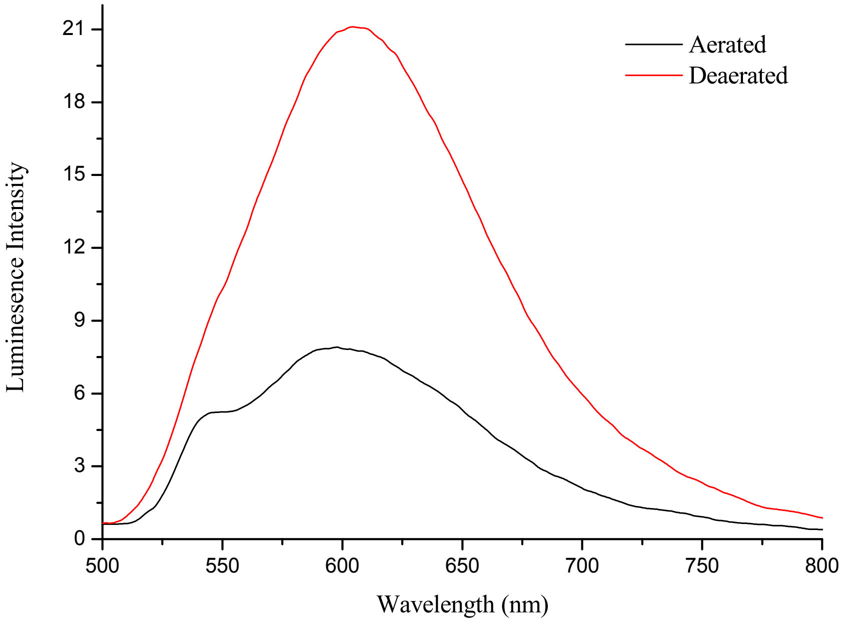

Figure C15. *aerated & deaerated emsn for complex 2 in ACN (1E-05)*

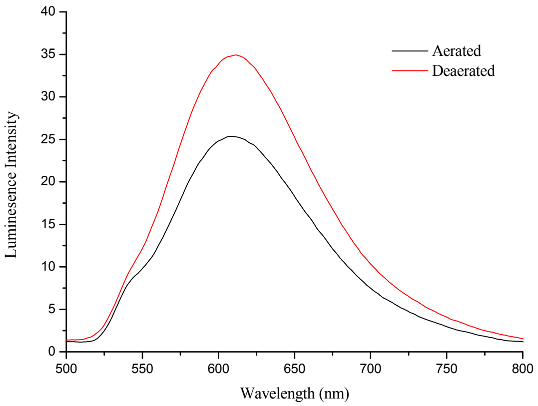

Figure C16*. aerated & deaerated emsn for complex 2 in MeOH (1E-05)*

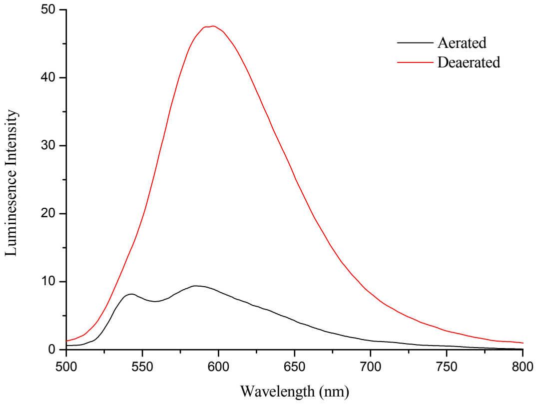

Figure C17*. aerated & deaerated emsn for complex 2 in* $CHCl_3$ *(1E-05)*

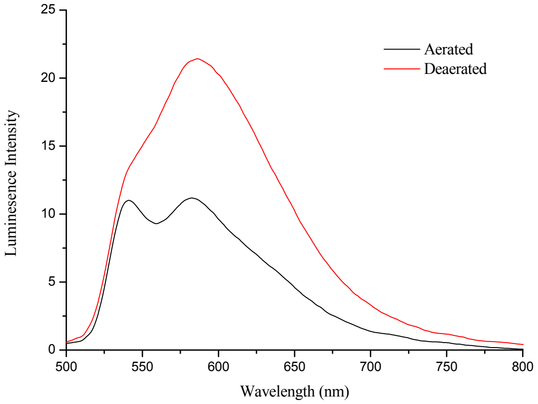

Figure C18*. aerated & deaerated emsn for complex 2 in DCM (1E-05)*

Complex 3: $[Ir(ppy)_2(BPP)PdCl]_2(PF_6)_2$ Photophysics

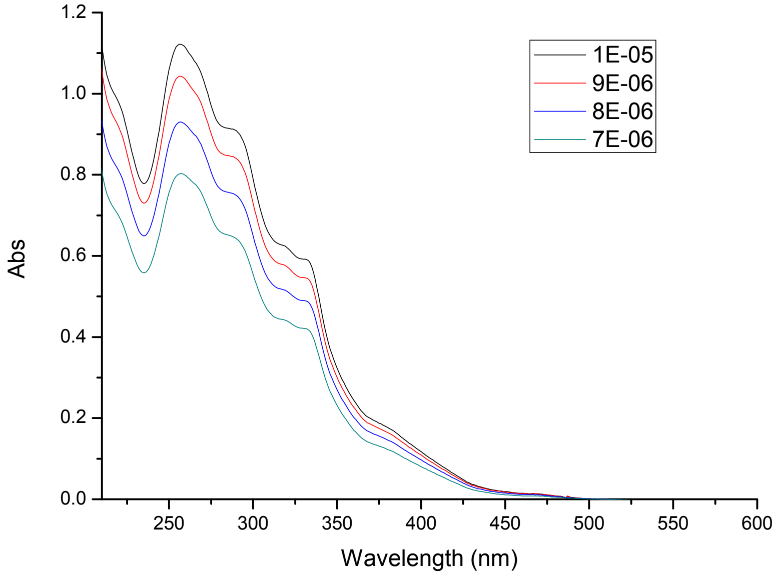

***Figure C19**. Conc. Dep abs for complex 3 in ACN*

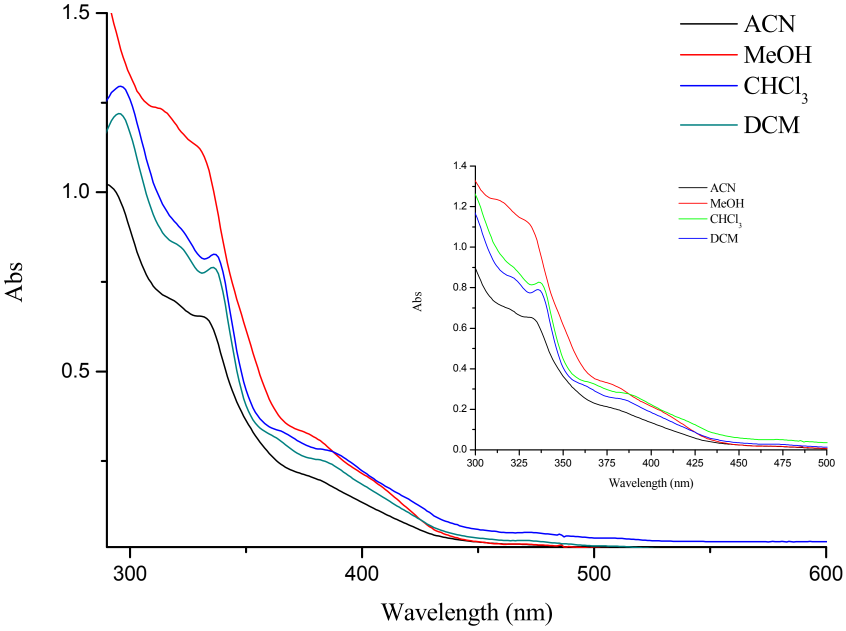

***Figure C20**. Solvent Dep abs for complex 3 (conc. 1E-05)*

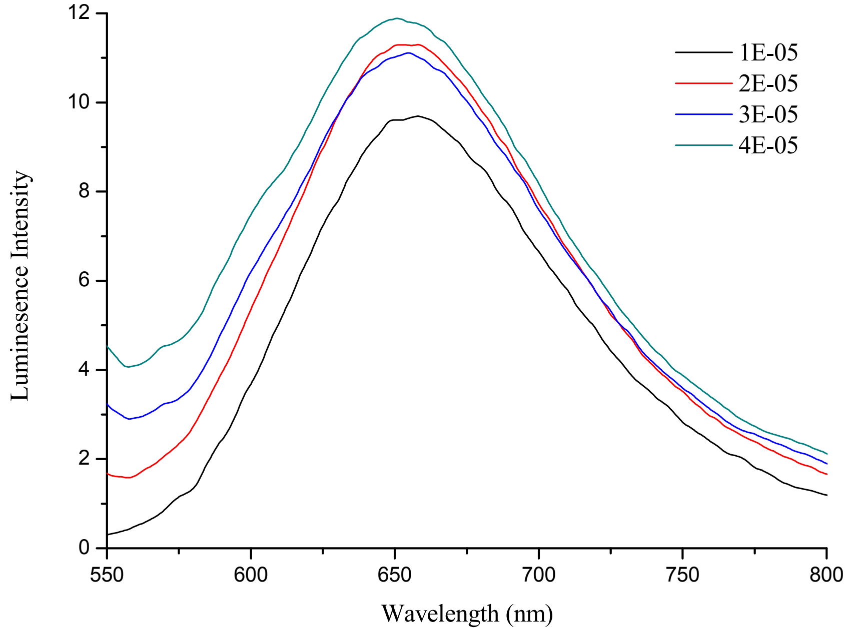

Figure C21. *Conc. Dependant Emsn Spectra of Complex 3 in ACN*

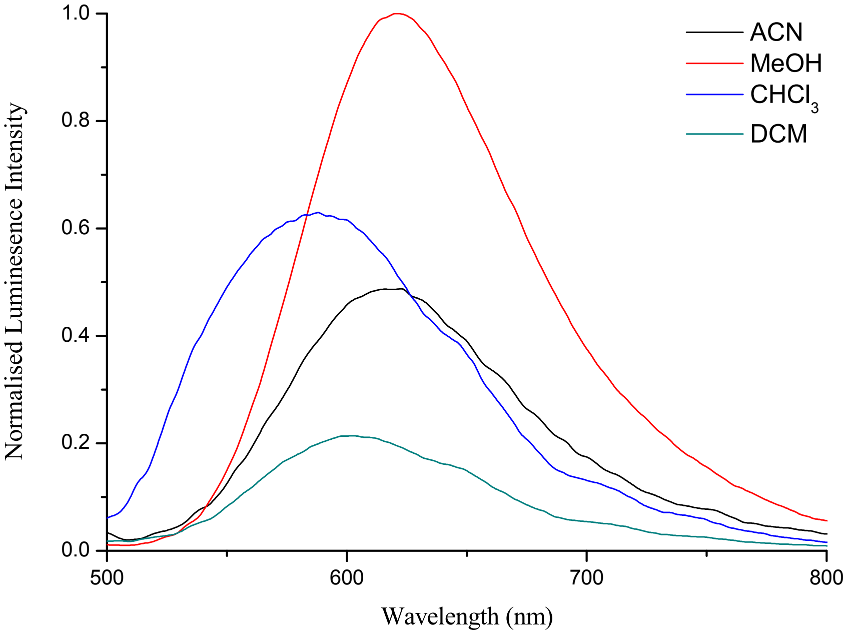

Figure C22. *Solvent Dependant Emsn Spectra of Complex 3 (1E-05)*

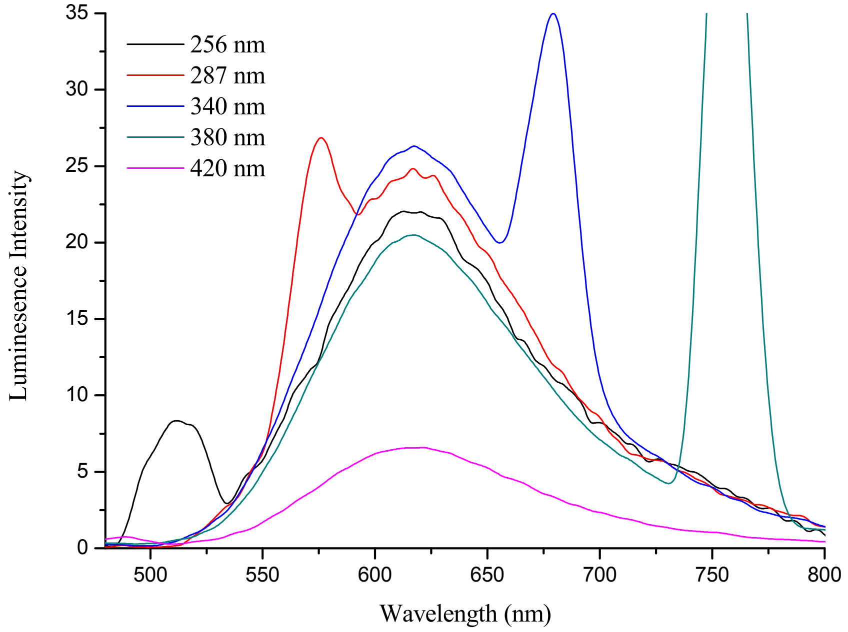

Figure C23. *Excitation wavelength dependant emission for complex 3 in ACN (1E-05)*

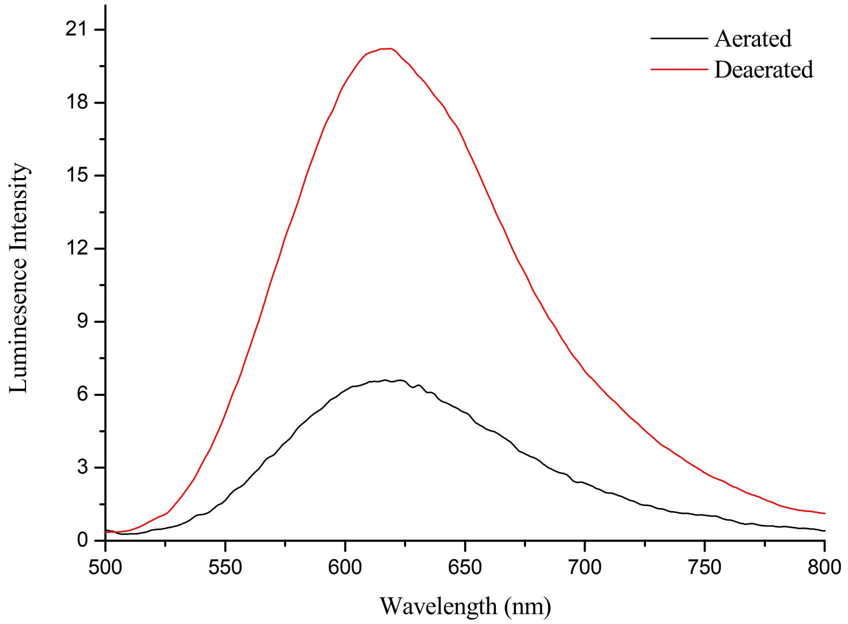

Figure C24. *Aerated & Deaerated emission for complex 3 in ACN (1E-05)*

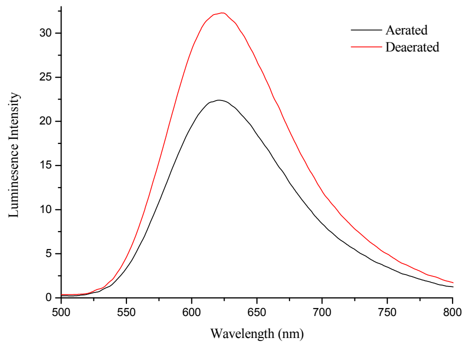

***Figure C25**. Aerated & Deaerated emission for complex 3 in MeOH (1E-05)*

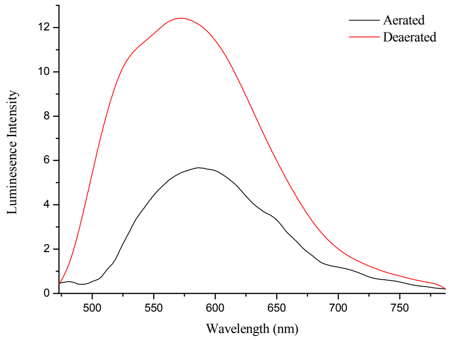

***Figure C26.** Aerated & Deaerated emission for complex 3 in $CHCl_3$ (1E-05)*

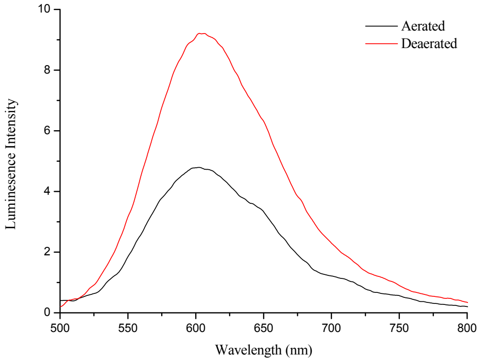

***Figure C27**. Aerated & Deaerated emission for complex 3 in DCM (1E-05)*

Temperature dependent lifetime data for Ir-Pt complex $[Ir(ppy)_2(bpp)PtCl]_2(PF_6)_2$ (2) measured in a temperature of 77 K to 290 K is tabulated below

Temperature	Wavelength λ	Lifetime, μs	Relative %	Avg Life time, ns
77K	527	$\tau = 3322$	100	3322
		$\chi^2 = 1.012$		
	567	$\tau_1 = 635$	11.57	3066
		$\tau_2 = 3130$	88.43	
		$\chi^2 = 1.035$		
90K	527	$\tau = 2987$	100	2987
		$\chi^2 = 1.124$		
	567	$\tau_1 = 552.33$	12.75	2746
		$\tau_2 = 2809$	87.25	
		$\chi^2 = 1.184$		
100K	527	$\tau = 2776$	100	2776
		$\chi^2 = 1.088$		
	567	$\tau_1 = 469.74$	11.85	2495
		$\tau_2 = 2545$	88.15	
		$\chi^2 = 1.192$		
110K	527	$\tau = 2564$	100	2564
		$\chi^2 = 1.073$		
	567	$\tau_1 = 539$	15.79	2255
		$\tau_2 = 2329$	84.21	
		$\chi^2 = 1.003$		
120K	529	$\tau_1 = 361.26$	9.89	1938
		$\tau_2 = 1970$	90.11	
		$\chi^2 = 1.110$		
	570	$\tau_1 = 298.35$	12.64	1291
		$\tau_2 = 1323$	87.36	
		$\chi^2 = 1.138$		
125K	534	$\tau_1 = 106.20$	20.11	972
		$\tau_2 = 994.77$	79.89	
		$\chi^2 = 1.098$		
	572	$\tau_1 = 283.20$	21.83	1044
		$\tau_2 = 1099$	78.17	
		$\chi^2 = 1.138$		
130K	536	$\tau_1 = 71.43$	35.33	508
		$\tau_2 = 539.91$	64.67	
		$\chi^2 = 1.063$		
	576	$\tau_1 = 147.54$	15	747
		$\tau_2 = 767.68$	85	
		$\chi^2 = 1.051$		
135K	579	$\tau_1 = 160.64$	20.97	734
		$\tau_2 = 766.34$	79.03	
		$\chi^2 = 1.078$		
140K	582	$\tau_1 = 122.57$	19.60	679
		$\tau_2 = 702.93$	80.40	
		$\chi^2 = 1.114$		

150K	585	τ_1= 115.82	19.47	632
		τ_2= 653.71	80.53	
		χ^2= 1.063		
160	588	τ_1= 106.38	20.40	575
		τ_2= 596.14	79.60	
		χ^2= 1.102		
170K	544	τ_1= 49.73	42.57	256
		τ_2= 283.14	57.43	
		χ^2= 1.146		
	587	τ_1= 103.19	22.11	501
		τ_2= 522.75	77.89	
		χ^2= 1.106		
180K	543	τ_1= 40.02	40.35	198
		τ_2= 217.16	59.65	
		χ^2= 1.137		
	587	τ_1= 78.83	18.81	400
		τ_2= 414.10	81.19	
		χ^2= 1.107		
190K	543	τ_1= 39	41.64	169
		τ_2= 188.40	58.36	
		χ^2= 1.123		
	589	τ_1= 72.83	23.69	334
		τ_2= 351.22	76.31	
		χ^2= 1.192		
200K	543	τ_1= 34.89	42.78	147
		τ_2= 164.18	57.22	
		χ^2= 1.097		
	589	τ_1= 69.41	25.70	280
		τ_2= 296.89	74.30	
		χ^2= 1.111		
210K	543	τ_1= 31.52	40.72	125
		τ_2= 139.77	59.28	
		χ^2= 1.058		
	589	τ_1= 66.58	31.95	252
		τ_2= 272.97	68.05	
		χ^2= 1.065		
220	543	τ_1= 29.13	43.53	117
		τ_2= 131.66	56.47	
		χ^2= 1.055		
	589	τ_1= 64.45	35.23	222
		τ_2= 244.36	64.77	
		χ^2= 1.089		
230K	543	τ_1= 28.49	42.28	101
		τ_2= 114.67	57.72	
		χ^2= 1.085		
	589	τ_1= 61.79	43.86	195
		τ_2= 223.66	56.14	
		χ^2= 1.114		

240K	543	τ_1= 27	47.33	91
		τ_2= 105.29	52.67	
		χ^2= 1.090		
	587	τ_1= 38.16	30.74	143
		τ_2= 154.43	69.26	
		χ^2= 1.117		
250K	543	τ_1= 24.07	45.57	80
		τ_2= 92.44	54.43	
		χ^2= 1.100		
	587	τ_1= 35.57	38.32	138
		τ_2= 152,36	61.68	
		χ^2= 1.069		
260K	543	τ_1= 18.28	35.67	65
		τ_2= 72	64.33	
		χ^2= 1.042		
	587	τ_1= 25.53	23.48	103
		τ_2= 108.57	76.52	
		χ^2= 1.151		
270K	543	τ_1= 17.56	34.02	63
		τ_2= 68.69	65.98	
		χ^2= 1.046		
	587	τ_1= 22.38	23.39	94
		τ_2= 98.80	76.61	
		χ^2= 1.056		
280K	543	τ_1= 17.41	39.63	60
		τ_2= 67.08	60.37	
		χ^2= 1.083		
	587	τ_1= 21.73	24.54	92
		τ_2= 97.47	75.46	
		χ^2= 1.059		
290	543	τ_1= 12.21	24.71	44
		τ_2= 46.96	75.29	
		χ^2= 1.105		
	587	τ_1= 21.22	25.84	89
		τ_2= 94.21	74.16	
		χ^2= 1.107		

Temperature dependent lifetime data for Ir-Pd complex $[Ir(ppy)_2(bpp)PdCl]_2(PF_6)_2$ (3) measured in a temperature of 77 K to 290 K is tabulated below

Temperature	Wavelength λ	Lifetime, µs	Relative %	Avg Life time, ns
77 K	544	τ_1= 455	4.64	3174
		τ_2= 3193	95.36	
		χ^2= 1.059		
90 K	545	τ_1= 307.81	3.74	2795
		τ_2= 2806	96.26	
		χ^2= 1.012		
100 K	545	τ_1= 223.62	3.38	2572
		τ_2= 2579	96.62	
		χ^2= 1.000		
110 K	555	τ = 169.23	3.45	2496
		τ_2= 2502	96.55	
		χ^2= 1.064		
120 K	564	τ_1= 144.35	2.78	2275
		τ_2= 2279	97.22	
		χ^2= 1.001		
130 K	579	τ_1= 128.49	2.67	1500
		τ_2= 1503	97.33	
		χ^2= 1.057		
140 K	587	τ_1= 122.12	32.05	603
		τ_2= 646.24	67.95	
		χ^2= 1.114		
150 K	601	τ_1= 77.75	19.43	433
		τ_2= 447.63	80.57	
		χ^2= 1.093		
160 K	603	τ_1= 53.08	13.78	376
		τ_2= 383.33	86.22	
		χ^2= 1.048		
170 K	606	τ_1= 35.83	9.98	341
		τ_2= 344.97	90.02	
		χ^2= 1.109		
180 K	607	τ_1= 34.00	6.18	274
		τ_2= 275.85	93.82	
		χ^2= 1.006		
190 K	608	τ_1= 10.48	2.67	191
		τ_2= 191.07	97.33	
		χ^2= 1.103		

200 K	609	τ_1= 9.03	0.81	153
		τ_2= 152.63	99.19	
		χ^2= 1.084		
210 K	610	τ_1= 5.11	1.55	138
		τ_2= 138.12	98.45	
		χ^2= 1.089		
220 K	611	τ_1= 1.76	0.96	121
		τ_2= 120.86	99.04	
		χ^2= 1.112		
230 K	614	τ = 1.24	0.46	98
		τ_2= 97.53	99.54	
		χ^2= 1.072		
240 K	615	τ_1= 0.62	0.28	88
		τ_2= 88.34	99.72	
		χ^2= 1.045		
250 K	615	τ_1= 0.539	0.19	83
		τ_2= 82.54	99.81	
		χ^2= 1.079		
260 K	615	τ_1= 0.42	2.17	76
		τ_2= 76.21	97.83	
		χ^2= 1.042		
270 K	615	τ_1= 0.34	1	74
		τ_2= 73.53	99	
		χ^2= 1.075		
280 K	615	τ_1= 0.52	2.52	70
		τ_2= 70.06	97.48	
		χ^2= 1.035		
290 K	615	τ_1= 0.56	2.05	69
		τ_2= 69.63	97.95	
		χ^2= 1.007		

Temperature dependent emission curves for ester analogous complexes [Ir(ppy-COOCH$_3$)$_2$(bpp)](PF$_6$), [Ir(ppy-COOCH$_3$)$_2$(bpp)PtCl]$_2$(PF$_6$)$_2$ and [Ir(ppy-COOCH$_3$)$_2$(bpp)PdCl]$_2$(PF$_6$)$_2$.

(a) Temperature dependent emission curves for [Ir(ppy-COOCH$_3$)$_2$(bpp)](PF$_6$)

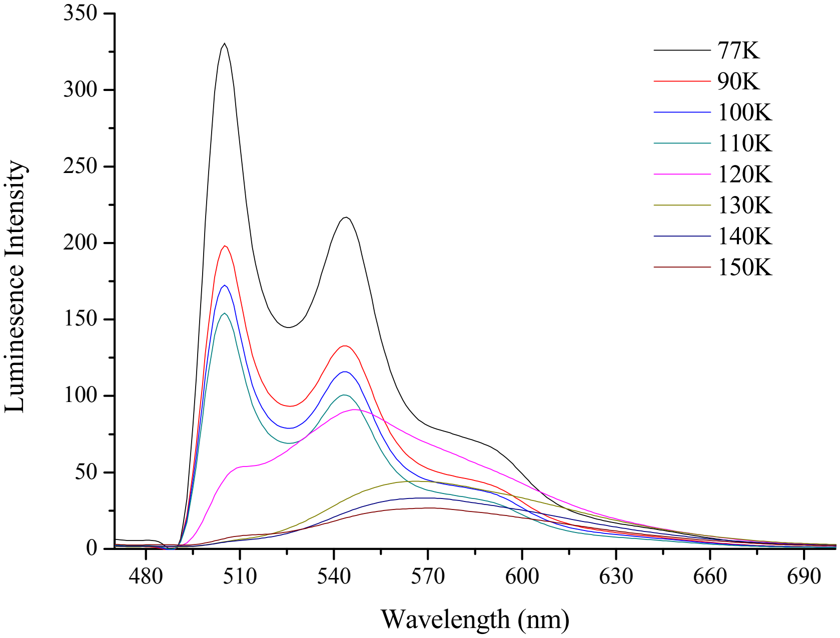

***Figure C28**. Temperature dependent emission spectrum for [Ir(ppy-COOCH$_3$)$_2$(bpp)](PF$_6$) from 77 K to 150 K in every 10 K difference measured in EtOH:MeOH (4:1) glass.*

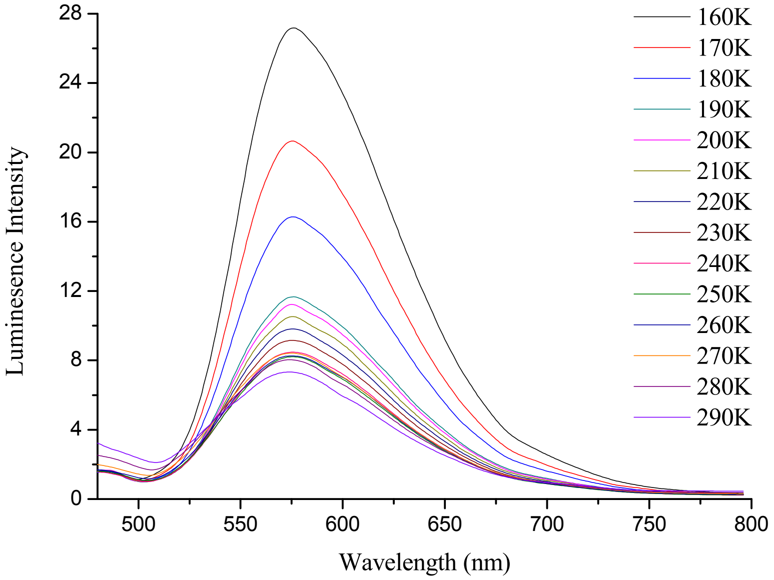

Figure C29. *Temperature dependent emission spectrum for [Ir(ppy-COOCH$_3$)$_2$(bpp)](PF$_6$) from 160 K to 290 K in every 10 K difference measured in EtOH:MeOH (4:1) glass.*

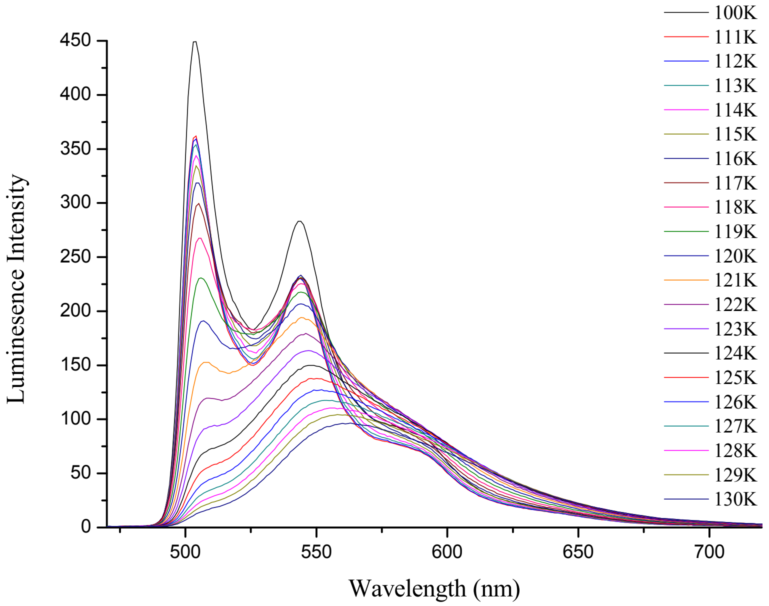

Figure C30. *Temperature dependent emission spectrum for [Ir(ppy-COOCH$_3$)$_2$(bpp)](PF$_6$) from 100 K to 130 K in every 1 K difference of temperature measured in EtOH:MeOH (4:1) glass.*

(b) Temperature dependent emission curves for $[Ir(ppy\text{-}COOCH_3)_2(bpp)PtCl]_2(PF_6)_2$

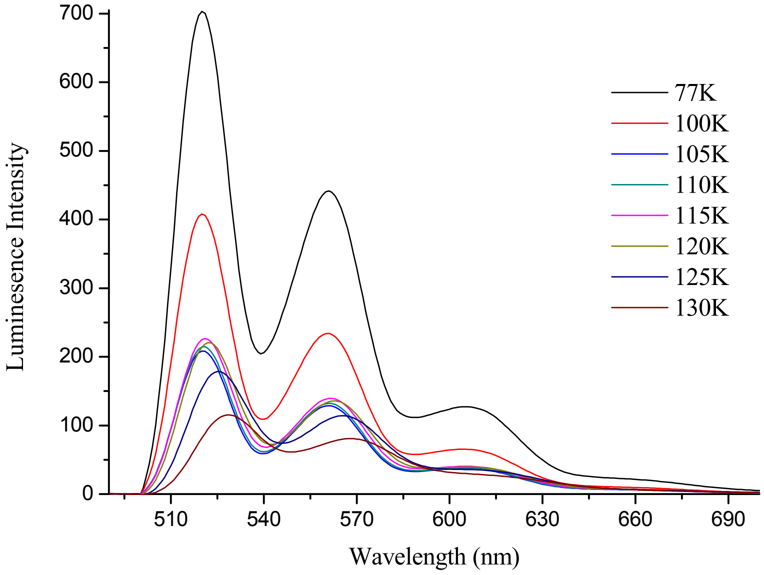

Figure C31. *Temperature dependent emission spectrum for* $[Ir(ppy\text{-}COOCH_3)_2(bpp)PtCl]_2(PF_6)_2$ *from 77 K to 130 K in every 10K difference of temperature measured in EtOH:MeOH(4:1) glass.*

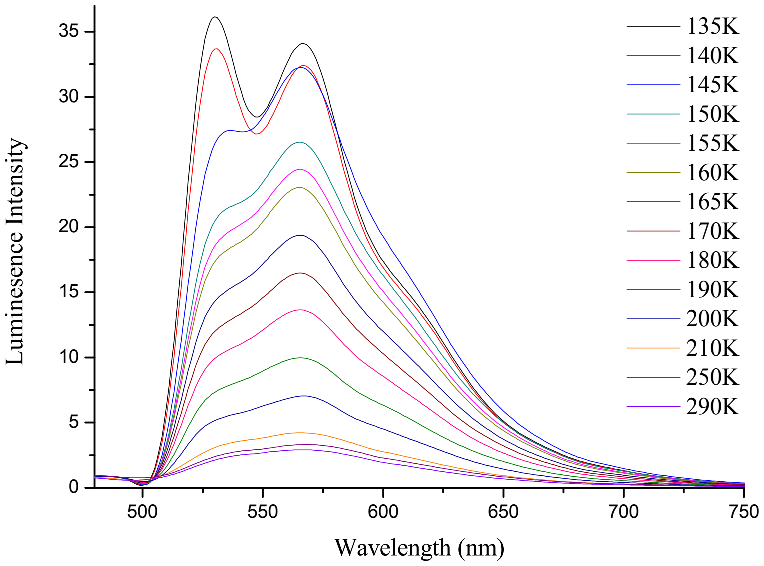

Figure C32. *Temperature dependent emission spectrum for* $[Ir(ppy\text{-}COOCH_3)_2(bpp)PtCl]_2(PF_6)_2$ *from 135K to 290K in every 10K difference of temperature measured in EtOH:MeOH(4:1) glass.*

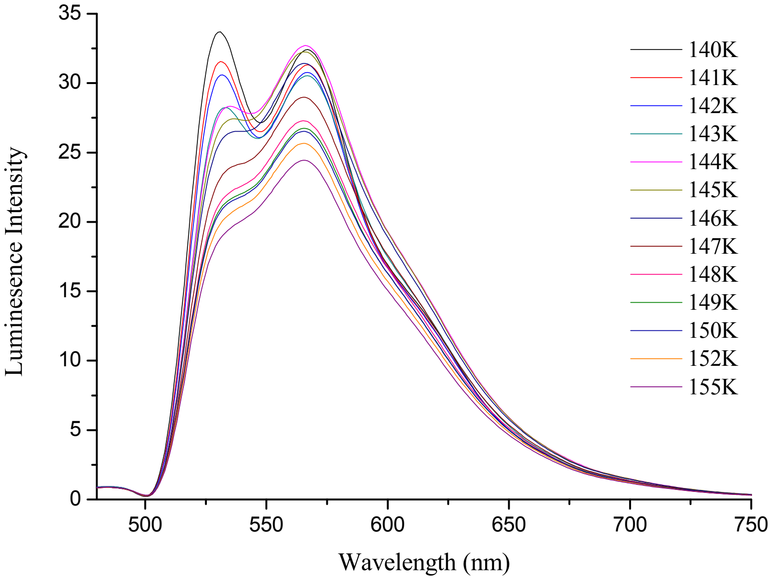

Figure C33. *Temperature dependent emission spectrum for[Ir(ppy-COOCH$_3$)$_2$(bpp)PtCl]$_2$(PF$_6$)$_2$ from 140K to 155K in every 1K difference of temperature measured in EtOH:MeOH(4:1) glass.*

(c) Temperature dependent emission curves for [Ir(ppy-COOCH$_3$)$_2$(bpp)PdCl]$_2$(PF$_6$)$_2$

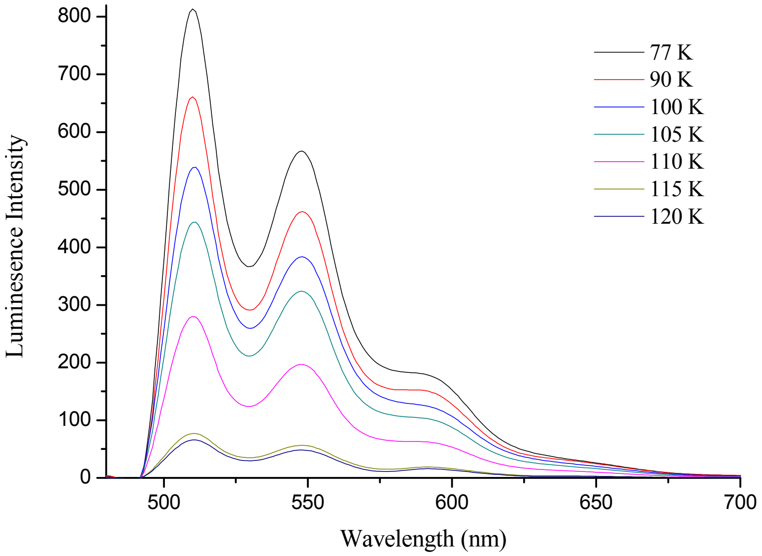

Figure C34. *Temperature dependent emission spectrumfor[Ir(ppy-COOCH$_3$)$_2$(bpp)PdCl]$_2$(PF$_6$)$_2$ from 77K to 120K in every 5K difference of temperature measured in EtOH:MeOH(4:1) glass.*

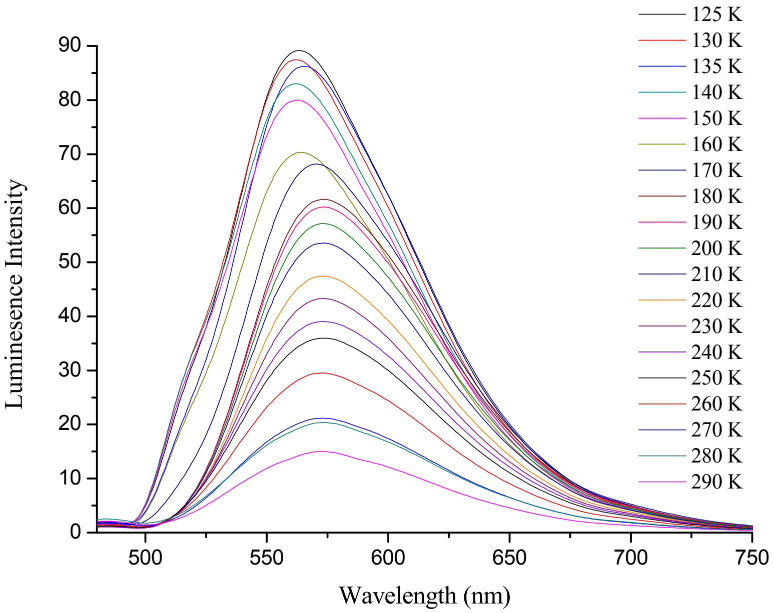

***Figure C35**. Temperature dependent emission spectrumfor*$[Ir(ppy\text{-}COOCH_3)_2(bpp)PdCl]_2(PF_6)_2$ *from 125K to 290K in every 10K difference of temperature measured in EtOH:MeOH(4:1) glass.*

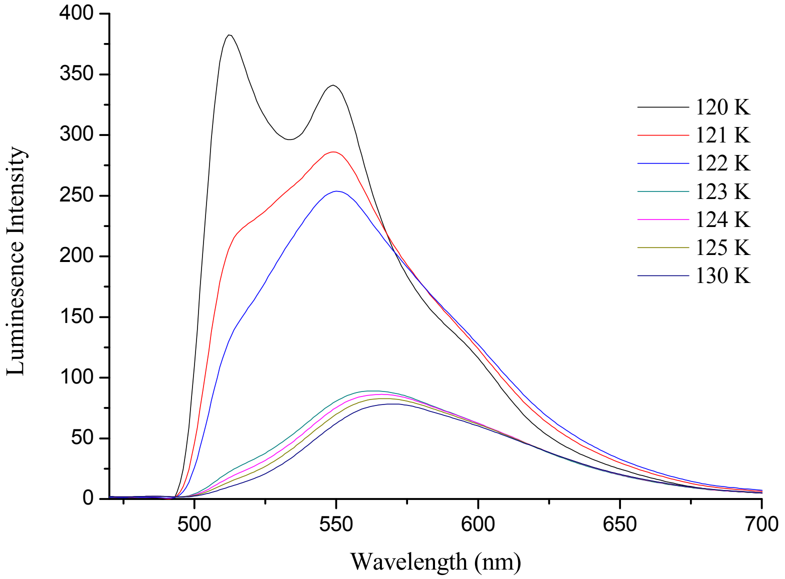

***Figure C36**. Temperature dependent emission spectrumfor*$[Ir(ppy\text{-}COOCH_3)_2(bpp)PdCl]_2(PF_6)_2$ *from 120K to 125K in every 1K difference of temperature measured in EtOH:MeOH(4:1) glass.*

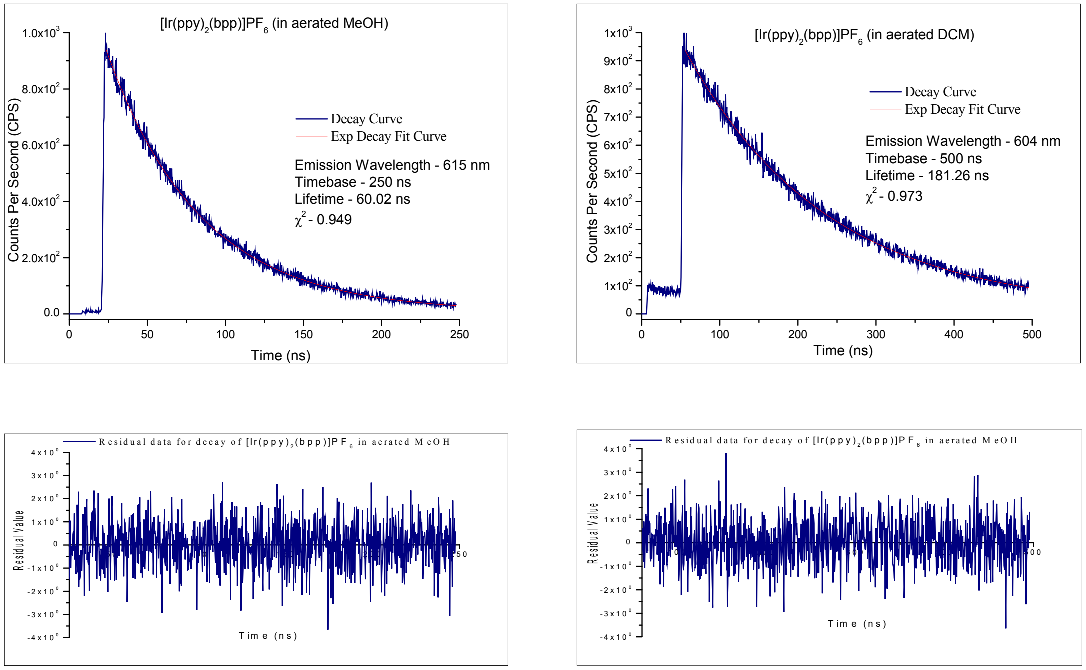

***Figure C37**. Lifetime decay plots for[Ir(ppy)$_2$(bpp)](PF$_6$) in MeOH and DCM.*

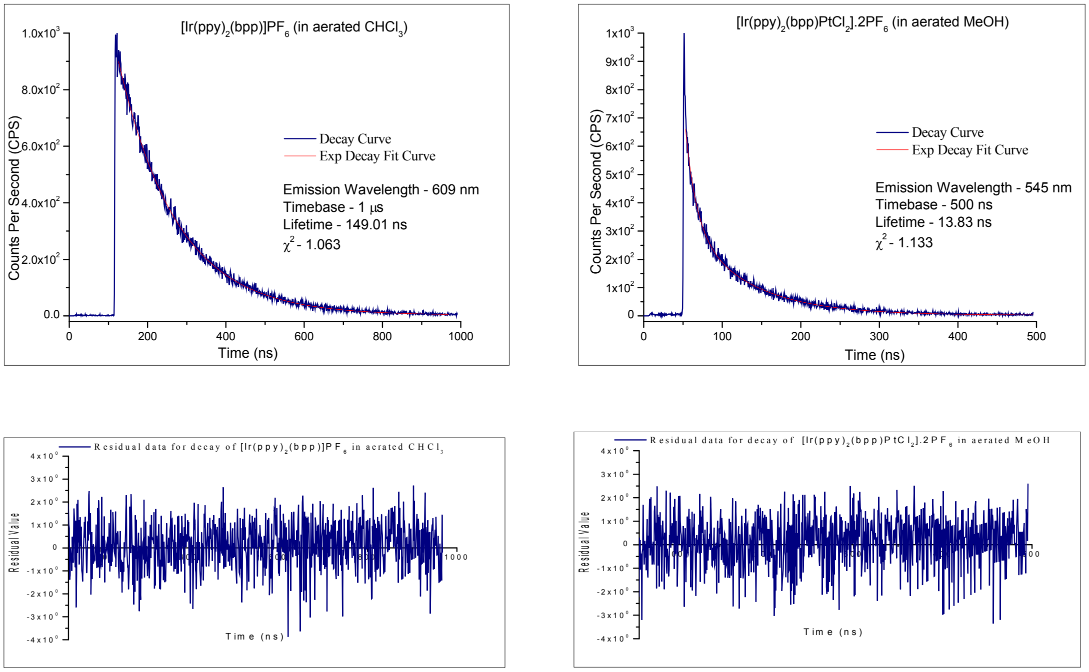

***Figure C38**. Lifetime decay plots for[Ir(ppy)$_2$(bpp)](PF$_6$) and [Ir(ppy-COOCH$_3$)$_2$(bpp)PdCl]$_2$ (PF$_6$)$_2$ in CHCl$_3$ and MeOH.*

Appendix D

Supplementary data from chapter 5

Synthesis of [Ir(bpy)$_3$]PF$_6$ (XVII)

10 ml ethylene glycol was taken in a 2 necked RB through which N_2 was bubbled , bpy (0.163 g, 1.05 mmol) was added and stirred to which [Ir(bpy)$_2$(OSO$_2$CF$_3$)$_2$]CF$_3$SO$_3$ (0.05 g, 0.052523 mmol) was added and refluxed for 5 hour. The reaction mixture was cooled, water was added, filtered and to the filtrate saturated aq KPF$_6$ was added resulting in the precipitation of the complex as pale yellow white solid which was vacuum filtered , washed with water and diethyl ether and dried to get the product in full purity. Yield (0.042 g, 72 %). ^{1}H NMR (400 MHz, DMSO), δ (ppm): 7.74 (t, 1H), 7.845 (d, 1H), 8.49 (t, 1H), 9.01 (d, 1H). Elemental Analysis for complex XVII, $C_{30}H_{24}F_{18}IrN_6P_3$; (calculated) : C : 32.89, H : 2.21, N : 7.67; (found) : C : 32.96, H : 2.04, N : 7.95

Synthesis of [Ir(bpy)$_2$(bpm)](PF$_6$)$_3$ (XVIII)

10 ml ethylene glycol was taken in a 2 necked RB through which N_2 was bubbled , bipyrimidine ligand (bpm) (0.0.083 g) was added and stirred to which [Ir(bpy)$_2$(OSO$_2$CF$_3$)]CF$_3$SO$_3$ (0.025g, 0.026261mmol) was added and refluxed for 5 hour. The reaction mixture was cooled, water was added, filtered and to the filtrate saturated aq KPF$_6$ was added resulting in the precipitation of the complex which was vacuum filtered , washed with water and diethyl ether and dried to get the product. The product was not completly pure as seen from the NMR and the yield was lower. The nmr obtaned is given in the supplimentary information.

NMR Spectrum of d8 & (h8+d8) [Ir^{III}(bpy-N,N')$_2$Cl$_2$]$^+$

The nmr specrtrum of complexes are measured in 400MHz instrument using DMSO in which all of them are completly soluble.

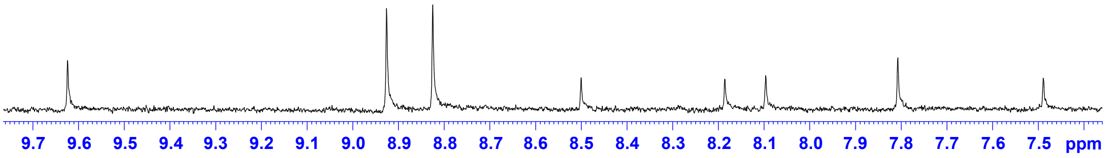

Figure D1. NMR spectrum of purified d8-[Ir^{III}(bpy-N,N')$_2$Cl$_2$]$^+$

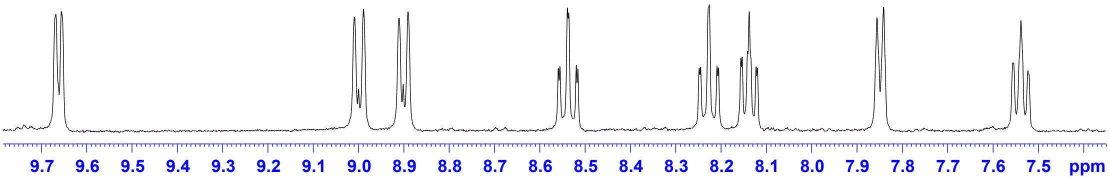

Figure D2. NMR spectrum of purified(h8+ d8) - [Ir^{III}(bpy-N,N')$_2$Cl$_2$]$^+$

NMR Spectrum of d8 & (h8+d8) [Ir^{III}(bpy-N,N')$_2$(bpy-C,N')$^-$]$^{2+}$

The nmr specrtrum of complexes are measured in 600MHz instrument using DMSO in which all of them are completly soluble.

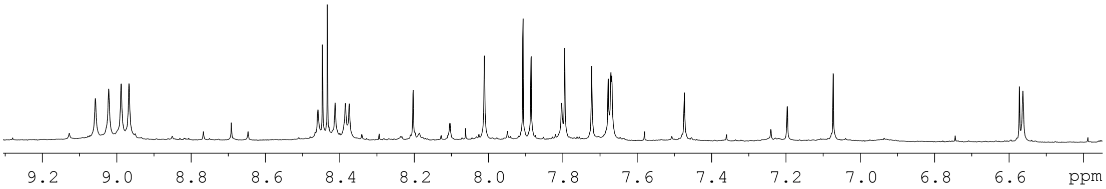

Figure D3. NMR spectrum of purified d8-[Ir^{III}(bpy-N,N')$_2$(bpy-C,N')$^-$]$^{2+}$

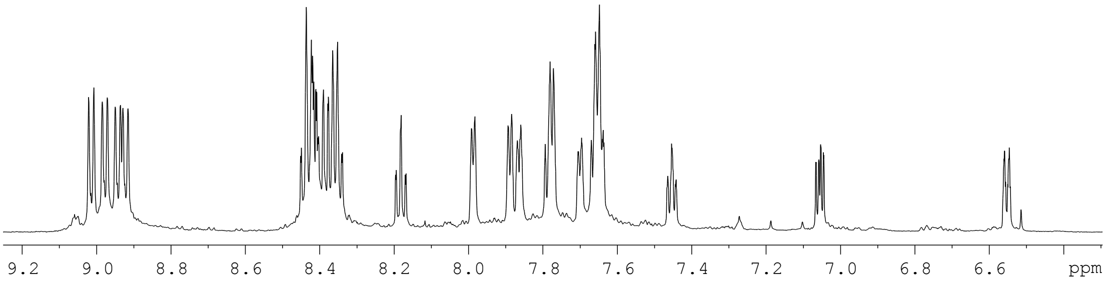

Figure D4. NMR spectrum of purified (h8+d8)-[Ir^{III}(bpy-N,N')$_2$(bpy-C,N')$^-$]$^{2+}$

COSY Spectrum of h8-[Ir^{III}(bpy-N,N')$_2$Cl$_2$]$^+$ & h8-[Ir^{III}(bpy-N,N')$_2$(bpy-C,N')$^-$]$^{2+}$

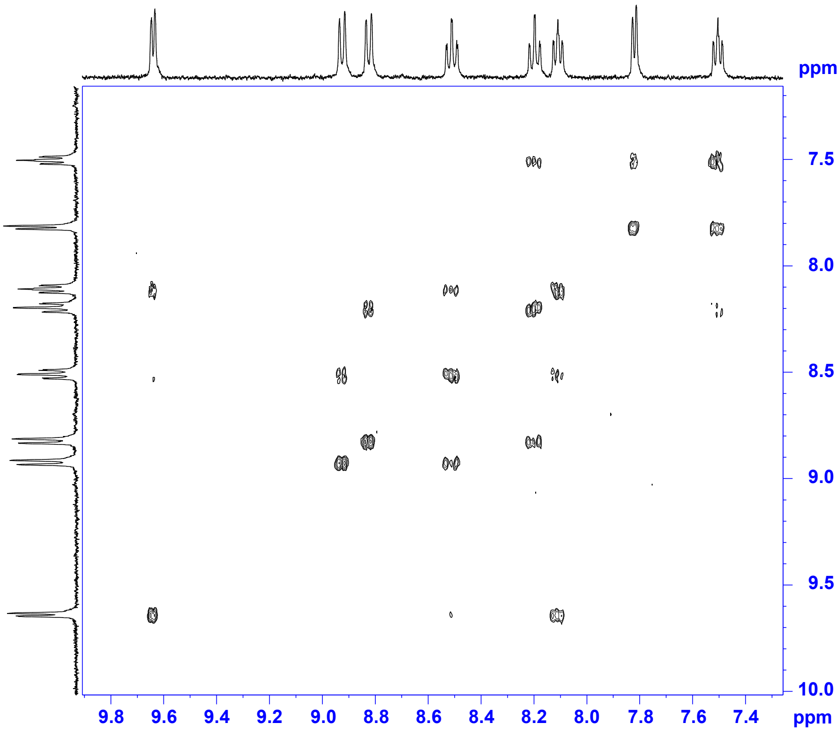

Figure D5. COSY spectrum of purified h8-[Ir^{III}(bpy-N,N')$_2$Cl$_2$]$^+$ taken in deuteriated DMSO.

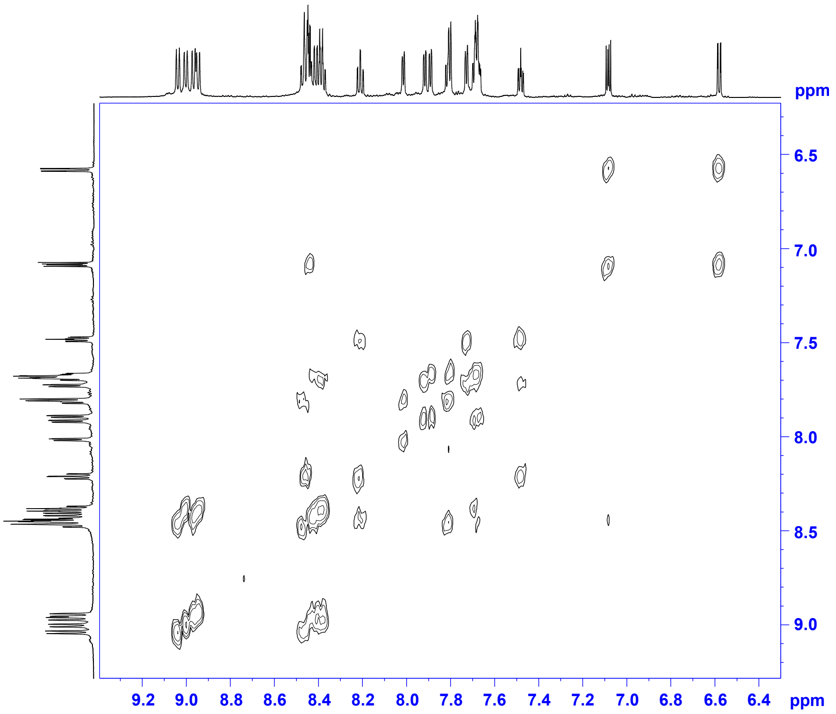

Figure D6. COSY spectrum of purified h8-[Ir^{III}(bpy-N,N')$_2$(bpy-C,N')$^-$]$^{2+}$ taken in deuteriated DMSO.

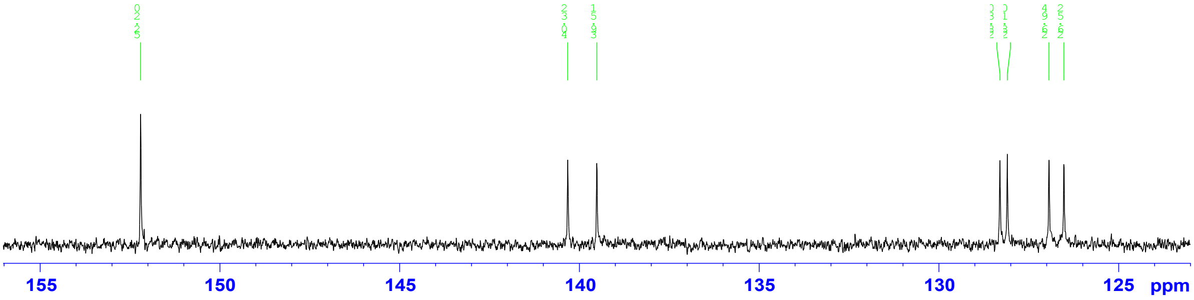

Figure D7. DEPT-135 spectrum of purified [Ir^{III}(phen)$_2$Cl$_2$].PF$_6$ (**V**) taken in deuteriated DMSO.

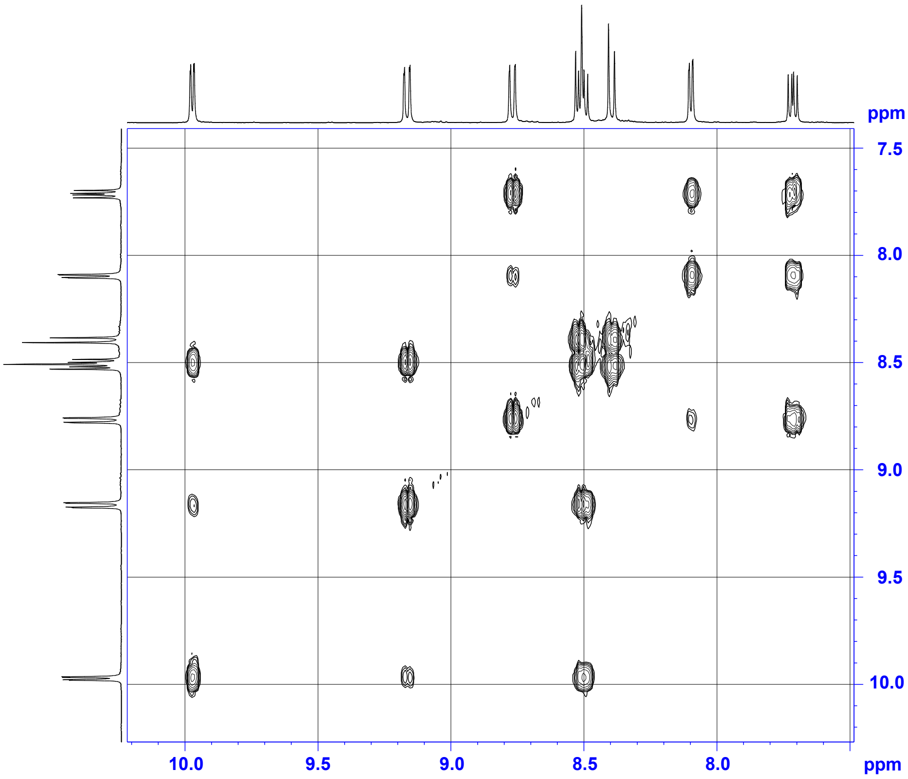

Figure D8. COSY spectrum of purified [Ir^{III}(phen)$_2$Cl$_2$].PF$_6$ (**V**) taken in deuteriated DMSO.

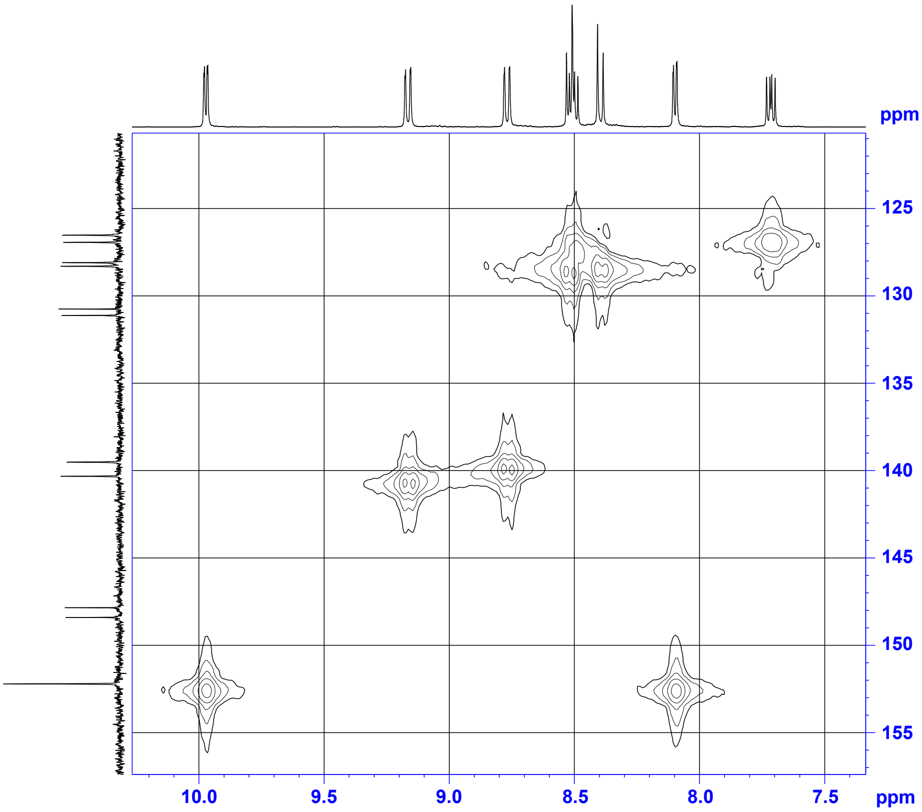

Figure D9. 1H-13C HSQC spectrum of purified [Ir^{III}(phen)$_2$Cl$_2$].PF$_6$ (**V**) taken in deuteriated DMSO.

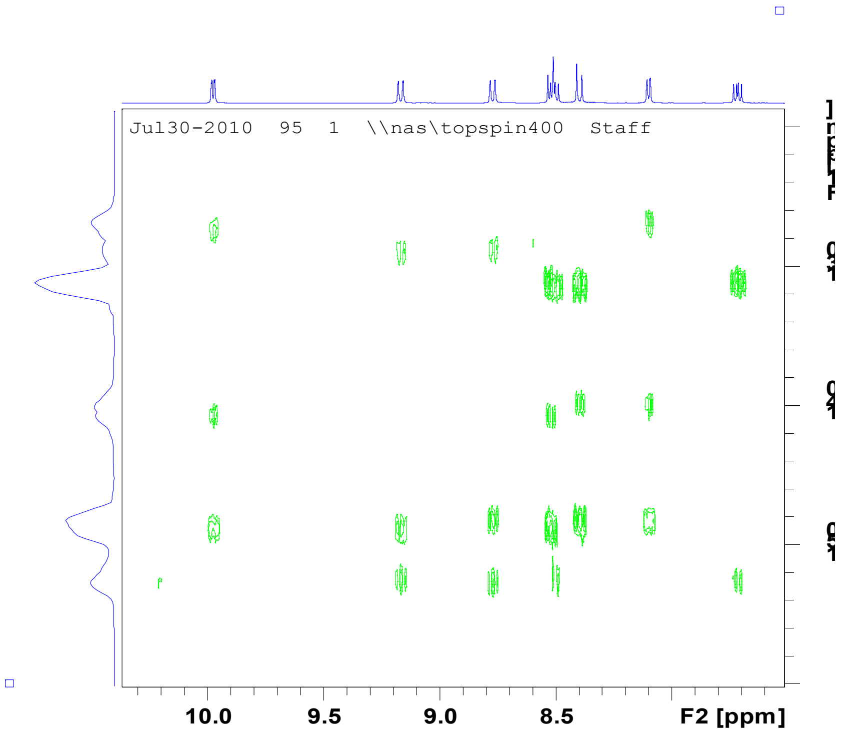

Figure D10. HMBC spectrum of purified [Ir^{III}(phen)$_2$Cl$_2$].PF$_6$ (**V**) taken in deuteriated DMSO.

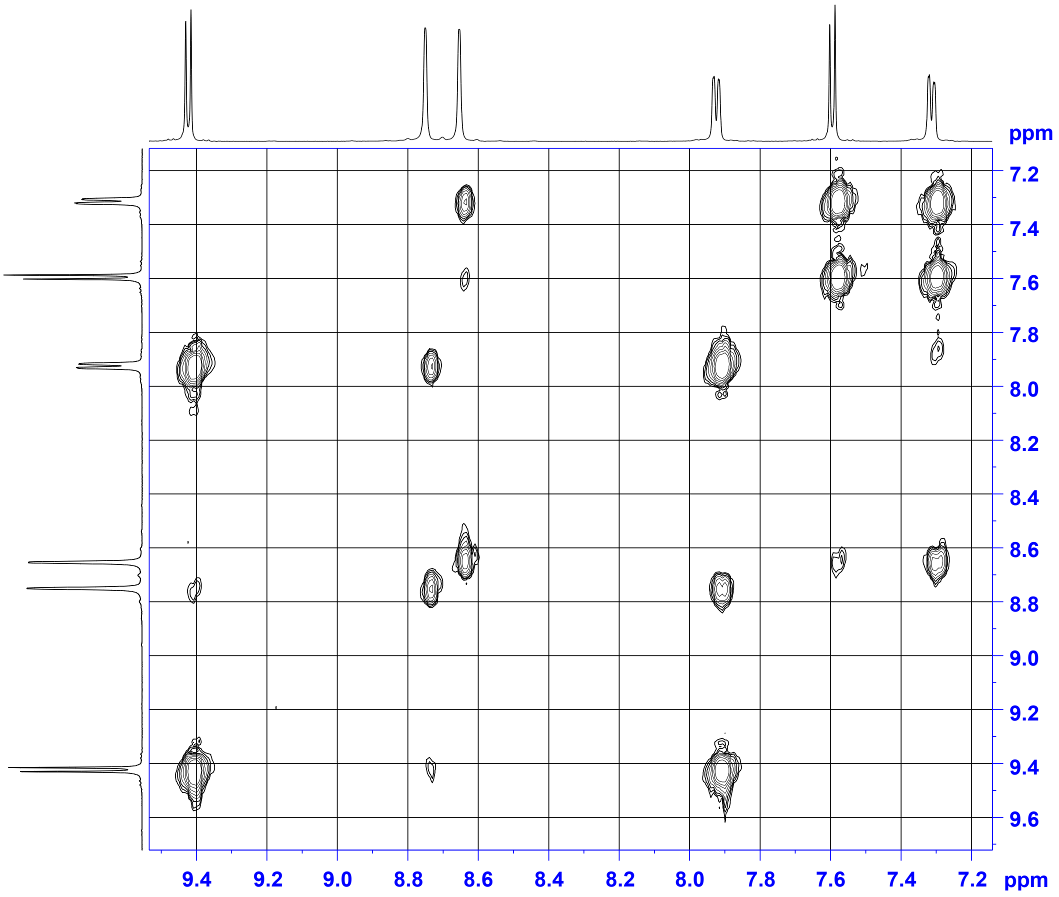

Figure D11. COSY spectrum of purified [Ir^{III}(dmbpy)$_2$Cl$_2$]$^+$Cl (**VII**) taken in deuteriated DMSO.

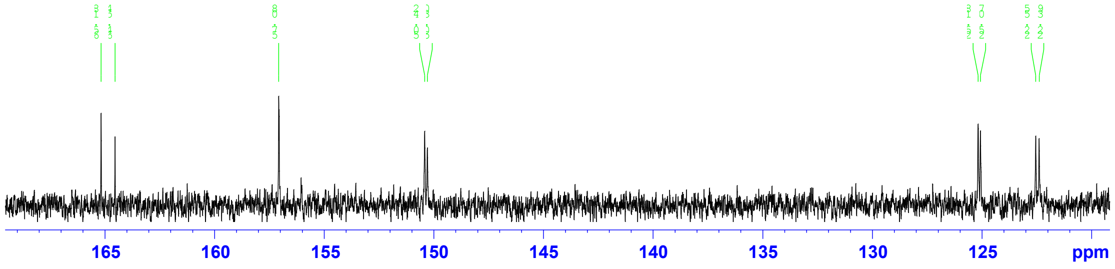

Figure D12. ^{13}C spectrum of purified [Ir^{III}(dtbpy)$_2$Cl$_2$].PF$_6$ (**IX**) taken in deuteriated DMSO.

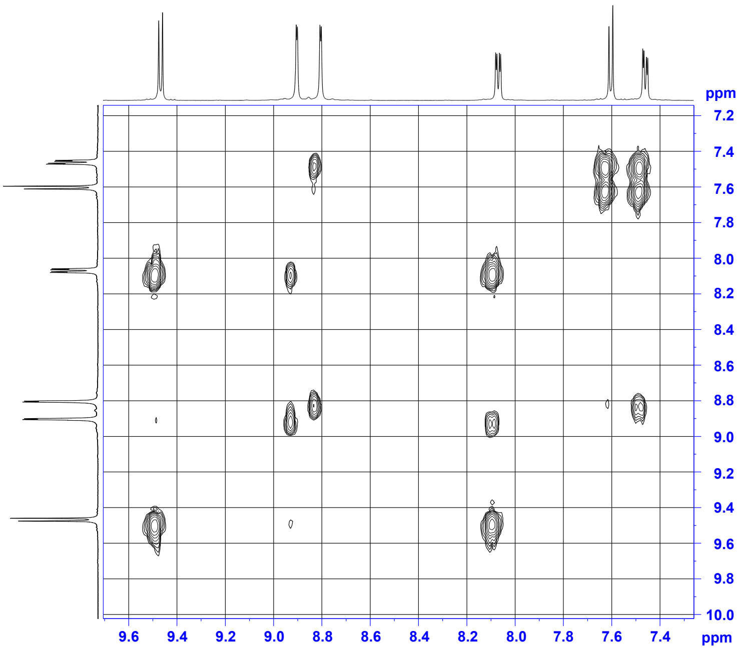

Figure D13. COSY spectrum of purified [Ir^{III}(dtbpy)$_2$Cl$_2$].PF$_6$ (**IX**) taken in deuteriated DMSO.

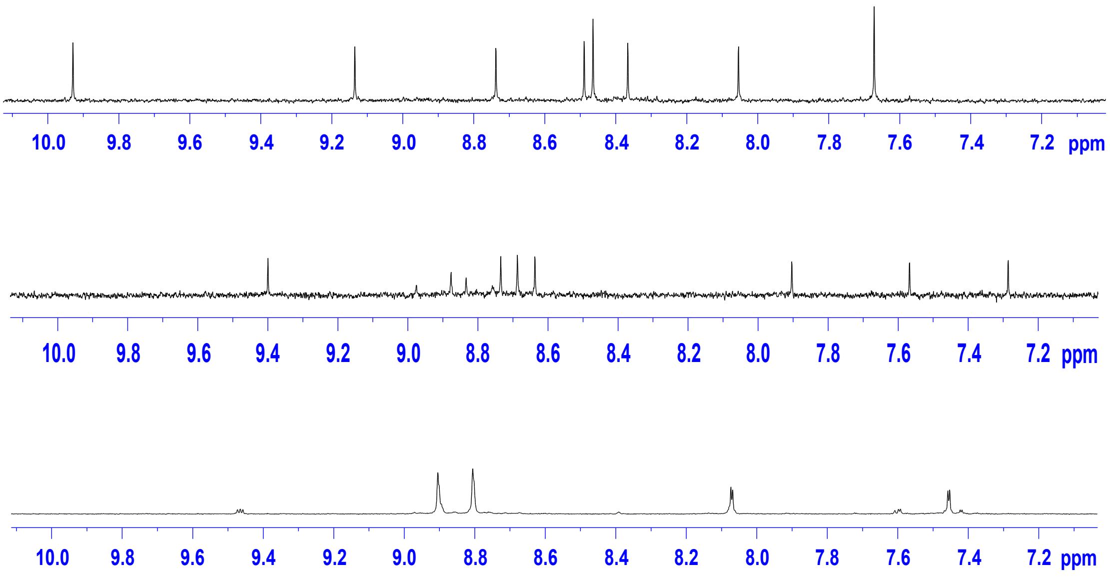

Figure D14. ^{1}H NMR spectrum of purified **VI, VIII, X** taken in deuteriated DMSO.

Time Dependent Study of the reaction mechanism of $IrCl_3$ with h8 bpy using HPLC and NMR

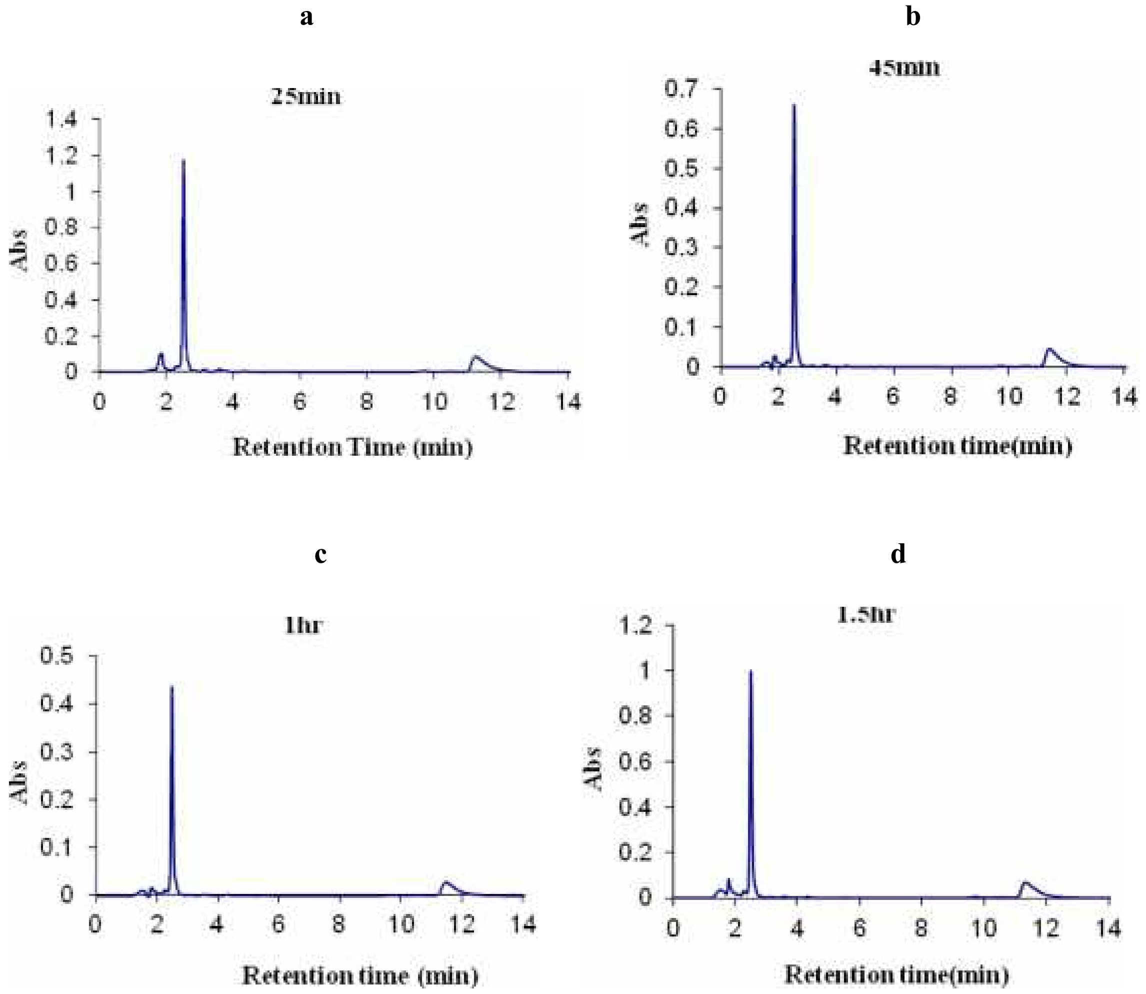

Figure D15. *Time dependent HPLC data for reaction of $IrCl_3$ with h8 bpy at different time intervals ranging from 25min to 1.5hour. a) 25min b) 45min c)1hr d) 1.5hr.*

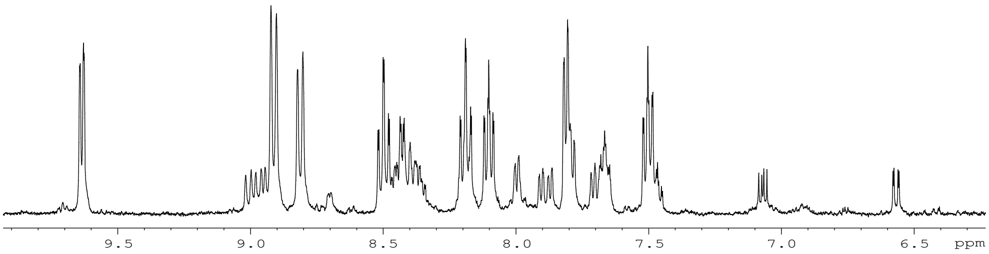

a) 25min

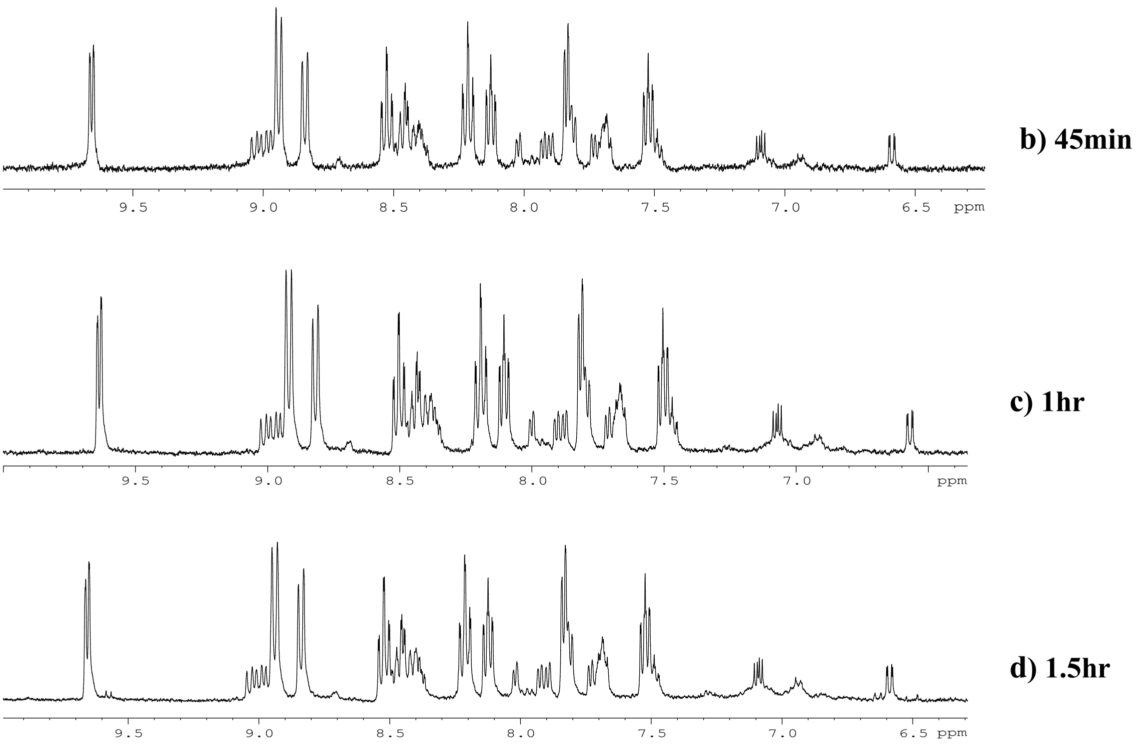

Figure D16. *Time dependent nmr data for the reaction of $IrCl_3$ with h8 bpy at different time intervals ranging from 25min to 1.5hour. a) 25min b) 45min c) 1hr d) 1.5hr.*

Photophysics

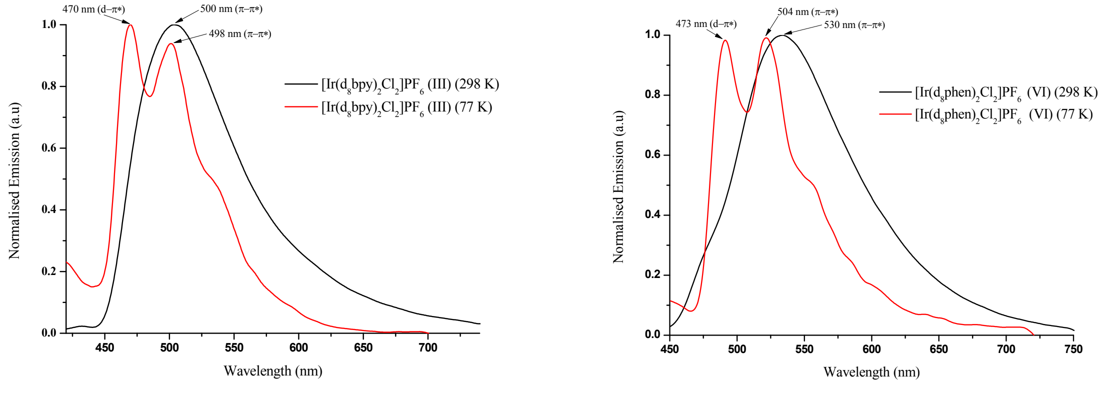

(a) **(b)**

Figure S17. (a) *Normalised emission spectra of complex III at 298 K (—) measured in spec grade ACN and 77 K (—) measured in EtOH : MeOH (4:1) glass. λ_{ex}=380 nm.* ***(b)*** *Normalised emission spectra of complex VI at 298 K (—) measured in spec grade ACN and 77 K (—) measured in EtOH : MeOH (4:1) glass. λ_{ex}=380 nm.*

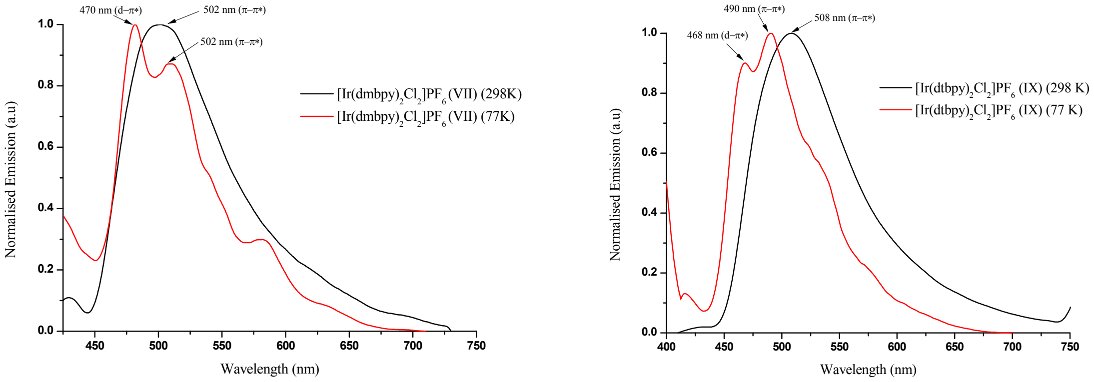

(a) **(b)**

Figure S18 (a) *Normalised emission spectra of complex VII at 298 K (—) measured in spec grade ACN and 77 K (—) measured in EtOH : MeOH (4:1) glass.* λ_{ex}*=380 nm.* ***(b)*** *Normalised emission spectra of complex IX at 298 K (—) measured in spec grade ACN and 77 K (—) measured in EtOH : MeOH (4:1) glass.* λ_{ex}*=380 nm.*

Life Time Measurements done using Laser

$[Ir(d_8\text{-}bpy)_2Cl_2]PF_6$

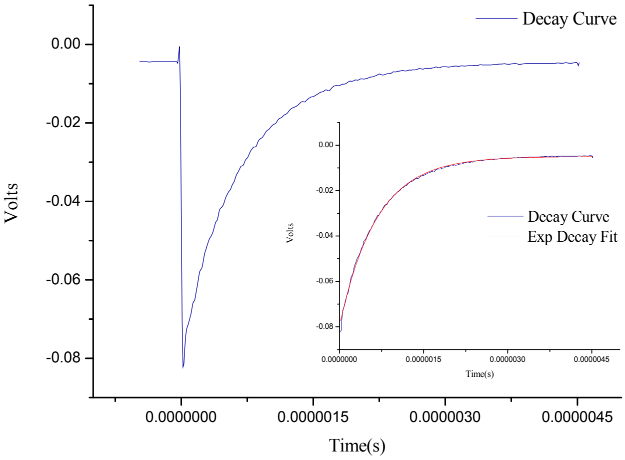

[Ir(h8-bpy)$_2$(h8-bpy)$^-$]2PF$_6$

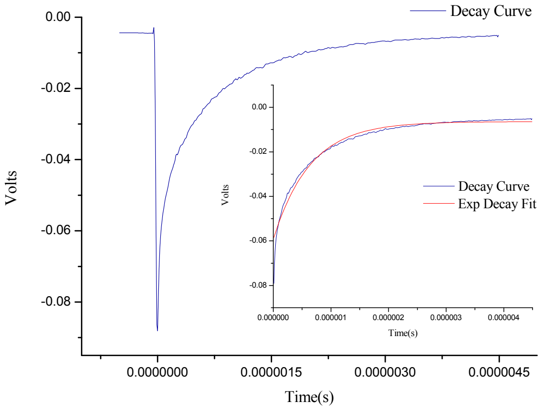

[Ir(d8-bpy)$_2$(d8-bpy)$^-$]2PF$_6$

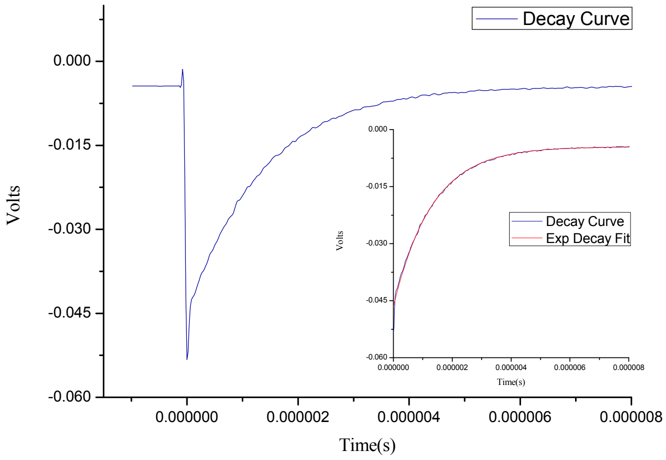

[Ir^{III}(phen)$_2$Cl$_2$]PF$_6$ (V) (Emission maxima taken, λ_{em} = 473 nm)

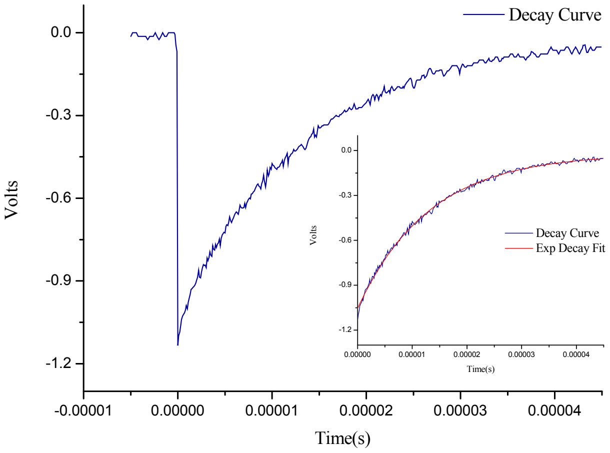

$[Ir^{III}(phen)_2Cl_2]PF_6$ (V) (Emission maxima taken, λ_{em} = 504 nm)

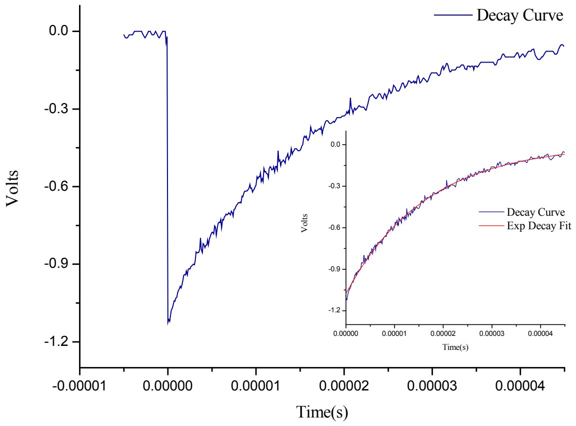

$[Ir^{III}(d8\text{-}phen)_2Cl_2]PF_6$ (VI) (Emission maxima taken, λ_{em} = 473 nm)

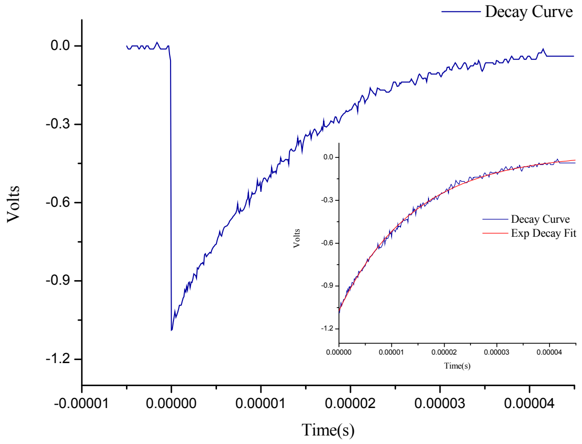

$[Ir^{III}(d8\text{-}phen)_2Cl_2]PF_6$ (VI) (Emission maxima taken, λ_{em} = 504 nm)

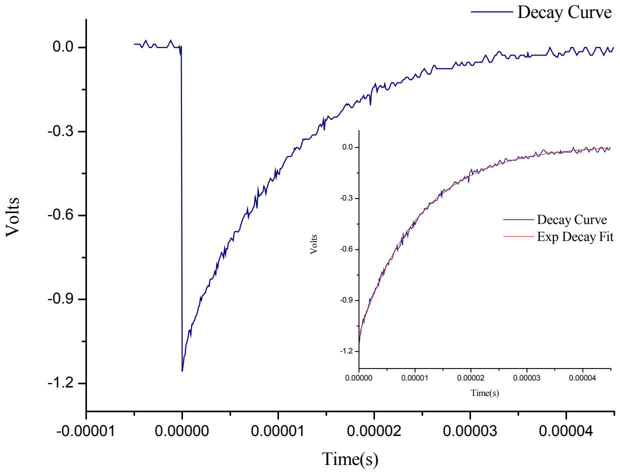

[Ir^{III}(dmbpy)$_2$Cl$_2$]PF$_6$ (VII) (Emission maxima taken, λ_{em} = 470 nm)

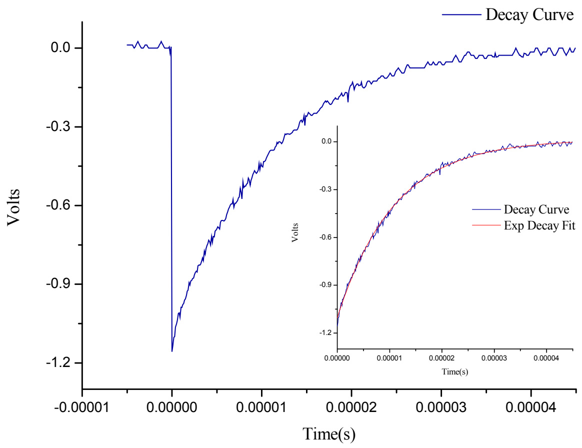

[Ir^{III}(dmbpy)$_2$Cl$_2$]PF$_6$ (VII) (Emission maxima taken, λ_{em} = 502 nm

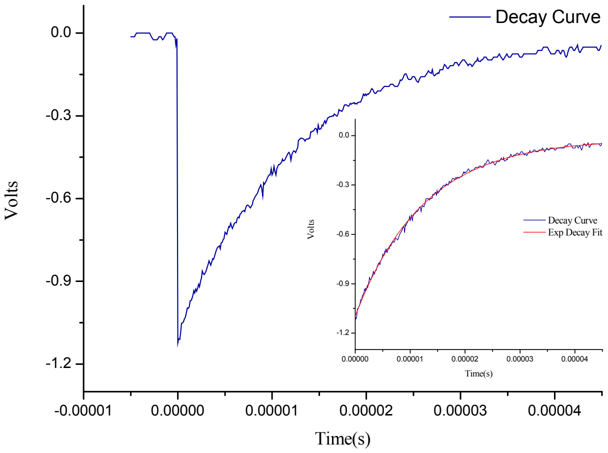

[Ir^{III}(d12-dmbpy)$_2$Cl$_2$]PF$_6$ (VIII) (Emission maxima taken, λ_{em} = 470 nm)

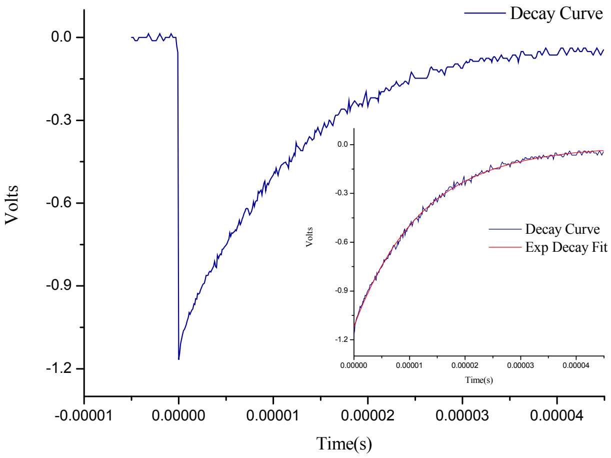

$[Ir^{III}(d12\text{-}dmbpy)_2Cl_2]PF_6$ (VIII) (Emission maxima taken, λ_{em} = 502 nm)

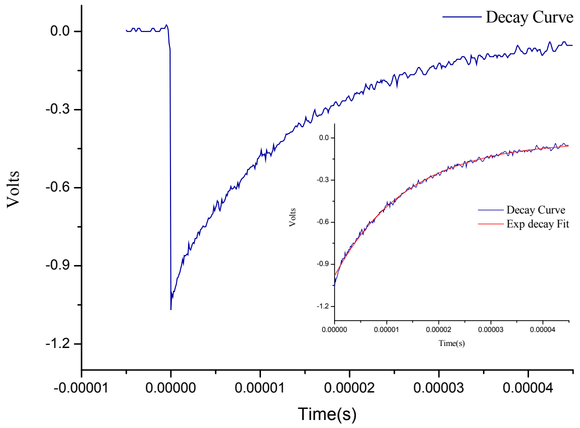

$[Ir^{III}(dtbpy)_2Cl_2]PF_6$ (IX) (Emission maxima taken, λ_{em} = 468 nm)

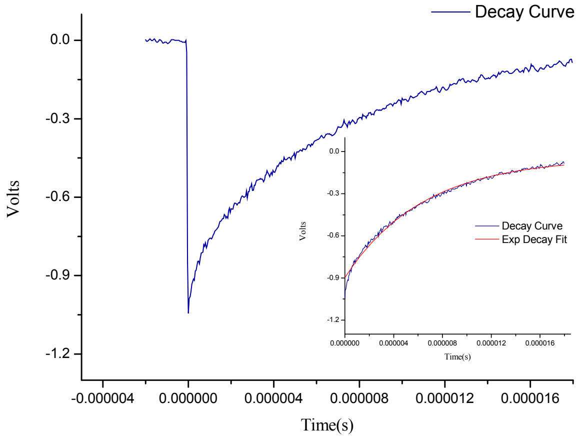

$[Ir^{III}(dtbpy)_2Cl_2]PF_6$ (IX) (Emission maxima taken, λ_{em} = 490 nm)

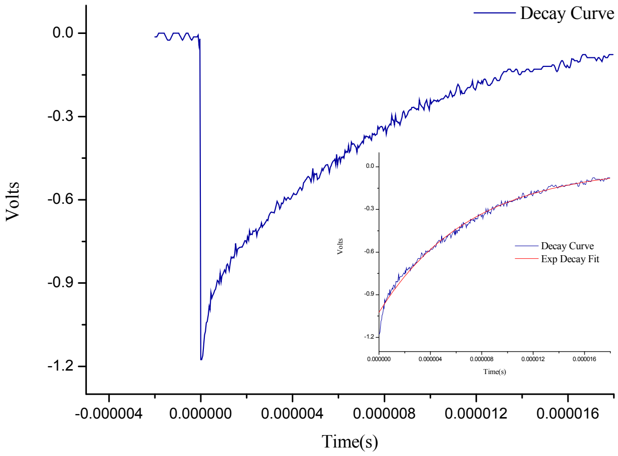

[Ir^{III}(d24-dtbpy)$_2$Cl$_2$]PF$_6$ (X) (Emission maxima taken, λ_{em} = 468 nm)

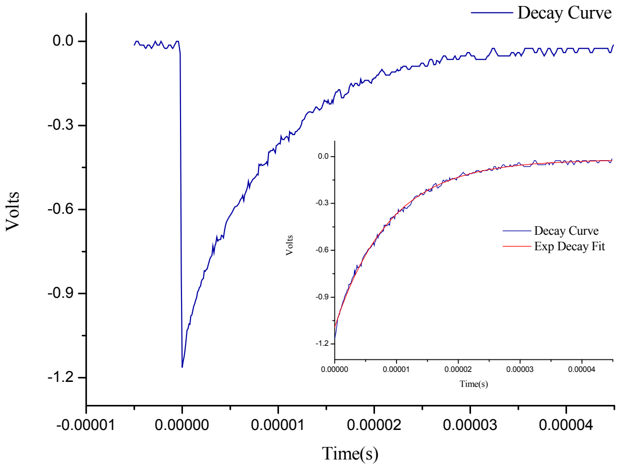

[Ir^{III}(d24-dtbpy)$_2$Cl$_2$]PF$_6$ (X) (Emission maxima taken, λ_{em} = 490 nm)

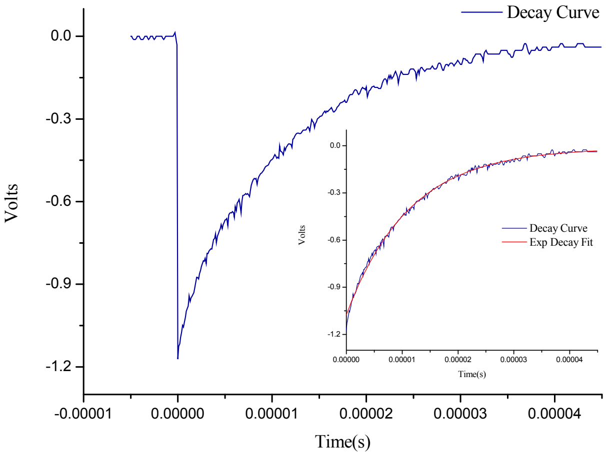

Appendix E

Synthesis of $[Ru(bpy)_2(pztr)]^+$ Separation of its Isomers and Photophysics

Introduction

Over the last decade the work done by Han Vos Research Group has been focused on the spectroscopic properties of Ru (II) polypyridine complexes incorporating the strong σ-donor 1,2,4-triazole group. The pH and coordination mode (N2 / N4) dependent photophysical and photochemical properties have been particular interest. The use of pyridyl and pyrazyl groups within these complexes has demonstrated their versatility towards synthetic tunability of ground and excited state properties. The work we done contains the synthesis of pyridyl, pyrazyl and 1,2,4-triazole ligands and complexes and photochemical studies of complexes containing 5-pyridin-2-yl-4H-[1,2,4]triazoles and 5-pyrazyl-4H-[1,2,4]triazoles.

Synthetic Scheme for $[Ru(bpy)_2(pztr)]^+$

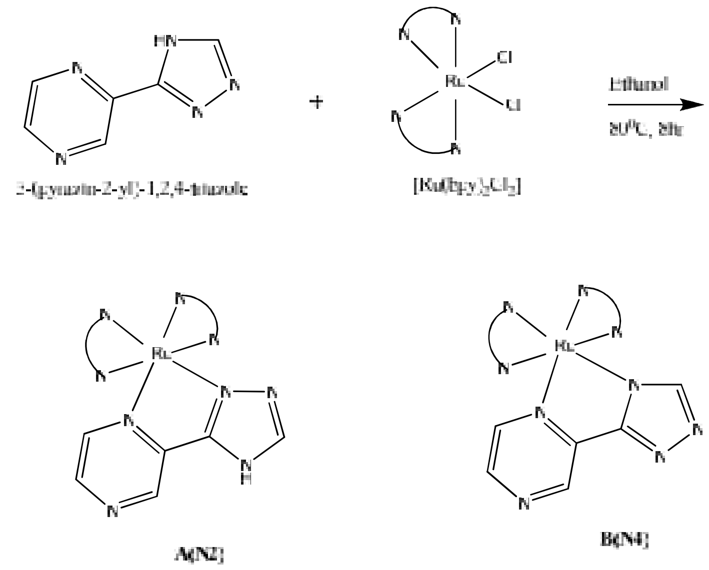

To a suspension of EtOH (30 mL) and H_2O (30 mL) was added *cis*-$[Ru(bpy)_2Cl_2].2H_2O$ (185 mg, 0.36 mmol) and Pztr-H (80 mg, 0.54 mmol). After refluxing for 8 h, EtOH was evaporated and the mixture was left in the fumehood overnight. The crude product was flash chromatographed on a silica column with 7:3 CH_3CN / H_2O saturated with KNO_3. To each of the two fractions was added a drop of NH_3 solution and NH_4PF_6 (30 mg, 0.18 mmol). Each mixture was extracted with dichloromethane (3x20 mL) and the solvent was evaporated. The N2-isomer (second fraction of silica column) was chromatographed on an alumina column (neutral) with

CH_3CN. After the solvent was evaporated, it was recrystallised with 2:1 MeOH / H_2O. The N4-isomer (first fraction of silica column) was chromatographed on an alumina column (neutral) with first CH_3CN, then 1:20 MeOH / CH_3CN, 1:10 MeOH / CH_3CN and 1:5 MeOH / CH_3CN. After the solvent was evaporated, it was recrystallised with 2:1 MeOH / H_2O. Yield: 51 mg N2-isomer (0.07 mmol, 41 %), 90 mg N4-isomer (0.13 mmol, 71 %).

^{1}H NMR and COSY Spectrum for N2 and N4 Isomers

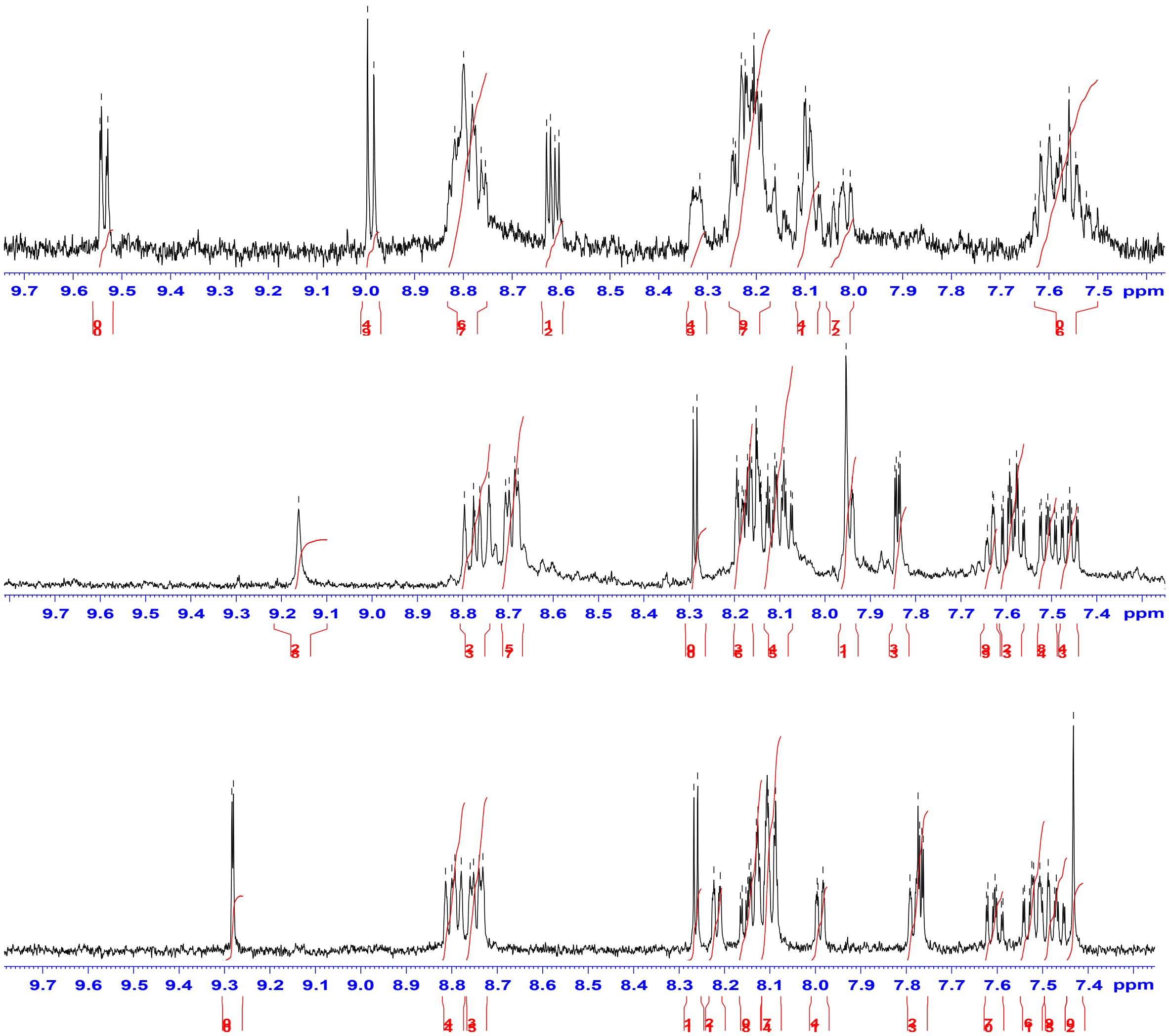

Figure S1 (a) ^{1}H NMR spectrum of $[Ru(bpy)_2(pztr)]^+$ containing both isomers taken in d6 DMSO, (b) ^{1}H NMR spectrum of N2 isomer of $[Ru(bpy)_2(pztr)]^+$ taken in d6 DMSO and (c) ^{1}H NMR spectrum of N4 isomer of $[Ru(bpy)_2(pztr)]^+$ taken in d6 DMSO.

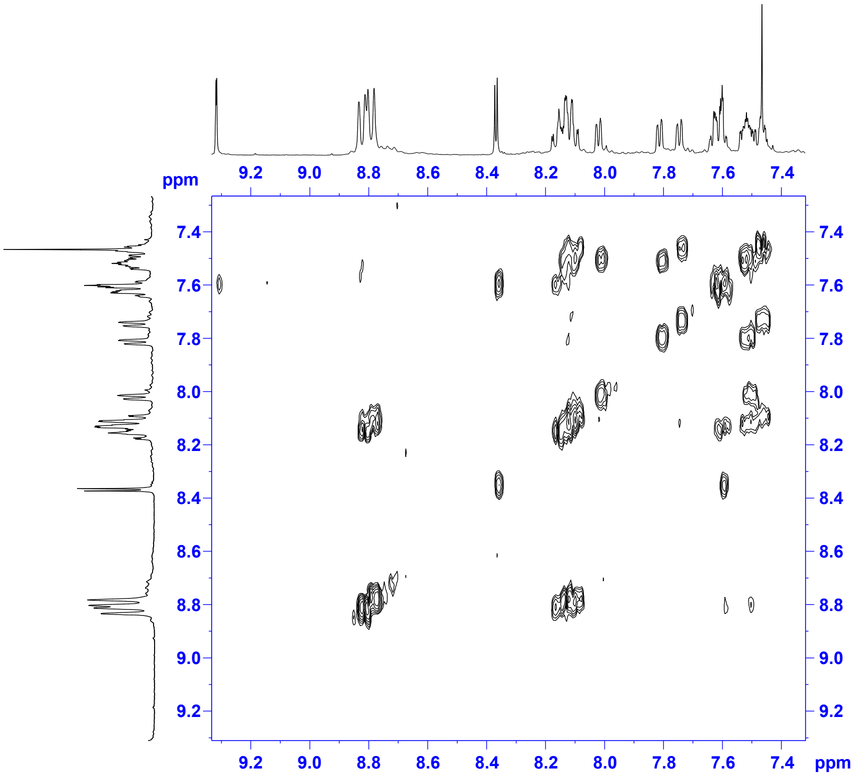

COSY Spectrum for the N4 Isomer

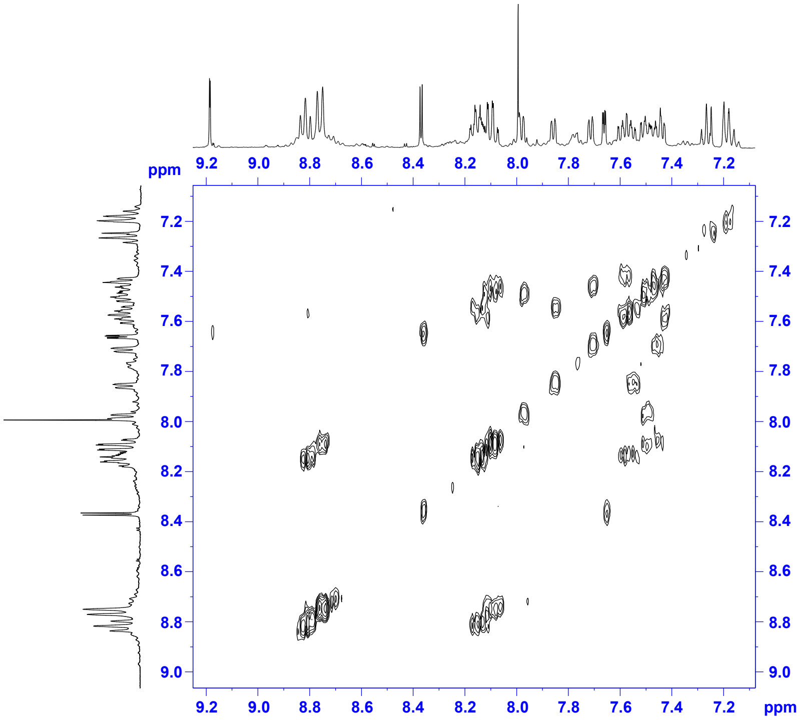

COSY Spectrum for the N2 Isomer

HPLC Seperation of N2 and N4 Isomers

High-Performance Liquid Chromatography (HPLC) was carried out using a Varain ProStar (model 335.71) photodiode array Detector, HPLC conjunction with Varian Star software, a Varian (model 210) pump, a 20 µl injector loop and a strong cation exchange Luna SCX 100A column (25cm X 4.6mm) provided by phenomenex . This column is silica- based sorbent derivatized with benzene sulphuric acid phase. The column is placed with 5 µm particles and the operating pH range is between 2 and 8. The mobile phase for this work was 75:20:5 CH_3CN: H_2O: CH_3OH containing 0.1 M KNO_3. Filtered and degassed prior using the flow rate ranged 1.5 and 2 cm^3/min^{-1}. The detection wavelength was 280 nm where the most intense band in the adsorption spectra (π-π*), for ruthenium complexes studied in this work. All Samples were dissolved in the pure acetonitrile HPLC gradient grade ≥99.9 % and filtered through 0.45 micron filter prior to injection. All solvents employed were of HPLC grade or better and used as received unless otherwise stated. These measurements were carried out by Mr. Hamid M. Y. Ahmed.

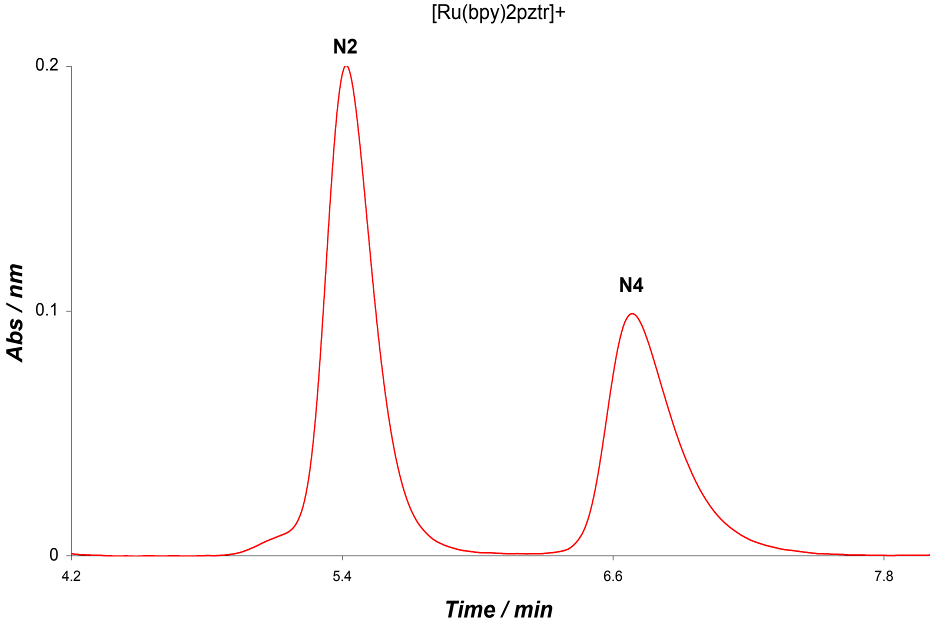

HPLC separation of N2 / N4 isomers of $[Ru(bpy)_2(Hpztr)]^+$ *in acetonitrile (Mobile phase* CH_3CN: H_2O: CH_3OH *with volume ratio 75:20:5 0.12 M* KNO_3*). Flow rate: 2.0* cm^3 min^{-1}*; detection wavelength: 430 nm.*

Photochemistry:

Absorption & Emission Spectra for N2 & N4 isomers of $[Ru(bpy)_2(pztr)]^+$ and the effect of adding 100 µl of 1eq CF_3COOH to the solution

Absorption Spectra for N2 Isomer

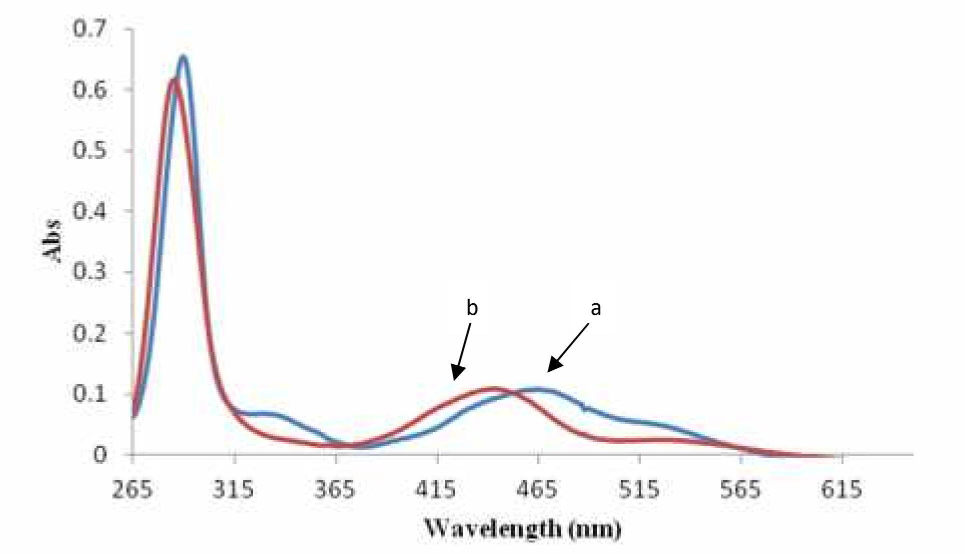

Fig S2: a) absorption spectra of N2 isomer taken in spectroscopic grade ACN having an abs maximum of 464 nm. at an optical density of 0.108 b) absorption spectra of N2 isomer after adding 100 µl of 1equivalent CF_3COOH having an abs maximum of 443 nm at an optical density of 0.108.

Emission Spectra for N2 Isomer

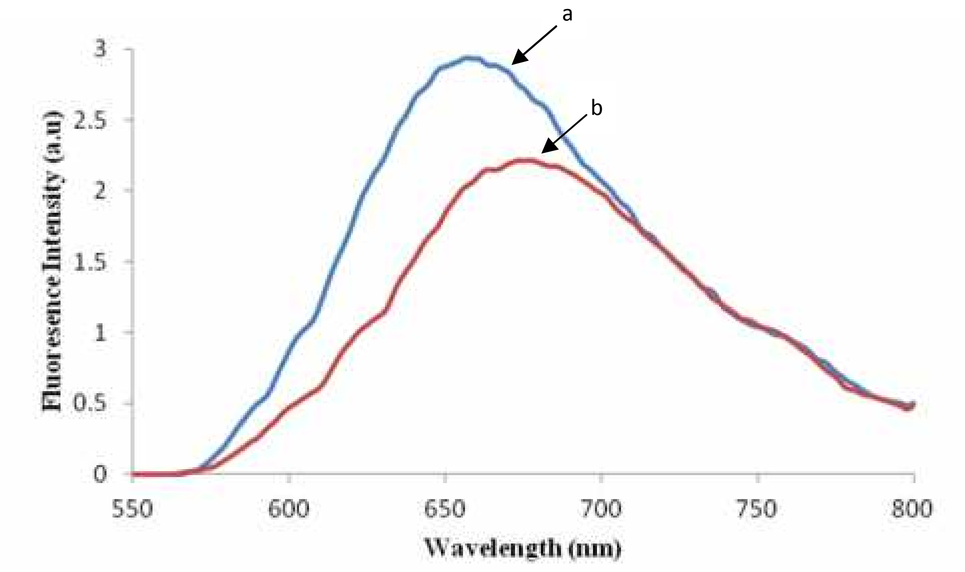

Fig S3: a) emission spectra of N2 isomer taken in spectroscopic grade ACN at an excitation wavelength of 464 nm. b) emission spectra of N2 isomer after adding 100 µl 1eq of CF_3COOH taken at excitation wavelength of 443 nm.

Absorption Spectra for N4 Isomer

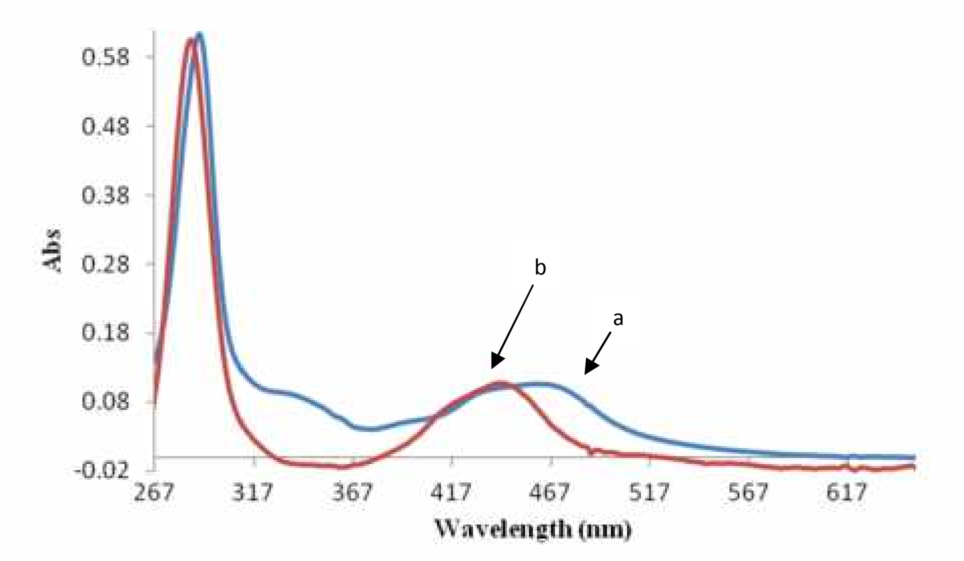

Fig S4: a) absorption spectra of N4 isomer taken in spectroscopic grade ACN having an abs maximum of 460 nm at an optical density of 0.107 b) absorption spectra of N4 isomer after adding 100 µl 1eq of CF_3COOH having an abs maximum of 441 nm at an optical density of 0.107

Emission Spectra for N2 Isomer

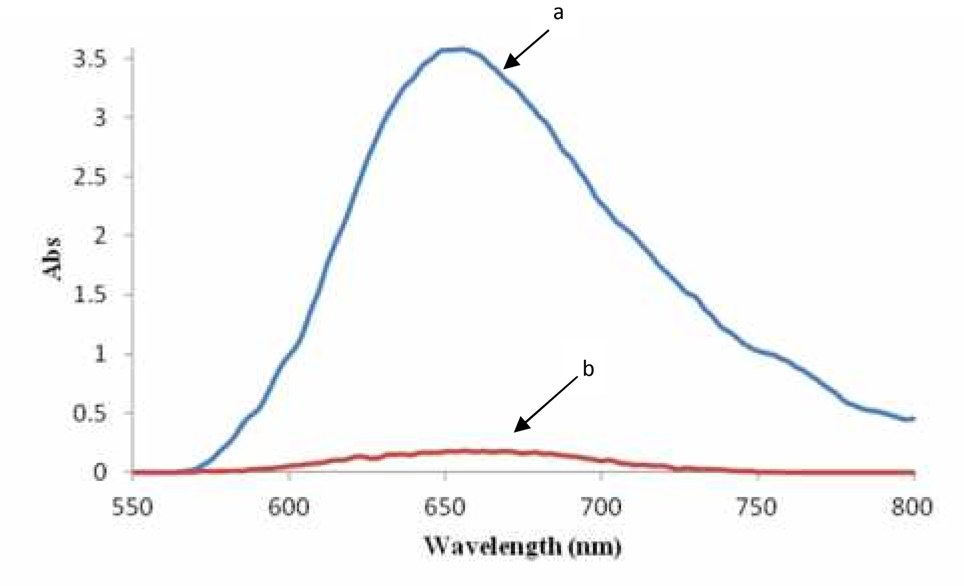

Fig S5: a) emission spectra of N4 isomer taken in spectroscopic grade ACN at an excitation wavelength of 460 nm. b) emission spectra of N4 isomer after adding 100 µl 1eq of CF_3COOH taken at excitation wavelength of 441 nm.

[Note: In all the graphs the blue line indicates the sample in spectrometric grade ACN and red line indicates the sample after addition of 100µl 1eq of CF_3COOH, the optical densities at the abs]

Heteroleptic Ru (II) complexes containing 1,2,4-triazole based ligands have been proven to be amongst the most photostable Ru (II) diimine complexes known in basic conditions. However, in acidic conditions these complexes exhibit an extensive and interesting photochemistry, which includes coordination isomerisation and reversible ligand substitution. The photochemistry of several complexes of this type are discussed in this section

The photochemical experiments were carried out at room temperature in air-equilibrated solution in a 1 cm quartz cell using two 9.6 VA and 250-W tungsten lamp, a glass filter ($\lambda > 390$ nm) to prevent UV radiation reaching the sample, and a water filter to prevent any thermal reactions taking place.

Appendix F

Photophysics of Ru (II) Complexes

Lifetime measurements for Ru Monomers & Ru-Pt, Ru-Pd Dimers

All the complexes was given to me for measurement by Mr.Gurmeet Singh Bindra

Measurements were carried out in doubly distilled spectrometric grade ACN. For deaeration N_2 was passed through the solution for 20 min.

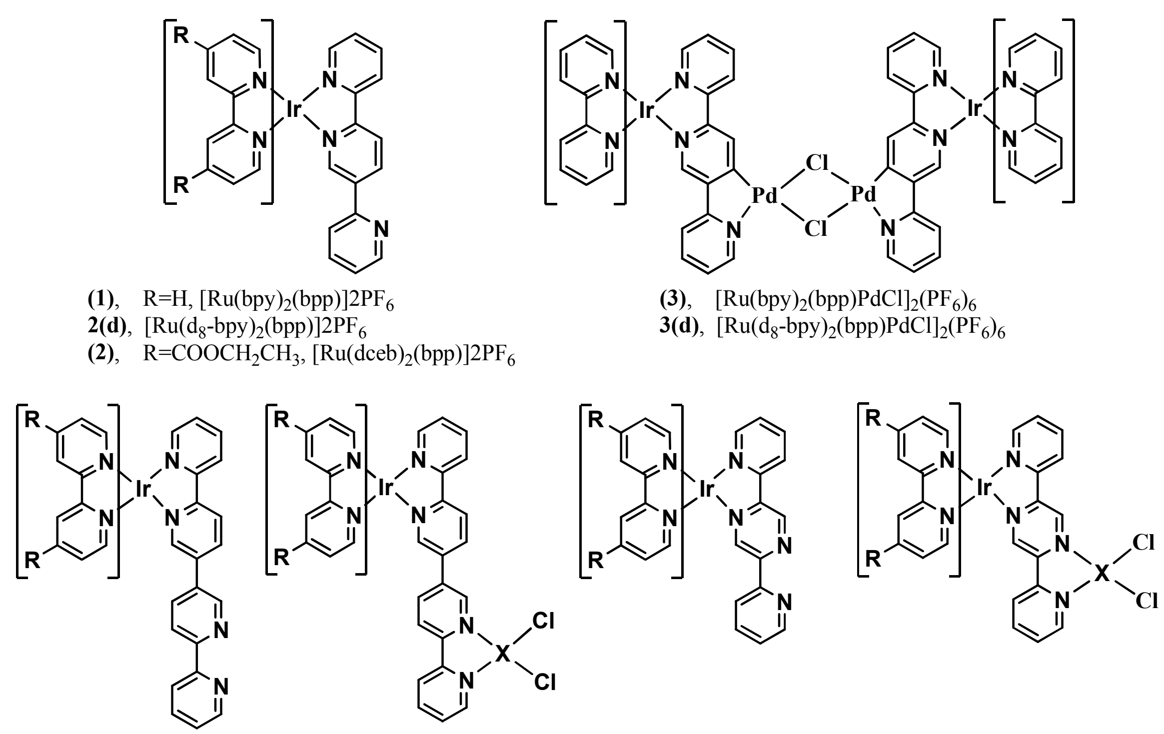

(1), R=H, $[Ru(bpy)_2(bpp)]2PF_6$
2(d), $[Ru(d_8\text{-}bpy)_2(bpp)]2PF_6$
(2), $R=COOCH_2CH_3$, $[Ru(dceb)_2(bpp)]2PF_6$

(3), $[Ru(bpy)_2(bpp)PdCl]_2(PF_6)_6$
3(d), $[Ru(d_8\text{-}bpy)_2(bpp)PdCl]_2(PF_6)_6$

(5), R=H, $[Ru(bpy)_2(bis\text{-}bpy)]_2PF_6$
(6), R=COOEt,

(7), R=H, X=Pt
(8), R=H, X=Pd
(9), R=COOEt, X=Pt
(10), R=COOEt, X=Pd
(11), R=COOH, X=Pt

(12), R=COOEt

(13), R=COOEt, X=Pt
(14), R=COOEt, X=Pd

Figure F1. *Schematic representation of the Ru monomers, Ru-Pt and Ru-Pd dimers with ligands bpp, bis-bpy and dpp*

Complex	**ID**	**Lifetime (aerated), 298 K**		**Lifetime (deaerated), 298 K**	
		ns	Reduced r^2 value	ns	Reduced r^2 value
$[Ru(bpy)_2(bpp)]2PF_6$	1	222	0.99047	442	0.98362
$[Ru(d_8\text{-}bpy)_2(bpp)]2PF_6$	1(d)	226	0.99287	521	0.9879
$[Ru(dceb)_2(bpp)]2PF_6$	2	440	0.97416	1080	0.90653
$[Ru(bpy)_2(bpp)PdCl]_2(PF_6)_6$	3	79	0.99175	105	1.090
$[Ru(d_8\text{-}bpy)_2(bpp)PdCl]_2(PF_6)_6$	3(d)	86	0.9872	116	1.048
$[Ru(bpy)_2(bis\text{-}bpy)]2PF_6$	5	240	0.99363	755	0.96806
$[Ru(dceb)_2(bis\text{-}bpy)]2PF_6$	6	440	0.96239	825	0.9781
$[Ru(bpy)_2(bis\text{-}bpy)PdCl_2]2PF_6$	7	16	0.98706	17	0.98573
$[Ru(bpy)_2(bis\text{-}bpy)PtCl_2]2PF_6$	8	206	0.98632	331	0.97698
$[Ru(dceb)_2(bis\text{-}bpy)PdCl_2]2PF_6$	9	49	0.99479	53	0.98995
$[Ru(dceb)_2(bis\text{-}bpy)PtCl_2]2PF_6$	10	400	0.96953	534	0.95088
$[Ru(dcab)_2(bis\text{-}bpy)PtCl_2]2PF_6$	11	110 (0.5)	0.87832		
$[Ru(dceb)_2(2,5\text{-}dpp)]2PF_6$	12	564	0.96287	1895	0.91842
$[Ru(dceb)_2(2,5\text{-}dpp)PtCl_2]2PF_6$	13	Life time is < 0.5ns not able to measure using SPC as its taking long time			
$[Ru(dceb)_2(2,5\text{-}dpp)PdCl_2]2PF_6$	14	Life time is < 0.5ns not able to measure using SPC as its taking long time			

Table F1. *Tabulated data for lifetimes in aerated and deaerated ACN for Ru monomers, Ru-Pt dimers and Ru-Pd dimer complexes*

77 K measurement done for Ru complexes with ligand dpp in EtOH:MeOH (4:1) mixture

1) $[Ru(bpy)_2(dpp)]PF_6$ - 3.6us
2) $[Ru(d_8\text{-}bpy)_2(dpp)]PF_6$ - 4.1us
3) $[Ru(bpy)_2(d_{10}\text{-}dpp)]PF_6$ - 4.5us

Emission at 77 K and lifetimes at both room temperature (298 K) and low temperature (77 K) with various Ru-Re complexes

All the complexes were given to me for measurement by Mr.Avishek Paul.

Measurements were carried out in doubly distilled spectrometric grade ACN. For Deaeration N_2 was passed through the solution for 20 min.

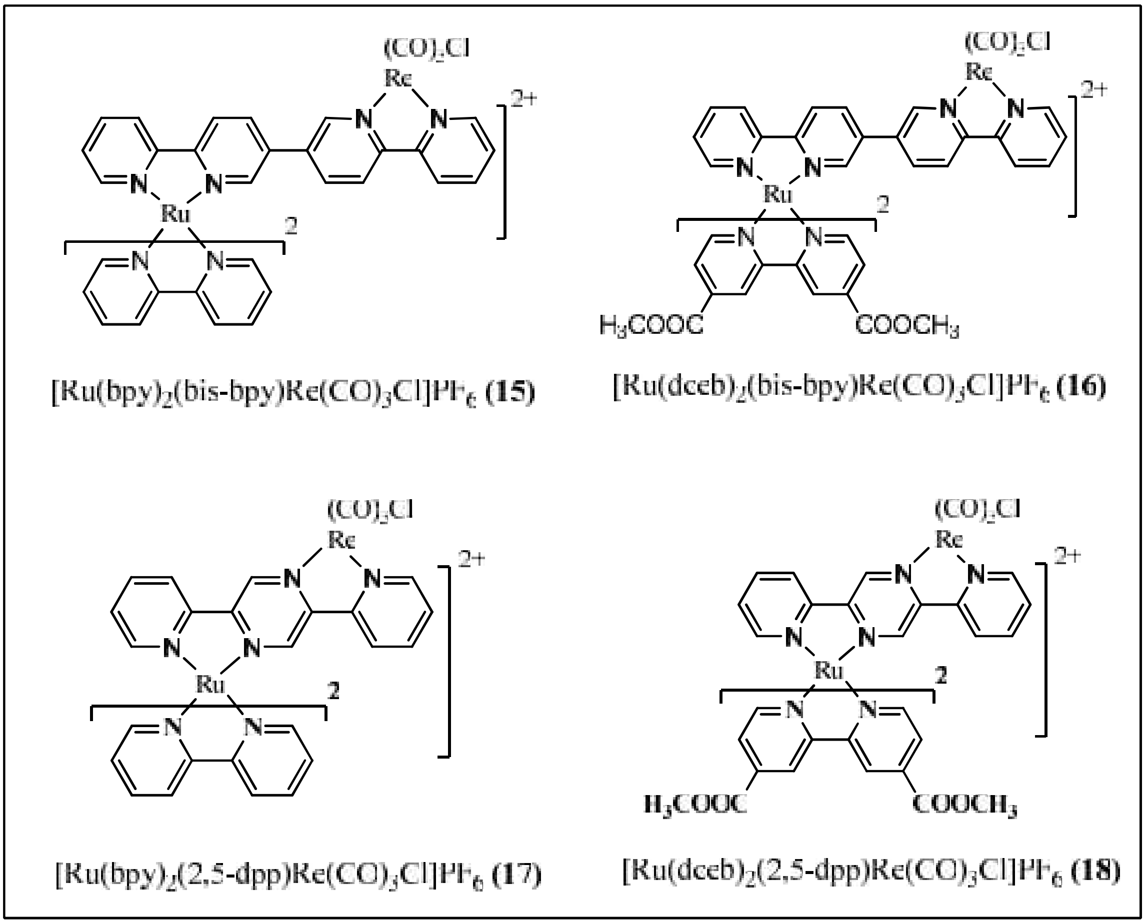

[Ru(bpy)$_2$(bis-bpy)Re(CO)$_3$Cl]PF$_6$ **(15)**

[Ru(dceb)$_2$(bis-bpy)Re(CO)$_3$Cl]PF$_6$ **(16)**

[Ru(bpy)$_2$(2,5-dpp)Re(CO)$_3$Cl]PF$_6$ **(17)**

[Ru(dceb)$_2$(2,5-dpp)Re(CO)$_3$Cl]PF$_6$ **(18)**

Figure F2. *Schematic representation of the Ru-Re complexes*

Complex	Emission (77K),(nm)	Lifetime(298K) (aerated)	Lifetime (77K)
[Ru(bpy)2(bis-bpy)Re(CO)$_3$Cl]PF$_6$ **(15)**	610	217.46ns	6.64µs
[Ru(dceb)2(bis-bpy)Re(CO)$_3$Cl]PF$_6$ **(16)**	616	355.62ns	1.66µs
[Ru(bpy)2(2,5-dpp)Re(CO)$_3$Cl]PF$_6$ **(17)**	748	0.532ns	10.23µs
[Ru(dceb)2(2,5-dpp)Re(CO)$_3$Cl]PF$_6$ **(18)**	706	0.527ns	4.2µs

Table F2. *Tabulated emission (77 K) and lifetime (77 K & 298 K) for Ru-Re complexes. (298K measurements were done in ACN and 77 K measurements in EtOH:MeOH (4:1) mixture)*

Lifetime decay curves and decay fit curve with results for Ru (II) complexes (1) to (14) in aerated and deaerated ACN

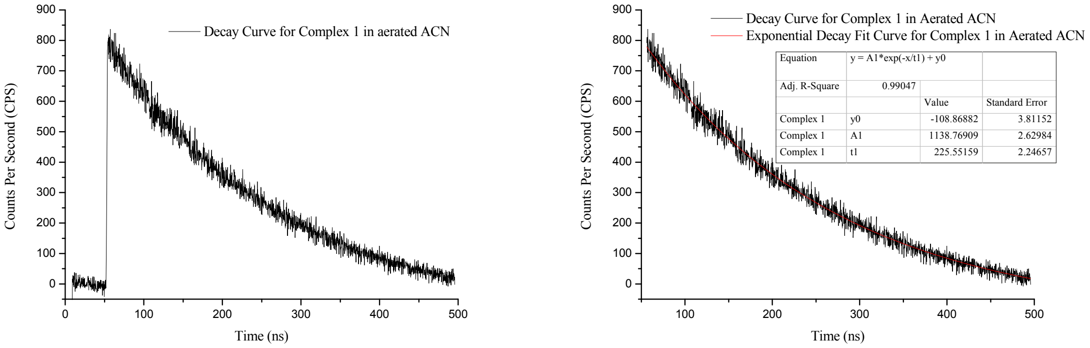

Equation	y = A1*exp(-x/t1) + y0		
Adj. R-Square	0.99047		
		Value	Standard Error
Complex 1	y0	-108.86882	3.81152
Complex 1	A1	1138.76909	2.62984
Complex 1	t1	225.55159	2.24657

Figure F3. *Decay curve and decay fit curve for complex [Ru(bpy)$_2$(bpp)]PF$_6$* ***(1)*** *in aerated ACN*

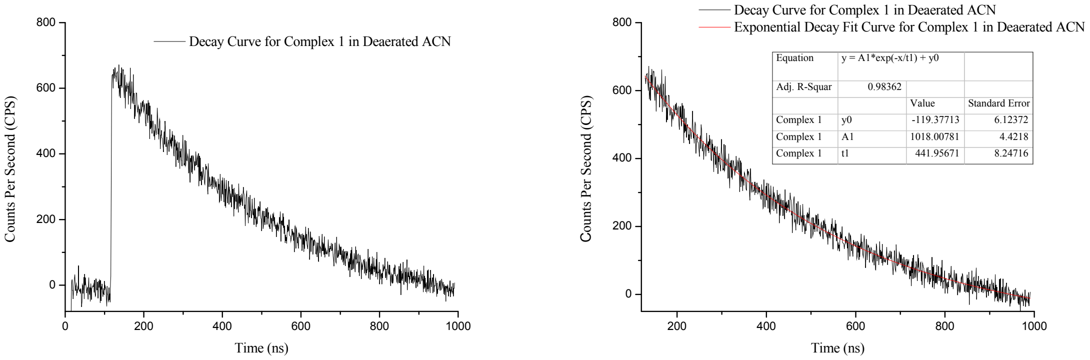

Equation	y = A1*exp(-x/t1) + y0		
Adj. R-Squar	0.98362		
		Value	Standard Error
Complex 1	y0	-119.37713	6.12372
Complex 1	A1	1018.00781	4.4218
Complex 1	t1	441.95671	8.24716

Figure F4. *Decay curve and decay fit curve for complex [Ru(bpy)$_2$(bpp)]PF$_6$* ***(1)*** *in deaerated ACN*

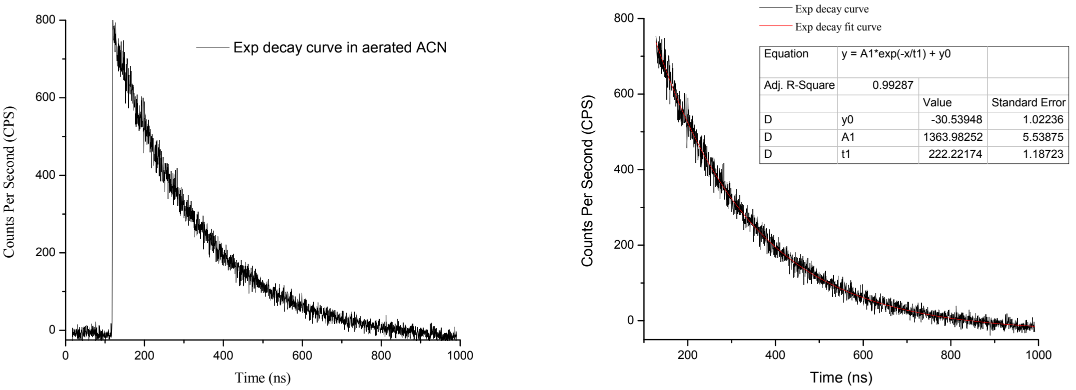

Equation	y = A1*exp(-x/t1) + y0		
Adj. R-Square	0.99287		
		Value	Standard Error
D	y0	-30.53948	1.02236
D	A1	1363.98252	5.53875
D	t1	222.22174	1.18723

Figure F5. *Decay curve and decay fit curve for complex [Ru(d$_8$-bpy)$_2$(bpp)]PF$_6$* ***1(d)*** *in aerated ACN*

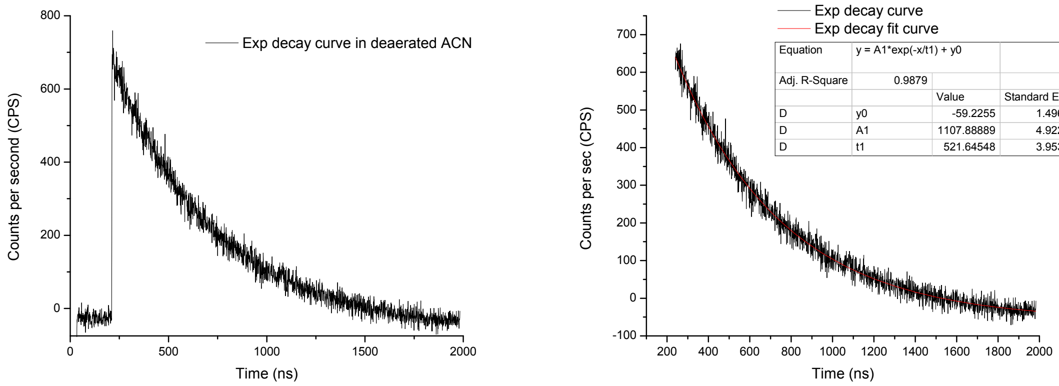

Equation	y = A1*exp(-x/t1) + y0		
Adj. R-Square	0.9879		
		Value	Standard Error
D	y0	-59.2255	1.49678
D	A1	1107.88889	4.92205
D	t1	521.64548	3.95319

Figure F6. *Decay curve and decay fit curve for complex [Ru(d_8-bpy)$_2$(bpp)]PF_6* ***1(d)*** *in deaerated ACN*

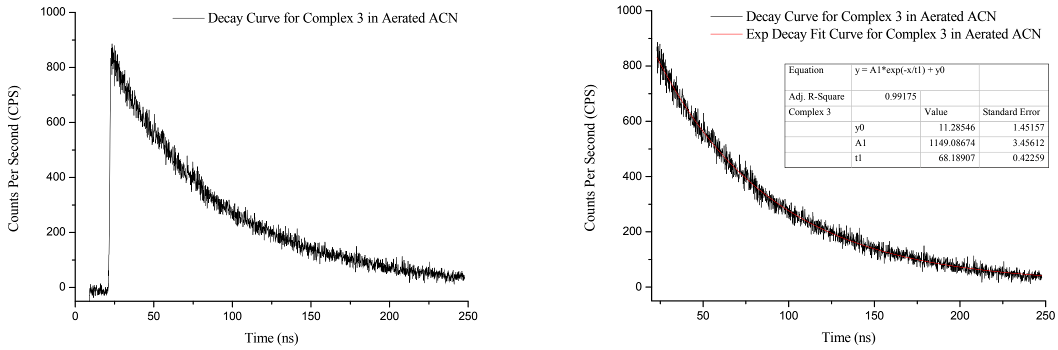

Equation	y = A1*exp(-x/t1) + y0		
Adj. R-Square	0.99175		
Complex 3		Value	Standard Error
	y0	11.28546	1.45157
	A1	1149.08674	3.45612
	t1	68.18907	0.42259

Figure F7. *Decay curve and decay fit curve for complex [Ru(bpy)$_2$(bpp)PdCl]$_2$(PF_6)$_6$* ***(3)*** *in aerated ACN*

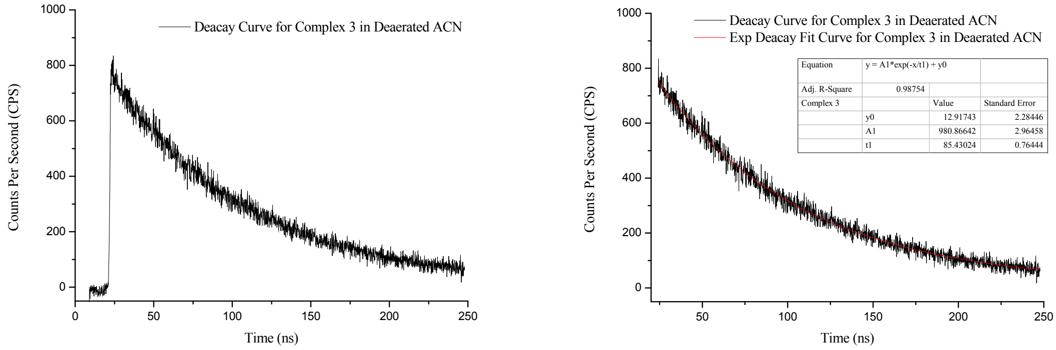

Equation	y = A1*exp(-x/t1) + y0		
Adj. R-Square	0.98754		
Complex 3		Value	Standard Error
	y0	12.91743	2.28446
	A1	980.86642	2.96458
	t1	85.43024	0.76444

Figure F8. *Decay curve and decay fit curve for complex [Ru(bpy)$_2$(bpp)PdCl]$_2$(PF_6)$_6$* ***(3)*** *in deaerated ACN*

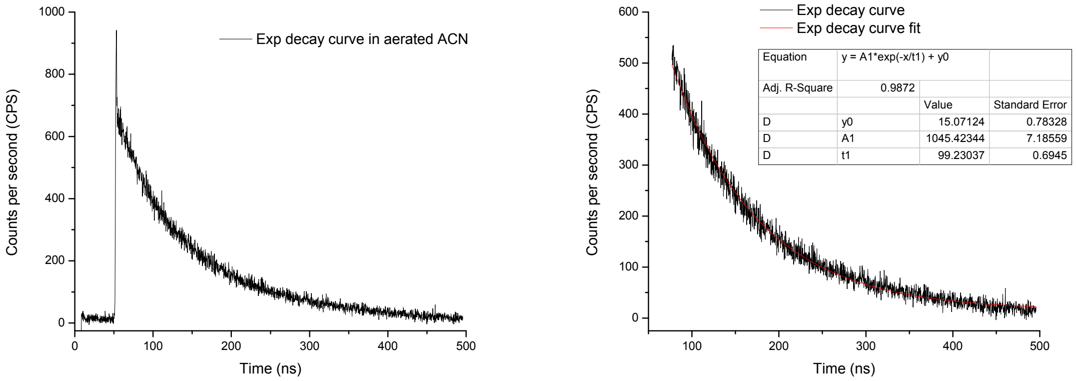

Equation	y = A1*exp(-x/t1) + y0		
Adj. R-Square	0.9872		
		Value	Standard Error
D	y0	15.07124	0.78328
D	A1	1045.42344	7.18559
D	t1	99.23037	0.6945

Figure F9. *Decay curve and decay fit curve for complex [Ru(d*$_8$*-bpy)*$_2$*(bpp)PdCl]*$_2$*(PF*$_6$*)*$_6$ ***(3d)*** *in aerated ACN*

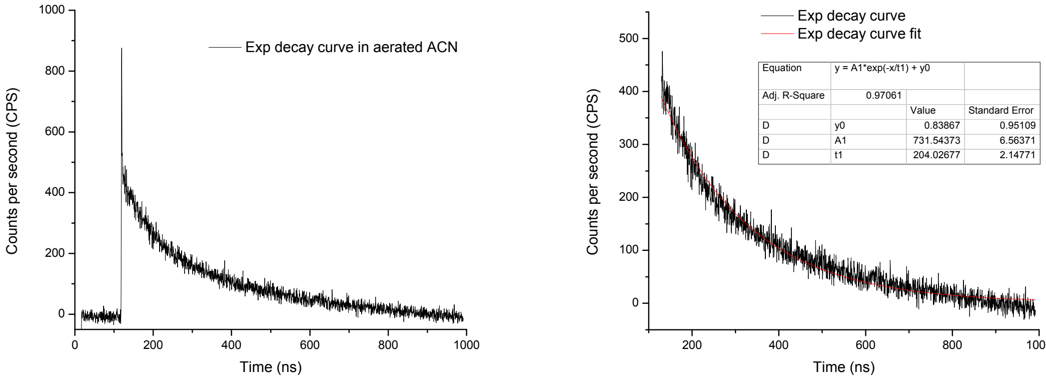

Equation	y = A1*exp(-x/t1) + y0		
Adj. R-Square	0.97061		
		Value	Standard Error
D	y0	0.83867	0.95109
D	A1	731.54373	6.56371
D	t1	204.02677	2.14771

Figure F10. *Decay curve and decay fit curve for complex [Ru(d*$_8$*-bpy)*$_2$*(bpp)PdCl]*$_2$*(PF*$_6$*)*$_6$ ***(3d)*** *in deaerated ACN*

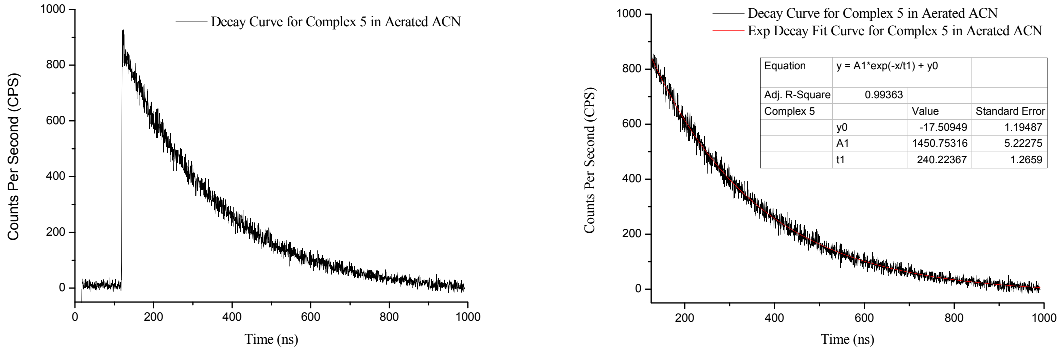

Equation	y = A1*exp(-x/t1) + y0		
Adj. R-Square	0.99363		
Complex 5		Value	Standard Error
	y0	-17.50949	1.19487
	A1	1450.75316	5.22275
	t1	240.22367	1.2659

Figure F11. *Decay curve and decay fit curve for complex [Ru(bpy)*$_2$*(bis-bpy)]2PF*$_6$ ***(5)*** *in aerated ACN*

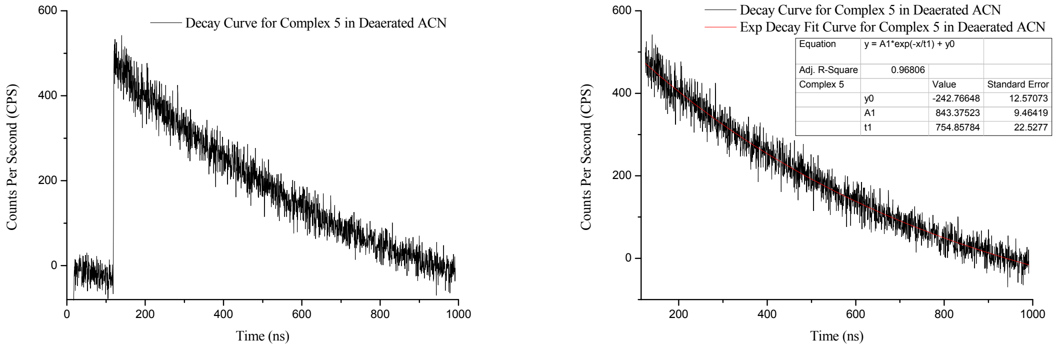

Equation	y = A1*exp(-x/t1) + y0		
Adj. R-Square	0.96806		
Complex 5		Value	Standard Error
	y0	-242.76648	12.57073
	A1	843.37523	9.46419
	t1	754.85784	22.5277

***Figure F12**. Decay curve and decay fit curve for complex [Ru(bpy)$_2$(bis-bpy)]2PF$_6$ **(5)** in deaerated ACN*

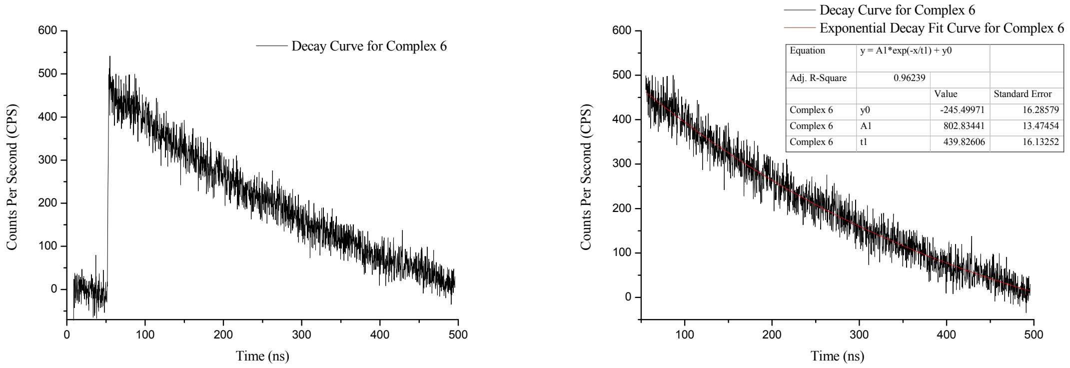

Equation	y = A1*exp(-x/t1) + y0		
Adj. R-Square	0.96239		
		Value	Standard Error
Complex 6	y0	-245.49971	16.28579
Complex 6	A1	802.83441	13.47454
Complex 6	t1	439.82606	16.13252

***Figure F13**. Decay curve and decay fit curve for complex [Ru(dceb)$_2$(bis-bpy)]2PF$_6$ **(6)** in aerated ACN*

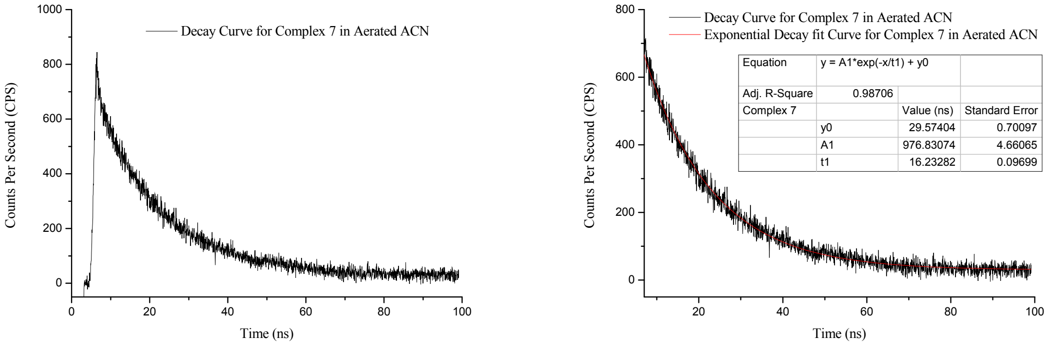

Equation	y = A1*exp(-x/t1) + y0		
Adj. R-Square	0.98706		
Complex 7		Value (ns)	Standard Error
	y0	29.57404	0.70097
	A1	976.83074	4.66065
	t1	16.23282	0.09699

***Figure F14**. Decay curve and decay fit curve for complex [Ru(bpy)$_2$(bis-bpy)PdCl$_2$]2PF$_6$ **(7)** in aerated ACN*

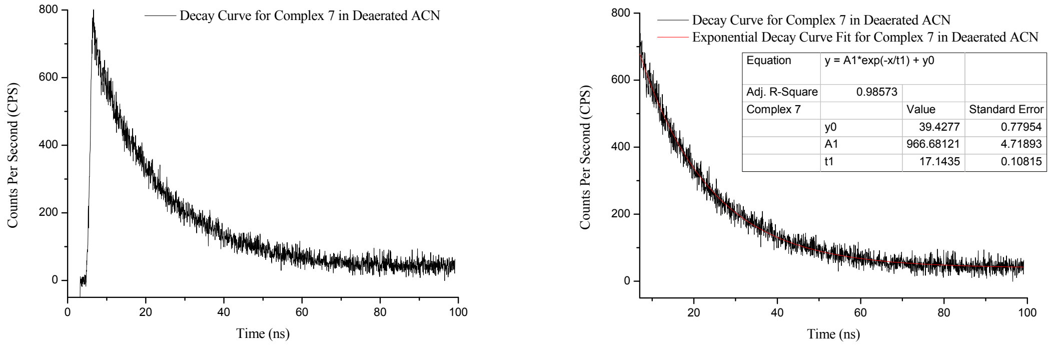

Equation	y = A1*exp(-x/t1) + y0		
Adj. R-Square	0.98573		
Complex 7		Value	Standard Error
	y0	39.4277	0.77954
	A1	966.68121	4.71893
	t1	17.1435	0.10815

***Figure F15**. Decay curve and decay fit curve for complex [Ru(bpy)$_2$(bis-bpy)PdCl$_2$]2PF$_6$ **(7)** in deaerated ACN*

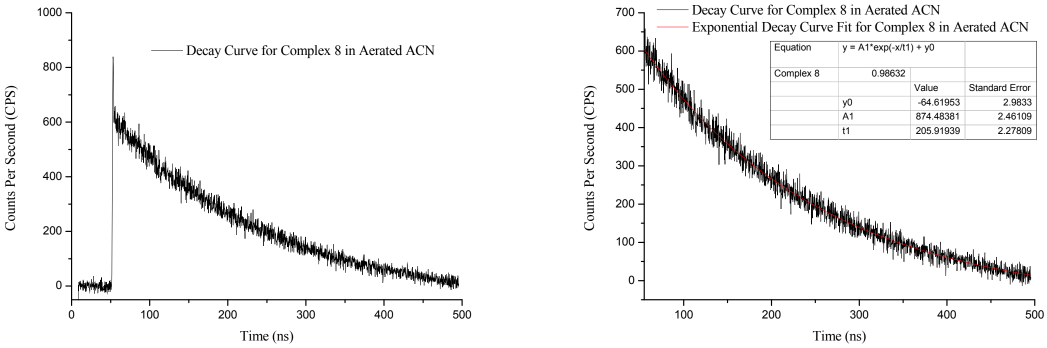

Equation	y = A1*exp(-x/t1) + y0		
Complex 8	0.98632		
		Value	Standard Error
	y0	-64.61953	2.9833
	A1	874.48381	2.46109
	t1	205.91939	2.27809

***Figure F16**. Decay curve and decay fit curve for complex [Ru(bpy)$_2$(bis-bpy)PtCl$_2$]2PF$_6$ **(8)** in aerated ACN*

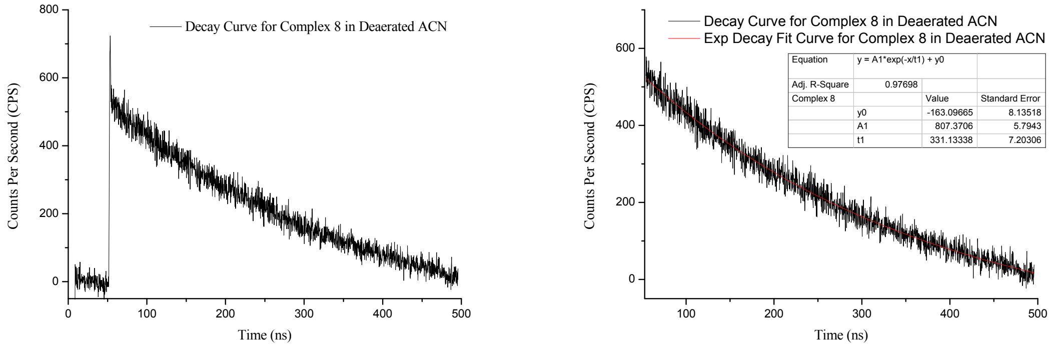

Equation	y = A1*exp(-x/t1) + y0		
Adj. R-Square	0.97698		
Complex 8		Value	Standard Error
	y0	-163.09665	8.13518
	A1	807.3706	5.7943
	t1	331.13338	7.20306

***Figure F17**. Decay curve and decay fit curve for complex [Ru(bpy)$_2$(bis-bpy)PtCl$_2$]2PF$_6$ **(8)** in deaerated ACN*

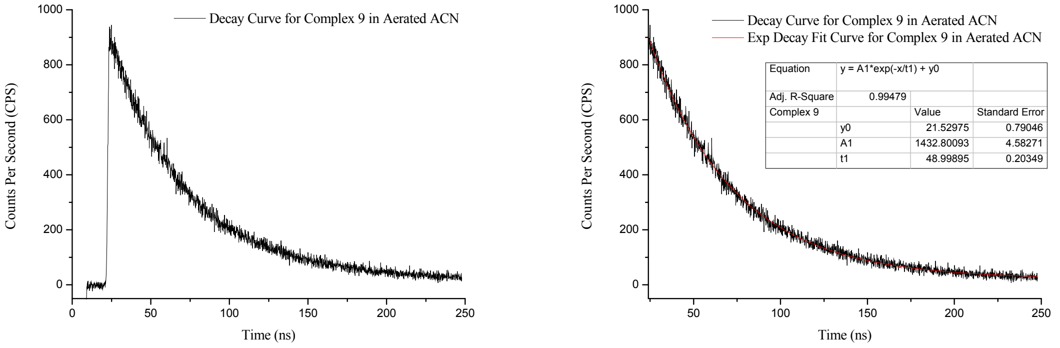

Equation	y = A1*exp(-x/t1) + y0		
Adj. R-Square	0.99479		
Complex 9		Value	Standard Error
	y0	21.52975	0.79046
	A1	1432.80093	4.58271
	t1	48.99895	0.20349

***Figure F18**. Decay curve and decay fit curve for complex* $[Ru(dceb)_2(bis\text{-}bpy)PdCl_2]2PF_6$ ***(9)** in aerated ACN*

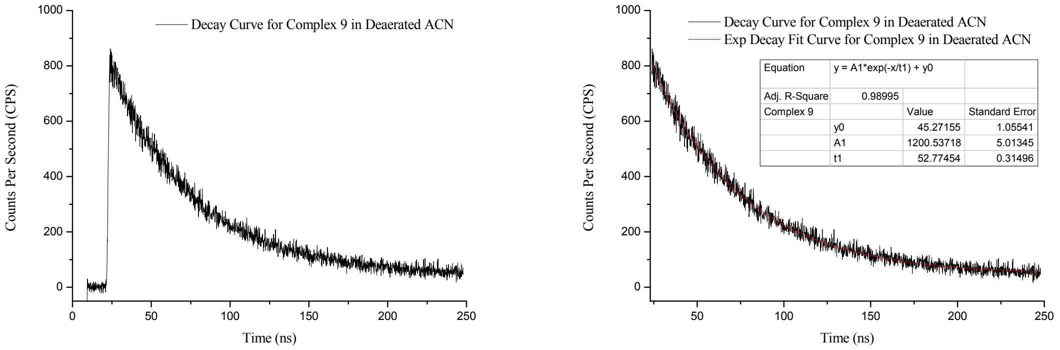

Equation	y = A1*exp(-x/t1) + y0		
Adj. R-Square	0.98995		
Complex 9		Value	Standard Error
	y0	45.27155	1.05541
	A1	1200.53718	5.01345
	t1	52.77454	0.31496

***Figure F19**. Decay curve and decay fit curve for complex* $[Ru(dceb)_2(bis\text{-}bpy)PdCl_2]2PF_6$ ***(9)** in deaerated ACN*

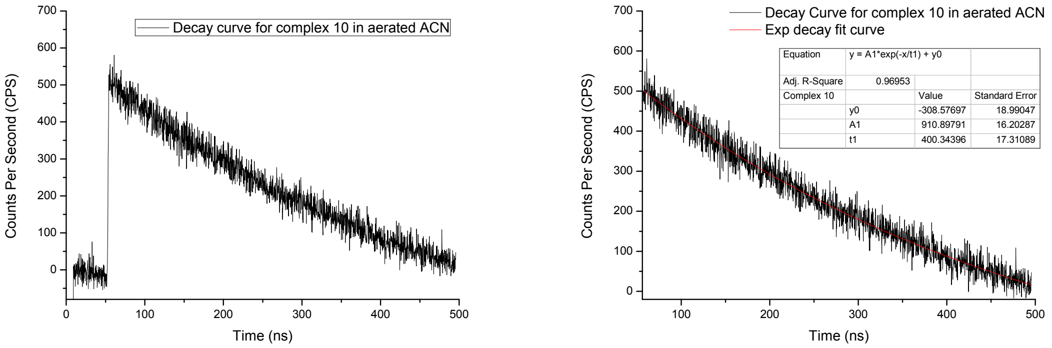

Equation	y = A1*exp(-x/t1) + y0		
Adj. R-Square	0.96953		
Complex 10		Value	Standard Error
	y0	-308.57697	18.99047
	A1	910.89791	16.20287
	t1	400.34396	17.31089

***Figure F20**. Decay curve and decay fit curve for complex* $[Ru(dceb)_2(bis\text{-}bpy)PtCl_2]2PF_6$ ***(10)** in aerated ACN*

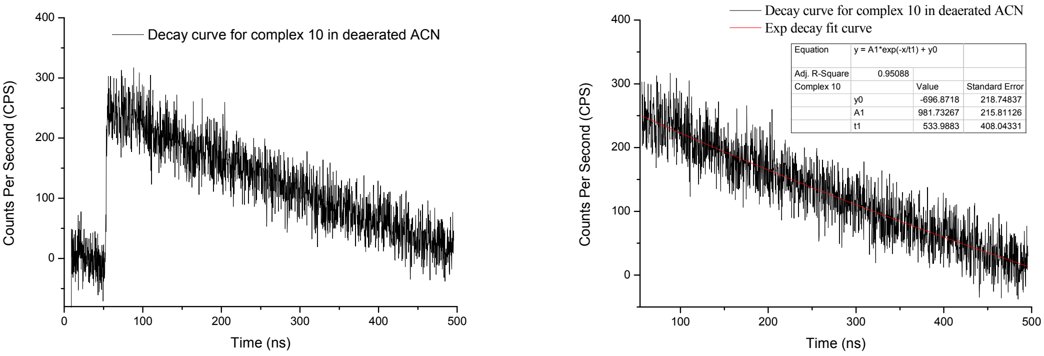

Equation	y = A1*exp(-x/t1) + y0		
Adj. R-Square	0.95088		
Complex 10		Value	Standard Error
	y0	-696.8718	218.74837
	A1	981.73267	215.81126
	t1	533.9883	408.04331

Figure F21. *Decay curve and decay fit curve for complex [Ru(dceb)$_2$(bis-bpy)PtCl$_2$]2PF$_6$* ***(10)*** *in deaerated ACN*

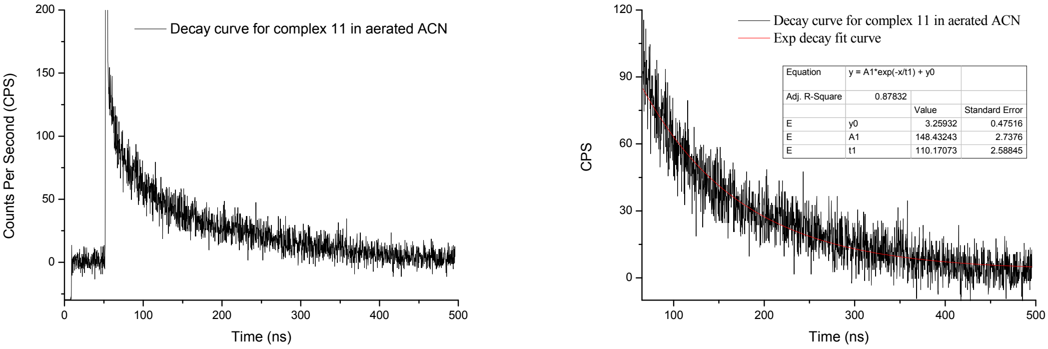

Equation	y = A1*exp(-x/t1) + y0		
Adj. R-Square	0.87832		
		Value	Standard Error
E	y0	3.25932	0.47516
E	A1	148.43243	2.7376
E	t1	110.17073	2.58845

Figure F22. *Decay curve and decay fit curve for complex [Ru(dcab)$_2$(bis-bpy)PtCl$_2$]2PF$_6$* ***(11)*** *in aerated ACN*

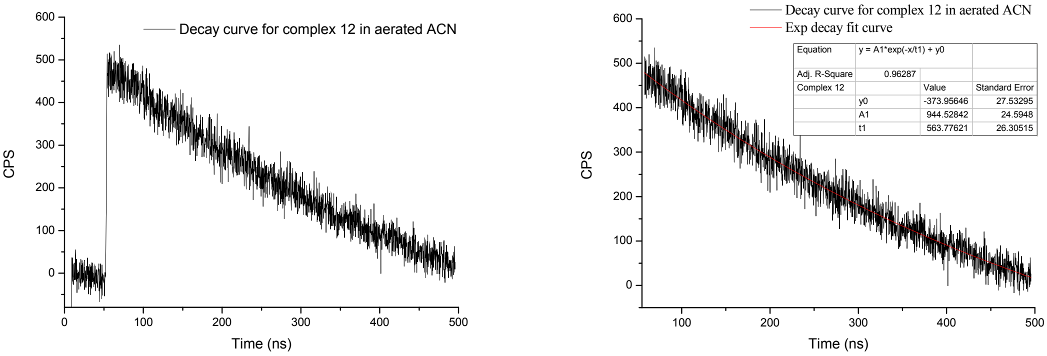

Equation	y = A1*exp(-x/t1) + y0		
Adj. R-Square	0.96287		
Complex 12		Value	Standard Error
	y0	-373.95646	27.53295
	A1	944.52842	24.5948
	t1	563.77621	26.30515

Figure F23. *Decay curve and decay fit curve for complex [Ru(dceb)$_2$(2,5-dpp)]2PF$_6$* ***(12)*** *in aerated ACN*

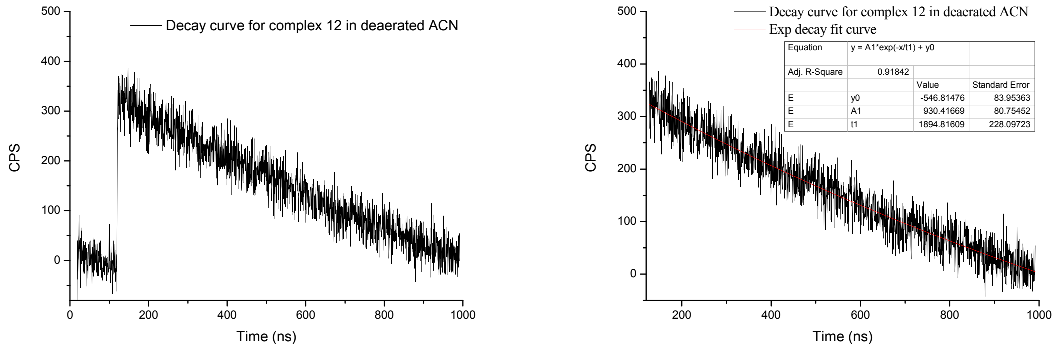

Equation	y = A1*exp(-x/t1) + y0		
Adj. R-Square	0.91842		
		Value	Standard Error
E	y0	-546.81476	83.95363
E	A1	930.41669	80.75452
E	t1	1894.81609	228.09723

***Figure F24**. Decay curve and decay fit curve for complex [Ru(dceb)$_2$(2,5-dpp)]2PF$_6$ **(12)** in deaerated ACN*